A Selection of published/presented papers

Volume V (2)
(2009)

Papers 1-20

S Lee

A Selection of published/presented papers
Volume V Part 2

(2009)

S Lee

1 Response to "Comment on 'Current Limitation Effect in Plasma Focus'" [Appl Phys Lett 94, 076101 (2009)]
S Lee and S H Saw
Appl. Phys. Lett. 94, 076102 (2009), DOI:10.1063/1.3081405

2 Optimizing UNU/ICTP PFF Plasma Focus for Neon Soft X-ray Operation
S H Saw, P C K Lee, R S Rawat and S Lee
IEEE Trans Plasma Sci, VOL. 37, NO. 7, 1276-1382 July 2009

3 Soft x-ray yield from NX2 plasma focus
S. Lee, R. S. Rawat, P. Lee and S. H. Saw
J. Appl. Phys. 106, 023309 (2009) (*6 pages*)
Online Publication Date: 30 July 2009

4 Numerical experiments on plasma focus neon soft x-ray scaling
S Lee, S H Saw, P Lee and R S Rawat
Plasma Phys. Control. Fusion 51 (2009) 105013 (8pp) doi:10.1088/0741-3335/51/10/105013
Online at stacks.iop.org/PPCF/51/105013

5 Numerical experiments on plasma focus neutron yield versus pressure compared with laboratory experiments
S Lee, S H Saw, L Soto, S V Springham and S P Moo
Plasma Phys. Control. Fusion 51 (2009) 075006 (11pp)
http://www.iop.org/EJ/abstract/0741-3335/51/7/075006/ doi: 10.1088/0741-3335/51/7/075006

6 Numerical Experiments on Soft X-Ray Emission Optimization of Nitrogen Plasma in 3 kJ Plasma Focus SY-1 Using Modified Lee Model
M. Akel, Sh. Al- Hawat and S Lee
J Fusion Energy (2009) DOI 10.1007/s10894-009-9203-4 Online First May 19 2009
http://www.springerlink.com/content/6n73j86044542676/?p=6dabe9c2a0714490975c710a1c0a3198&pi=0

7 Pinch Current and Soft x-ray yield limitation by numerical experiments on Nitrogen Plasma Focus
M Akel, S Hawat, S Lee
J Fusion Energy (21 August 2009) DOI 10.1007/s10894-009-9238-6 First online 21 August 2009

8 Numerical Experiments on Oxygen Soft X-Ray Emissions from Low Energy Plasma Focus Using Lee Model
M. Akel, Sh. Al- Hawat, S. H. Saw and S Lee
Journal of Fusion Energy DOI 10.1007/s10894-009-9262-6 First online 22 November 2009

9 Neutron Yield Saturation in Plasma Focus-A fundamental cause
S. Lee
App Phys Lett 95, 151503 (2009) published online 15 October 2009
URL: http://link.aip.org/link/?APL/95/151503

10 Diagnostics and Insights from Current waveform and Modelling of Plasma Focus
S Lee
Keynote address: International Workshop on Plasma Diagnostics & Applications, Singapore 2-3 July (2009) powerpoint

11 Scaling laws for plasma focus machines from numerical experiments
S H Saw & S Lee
Invited paper: International Workshop on Plasma Diagnostics and Applications, Singapore 2-3 July (2009)

12 Fusion Energy and the Plasma Focus powerpoint
S Lee
Keynote Paper TUBAV Conferences: Nuclear & Renewable Energy Sources Ankara, Turkey, 28 & 29 September 2009. Procs: pg 9-18

13 Scaling the plasma focus for fusion energy considerations
Sor Heoh Saw and Sing Lee
Invited Paper TUBAV Conferences: Nuclear & Renewable Energy Sources Ankara, Turkey, 28 & 29 September 2009. Procs: pg 61-70

14 Latest Trends in fusion studies with plasma focus devices
S Lee & S H Saw
Invited talk presented at Saraykoy Nuclear Research Training Centre, Ankara, Turkey; 1 October 2009

15 Energy gain from thermonuclear fusion
S Lee & S H Saw
Invited talk presented at Turkish Science & Research Foundation, Ankara, Turkey 1 October 6 p.m

16 Plasma focus fusion devices
S Lee & S H Saw
Invited talk, presented at Gazi University, Technical Education Faculty, 2 October 2009

17 Plasma Fusion Energy Technology powerpoint
S Lee & S H Saw
Invited First Keynote address presented by S H Saw at iCREATE 2009 at Pan Pacific Hotel, KLIA, Malaysia , 23-24 November 2009

18 The effect of anode shape on neon soft x-ray emissions and current sheath configuration in plasma focus device
M A Mohammadi, S Sobhanian, C S Wong, S Lee, P Lee and R S Rawat
J. Phys. D: Appl. Phys. 42 (2009) 045203 (10pp)

19 Backward high energy ion beams from plasma focus
M. V. Roshan, P. Lee, S. Lee, A. Talebitaher, R. S. Rawat, and S. V. Springham
Phys of Plasmas, 074506 2009

20 Effect of cathode structure on neutron yield performance of a miniature plasma focus device
Rishi Verma, R.S. Rawat, P. Lee, S. Lee, S.V. Springham, T.L. Tan, M. Krishnan

The Universal Plasma Focus Facility was set up at INTI-UC on 20

Phys Letts A 373 (2009) 2568 – 2571

Response to "Comment on 'Pinch current limitation effect in plasma focus'" [Appl. Phys. Lett. 94, 076101 (2009)]

S. Lee[1,2,a] and S. H. Saw[2]
[1]*Institute for Plasma Focus Studies, 32 Oakpark Drive, Chadstone, Victoria 3148, Australia and National Institute of Education, Nanyang Technological University, Singapore 637616, Singapore*
[2]*INTI International University College, 71800 Nilai, Malaysia*

(Received 5 January 2009; accepted 19 January 2009; published online 17 February 2009)

The main point of the comment [Appl. Phys. Lett. **94**, 076101 (2009)] is that Eq. (2) and consequentially Eq. (3) of the commented paper [Appl. Phys. Lett. **92**, 021503 (2008)] require correction. The alternative equation suggested in the comment is derived using Kirchhoff's voltage rule. The comment consider only the energy distribution in the inductive components and the resultant equation confirms a progressive lowering of the $I_{\text{pinch}}/I_{\text{peak}}$ ratio as the static inductance L_0 is reduced, lowering from 0.87 to 0.31 as L_0 is reduced from 100 to 5 nH according to the revised formula corresponding to Eq. (3), compared to 0.63–0.25 according to Eq. (3). This progressive lowering of the ratio $I_{\text{pinch}}/I_{\text{peak}}$ due to the inductive energy distribution is one of two factors responsible for the pinch current limitation. The other factor is the progressive reduction in the *L-C* interaction time compared to the current dip duration denoted by δ_{cap} in Eq. (2). The comment does not deal with δ_{cap} at all; hence, its conclusion based on inductive energy distribution only is not useful, since in the low L_0 region when pinch current limitation begins to manifest, δ_{cap} becomes more and more the dominant factor. In any case, the results of the paper do not depend on Eqs. (2) and (3), which are used in the paper only for illustrative purposes. © *2009 American Institute of Physics*. [DOI: 10.1063/1.3081405] [DOI: 10.1063/1.3081405]

The paper[1] has one primary point: that for any given capacitance, the pinch current does not increase beyond a certain value however low the static inductance is decreased to. This point is demonstrated by using the Lee model code, which couples the electrical circuit with plasma focus motion, numerically solving these coupled equations point by point through time. All interactions of inductances, capacitance, stray resistance, and motional impedances are taken care of in the code. The formulation of the code is completely consistent with Kirchhoff's voltage and current rules. Equation 2, approximated for brevity, is not used in the code, nor is the further approximated Eq. (3). Their role in the paper is simply to highlight the factors responsible for the pinch current limitation. These factors are now explained as follows:

(a) Lowering L_0 increases I_{peak}, leading necessarily to an increase in "a," hence z_p, hence L_p. The net result is a drop in the fraction $I_{\text{pinch}}/I_{\text{peak}}$.
(b) Lowering L_0 reduces the *L-C* interaction time of the bank while increasing the radial current dip duration. As L_0 is reduced the capacitor bank is more and more coupled to the inductive energy transfer processes. In other words δ_{cap} in Eq. (2) becomes more and more important. I_{pinch} is already reduced by the effect considered in point (a) above, and then δ_{cap} adds in to cause the limitation to I_{pinch} as L_0 is reduced further.

In the paper,[1] Eq. (2) was derived by an inspection of the energy distribution to bring out the two points above. The alternative equation suggested by the comment[2] may be a better representation as far as the inductive components are concerned. However in the low L_0 situations under discussion, this increased accuracy (of *one* of the factors) serves little purpose since the *other* factor of increasing capacitance-coupling (δ_{cap}) is really the dominant factor.

Moreover Eq. (2) serves its purposes to show points (a) and (b) sufficiently clearly. The alternative equations of the comment do not show anything more or new in that respect.

The comment also suggest that keeping the filling pressure constant is "not too reasonable since experimentally changing the filling pressure is far simpler than changing the electrodes geometry and/or the circuit connections." This seems to present the viewpoint of the "hardware" experimentalist. The numerical experimentalist may suggest that the freedom to change any parameter easily makes the numerical experiments more wide-ranging, enabling a greater range of phenomena to be explored. The comment further claim that the "discussed pinch current limitation starts to manifest when the electrodes switches from Mather-type to a Filippov-type and … assumption that $z_p \sim a$ still holds is rather dubious and does not have … experimental support." Contrary to what the comment implies, the regime of current limitation typically starts with electrode parameters still within Mather-type. For example for computations based on the PF1000, current limitation is computed[3] to start as the static inductance is reduced to $L_0 \sim 40$ nH, $z_0 \sim 55$ cm with $a = 15.5$ cm. This is still a Mather-type configuration. Current waveform data[1] of PF1000 show that its static inductance of 33 nH is already low enough to be pinch current limited (i.e., lowering its L_0 further will not increase I_{pinch}). PF1000 has published results[4] of visible and x-ray images

[a]Electronic mail: leesing@optusnet.com.au.

showing $z_p \sim 0.7a - 0.9a$. One further note on a remark by the comment that the radial phase is treated as "a sort of snow plough model." In fact, our code uses a slug model[5,6] for the radial phase. However, we point out that the left hand side of Eq. (1)[1] should be multiplied by a factor n_i.

[1]S. Lee and S. H. Saw, Appl. Phys. Lett. **92**, 021503 (2008).
[2]H. Bruzzone and H. Acuna, Appl. Phys. Lett. **94**, 076101 (2009), preceding comment.
[3]S. Lee, P. Lee, S. H. Saw, and R. S. Rawat, Plasma Phys. Controlled Fusion **50**, 065012 (2008).
[4]V. A. Gribkov, B. Bienkowska, M. Borowiecki, A. V. Dubrovsky, I. Ivanova-Stanik, L. Karpinski, R. A. Miklaszewski, M. Paduch, M. Scholz, and K. Tomaszewski, J. Phys. D: Appl. Phys. **40**, 1977 (2007).
[5]D. E. Potter, Phys. Fluids **14**, 1911 (1971).
[6]S. Lee, radiative dense plasma focus computation package RADPF http://www.plasmafocus.net/IPFS%20folders/modelpackage/File2Theory.pdf.

Optimizing UNU/ICTP PFF Plasma Focus for Neon Soft X-ray Operation

Sor Heoh Saw, Paul Choon Keat Lee, Rajdeep Singh Rawat, and Sing Lee

***Abstract*—The United Nations University/International Centre for Theoretical Physics Plasma Focus Facility (UNU/ICTP PFF), a 3.3-kJ plasma focus, was designed for operation in deuterium with a speed factor S such that the axial run-down time matches the current rise time at an end axial speed of nearly 10 cm/μs. For operation in neon, we first consider that a focus pinch temperature between 200 and 500 eV may be suitable for a good yield of neon soft X-rays, which corresponds to an end axial speed of 6–7 cm/μs. On this basis, for operation in neon, the standard UNU/ICTP PFF needs to have its anode length z_0 reduced by some 30%–40% to maintain the time matching. Numerical experiments using the Lee model code are carried out to determine the optimum configuration of the electrodes for the UNU/ICTP PFF capacitor system. The results show that an even more drastic shortening of anode length z_0 is required, from the original 16 to 7 cm, at the same time, increasing the anode radius "a" from 0.95 to 1.2 cm, to obtain an optimum yield of $Y_{\mathrm{sxr}} = 9.5$ J. This represents a two- to threefold increase in the Y_{sxr} from that computed for the standard UNU/ICTP PFF.**

***Index Terms*—Dense plasma focus, neon plasma, numerical experiments, soft X-ray (SXR) source.**

I. Introduction

THE UNITED Nations University/International Centre for Theoretical Physics Plasma Focus Facility (UNU/ICTP PFF) has a unique standing in the study of plasma focus. This plasma focus system was developed under the funding and support of UNU, ICTP, and the Asian African Association for Plasma Training to initiate and promote practical knowledge and skills in plasma physics, including fusion, in developing countries [1]. It is the only plasma focus machine operating in nine research laboratories in seven countries. Research studies carried out using the UNU/ICTP PFFs have led, at last count, 11 years ago [2], to the publication of more than 200 research papers, 20 Ph.D. degrees, and 40 master's degrees. It has been successful in achieving its objectives and remains one of the most cost-effective and reliable plasma focus machines for the studies of dense multiradiation plasma sources.

Manuscript received March 4, 2009; revised April 17, 2009. First published June 12, 2009; current version published July 9, 2009.

S. H. Saw is with the Institute for Plasma Focus Studies, Melbourne, Vic. 3148, Australia, and also with the Centre for Plasma Research, INTI University College, Nilai 71800, Malaysia (e-mail: saw_sorheoh@intimal.edu.my).

P. C. K. Lee and R. S. Rawat are with the Radiation Sources Laboratory, Natural Sciences and Science Education, National Institute of Education, Nanyang Technological University, Singapore 637616 (e-mail: paul.lee@nie.edu.sq; Rajdeep.rawat@nie.edu.sq).

S. Lee is with the Institute for Plasma Focus Studies, Melbourne, Vic. 3148, Australia, with INTI University College, Nilai 71800, Malaysia, and with the Natural Sciences and Science Education, National Institute of Education, Nanyang Technological University, Singapore 637616 (e-mail: leesing@optusnet.com.au).

Digital Object Identifier 10.1109/TPS.2009.2022167

The UNU/ICTP PFF is a 3.3-kJ Mather-type plasma focus system powered by a single 15-kV 30-μF Maxwell capacitor switched on by a simple parallel-plate swinging cascade air gap [3]. The system produces remarkably consistent focusing actions and neutron yields of $0.5-1.0 \times 10^8$ neutrons per discharge at 3.0 torr of deuterium operating at 15 kV and 180 kA [3], [4]. This was not unexpected as the UNU/ICTP PFF was designed for optimum neutron yield in deuterium. It has a speed factor $S = (I/a)/P_0^{0.5}$ of 97 kA/cm per $[\text{torr of deuterium}]^{1/2}$ that is consistent with the range of other neutron-optimized plasma focus devices operating in deuterium [5]. The speed factor determines the speed in both the axial and radial phases. For operation in deuterium, this corresponds to just under 10 cm/μs for the end axial phase (just before the start of the radial phase) and a radial speed of 25 cm/μs when the imploding shock nears the axis. The ratio of average to end axial speed for a typical focus device is around 0.6. Thus, the UNU/ICTP PFF is designed for an average axial speed of 6 cm/μs running over an anode length of 16 cm. This ensures that the axial run-down time matches the effective current rise time of 2.6 μs at an end axial speed of nearly 10 cm/μs [3].

However, for operation in neon, Liu [6] and Bing [7] have shown that a focus pinch compression temperature of 200–500 eV is suitable for a good yield of neon soft X-rays (SXRs). For the UNU/ICTP PFF, Liu has shown that the required end axial speed is around 6–7 cm/μs, giving an average axial speed of around 4 cm/μs. In terms of time matching, this means that, for operation in neon, the standard UNU/ICTP PFF has too long an anode and that this anode has to be reduced by some 30%–40% to maintain the time matching. These factors in design consideration are basic and have been discussed in more detail in an introductory document (paragraph titled "Designing a new plasma focus") of the Lee model code [8]. We use these considerations as a starting point in our optimization of the UNU/ICTP PFF for neon operation. The numerical experiments, as will be seen, then go on to show that the required reduction on anode length z_0 is more drastic than expected.

II. Lee Model Code Incorporating Line Radiation

The Lee model code couples the electrical circuit with plasma focus dynamics, thermodynamics, and radiation, enabling a realistic simulation of all gross focus properties. The basic model, described in 1984 [9], was successfully used to assist several projects [3], [10], [11]. Radiation-coupled dynamics was included in the five-phase code, leading to numerical experiments on radiation cooling [12]. The vital role of a finite small disturbance speed discussed by Potter in a Z-pinch situation

[13] was incorporated together with real gas thermodynamics and radiation-yield terms. Before this "communication delay effect" was incorporated, the model consistently overestimated the radial speeds. This is serious from the point of view of neutron yields. A factor of two in shock speeds gives a factor of four in temperatures, leading to a difference in fusion cross sections of approximately 1000 at the range of temperatures that we are dealing with. This version of the code assisted other research projects [5]–[7], [14]–[16] and was web published in 2000 [17] and 2005 [18]. Plasma self-absorption was included in 2007 [16], improving the SXR yield simulation. The code has been used extensively in several machines including UNU/ICTP PFF [2]–[6], [14], [15], [19], NX2 [7], [16], [20], and NX1 [20], [21] and has been adapted for the Filippov-type plasma focus DENA [22]. A recent development is the inclusion of the neutron yield Y_n using a beam–target mechanism [23]–[27], incorporated in recent versions [8] of the code (versions later than RADPFV5.13), resulting in realistic Y_n scaling with I_{pinch} [23], [24]. The versatility and utility of the model are demonstrated in its clear distinction of I_{pinch} from I_{peak} [28] and the recent uncovering of a plasma focus pinch current limitation effect [25], [26]. The description, theory, code, and a broad range of results of this "Universal Plasma Focus Laboratory Facility" are available for download from [8].

A brief description of the code is given in the following. The five phases are summarized as follows.

1) Axial phase: Described by a snowplow model with an equation of motion coupled to a circuit equation. The equation of motion incorporates the axial phase model parameters: mass and current factors f_m and f_c, respectively. The mass swept-up factor f_m accounts for not only the porosity of the current sheet but also for the inclination of the moving current sheet—shock front structure and all other unspecified effects which have effects equivalent to increasing or reducing the amount of mass in the moving structure—during the axial phase. The current factor f_c accounts for the fraction of current effectively flowing in the moving structure (due to all effects such as current shedding at or near the back-wall and current-sheet inclination). This defines the fraction of current effectively driving the structure during the axial phase.
2) Radial inward shock phase: Described by four coupled equations using an elongating slug model. The first equation computes the radial inward shock speed from the driving magnetic pressure. The second equation computes the axial elongation speed of the column. The third equation computes the speed of the current sheath, also called the magnetic piston, allowing the current sheath to separate from the shock front by applying an adiabatic approximation. The fourth is the circuit equation. Thermodynamic effects due to ionization and excitation are incorporated into these equations, these effects being important for gases other than hydrogen and deuterium. Temperature and number densities are computed during this phase. A communication delay between shock front and current sheath due to the finite small disturbance speed is crucially implemented in this phase. The model parameters, radial phase mass swept-up and current factors f_{mr} and f_{cr} are incorporated in all three radial phases. The mass swept-up factor f_{mr} accounts for all mechanisms which have effects equivalent to increasing or reducing the amount of mass in the moving slug during the radial phase. The current factor f_{cr} accounts for the fraction of current effectively flowing in the moving piston forming the back of the slug (due to all effects). This defines the fraction of current effectively driving the radial slug.
3) Radial reflected shock (RS) phase: When the shock front hits the axis, because the plasma focus is collisional, an RS develops, which moves radially outward, while the radial current-sheath piston continues to move inward. Four coupled equations are also used to describe this phase, these being for the RS moving radially outward, the piston moving radially inward, the elongation of the annular column, and the circuit. The same model parameters f_{mr} and f_{cr} are used as in the previous radial phase. The plasma temperature behind the RS undergoes a jump by a factor of approximately two.
4) Slow compression (quiescent) or pinch phase: When the outgoing RS hits the incoming piston, the compression enters a radiative phase in which, for gases such as neon, radiation emission may actually enhance the compression, where we have included energy loss/gain terms from Joule heating and radiation losses into the piston equation of motion. Three coupled equations describe this phase, these being the piston radial motion equation, the pinch column elongation equation, and the circuit equation, incorporating the same model parameters as in the previous two phases. Thermodynamic effects are incorporated into this phase. The duration of this slow compression phase is set as the time of transit of small disturbances across the pinched plasma column. The computation of this phase is terminated at the end of this duration.
5) Expanded column phase: To simulate the current trace beyond this point, we allow the column to suddenly attain the radius of the anode and use the expanded column inductance for further integration. In this final phase, the snowplow model is used, and two coupled equations are used, similar to the axial phase aforementioned. This phase is not considered important as it occurs after the focus pinch.

We note that the transition from Phase 4 to 5 is observed in laboratory measurements to occur in an extremely short time with plasma/current disruptions, resulting in localized regions of high densities and temperatures. These localized regions are not modeled in the code, which consequently computes only average uniform density and temperature, which are considerably lower than the measured peak density and temperature. However, because the four model parameters are obtained by fitting the computed to the measured total current waveform, the model incorporates the energy and mass balances equivalent, at least in the gross sense, to all the processes which are not even specifically modeled. Hence, the computed gross features such as speeds and trajectories and integrated SXR yields have been

TABLE I
COMPUTED $Y_{\rm sxr}$ ($Q_{\rm line}$) VERSUS P_0 FOR STANDARD UNU/ICTP PFF WITH $L_0 = 110$ nH, $C_0 = 30$ μF, $RESF = 0.2$, $b = 3.2$ cm, $a = 0.95$ cm, AND $z_0 = 16$ cm OPERATING AT 14 kV WITH FITTED MODEL PARAMETERS $f_m = 0.05$, $f_c = 0.7$, $f_{\rm mr} = 0.2$, AND $f_{\rm cr} = 0.8$. PEAK AXIAL, RADIAL SHOCK, AND RADIAL PISTON SPEEDS v_a, v_s, AND v_p ARE ALSO TABULATED. MEASURED DATA ARE FROM THE Ph.D. THESIS OF LIU [6] PUBLISHED IN [20, FIG. 6(c)]

Computed Y_{sxr} vs P_0								Measured data (Liu[6])		
P_0 (Torr)	I_{peak} (kA)	I_{pinch} (kA)	Peak v_a (cm/μs)	Peak v_s (cm/μs)	Peak v_p (cm/μs)	S (kA/cm[Torr Ne]$^{0.5}$)	Q_{line} (J)	P_0 (Torr)	Q_{line} (J)	error range ±
4.2	182	90	4.7	16.0	12.3	94	0.00	5.6	0.1	0.1
4.0	182	94	4.8	17.2	12.9	96	0.10	4.5	1.9	0.3
3.7	181	99	5.0	18.8	13.8	99	1.61	3.8	4.1	0.4
3.5	181	103	5.2	20.2	14.3	102	3.19	3.5	4.1	0.7
3.3	180	103	5.4	21.4	14.7	105	3.92	3.0	5.4	1.0
3.2	180	108	5.5	22.3	14.9	106	3.66	2.7	3.7	0.4
3.1	180	110	5.6	23.0	15.1	108	3.19	2.6	4.1	0.8
2.5	178	119	6.3	25.2	16.4	119	1.36	2.2	0.9	0.3
2.0	176	125	7.0	26.7	17.7	131	0.62	1.6	0.4	0.1
1.5	173	129	8.0	29.6	20.5	149	0.24			
1.0	169	130	9.4	34.6	24.9	178	0.07			

extensively tested in numerical experiments for several machines and are found to be comparable with measured values.

In the code [8], neon line radiation Q_L is calculated as follows:

$$\frac{dQ_L}{dt} = -4.6 \times 10^{-31} n_i^2 Z Z_n^4 \left(\pi r_p^2\right) z_f / T \qquad (1)$$

where, for the temperatures of interest in our experiments, we take the SXR yield $Y_{\rm sxr} = Q_L$. Z_n is the atomic number.

Since, in our code, Q_L is obtained by integrating over the pinch duration, the SXR energy generated within the plasma pinch depends on the following properties: number density n_i, effective charge number Z, pinch radius r_p, pinch length z_f and temperature T, and pinch duration.

This generated energy is then reduced by the plasma self-absorption which depends primarily on density and temperature; the reduced quantity of energy is then emitted as the SXR yield. These effects are included in the modeling by computing volumetric plasma self-absorption factor "A" derived from the photonic excitation number M which is a function of Z_n, n_i, Z, and T. However, in our range of operation, the numerical experiments show that the self-absorption is not significant. It was first pointed out by Liu [6] that a temperature around 300 eV is optimum for SXR production. Bing's subsequent work [7] and our experience through numerical experiments suggest that around 2×10^6 K (below 200 eV) or even a little lower could be better. Hence, unlike the case of neutron scaling, for SXR scaling, there is an optimum small range of temperatures (T windows) to operate.

III. NUMERICAL EXPERIMENTS ON STANDARD UNU/ICTP PFF

To start the numerical experiments, we select a discharge current trace of the UNU/ICTP PFF taken with a Rogowski coil. The following bank, tube, and operation parameters (near the peak SXR yield) are used:

1) bank: static inductance $L_0 = 110$ nH, $C_0 = 30$ μF, and stray resistance $r_0 = 12$ mΩ;

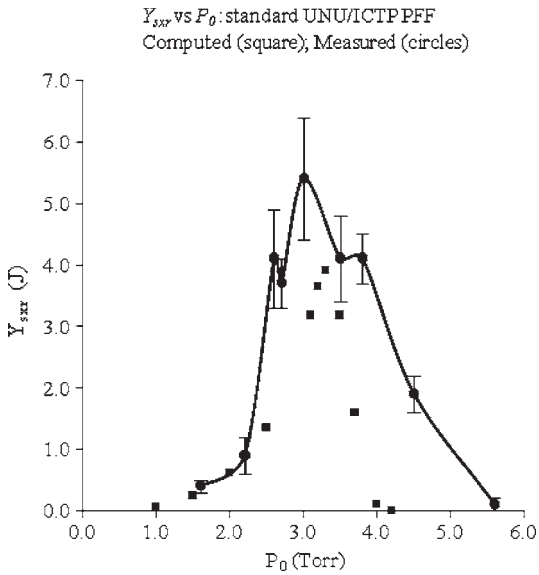

Fig. 1. Computed $Y_{\rm sxr}$ versus P_0 compared to measured [6] $Y_{\rm sxr}$ versus P_0 for standard UNU/ICTP PFF with $L_0 = 110$ nH, $C_0 = 30$ μF, $RESF = 0.2$, $b = 3.2$ cm, $a = 0.95$ cm, and $z_0 = 16$ cm operated at 14 kV in neon, with fitted model parameters $f_m = 0.05$, $f_c = 0.7$, $f_{\rm mr} = 0.2$, and $f_{\rm cr} = 0.8$.

2) tube: cathode radius $b = 3.2$ cm, anode radius $a = 0.95$ cm, and anode length $z_0 = 16$ cm;
3) operation: voltage $V_0 = 14$ kV and pressure $P_0 = 3$ torr neon.

The computed total discharge current waveform is fitted to the measured values by varying model parameters f_m, f_c, $f_{\rm mr}$, and $f_{\rm cr}$ one by one until the computed waveform agrees with the measured waveform. First, the axial model factors f_m and f_c are adjusted (fitted) until the computed rising slope of the total current trace and the rounding off of the peak current as well as the peak current itself are in reasonable (typically good) fit with the measured total current trace. Then, we proceed to adjust (fit) the radial phase model factors $f_{\rm mr}$ and $f_{\rm cr}$ until the computed slope and depth of the dip agree with the measured values. In this case, the following fitted model parameters are obtained: $f_m = 0.05$, $f_c = 0.7$, $f_{\rm mr} = 0.2$, and $f_{\rm cr} = 0.8$.

TABLE II
COMPUTED $Y_{\rm sxr}$ ($Q_{\rm line}$) VERSUS P_0 FOR OPTIMIZED UNU/ICTP PFF WITH $L_0 = 110$ nH, $C_0 = 30$ μF, AND $RESF = 0.2$, OPERATING AT 14 kV WITH FITTED MODEL PARAMETERS $f_m = 0.05$, $f_c = 0.7$, $f_{\rm mr} = 0.2$, AND $f_{\rm cr} = 0.8$. OPTIMIZATION CARRIED OUT WITH FIXED $c = 3.4$ BUT ALLOWING z_0 AND a TO BE VARIED AT EACH P_0, UNTIL AN OPTIMUM COMBINATION OF z_0 AND a IS OBTAINED FOR EACH P_0

b (cm)	a (cm)	z_0 (cm)	P_0 (Torr)	I_{peak} (kA)	I_{pinch} (kA)	Peak v_a (cm/μs)	Peak v_s (cm/μs)	Peak v_p (cm/μs)	S (kA/cm[Torr Ne]$^{0.5}$)	Q_{line} (J)
3.20	0.951	6.0	5.0	182	140	4.3	23.1	15.1	86	6.44
3.80	1.129	7.0	3.5	183	140	4.5	23.3	15.1	87	7.58
4.09	1.213	7.0	3.0	183	139	4.5	23.0	15.1	87	8.04
4.45	1.322	7.0	2.5	183	138	4.5	23.2	15.1	88	8.01
4.94	1.466	7.0	2.0	183	137	4.6	23.2	15.1	88	8.00
5.63	1.673	6.0	1.5	181	136	4.4	23.1	15.1	88	7.96
6.78	2.014	6.0	1.0	180	134	4.5	23.3	15.1	90	7.22

These fitted values of the model parameters are then used for the computation of all the discharges at various pressures to obtain Table I.

It is evident from Table I that the peak value of the total discharge current $I_{\rm peak}$ decreases with decreasing pressure. This is due to the increasing dynamic resistance (rate of change of plasma inductance dL/dt gives rise to a dynamic resistance equal to 0.5 dL/dt) due to the increasing current-sheath speed as pressure is decreased. We note that, on the contrary, the current $I_{\rm pinch}$ that flows through the pinched plasma column increases with decreasing pressure. This is due to the shifting of the pinch time closer and closer toward the time of peak current as the current sheet moves faster and faster. Even at 1 torr, the current sheet (with a peak end axial value of 9.4 cm/μs) is still not quite fast enough for best matching and reaches the end just after the peak of the circuit current (which peaks at 2.6 μs, a little earlier than the unloaded rise time). For the standard UNU/ICTP PFF with an anode length of 16 cm, the operating pressure has to be just below 0.9 torr in neon for the current sheet to reach the end of the anode at peak total current. Below 0.9 torr, the $I_{\rm pinch}$ starts to decrease as the pinch time now occurs before current peak time. Moreover, $I_{\rm peak}$ is also dropping because of the still increasing dynamic resistance. As the pressure is decreased, the increase in $I_{\rm pinch}$ may be expected to favor $Y_{\rm sxr}$; however, there is a competing effect that decreasing pressure reduces the number density. The interaction of these competing effects will decide on the actual yield versus pressure behavior as shown in the computed results.

A plot of $Y_{\rm sxr}$ versus P_0 is shown in Fig. 1. The data of measured $Y_{\rm sxr}$ with P_0 were obtained by Liu [6] using a five-channel p-i-n SXR detector confirmed by a calorimeter. Comparing computed $Y_{\rm sxr}$ versus P_0 data with the measured $Y_{\rm sxr}$ versus P_0 data shows general agreement between our computed curve and the measured curve. The differences are as follows. Liu's measured optimum point is at 3.0 torr and has an optimum $Y_{\rm sxr}$ of 5.4 $\pm$ 1 J. This compares with our computed optimum pressure of 3.3 torr and computed optimum $Y_{\rm sxr}$ of 3.9 J. The drop-off of $Y_{\rm sxr}$ on the low-pressure side is very similar, but our computed drop-off on the high P_0 side shows a sharper drop-off compared with Liu's data. This comparison of data from our numerical experiments with Liu's careful measurements gives us confidence that the numerical experiments provide realistic values and pressure dependence of neon $Y_{\rm sxr}$ comparable with measured neon $Y_{\rm sxr}$ versus P_0 data, although the computed values appear to be significantly on the low side.

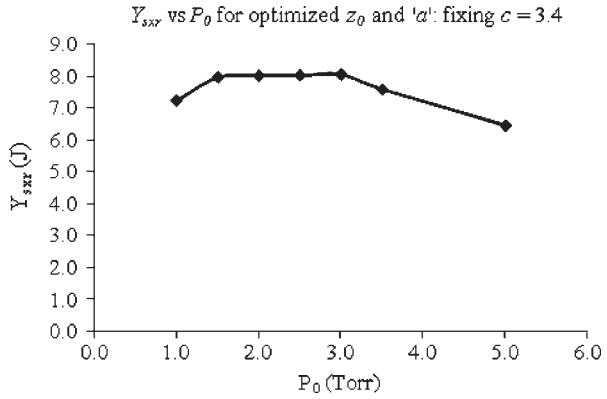

Fig. 2. Computed $Y_{\rm sxr}$ ($Q_{\rm line}$) versus P_0 for optimized UNU/ICTP PFF with $L_0 = 110$ nH, $C_0 = 30$ μF, and $RESF = 0.2$, operated at 14 kV in neon, with fitted model parameters $f_m = 0.05$, $f_c = 0.7$, $f_{\rm mr} = 0.2$, and $f_{\rm cr} = 0.8$. Optimization is carried out with fixed $c = 3.4$ but allowing z_0 and a to be varied at each P_0, until an optimum combination of z_0 and a is obtained for each P_0.

IV. OPTIMIZING FOR A PRACTICAL OPTIMUM CONFIGURATION

Next, we carry out numerical experiments to determine the optimum configuration for the electrodes using the UNU/ICTP PFF capacitor system. We retain the capacitor bank parameters of the UNU/ICTP PFF operating at 14 kV in neon with $L_0 = 110$ nH, $C_0 = 30$ μF, and $RESF = 0.2$. We also kept the ratio of the outer to inner electrode constant at $c = b/a = 3.4$ and retained model parameters $f_m = 0.05$, $f_c = 0.7$, $f_{\rm mr} = 0.2$, and $f_{\rm cr} = 0.8$. To check that it is reasonable to retain model parameters, we ran the code for $z_0 = 18$ cm and $a = 0.85$ cm and found that the maximum SXR yield of 2.6 J at 3.3 torr also compares well with the measurements by Mohammadi *et al.* [29].

We then parametrically varied P_0, z_0, and "a" in that parametric order and obtained Table II which gives us the optimum combination of z_0 and a for each given P_0, each optimum combination being the result of a series of numerical experiments systematically varying z_0 and a. From Table II, for a computed optimized $Y_{\rm sxr}$, Fig. 2 is shown.

From the numerical experiments, for $c = 3.4$, the optimum $Y_{\rm sxr}$ is 8.04 J at $a = 1.213$ cm, $z_0 = 7$ cm, and $P_0 = 3$ torr. This compares with a pressure-optimum yield of $Y_{\rm sxr} = 3.9$ J at 3.3 torr for the standard UNU/ICTP PFF which is operated with a fixed combination of $z_0 = 16$ cm and $a = 0.95$ cm.

TABLE III
COMPUTED $Y_{\rm sxr}$ ($Q_{\rm line}$) VERSUS P_0 FOR PRACTICAL OPTIMIZED UNU/ICTP PFF WITH $L_0 = 110$ nH, $C_0 = 30$ μF, AND $RESF = 0.2$, OPERATING AT 14 kV WITH FITTED MODEL PARAMETERS $f_m = 0.05$, $f_c = 0.7$, $f_{\rm mr} = 0.2$, AND $f_{\rm cr} = 0.8$; USING OPTIMIZED COMBINATION of $z_0 = 7$ cm AND $a = 1.2$ cm BUT WITH A CATHODE RADIUS FIXED AT $b = 3.2$ cm

P_0 (Torr)	I_{peak} (kA)	I_{pinch} (kA)	Peak v_a (cm/μs)	Peak v_s (cm/μs)	Peak v_p (cm/μs)	S (kA/cm[Torr Ne]$^{0.5}$)	Q_{line} (J)
6.0	188	140	3.9	16.3	12.4	64	0.00
5.0	187	141	4.3	18.1	13.5	70	0.12
4.0	186	141	4.6	20.4	14.3	77	6.41
3.5	184	141	4.9	21.7	14.8	82	9.47
3.2	183	140	5.0	22.9	15.0	85	8.59
3.1	182	140	5.1	23.2	15.1	86	8.15
3.0	182	139	5.2	23.5	15.2	88	7.31
2.5	179	138	5.5	25.1	15.8	94	4.26
2.0	175	135	5.9	25.3	16.4	103	2.22
1.5	168	130	6.5	26.2	17.1	114	0.98
1.0	158	123	7.4	28.1	19.1	132	0.33

The length of the optimum anode may seem to be surprisingly short compared with our initial expectations. This is because the numerical experiments show that the optimum end axial speed (which is also the peak axial speed) for the case of $c = b/a = 3.4$ is 4.5 cm/μs. The axial transit time then computes to be 2.54 μs, which, added to a radial transit time of 0.15 μs, means that the pinch time occurs at 2.69 μs, which is only 0.1 μs from the loaded capacitor bank current rise time of 2.6 μs. The computation shows that this time matches the loaded capacitor bank discharge characteristics best in terms of energy transfer efficiency.

We next note that, practically, it is technically difficult to change the dimensions of outer radius b, unless the whole electrode system and input flange system of the device is completely redesigned. On the other hand, if we keep the outer electrode unchanged and use a screw-on anode, the screw-on part can be designed to be screwed onto an anode stub that keeps the original radius until it just emerges out of the insulator sleeve, at which point it is cut short and has its radius converted to that of the screw-on part. Then, the screw-on part of the anode can have the optimized radius a and anode length z_0. The length of the cathode can be correspondingly shortened.

We therefore continue with the numerical experiments, keeping $b =$ constant at the original value of 3.2 cm, changing a to 1.2 cm with $z_0 = 7$ cm, and varying pressure to find this "practical optimum." The results are shown in Table III.

This gives us a practical optimum configuration of $b =$ 3.2 cm (unchanged from the original cathode radius of the standard UNU/ICTP PFF), $a = 1.2$ cm, and $z_0 = 7$ cm, giving a practical optimum yield of 9.5 J at a P_0 of 3.5 torr. The slightly higher yield compared with that in Table II is due to the reduced ratio "c" from 3.4 to 2.7. An earlier study has shown that reducing c, down to certain limits, has a beneficial effect in the case of neutron production operating in deuterium [24], and we have also confirmed through numerical experiments that this effect is also observed for neon $Y_{\rm sxr}$. The practical optimized results are shown in Fig. 3.

We could, of course, proceed to reduce c further and continue with further parametric variations of anode radius a and length z_0 to obtain small incremental improvements in SXR yields. However, for a small device, reducing c further will have difficulties in terms of a very small channel width. Moreover, we are confident that the practical optimum configuration we have found will form a good basis for an easily achievable practical design to optimize the UNU/ICTP PFF for neon SXR operation. We also observed that the optimum configuration for neon SXR operation has remarkably little variation in the S values, the values ranging from 82 to 87 kA/cm per [torr of neon]$^{1/2}$.

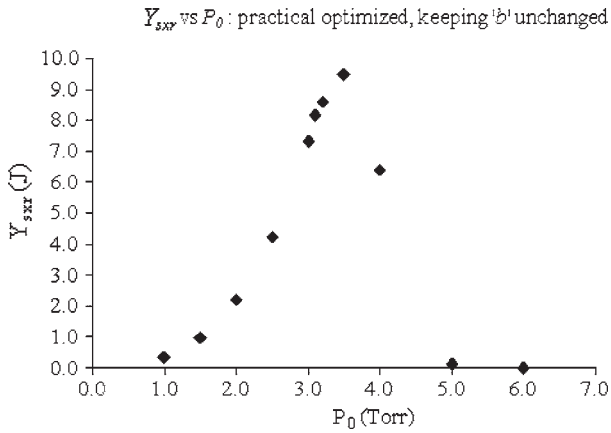

Fig. 3. Computed $Y_{\rm sxr}$ ($Q_{\rm line}$) versus P_0 for practical optimized UNU/ICTP PFF with $L_0 = 110$ nH, $C_0 = 30$ μF, and $RESF = 0.2$, operated at 14 kV in neon, with fitted model parameters $f_m = 0.05$, $f_c = 0.7$, $f_{\rm mr} = 0.2$, and $f_{\rm cr} = 0.8$, using optimized combination of $z_0 = 7$ cm and $a = 1.2$ cm but with cathode radius $b = 3.2$ cm.

V. CONCLUSION

A practical optimum configuration for UNU/ICTP PFF plasma focus for neon SXR operation is rigorously determined from numerical experiments using the Lee model code. By shortening the anode length z_0 from 16 to 7 cm and increasing the anode radius a from 0.95 to 1.2 cm, it is predicted that an optimum yield of $Y_{\rm sxr} = 9.5$ J can be achieved. Moreover, keeping cathode design unchanged with b unchanged at 3.2 cm, it is a simple matter, technically, to use a screw-on part to increase the anode radius. It would be interesting to see if the predicted two- to threefold increase in $Y_{\rm sxr}$ going from the standard UNU/ICTP PFF anode to the optimized anode may be achieved in the laboratory. We note that an examination

of Liu's data and the more recent data of Rawat *et al.* [30] seems to indicate the possibility that our numerical experiments may be systematically underestimating the Y_{sxr} of the standard UNU/ICTP PFF. It is important then that, when laboratory experiments are carried out, the measured Y_{sxr} from the practical optimized UNU/ICTP PFF should be compared with that from the standard device, simply by switching anodes and relevant pressures, everything else being kept constant.

REFERENCES

[1] S. Lee and C. S. Wong, "Initiating and strengthening plasma research in developing countries," *Phys. Today*, vol. 59, no. 5, pp. 31–36, May 2006. ICTP Open Access Archive. [Online]. Available: http://eprints.ictp.it/273/

[2] S. Lee, in *Twelve Years of UNU/ICTP PFF—A Review*. Trieste, Italy: Abdus Salam ICTP, 1998, pp. 5–34. IC/ 98/ 231, ICTP Open Access Archive. [Online]. Available: http://eprints.ictp.it/31/

[3] S. Lee, T. Y. Tou, S. P. Moo, M. A. Eissa, A. V. Gholap, K. H. Kwek, S. Mulyodrono, A. J. Smith, S. Suryadi, W. Usada, and M. Zakaullah, "A simple facility for the teaching of plasma dynamics and plasma nuclear fusion," *Amer. J. Phys.*, vol. 56, no. 1, pp. 62–68, Jan. 1988.

[4] S. V. Springham, S. Lee, and M. S. Rafique, "Correlated deuteron energy spectra and neutron yield for a 3 kJ plasma focus," *Plasma Phys. Control. Fusion*, vol. 42, no. 10, pp. 1023–1032, Oct. 2000.

[5] S. Lee and A. Serban, "Dimensions and lifetime of the plasma focus pinch," *IEEE Trans. Plasma Sci.*, vol. 24, no. 3, pp. 1101–1105, Jun. 1996.

[6] M. Liu, "Soft X-rays from compact plasma focus," Ph.D. dissertation, NIE, Nanyang Technological Univ., Singapore, 2006. ICTP Open Access Archive. [Online]. Available: http://eprints.ictp.it/327/

[7] S. Bing, "Plasma dynamics and X-ray emission of the plasma focus," Ph.D. dissertation, NIE, Nanyang Technological Univ., Singapore, 2000. ICTP Open Access Archive. [Online]. Available: http://eprints.ictp.it/99/

[8] S. Lee, *Radiative Dense Plasma Focus Computation Package: RADPF*. [Online]. Available: http://www.intimal.edu.my/school/fas/UFLF/File1RADPF.htm, http://www.plasmafocus.net/IPFS/modelpackage/File1RADPF.htm

[9] S. Lee, "Plasma focus model yielding trajectory and structure," in *Radiations in Plasmas*, vol. II, B. McNamara, Ed. Singapore: World Scientific, 1984, pp. 978–987.

[10] T. Y. Tou, S. Lee, and K. H. Kwek, "Non perturbing plasma focus measurements in the run-down phase," *IEEE Trans. Plasma Sci.*, vol. 17, no. 2, pp. 311–315, Apr. 1989.

[11] S. Lee, "A sequential plasma focus," *IEEE Trans. Plasma Sci.*, vol. 19, no. 5, pp. 912–919, Oct. 1991.

[12] J. bin Ali, "Development and studies of a small plasma focus," Ph.D. dissertation, Universiti Teknologi Malaysia, Malaysia, 1990.

[13] D. E. Potter, "The formation of high-density z-pinches," *Nucl. Fus.*, vol. 18, pp. 813–823, 1978.

[14] A. Serban and S. Lee, "Experiments on speed-enhanced neutron yield from a small plasma focus," *J. Plasma Phys.*, vol. 60, no. 1, pt. 1, pp. 3–15, Aug. 1998.

[15] M. H. Liu, X. P. Feng, S. V. Springham, and S. Lee, "Soft X-ray measurement in a small plasma focus operated in neon," *IEEE Trans. Plasma Sci.*, vol. 26, no. 2, pp. 135–140, Apr. 1998.

[16] D. Wong, P. Lee, T. Zhang, A. Patran, T. L. Tan, R. S. Rawat, and S. Lee, "An improved radiative plasma focus model calibrated for neon-filled NX2 using a tapered anode," *Plasma Sources Sci. Technol.*, vol. 16, no. 1, pp. 116–123, Feb. 2007.

[17] S. Lee, 2000–2007. [Online]. Available: http://ckplee.myplace.nie.edu.sg/plasmaphysics/

[18] S. Lee, *ICTP Open Access Archive*, 2005. [Online]. Available: http://eprints.ictp.it/85/

[19] M. A. Mohammadi, S. Sobhanian, C. S. Wong, S. Lee, P. Lee, and R. S. Rawat, "The effect of anode shape on neon soft X-ray emissions and current sheath configuration in plasma focus device," *J. Phys. D, Appl. Phys.*, vol. 42, no. 4, Feb. 2009. 045 203 (10pp).

[20] S. Lee, P. Lee, G. Zhang, X. Feng, V. A. Gribkov, M. Liu, A. Serban, and T. Wong, "High rep rate high performance plasma focus as a powerful radiation source," *IEEE Trans. Plasma Sci.*, vol. 26, no. 4, pp. 1119–1126, Aug. 1998.

[21] E. P. Bogolyubov, V. D. Bochkov, V. A. Veretennikov, L. T. Vekhoreva, V. A. Gribkov, A. V. Dubrovskii, Y. P. Ivanov, A. I. Isakov, O. N. Krokhin, P. Lee, S. Lee, V. Y. Nikulin, A. Serban, P. V. Silin, X. Feng, and G. X. Zhang, "A powerful soft X-ray source for X-ray lithography based on plasma focusing," *Phys. Scr.*, vol. 57, no. 4, pp. 488–494, 1998.

[22] V. Siahpoush, M. A. Tafreshi, S. Sobhanian, and S. Khorram, "Adaptation of Sing Lee's model to the Filippov type plasma focus geometry," *Plasma Phys. Control. Fusion*, vol. 47, no. 7, pp. 1065–1075, Jul. 2005.

[23] S. Lee and S. H. Saw, "Neutron scaling laws from numerical experiments," *J. Fusion Energy*, vol. 27, no. 4, pp. 292–295, Dec. 2008.

[24] S. Lee, "Current and neutron scaling for megajoule plasma focus machines," *Plasma Phys. Control. Fusion*, vol. 50, no. 10, p. 105 005 (14pp), Oct. 2008.

[25] S. Lee and S. H. Saw, "Pinch current limitation effect in plasma focus," *Appl. Phys. Lett.*, vol. 92, no. 2, p. 021 503, Jan. 2008.

[26] S. Lee, P. Lee, S. H. Saw, and R. S. Rawat, "Numerical experiments on plasma focus pinch current limitation," *Plasma Phys. Control. Fusion*, vol. 50, no. 6, Jun. 2008. 065 012 (8pp).

[27] V. A. Gribkov, A. Banaszak, B. Bienkowska, A. V. Dubrovsky, I. Ivanova-Stanik, L. Jakubowski, L. Karpinski, R. A. Miklaszewski, M. Paduch, M. J. Sadowski, M. Scholz, A. Szydlowski, and K. Tomaszewski, "Plasma dynamics in the PF-1000 device under full-scale energy storage: II. Fast electron and ion characteristics versus neutron emission parameters and gun optimization perspectives," *J. Phys. D, Appl. Phys.*, vol. 40, no. 12, pp. 3592–3607, Jun. 2007.

[28] S. Lee, S. H. Saw, P. C. K. Lee, R. S. Rawat, and H. Schmidt, "Computing plasma focus pinch current from total current measurement," *Appl. Phys. Lett.*, vol. 92, no. 11, p. 111 501, Mar. 2008.

[29] M. A. Mohammadi, R. Verma, S. Sobhanian, C. S. Wong, S. Lee, S. V. Springham, T. L. Tan, P. Lee, and R. S. Rawat, "Neon soft X-ray emission studies from the UNU-ICTP plasma focus operated with longer than optimal anode length," *Plasma Sources Sci. Technol.*, vol. 16, no. 4, pp. 785–790, Nov. 2007.

[30] R. S. Rawat, T. Zhang, C. B. L. Phua, J. X. Y. Then, K. A. Chandra, X. Lin, A. Patran, and P. Lee, "Effect of insulator sleeve length on soft X-ray emission from a neon-filled plasma focus device," *Plasma Sources Sci. Technol.*, vol. 13, no. 4, pp. 569–575, Nov. 2004.

Sor Heoh Saw received the B.Sc. (with honors) and Ph.D. degrees in physics from the University of Malaya, Kuala Lumpur, Malaysia, in 1985 and 1991, respectively, and the M.A. degree in educational management from the University of Nottingham, Nottingham, U.K., in 1997.

She is an Associate Professor and the Vice-President for Teaching and Learning with the INTI University College, Nilai, Malaysia, where she currently heads the Centre for Plasma Research. She is also an Associate with the Institute of Plasma Focus Studies, Melbourne, Australia, and the designated delegate of the INTI University College for Asian African Association for Plasma Training. Her current research interests include plasma physics and improving teaching.

Paul Choon Keat Lee received the B.Sc. (with honors) and Ph.D. degrees from the Imperial College, London, U.K., in 1992 and 1996, respectively, and the PGDipTHE from Nanyang Technological University, Singapore, in 1999.

He is currently an Associate Professor with the Radiation Sources Laboratory, Natural Sciences and Science Education, National Institute of Education, Nanyang Technological University. He was a Visiting Associate Professor at the University of Washington, Seattle, and at the Technological Educational Institute, Crete, in 2007. His current research interests include plasma physics, materials science, and physics education.

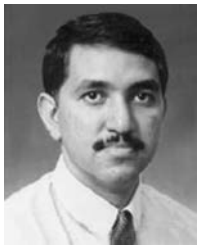

Rajdeep Singh Rawat received the B.Sc. (with honors), M.Sc., and Ph.D. degrees from the University of Delhi, Delhi, India, in 1985, 1987, and 1994, respectively.

He is currently an Associate Professor with the Radiation Sources Laboratory, Natural Sciences and Science Education, National Institute of Education, Nanyang Technological University, Singapore. He has authored 79 research papers in journals of international repute and about 45 research papers in conference proceedings. His current research interests include the development of repetitive miniature plasma focus devices as portable neutron source, charged particle and radiation emission from focus devices for nanophase material synthesis, ion-implantations and lithography applications, magnetic nanoparticles/nanocomposites, and diluted magnetic semiconductor thin films of transition-metal-doped ZnO using pulsed laser depositions.

Dr. Rawat is currently the Honorary Secretary of the Asian African Association for Plasma Training and a Council Member of the Institute of Physics, Singapore.

Sing Lee received the B.Sc. and M.Sc. degrees from the University of Malaya (UM), Kuala Lumpur, Malaysia, in 1964 and 1966, respectively, and the Ph.D. degree from the Australian National University, Canberra, Australia, in 1970.

He was an Alexander von Humboldt Fellow (1975–1976) with Kernforschunglange, Juelich, West Germany, a Commonwealth Academic Staff Fellow (1981–1982) with the Imperial College, London, U.K., and a Visiting Professor and a United Nations University Special Fellow (1986–1987) at Flinders University, South Australia. He was a Professor of Applied Physics with UM, where he headed research groups in plasma and pulse technology and the Physics Department. He was the Head of the Division of Physics and the Head of the Academic Group of Natural Sciences, National Institute of Education, Nanyang Technological University (NTU/NIE), Singapore. He is currently the Founder Principal of the (web-based) Institute for Plasma Focus Studies, Melbourne, Australia, and an Adjunct Professor (honorary) with the Natural Sciences and Science Education, NTU/NIE, and with INTI University College, Nilai, Malaysia.

Dr. Lee was the Founder President of the Asian African Association for Plasma Training (AAAPT), the Associate Director of the AAAPT Research and Training Centre, Institute of Physics, Academia Sinica, Beijing, the Far Eastern Representative of the International Centre for Theoretical Physics, and an ardent advocate and implementor of south–south technology creation and transfer, particularly in plasma fusion, laser, and pulse technology. He is also a Chartered Physicist and Fellow of the Institute of Physics (U.K.), a Life and Honorary Fellow of the Institute of Physics, Malaysia, and a Life Fellow of the Singapore Institute of Physics and the Samahang Pisika ng Pilipinas.

Soft x-ray yield from NX2 plasma focus

S. Lee,[1,2,3] R. S. Rawat,[2,a)] P. Lee,[2] and S. H. Saw[1,3]
[1]*Institute for Plasma Focus Studies, 32 Oakpark Drive, Chadstone, Victoria 3148, Australia*
[2]*Natural Sciences and Science Education, National Institute of Education, Nanyang Technological University, Singapore 637616, Singapore*
[3]*INTI University College, 71800 Nilai, Malaysia*

(Received 25 February 2009; accepted 15 June 2009; published online 30 July 2009)

The Lee model code is used to compute neon soft x-ray yield Y_{sxr} for the NX2 plasma focus as a function of pressure. Comparison with measured Y_{sxr} shows reasonable agreement in the Y_{sxr} versus pressure curve, the absolute maximum yield as well as the optimum pressure. This gives confidence that the code gives a good representation of the neon plasma focus in terms of gross properties including speeds and trajectories and soft x-ray yields, despite its lack of modeling localized regions of higher densities and temperatures. Computed current curves versus pressure are presented and discussed particularly in terms of the dynamic resistance of the axial phase. Computed gross properties of the plasma focus including peak discharge current I_{peak}, pinch current I_{pinch}, minimum pinch radius r_{min}, plasma density at the middle duration of pinch n_{pinch}, and plasma temperature at middle duration of pinch T_{pinch} are presented and the trends in variation of these are discussed to explain the peaking of Y_{sxr} at optimum pressure. © *2009 American Institute of Physics*.
[DOI: 10.1063/1.3176489]

I. INTRODUCTION

Plasma focus has been demonstrated as potential x-ray source for various medicobiological and industrial applications such as lithography[1–4] (using ~0.9–1.5 keV photons), radiography,[5,6] microscopy[7,8] (using ~0.25–2.5 keV radiations), and micromachining[9] (using ~4 keV photos). This has led to an increasing interest in exploiting the plasma focus device as a viable intense x-ray source due to some clear advantages such as being relatively cheap, compact, and ease of construction. The x-ray emissions from plasma focus devices have been explored over the wide range of capacitor bank energies ranging from large megajoule and few hundred kilojoule banks[10] to medium sized kilojoule banks[4,11–14] to subkilojoule banks of miniature sized focus devices.[15,16] In the past few years various efforts have been made for enhancing the x-ray yield by changing various experimental parameters such as bank energy,[17] discharge current, electrode configuration (shape and material),[11,13] insulator material and dimensions,[11] gas composition, and filling gas pressure.[5] Thus, soft x-ray yield optimization studies on the plasma focus devices operating over the wide range of bank energies have been one of the actively pursued fields of plasma focus research owing to their vast possible applications. Currently used systematic trial and error experimental procedure to obtain the optimized conditions for maximum radiation yield is highly time-consuming. Hence, the quicker optimization of plasma focus device is highly desirable, which can be achieved if the reliable focus model and corresponding simulation code to predict the x-ray yields from plasma focus device can be developed and used. Obviously the computed yields need to be checked against corresponding measured yields. Further, if the computed soft x-ray yields are consistently reliable against measured values; then it is reasonable to use the computed gross plasma properties as indicative of what we can expect when these plasma properties are measured. In this way, a reliable model code cannot only be used to compute radiation yields, but also be used as a good indicative diagnostic tool for multiple gross plasma properties of the plasma focus.

In the present paper, we used the Lee model code version 13.6b to carry out the numerical experiments on NX2 plasma focus device to compute its neon soft x-ray yield Y_{sxr} as a function of filling gas pressure. The NX2 is a 3 kJ plasma focus originally designed to operate as a neon soft x-ray source with 20 J per shot at 16 shots/s with burst durations of several minutes.[4] Its performance in repetitive mode has been extensively studied, especially in regards to its discharge currents and soft x-ray yield Y_{sxr}. In this paper, we have simulated the operation of NX2 focus device in numerical experiments which are designed to compare its currents, dynamics, and some plasma pinch gross properties at various pressures so as to examine the role played by various relevant plasma properties on the way the Y_{sxr} peaks at the optimum pressure.

II. THE MODEL CODE USED FOR NUMERICAL EXPERIMENTS

The Lee model couples the electrical circuit with plasma focus dynamics, thermodynamics, and radiation, enabling realistic simulation of all gross focus properties. The basic model, described in 1984,[18] was successfully used to assist several projects.[14,19–21] Radiation-coupled dynamics was included in the five-phase code leading to numerical experiments on radiation cooling.[22] The vital role of a finite small disturbance speed discussed by Potter[23] in a Z-pinch situation was incorporated together with real gas thermodynamics and radiation-yield terms;[24] this version of the code assisted

a)Electronic mail: rajdeep.rawat@nie.edu.sg.

other research projects[4,25,26] and was web-published in 2000[27] and 2005.[28] Plasma self-absorption was included in 2007 (Ref. 27) improving soft x-ray yield simulation. The code has been used extensively in several machines including UNU/ICTP PFF,[4,14,21,25,29] NX2,[4,26] NX1,[4] and adapted for the Filippov-type plasma focus DENA.[30] A recent development is the inclusion of the neutron yield Y_n using a beam-target mechanism,[31–34] incorporated in the present version[35] of the code RADPFV5.13, resulting in realistic Y_n scaling with pinch current I_{pinch}.[31,32] The versatility and utility of the model is demonstrated in its clear distinction of pinch current I_{pinch} from peak discharge current I_{peak} (Ref. 36) and the recent uncovering of a plasma focus pinch current limitation effect[31,33] as well as elucidation of neutron scaling laws to multimega-Joule facilities.[34] The description, theory, code and a broad range of results of this "Universal Plasma Focus Laboratory Facility" is available for download from world wide web.[35]

A brief description, however, of the five phases incorporated in the Lee model code is as follows.

(1) Axial phase: the axial phase is described by a snowplow model with an equation of motion which is coupled to a circuit equation. The equation of motion incorporates the axial phase model parameters: mass and current factors f_m and f_c. The mass swept-up factor f_m accounts for not only the porosity of the current sheath but also for the inclination of the moving current sheath-shock front structure and all other unspecified effects which have effects equivalent to increasing or reducing the amount of mass in the moving structure, during the axial phase. The current factor f_c accounts for the fraction of current effectively flowing in the moving structure (due to all effects such as current shedding at or near the back-wall, current sheet inclination). This defines the fraction of current effectively driving the structure, during the axial phase.

(2) Radial inward shock phase: it is described by four coupled equations using an elongating slug model. The first equation computes the radial inward shock speed from the driving magnetic pressure. The second equation computes the axial elongation speed of the column. The third equation computes the speed of the current sheath, also called the magnetic piston, allowing the current sheath to separate from the shock front by applying an adiabatic approximation. The fourth is the circuit equation. Thermodynamic effects due to ionization and excitation are incorporated into these equations, these effects being important for gases other than hydrogen and deuterium. Temperature and number densities are computed during this phase. A communication delay between shock front and current sheath due to the finite small disturbance speed is crucially implemented in this phase. The model parameters, radial phase mass swept up, and current factors f_{mr} and f_{cr} are incorporated in all three radial phases. The mass swept-up factor f_{mr} accounts for all mechanisms which have effects equivalent to increasing or reducing the amount of mass in the moving slug, during the radial phase not least of which could be axial ejection of mass. The current factor f_{cr} accounts for the fraction of current effectively flowing in the moving piston forming the back of the slug (due to all effects). This defines the fraction of current effectively driving the radial slug.

(3) Radial reflected shock (RS) phase: when the shock front hits the axis, because the focus plasma is collisional, a RS develops which moves radially outwards, while the radial current sheath piston continues to move inwards. Four coupled equations are also used to describe this phase, these being for the RS moving radially outwards, the piston moving radially inwards, the elongation of the annular column and the circuit equation. The same model parameters f_{mr} and f_{cr} are used as in the previous radial phase. The plasma temperature behind the RS undergoes a jump by a factor nearly 2.

(4) Slow compression (quiescent) or pinch phase: when the outgoing RS hits the ingoing piston the compression enters a radiative phase in which for gases such as neon, the radiation emission may actually enhance the compression where we have included energy loss/gain terms from Joule heating and radiation losses into the piston equation of motion. Three coupled equations describe this phase; these being the piston radial motion equation, the pinch column elongation equation and the circuit equation, incorporating the same model parameters as in the previous two phases. Thermodynamic effects are incorporated into this phase. The duration of this slow compression phase is set as the time of transit of small disturbances across the pinched plasma column. The computation of this phase is terminated at the end of this duration.

(5) Expanded column phase: to simulate the current trace beyond this point we allow the column to suddenly attain the radius of the anode, and use the expanded column inductance for further integration. In this final phase the snow plow model is used and two coupled equations are used similar to the axial phase above. This phase is not considered important as it occurs after the focus pinch.

We note that in radial phases 2, 3, and 4, axial acceleration and ejection of mass caused by necking curvatures of the pinching current sheath result in time dependent strongly center-peaked density distributions. Moreover the transition from phase 4 to phase 5 is observed in laboratory measurements to occur in an extremely short time with plasma/current disruptions resulting in localized regions of high densities and temperatures. These center-peaking density effects and localized regions are not modeled in the code, which consequently computes only an average uniform density and an average uniform temperature which are considerably lower than measured peak density and temperature (we thank a Reviewer for his comments regarding this point). However, because the four model parameters are obtained by fitting the computed total current waveform to the measured total current waveform, the model incorporates the energy and mass balances equivalent, at least in the gross sense to all the processes, which are not even specifically modeled. Hence

the computed gross features such as speeds and trajectories and integrated soft x-ray yields have been extensively tested in numerical experiments for several machines and are found to be comparable with measured values.

III. X-RAY EMISSIONS IN PLASMA FOCUS AND ITS INCORPORATION IN MODEL CODE

The focused plasma, with electron temperature of a few hundreds of eV to about keV and high enough electron density, is a copious source of x rays. The plasma focus emits both soft (thermal) as well as hard (nonthermal) x rays but for the scope of this paper, we will concentrate only on soft thermal x rays. The plasma focus emits soft thermal x rays by three processes,[37,38] namely: bremsstrahlung (free-free transition) from the Coulomb interactions between electrons and ions; recombination radiation (free-bound transition) emitted by an initially free electron as it loses energy on recombination with an ion; and de-excitation radiation (bound-bound transition) when a bound electron loses energy by falling to a lower ionic energy state. The first two processes give rise to the continuum of the x-ray spectrum, while the third process produces the characteristic line radiation of the plasma. The relative strengths of the continuum and line emissions depend on how the plasma was formed; typically, for a plasma formed from a high-Z material continuum emission dominates, while for a low-Z material line emission can be stronger. The calculation of the power emitted by processes within the plasma depends on assumptions made about the state of the plasma. Following the spectral data obtained by Mahe[24] and Liu *et al.*[25] for the soft x rays from neon operated 3.3 kJ UNU-ICTP plasma focus device, it was found that 64% of soft x-ray emission can be attributed to line radiations at 922 eV (Ly-α) and 1022 eV (He-α) and the remaining 36% by the rest, mainly recombination radiation, for optimized operations. For NX2 plasma focus device, Zhang[39] reported the contribution of line radiation rising to about 80%. It is for these reasons, and also for the temperatures of interest in our numerical experiments on NX2 device we take the neon soft x-ray yield to be equivalent to line radiation yield, i.e., $Y_{\mathrm{sxr}}=Q_L$.

In the code in phase 4, pinch phase neon line radiation Q_L is calculated using the relation

$$\frac{dQ_L}{dt} = -4.6\times 10^{-31} n_i^2 Z Z_n^4 (\pi r_p^2) z_f / T,$$

after being integrated over the pinch duration. Hence the SXR energy generated within the plasma pinch depends on the properties: number density n_i, effective charge number Z, atomic number of gas Z_n, pinch radius r_p, pinch length z_f, plasma temperature T, and the pinch duration.

This generated energy is then reduced by the plasma self-absorption, which depends primarily on density and temperature; the reduced quantity of energy is then emitted as the SXR yield. It was first pointed by Mahe[24] that a temperature around 300 eV is optimum for SXR production from neon operated plasma. Bing's[26] subsequent work and our subsequent experience through numerical experiments suggest that around 2×10^6 K (below 200 eV) seems to be better. Hence unlike the case of neutron scaling, for neon SXR scaling there is an optimum small range of temperatures (T window) to operate.

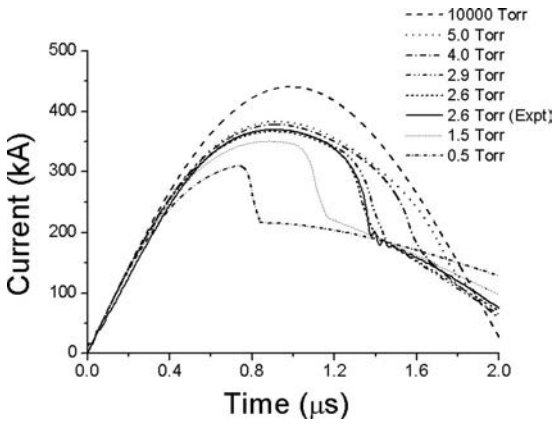

FIG. 1. Fine tuning of Lee model parameter by fitting of computed total current waveform of numerical experiment conducted at 2.6 Torr to that of experimentally measured waveform at same 2.6 Torr of neon. Plots of discharge current waveforms from numerical experiments performed over wide range of neon filling gas pressures are also shown for comparison.

IV. NUMERICAL EXPERIMENTS AND COMPARISON WITH EXPERIMENTAL RESULTS

To start the numerical experiments we select a discharge current trace of the NX2 taken with a Rogowski coil. The selected measured waveform is of a shot at 2.6 Torr neon, near optimum Y_{sxr} yield. The following bank, tube, and operation parameters are used; bank: static inductance $L_0=15$ nH, $C_0=28$ μF, stray resistance $r_0=2.2$ mΩ; tube: cathode radius $b=4.1$ cm, anode radius $a=1.9$ cm, anode length $z_0=5$ cm; and operation: voltage $V_0=11$ kV, pressure $P_0=2.6$ Torr.

The computed total current waveform is fitted to the measured waveform by varying model parameters f_m, f_c, f_{mr}, and f_{cr} one by one until the computed waveform agrees with the measured waveform. First, the axial model factors f_m and f_c are adjusted (fitted) until the computed rising slope of the total current trace and the rounding off of the peak current as well as the peak current itself are in reasonable (typically very good) fit with the measured total current trace (see Fig. 1, e.g., 2.6 Torr measured trace and computed trace). Then we proceed to adjust (fit) the radial phase model factors f_{mr} and f_{cr} until the computed slope and depth of the dip agree with the measured. In this case, the following fitted model parameters are obtained: $f_m=0.1$, $f_c=0.7$, $f_{\mathrm{mr}}=0.12$, and $f_{\mathrm{cr}}=0.68$. These fitted values of the model parameters are then used for the computation of all the discharges at various pressures.

The code is used for each pressure, starting at high pressure (about 10 000 Torr, which is not an issue in numerical experiments although we would not use such pressures in "hardware" experiments) so that the discharge current stayed at the backwall with hardly any motion and hence can be treated as short circuit discharge. The discharge current then resembles that of a simple L-C-R discharge, which is a damped sinusoid. The pressure is then lowered for another

TABLE I. Computed plasma dynamics and pinch plasma parameters for different neon filling gas pressures by numerical experiments conducted on NX2 device using Lee model code. [Parameters used in the table are: I_{peak} is the peak value of the total discharge current; I_{pinch} is the pinch current, taking its value at the start of the pinch phase; peak v_a=peak axial speed, typically end axial speed; S=speed parameter (in kA/cm/Torr$^{1/2}$); peak v_s, v_p=peak radial shock and piston speeds, respectively; r_{min}=minimum radius or focus pinch radius at maximum compression; z_{max}=maximum length of focus pinch at time of maximum compression (note that the anode is hollow); T_{pinch}=plasma temperature at middle of pinch duration; n_i pinch=ion density at the middle of pinch duration; Z=effective charge of the neon plasma at middle of pinch duration; and EINP=work done by the dynamic resistance during radial phase expressed as % of E_0.]

P_0 (Torr)	I_{peak} (kA)	I_{pinch} (kA)	Peak v_a (cm/μs)	S	Peak v_s (cm/μs)	Peak v_p (cm/μs)	r_{min} (cm)	z_{max} (cm)	Pinch duration (ns)	T_{pinch} 10^6 K	n_i pinch (10^{23}/m^3)	Z	EINP (%)	Y_{sxr} (J)
High	440									Middle of pinch				
5	383	76	4.6	90	11.1	8.6	0.86	2.84	100	0.3	1.1	5.5	6.3	0
4.5	381	99	4.8	94	12.2	9.5	0.42	2.7	60	0.47	2.4	7.7	8.6	0
4	378	114	5	99	14.9	11.6	0.29	2.7	46	0.7	3.2	8	10.7	0
3.5	374	128	5.3	105	17	12.8	0.22	2.75	37	1.03	3.9	8	12.9	4.5
3.2	372	135	5.6	109	18.8	13.7	0.19	2.79	34	1.23	4.1	8	14.4	14.6
3	370	140	5.7	113	20	14.1	0.18	2.8	32	1.4	4.1	8	15.2	19.9
2.9	369	142	5.8	114	20.6	14.5	0.17	2.79	30.6	1.51	4	8	15.5	20.8
2.8	369	144	5.9	116	21.1	14.8	0.17	2.79	29.6	1.61	3.8	8	15.7	20
2.7	368	146	6	118	21.8	15	0.18	2.78	28.8	1.72	3.5	8	15.8	17.9
2.6	367	148	6.1	120	22.5	15.3	0.19	2.75	27.3	1.86	3	8	15.8	14.4
2.4	364	152	6.3	124	24.4	15.4	0.22	2.7	23.5	2.18	2.3	8	15.6	8
2	359	159	6.8	134	25.2	16.7	0.25	2.73	23.6	2.8	1.6	8.2	16.2	3.9
1.5	350	164	7.6	151	27.6	18.8	0.26	2.77	22.4	3.9	1.1	8.7	16.7	1.5
1	338	165	8.8	178	32	22.7	0.26	2.77	19.3	5.5	0.7	9.3	16.5	0.4
0.5	310	157	11.1	230	41	28.6	0.26	2.78	15.5	9.4	0.35	10	14.4	0.05

run. This is repeated each time lowering the filling neon pressure. Figure 1 records the discharge current waveforms for some of the selected pressures covering a wide range of neon operating pressures from 5 Torr down to 0.5 Torr. The Fig. 1 also includes the simulated waveform for high pressure shot and measured waveform at 2.6 Torr. It may be noticed that computed total current waveform at 2.6 Torr numerical experiment is almost identical to the measured total current waveform for the 2.6 Torr actual experiment conducted by Zhang indicating an extremely good fine tuning of Lee model parameters, i.e., f_m, f_c, f_{mr}, and f_{cr} [0.1, 0.7, 0.12, and 0.68, respectively, for this shot] and hence provide confidence in simulated results of the gross properties. Figure 1 shows that the unloaded (dynamically) high pressure discharge waveform peaks at about 440 kA just before 1.1 μs. At 5 Torr, the peak of the total current I_{peak} is 380 kA and a small current dip is seen at 1.8 μs which is well after peak current with the total discharge current having dropped to 150 kA at the start of the dip. At successive lower pressure, I_{peak} reduces progressively while the current dip appears at progressively earlier times. At 1.5 Torr, I_{peak} has dropped to 350 kA and the dip starts at about the time of peak current of the high pressure shot. It is reasonable to correlate the current dip with the radial phase, so the shifting of the current dip earlier and earlier at lower and lower pressures is consistent with higher and higher axial speeds. The higher speeds lead to correspondingly higher dynamic resistance (which is numerically half the rate of change of inductance; thus is proportional to the axial speed for an axial run-down tube of constant cross-sectional dimensions). We also tabulate some properties of the dynamics and the pinch plasma as a function of the pressure as computed by numerical experiments. This is shown in Table I.

From the Table I it is seen that optimum Y_{sxr} is computed at P_0=2.9 Torr from the numerical experiments. In order to plot all the properties in one figure each quantity is normalized to its value at optimum, i.e., the value obtained for 2.9 Torr operation. The normalized pinch plasma parameters and absolute Y_{sxr} are then plotted as a function of filling gas pressure of neon (P_0) in Figs. 2(a) and 2(b), respectively. The experimentally measured Y_{sxr} of NX2 operated under similar conditions is also included for comparison. The experimental data in Fig. 2(b) is taken from Fig. 6b of Ref. 4 and also from Fig. 6.7b on page 206 of Ref. 37, and hence the numerical experiments were performed for NX2 device with 5 cm long anode with the device being operated at 11.5 kV. It is evident from Fig. 2(b) (also from Table I) that the Y_{sxr} values from numerical experiments fit the experimentally measured yields reasonably well. It is also necessary to point out here that our computed n_i (being an averaged uniform value) is considerably lower than values measured experimentally. From shock theory we compute for this case (2.6 Torr neon in NX2) a peak on-axis RS value of 2.63×10^{24} ions/m^{-3}. Similarly we compute a peak on-axis RS temperature of 2.7×10^6 K. This illustrates that consideration of density and temperature distributions can allow more realistic estimation of these quantities and even their spatial and temporal distributions. Hence, though our model gives only mean values of the key plasma parameters (such as that of n_i and T) and is unable to trace their evolution with an accuracy that probably can be achieved by modern diagnostics technique, but at the same time we also point out that our average methods allow us to compute realistic gross quantities such as trajectories, speeds, and soft x-ray yields.

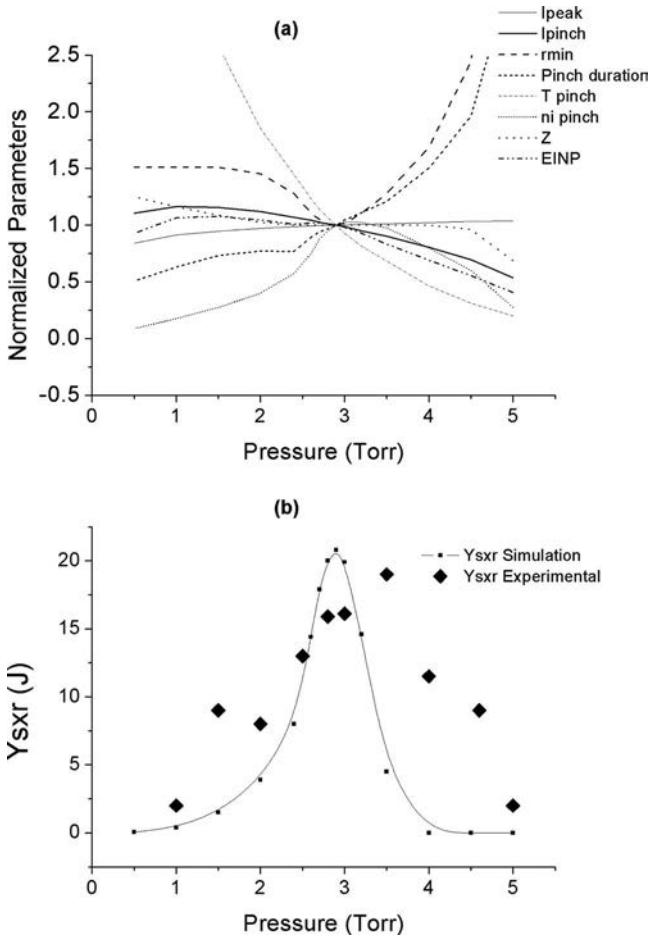

FIG. 2. Effect of operating gas pressure on (a) some key pinch plasma parameters (all normalized using value at optimum operating pressure of 2.9 Torr) and (b) Y_{sxr}; as estimated by numerical experiments. The experimentally measured Y_{sxr} of NX2 operated under similar conditions is also included in (b) for comparison.

V. DISCUSSION OF RESULTS

It is evident from Fig. 2(a) that the peak value of total discharge current I_{peak} decreases with decreasing pressure. This is attributed to increasing dynamic resistance (i.e., increasing rate of change of plasma inductance, dL/dt) due to the increasing current sheath speed as pressure is decreased. We note that, on the contrary, the current I_{pinch} that flows through the pinched plasma column, increases with decreasing pressure. This is due to the shifting of the pinch time toward the time of peak current until the pressure nears 1.2 Torr. As the pressure is decreased below 1.2 Torr, the I_{pinch} starts to decrease as the pinch time now occurs before current peak time. The T_{pinch}, which is the temperature at the middle of the pinch, keeps increasing as pressure is decreased. The n_{pinch}, which is the ion density at middle of the pinch, increases as pressure decreases peaking around 3 Torr and then dropping at lower pressures. The r_{min}, which is the minimum radius of the pinch, has a complementary trend with a minimum at around 3 Torr. This shows that as the operating pressure is reduced toward 3 Torr, the increasing I_{pinch} increases the compression sufficiently so that despite the drop in ambient number density, the pinch n_i is still able to reach a higher value at 3 Torr. As the operating pressure is reduced below 3 Torr, the increase in I_{pinch} does not appear to be sufficient to further increase n_i or indeed even to compress the pinch to a smaller radius than at 3 Torr. To clarify this situation we briefly explain the plasma dynamics during the radial collapse phase.

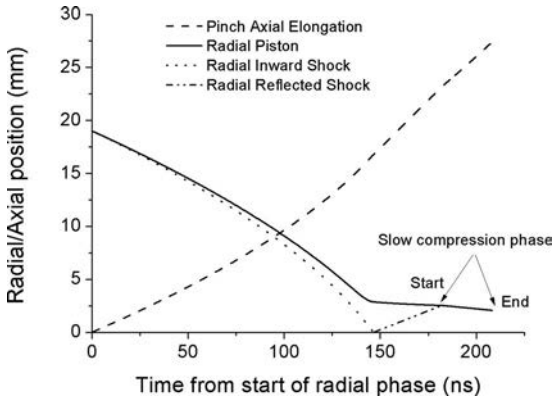

FIG. 3. The currents sheath (radial piston) continues to move in slow compression phase after the radial RS hits it and reaches minimum pinch radius r_{min} at the end of slow compression phase.

The radial phase uses a slug model with an imploding cylindrical shock wave forming the front of the slug, driven by a cylindrical magnetically driven current sheath piston at the rear of the slug. Between the shock wave and the current sheath is the shock heated plasma. When the shock front implodes onto the tube axis, because the plasma is collisional, a RS develops. The RS front moves radially outwards into the inwardly streaming particles of the plasma slug, leaving behind it a stationary doubly shocked plasma with a higher temperature and density than the singly shocked plasma ahead of it. When the RS reaches the incoming current sheath, typically the magnetic pressure exceeds the doubly shocked plasma pressure, in which case the current sheath continues inwards in a further slow compression, until the end of this quasiequilibrium phase. The duration of this slow compression phase may be defined by the transit time of small disturbances. For a well-designed and operated plasma focus there is a slow compression throughout this whole duration and the pinch radius reaches its minimum r_{min} at the end of the phase. These various phases/phenomena can be seen in Fig. 3. The radiation yield depends on: (a) the absolute density (which depends on the ambient density and the compression of which r_{min} is a measure, the smaller r_{min}/a where a is the anode radius, the greater the compression), (b) the temperature (which depends on the imploding speeds [the lower the operating pressure, the higher the imploding speeds, noting that shocked temperatures depends on the square of the shock speeds] and the further compression), (c) the duration of the slow compression phase (which scales inversely as the square root of the pinch temperature), and (d) the volume of the pinched plasma during the slow compression phase (which predominantly scales as a). Thus, in this particular example, as the operating pressure is reduced below 3 Torr, although I_{pinch} still increases, speeds also increase, increasing the temperature, which tends to oppose the severity of the compression during the slow compression phase, although the decreased ambient number density tends

to work in the opposite direction. The interaction of all these factors are taken care of in the code and manifests in the peaking of n_i at 3.1 Torr and the minimum value of r_{min} at 2.9 Torr. Moreover, as can be seen in Table I, the pinch duration progressively reduces, as the temperature increases with lowering pressure; while the radiating plasma volume reaches a minimum around 2.9 Torr. The interactions of all the behavior of r_{min}, n_i, and T_{pinch}, pinch duration and plasma volume all contribute to the peak in Y_{sxr} as a function of operating pressure. Looking at the Table I and Fig. 2(a) it does appear that the peaking of n_{pinch} at 3.1 Torr is a notable factor for the peaking of Y_{sxr} at 2.9 Torr.

The Fig. 2(b) shows reasonable agreement the results of numerical experiments and experimentally measured; in terms of absolute value of Y_{sxr} at optimum pressure (about 20.8 J by numerical experiment, refer Table I, and about 16.1 J as experimentally measured[4,39]) as well as the optimum pressure value itself. The computed curve falls off more sharply on both sides of the optimum pressure. This agreement validates our views that the fitting of the computed total current waveform with the measured waveform enables the model to be energetically correct in all the gross properties of the radial dynamics including speeds and trajectories and soft x-ray yields despite the lack of fine features in the modeling.

VI. CONCLUSIONS

To conclude, the Lee model code has been successfully used to perform numerical experiments to compute neon soft x-ray yield for the NX2 as a function of pressure with reasonable degree of agreement in (i) the Y_{sxr} versus pressure curve trends, (ii) the absolute maximum yield, and (iii) the optimum pressure value. The only input required is a measured total current waveform. This reasonably good agreement, against the background of an extremely complicated situation to model, moreover the difficulties in measuring Y_{sxr}, gives confidence that the model is sufficiently realistic in describing the plasma focus dynamics and soft x-ray emission for NX2 operating in Neon. This encourages us to present Table I and to present the above views regarding the factors contributing to the peaking of Y_{sxr} at an optimum pressure.

[1]D. Wong, A. Patran, T. L. Tan, R. S. Rawat, and P. Lee, IEEE Trans. Plasma Sci. **32**, 2227 (2004).
[2]R. Petr, A. Bykanov, J. Freshman, D. Reilly, J. Mangano, M. Roche, J. Dickenson, M. Burte, and J. Heaton, Rev. Sci. Instrum. **75**, 2551 (2004).
[3]Y. Kato, I. Ochiai, Y. Watanabe, and S. Murayama, J. Vac. Sci. Technol. B **6**, 195 (1988).
[4]S. Lee, P. Lee, G. Zhang, X. Feng, V. A. Gribkov, M. Liu, A. Serban, and T. K. S. Wong, IEEE Trans. Plasma Sci. **26**, 1119 (1998).
[5]F. N. Beg, I. Ross, A. Lorena, J. F. Worley, A. E. Dangor, and M. G. Haines, J. Appl. Phys. **88**, 3225 (2000).
[6]S. Hussain, M. Shafiq, R. Ahmad, A. Waheed, and M. Zakaullah, Plasma Sources Sci. Technol. **14**, 61 (2005).
[7]F. Castillo-Mejia, M. M. Milanese, R. L. Moroso, J. O. Pouzo, and M. A. Santiago, IEEE Trans. Plasma Sci. **29**, 921 (2001).
[8]R. S. Rawat, T. Zhang, G. J. Lim, W. H. Tan, S. J. Ng, A. Patran, S. M. Hassan, S. V. Springham, T. L. Tan, M. Zakaullah, S. Lee, and P. Lee, J. Fusion Energy **23**, 49 (2004).
[9]V. A. Gribkov, A. Srivastava, P. L. C. Keat, V. Kudryashov, and S. Lee, IEEE Trans. Plasma Sci. **30**, 1331 (2002).
[10]V. A. Gribkov, B. Bienkowska, M. Borowiecki, A. V. Dubrovsky, I. Ivanova-Stanik, L. Karpinski, R. A. Miklaszewski, M. Paduch, M. Scholz, and K. Tomaszewski, J. Phys. D **40**, 1977 (2007).
[11]M. Zakullah, K. Alamgir, M. Shafiq, S. M. Hassan, M. Sharif, S. Hussain, and A. Waheed, Plasma Sources Sci. Technol. **11**, 377 (2002).
[12]R. S. Rawat, T. Zhang, C. B. L. Phua, J. X. Y. Then, K. A. Chandra, X. Lin, A. Patran, and P. Lee, Plasma Sources Sci. Technol. **13**, 569 (2004).
[13]H. Bhuyan, S. R. Mohanty, N. K. Neog, S. Bujarbarua, and R. K. Rout, J. Appl. Phys. **95**, 2975 (2004).
[14]S. Lee, T. Y. Tou, S. P. Moo, M. A. Eissa, A. V. Gholap, K. H. Kwek, S. Mulyodrono, A. J. Smith, Suryadi, W. Usada, and M. Zakaullah, Am. J. Phys. **56**, 62 (1988).
[15]R. Verma, P. Lee, S. V. Springham, T. L. Tan, M. Krishnan, and R. S. Rawat, Appl. Phys. Lett. **92**, 011506 (2008).
[16]P. Silva, J. Moreno, C. Pavez, L. Soto, and J. Arancibia, J. Phys.: Conf. Ser. **134**, 012044 (2008).
[17]P. G. Burkhalter, G. Mehlman, D. A. Newman, M. Krishnan, and R. R. Prasad, Rev. Sci. Instrum. **63**, 5052 (1992).
[18]S. Lee, in *Radiations in Plasmas*, edited by B. McNamara (World Scientific, Singapore, 1984), p. 978.
[19]T. Y. Tou, S. Lee, and K. H. Kwek, IEEE Trans. Plasma Sci. **17**, 311 (1989).
[20]S. Lee, IEEE Trans. Plasma Sci. **19**, 912 (1991).
[21]A. Serban and S. Lee, J. Plasma Phys. **60**, 3 (1998).
[22]J. b. Ali, "Development and studies of a small plasma focus," Ph.D. thesis, Universiti Teknologi Malaysia, 1990.
[23]D. E. Potter, Nucl. Fusion **18**, 813 (1978).
[24]L. Mahe, "Soft x-rays from compact plasma focus," Ph.D. thesis, Nanyang Technological University, 1996.
[25]M. Liu, X. P. Feng, S. V. Springham, and S. Lee, IEEE Trans. Plasma Sci. **26**, 135 (1998).
[26]S. Bing, "Plasma dynamics and x-ray emission of the plasma focus," Ph.D. thesis, Nanyang Technological University, 2000; ICTP Open Access Archive: http://eprints.ictp.it/99/.
[27]S. Lee, http://ckplee.myplace.nie.edu.sg/plasmaphysics/, 2000.
[28]S. Lee, ICTP Open Access Archive: http://eprints.ictp.it/85/13, 2005.
[29]S. Lee, Twelve Years of UNU/ICTP PFF—A Review IC 98 (231), Miramare, Trieste, 1998 (unpublished).
[30]V. Siahpoush, M. A. Tafreshi, S. Sobhanian, and S. Khorram, Plasma Phys. Controlled Fusion **47**, 1065 (2005).
[31]S. Lee and S. H. Saw, Appl. Phys. Lett. **92**, 021503 (2008).
[32]S. Lee and S. H. Saw, J. Fusion Energy **27**, 292 (2008).
[33]S. Lee, P. Lee, S. H. Saw, and R. S. Rawat, Plasma Phys. Controlled Fusion **50**, 065012 (2008).
[34]S. Lee, Plasma Phys. Controlled Fusion **50**, 105005 (2008).
[35]S. Lee, Radiative Dense Plasma Focus Computation Package: RADPF http://www.intimal.edu.my/school/fas/UFLF/.
[36]S. Lee, S. H. Saw, P. C. K. Lee, R. S. Rawat, and H. Schmidt, Appl. Phys. Lett. **92**, 111501 (2008).
[37]E. H. Beckner, J. Appl. Phys. **37**, 4944 (1966).
[38]W. H. Bostic, V. Nardi, and W. Prior, J. Plasma Phys. **8**, 1 (1972).
[39]Z. Guixin, "Plasma soft x-ray source for microelectronic lithography," Ph.D. thesis, Nanyang Technological University, 1999.

Numerical experiments on plasma focus neon soft x-ray scaling

2009 Plasma Phys. Control. Fusion 51 105013

(http://iopscience.iop.org/0741-3335/51/10/105013)

Plasma Phys. Control. Fusion **51** (2009) 105013 (8pp) doi:10.1088/0741-3335/51/10/105013

Numerical experiments on plasma focus neon soft x-ray scaling

S Lee[1,2,3], **S H Saw**[3], **P Lee**[2] **and R S Rawat**[2]

[1] Institute for Plasma Focus Studies, 32 Oakpark Drive, Chadstone, VIC3148, Australia
[2] NSSE, National Institute of Education, Nanyang Technological University, Singapore 637616, Singapore
[3] INTI University College, 71800 Nilai, Malaysia

E-mail: leesing@optusnet.com.au

Received 25 February 2009, in final form 1 August 2009
Published 21 September 2009
Online at stacks.iop.org/PPCF/51/105013

Abstract

Numerical experiments are carried out systematically to determine the neon soft x-ray yield Y_{sxr} for optimized neon plasma focus with storage energy E_0 from 0.2 kJ to 1 MJ. The ratio $c = b/a$, of outer to inner electrode radii, and the operating voltage V_0 are kept constant. E_0 is varied by changing the capacitance C_0. Parametric variation at each E_0 follows the order operating pressure P_0, anode length z_0 and anode radius a until all realistic combinations of P_0, z_0 and a are investigated. At each E_0, the optimum combination of P_0, z_0 and a is found that produces the biggest Y_{sxr}. At low energies the soft x-ray yield scales as $Y_{sxr} \sim E_0^{1.6}$ whilst towards 1 MJ it becomes $Y_{sxr} \sim E_0^{0.8}$. The Y_{sxr} scaling laws are found to be $Y_{sxr} \sim I_{peak}^{3.2}$ (0.1–2.4 MA) and $Y_{sxr} \sim I_{pinch}^{3.6}$ (0.07–1.3 MA) throughout the range investigated. When numerical experimental points with other c values and mixed parameters are included, there is evidence that the Y_{sxr} versus I_{pinch} scaling is more robust and universal, remaining unchanged whilst the Y_{sxr} versus I_{peak} scaling changes slightly, with more scatter becoming evident.

1. Introduction

Plasma focus machines operated in neon have been studied as intense sources of soft x-rays (SXRs) with potential applications [1–3]. Whilst many recent experiments have concentrated efforts on low energy devices [1–3] with a view of operating these as repetitively pulsed sources, other experiments have looked at x-ray pulses from larger plasma focus devices [4, 5] extending to the megajoule regime. However, numerical experiments simulating x-ray pulses from plasma focus devices are gaining more interest in the public domain. For example, the Institute of Plasma Focus Studies [6] conducted a recent International Internet Workshop on Plasma Focus Numerical Experiments [7], at which it was demonstrated that the Lee model code [8] not only computes realistic focus pinch parameters, but also absolute values of SXR yield Y_{sxr} which are consistent with those measured experimentally. A comparison was made

for the case of the NX2 machine [3], showing good agreement between computed and measured Y_{sxr} as a function of P_0 [7, 9]. This gives confidence that the Lee model code gives realistic results in the computation of Y_{sxr}. In this paper, we report on a comprehensive range of numerical experiments with storage energies E_0 in the range 0.2 kJ–1 MJ in order to derive the scaling laws for plasma focus neon Y_{sxr}, in terms of E_0, peak discharge current I_{peak} and focus pinch current I_{pinch}.

Numerical experiments for deriving scaling laws on neutron yield Y_n have already been reported [10, 11]. These have shown that in terms of storage energy E_0, $Y_n \sim E_0^2$ at small E_0 of kilojoules, the scaling 'slowing' with increasing E_0, becoming $Y_n \sim E_0$ in the higher energy ranges of megajoules. In terms of I_{peak}, a single power law covers the scaling, this being $Y_n \sim I_{peak}^{3.8}$; likewise another single power law for I_{pinch}, this being $Y_n \sim I_{pinch}^{4.5}$. These scaling laws apply from kJ to 25 MJ with corresponding I_{peak} from 0.1 to 5.7 MA and I_{pinch} from 0.08 to 2.4 MA. It needs to be stressed that these scaling rules only apply to optimized operational points. It also needs to be pointed out that the distinction of I_{pinch} from I_{peak} is of basic importance [12–14]. The scaling with I_{pinch} is the more fundamental and robust one, since obviously there are situations (no pinching or poor pinching however optimized) where I_{peak} may be large but Y_n is zero or small, whereas the scaling with I_{pinch} is certainly more consistent with all situations. In these works the primary importance of I_{pinch} for scaling plasma focus properties including neutron yield Y_n has been firmly established [10–14].

This primary importance of I_{pinch} has been borne in mind in our numerical experiments on neon plasma focus. In the context of neon Y_{sxr} scaling, not much work appears to have been reported in the literature. Gates, in optimization studies, had proposed [15] that the total energy emitted as x-rays may scale as $Y_x \sim I_{peak}^4/(\text{pinchradius})^2$. This scaling rule is not very useful for predictive purposes since for a given capacitor bank whilst I_{peak} may be estimated, the focus pinch radius is difficult to quantify. Moreover if one considers a certain gas, say, neon, then for an optimum operation one really needs to fix an axial speed, in which case the speed factor $S = (I_{peak}/a)/P_0^{0.5}$ (where a is the anode radius and P_0 is the operating pressure)is fixed [16]. Moreover for optimum operation in neon, the pinch radius has a fixed relationship to a [17]. This means that the Gates scaling rule reduces to $Y_x \sim P_0 I_{peak}^2$. In this context, it is of greater interest to note that Filippov *et al* [5] had compared the experimental data of two Filippov-type plasma focus operated at 0.9 MJ and 5 kJ, respectively, and on the basis of the experimental results of just these two machines had proposed a scaling for the K-shell lines of neon $Y_x \sim I_{pinch}^{3.5–4}$. They further stated that such a scaling is in conformity to the resistive heating mechanism of neon plasma. It is unlikely that Filippov's $Y_x \sim I_{pinch}^{3.5–4}$ is compatible with Gates' $Y_x \sim I_{peak}^4/(\text{pinchradius})^2$. It is against this background of rather scanty experimental data that our numerical experiments are designed to comprehensively cover the range of E_0 from 0.2 kJ to 1 MJ using the Lee model code which models the Mather-type configurations.

2. The Lee model code for neon SXR yields

The Lee model couples the electrical circuit with plasma focus dynamics, thermodynamics and radiation, enabling realistic simulation of all gross focus properties. This approach focusing on gross properties is different from magnetohydrodynamic (MHD) codes where spatially resolved and detailed description of plasma properties is calculated. Many authors have developed and used MHD and fluid models of the plasma focus. Behler and Bruhns [18] developed a 2D three-fluid code. Garanin and Mamyshev [19] introduced the MHD model, which takes into account anomalous resistivity. However, none of these studies [18–23] has

resulted in published data on SXR yields, nor any comparison with laboratory experiments on SXR yields [18–23].

Our basic model, described in 1984 [24], was successfully used to assist several projects [25–27]. Radiation-coupled dynamics was included in the five-phase code leading to numerical experiments on radiation cooling [28]. The vital role of a finite small disturbance speed discussed by Potter in a Z-pinch situation [29] was incorporated together with real gas thermodynamics and radiation-yield terms. Before this 'communication delay effect' was incorporated, the model consistently over-estimated the radial speeds by a factor of ∼2 and shock temperatures by a factor ∼4. This version, using the 'signal-delay slug', which became a must-have feature in all subsequent versions, assisted other research projects [30–33] and was web-published in 2000 [34] and 2005 [35]. Plasma self-absorption was included in 2007 [34] improving SXR yield simulation. The code has been used extensively in several machines including UNU/ICTP PFF [25, 28, 30, 31, 36–38], NX2 [3, 32, 33], NX1 [2, 3] and adapted for the Filippov-type plasma focus DENA [39]. A recent development is the inclusion of the neutron yield, Y_{n}, using a beam–target mechanism [10, 11, 13, 40, 41], incorporated in recent versions [8] of the code (later than RADPFV5.13), resulting in realistic Y_{n} scaling with I_{pinch} [10, 11]. The versatility and the utility of the model are demonstrated in its clear distinction of I_{pinch} from I_{peak} [12] and the recent uncovering of a plasma focus pinch current limitation effect [13, 14]. The description, theory, code and a broad range of results of this 'Universal Plasma Focus Laboratory Facility' are available for download from [8].

In the code, neon line radiation Q_{L} is calculated as follows:

$$\frac{\mathrm{d}Q_{\mathrm{L}}}{\mathrm{d}t} = -4.6 \times 10^{-31} n_i^2 Z Z_n^4 (\pi r_{\mathrm{p}}^2) z_{\mathrm{f}} / T,$$

where for the temperatures of interest in our experiments we take $Y_{\mathrm{sxr}} = Q_{\mathrm{L}}$.

Hence the SXR energy generated within the plasma pinch depends on the following properties: number density n_i, effective charge number Z, pinch radius r_{p}, pinch length z_{f}, temperature T and pinch duration, since in our code Q_{L} is obtained by integrating over the pinch duration.

This generated energy is then reduced by the plasma self-absorption which depends primarily on density and temperature; the reduced quantity of energy is then emitted as the SXR yield. It was first pointed out by Mahe [37] that a temperature around 300 eV is optimum for SXR production. Bing's subsequent work [32] and our experience through numerical experiments suggest that around 2×10^6 K (below 200 eV) or even a little lower seems to be better in providing the best mix of helium-like and hydrogen-like neon ions radiating SXR lines in the spectral range 1–1.3 nm. Hence unlike the case of neutron scaling, for SXR scaling there is an optimum small range of temperatures (T window) in which to operate.

3. Numerical experiments and their results

We use the Lee model code to carry out a series of numerical experiments over the energy range 0.2 kJ–1 MJ. For the neon operation, the Lee model code had previously been designed to compute the line radiation yield. For this work we want to distinguish that part of the line yield that is SXRs. Reviewing previous experimental and numerical work by Mahe [37] and more detailed numerical work by Bing [32], we are able to fix a temperature range for neon at which the radiation is predominantly SXR coming from He-like and H-like neon ions. Bing, in particular, carried out a line-by-line computation using a corona method and computed the relative intensities of each of the four neon SXR lines (He- and H-like) as functions of temperature. From this paper we set the following temperature range: 2.3–5.1 $\times 10^6$ K as that

Table 1. Optimized configuration found for each E_0. Optimization carried out with RESF = 0.1, $c = 1.5$, $L_0 = 30$ nH and $V_0 = 20$ kV and model parameters f_m, f_c, f_{mr}, f_{cr} are fixed at 0.06, 0.7, 0.16 and 0.7, respectively. The v_a, v_s and v_p are the peak axial, radial shock and radial piston speeds, respectively.

E_0 (kJ)	C_0 (μF)	a (cm)	z_0 (cm)	P_0 (Torr)	I_{peak} (kA)	I_{pinch} (kA)	v_a (cm μs^{-1})	v_s (cm μs^{-1})	v_p (cm μs^{-1})	Y_{sxr} (J)	Efficiency (%)
0.2	1	0.58	0.5	4.0	100	68	5.6	22.5	14.9	0.44	0.2
1	5	1.18	1.5	4.0	224	143	6.6	23.3	15.1	7.5	0.8
2	10	1.52	2.1	4.0	300	186	6.8	23.6	15.2	20	1.0
6	30	2.29	5.2	4.2	512	294	8.1	24.5	15.6	98	1.6
10	50	2.79	7.5	4.0	642	356	8.7	24.6	15.7	190	1.9
20	100	3.50	13	4.0	861	456	9.6	24.6	16.0	470	2.4
40	200	4.55	20	3.5	1 109	565	10.3	24.7	16.2	1 000	2.5
100	500	6.21	42	3.0	1 477	727	11.2	24.8	16.4	2 700	2.7
200	1 000	7.42	63	3.0	1 778	876	11.4	24.8	16.5	5 300	2.7
400	2 000	8.70	98	3.0	2 079	1 036	11.4	24.9	16.5	9 400	2.4
500	2 500	9.10	105	2.9	2 157	1 086	11.5	25.1	16.7	11 000	2.2
1 000	5 000	10.2	160	3.0	2 428	1 261	11.4	25.2	16.7	18 000	1.8

relevant to the production of neon SXRs. In any shot, for the duration of the focus pinch, whenever the focus pinch temperature is within this range, the line radiation is counted as neon SXRs. Whenever the pinch temperature is outside this range, the line radiation is not included as neon SXRs.

The following parameters are kept constant: (i) the ratio $b = c/a$ (kept at 1.5, which is practically optimum according to our preliminary numerical trials), (ii) the operating voltage V_0 (kept at 20 kV), (iii) static inductance L_0 (kept at 30 nH, which is already low enough to reach the I_{pinch} limitation regime [13, 14] over most of the range of E_0 we are covering) and (iv) the ratio of stray resistance to surge impedance, RESF (kept at 0.1). The model parameters [7, 8, 10–14] f_m, f_c, f_{mr}, f_{cr} are also kept at fixed values of 0.06, 0.7, 0.16 and 0.7.

The storage energy E_0 is changed by changing the capacitance C_0. Parameters that are varied are operating pressure P_0, anode length z_0 and anode radius a. Parametric variation at each E_0 follows the order P_0, z_0 and a until all realistic combinations of P_0, z_0 and a are investigated. At each E_0, the optimum combination of P_0, z_0 and a is found that produces the biggest Y_{sxr}. In other words at each E_0, a P_0 is fixed, a z_0 is chosen and a is varied until the largest Y_{sxr} is found. Then keeping the same values of E_0 and P_0, another z_0 is chosen and a is varied until the largest Y_{sxr} is found. This procedure is repeated until for that E_0 and P_0, the optimum combination of z_0 and a is found. Then keeping the same value of E_0, another P_0 is selected. The procedure for parametric variation of z_0 and a as described above is then carried out for this E_0 and new P_0 until the optimum combination of z_0 and a is found. This procedure is repeated until for a fixed value of E_0, the optimum combination of P_0, z_0 and a is found.

The procedure is then repeated with a new value of E_0. In this manner after systematically carrying out some 2000 runs, the optimized runs for various energies are tabulated in table 1. From the data of table 1, we plot Y_{sxr} against E_0 as shown in figure 1.

Figure 1 shows that Y_{sxr} scales as $E_0^{1.6}$ at low energies in the 0.2 to several kJ region. The scaling 'drops' as E_0 is increased and Y_{sxr} scales as $E_0^{0.76}$ at high energies towards 1 MJ.

We then plot Y_{sxr} against I_{peak} and I_{pinch} and obtain figure 2

Figure 2 shows that the yield scales as $Y_{sxr} \sim I_{pinch}^{3.6}$ and $Y_{sxr} \sim I_{peak}^{3.2}$. The I_{pinch} scaling has less scatter than the I_{peak} scaling.

We next test the scaling when the fixed parameters RESF, c, L_0 and V_0 and model parameters f_m, f_c, f_{mr}, f_{cr} are varied. We add in the results of some numerical experiments

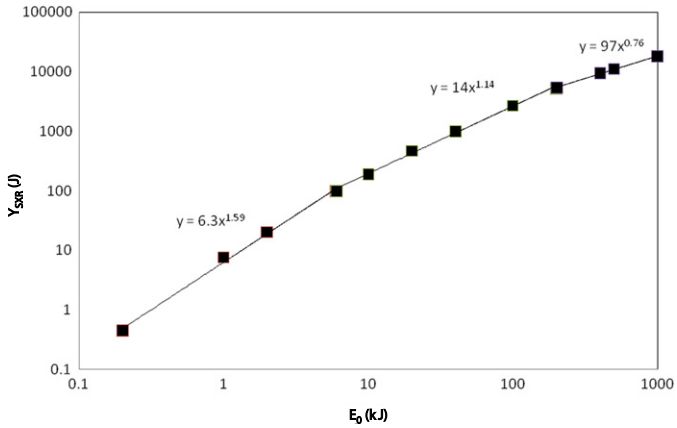

Figure 1. Y_{sxr} versus E_0. The parameters kept constant are: RESF $= 0.1$, $c = 1.5$, $L_0 = 30$ nH and $V_0 = 20$ kV and model parameters f_{m}, f_{c}, f_{mr}, f_{cr} at 0.06, 0.7, 0.16 and 0.7, respectively.

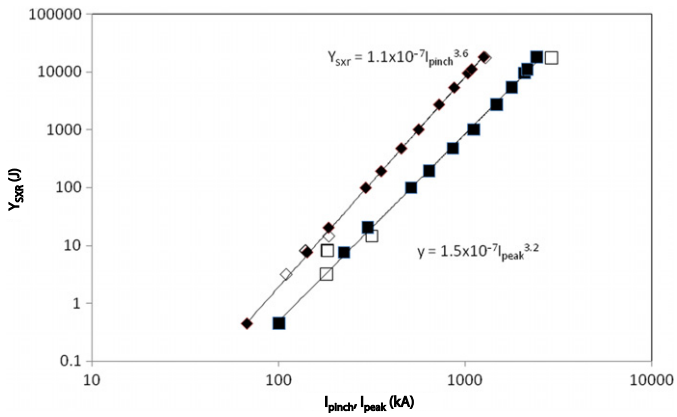

Figure 2. Y_{sxr} versus I_{pinch}, I_{peak}. The parameters kept constant for the black data points are RESF $= 0.1$, $c = 1.5$, $L_0 = 30$ nH and $V_0 = 20$ kV and model parameters f_{m}, f_{c}, f_{mr}, f_{cr} at 0.06, 0.7, 0.16 and 0.7, respectively. The white data points are for specific machines which have different values for the parameters c, L_0 and V_0.

using the parameters of several existing plasma focus devices including the UNU/ICTP PFF (RESF $= 0.2$, $c = 3.4$, $L_0 = 110$ nH and $V_0 = 14$ kV with fitted model parameters $f_{\mathrm{m}} = 0.05$, $f_{\mathrm{c}} = 0.7$, $f_{\mathrm{mr}} = 0.2$, $f_{\mathrm{cr}} = 0.8$) [6–8, 37], the NX2 (RESF $= 0.1$, $c = 2.2$, $L_0 = 20$ nH and $V_0 = 11$ kV with fitted model parameters $f_{\mathrm{m}} = 0.06$, $f_{\mathrm{c}} = 0.7$, $f_{\mathrm{mr}} = 0.16$, $f_{\mathrm{cr}} = 0.7$) [6–9, 32] and PF1000 (RESF $= 0.1$, $c = 1.39$, $L_0 = 33$ nH and $V_0 = 27$ kV with fitted model parameters $f_{\mathrm{m}} = 0.1$, $f_{\mathrm{c}} = 0.7$, $f_{\mathrm{mr}} = 0.15$, $f_{\mathrm{cr}} = 0.7$) [6–8, 13]. These new data points (white data points in figure 2) contain wide ranges of c, V_0, L_0 and model parameters. The resulting Y_{sxr} versus I_{pinch} log–log curve remains a straight line, with the scaling index 3.6 unchanged and with no more scatter than before. However, the resulting Y_{sxr} versus I_{peak} curve now exhibits considerably larger scatter and the scaling index has changed.

Another way of looking at the comparison of the I_{pinch} scaling and the I_{peak} scaling is to consider some unoptimized cases, e.g. at very high or very low pressures. In these cases, Y_{sxr} is zero and I_{pinch} is zero but there is a value for I_{peak}. This is an argument that the I_{pinch} scaling is more robust. However, it must be noted that both scalings are applicable only to optimized

points. Nevertheless, noting that the $Y_{sxr} \sim I_{pinch}$ scaling has less scatter than the $Y_{sxr} \sim I_{peak}$ scaling particularly when mixed-parameter cases are included, the conclusion is that the I_{pinch} scaling is the more universal and robust one.

4. Discussion of results

The numerical experiments with neon plasma focus over the storage energy range of 0.2 kJ–1 MJ show that within the stated constraints of these experiments, scaling with E_0 is $Y_{sxr} \sim E_0^{1.6}$ in the low energy range towards sub kJ and 'decreases' to $Y_{sxr} \sim E_0^{0.8}$ in the high energy range investigated towards 1 MJ. A single power law applies for the I_{peak} scaling: $Y_{sxr} \sim I_{peak}^{3.2}$, in the range 0.1–2.4 MA; likewise for I_{pinch} scaling: $Y_{sxr} \sim I_{pinch}^{3.6}$, in the range 0.07–1.3 MA. The observation of the numerical experiments, bolstered by fundamental considerations, is that the I_{pinch} scaling is the more universal and robust one. It may also be worth noting that our comprehensively surveyed numerical experiments for Mather configurations in the range of energies 1 kJ–1 MJ produce an I_{pinch} scaling rule not compatible with Gates' rule [15]. However, it is remarkable that our I_{pinch} scaling index of 3.6, obtained through a set of comprehensive numerical experiments over a range of 0.2 kJ–1 MJ, on the Mather-type devices is within the range 3.5–4 postulated on the basis of sparse experimental data (basically just two machines one at 5 kJ and the other at 0.9 MJ) by Filippov [5], for Filippov configurations in the range of energies 5 kJ–1 MJ.

It must be pointed out that the results represent scaling for comparison with baseline plasma focus devices that have been optimized in terms of electrode dimensions. It must also be emphasized that the scaling with I_{pinch} works well even when there are some variations in the actual device from $L_0 = 30$ nH, $V_0 = 20$ kV and $c = 1.5$. However, there may be many other parameters which can change which could lead to a further enhancement of x-ray yield. For example, 100 J SXR yields have been reported for the 2–3 kJ devices NX1 [3] and NX2+ [33]. The enhancement in yield in those cases may be due to an enhanced I_{pinch}, which may in turn be due to an insulator sleeve arrangement which organizes a good initial breakdown; NX1 has a special high dielectric constant insulator sleeve and NX2+ has an insulator sleeve geometry instead of the insulator disc geometry of NX2 [3]. On the other hand, the yield enhancement could also be due to the anode shape since NX1 is rounded, with specially shaped anode and cathode, and NX2+ is tapered, which may cause changes in the plasma parameters, e.g. plasma density even at the same I_{pinch}. The explanation for x-ray yield enhancement being due to a change in plasma density when tapering the anode is supported by the Lee code [8] and computed by Wong *et al* [33]. Some examples of experimental techniques which may enhance x-ray yields are changing the anode shape, changing the insulator sleeve material, pre-ionization of the ambient gas, pre-ionization of the insulator sleeve, introduction of gas mixture, introduction of density variations in the plasma focus tube by gas puffing (both at the insulator and at the anode tip), changing the insulator sleeve length and thus the plasma sheath curvature, varying the operating voltage, changing the cathode geometry and changing the anode material. Some of these experimental variations may yield significant changes in f_m, f_c, f_{mr}, f_{cr} while others might not be easily simulated by the Lee model in its current form.

5. Conclusions

In conclusion, this paper has shown that within the scope of this paper, neon x-ray yields scale well with $Y_{sxr} = 1.07 \times 10^{-7} I_{pinch}^{3.63}$ (where yield is in joules and current in kiloamperes). This

implies that for applications requiring high x-ray yield, the plasma focus must be designed to optimize I_{pinch}. For example from table 1, it can be seen that the optimum efficiency for SXR yield is with a capacitor bank energy of 100 kJ. One factor may be that beyond 100 kJ, I_{pinch} does not increase well with bank energy due to the increase in the impedance of the plasma focus in comparison with that of the bank impedance. Therefore for larger devices, it may be necessary to operate at a higher voltage and use higher driver impedance to ensure increasing x-ray yield efficiency beyond 100 kJ. Based on the scaling law proposed here, it is possible to classify experimental yield enhancements into three categories: (i) 'compensating for unoptimized focus' where experiments start off with a focus showing unexpectedly low yield, i.e. below the scaling law and then the yield is 'enhanced' by techniques other than changing of anode dimensions to follow the scaling law, (ii) 'increasing I_{pinch}' for example by reducing the current shedding or increasing the current by current stepping with novel driver circuits where the enhanced device still follows the same scaling law and (iii) 'new regime of operation' where plasma parameters such as density, dimensions and lifetime are changed at the same I_{pinch} and yield is beyond the scaling law.

References

[1] Kato Y and Be S H 1986 *Appl. Phys. Lett.* **48** 686
[2] Bogolyubov E P *et al* 1998 *Phys. Scr.* **57** 488–94
[3] Lee S, Lee P, Zhang G, Feng X, Gribkov V A, Mahe L, Serban A and Wong T K S 1998 *IEEE Trans. Plasma Sci.* **26** 1119
[4] Filippov N V *et al* 1996 *IEEE Trans Plasma Sci.* **24** 1215–23
[5] Filippov N V, Filippova T I, Khutoretskaia I V, Mialton V V and Vinogradov V P 1996 *Phys. Lett.* A **211** 168–171
[6] Institute for Plasma Focus Studies http://www.plasmafocus.net
[7] 2008 *Internet Workshop on Plasma Focus Numerical Experiments (IPFS-IBC1) (14 April–19 May 2008)* http://www.plasmafocus.net/IPFS/Papers/IWPCAkeynote2ResultsofInternet-basedWorkshop.doc
[8] Lee S *Radiative Dense Plasma Focus Computation Package: RADPF* http://www.intimal.edu.my/school/fas/UFLF/File1RADPF.htm; http://www.plasmafocus.net/IPFS/modelpackage/File1RADPF.htm
[9] Lee S, Rawat R S, Lee P and Saw S H 2009 *J. Appl. Phys.* **106** 023309
[10] Lee S and Saw S H 2008 *J. Fusion Energy* **27** 292–5
[11] Lee S 2008 *Plasma Phys. Control. Fusion* **50** 105005
[12] Lee S, Saw S H, Lee P C K, Rawat R S and Schmidt H 2008 *Appl. Phys. Lett.* **92** 111501
[13] Lee S and Saw S H 2008 *Appl. Phys. Lett.* **92** 021503
[14] Lee S, Lee P, Saw S H and Rawat R S 2008 *Plasma Phys. Control. Fusion* **50** 065012
[15] Gates D C 1983 *Proc. 2nd Int. Conf. on Energy Storage, Compression and Switching (Venice, Italy, 1978)* vol 2 (New York: Plenum) p 329
[16] Lee S and Serban A 1996 *IEEE Trans. Plasma Sci.* **24** 1101
[17] Lee S 1998 Scaling of the plasma focus *Int. Workshop on Plasma Focus Research (PF98) (Kudowa, Poland, July 1998)* http://eprints.ictp.it/109/ (also in *1st Conf. on Plasma Physics Applications (Julich, Germany, 2004)* (*International Cooperation Bilateral Seminars* vol 34) (Julich: Forschungszentrum Julich Gmbh) pp 27–33)
[18] Behler K and Bruhns H 1987 *Phys. Fluids* **30** 3767
[19] Garanin S F and Mamyshev V I 2008 *Plasma Phys. Rep.* **34** 639–49
[20] Potter D E 1971 *Phys. Fluids* **14** 1911 doi:10.1063/1.1693700
[21] Vikhrev V, Ivanov V V and Rosanova G A 1993 *Nucl. Fusion* **33** 311
[22] Stepniewski W 2006 *J. Phys.: Conf. Ser.* **44** 215–220 doi:10.1088/1742-6596/44/1/031 (*1st Int. Workshop and Summer School on Plasma Physics (IWSSPP'05) (Kiten, Bulgaria, 8–12 June 2005)*)
[23] Yordanov V, Ivanova–Stanik I and Blagoev A 2006 *J. Phys.: Conf. Ser.* **44** 215–20 doi:10.1088/1742-6596/44/1/031 (*1st Int. Workshop and Summer School on Plasma Physics (IWSSPP'05) (Kiten, Bulgaria, 8–12 June 2005)*)
[24] Lee S 1984 Plasma focus model yielding trajectory and structure *Radiations in Plasmas* vol II ed B McNamara (Singapore: World Scientific) ISBN 9971-966-37-9 pp 978–87
[25] Lee S *et al* 1988 *Am. J. Phys.* **56** 62
[26] Tou T Y, Lee S and Kwek K H 1989 *IEEE Trans. Plasma Sci.* **17** 311
[27] S Lee 1991 *IEEE Trans. Plasma Sci.* **19** 912

[28] Ali J b 1990 Development and studies of a small plasma focus *PhD Thesis* Universiti Teknologi Malaysia, Malaysia
[29] Potter D E 1978 *Nucl. Fusion* **18** 813–23
[30] Lee S and Serban A 1998 *J. Plasma Phys.* **60** 3–15
[31] Liu M H, Feng X P, Springham S V and Lee S 1998 *IEEE Trans. Plasma Sci.* **26** 135–40
[32] Bing S 2000 Plasma dynamics and x-ray emission of the plasma focus *PhD Thesis* NIE ICTP Open Access Archive: http://eprints.ictp.it/99/
[33] Wong D, Lee P, Zhang T, Patran A, Tan T L, Rawat R S and Lee S 2007 *Plasma Sources Sci. Technol.* **16** 116–23
[34] Lee S 2000–2007 http://ckplee.myplace.nie.edu.sg/plasmaphysics/
[35] Lee S 2005 ICTP Open Access Archive: http://eprints.ictp.it/85/
[36] Lee S 1998 *Twelve Years of UNU/ICTP PFF—A Review* IC 98 (231) Abdus Salam ICTP, Miramare, Trieste; ICTP OAA: http://eprints.ictp.it/31/
[37] Mahe L 1996 Soft x-rays from compact plasma focus *PhD Thesis* Nanyang Technological University Singapore. ICTP Open Access Archive: http://eprints.ictp.it/327/
[38] Saw S H, Lee P, Rawat R S and Lee S 2009 *IEEE Trans. Plasma Sci.* **37** 1276–82
[39] Siahpoush V, Tafreshi M A, Sobhanian S and Khorram S 2005 *Plasma Phys. Control. Fusion* **47** 1065
[40] Gribkov V A *et al* 2007 *J. Phys. D: Appl. Phys.* **40** 3592
[41] Springham S V, Lee S and Rafique M S 2000 *Plasma Phys. Control. Fusion* **42** 1023

Plasma Phys. Control. Fusion **51** (2009) 075006 (11pp) doi:10.1088/0741-3335/51/7/075006

Numerical experiments on plasma focus neutron yield versus pressure compared with laboratory experiments

S Lee[1,2,3], S H Saw[1,2], L Soto[1,4,5], S V Springham[3] and S P Moo[1]

[1] Institute for Plasma Focus Studies, 32 Oakpark Drive, Chadstone, VIC3148, Australia
[2] INTI University College, 71800 Nilai, Malaysia
[3] National Institute of Education, Nanyang Technological University, Singapore 637616, Singapore
[4] Comisión Chilena de Energía Nuclear, Casilla 188-D, Santiago, Chile
[5] Center for Research and Applications in Plasma Physics and Pulsed Power, P[4], Santiago-Curicó, Chile

E-mail: leesing@optusnet.com.au

Received 21 February 2009, in final form 16 April 2009
Published 19 May 2009
Online at stacks.iop.org/PPCF/51/075006

Abstract

Published literature shows that the neutron yield of the plasma focus has been modeled in two papers using a thermonuclear mechanism. However, it is more widely held that plasma focus neutrons are produced mainly by non-thermalized mechanisms such as beam–target. Moreover these papers use several parameters which are adjusted for each machine until the computed neutron yield Y_n data agree with measured Y_n data. For this paper numerical experiments are carried out, using the Lee model code, incorporating a beam–target mechanism to compute the Y_n versus pressure data of plasma focus devices PF-400 J and FN-II. The Lee model code is first configured for each of these two machines by fitting the computed current waveform against a measured current waveform. Thereafter all results are computed without adjusting any parameters. Computed results of Y_n versus pressure for each device are compared with the measured Y_n versus pressure data. The comparison shows degrees of agreement between the laboratory measurements and the computed results.

1. Introduction

The dense plasma focus produces copious multi-radiation, including a wide spectrum of photons and particles, which is the subject of many studies and applications. From many devices and experiments have been gathered a large array of data and information leading to interesting discussions. For example, to explain the observed fast particles with energies up to megaelectronvolt emitted from devices operating at tens of kilovolts, mechanisms such

as micro-instabilities, magnetohydrodynamic instabilities, acceleration by turbulence and 'anomalous' plasma resistance have been postulated [1, 2]. Working with these ideas enables some numbers to be estimated regarding, for example, beam particle energies.

One of the most important emissions of the plasma focus is the fusion neutrons, which for a deuterium focus derive from the D–D fusion reaction, resulting in 2.45 MeV neutrons. Much data have been accumulated experimentally including pulse duration and time characteristics of emission, neutron spectra and spatial anisotropy of emission and yields [1]. From these data, scaling rules of neutron yield Y_n versus storage energy E_0 or discharge current, I, have been deduced. The yield Y_n was found to be much higher than could be from thermonuclear reactions, given the measured parameters of the plasma focus pinch. Mechanisms such as moving boiler, beam–target, gyrating particles [1–5] and others such as quasi-Maxwellian hot plasmoids [6] have been invoked to explain the high measured Y_n. These neutron generating mechanisms are assumed to be consequential to the instabilities, etc discussed in the last paragraph. Again from such mechanisms come forth general results such as the temporal and spatial characteristics of the neutron pulses, and representative yield numbers put forward to illustrate the validity of the assumed mechanism. There do not appear to be any published results demonstrating non-thermonuclear modeling which may be applied to any particular machine to derive Y_n in a manner where such modeled data may be compared with specific experiments.

Given that it is widely held that the neutron yield from the plasma focus is predominantly from non-thermonuclear mechanisms [1–5] it is interesting that model codes have been developed using a thermonuclear mechanism that claim to have achieved agreement with laboratory measurements for Y_n data [7, 8]. It may be commented that both these papers use parameters such as axial sweeping and radial sweeping efficiency factors which are adjusted until the computed Y_n data agree with the measured Y_n data. Moreover, the kind of temperatures needed in the computation for the gross pinch (as distinct from hot spots), several kiloelectronvolts, is unlikely to be achieved in the actual plasma focus pinch. Specifically it may be commented that figure 16 of Gonzalez *et al* [8] shows a computed peak radial speed of $72\,\mathrm{cm}\,\mu\mathrm{s}^{-1}$, which is a factor of at least 2 higher than that observed experimentally for typical neutron optimized operation [1, 2]. Such a speed generates, in a deuterium plasma, as can be shown from shock equations, a temperature of 2.1 keV, which is 4 times higher than that computed were the speed to be half the claimed value. The reflected shock raises the temperature further to 5 keV, and then follows the pinch compression raising the temperature still higher. In this range of temperature, a factor of 4 in temperature gives a factor $\sim$1000 times in the themalized D–D fusion cross-section [9]. One might wish to ponder how their modeling gives such unrealistically high temperatures.

Reference [8] states that in their model, the 'kinematics' of the current sheet follows Lee's model, quoting [10], of 1983 vintage. A critical problem of the Lee model code, versions up to 1995, was that the computed speeds of the radial phase were too high by a factor of about 2. The modeling of the radial phase considers an imploding slug (of plasma) the front of which is a shock wave and the rear of which is the magnetic piston driving the imploding shock front. In modeling such an imploding slug, there is an implicit assumption that the shock front and the magnetic piston are in instantaneous communication. It was pointed out by Potter [11] that the non-infinite speed of small disturbances means that as the axis is approached, the communication delay between the front and the back of the slug becomes significant. When this communication delay was implemented into the Lee model code [12, 13] the modeled speeds reduced by a factor of about 2 and became more realistic when compared with experimental observations. This critical feature, of a 'signal-delay slug' has since been built into every version of the Lee model code [12, 13].

The imploding radial layer modeled by [8] does not have this vital 'signal-delay' mechanism, and thus ends up computing unrealistic high speeds (factor of 2 too high), which would lead to equally unrealistic high temperatures (factor of 4 too high; hence a factor of ∼1000 times too high in thermonuclear fusion cross-section) in their modeling of the pinch compression phase. Without this unrealistically modeled high speeds it is doubtful that even the most extreme adjustments of the sweeping factors would enable agreement of the computed thermonuclear Y_n with the measured Y_n.

Recently, the Lee model code was equipped with a beam–target mechanism which computes the Y_n for a wide range of plasma focus machines ranging from the sub-kilojoule PF-400 J to the megajoule PF1000. The computed yields are typically within a factor of 2 compared with the measured Y_n [14, 15]. Numerical experiments using this code over a wide range of plasma focus machines and energies have derived scaling rules of Y_n.

In this paper we show that the Lee model code is not only able to compute Y_n for various machines but that it is able to compute data such as Y_n versus P_0. We choose two specific machines the PF-400 J [16] and FN-II [17] (Fuego Nuevo II) which have well-documented published data on Y_n versus P_0 as well as sufficient published machine parameters and measured current traces, so that numerical experiments may be carried out with the Lee model code. The computed Y_n versus P_0 curve in each case is compared with the published measured Y_n versus P_0 data.

The Lee model couples the electrical circuit with plasma focus dynamics, thermodynamics and radiation, enabling realistic simulation of all gross focus properties. The basic model, described in 1984 [10], was successfully used to assist several experiments [18–21]. Radiation-coupled dynamics was included in the five-phase code leading to numerical experiments on radiation cooling [22]. The signal-delay slug, so crucial to radial simulation, was incorporated together with real gas thermodynamics and radiation-yield terms and assisted other research projects [23, 25, 26] and was web-published in 2000 [12] and 2005 [13]. All subsequent versions of the Lee model code incorporate the 'signal-delay slug' as a must-have feature. Plasma self-absorption was included in 2007 [12], improving soft x-ray yield simulation. The code has been used extensively in several machines including UNU/ICTP PFF [18, 21–24], NX2 [25, 26] NX1 [25], and adapted for the Filippov-type plasma focus DENA [27]. A recent development is the inclusion of neutron yield, Y_n, using a beam–target mechanism [3], incorporated in the present version [28] of the code RADPFV5.13.b (and later versions), resulting in realistic Y_n scaling with I_{pinch} [14, 15]. The versatility and utility of the Lee model is demonstrated in its clear distinction of I_{pinch} from I_{peak} [29] and the recent uncovering of a plasma focus pinch current limitation effect [30, 31]. The description, theory, and up-to-date code and a broad range of results of this 'Universal Plasma Focus Laboratory Facility' are available for download [28].

The neutron yield is computed using a phenomenological beam–target neutron generating mechanism described recently by Gribkov *et al* [3] and adapted to yield the following equation. A beam of fast deuteron ions is produced by diode action in a thin layer close to the anode, with plasma disruptions generating the necessary high voltages. The beam interacts with the hot dense plasma of the focus pinch column to produce the fusion neutrons. The beam–target yield is derived [14, 15, 28, 31] as

$$Y_{b-t} = C_n n_i I_{pinch}^2 z_p^2 (\ln(b/r_p))\sigma/U^{0.5},$$

where n_i is the ion density, b is the cathode radius, r_p is the radius of the plasma pinch with length z_p, σ the cross-section of the D–D fusion reaction, n-branch [9] and U, the beam energy. C_n is treated as a calibration constant combining various constants in the derivation process.

The D–D cross-section is sensitive to the beam energy in the range 15–150 kV; so it is necessary to use the appropriate range of beam energy to compute σ. The code computes induced voltages (due to current motion inductive effects) $V_{\max}$ of the order of only 15–50 kV. However it is known, from experiments that the ion energy responsible for the beam–target neutrons is in the range 50–150 keV [3], and for smaller lower voltage machines the relevant energy could be lower at 30–60 keV [5]. Thus in line with the experimental observations the D–D cross section σ is reasonably obtained by using $U = 3V_{\max}$. This fit was tested by using U equal to various multiples of $V_{\max}$. A reasonably good fit of the computed neutron yields to the measured published neutron yields at energy levels from sub-kilojoule to near megajoule was obtained when the multiple of 3 was used; with poor agreement for most of the data points when, for example, a multiple of 1 or 2 or 4 or 5 was used. The model uses a value of $C_n = 2.7 \times 10^7$ obtained by calibrating the yield [28, 31] at an experimental point of 0.5 MA.

The thermonuclear component is also computed in every case and it is found that this component is negligible when compared with the beam–target component.

2. Procedures for the numerical experiments

The Lee model code is configured to work as any plasma focus by inputting the bank parameters, L_0, C_0 and stray circuit resistance r_0; the tube parameters b, a and z_0 and operational parameters V_0 and P_0 and the fill gas. The standard practice is to fit the computed total current waveform to an experimentally measured total current waveform [12–15, 28–31] using four model parameters representing the mass swept-up factor f_m, the plasma current factor f_c for the axial phase and factors f_{mr} and f_{cr} for the radial phases. The mass swept-up factor f_m accounts for not only the porosity of the current sheet but also for the inclination of the moving current sheet–shock front structure, contact layers and all other unspecified mechanisms which have effects equivalent to increasing or reducing the amount of mass in the moving structure, during the axial phase. The current factor f_c accounts for the fraction of current effectively flowing in the moving structure (due to all effects such as current shedding at or near the back-wall and current sheet inclination). This defines the fraction of current effectively driving the structure, during the axial phase. Likewise the radial phase mass swept-up and current factors f_{mr} and f_{cr} are incorporated in all three radial phases. The mass swept-up factor f_{mr} accounts for all mechanisms which have effects equivalent to increasing or reducing the amount of mass in the moving slug, during the radial phase, not the least of which could be the ejection of mass in the axial direction. The current factor f_{cr} accounts for the fraction of current effectively flowing in the moving piston forming the back of the slug (due to all effects). This defines the fraction of current effectively driving the radial slug. The pinch current I_{pinch} is therefore obtained by multiplying the total (circuit) current at the time of pinch by f_{cr}.

From experience it is known that the current trace of the focus is one of the best indicators of gross performance. The axial and radial phase dynamics and the crucial energy transfer into the focus pinch are among the important information that is quickly apparent from the current trace.

The exact time profile of the total current trace is governed by the bank parameters, by the focus tube geometry and the operational parameters. It also depends on the fraction of mass swept-up and the fraction of sheath current and the variation of these fractions through the axial and radial phases. These parameters determine the axial and radial dynamics, specifically the axial and radial speeds which in turn affect the profile and magnitudes of the discharge current. The detailed profile of the discharge current during the pinch phase also reflects the Joule heating and radiative yields. At the end of the pinch phase the total current profile also reflects the sudden transition of the current flow from a constricted pinch to a large column

flow. Thus the discharge current powers all dynamic, electrodynamic, thermodynamic and radiation processes in the various phases of the plasma focus. Conversely all the dynamic, electrodynamic, thermodynamic and radiation processes in the various phases of the plasma focus affect the discharge current. It is then no exaggeration to say that the discharge current waveform contains information on all the dynamic, electrodynamic, thermodynamic and radiation processes that occur in the various phases of the plasma focus. This explains the importance attached to matching the computed current trace to the measured current trace in the procedure adopted by the Lee model code.

Once the current matching is done, and the model parameters are fixed, with adjustments to L_0, C_0, r_0 and z_0 as required by the current matching, all these parameters are fixed and no further adjustment is made to any of the bank, tube and model parameters.

It is observed in laboratory measurements that towards the end of the focus pinch phase plasma/current disruptions occur resulting in localized regions of high densities and temperatures. These localized regions are not modeled in the code, which consequently computes only an average uniform density and an average uniform temperature which are considerably lower than measured peak density and temperature. However, because the four model parameters are obtained by fitting the computed total current waveform to the measured total current waveform, the model incorporates the energy and mass balances equivalent, at least in the gross sense, to all the processes which are not even specifically modeled. Hence, computed gross features such as speeds and trajectories and integrated soft x-ray yields have been extensively tested in numerical experiments on several machines, and found to be comparable with the measured values. Although these current/plasma disruptions are not specifically modeled, as explained earlier, our beam–target mechanism for neutron production is based on such disruptions.

3. PF-400 J—the numerical experiments

3.1. Fitting the computed current trace to obtain the model parameters

Silva *et al* had published a paper [16] with laboratory measurements from the PF-400 J, including a typical current waveform at 6.6 Torr deuterium, and a graph of neutron yield versus pressure. We first fit the computed current waveform to the published measured waveform [16] in the following manner.

We configure the Lee model code (version RADPF05.13.9b) to operate as the PF-400 J, starting with the following published [16] bank and tube parameters:

Bank parameters: $L_0 = 38$ nH, $C_0 = 0.88\,\mu$F, $r_0 =$ not given
Tube parameters: $b = 1.55$ cm, $a = 0.6$ cm, $z_0 = 2.8$ cm
Operating parameters: $V_0 = 28$ kV, $P_0 = 6.6$ Torr deuterium,

where L_0 is the static inductance (nominal), C_0 the storage capacitance (nominal), b the tube outer radius, a the inner radius, z_0 the anode length, V_0 the operating voltage and P_0 the operating initial pressure.

The computed total discharge current waveform is fitted to the measured by varying model parameters f_{m}, f_{c}, f_{mr} and f_{cr} one by one until the computed waveform agrees with the measured waveform. First, the axial model factors f_{m}, f_{c} are adjusted (fitted) until the computed rising slope of the total current trace and the rounding off of the peak current as well as the peak current itself are in reasonable (typically good) fit with the measured total current trace. Then we proceed to adjust (fit) the radial phase model factors f_{mr} and f_{cr} until the computed slope and depth of the dip agree with the measured. This procedure is quite

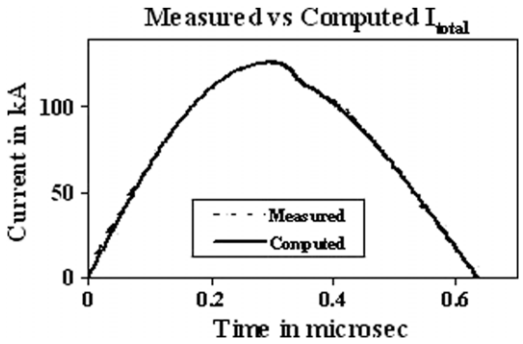

Figure 1. PF-400 J: computed discharge current compared with the published measured current [16].

sensitive and robust in that if any bank parameter such as L_0 or C_0 is not correctly given, no good fit is obtainable (i.e. the computed total current trace will not be matchable with the measured waveform no matter how the four model parameters are varied).

In the case of PF-400 J, to obtain a reasonably good fit of the computed current waveform with the measured current waveform, the following bank and tube parameters (L_0, C_0 and z_0 refitted and r_0 fitted) have to be used:

Bank parameters: $L_0 = 40\,\text{nH}$, $C_0 = 0.95\,\mu\text{F}$, $r_0 = 10\,\text{m}\Omega$
Tube parameters: $b = 1.55\,\text{cm}$, $a = 0.6\,\text{cm}$, $z_0 = 1.7\,\text{cm}$
Operating parameters: $V_0 = 28\,\text{kV}$, $P_0 = 6.6\,\text{Torr}$ deuterium

together with the following fitted model parameters:

$$f_\text{m} = 0.08, \qquad f_\text{c} = 0.7, \qquad f_\text{mr} = 0.11 \qquad \text{and} \qquad f_\text{cr} = 0.7.$$

The fitted computed current waveform is compared with the published waveform in figure 1, showing good agreement, the two traces practically inseparable.

3.2. Computing the neutron yield as a function of operating pressure

The code is configured to operate as the PF-400 J using the bank and tube parameters last mentioned above and using the fitted model parameters. Numerical experiments are then carried out at an operating voltage of 28 kV and at various initial pressures in deuterium. The neutron yields Y_n are then tabulated in Table 1 together with some of the computed properties of the focus pinch. The computed Y_n versus P_0 curve is compared with the published data [16] in figure 2.

Figure 2 shows that the computed neutron yield versus pressure curve agrees reasonably with the published curve. The main features for comparison include the peak Y_n (computed value of 1.16×10^6 against a measured value of 1.06×10^6 neutrons per shot); optimum P_0 (computed value of 6–7 mb against the measured value of 9 mb) and the drop-off of Y_n on both sides of the optimum, although the computed drop-offs are more gradual than the measured.

4. FN-II—the numerical experiments

4.1. Fitting the computed current trace to obtain the model parameters

Castillo *et al* published a paper [17] with laboratory measurements from the FN-II including a typical current derivative waveform and data on neutron yield flux (end-on and side-on)

Table 1. PF-400 J: computed Y_n as a function of pressure, together with some computed pinch properties. I_{peak} is the peak value of the total current, I_{pinch} the plasma pinch current at start of pinch, T_{pinch} the pinch temperature, v_a the axial speed, v_s, v_p the radial shock and piston speeds, r_{min} the minimum radius of focus, z_{max} the maximum length of pinch column, 'pinch dur' the pinch duration, V_{max} the maximum induced voltage and n_i the ion number density.

P_0 (mb)	Y_n (10^6 neutrons)	I_{peak} (kA)	I_{pinch} (kA)	Min T_{pinch} (10^6)	Max T_{pinch} (10^6)	Peak v_a (cm μs^{-1})	Peak v_s (cm μs^{-1})	Peak v_p (cm μs^{-1})	Pinch r_{min} (cm)	Pinch z_{max} (cm)	Pinch dur (ns)	V_{max} (kV)	n_i (10^{23} m^{-3})
15.0	0.27	127	70	2.5	2.7	7.0	23.5	16.0	0.09	0.8	8.0	9.3	6.18
14.0	0.38	127	73	2.9	3.1	7.3	24.8	16.9	0.09	0.8	7.5	10.3	5.95
13.0	0.50	127	75	3.3	3.5	7.5	26.3	17.8	0.09	0.8	7.0	11.4	5.70
12.0	0.64	127	77	3.8	4.0	7.8	27.9	18.8	0.09	0.8	6.6	12.5	5.40
11.0	0.77	126	78	4.3	4.5	8.1	29.6	19.9	0.09	0.8	6.1	13.7	5.06
10.0	0.90	126	80	5.0	5.2	8.5	31.5	21.1	0.09	0.8	5.7	15.0	4.69
9.0	1.02	126	81	5.7	5.9	8.9	33.5	22.5	0.09	0.8	5.4	16.3	4.30
8.7	1.05	126	81	6.0	6.2	9.0	34.3	22.9	0.09	0.8	5.2	16.8	4.17
8.0	1.11	126	82	6.6	6.8	9.3	35.8	24.0	0.09	0.8	5.0	17.8	3.88
7.0	1.16	125	83	7.7	7.9	9.8	38.5	25.7	0.08	0.8	4.6	19.3	3.45
6.0	1.16	124	83	9.1	9.3	10.4	41.5	27.8	0.08	0.8	4.3	21.0	2.99
5.0	1.11	123	83	10.8	11.1	11.1	45.2	30.2	0.08	0.8	3.9	22.9	2.52
4.0	1.00	121	82	13.2	13.6	12.0	49.7	33.3	0.08	0.8	3.5	25.1	2.05
3.0	0.81	117	80	16.8	17.2	13.3	55.8	37.3	0.08	0.8	3.1	27.6	1.55
2.0	0.55	111	76	22.9	23.3	15.1	64.8	43.3	0.08	0.8	2.7	30.5	1.05
1.0	0.25	99	68	36.7	37.2	18.6	81.6	54.5	0.08	0.8	2.1	34.6	0.53

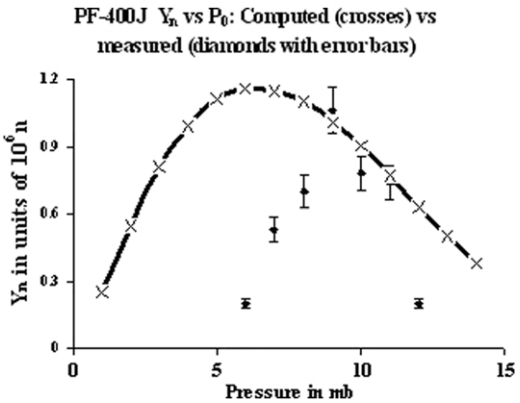

Figure 2. PF-400 J: computed (crosses) compared with the measured [16] (diamonds with error bars) Y_n as functions of P_0. Vertical scale is in units of 10^6 neutrons per shot.

together with emission anisotropy data from which can be deduced the Y_n versus P_0 curve. We first digitize the measured current derivative waveform [17] using an open access source digitizing program, Engauge [32] and then integrate the data with time to obtain the current waveform. Then we fit the computed current waveform to the published measured waveform as follows:

We configure the Lee model code to operate as the FN-II (electrode II) starting with the following published [17] bank and tube parameters:

Bank parameters: $L_0 = 54$ nH, $C_0 = 7.45\,\mu$F, $r_0 =$ not given
Tube parameters: b = 5 cm, a = 2.5 cm, $z_0 = 3$ cm

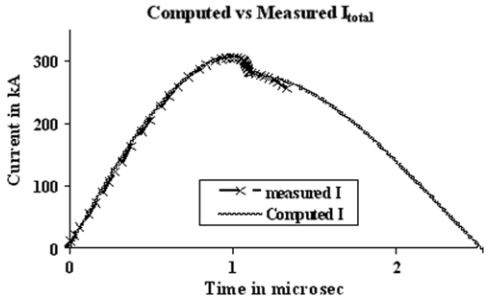

Figure 3. FN-II: computed discharge current compared with the published measured current [17] (derived) for FN-II. The measured discharge current is integrated to just beyond the bottom of the current dip, up to only 1.4 μs.

Operating parameters: $V_0 = 36$ kV, $P_0 = 2.75$ Torr deuterium.

To obtain a reasonably good fit the following bank and tube parameters (L_0, C_0 and z_0 refitted and r_0 fitted) are used:

Bank parameters: $L_0 = 75$ nH, $C_0 = 7.45\,\mu$F, $r_0 = 10\,\text{m}\Omega$
Tube parameters: $b = 5$ cm, $a = 2.5$ cm, $z_0 = 4$ cm
Operating parameters: $V_0 = 36$ kV, $P_0 = 2.75$ Torr deuterium

together with the following fitted model parameters:

$$f_m = 0.12, \qquad f_c = 0.7, \qquad f_{mr} = 0.13 \qquad \text{and} \qquad f_{cr} = 0.7.$$

It can be seen that the computed discharge current waveform agrees well with the published measured current waveform up to and slightly beyond the bottom of the current dip (figure 3). This means that the agreement covers all the regions of interest from axial to radial phases up to the end of the pinch phase; all five plasma focus phases of interest to us.

4.2. Computing the neutron yield as a function of operating pressure

Using the fitted model parameters, numerical experiments are then carried out at various initial pressures in deuterium. The neutron yields Y_n are then tabulated in table 2 and compared with the published measured values [17] in figure 4. The values of Y_n in table 2 are derived from the measured side-on differential yield per solid angle by multiplying each value by 4π and 1.11 as suggested by the discussion of anisotropy in [17]. Using this method the optimum Y_n at 2.75 Torr attains a value of 2.2×10^8 instead of the value of 1.66×10^8 quoted by Castillo *et al* [17]. It appears that this difference is due to the different readings of the Ag counters in their two sets of measurements. To simplify matters we are actually presenting the results without taking into account this difference. That is, we are using a peak value of 2.2×10^8 (using the multiplying factor suggested by the paper) instead of the peak value of 1.66×10^8 which is quoted as the peak value of Y_n. This gives us a less degree of agreement than if we had adjusted the Y_n values so that the peak were 1.66×10^8. This way we are more conservative in claiming the degree of agreement.

Figure 4 shows that the computed neutron yield versus pressure curve agrees reasonably with the published curve. Features of comparison include peak Y_n (computed value of 1.35×10^8 compared with the measured of 2.2×10^8 which agrees to better than factor of 2), optimum P_0 (computed value of 4 Torr compared with the measured value of 2.75 Torr)

Table 2. FN-II: Computed Yn as a function of pressure, together with some computed pinch properties. I_{peak} is the peak value of the total current, I_{pinch} the plasma pinch current at start of pinch, T_{pinch} the pinch temperature, v_a the axial speed, v_s, v_p the radial shock and piston speeds, r_{min} the minimum radius of focus, z_{max} the maximum length of pinch column, 'Pinch dur' the pinch duration, V_{max} the maximum induced voltage and n_i the ion number density.

P_0 (Torr)	Y_n (10^8)	I_{peak} (kA)	I_{pinch} (kA)	Min T_{pinch} (10^6)	Max T_{pinch} (10^6)	Peak v_a (cm μs^{-1})	Peak v_s (cm μs^{-1})	Peak v_p (cm μs^{-1})	r_{min} (cm)	z_{max} (cm)	pinch dur (ns)	V_{max} (kV)	n_i (10^{23} m^{-3})
8.0	0.47	322	168	0.91	1.06	4.9	15.6	10.5	0.44	3.6	54.5	14.1	4.0
6.0	1.01	320	187	1.59	1.75	5.5	19.2	12.9	0.40	3.6	41.8	19.8	3.6
5.0	1.24	319	194	2.09	2.26	6.0	21.5	14.4	0.39	3.6	36.8	23.2	3.2
4.0	1.35	316	198	2.77	2.95	6.5	24.2	16.2	0.38	3.6	32.0	27.1	2.7
3.0	1.28	311	200	3.78	4.00	7.2	27.8	18.6	0.37	3.6	27.5	31.6	2.1
2.8	1.24	309	199	4.05	4.27	7.4	28.7	19.2	0.37	3.6	26.6	32.6	2.0
2.0	0.99	299	196	5.51	5.76	8.3	33.1	22.1	0.36	3.6	22.9	37.1	1.5
1.0	0.50	272	181	9.49	9.83	10.3	42.8	28.5	0.36	3.6	17.5	44.7	0.8

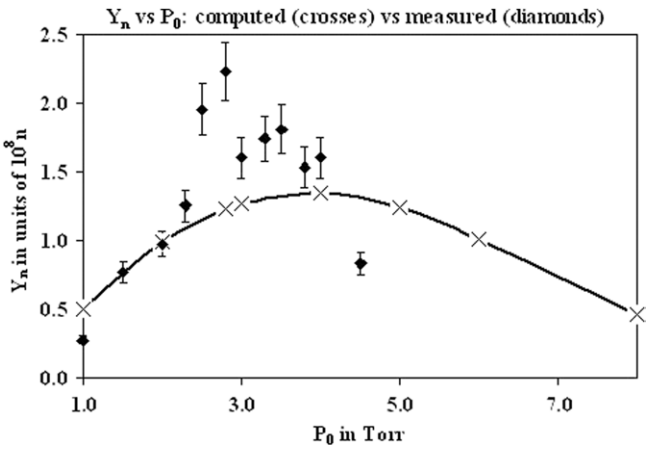

Figure 4. FN-II: computed compared with the measured [17] Y_n as functions of pressure. Vertical scale is in units of 10^8 neutrons per shot.

and the drop-off of Y_n on both sides of the optimum P_0, although the drop-off is more gradual for the computed curve than that for the measured curve.

The agreement between computed Y_n versus P_0 data and measured Y_n versus P_0 for each machine is even more remarkable when we note that model parameters are fitted by comparison of current traces; after fitting no more adjustments are done to any parameters. The same model code also shows reasonable agreement in neutron yield when compared with the published results of the PF1000 [3]; and it may be worthwhile to note that the PF-400 J is a small plasma focus of 400 J, the FN-II is 10 times bigger in storage energy, whilst the PF1000 is one of the biggest plasma focus in the world at 1 MJ. Thus the code computes realistic Y_n across practically the whole range of existing plasma focus devices.

Despite all the discussions in the literature [1, 2] about neutron production mechanisms such as beam–target, gyrating ions, moving boiler and others, the state of the art is not able to do better than make order of magnitude estimates, except in the case of thermonuclear models [7, 8], and those cases require parameters specifically adjusted to make the computed Y_n agree with the measured Y_n. On the other hand, our figures 2 and 4 are modeled with a more

acceptable beam–target mechanism using a more realistic code without adjusting parameters to fit the neutron yield to any specific machine.

5. Conclusion

The Lee model code is used to compute the neutron yield versus pressure curve of the Chilean PF-400 J and the Mexican FN-II. The computed results agree reasonably well with the published curves and give confidence that the Lee model code computes not just optimum neutron yields but also the behavior of neutron yield with pressure for specific plasma focus machines. The results indicate that this code, now incorporated with a beam–target mechanism, gives realistic plasma dynamics and focus properties together with a realistic neutron yield, applicable to a wide range of plasma focus devices, without the need of any adjustable parameters, needing only to fit the computed current trace to a measured current trace.

We may also remark that to do a better evaluation of any model for the mechanism of neutron production in plasma focus devices, it is necessary to use experimental diagnostics with high spatial and temporal resolution. Temporal and spatial resolution close to the pinch moment are crucial to describe properly the plasma heating. For example, to study radial velocities higher than 20 cm μs^{-1} (200 μm ns^{-1}) with optical refractive diagnostics requires shuttering pulses shorter than 100 ps; to obtain the necessary spatial resolution of 20μm for the imploding on-axis shock front. Visible streak camera of sufficient time and space resolution could also be used to assess the radial velocity and the duration of the pinch. Experimental measurements of the ion density and temperature with temporal resolution of the order of nanoseconds are also required for devices in the range of sub-kilojoule to a few kilojoules.

Acknowledgment

L Soto is supported by the Chile Bicentennial Program in Science and Technology grant ACT 26, Center of Research and Applications in Plasma Physics and Pulsed Power Technology (P^4-Project).

References

[1] Bernard A, Bruzzone H, Choi P, Chuaqui H, Gribkov V, Herrera J, Hirano K, Krejci A, Lee S and Luo C 1998 *J. Moscow Phys. Soc.* **8** 93–170
[2] Soto L 2005 *Plasma Phys. Control. Fusion* **47** A361
[3] Gribkov V A *et al* 2007 *J. Phys. D: Appl. Phys.* **40** 3592
[4] Moo S P, Chakrabarty C K and Lee S 1991 *IEEE Trans. Plasma Sci.* **19** 515
[5] Springham S V, Lee S and Rafique M S 2000 *Plasma Phys. Control. Fusion* **42** 1023
[6] Lerner E 2004 arXiv:physics/0401126
[7] Moreno C, Bruzzone H, Martínez J and Clausse A 2000 *IEEE Trans. Plasma Sci.* **28** 1735
[8] González J H, Clausse A, Bruzzone H and Florido P C 2004 *IEEE Trans. Plasma Sci.* **32** 1383
[9] Huba J D 2006 *Plasma Formulary* p 44 http://wwwppd.nrl.navy.mil/nrlformulary/NRL_FORMULARY_07.pdf
[10] Lee S 1984 *Proc. 1983 College on Plasma Physics, ICTP (Trieste, Italy) Radiations in Plasmas* vol 2 ed B McNamara (Singapore: World Scientific) pp 978–87
[11] Potter D E 1971 *Phys. Fluids* **14** 1911
[12] Lee S 2000/2007 http://ckplee.myplace.nie.edu.sg/plasmaphysics/
[13] Lee S 2005 ICTP Open Access Archive http://eprints.ictp.it/85/
[14] Lee S and Saw S H 2008 *J. Fusion Energy* **27** 292–5
[15] Lee S 2008 *Plasma Phys. Control. Fusion* **50** 105005
[16] Silva P, Moreno J, Soto L, Birstein L, Mayer R E and Kies W 2003. *Appl. Phys. Lett.* **83** 3269
[17] Castillo F, Herrera J J E, Rangel J, Alfaro A, Maza M A and Sakaguchi V 2002 *Braz. J. Phys.* **32** 3–12
[18] Lee S *et al* 1988 *Am. J. Phys.* **56** 62

[19] Tou T Y, Lee S and Kwek K H 1989 *IEEE Trans. Plasma Sci.* **17** 311
[20] Lee S 1991 *IEEE Trans. Plasma Sci.* **19** 912
[21] Lee S and Serban A 1996 *IEEE Trans. Plasma Sci.* **24** 1101–5
[22] Ali J b 1990 Development and studies of a small plasma focus *PhD Thesis* Universiti Teknologi Malaysia, Malaysia
[23] Liu M H, Feng X P, Springham S V and Lee S 1998 *IEEE Trans. Plasma Sci.* **26** 135–40
[24] Lee S 1998 *Twelve years of UNU/ICTP PFF—a review IC*, 98 (231) Abdus Salam ICTP, Miramare, Trieste; ICTP OAA: http://eprints.ictp.it/31/
[25] Lee S, Lee P, Zhang G, Feng X, Gribkov V A, Liu M, Serban A and Wong T 1998 *IEEE Trans. Plasma Sci.* **26** 1119
[26] Bing S 2000 Plasma dynamics and x-ray emission of the plasma focus *PhD Thesis* NIE ICTP Open Access Archive http://eprints.ictp.it/99/
[27] Siahpoush V, Tafreshi M A, Sobhanian S and Khorram S 2005 *Plasma Phys. Control. Fusion* **47** 1065
[28] Lee S *Radiative Dense Plasma Focus Computation Package: RADPF* http://www.intimal.edu.my/school/fas/UFLF/; http://www.plasmafocus.net/IPFS/modelpackage/File1RADPF.htm
[29] Lee S, Saw S H, Lee P C K, Rawat R S and Schmidt H 2008 *Appl. Phys. Lett.* **92** 111501
[30] Lee S, Lee P, Saw S H and Rawat R S 2008 *Plasma Phys. Control. Fusion* **50** 065012
[31] Lee S and Saw S H 2008 *Appl. Phys. Lett.* **92** 021503
[32] 2009 http://sourceforge.net/project/showfiles.php?group_id=67696&package_id=130007&release_id=500277

J Fusion Energ
DOI 10.1007/s10894-009-9203-4

ORIGINAL PAPER

Numerical Experiments on Soft X-ray Emission Optimization of Nitrogen Plasma in 3 kJ Plasma Focus SY-1 Using Modified Lee Model

M. Akel · Sh. Al-Hawat · S. Lee

Abstract The X-ray emission properties of nitrogen plasmas are numerically investigated using corona plasma equilibrium model. The X-ray emission intensities of nitrogen Ly_{α}, Ly_{β} and He_{α}, He_{β} lines are calculated. The optimum plasma temperature for nitrogen X-ray output is concluded to be around 160 eV. The Lee model is modified to include nitrogen in addition to other gasses (H_2, D_2, He, Ne, Ar, Xe). It is then applied to characterize the 2.8 kJ plasma focus PF-SY1, finding a nitrogen soft X-ray yield (Ysxr) of 8.7 mJ in its typical operation. Keeping the bank parameters and operational voltage unchanged but systematically changing other parameters, numerical experiments were performed finding the optimum combination of pressure = 0.09 Torr, anode length = 7.2 cm and anode radius = 2.58 cm. The optimum Ysxr was 64 mJ. Thus we expect to increase the nitrogen Ysxr of PF-SY1 sevenfold from its present typical operation; without changing the capacitor bank, merely by changing the electrode configuration and operating pressure.

M. Akel (✉) · Sh. Al-Hawat
Department of Physics, Atomic Energy Commission,
P.O. Box 6091, Damascus, Syria
e-mail: scientific@aec.org.sy

S. Lee
Institute for Plasma Focus Studies, 32 Oakpark Drive,
Chadstone, VIC 3148, Australia

S. Lee
National Institute of Education, Nanyang Technological
University, Singapore 637616, Singapore

S. Lee
INTI International University College, 71800 Nilai, Malaysia

Keywords Plasma focus SY1 · Soft X-ray · Nitrogen gas · Lee model RADPF5.15a

Introduction

The dynamics of plasma focus discharges is complicated; for this purpose, to investigate the plasma focus phenomena, the Lee model couples the electrical circuit with plasma focus dynamics, thermodynamics and radiation, enabling realistic simulation of all gross focus properties. The model provides a useful tool to conduct scoping studies, as it is not purely a theoretical code, but offers means to conduct phenomenological scaling studies for any plasma focus device from low energy to high energy levels.

The model in its two-phase form was described in 1984 [1]. It was successfully used to assist in the design and interpretation of several experiments [2–6]. Radiation-coupled dynamics was included in the five-phase code leading to numerical experiments on radiation cooling [7]. The vital role of a finite small disturbance speed discussed by Potter in a Z-pinch situation [8] was incorporated together with real gas thermodynamics and radiation-yield terms. Before this 'communication delay effect' was incorporated, the model consistently over-estimated the radial speeds by a factor of ~ 2 and shock temperatures by a factor ~ 4. This version using the 'signal-delay slug' assisted other research projects [9–11] and was web-published in 2000 [12] and 2005 [13]. All subsequent versions of the Lee model code incorporate the 'signal-delay slug' as a must-have feature. Plasma self-absorption was included in 2007 [12] improving soft X-ray yield simulation in neon, argon and xenon among other gasses. The model has been used extensively as a complementary facility in several machines, for example, UNU/ICTP PFF [2, 5, 9, 10,

Published online: 19 May 2009

J Fusion Energ
DOI 10.1007/s10894-009-9238-6

ORIGINAL PAPER

Pinch Current and Soft X-Ray Yield Limitations by Numerical Experiments on Nitrogen Plasma Focus

M. Akel · Sh. Al-Hawat · S. Lee

Abstract The modified version of the Lee model code RADPF5-15a is used to run numerical experiments with nitrogen gas, for optimizing the nitrogen soft X-ray yield on PF-SY1. The static inductance L_0 of the capacitor bank is progressively reduced to assess the effect on pinch current I_{pinch}. The experiments confirm the I_{pinch}, limitation effect in plasma focus, where there is an optimum L_0 below which although the peak total current, I_{peak}, continues to increase progressively with progressively reduced inductance L_0, the I_{pinch} and consequently the soft X-ray yield, Ysxr, of that plasma focus would not increase, but instead decreases. For the PF-SY1 with capacitance of 25 μF, the optimum $L_0 = 5$ nH, at which $I_{pinch} = 254$ kA, Ysxr = 5 J; reducing L_0 further increases neither I_{pinch} nor nitrogen Ysxr. The obtained results indicate that reducing the present L_0 of the PF-SY1 device will increase the nitrogen soft X-ray yield.

Keywords Plasma focus SY1 · Pinch current limitation · Soft X-ray · Nitrogen gas · Lee model RADPF5.15a

M. Akel (✉) · Sh. Al-Hawat
Department of Physics, Atomic Energy Commission,
P.O. Box 6091, Damascus, Syria
e-mail: scientific@aec.org.sy

S. Lee
Institute for Plasma Focus Studies, 32 Oakpark Drive,
Chadstone, VIC 3148, Australia

S. Lee
Nanyang Technological University, National Institute
of Education, Singapore 637616, Singapore

S. Lee
INTI University College, 71800 Nilai, Malaysia

Introduction

The plasma focus is well known as a source of fusion neutrons and X-rays. Besides being a ready source of hot dense plasma and fusion neutrons, the focus also emits plentiful amounts of soft X-rays, especially when operated with high Z gases rather than deuterium. Because of its simple construction, cost-effectiveness and easy maintenance, the plasma focus appears to be a promising device for X-ray generation, with enhanced efficiency. The nitrogen plasma focus is used as an emitter of the X-ray radiation [1–3].

The total current I_{total} waveform, which is a "fingerprint" of the plasma focus discharge, is easily measured using a Rogowski coil, and from experience, it is known that the current trace of the focus is one of the best indicators of gross performance [4–9]. The focus pinch current I_{pinch}, which is defined as the value of the plasma sheath current at the start of pinch, is difficult to measure and this is the reason that the total current I_{peak} is experimentally used instead of I_{pinch}, despite the fact that yields should more consistently be scaled to the focus pinch current I_{pinch}, since it is I_{pinch} which directly powers the emission processes. The numerical method to consistently deduce I_{pinch} from any measured trace of I_{total} was developed in numerical experiments using the Lee Model [4–9].

For enhancing of the neutron and X-ray yields from plasma focus devices, many experiments have been investigated by some modifications on the bank, tube and operating parameters of the devices; for example, the two plasma focus devices UNU/ICTP PFF and the NX2 both have capacitance of about 30 μF and maximum operating voltage V_0 of 15 kV. The UNU/ICTP PFF has L_0 of 110 nH whilst the NX2 was designed for much higher performance with $L_0 = 20$ nH. As a result of the much

Published online: 21 August 2009

J Fusion Energ (2010) 29:223–231
DOI 10.1007/s10894-009-9262-6

ORIGINAL PAPER

Numerical Experiments on Oxygen Soft X-Ray Emissions from Low Energy Plasma Focus Using Lee Model

M. Akel · Sh. Al-Hawat · S. H. Saw · S. Lee

Published online: 22 November 2009

Abstract The X-ray emission properties of oxygen plasmas are numerically investigated using corona plasma equilibrium model. The Lee model is here modified to include oxygen in addition to other gases. It is then applied to characterize the Rico Plasma Focus (1 kJ), finding a oxygen soft X-ray yield (Ysxr) of 0.04 mJ in its typical operation. Keeping the bank parameters and operational voltage unchanged but systematically changing other parameters, numerical experiments were performed finding the optimum combination of pressure = 3 Torr, anode length = 1.5 cm and anode radius = 1.29 cm. The optimum Ysxr was 43 mJ. Thus we expect to increase the oxygen Ysxr of PF-1 kJ thousand-fold from its present typical operation; without changing the capacitor bank, merely by changing the electrode configuration and operating pressure. The modified version of the Lee model code is also used to run numerical experiments with oxygen gas, for optimizing the oxygen soft X-ray yield on the new plasma focus device PF-SY2 (2.8 kJ). The static inductance L_0 of the capacitor bank is progressively reduced to assess the effect on pinch current I_{pinch}. The experiments confirm the I_{pinch}, limitation effect in plasma focus, where there is an optimum L_0 below which although the peak total current, I_{peak}, continues to increase progressively with progressively reduced inductance L_0, the I_{pinch} and consequently the soft X-ray yield, Ysxr, of that plasma focus would not increase, but instead decreases. The obtained results indicate that reducing the present L_0 of the PF-SY2 device will increase the oxygen soft X-ray yield till the maximum value after that the Ysxr will decrease with I_{pinch} decreasing.

Keywords Low energy plasma focus · Soft X-ray · Oxygen gas · Lee Model RADPF5.15 K

M. Akel (✉) · Sh. Al-Hawat
Department of Physics, Atomic Energy Commission, P.O. Box 6091, Damascus, Syria
e-mail: scientific@aec.org.sy

S. H. Saw · S. Lee
Institute for Plasma Focus Studies, 32 Oakpark Drive, Chadstone, VIC 3148, Australia

S. Lee
National Institute of Education, Nanyang Technological University, Singapore 637616, Singapore

S. H. Saw · S. Lee
INTI International University College, 71800 Nilai, Malaysia

Introduction

The dynamics of plasma focus discharges is complicated; for this purpose, to investigate the plasma focus phenomena, the Lee model couples the electrical circuit with plasma focus dynamics, thermodynamics and radiation, enabling realistic simulation of all gross focus properties.

In the radial phases, axial acceleration and ejection of mass are caused by necking curvatures of the pinching current sheath result in time-dependent strongly center-peaked density distributions. Moreover laboratory measurements show that rapid plasma/current disruptions result in localized regions of high densities and temperatures particularly in the heavy gases like xenon. We need to point out that these center-peaking density effects and localized regions are not modeled in the code, which consequently computes only an average uniform density and an average uniform temperature which are considerably lower than measured peak density and temperature. However, because the 4-model parameters are obtained by

fitting the computed total current waveform to the measured total current waveform, the model incorporates the energy and mass balances equivalent, at least in the gross sense, to all the processes which are not even specifically modeled. Hence the computed gross features such as speeds and trajectories and integrated soft X-ray yields have been extensively tested in numerical experiments for several machines and are found to be comparable with measured values.

Thus the code provides a useful tool to conduct scoping studies, as it is not purely a theoretical code, but offers means to conduct phenomenological scaling studies for any plasma focus device from low energy to high energy machines.

The model in its two-phase form was described in 1984 [1]. It was successfully used to assist in the design and interpretation of several experiments [2–6]. Radiation-coupled dynamics was included in the five-phase code leading to numerical experiments on radiation cooling [7]. The vital role of a finite small disturbance speed discussed by Potter [8] in a Z-pinch situation was incorporated together with real gas thermodynamics and radiation-yield terms. Before this 'communication delay effect' was incorporated, the model consistently over-estimated the radial speeds by a factor of ~ 2 and shock temperatures by a factor ~ 4. This version using the 'signal-delay slug' assisted other research projects [9–11] and was web-published in 2000 [12] and 2005 [13]. All subsequent versions of the Lee model code incorporate the 'signal-delay slug' as a must-have feature. Plasma self-absorption was included in 2007 [12] improving soft X-ray yield simulation in neon, argon and xenon among other gases. The model has been used extensively as a complementary facility in several machines, for example, UNU/ICTP PFF [2, 5, 9, 10, 14–17], NX1 [10, 18] NX2 [10, 11] and DENA [19]. It has also been used in other machines for design and interpretation including sub-kJ plasma focus machines [20]. Information obtained from the model includes axial and radial velocities and dynamics [19], dimensions and duration of the focus pinch, gross information of temperatures and densities within the pinch, soft X-ray emission characteristics and yield [10, 11, 21], design and optimization [20, 21], of machines, and adaptation to other machine types such as the Filippov-type DENA [19]. The versatility and utility of the improved model is demonstrated in the clear distinction of pinch current from the peak current [22] and the recent uncovering of a plasma focus pinch current limitation effect [23–26]. The detailed description, theory, latest code and a broad range of results of this 'Universal Plasma Focus Laboratory Facility' are available for download from ref. [27].

Oxygen has been used in plasma focus devices as a rich ion source for material science applications [28, 29]. To characterize the plasma focus device operated in oxygen, in this work the Lee model code was modified to include oxygen gas. For this purpose, the oxygen ionization energy data was extracted from NIST [30], and using the corona-model sub-routines available on the IPFS website [27], thermodynamic data such as ionization curves, effective charge numbers and specific heat ratios for oxygen were calculated. Next, these data were fed into the latest Lee code RADPF5.15 K using the 6-polynomials method for the oxygen thermodynamic data.

This work has progressed the Lee model code to the version RADPF5.15 K, which enables to run numerical experiments with the following gases: hydrogen, deuterium, deuterium-tritium, helium, neon, argon, xenon, krypton, nitrogen and oxygen.

In this paper, the Lee Model RADPF5.15 K was used in numerical experiments on two low energy plasma focus devices: Rico Plasma focus (1 kJ) [28, 29] and PF-SY2 (2.8 kJ) operating with oxygen gas.

Calculations of Oxygen Plasma Parameters Using Corona Model

The X-ray radiation properties of plasma are dependent on the plasma temperature, ionization states and density. Plasma equilibrium model can be used to calculate the ion fraction α, the effective ionic charge number Z_{eff}, the effective specific heat ratio γ and X-ray emission of the plasma at different temperatures.

The corona model [11, 27, 31–33] has been used as an approximation for computing the thermodynamic data of the oxygen plasma in the plasma focus. The data of ionization potentials and X-ray emission spectrum of highly ionized oxygen plasma are taken from NIST [30]. Based on the corona model, the ion fraction, effective ionic charge number and effective specific heat ratio for oxygen plasma have been calculated at different temperatures, for more details see [11, 32]. The obtained results for the ion fraction and effective ionic charge number are shown in Figs. 1, 2.

Looking at the results displayed in Fig. 1, the suitable temperature range for generating H-like 1s-2p, O_2: 18.97 A^o ($h\nu_1 = 653.68$ eV), 1s-3p, O_2: 16 A^o ($h\nu_2 = 774.634$ eV) and He– like $1s^2$-1s2p, O_2: 21.6 A^o ($h\nu_3 = 573.947$ eV), $1s^2$-1s3p, O_2: 18.62 A ($h\nu_4 = 665.615$) ions in oxygen plasma (therefore soft X-ray emissions) is between 119–260 eV (1.38×10^6–3×10^6 K). Also the important feature can be seen from Fig. 2, that the temperatures range 49.44–80.53 eV corresponds to the $1s^2$ close shell for the oxygen ions. Therefore, the yield from X-ray line emissions is low in this temperature range from oxygen. And it can be noticed that the oxygen atoms become fully ionized around 2,000–3,000 eV.

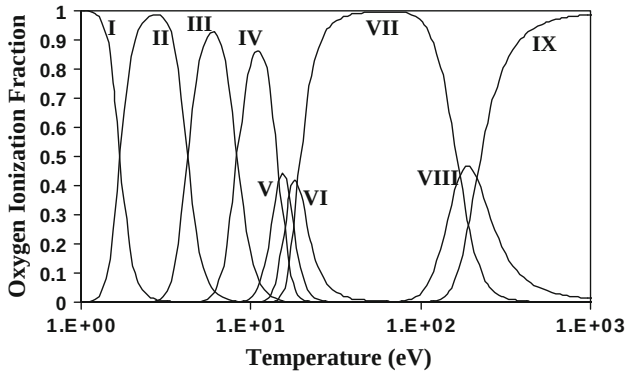

Fig. 1 Oxygen ion fractions at different temperature, where IX indicates the ion O^{+8}

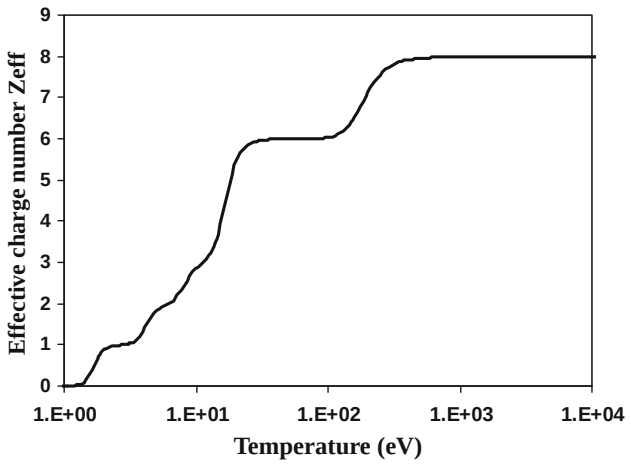

Fig. 2 Effective ionization number Z_{eff} of oxygen (calculated by corona model)

The power of line emissions can also be calculated [11, 32], and the intensities of Lyman—alpha (Ly_α), helium—alpha (He_α) lines are proportional to the H-like and He-like ion densities , respectively. Using the following equations the radiation power of Ly_α, Ly_β and He_α, He_β lines for oxygen as functions of photon energy hν are [11]:

$$P_{Ly\alpha(1s-2p)} = k_1 \cdot N_i^2 \cdot \alpha_7 \cdot Z_{eff} \cdot e^{\left(\frac{-h\nu_1}{T_{ev}}\right)} / \sqrt{T_{eV}} \quad (1)$$

$$P_{Ly\beta(1s-3p)} = k_2 \cdot N_i^2 \cdot \alpha_7 \cdot Z_{eff} \cdot e^{\left(\frac{-h\nu_2}{T_{ev}}\right)} / \sqrt{T_{eV}} \quad (2)$$

$$P_{He\alpha(1s^2-1s2p)} = k_3 \cdot N_i^2 \cdot \alpha_6 \cdot Z_{eff} \cdot e^{\left(\frac{-h\nu_3}{T_{ev}}\right)} / \sqrt{T_{eV}} \quad (3)$$

$$P_{He\beta(1s^2-1s3p)} = k_4 \cdot N_i^2 \cdot \alpha_6 \cdot Z_{eff} \cdot e^{\left(\frac{-h\nu_4}{T_{ev}}\right)} / \sqrt{T_{eV}} \quad (4)$$

where: $k_1 = 2 \times 10^{-31}$, $k_2 = 4 \times 10^{-32}$, $k_3 = 1.3 \times 10^{-31}$, $k_4 = 3 \times 10^{-32}$.From these equations it can be seen that the radiation power is proportional to the density squared, ion fraction and Z_{eff}. Then the normalized emission intensity can be calculated by putting $N_i = 1$. The calculated Ly and He emission intensities from one oxygen ion at unit density are given in Fig. 3. The related ion fractions are also plotted in this figure, which clearly shows the relationship between the line emission intensity with corresponding ions. The peaks of the Ly and He lines are located at the higher temperature side of the H-like and He-like ion distributions. It means the ions need to be heated to excited states to give X-ray emissions. The locations of the peaks give us a rough knowledge of the optimum temperatures for generating X-rays from oxygen plasma, i.e. 225 eV. Choice of optimum temperature is made in comparison with the optimum temperatures chosen for nitrogen [33], neon and argon in Shan Bing's work [11]. The comparison is shown in Table 1. It can be seen that much more energy is required to heat the argon to its X-ray optimum temperature. Hence the usual method for increasing the plasma temperature (by increase the energy density) is to decrease the filling gas pressure. However, the X-ray yield is also related to the total number of X-ray emitters which is proportional to the gas pressure. Therefore, the optimum oxygen X-ray yield temperature may be lower than 260 eV in a plasma focus.

X-Ray Emissions in Plasma Focus and its Incorporation in Model Code

The focused plasma, with electron temperature of a few hundreds eV to about keV and high enough electron density, is a copious source of X-rays. The plasma focus emits both soft (thermal) as well as hard (non-thermal) X-rays but for the scope of this paper we will concentrate only on soft thermal X-rays. The plasma focus emits soft thermal X-rays by three processes [34, 35], namely: Bremsstrahlung (free-free transition) from the coulomb interactions between electrons and ions; recombination radiation (free-bound transition) emitted by an initially free electron as it

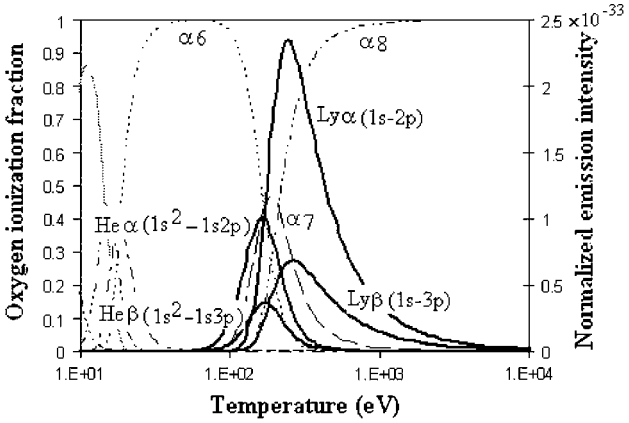

Fig. 3 Calculated X-ray line emission intensities from oxygen Ly and He lines vs temperature. The *dot lines* are the ions fractions (calculated by corona model)

Table 1 Optimization conditions for X-ray radiative plasma of Oxygen, Nitrogen, Neon and Argon

Gas	Temperature	Z_{eff}	$E_{ion} = E_i + (3/2)(1 + Z_{eff})kT$
Oxygen	~225 eV	7.38	1.59 + 2.82 keV
Nitrogen	~160 eV	6.48	1.16 + 1.79 keV [33]
Neon	~420 eV	9.38	2.69 + 4.36 keV [11]
Argon	~3 keV	17.00	11.03 + 54 keV [11]

loses energy on recombination with an ion; and de-excitation radiation (bound-bound transition) when a bound electron loses energy by falling to a lower ionic energy state. The first two processes give rise to the continuum of the X-ray spectrum while the third process produces the characteristic line radiation of the plasma. The relative strengths of the continuum and line emissions depend on how the plasma was formed; typically, for plasma formed from a high-Z material continuum emission dominates, while for a low-Z material line emission can be stronger. The calculation of the power emitted by processes within the plasma depends on assumptions made about the state of the plasma.In the code [27, 36–38] in pinch phase, line radiation Q_L is calculated using the relation

$$\frac{dQ_L}{dt} = -4.6 \times 10^{-31} N_i^2 Z_{eff} Z_n^4 \left(\pi a_{min}^2\right) Z_{max}/T \quad (5)$$

after being integrated over the pinch duration. Hence the soft X-ray energy generated within the plasma pinch depends on the properties: number density N_i, effective charge number Z_{eff}, atomic number of gas Z_n, pinch radius a_{min}, pinch length Z_{max}, plasma temperature T and the pinch duration. This generated energy is then reduced by the plasma self-absorption which depends primarily on density and temperature; the reduced quantity of energy is then emitted as the soft X-ray yield.

Based on the corona model, in the code we take the oxygen soft X-ray yield (generation H-like and He-like ions) to be equivalent to line radiation yield i.e. $Y_{sxr} = Q_L$ at the following temperature range 119–260 eV.

Procedures for Numerical Experiments Using RADPF5.15 K

The Lee code is configured to work as any plasma focus by inputting the bank parameters, the tube parameters, operational parameters and the fill gas. The standard practice is to fit the computed total current waveform to an experimentally measured total current waveform using four model parameters representing the mass swept-up factor f_m, the plasma current factor f_c for the axial phase and factors f_{mr} and f_{cr} for the radial phase.

The axial and radial phase dynamics and the crucial energy transfer into the focus pinch are among the important information that is quickly apparent from the current trace. The exact time profile of the total current trace is governed by the bank parameters, by the focus tube geometry and the operational parameters. It also depends on the fraction of the mass swept up and the fraction of sheath current and the variation of these fractions through the axial and radial phases. These parameters determine the axial and radial dynamics, specifically the axial and radial speeds which in turn affect the profile and magnitudes of the discharge current. The detailed profile of the discharge current during the pinch phase also reflects the Joule heating and radiative yields. At the end of the pinch phase the total current profile also reflects the sudden transition of the current flow from a constricted pinch to a large column flow. Thus, the discharge current powers all dynamic, electrodynamic, thermodynamic and radiation processes in the various phases of the plasma focus. Conversely all the dynamic, electrodynamic, thermodynamic and radiation processes in the various phases of the plasma focus affect the discharge current. It is then no exaggeration to say that the discharge current waveform contains information on all the dynamic, electrodynamic, thermodynamic and radiation processes that occur in the various phases of the plasma focus. This explains the importance attached to matching the computed current trace to the measured current trace in the procedure adopted by the Lee model code [12, 13, 22–24, 39, 40].

The numerical experiments for soft X-ray optimization from oxygen plasma were investigated on two low energy plasma focus devices: Rico Plasma focus (1 kJ) and PF-SY2.

PF-1 kJ-:The Numerical Experiments

The Rico Plasma focus (1 kJ) [28, 29] operated with oxygen filling gas at the following bank and tube parameters:

Bank parameters: $L_0 = 65$ nH, $C_0 = 3.86$ μF, $r_0 = 22$ mΩ,
Tube parameters: $a = 1.75$ cm, $b = 4.9$ cm, $z_0 = 6.75$ cm,
Operating parameters: $V_0 = 14.9$ kV, $p_0 = 0.2$ Torr, oxygen gas,

where L_0 is the static inductance (nominal), C_0 the storage capacitance (nominal), b the tube outer radius, a the inner radius, z_0 the anode length, V_0 the operating voltage and p_0 the operating initial pressure. The measured current derivative waveform at the above conditions is shown in Fig. 4.

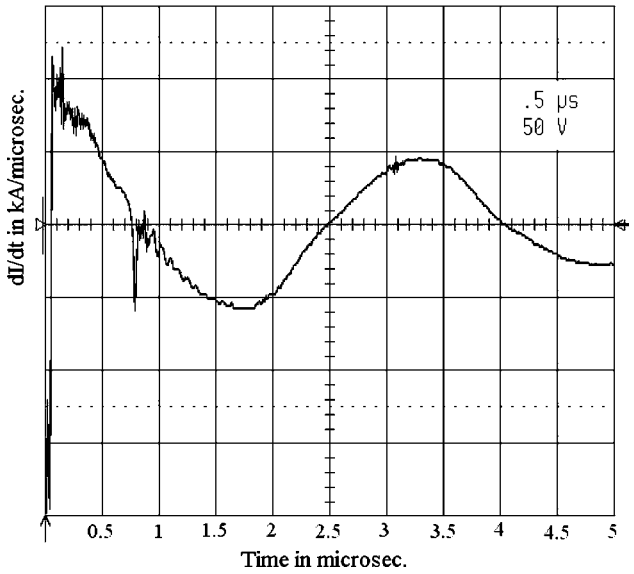

Fig. 4 The temporal evolution of derivative current of the oxygen discharge during the plasma focus formation in PF-1 kJ. $V_0 = 14.9$ kV, $p_0 = 0.2$ Torr, $C_0 = 3.86$ μF, $L_0 = 65$ nH, $r_0 = 22$ mΩ

We first digitize the measured current derivative waveform using an open access source digitizing program, Engauge [41] and then integrate the data with time to obtain the current waveform. Then we fit the computed current waveform to the measured waveform as follows:

We configure the Lee model code (version RADPF5.15 K) to operate as the Rico Plasma focus (1 kJ) starting with the above bank and tube parameters.

To obtain a reasonably good fit the following parameters are used:

Bank parameters: $L_0 = 69$ nH, $C_0 = 3.86$ μF, $r_0 = 20$ mΩ,
Tube parameters: $b = 4.9$ cm, $a = 1.75$ cm, $z_0 = 6.75$ cm,
Operating parameters: $V_0 = 14.9$ kV, $p_0 = 0.2$ Torr, oxygen gas,

together with the following fitted model parameters:
$f_m = 0.004$, $f_c = 0.7$, $f_{mr} = 0.015$ and $f_{cr} = 0.45$.

It can be seen that the computed discharge current waveform agrees well with the measured current waveform up to and slightly beyond the bottom of the current dip (Fig. 5). This means that the agreement covers all the regions of interest from axial to radial phases up to the end of the pinch phase; all five plasma focus phases of interest to us.

The numerical experiments using RADPF5.15 K at the bank and tube parameters last mentioned above and using the fitted model parameters give then the following results: the end axial speed to be $V_a = 17.6$ cm/μs, the final plasma column is 0.19 cm in radius, and 2.1 cm in length.

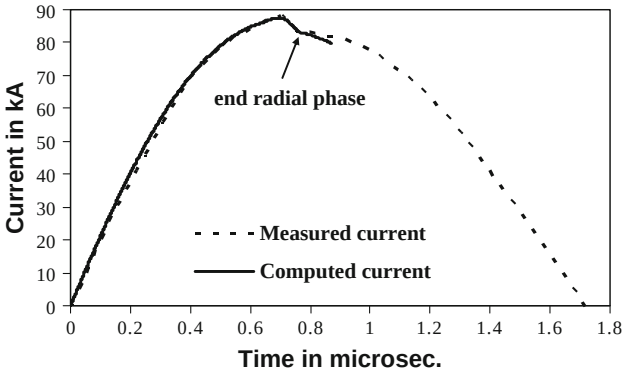

Fig. 5 Comparison of the computed current trace (*solid smooth line*) with the experimental one (*dotted line*) of the PF- 1 kJ at 14.9 kV, 0.2 Torr at oxygen filling gas

Also the Ysxr emitted from the oxygen plasma is calculated at the above conditions, to be 0.04 mJ (see Table 2). Form Table 2 at $p_0 = 0.2$ Torr, it can be found, that the axial speed is very high, and consequently the temperature will be higher than suitable for soft X-ray generation. This low soft X-ray yield from Rico Plasma focus (1 kJ) at experimental conditions is already expected, since Rico Plasma focus (1 kJ) was modified to use as ion beam source for material science applications, and not to generate soft X-ray or line radiation.

As the first step, the code RADPF5.15 K was run to optimize X-ray yield from PF-1 kJ with oxygen gas as function of only pressure; fixing all the mentioned above parameters. The pressure was varied from 0.2 to 0.9 Torr.

As is well known, when the operating pressure is increased, the plasma speeds decrease; hence, the duration of the axial phase increases. From Table 2 it is seen that the Ysxr increases with increasing pressure until it reaches the maximum value about 6.8 mJ at $p_0 = 0.745$ Torr, after which it decreases with higher pressures. As expected as p_0 is increased, the end axial speed, the inward shock speed and the radial piston speed all reduced. The decrease in speeds lead to lowering of plasma temperatures below that needed for soft X-ray production. From Table 2 we note that a shift of operating pressure to 0.745 Torr would increase the computed Ysxr to 6.8 mJ.

To optimize the soft X-ray yield from Rico Plasma focus (1 kJ) with oxygen gas, more numerical experiments were carried out with the above model parameters; but varying p_0, z_0 and 'a' keeping $c = b/a$ constant at value $c = 2.8$. The pressure p_0 was varied from 1 to 15 Torr.

The following procedure was used [33]:

– At each p_0, the anode length z_0 was fixed at a certain value,
– Then the anode radius 'a' was smoothly varied, till the maximum X-ray yield (Ysxr) was obtained for this certain value of z_0.

Table 2 Variation PF-1 kJ parameters with pressure at: $L_0 = 69$ nH, $C_0 = 3.86$ μF, $r_0 = 20$ mΩ, $V_0 = 14.9$ kV, RESF = 0.150, c = b/a = 2.8, $f_m = 0.004$, $f_c = 0.7$, $f_{mr} = 0.015$, $f_{cr} = 0.45$, oxygen gas

p_0 (Torr)	I_{peak} (kA)	I_{pinch} (kA)	V_a (cm/μs)	V_s (cm/μs)	V_p (cm/μs)	Pinch dur. (ns)	T_{pinch} (10^6 K)	Ysxr (mJ)
0.2	87	38	17.6	35.3	24.4	12.7	8.39	0.04
0.3	89	38	15.2	29.8	20.9	14.8	5.62	0.16
0.5	91	35	12.4	22.8	16.3	19.2	2.94	1.2
0.7	92	30	10.6	17.9	13.1	24.9	1.60	5.1
0.72	92	30	10.5	17.5	12.8	25.6	1.50	5.7
0.73	92	29	10.4	17.2	12.7	25.9	1.45	6.1
0.74	92	29	10.4	17.0	12.5	26.2	1.41	6.5
0.745	92	29	10.3	16.9	12.5	26.5	1.38	6.8
0.75	92	29	10.3	16.8	12.4	26.7	1.36	6
0.77	93	28	10.2	16.4	12.1	27.6	1.27	2
0.8	93	27	10.0	15.8	11.7	28.9	1.14	0
0.9	93	24	9.4	13.8	10.4	34.5	0.78	0

- After that, we chose another value of z_0, varying the value of 'a' looking for the maximum of Ysxr, until we found the optimum combination of z_0 and 'a' for the best X-ray yield at the fixed p_0.
- Then we changed p_0 and repeated the above procedure to find the optimum combination of z_0 and 'a' corresponding to this new value of p_0. We proceed until we had obtained the optimum combination of p_0, z_0 and 'a' for the maximum soft X-ray yield.

For optimum oxygen Ysxr, as mentioned earlier, there is an optimum temperature. This implies that there is an optimum speed factor [6] $S = (I_{peak}/a)/p_0^{0.5}$. As p_0 was increased in order to maintain the optimum S, (I_{peak}/a) had to be correspondingly increased, by a reduction of 'a'. The numerical experiments also showed that z_0 needed to be increased to optimize the Ysxr (see Table 3). Thus whilst external inductance L_0 is fixed at a constant value and an axial section inductance L_a is increased due to increasing the anode length, the pinch inductance L_p is reduced due to decreasing the pinch length [6, 23].

The optimized results for each value of p_0 are shown in table 3. The table shows that as p_0 is increased, anode length z_0 rises and inner radius 'a' decreases with each increase in p_0, while the soft X-ray yield slightly increases with increasing p_0 until it reaches a maximum value of 43 mJ at $p_0 = 3$ Torr; then the Ysxr decreases with further pressure increase.

Nevertheless the numerical experiments have shown that with the present capacitor bank, Rico Plasma focus (1 kJ) can be improved from its present computed Ysxr of 0.04 mJ corresponding to the yield with its present geometry and usual operating pressure. The optimum geometry requires making the anode length and the anode radius shorter, at the same time increasing its operational pressure.

PF-SY2 (2.8 kJ)-The Numerical Experiments

The numerical experiments were investigated using the parameters of the low energy plasma focus PF-SY2 and optimizing for a X-ray source. The bank parameters were $L_0 = 200$ nH, $C_0 = 25$ μF and $r_0 = 14$ mΩ. The tube parameters were the outer radius b = 3.2 cm, the inner radius a = 0.95 cm, and the anode length $z_0 = 16$ cm. The operating parameters were $V_0 = 15$ kV, and $p_0 = 10$ Torr, filling oxygen gas. The above mentioned parameters were put into the code RADPF5.15 K.

Table 3 X-ray yield optimization from PF-1 kJ for each value of p_0 varying z_0 and 'a' at filling oxygen gas

p_0 (Torr)	z_0 (cm)	a (cm)	I_{peak} (kA)	I_{pinch} (kA)	Ysxr (mJ)	V_a (cm/μs)	a_{min} (cm)	z_{max} (cm)
1.0	1.0	2.18	92	40	41	4.8	0.20	2.7
2.0	1.3	1.57	92	41	42	5.3	0.14	1.9
3.0	1.5	1.29	92	41	43	5.6	0.12	1.6
5.0	1.8	1.01	93	41	42	5.9	0.09	1.2
10.0	2.8	0.71	95	42	37	6.7	0.07	0.9
15.0	3.0	0.58	95	42	33	6.8	0.05	0.7

$L_0 = 69$ nH, $C_0 = 3.86$ μF, $r_0 = 20$ mΩ, $V_0 = 14.9$ kV, RESF = 0.150, c = b/a = 2.8, $f_m = 0.004$, $f_c = 0.7$, $f_{mr} = 0.015$, $f_{cr} = 0.45$

In this work we would like to present the Mather-type plasma focus device PF-SY2 as a X-ray source with oxygen filling gas using Lee model RADPF5.15 K.

The numerical experiments were conducted using a constant value of a factor RESF = 0.157 (RESF = stray resistance/surge impedance), where at each L_0 the corresponding resistance value was found. Also at each L_0 the ratio (c = b/a) was kept constant at value c = 3.368.

To optimize the soft X-ray yield from PF-SY2 with oxygen gas, varying L_0, z_0 and 'a' keeping 'c' and RESF constant. The external inductance L_0 was varied from 200 to 1 nH.

As we haven't any oxygen measured current trace from PF-SY2, the numerical experiments for optimization soft X-ray from oxygen plasma were carried out with the two different model parameters:

The first model parameters: $f_m = 0.05$, $f_c = 0.7$, $f_{mr} = 0.1$, and $f_{cr} = 0.7$,
The second model parameters: $f_m = 0.03$, $f_c = 0.7$, $f_{mr} = 0.08$, and $f_{cr} = 0.7$.

The following procedures were used:

At each L_0, the pressure was fixed at constant value (in our case $p_0 = 10$ Torr) and also the anode length was fixed at a certain value:

- Then the inner radius 'a' was varied, whilst keeping c = 3.368, until the maximum X-ray yield was obtained for this certain value of z_0.
- After that we chose another value of z_0, varying 'a' until maximum X-ray yield and so on, until we have obtained the combination of z_0 and 'a' for the best maximum X-ray yield at a fixed L_0 (Ysxr vs z_0 and 'a' at fixed L_0 and p_0).
- We repeated the above procedure for progressively smaller L_0 until $L_0 = 1$ nH.

At each L_0, after z_0 was varied, the inner radius 'a' was adjusted to obtain the optimum X-ray yield, which we find to correspond closely to the largest I_{pinch}.

The soft X-ray optimization for each value of L_0, varying z_0 and 'a' is shown in Tables 4, 5. The tables show that as L_0 is reduced, I_{peak} increases with each reduction in L_0 with no sign of any limitation as function of L_0. However, I_{pinch} reaches a maximum value at $L_0 = 5$ nH, then it decreases with each reduction in L_0, but the ratio I_{pinch}/I_{peak} drops progressively as L_0 decreases. Thus I_{peak} does not show any limitation as L_0 is progressively reduced. However, I_{pinch} has a maximum value. This pinch current limitation effect is not a simple, but it is a combination of the two complex effects: the interplay of the various inductances involved in the plasma focus processes abetted by the increasing coupling of C_0 to the inductive energetic processes, as L_0 is reduced [23, 25].

From Tables 4, 5 it can be seen, that as L_0 is decreased, the soft X-ray yield increases until it reaches a maximum value of 10 J at $L_0 = 5$ nH (where I_{pinch} also has maximum); beyond which the soft X-ray yield does not increase with reducing L_0. Thus with decreasing L_0 the pinch current I_{pinch} and the soft X-ray yield show limitation. The obtained results confirm the pinch current limitation effect in oxygen plasma focus, and consequently the soft X-ray yield. Figures 6, 7 represent I_{pinch} and X-ray limitation effects in oxygen plasma focus at 10 Torr as L_0 is reduced from 200 to 1 nH.

Looking at Tables 4 and 5, it is noticed that as L_0 was progressively reduced, to optimize 'a' had to be progressively increased and z_0 progressively decreased. Also the plasma pinch dimensions (pinch radius a_{min} and pinch length Z_{max}) increased as L_0 was reduced.

As the external inductance L_0 is lowered from 200 to 1 nH, the tube inductance ($L_a = 2\times10^{-7}$ ln (b/a) Z_0) is decreased and the focus pinch inductance ($L_p = \sim$ln (b/a_{min}) Z_{max}) is increased [23, 39].

Based on the obtained results of these sets of numerical experiments on PF-SY2 with oxygen gas, we can say that to improve the soft X-ray yield, L_0 should be reduced to a value around 10–15 nH (which is an achievable range incorporating low inductance technology [10]), below which the pinch current I_{pinch} and the soft X-ray yield Ysxr would not be improved much, if at all. These experiments confirm the pinch current limitation effect, and consequently the soft X-ray yield for the oxygen plasma focus. Finally, we would like to emphasize that we, practically, have no intention (or ambition) to go below 10–15 nH (which is an achievable range), but in our numerical experiments using RADPF5.15 K we go down to low values (5–1 nH) just to find the pinch current limitation effect.

Conclusions

The required oxygen plasma thermodynamic parameters (the ion fraction, effective ionic charge number and effective specific heat ratio) were calculated at different temperatures and the X-ray emission properties of oxygen plasma were investigated using corona model.

The Lee model RADPF5.15a was modified to get RADPF5.15 K which includes oxygen gas and it was used to characterize the Rico Plasma focus (1 kJ) using its experimental parameters. The soft X-ray yield was found to be 0.04 mJ at the usual operating pressure $p_0 = 0.2$ Torr. By changing p_0 to 0.745 Torr the Ysxr will increase to 6.8 mJ, as the optimum value for Rico Plasma focus (1 kJ).

The optimum combination of p_0, z_0 and 'a' for optimum soft X-ray yield was found to be: $p_0 = 3$ Torr, $z_0 = 1.5$ cm, a = 1.29 cm and Ysxr = 43 mJ. From these

Table 4 For each L_0 the optimization combination of z_0 and 'a' were found and are listed here

L_0 (nH)	z_0 (cm)	a (cm)	b (cm)	I_{peak} (kA)	I_{pinch} (kA)	I_{pinch} /I_{peak}	a_{min} (cm)	Z_{max} (cm)	Ysxr (J)
200.0	6.1	0.5900	2.0	143	99	0.692	0.06	0.8	0.36
100.0	4.5	0.7700	2.6	198	134	0.676	0.07	1.0	1.03
50.0	3.2	0.9900	3.3	271	175	0.645	0.09	1.4	2.64
40.0	2.8	1.1000	3.7	300	189	0.63	0.11	1.5	3.27
25.0	2.5	1.2000	4.0	365	215	0.589	0.12	1.7	5.52
15.0	2.1	1.3000	4.4	443	237	0.534	0.14	1.8	7.75
10.0	1.7	1.4000	4.7	510	247	0.484	0.17	2.0	9.44
5.0	1.6	1.4600	4.9	627	249	0.397	0.21	2.1	10.06
3.0	1.6	1.4500	4.9	699	244	0.349	0.23	2.1	9.45
1.0	1.6	1.3600	4.6	799	230	0.288	0.234	2.0	7.47

PF-SY2: Bank parameters: $L_0 = 200$ nH, $C_0 = 25$ μF, $r_0 = 14$ mΩ; tube parameter: $c = b/a = 3.368$; model parameters: $f_m = 0.05$, $f_c = 0.7$, $f_{mr} = 0.1$, $f_{cr} = 0.7$; operating at 10 Torr oxygen gas, $V_0 = 15$ kV

Table 5 For each L_0 the optimization combination of z_0 and 'a' were found and are listed here

L_0 (nH)	z_0 (cm)	a (cm)	b (cm)	I_{peak} (kA)	I_{pinch} (kA)	I_{pinch} /I_{peak}	a_{min} (cm)	Z_{max} (cm)	Ysxr (J)
200.0	6.1	0.6700	2.3	141	98	0.695	0.06	0.9	0.43
100.0	4.7	0.8800	3.0	196	133	0.678	0.08	1.2	1.22
50.0	3.2	1.1000	3.7	265	172	0.649	0.10	1.5	3.02
40.0	3.0	1.2000	4.0	293	185	0.631	0.11	1.6	3.91
25.0	2.5	1.4000	4.7	358	209	0.583	0.14	1.9	5.90
15.0	2.1	1.5000	5.1	432	228	0.527	0.17	2.1	8.65
10.0	1.7	1.6000	5.4	494	236	0.477	0.20	2.24	9.97
5.0	1.4	1.6100	5.4	595	239	0.401	0.23	2.29	10.81
3.0	1.2	1.5700	5.3	656	234	0.356	0.24	2.26	9.87
1.0	1.2	1.4600	4.9	741	219	0.295	0.25	2.1	7.22

PF-SY2: Bank parameters: $L_0 = 200$ nH, $C_0 = 25$ μF, $r_0 = 14$ mΩ; tube parameter: $c = b/a = 3.368$; model parameters: $f_m = 0.03$, $f_c = 0.7$, $f_{mr} = 0.08$, $f_{cr} = 0.7$; operating at 10 Torr oxygen gas, $V_0 = 15$ kV

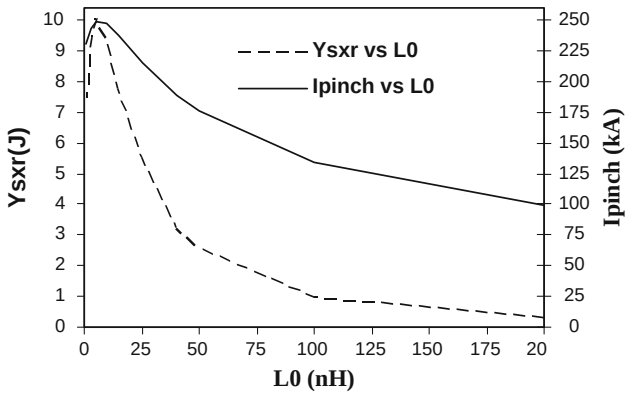

Fig. 6 The X-ray yield from PF-SY2 and I_{pinch} (computed) vs L_0 (200 to 1 nH), model parameters: $f_m = 0.05$, $f_c = 0.7$, $f_{mr} = 0.1$, $f_{cr} = 0.7$; operating at 10 Torr oxygen gas, $V_0 = 15$ kV

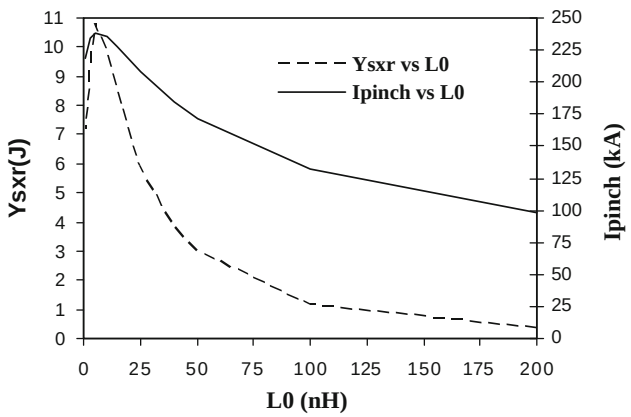

Fig. 7 The X-ray yield from PF-SY2 and I_{pinch} (computed) vs L_0 (200 to 1 nH), model parameters: $f_m = 0.03$, $f_c = 0.7$, $f_{mr} = 0.08$, $f_{cr} = 0.7$; operating at 10 Torr oxygen gas, $V_0 = 15$ kV

numerical experiments we expect to increase the oxygen Ysxr of PF-1 kJ thousand-fold from its present typical operation or hundred-fold from its pressure–optimized present configuration; without changing its capacitor bank, merely by changing its electrode configuration and operating pressure.

The Lee model code RADPF5-15 K was also used to run numerical experiments on PF-SY2 with oxygen gas for optimizing soft X-ray yield with reducing L_0, varying z_0 and 'a'. Contrary to the general expectation that performance of a plasma focus would progressively improve with progressive reduction of its external inductance L_0, the pinch current limitation effect in plasma focus was confirmed with reducing L_0, and consequently the maximum soft X-ray yield was computed as 10 J at $L_0 = 5$ nH; operating the inductance-reduced PF-SY2 at 15 kV, 10 Torr oxygen pressure.

From these numerical experiments we expect to increase the oxygen Ysxr of PF-SY2 with reducing L_0, from the present 0.4 J at $L_0 = 200$ nH to maximum value of near 8 J at an achievable $L_0 = 15$ nH. Because of the current limitation effect, there is little to gain to try to reduce L_0 to 5 nH (which is technically very difficult); and even a loss to reduce L_0 below 5 nH.

Acknowledgments The authors would like to thank Director General of AECS, for encouragement and permanent support. The authors express thanks and appreciation to Dr. L. Rico (Instituto de Fı'sica Rosario (CONICET-UNR), Bvrd. 27 de Febrero 210 Bis, S2000EZP Rosario, Argentina) who provided the Rico Plasma focus (1 kJ) parameters and the measured derivative current waveform of the plasma focus operating with oxygen filling gas. M. Akel would also like to express thanks to Mrs. Sheren Isamael, who collaborated going through all the numerical experiments using Lee Model.

References

1. S. Lee, in *Radiations in Plasmas*, ed. by B. McNamara (World Scientific, Singapore, 1984), pp. 978–987
2. S. Lee et al., Am. J. Phys. **56**, 62 (1988)
3. T.Y. Tou, S. Lee, K.H. Kwek, IEEE Trans. Plasma Sci. **17**, 311 (1989)
4. S. Lee, IEEE Trans. Plasma Sci. **19**, 912 (1991)
5. A. Serban, S. Lee, J. Plasma Phys. **60**, 3–15 (1998)
6. S. Lee, A. Serban, IEEE Trans. Plasma. Sci. **24**, 1101–1105 (1996)
7. J.B. Ali, Development and studies of a small plasma focus PhD thesis, University Technology Malaysia, Kuala Lumpur, Malaysia, 1990
8. D.E. Potter, Nucl. Fusion **18**(6), 813–823 (1978)
9. M.H. Liu et al., IEEE Trans. Plasma. Sci. **26**, 135–140 (1998)
10. S. Lee et al., IEEE Trans. Plasma. Sci. **26**, 1119–1126 (1998)
11. S. Bing, Plasma dynamics and X-ray emission of the plasma focus, PhD thesis NIE ICTP Open Access Archive: http://eprints.ictp.it/99/, 2000
12. S. Lee, http://ckplee.myplace.nie.edu.sg/plasmaphysics/, (2000–2009)
13. S. Lee, ICTP Open Access Archive: http://eprints.ictp.it/85/13, (2005)
14. S. Lee, Twelve years of UNU/ICTP PFF—A Review IC, 98 (231) ICTP, Miramare, Trieste; ICTP OAA: http://eprints.ictp.it/31/, (1998)
15. S.V. Springham et al., Plasma Phys. Control Fusion **42**, 1023–1032 (2000)
16. A. Patran et al., Plasma Sources Sci. Technol. **14**(3), 549–560 (2005)
17. M.A. Mohammadi, S. Sobhanian, C.S. Wong, S. Lee, P.Lee and R.S. Rawat, J. Phys. D: Appl. Phys. **42**, 045203 (2009)
18. E.P. Bogolyubov et al., Phys. Scripta. **57**, 488–494 (1998)
19. V. Siahpoush et al., Plasma Phys. Control Fusion **47**, 1065 (2005)
20. L. Soto et al., Braz. J. Phys. **34**, 1814 (2004)
21. D. Wong et al., Plasma Sources Sci. Technol. **16**, 116–123 (2007)
22. S. Lee et al., Appl. Phys. Lett. **92** 111501 (2008)
23. S. Lee et al., Appl. Phys. Lett. **92** 021503 (2008)
24. S. Lee et al., Plasma Phys. Control Fusion **50** 065012 (2008)
25. S. Lee and S.H. Saw, Appl. Phys. Lett. **94** 076102, (2009)
26. M. Akel, Sh. Al-Hawat, S. Lee, J. Fusion Energ. (2009). doi: 10.1007/s10894-009-9238-6, published online 21 Aug
27. S. Lee, Radiative Dense Plasma Focus Computation Package: RADPF, http://www.intimal.edu.my/school/fas/UFLF/. http://www.plasmafocus.net/IPFS/modelpackage/File1RADPF.htm. (October 2009)
28. L. Rico, B.J. Gomez, J.N. Feugeas, O.de Sanctis, Appl. Surf. Sci. **254**, 193–196 (2007)
29. L. Rico, B.J. Gomez, M. Stachoitti, N. Pellegri, J.N. Feugeas, O.de Sanctis, Braz. J. Phys. **36**(3), 1009–1012 (2006)
30. http://physics.nist.gov/ NIST Atomic Spectra Database Levels Data, (September 2009)
31. S. Lee, Aust. J. Phys. **36**, 891 (1983)
32. M.H. Liu, Soft X-ray from compact plasma focus. PhD thesis, School of Science, Nanyang Technological University, December 1996
33. M. Akel, Sh. Al-Hawat, S. Lee, J. Fusion Energ. **28**(4), 355–363 (2009)
34. E.H. Beckner, J. Appl. Phys. **37**, 4944 (1966)
35. W.H. Bostic, V. Nardi, W. Prior, J. Plasma Phys. **8**, 1 (1972)
36. S.H. Al-Hawat, S. Saloum, Contrib. Plasma Phys. **49**(2), 5–14 (2009)
37. S.H. Saw et al., IEEE Trans. Plasma Sci. **37**(7), 1276–1282 (2009)
38. S. Lee et al., Plasma Phys. Control. Fusion **51**, 105013 (2009)
39. S. Lee, Plasma Phys. Control Fusion **50**, 105005 (2008)
40. S. Lee et al., J. Fusion Energ. **27**(4), 292 (2008)
41. http://sourceforge.net/project/showfiles.php?groupid=67696&package id=130007&release id=500277, (2009)

Neutron yield saturation in plasma focus: A fundamental cause

S. Lee[a)]
INTI University College, 71800 Nilai, Malaysia; Institute for Plasma Focus Studies, 32 Oakpark Dr, Chadstone VIC3148, Australia; and National Institute of Education, Nanyang Technological University, Singapore 637616, Singapore

(Received 28 July 2009; accepted 21 September 2009; published online 15 October 2009)

Plasma focus research in the direction of fusion energy faces the limitation of observed neutron saturation; the neutron yield Y_n falls away from $Y_n \sim E_0^2$, the scaling deteriorating as storage energy E_0 increases toward 1 MJ. Numerical experiments confirm that $Y_n \sim E_0^2$ applies at low energies and drops to $Y_n \sim E_0^{0.8}$ toward 25 MJ; deteriorating already at several hundred kilojoules. We point out that the cause is the dynamic resistance of the axial phase that is constant for all plasma foci. This dynamic resistance dominates the circuit as capacitor bank surge impedance becomes insignificant at large E_0, causing current, hence neutron "saturation." © *2009 American Institute of Physics*. [doi:10.1063/1.3246159]

It was observed early in plasma focus research[1] that neutron yield $Y_n \sim E_0^2$ where E_0 is the capacitor storage energy. Such scaling gave hopes of possible development as a fusion energy source. Devices were scaled up to higher E_0. It was then observed that the scaling deteriorated, with Y_n not increasing as much as suggested by the E_0^2 scaling. In fact some experiments were interpreted as evidence of a neutron saturation effect[2,3] as E_0 approached several hundreds of kilojoules. As recently as 2006, Kraus[4] and Scholz[5] (November 2007) have questioned whether the neutron saturation was due to a fundamental cause or to avoidable machine effects such as incorrect formation of plasma current sheath arising from impurities or sheath instabilities.[3] We should note here that the region of discussion (several hundreds of kilojoules approaching the megajoules region) is in contrast to the much higher energy region discussed by Schmidt[6] at which there might be expected to be a decrease in the role of beam target fusion processes.[3]

Recent extensive numerical experiments[7,8] also showed that whereas at energies up to tens of kilojoules the $Y_n \sim E_0^2$ scaling held, deterioration of this scaling became apparent above the low hundreds of kilojoules. This deteriorating trend worsened and tended toward $Y_n \sim E_0^{0.8}$ at tens of megajoules. The results of these numerical experiments are summarized in Fig. 1 with the solid line representing results from numerical experiments. Experimental results from 0.4 kJ to megajoules, compiled from several available published sources[3,9–14] are also included as squares in the same figure. The combined experimental and numerical experimental results[15] appear to have general agreement particularly with regards to the $Y_n \sim E_0^2$ at energies up to 100 kJ, and the deterioration of the scaling from low hundreds of kilojoules to the 1 MJ level. It is proposed here that the global data of Fig. 1 suggest that the apparently observed neutron saturation effect is overall not in significant variance with the deterioration of the scaling shown by the numerical experiments.

We wish now to provide a simple yet compelling analysis of the cause of this neutron saturation. In Fig. 2 is shown a schematic of the plasma dynamics in the axial phase of the Mather-type plasma focus.

We consider the simplest representation in which the current sheet is shown to go from the anode to the cathode perpendicularly. Observation shows that there is actually a canting of the current sheet[16] and also that only a fraction (typically 0.7) of the total current participates in driving the current sheet. These points are accounted for in the modeling[17–22] by model parameters f_m and f_c. For the moment we do not consider these two effects. The outer cathode radius is shown as b, inner anode radius as a and the moving current sheet is shown at position z in the axial phase.

By surveying published results of all Mather-type experiments we find that all deuterium plasma focus devices operate at practically the same speeds[23] and are characterized by a constancy of energy density (per unit mass) over the whole range of devices from the smallest subkilojoule to the largest megajoule devices. The time varying tube inductance is $L=(\mu/2\pi)\ln(c)z$, where $c=b/a$ and μ is the permeability of free space. The rate of change in inductance is $dL/dt=2\times10^{-7}(\ln c)\, dz/dt$ in SI units. Typically on switching, as the capacitor discharges, the current rises toward its peak value, the current sheet is accelerated, quickly reaching nearly its peak speed, and continues accelerating slightly toward its peak speed at the end of the axial phase. Thus for most of its

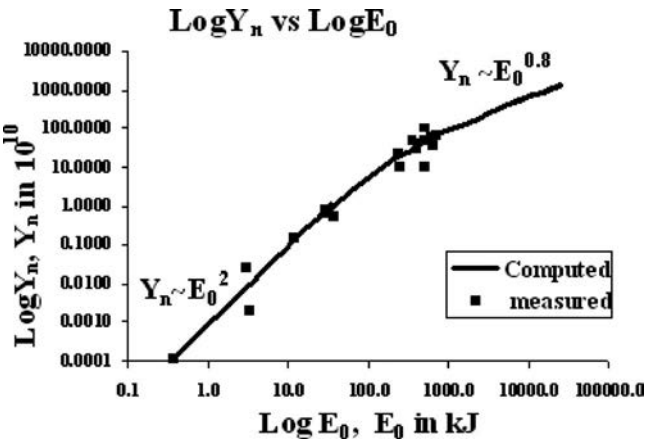

FIG. 1. Illustrating Y_n scaling deterioration observed in numerical experiments from 0.4 kJ to 25 MJ (solid line) using the Lee model code, compared to measurements compiled from publications (squares) of various machines from 0.4 kJ to 1 MJ.

[a)]Electronic mail: leesing@optusnet.com.au.

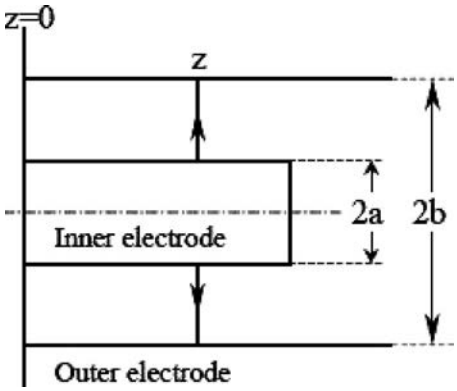

FIG. 2. Plasma focus schematic showing axial phase only.

axial distance the current sheet is traveling at a speed close to the end-axial speed. In deuterium the end-axial speed is observed to be about 10 $cm/\mu s$ over the whole range of devices. This fixes the rate of change in inductance dL/dt as 1.4×10^{-2} H/s for all the devices, if we take the radius ratio $c=b/a=2$. This value of dL/dt changes by at most a factor of 2, taking into account the variation in c from low values of 1.4 (generally for larger machines) to 4 (generally for smaller machines). This typical dL/dt may also be expressed as 14 mΩ.

We need now to inquire into the nature of the change in the inductance $L(t)$. Consider instantaneous power P delivered to $L(t)$ by a change in $L(t)$.

Induced voltage:

$$V = d(LI)/dt = I(dL/dt) + L(dI/dt). \tag{1}$$

Hence instantaneous power into $L(t)$,

$$P = VI = I^2(dL/dt) + LI(dI/dt). \tag{2}$$

Next, consider instantaneous power associated with the inductive energy $(1/2LI^2)$

$$P_L = d\left(\tfrac{1}{2}LI^2\right)/dt = \tfrac{1}{2}I^2(dL/dt) + LI(dI/dt). \tag{3}$$

We note that P_L of Eq. (3) is not the same as P of Eq. (2).

The difference $=P-P_L=\left(\frac{1}{2}\right)(dL/dt)I^2$ is not associated with the inductive energy stored in L. We conclude that whenever $L(t)$ changes with time, the instantaneous power delivered to $L(t)$ has a component that is not inductive. Hence this component of power $\left(\frac{1}{2}\right)(dL/dt)I^2$ must be resistive in nature; and the quantity $\left(\frac{1}{2}\right)(dL/dt)$ is identified as a resistance due to the motion associated with dL/dt, which we call the dynamic resistance.[15] Note that this is a general result and is independent of the actual processes involved. In the case of the plasma focus axial phase, the motion of the current sheet imparts power to the shock wave structure with consequential shock heating, Joule heating, ionization, radiation etc. The total power imparted at any instant is just the amount $\left(\frac{1}{2}\right)(dL/dt)I^2$, with this amount powering all consequential processes. We denote the dynamic resistance of the axial phase as DR_0.

We have thus identified for the axial phase of the plasma focus a typical dynamic resistance of 7 mΩ due to the motion of the current sheet at 10 $cm/\mu s$. It should be noted here that similar ideas of the role of dL/dt as a resistance was discussed by Bernard *et al.*[3] In that work the effect of dL/dt was discussed only for the radial phase. In our opinion the more important phase for the purpose of neutron saturation is actually the axial phase for the Mather-type plasma focus.

TABLE I. Discharge characteristics of equivalent plasma focus circuit, illustrating the saturation of I_{peak} with increase of E_0 to very large values. The last column presents results using circuit (LCR) computation, with a fixed resistance load of 7 mΩ, simulating the effect of the DR_0 and a stray resistance of value $0.1Z_0$.

E_0 (kJ)	C_0 (μF)	Z_0 (mΩ)	DR_0 (mΩ)	Z_{total} (mΩ)	$I_{peak}=V_0/Z_{total}$ (kA)	I_{peak}, LCR (kA)
0.45	1	173	7	197	152	156
4.5	10	55	7	67	447	464
45	100	17	7	26	1156	1234
135	300	10	7	18	1676	1819
450	1000	5.5	7	12.9	2321	2554
1080	2400	3.5	7	10.8	2781	3070
4500	10 000	1.7	7	8.8	3407	3722
45 000	100 000	0.55	7	7.6	4209	4250

We now resolve the problem into its most basic form as follows. We have a generator (the capacitor charged to 30 kV), with an impedance of $Z_0=(L_0/C_0)^{0.5}$ driving a load with a near constant resistance of 7 mΩ. We also assign a value for stray resistance of $0.1Z_0$. This situation may be shown in Table I where L_0 is given a typical value of 30 nH. We also include in the last column the results from a circuit (LCR) computation, discharging the capacitor with initial voltage 30 kV into a fixed resistance load of 7 mΩ, simulating the effect of the DR_0 and a stray resistance of value $0.1Z_0$.

Plotting the peak current as a function of E_0 we obtain Fig. 3, which shows the tendency of the peak current toward saturation as E_0 reaches large values; the deterioration of the curve becoming apparent at the several hundred kilojoule level. This is the case for $I_{peak}=V_0/Z_{tot}$ and also for the LCR discharge with simulated value of the DR_0. In both cases it is seen clearly that a capacitor bank of voltage V_0 discharging into a constant resistance such as DR_0 will have a peak current I_{peak} approaching an asymptotic value of $I_{peak}=V_0/DR_0$ when the bank capacitance C_0 is increased to such large values that the value of $Z_0=(L_0/C_0)^{0.5}\ll DR_0$. Thus DR_0 causes current saturation.

Recent numerical experiments[7,8] have shown agreement with accumulated laboratory data in deriving the relationship between Y_n and I_{peak} and I_{pinch} as follows:

$$Y_n \sim I_{pinch}^{4.5},$$

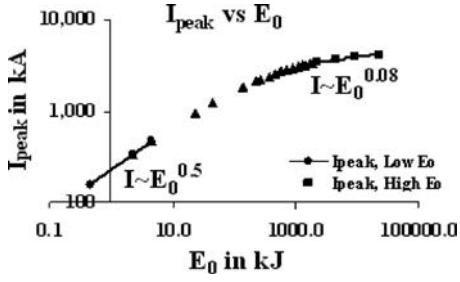

FIG. 3. I_{peak} vs E_0 on log-log scale, illustrating I_{peak} saturation at large E_0.

$$Y_n \sim I_{\text{peak}}^{3.8}.$$

Hence saturation of I_{peak} will lead to saturation of Y_n.

At this point we note that if we consider that only 0.7 of the total current takes part in driving the current sheet, as typically agreed upon from experimental observations, then there is a correction factor which reduces the axial dynamic resistance by some 40%. That would raise the asymptotic value of the current by some 40%, nevertheless there would still be saturation.

In this paper we have shown that current saturation is inevitable as E_0 is increased to very large values by an increase in C_0, simply due to the dominance of the axial phase dynamic resistance. This makes the total circuit impedance tend toward an asymptotic value which approaches the dynamic resistance at infinite values of E_0. The saturation of current inevitably leads to a saturation of neutron yield. Thus the apparently observed neutron "saturation" which is more accurately represented as a neutron scaling deterioration is inevitable because of the dynamic resistance. In line with current plasma focus terminology we will continue to refer to this scaling deterioration as saturation. The above analysis applies to the Mather-type plasma focus. The Filippov-type plasma focus does not have a clearly defined axial phase. Instead it has a liftoff phase and an extended prepinch radial phase which determine the value of I_{peak}. During these phases the inductance of the Filippov discharge is changing, and the changing $L(t)$ will develop a dynamic resistance which will also have the same current saturation effect as the Filippov bank capacitance becomes big enough.

Moreover the saturation as observed in presently available data is due also to the fact that all tabulated machines operate in a narrow range of voltages of 15–50 kV. Only the SPEED machines, most notably SPEED II (Ref. 24) operated at low hundreds of kilovolts. No extensive data have been published from the SPEED machines. Moreover SPEED II, using Marx technology, has a large bank surge impedance of 50 $\text{m}\Omega$, which itself would limit the current. If we operate a range of such high voltage machines at a fixed high voltage, say 300 kV, with ever larger E_0 until the surge impedance becomes negligible due to the very large value of C_0. then the saturation effect would still be there, but the level of saturation would be proportional to the voltage. In this way we can go far above presently observed levels of neutron saturation; moving the research, as it were into presently beyond-saturation regimes.

[1] H. Rapp, Phys. Lett. A **43**, 420 (1973).
[2] H. Herold, A. Jerzykiewicz, M. Sadowski, and H. Schmidt, Nucl. Fusion **29**, 1255 (1989).
[3] A. Bernard, H. Bruzzone, P. Choi, H. Chuaqui, V. Gribkov, J. Herrera, K. Hirano, A. Krejci, S. Lee, and C. Luo, J Moscow Physical Society **8**, 93 (1998).
[4] V. I. Krauz, Plasma Phys. Controlled Fusion **48**, B221 (2006).
[5] M. Scholz, Proceedings of the ICDMP Meeting, Warsaw, Poland, November 2007 (unpublished).
[6] H. Schmidt, Proceedings of Fifth International Workshop on Plasma Focus and *Z*-pinch Research, Toledo 1987 (unpublished), p. 65.
[7] S. Lee and S. H. Saw, J. Fusion Energy **27**, 292 (2008).
[8] S. Lee, Plasma Phys. Controlled Fusion **50**, 105005 (2008).
[9] W. Kies, in *Laser and Plasma Technology*, edited by S. Lee, B. C. Tan, C. S. Wong, A. C. Chew, K. S. Low, H. Ahmad, and Y. H. Chen (World Scientific, Singapore, 1988), pp. 86–137.
[10] H. Herold, in *Laser and Plasma Technology*, edited by C. S. Wong, S. Lee, B. C. Tan, A. C. Chew, K. S. Low, and S. P. Moo (World Scientific, Singapore, 1990), pp. 21–45.
[11] S. Lee, T. Y. Tou, S. P. Moo, M. A. Eissa, A. V. Gholap, K. H. Kwek, S. Mulyodrono, A. J. Smith, S. Suryadi, W. Usada, and M. Zakaullah, Am. J. Phys. **56**, 62 (1988).
[12] L. Soto, P. Silva, J. Moreno, G. Silvester, M. Zambra, C. Pavez, L. Altamirano, H. Bruzzone, M. Barbaglia, Y. Sidelnikov, and W. Kies, Braz. J. Phys. **34**, 1814 (2004).
[13] A. Patran, R. S. Rawat, J. M. Koh, S. V. Springham, T. L. Tan, P. Lee, and S. Lee, Proceedings of the 31st EPS Conference on Plasma Physics, London, 2004 (unpublished), Vol. 28G, p. 4.213.
[14] S. V. Springham, S. Lee, and M. S. Rafique, Plasma Phys. Controlled Fusion **42**, 1023 (2000).
[15] www.plasmafocus.net/IPFS/Papers/keynoteaddressIWPDA09.doc
[16] S. P. Chow, S. Lee, and B. C. Tan, J. Plasma Phys. **8**, 21 (1972).
[17] S. Lee, Radiative Dense Plasma Focus Computation Package: RADPF, www.intimal.edu.my/school/fas/UFLF/; www.plasmafocus.net/IPFS/modelpackage/File1RADPF.htm.
[18] S. Lee and S. H. Saw, Appl. Phys. Lett. **92**, 021503 (2008).
[19] S. Lee, P. Lee, S. H. Saw, and R. S. Rawat, Plasma Phys. Controlled Fusion **50**, 065012 (2008).
[20] S. Lee, S. H. Saw, P. C. K. Lee, R. S. Rawat, and H. Schmidt, Appl. Phys. Lett. **92**, 111501 (2008).
[21] S. H. Saw, P. Lee, R. S. Rawat, and S. Lee, IEEE Trans. Plasma Sci. **37**, 1276 (2009).
[22] S. Lee, S. H. Saw, L. Soto, S. V. Springham, and S. P. Moo, Plasma Phys. Controlled Fusion **51**, 075006 (2009).
[23] S. Lee and A. Serban, IEEE Trans. Plasma Sci. **24**, 1101 (1996).
[24] G. Decker, W. Kies, R. Nadolny, P. Röwekamp, F. Schmitz, G. Ziethen, K. N. Koshelev, and Yu. V. Sidelnikov, Plasma Sources Sci. Technol. **5**, 112 (1996).

Diagnostics and Insights from Current waveform and Modelling of Plasma Focus

S Lee

Institute for Plasma Focus Studies

(www.plasmafocus.net)

***Nanyang Technological University, National Institute of Education, Singapore* 637616**

INTI University College, 71800 Nilai, Malaysia

Keynote address: IWPDA, Singapore 2 July 2009

Plan of Talk

- **Introduction**
- **Diagnostics from modelling**
- **Insights from modelling:**

  - Scaling laws for radiation & neutrons

  -An explanation of neutron saturation in plasma focus
- **Conclusions & discussions:**

  Beyond saturation?

Introduction: Some landmarks:

Plasma Focus independently invented, early 1960's by

- **N V Filippov**
  (4th from left)
- **J W Mather**
  (3rd from left, front row)

1971: David Potter published " Numerical Studies of the Plasma Focus"- a two-dimensional fluid model

- **estimated neutron yield which agrees with experimental measurements**
- **concluded that these neutrons were the result of thermally reacting deuterons in the hot pinch region**

1988- formation of AAAPT

- **Leading to development of a network of small plasma focus devices.**
- **This enabled small research groups to play a role in plasma focus research, a role that has increased in significance with the passing years.**

1997 ICDMP **(International Centre for Dense Magnetised Plasmas)** established in Warsaw-now operates one of biggest plasma focus in the world, the PF1000

Introduction: Some general results from Decades of research

measuring all aspects of the plasma focus:

-imaging for dynamics

-interferometry for densities

-spectroscopy for temperatures

-neutrons, radiation yields, MeV particles

Result: commonly accepted picture today that mechanisms within the focus pinch :

- micro- & MHD instabilities

-acceleration by turbulence

- 'anomalous' plasma resistance

are important to plasma focus behaviour, and

neutron yields are non-thermonuclear in origin

Summarised in: Bernard A, Bruzzone H, Choi P, Chuaqui H, Gribkov V, Herrera J, Hirano K, Krejci A, Lee S, Luo C 1998 "Scientific status of plasma focus research" J Moscow Physical Society 8 93-170

Most important general property of the Plasma Focus

Energy density constancy.

The smallest sub-kJ plasma focus and the largest MJ plasma focus have practically:

- **the same energy density (per unit mass)**
- **the same temperatures,**
- **the same speeds.**

Plasma volumes & lifetimes; increase with anode radius ‘a’

pinch radius ~a

pinch length ~a

pinch lifetime ~a

radius a~ current I

Derived from model scaling, based on observation of constancy of speed factor across plasma focus devices

One of most exciting properties of plasma focus is its neutron yield Y_n

- **Early experiments show: $Y_n \sim E_0^2$**
- **Prospect was raised in those early research years that, breakeven could be attained at ~100 MJ.**
- **However quickly shown that as E_0 approaches 1 MJ, a neutron saturation effect was observed; in other words, Y_n does not increase much more as E_0 was progressively raised above several hundred kJ**
- **Question: Is there a fundamental reason for Y_n saturation?**
- **In Part 2 of this paper we will identify one simple fundamental factor for Y_n saturation; after we discuss the use of modelling for providing reference points for diagnostics.**

Diagnostics from modelling: The Model Schematic

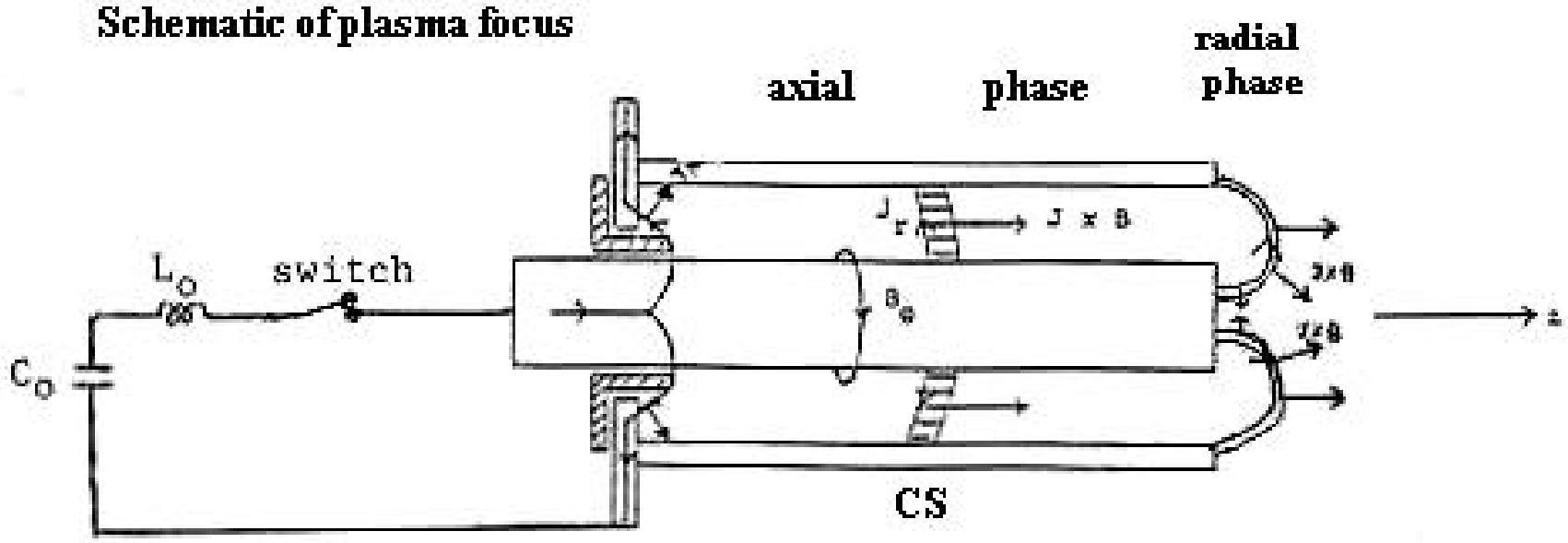

A capacitor bank discharges a large current into the coaxial tube. The current flows in a current sheath CS which is driven by the JXB force axially down the tube. At the end of the axial phase the CS implodes axially, forming an elongating pinch.

Dynamics in the Plasma Focus

(This animation courtesy Rajdeep Singh Rawat)

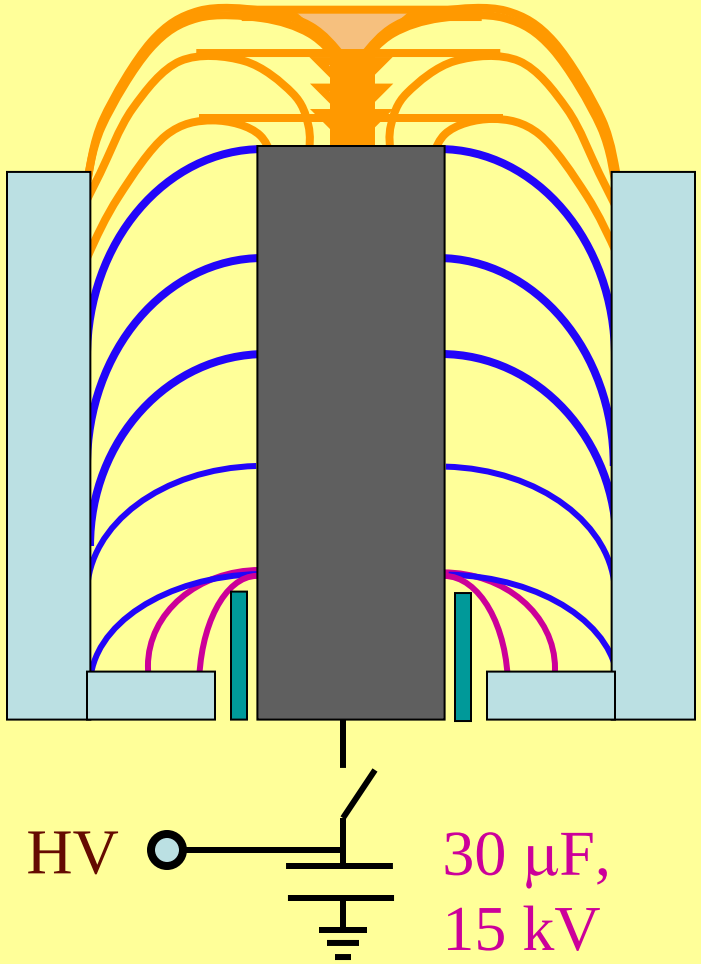

Radial Phase

~80 nanosec

Axial Accelaration Phase

~2.5 microsec

Inverse Pinch Phase

~0.2 microsec

Imaging the Radial Phases of the Plasma Focus

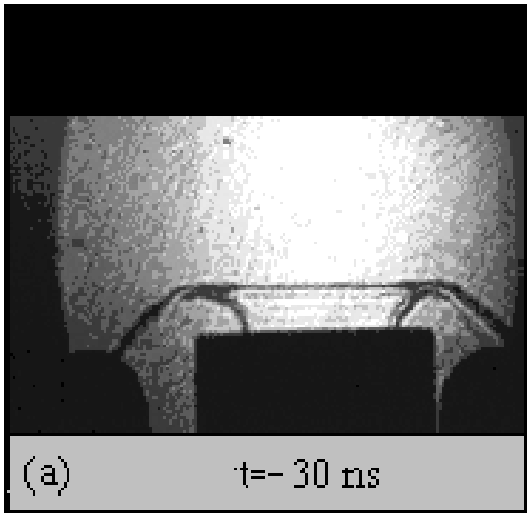

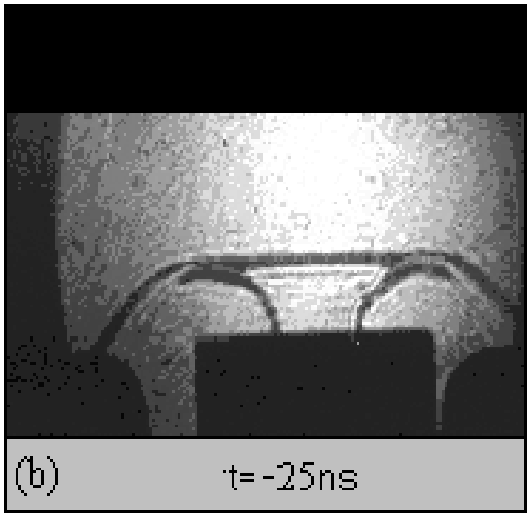

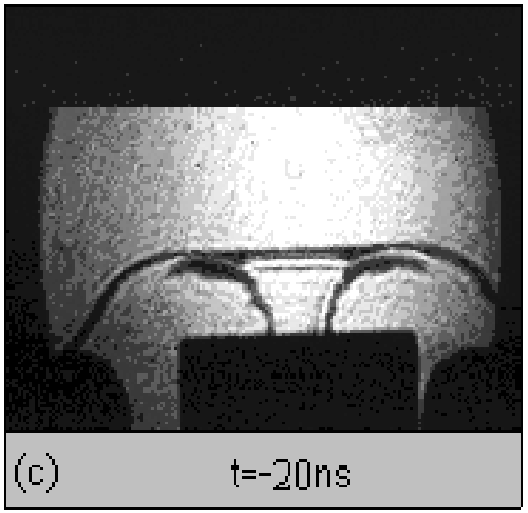

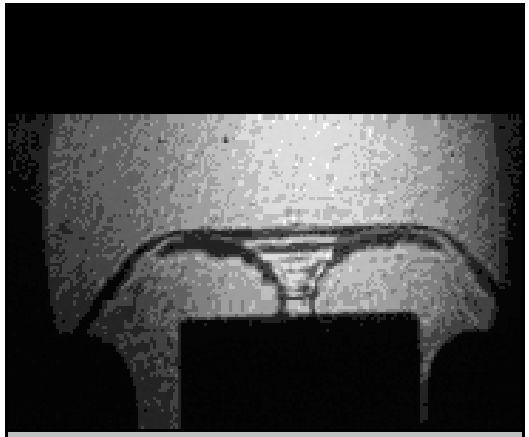

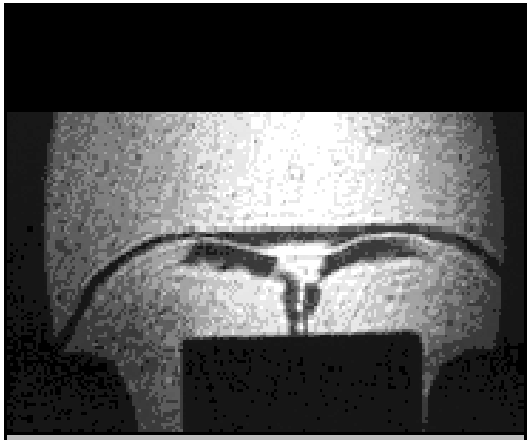

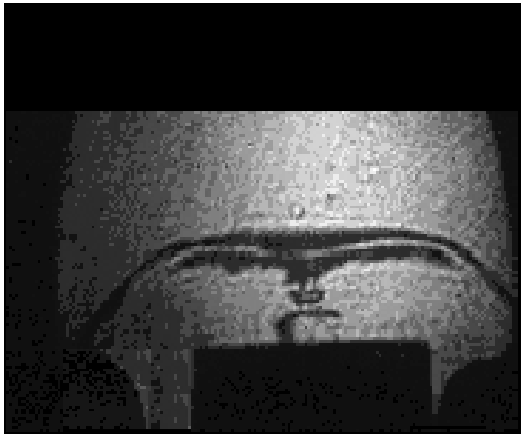

Axial Phase

Radial Phase

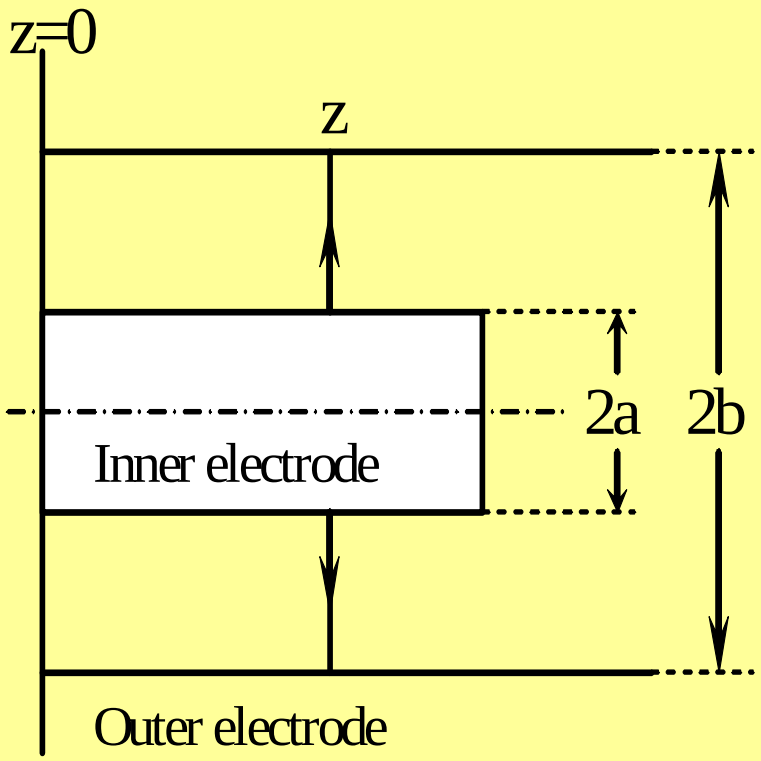

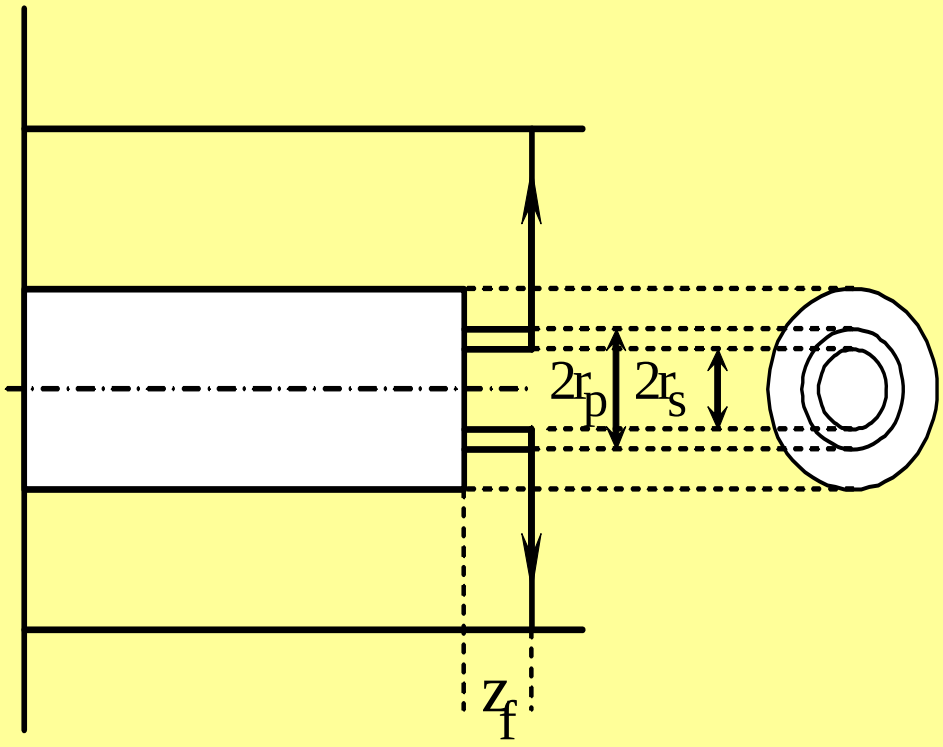

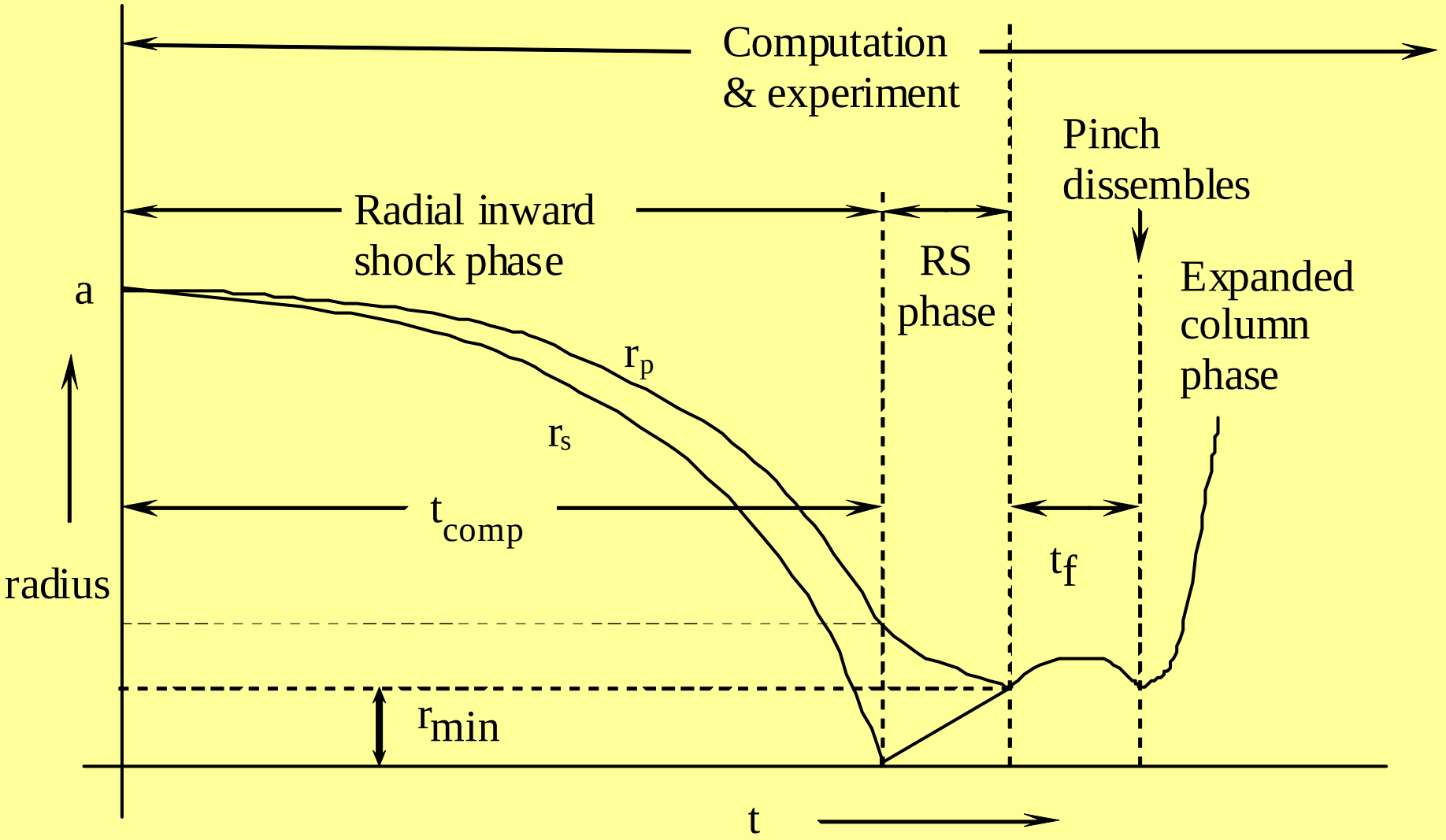

Fig 3. Schematic of radial phases

Schematic of Code

Computes:

- **Axial phase-snowplow model: 2 coupled equations-1 motion, coupled with 1 circuit. Incorporates mass swept-up fraction f_m, and plasma current fraction f_c. These model parameters account for all axial effects not specifically modelled.**
- **Radial implosion phase-, Shock Front-Current Sheet slug with thermodynamics: 4 coupled equations, 3 motion, coupled with 1 circuit; radial mass swept-up factor f_{mr} and current factor f_{cr}. These two model parameters are applied for the radial phases**
- **Reflected Shock Phase**
- **'Slow' compression radiative phase, including plasma self-absorption & possibility of radiative collapse**
- **Post-compression large radius phase**

Plasma focus circuit

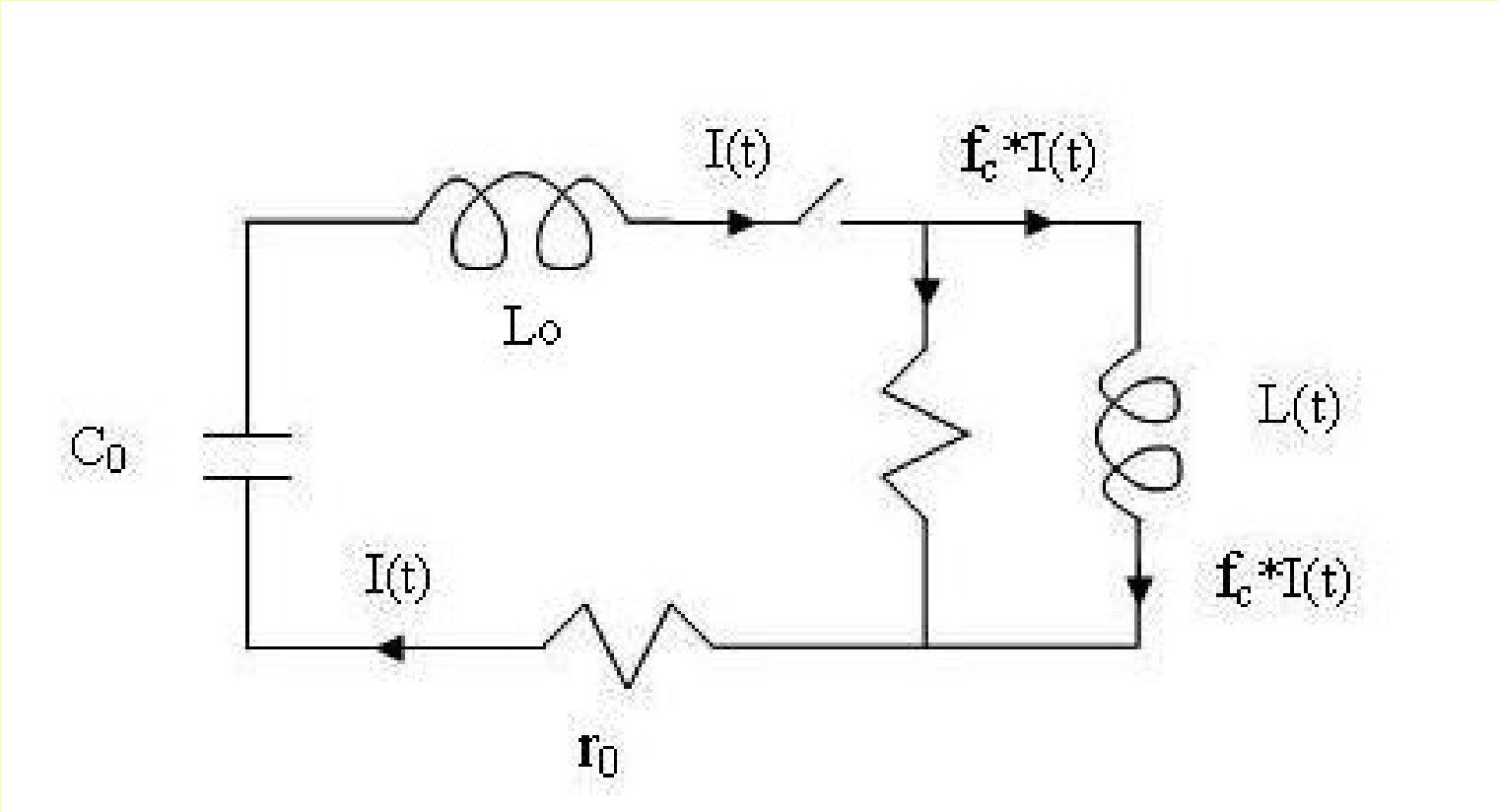

Inductances and dynamic resistance

- **Axial phase: $L(t)=2x10^{-7}\ln(b/a)\ z(t)$**

z(t) is the time varying axial position of the piston.

- **Radial phase: $L(t)= 2x10^{-7}\ln(b/r_p)(z_f)$**

  r_p is the time-varying radial position of the imploding CS (also called the magnetic piston) z_f is the time-varying length of the elongating radially imploding structure.

Whenever an inductance changes with time, a quantity of $0.5(dL/dt)I^2$ is dissipated non-conservatively as power to the system. The quantity half Ldot (we call dL/dt as Ldot) is an electrical RESISTANCE due to motion.

Hence we call the quantity half Ldot as DR, dynamic resistance.

Dynamic Resistance depends on speed

- **Axial phase:**

  DR_a= Half Ldot= 10^{-7}ln(c)(dz/dt))~7mOhm; for c=b/a=2 and axial speed of 10^5m/s.

  Depends on radius ratio 'c' & end axial speed dz/dt

  (Note 'c' & dz/dt are about the same for small and large plasma focus machines)

  Does not depend on size of plasma focus,

  Hence DR_a is the same for smallest to largest plasma focus machines.

- **Radial phase:**

  DR_r=Half Ldot= 10^{-7}[ln(b/r_p)(dz_f/dt)-(z_f/r_p)(dr_p/dt)]~100 mOhm

  Depends on speeds; also on 'c'

  Does not depend on size of Plasma Focus

It turns out that: Constancy of DR_a causes current saturation leading to neutron saturation:- more of this in Part 2 of talk.

Plasma focus and dynamic resistance

- **Magnetic piston (CS) is driven by the JXB force at highly supersonic speed, driving a shock wave ahead of it.**
- **Shocked plasma layer is thus imparted with kinetic and thermal energy, taking energy from the magnetic field in a dissipative manner.**
- **Amount of energy extracted from the electrical circuit is easily computed by integrating 0.5 (dL/dt) I^2**
- **Essentially, whatever happens to the plasma subsequently e.g. excitation and ionization, radiation, instabilities, plasma streaming, current/plasma disruption, beam acceleration the dynamic resistance powers all these effects, through a chain of mechanism; the first of which is the dynamic resistance DR.**

The role of the current

- Current trace: best indicators of gross performance. Dynamics and energy transfer immediately apparent from the current trace
- Profile of I_{total} is governed by the bank, tube and operational parameters; also depends on f_m and f_c and their variations through the phases.
- There are many underlying mechanisms in the axial & radial phase, not simply modelled (e.g.mass ejection, disruptions, hot spots), which are taken care of by the model parameters.
- The discharge current powers all dynamic, electrodynamic, thermodynamic and radiation processes in the various phases.
- Conversely all processes in the various phases of the focus affect I_{total}.
- The I_{total} waveform contains information on all the processes in the PF.
- Hence the importance of matching the computed Itotal trace to the measured I_{total} in the procedure.
- Once matched, the fitted model parameters assure that the computation proceeds with all physical mechanisms accounted for, at least in the gross energy and mass balance sense.

Significance of I_{total} current fitting

- **f_m: mass swept up factor, axial phase**
  accounts for all effects affecting mass swept up (structure inclination, porosity, boundary layer etc)

- **f_c: plasma current factor, axial phase**
  accounts for all effects affecting current flowing in the plasma (current leakage to backwall, shunting and fragmenting, CS inclination etc), defines the fraction of I_{total} effectively driving the magnetic piston

- **f_{mr}: mass swept up factor, radial phase**
  accounts for all effects affecting mass swept up (structure inclination, porosity, axial mass streaming etc)

- **f_{cr}: plasma current factor, radial phase**
  accounts for all effects affecting current flowing in the plasma (current leakage to backwall, CS bifurcation, current constriction/disruption etc) defines the fraction of I_{total} effectively driving the magnetic piston

We fit the computed I_{total} waveform to the measured because the I_{total} waveform is the one usually measured. Once the I_{total} waveform is fitted by adjusting the 4 model parameters, the I_{plasma} waveform is also implicitly fitted.

From Measured Current Waveform to Modelling for Diagnostics

Procedure to operate the code:

Step 1: Configure the specific plasma focus,

Input:

- **Bank parameters, L_0, C_0 and stray circuit resistance r_0;**
- **Tube parameters b, a and z_0 and**
- **Operational parameters V_0 and P_0 and the fill gas**

Step 2: Fitting the computed current waveform to the measured waveform-(connecting with reality)

- **A measured discharge current I_{total} waveform for the specific plasma focus is required**
- **The code is run successively. At each run the computed I_{total} waveform is fitted to the measured I_{total} waveform by varying model parameters f_m, f_c, f_{mr} and f_{cr} one by one, one step for each run, until computed waveform agrees with measured waveform.**

The 5-Point Fit:

- **First, the axial model factors f_m, f_c are adjusted (fitted) until**
  - **(1) computed rising slope of the I_{total} trace and**
  - **(2) the rounding off of the peak current as well as**
  - **(3) the peak current itself**

  are in reasonable (typically very good) fit with the measured I_{total} trace.
- **Next, adjust (fit) the radial phase model factors f_{mr} and f_{cr} until**
  - **(4) the computed slope and**
  - **(5) the depth of the dip**

  agree with the measured I_{total} waveform.

Fitting computed I_{total} waveform to measured I_{total} waveform: the 5-point fit

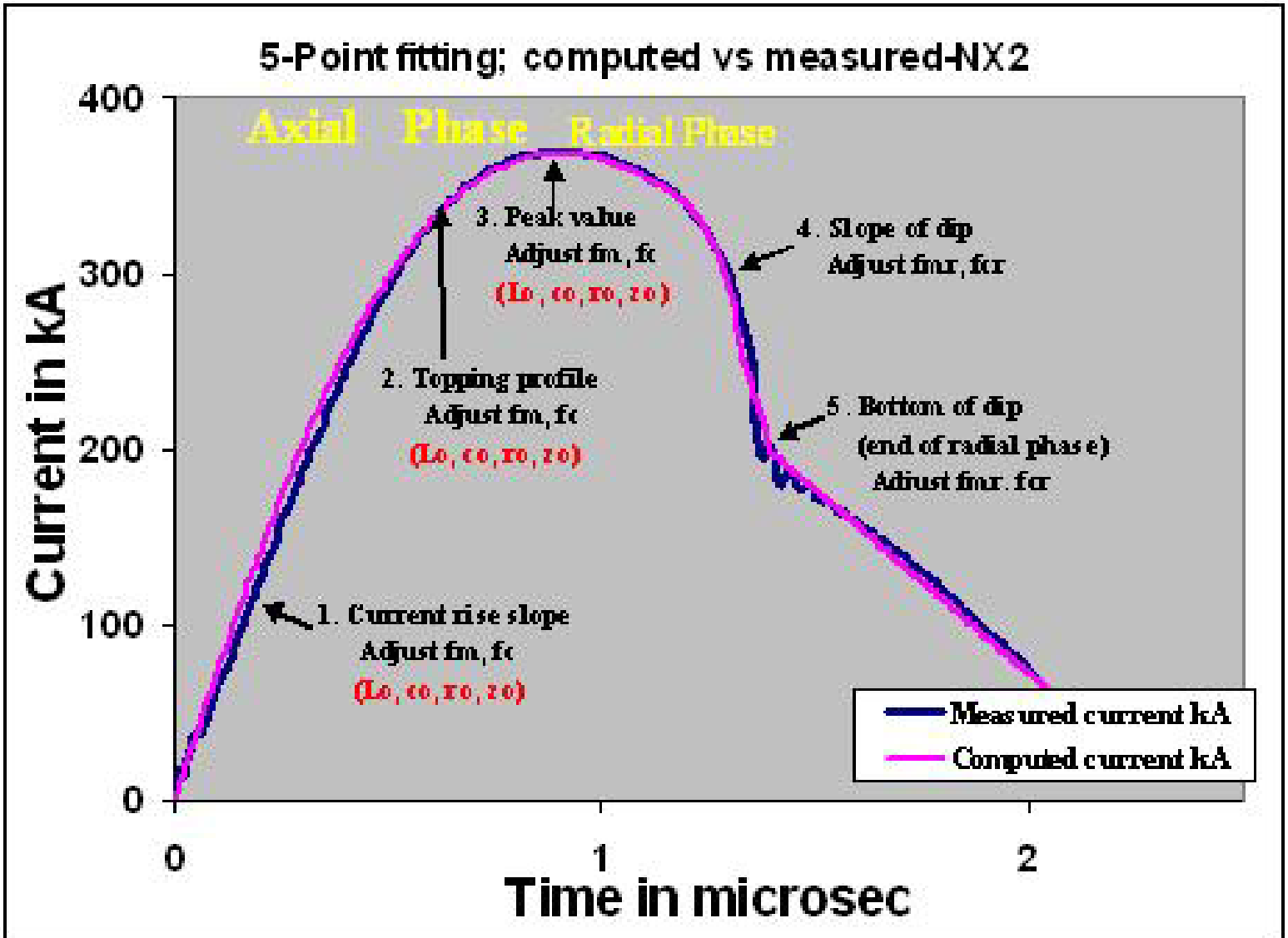

NX2; 11kV: 2.6 Torr neon

- **In this case, after fitting the 5 features (1) to (5) above, the following fitted model parameters are obtained:**

f_m=0.1

f_c=0.7

f_{mr}=0.12

f_{cr}=0.68

Diagnostics-Time histories of dynamics, energies and plasma properties computed by the code

Last adjustment, when the computed I_{total} trace is judged to be reasonably well fitted in all 5 features, computed times histories are presented (NX2 operated at 11 kV, 2.6 Torr neon)

Computed Itotal waveform fitted to measured

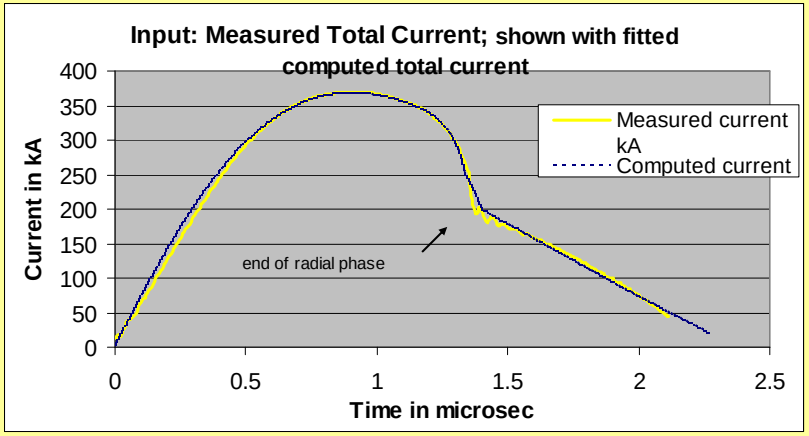

Computed Itotal & Iplasma

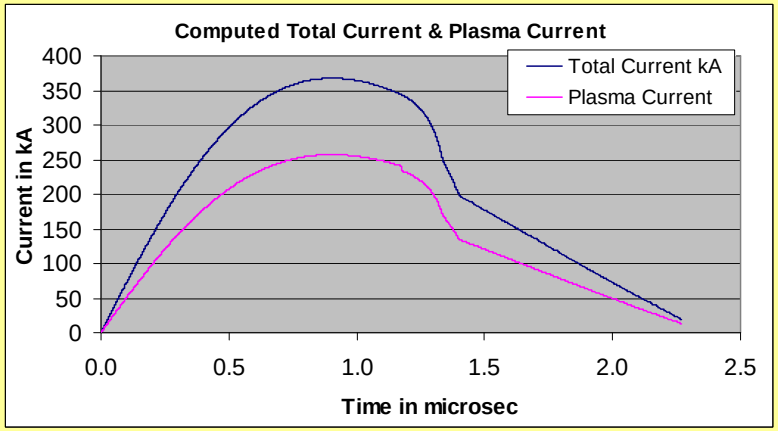

Computed Tube voltage

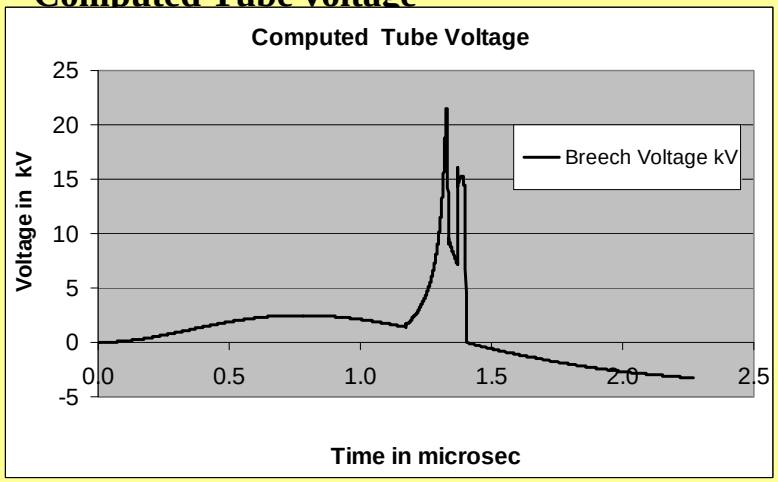

Computed axial trajectory & speed

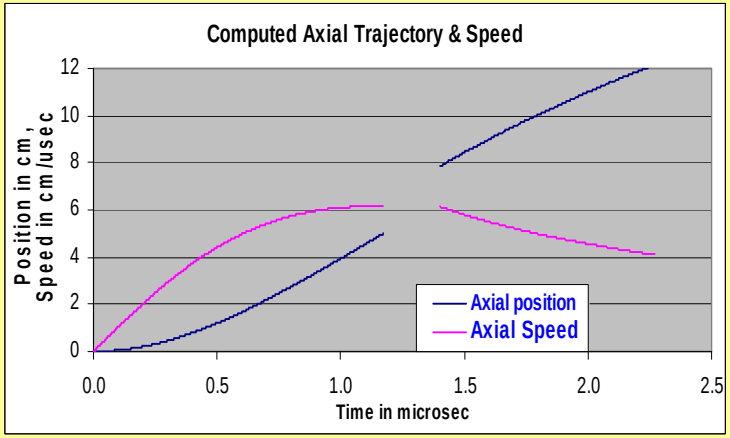

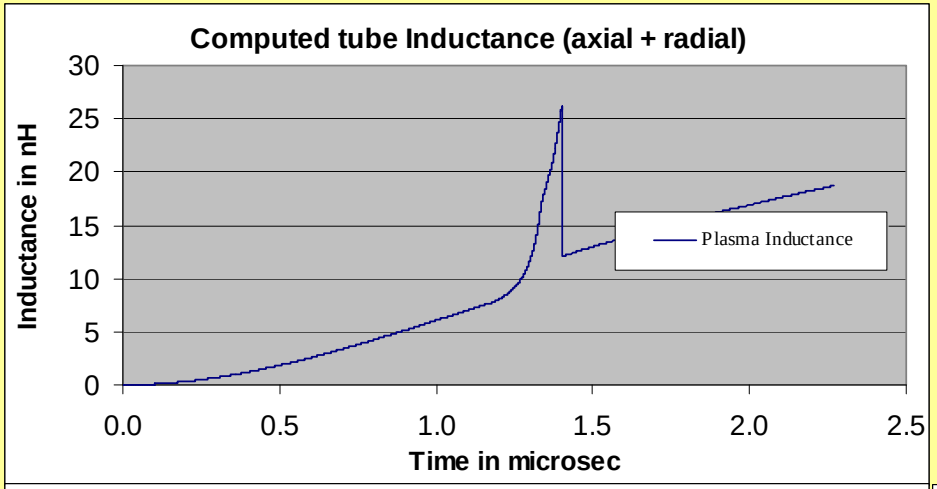
Computed tube Inductance (axial + radial)
Inductance in nH
Time in microsec
Plasma Inductance

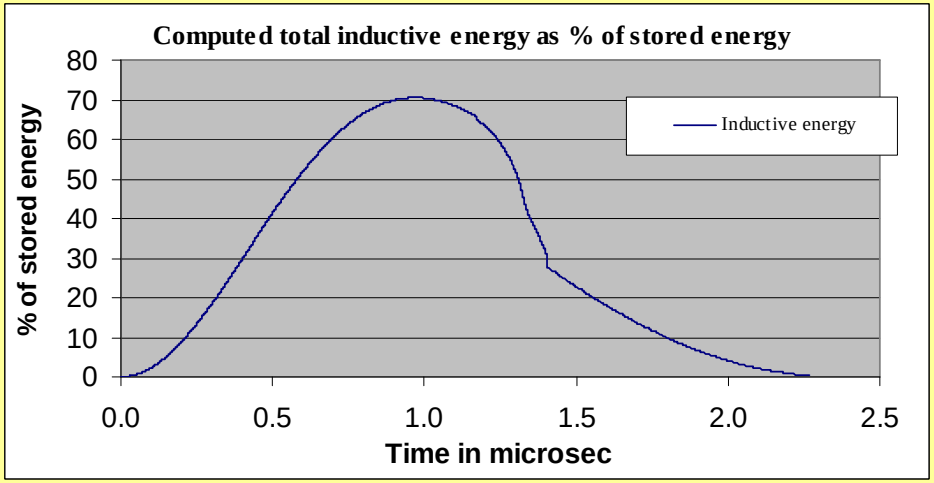
Computed total inductive energy as % of stored energy
% of stored energy
Time in microsec
Inductive energy

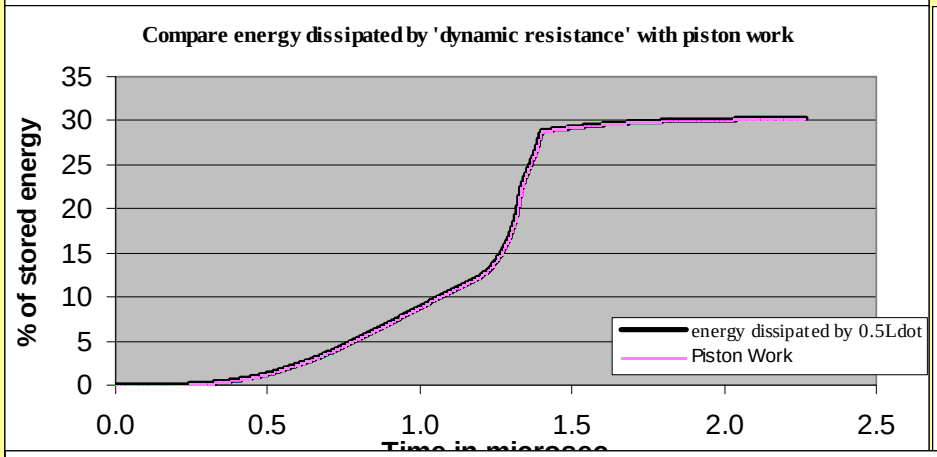
Compare energy dissipated by 'dynamic resistance' with piston work
% of stored energy
energy dissipated by 0.5Ldot
Piston Work

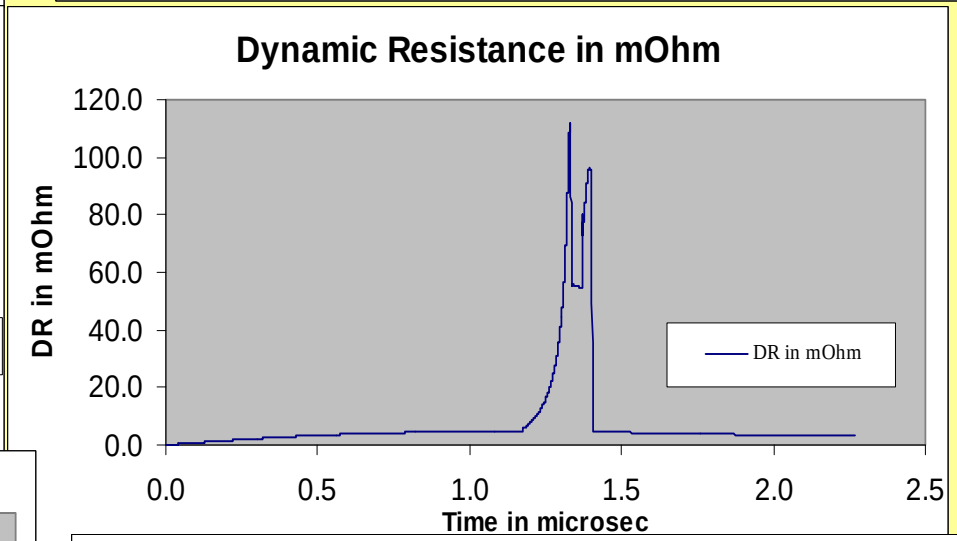
Dynamic Resistance in mOhm
DR in mOhm
Time in microsec
DR in mOhm

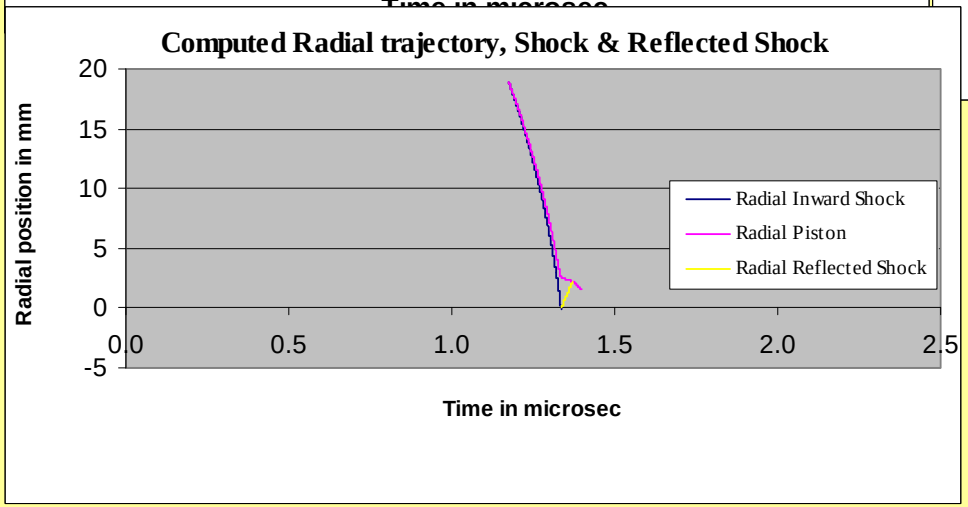
Computed Radial trajectory, Shock & Reflected Shock
Radial position in mm
Time in microsec
Radial Inward Shock
Radial Piston
Radial Reflected Shock

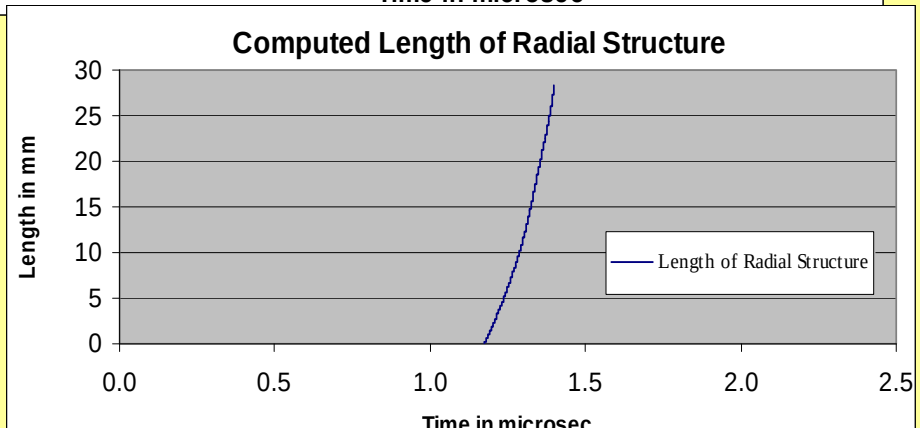
Computed Length of Radial Structure
Length in mm
Time in microsec
Length of Radial Structure

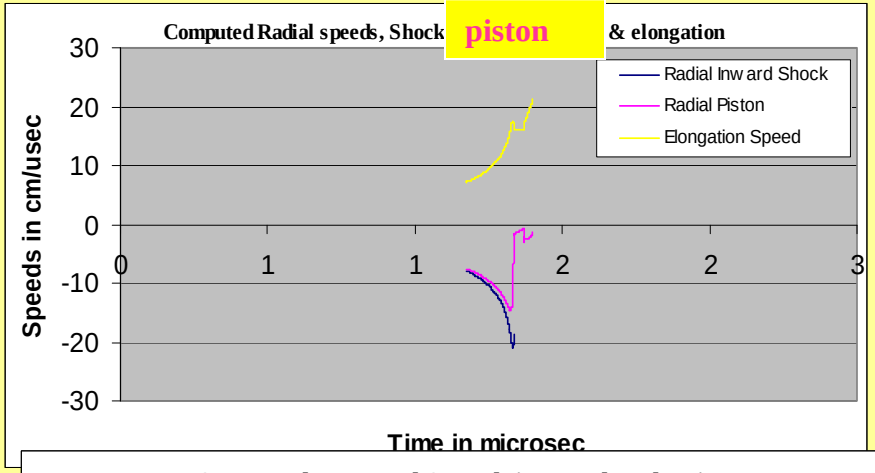
Computed Radial speeds, Shock piston & elongation
Radial Inward Shock
Radial Piston
Elongation Speed
Speeds in cm/usec
Time in microsec

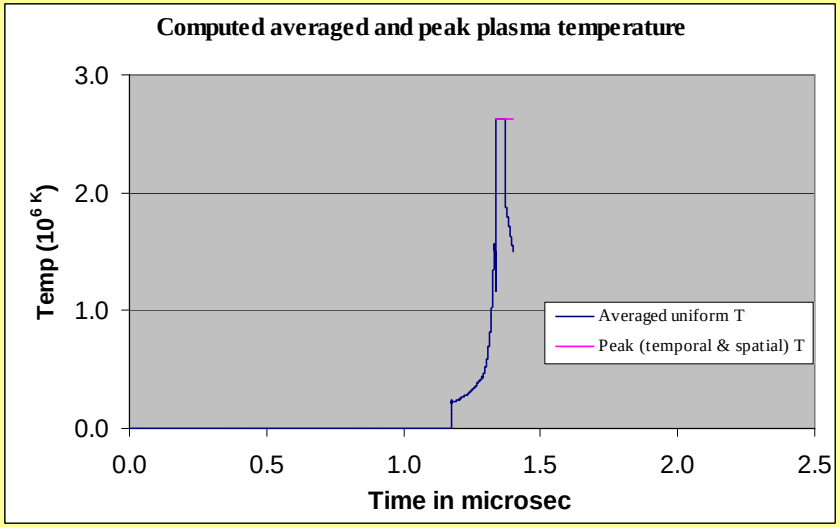
Computed averaged and peak plasma temperature
Averaged uniform T
Peak (temporal & spatial) T
Temp (10^6 K)
Time in microsec

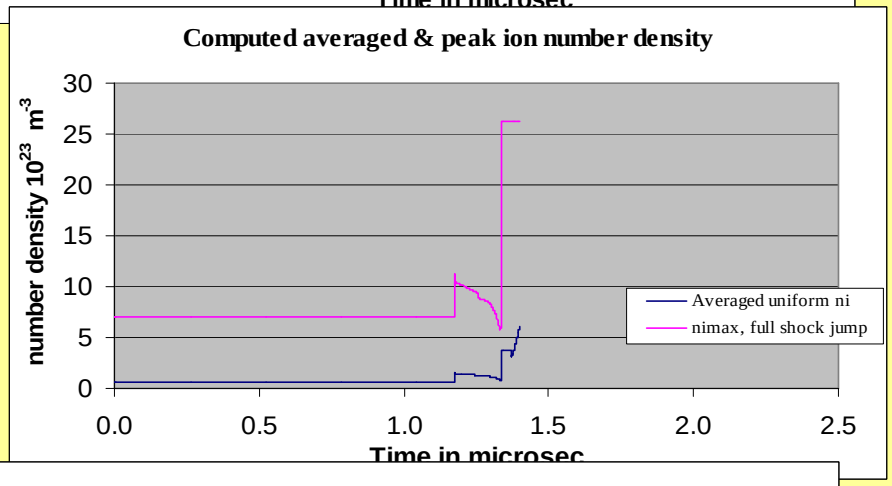
Computed averaged & peak ion number density
Averaged uniform ni
nimax, full shock jump
number density 10^23 m^-3
Time in microsec

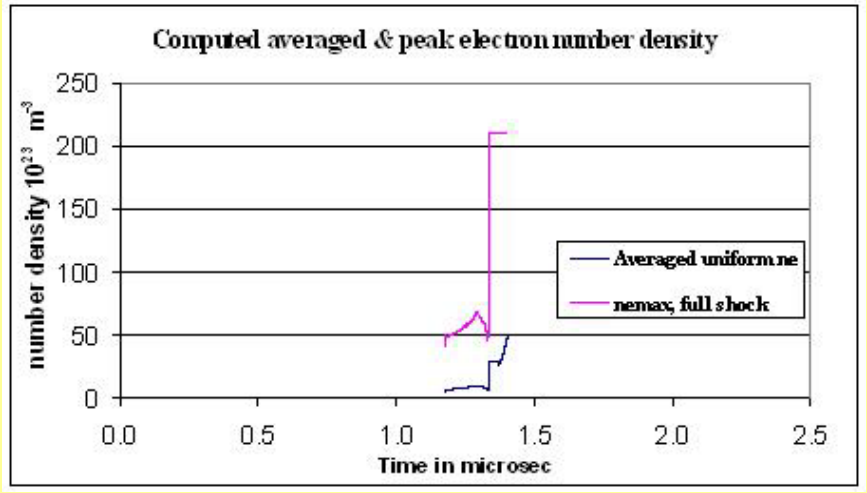
Computed averaged & peak electron number density
Averaged uniform ne
nemax, full shock
number density 10^23 m^-3
Time in microsec

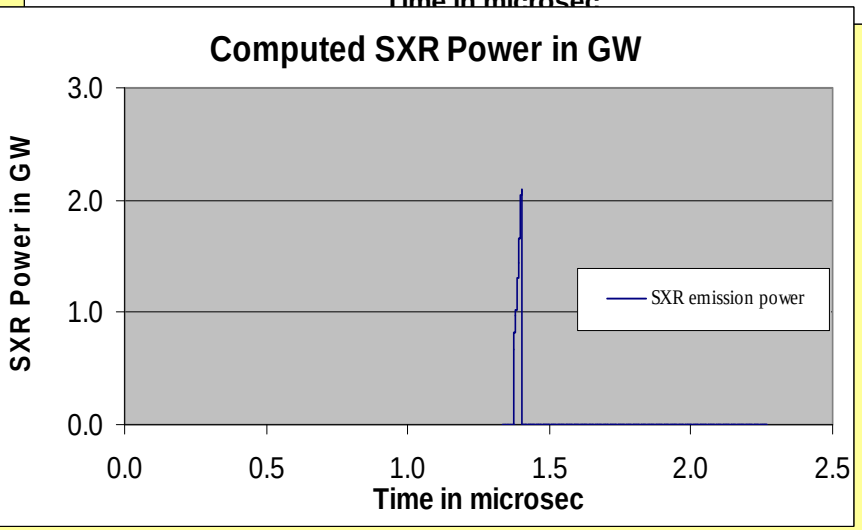
Computed SXR Power in GW
SXR emission power
SXR Power in GW
Time in microsec

Examining the radial phases

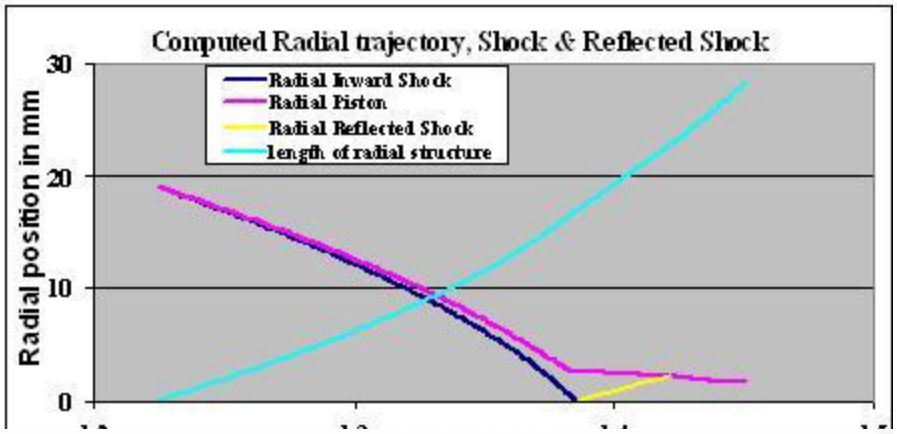

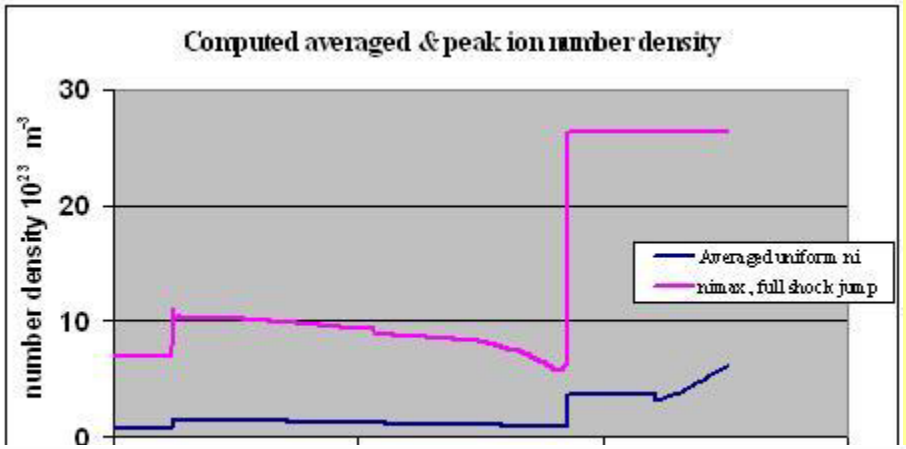

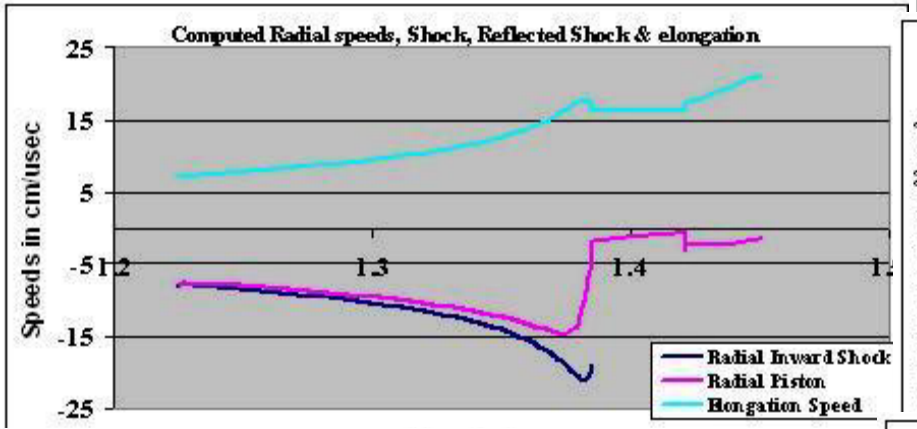

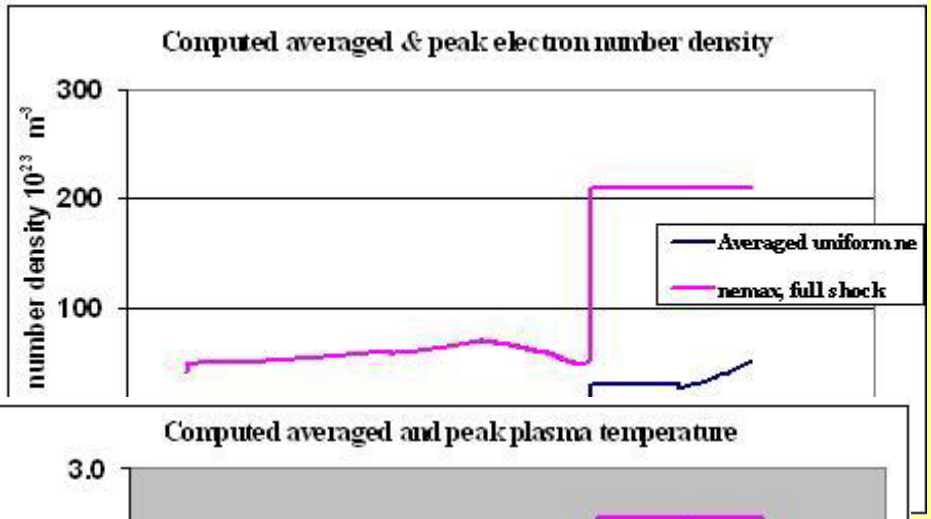

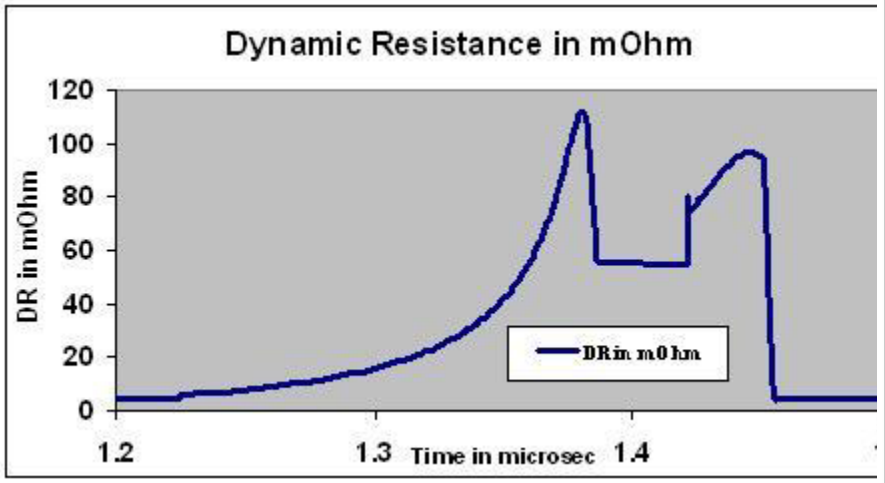

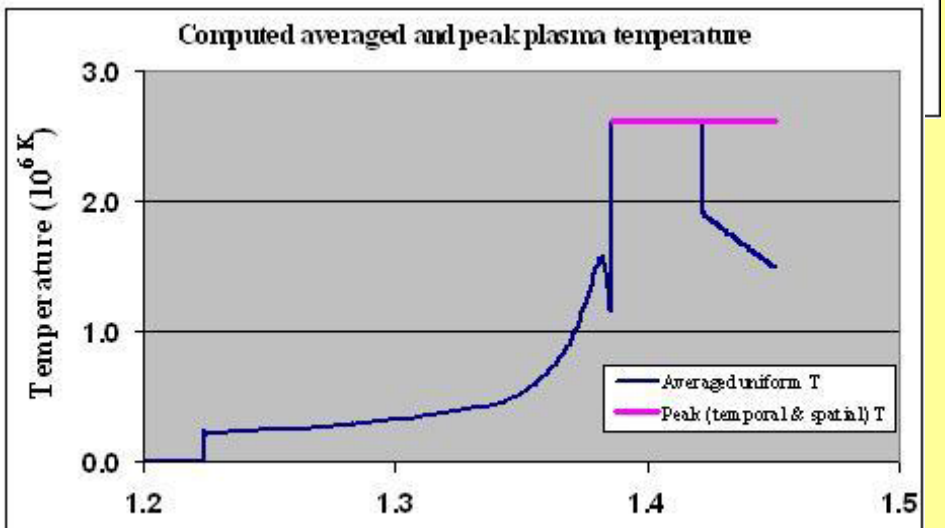

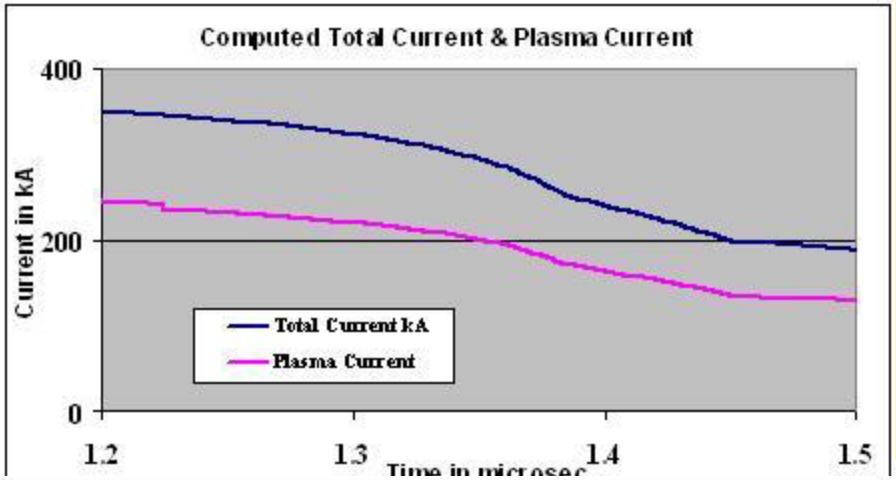
Computed Total Current & Plasma Current
Current in kA
400
200
0
Total Current kA
Plasma Current
1.2
1.3
1.4
1.5
Time in microsec

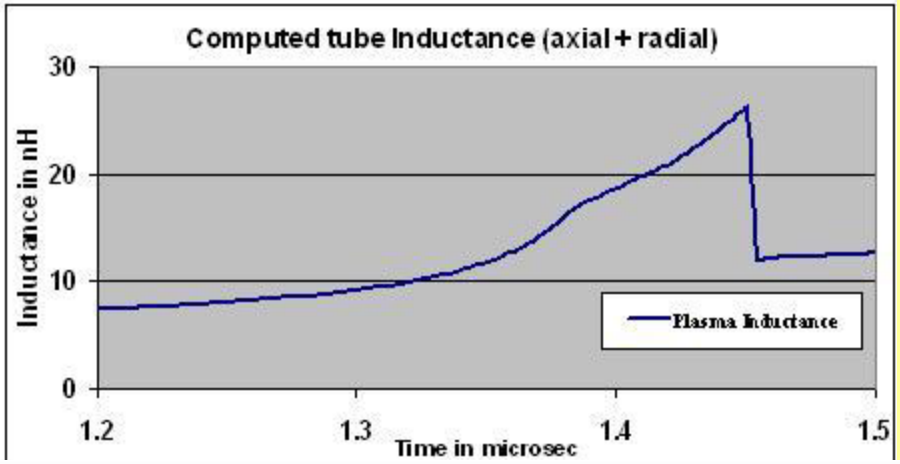
Computed tube Inductance (axial + radial)
Inductance in nH
30
20
10
0
Plasma Inductance
1.2
1.3
1.4
1.5
Time in microsec

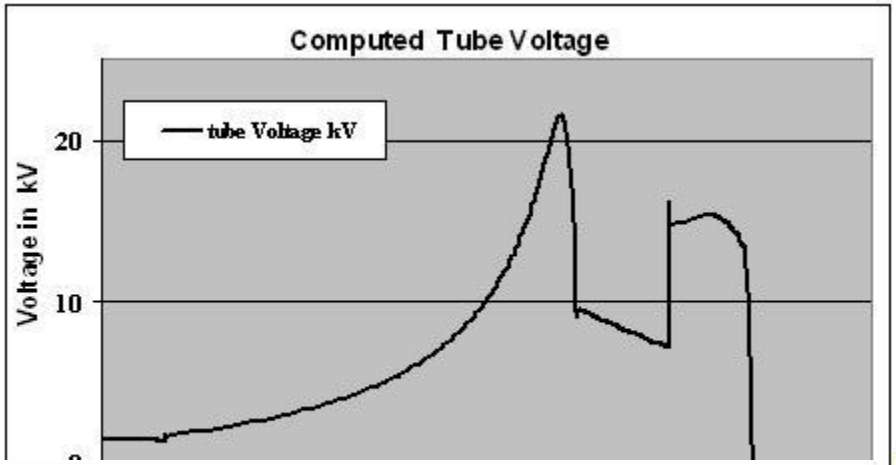
Computed Tube Voltage
Voltage in kV
20
10
tube Voltage kV

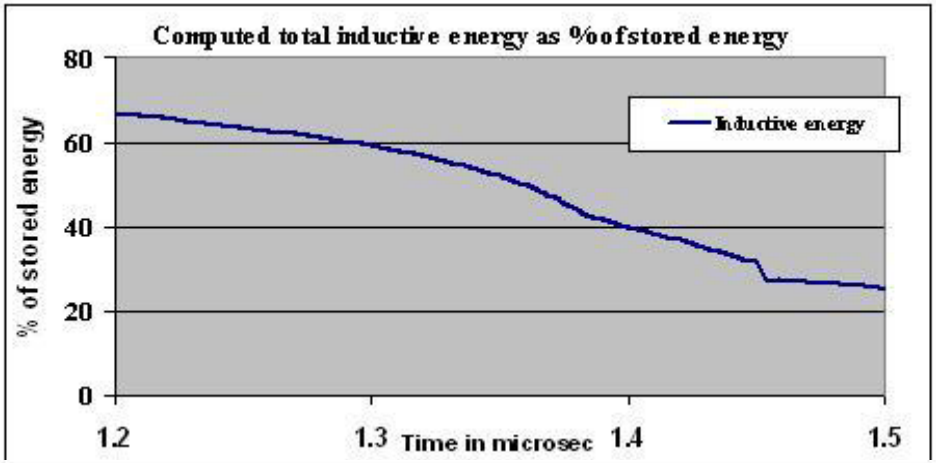
Computed total inductive energy as %of stored energy
% of stored energy
80
60
40
20
0
Inductive energy
1.2
1.3
1.4
1.5
Time in microsec

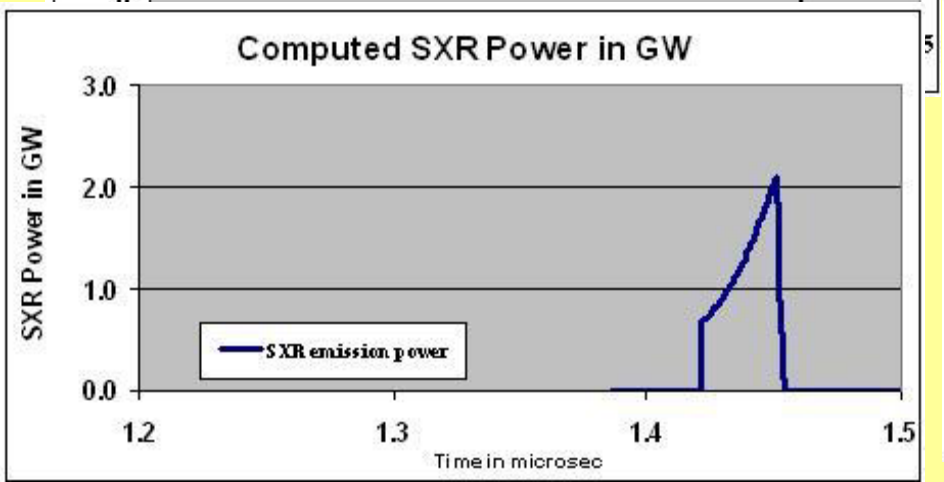
Computed SXR Power in GW
SXR Power in GW
3.0
2.0
1.0
0.0
SXR emission power
1.2
1.3
1.4
1.5
Time in microsec

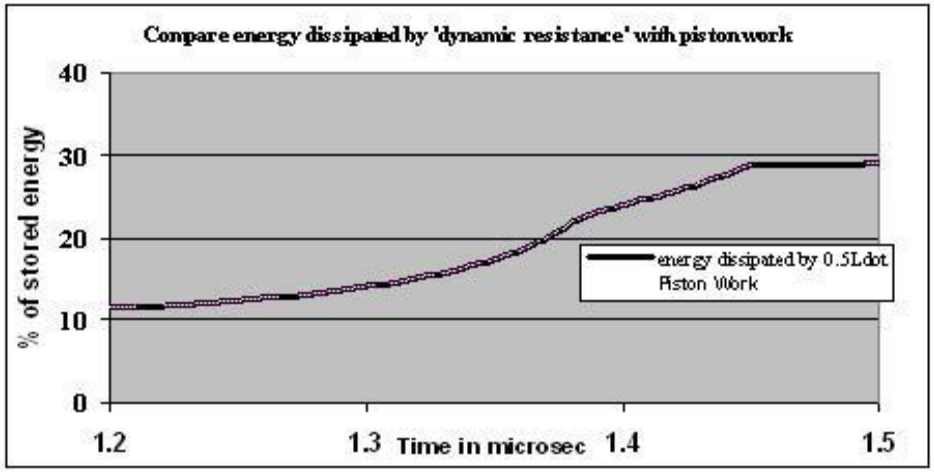
Compare energy dissipated by 'dynamic resistance' with piston work
% of stored energy
40
30
20
10
0
energy dissipated by 0.5Ldot
Piston Work
1.2
1.3
1.4
1.5
Time in microsec

Comments on computed quantities

- Computed I_{total} trace; typically fitted well with the measured.
- I_{plasma} is rarely measured. We had published a comparison of computed I_{plasma} with measured I_{plasma} for the Stuttgart PF78; which shows agreement of computed with measured I_{plasma}.
- Computed tube voltage is generally as expected.
- The computed axial trajectory & speed, agree with typical experimentally obtained time histories. Behaviour with pressure, agrees well with measurements.
- Computed inductance: steady increase, in axial phase, followed by sharp increase in radial phase .
- Inductive energy ($0.5LI^2$) peaks at 70% of E_0, then drops to 30% during the radial phase. Sharp drop of current more than offsets the effect of sharply increased inductance.
- Work done by magnetic piston (integrating force over distance) agrees with work dissipated by dynamic resistance, (integrating dynamic resistance xI^2over time). This validates the concept of half Ldot as a dynamic resistance. Piston work increases steadily to12% at end axial phase, then rises sharply to 30% in the radial phase.
- The value of the DR in the axial phase, together with the bank surge impedance, determine I_{peak}.
- Computed trajectories agree with scant experimental data. Computed speeds of radial shock front & piston; & elongation speed also shown.
- Ion number density: maximum value derived from shock-jump considerations, and averaged uniform value determined from overall energy and mass balance. The electron number density has similar profiles; modified by effective charge numbers due to ionization stages reached by the ions.
- Plasma temperature has a maximum value (derived from shock jump) & an averaged uniform value.
- Computed neon soft x-ray power profile is shown. Area of the curve is the soft x-ray yield in J.
- Pinch dimensions and lifetime: may be estimated from the radial trajectories.
- The model also computes the neutron yield, for operation in deuterium, using a phenomenological beam-target mechanism which has been calibrated at 0.5 MJ.

Desirable characteristics of a Model

- **Accurately descriptive**
- **Relates to reality**
- **Predictive, including extrapolative scaling**
- **Capable of providing insights**

Insight from modelling-Scaling Laws

Numerical experiments using the model have been carried out systematically over wide ranges of energy; optimizing pressure, anode length and radius, to obtain scaling laws:

Neutron yield, Y_n:

- $Y_n = 3.2 \times 10^{11} I_{pinch}^{4.5}$ I_{pinch} in MA (0.2 to 2.4 MA)
- $Y_n = 1.8 \times 10^{10} I_{peak}^{3.8}$ I_{peak} in MA (0.3 to 5.7 MA))
- $Y_n \sim E_0^{2.0}$ at tens of kJ to $Y_n \sim E_0^{0.84}$ at MJ level (up to 25MJ).

For neon soft x-rays:

- $Y_{sxr} = 8.3 \times 10^3 \times I_{pinch}^{3.6}$; I_{pinch} in MA (0.07 to1.3 MA)
- $Y_{sxr} = 600 \times I_{peak}^{3.2}$; I_{peak} in MA (0.1 to 2.4 MA),.
- $Y_{sxr} \sim E_0^{1.6}$ (kJ range) to $Y_{sxr} \sim E_0^{0.8}$ (towards MJ).

Our experience: the laws scaling yield with I_{pinch} are robust and more reliable than the others.

Insight into Neutron saturation

- Recently discussed by M. Scholz among others. Following Scholz we show a chart depicting the deterioration of the neutron scaling as E_0 increases; compared with the expected $Y_n \sim E_0^2$ scaling shown by lower energy experiments. This chart depicts the idea of Y_n saturation. Note that the capacitor banks all operate at several tens of kV and the increase of E_0 is essentially through increase of C_0.

Chart from M Scholz (November 2007 ICDMP)

Scaling

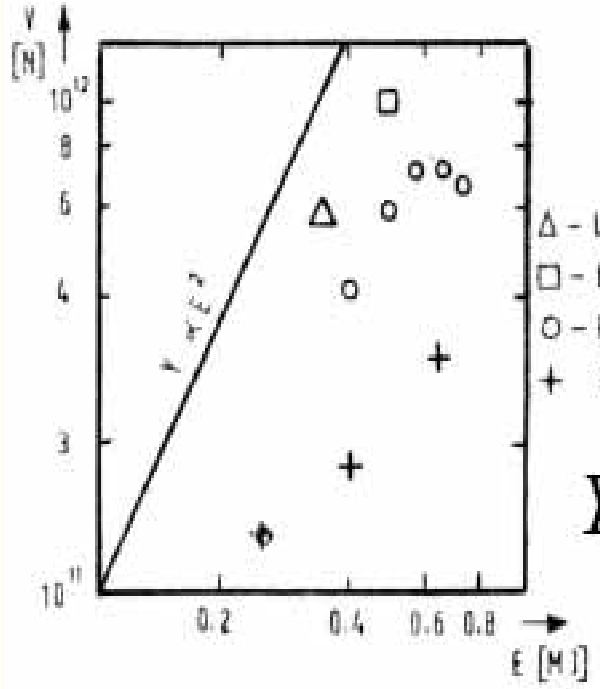

$$\frac{1}{2}(L+L_0)I^2 \cong \gamma E$$

$$L \cong L_0$$

$$Y_n \propto E^2$$

$$I^2 \propto E$$

Frascati (Program Euroatom), $E_b = 1MJ$; $U_b = 50$ kV;

Institute of Plasma Physics and Laser Microfusion
Warsaw, Poland

Illustrating Y_n 'saturation' observed in numerical experiments (small black crosses) compared to measurements on various machines (larger coloured crosses)

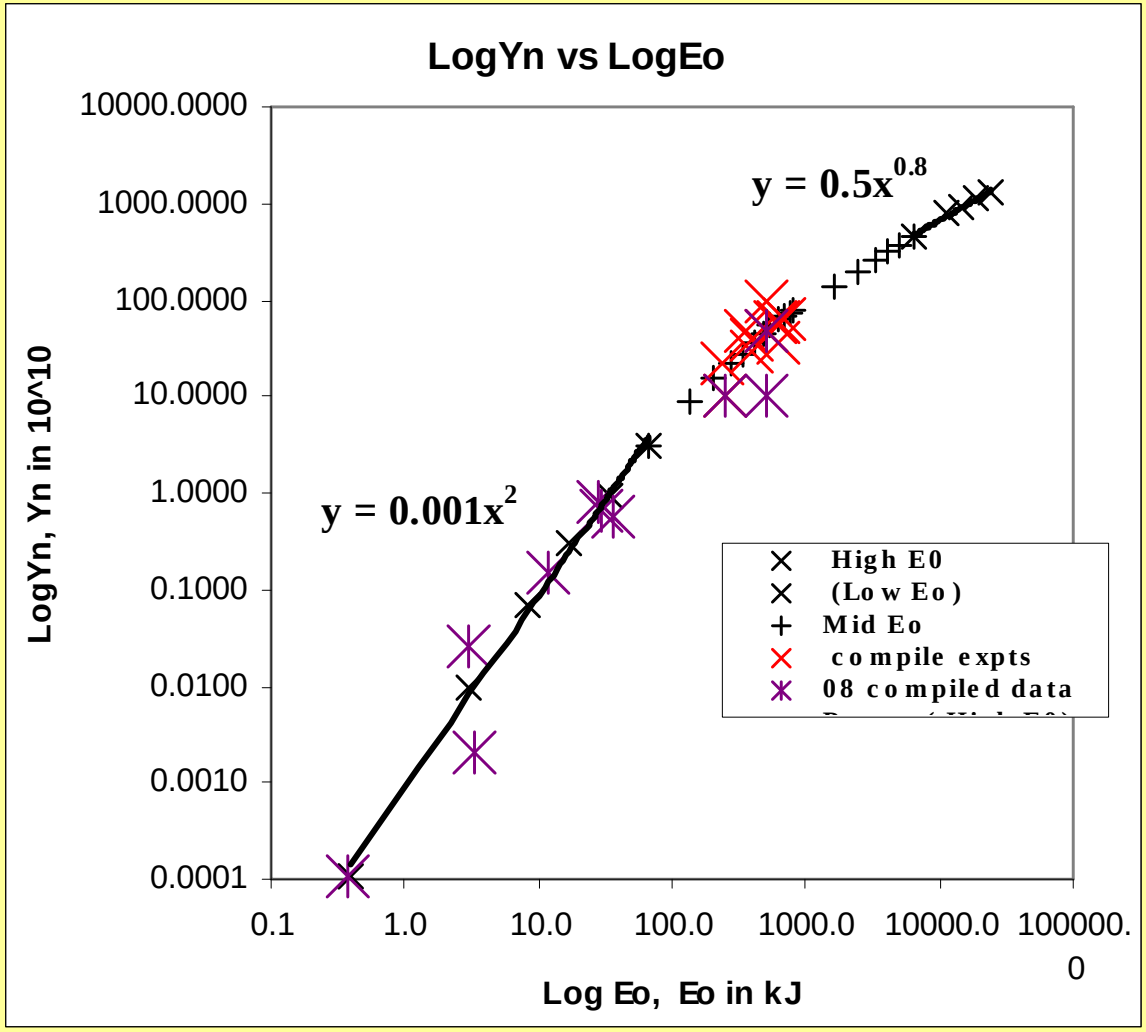

Y_n saturation trend already observed in numerical experiments

- **The deterioration of the Y_n scaling observed in numerical experiments agree generally with the measured data on Y_n yield of large experiments**
- **What is the physical basis of this scaling deterioration?**

Comparing I_{total} for small & large plasma focus

- **Small PF-400J; 0.4kJ 28 kV 6.6 Torr D2**
- **Large PF1000 (0.5 MJ) 27 kV 3.5 Torr D2**

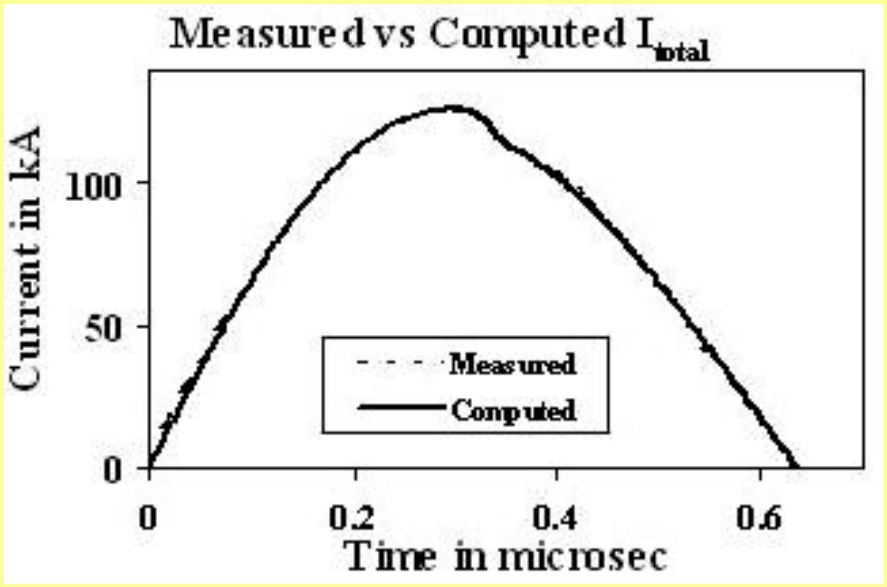

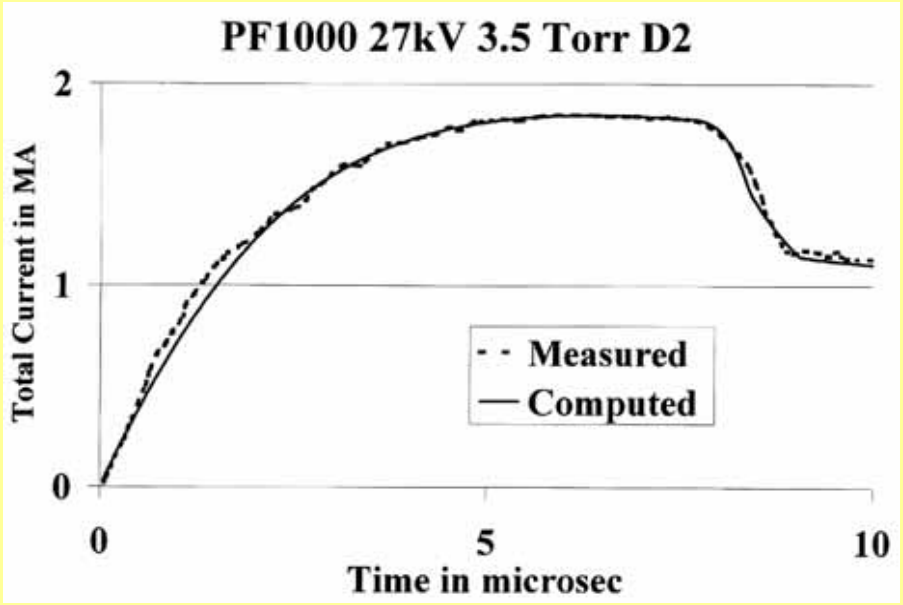

~300ns risetime; ~ 20ns current dip of <5%

End axial speed: 10cm/us

~8 us risetime; ~2 us current dip of 35%

End axial speed: 10cm/us

Comparing generator impedance & Dynamic Resistance of small & large plasma focus- before I_{peak}

PF	$Z_0 = (L_0/C_0)^{1/2}$	Axial DR_0	Axial dominance	I_{peak}
Small	100 mΩ	7 mΩ	Z_0	~ V_0/Z_0
Large	1 mΩ	7 mΩ	DR_0	~V_0/DR_0

As E_0 is increased by increasing C_0, with voltage kept around tens of kV, Z_0 continues to decrease and I_{peak} tends towards asymptotic value of V_0/DR_0

Illustrating the dominance of DR_0 as E_0 increases,

V_0=30kV, L_0=30nH; $Z_{total}=1.1Z_0+DR_0$

E_0	C_0	Z_0	DR_0	Z_{total}	$I_{peak} = V_0/Z_{total}$	I_{peak} from L-C-R	
kJ	uF	mΩ	mΩ	mΩ	kA	kA	
0.45	1	173	7	197	152	156	
4.5	10	55	7	67	447	464	
45	100	17	7	26	1156	1234	
135	300	10	7	18	1676	1819	
450	1000	5.5	7	12.9	2321	2554	
1080	2400	3.5	7	10.8	2781	3070	
4500	10000	1.7	7	8.8	3407	3722	
45000	100000	0.55	7	7.6	4209	4250	

Confirming I_{peak} saturation is due to constancy of DR_0

I_{peak} vs E_0 from DR_0 analysis compared to model simulation

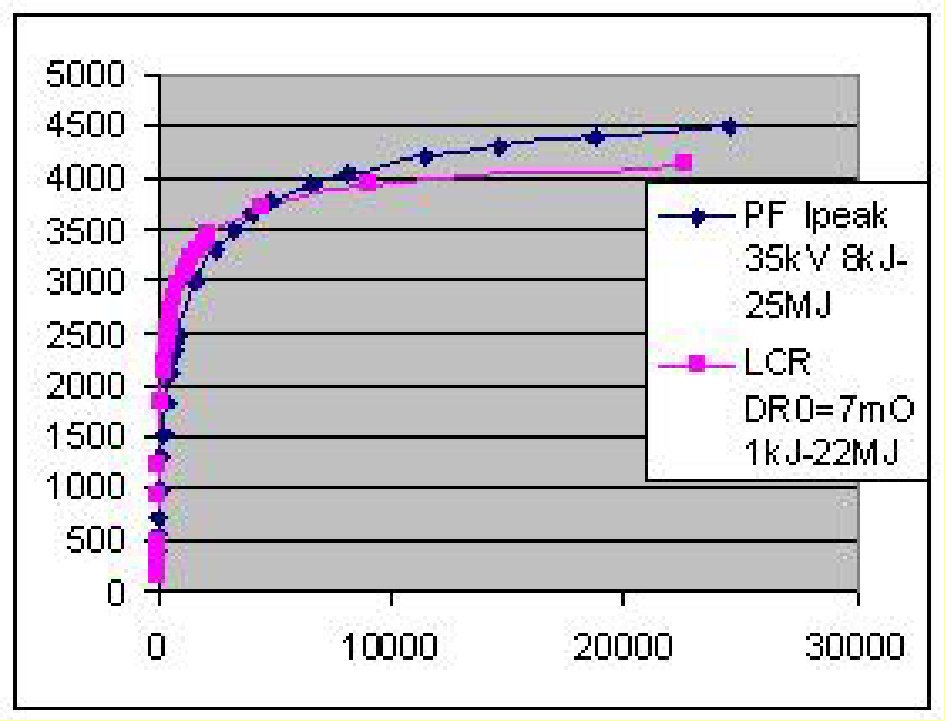

Model simulation gives higher I_{peak} due to a 'current overshoot effect' which lifts the value of I_{peak} before the axial DR_0 fully sets in

I_{peak} vs E_0 on log-log scale DR_0 analysis

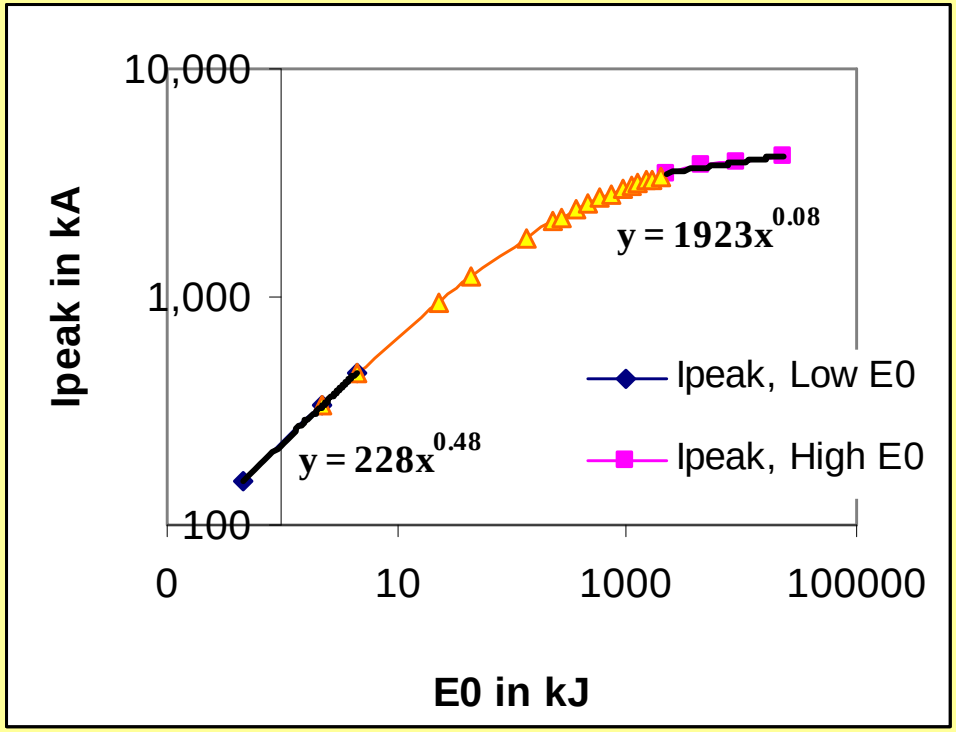

Confirming that I_{peak} scaling tends to saturate before 1 MJ

We have shown that: constancy of DR_0 leads to current 'saturation' as E_0 is increased by increasing C_0. Tendency to saturate occurs before 1 MJ

From both numerical experiments as well as from accumulated laboratory data

- $\mathbf{Y_n \sim I_{pinch}^{4.5}}$
- $\mathbf{Y_n \sim I_{peak}^{3.8}}$

Hence the 'saturation' of I_{peak} leads to saturation of neutron yield Y_n

Insight- neutron saturation

- **A major factor for ‘neutron saturation’ is simply: Axial Phase Dynamic Resistance**

Conclusions and Discussion

Diagnostics and scaling laws

- **Reference points for plasma focus diagnostics are provided by the model, giving realistic time histories of dynamics, energies, plasma properties and Y_{sxr}; also Y_n.**
- **Systematic numerical experiments then provide insight into Y_n and Y_{sxr} scaling laws, as functions of I_{pinch}, I_{peak} and E_0.**
- **These numerical experiments show tendency towards Y_n saturation, in agreement with laboratory experiments**

Conclusions and Discussion

Y_n saturation due to DR_0

- **Insight: Identification of a major factor contributing to Y_n saturation. It is current saturation due to DR_0. Nukulin & Polukhin [2007 paper] had discussed current saturation based on a wrong assumption of z_0 proportional to C_0. If their assumption were correct, reducing z_0 would overcome the current saturation. Unfortunately the causal mechanism is not length z_0, but speed dz/dt, more specifically DR_0.**

- **The same effect is expected to cause the saturation of other current –dependent radiation yields such as Y_{sxr}.**

Conclusions and Discussion

Beyond saturation?

Possible ways to improve Y_n:

- **Increase operating voltage. Eg SPEED II uses Marx technology: 300kV, driver impedance 60 mΩ. With E_0 of under 200 kJ, the system was designed to give I_{peak} of 5 MA and I_{pinch} just over 2 MA.**

- **Extend to 1MV?- would increase I_{peak} to 15 MA and I_{pinch} to 6 MA. Or multiple Blumleins at 1 MV, in parallel, could provide driver impedance matching radial phase DR, resulting in fast rise I_{peak} of 10 MA with 5 MA I_{pinch}. [at several MJ]**

- **Y_n enhancing methods such as doping deuterium with low % of krypton.**

- **Further increase in I_{pinch} by fast current-injection near the start of radial phase. This could be achieved with charged particle beams or by circuit manipulation such as current-stepping. This model is ideally suited for testing circuit manipulation schemes.**

We have discussed the following:

- **Diagnostics from modelling**
- **Insights from modelling:**
  - **Scaling laws for radiation & neutrons**
  - **Identifying the major factor causing neutron saturation in plasma focus**
  - **Suggest beyond saturation possibilities**

Thank You

Acknowledge contributions of S H Saw, Paul Lee, Rajdeep S Rawat, Liu Mahe, Mohamad Akel, Verma Rishi, H Schmidt, S P Moo, Leopoldo Soto, S V Springham & Sharif Al-Hawat to parts of this talk

This Keynote address is mainly based on the following 2008-2009 IPFS Papers :

- **S. Lee and S. H. Saw** — **Appl. Phys. Lett. 92 021503 (2008)**
- **S Lee and S H Saw** — **J of Fusion Energy 27 292-295 (2008)**
- **S Lee, P Lee, S H Saw and R S Rawat** — **Plasma Phys. Control. Fusion 50 (2008) 065012**
- **S. Lee, S. H. Saw, P. C. K. Lee, R. S. Rawat and H. Schmidt** — **Appl Phys Letters 92 111501 (2008)**
- **S Lee** — **Plasma Phys. Control. Fusion 50 (2008) 105005**
- **S Lee and S H Saw** — **Appl. Phys. Lett. 94 076102 (2009)**
- **S Lee, S H Saw, L Soto, S V Springham and S P Moo** — **Plasma Phys. Control. Fusion 51 (2009) 075006**
- **M. Akel, Sh. Al- Hawat and S Lee** — **J Fusion Energy (2009) Online First May 19 2009 DOI 10.1007/s10894-009-9203-4**
- **S H Saw, P C K Lee, R S Rawat and S Lee** — **IEEE Trans Plasma Sci (2009) In Press**
  Optimizing UNU/ICTP PFF Plasma Focus for Neon Soft X-ray Operation
- **S. Lee, R. S. Rawat, P. Lee and S. H. Saw** — **J Appl Phys (2009) In Press**
  Soft x-ray yield from NX2 plasma focus

S Lee, S H Saw, P Lee and R S Rawat — **Submitted to Plasma Phys. Control. Fusion (2009)**
Numerical experiments on plasma focus neon soft x-ray scaling

- **M Akel, S Hawat, S Lee** — **J Phys D: Appl Phys. (2009) In Press**
  Pinch Current and Soft x-ray yield limitation by numerical experiments on Nitrogen Plasma Focus

Thank you

IWPDA 2009, July 2, NIE Singapore

Appendix: Dynamic Resistance

Consider instantaneous power P delivered to L(t) by a change in L(t)

Induced voltage: $V=d(LI)/dt= I(dL/dt)+L(dI/dt)$

Hence instantaneous power into L(t): $P=VI= I^2(dL/dt)+LI(dI/dt)$

Consider instantanteous power associated with the inductive energy

$$P_L=d(\tfrac{1}{2}LI^2)/dt= (\tfrac{1}{2}I^2(dL/dt)+LI(dI/dt)$$

Note: P_L not the same as P

Difference=P- P_L = $(\tfrac{1}{2})(dL/dt)I^2$ is not associated with the inductive energy

Conclusion: Whenever L(t) changes with time, the instantaneous power delivered to L(t) has a component that is not inductive

- **This power component $(\tfrac{1}{2})(dL/dt)I^2$ is resistive in nature**
- **Thus identifying $(\tfrac{1}{2})(dL/dt)$ as a resistance due to the motion associated with dL/dt ; which we call the Dynamic Resistance** back 1

Scaling laws for plasma focus machines from numerical experiments

S H Saw[1,3] and S Lee[1,2,3]

[1]*INTI University College, 71800 Nilai, Malaysia*
[2]*NSSE, National Institute of Education, Nanyang Technological University, Singapore 637616*
[3]*Institute for Plasma Focus Studies, 32 Oakpark Drive, Chadstone, VIC3148, Australia*

Abstract

Numerical experiments carried out systematically using the Lee Model code unveil insightful and practical scaling laws for plasma focus machines. The experiments cover a range of plasma focus machines and over a range of storage energies. An essential feature and necessary first step of the numerical experiments involves the fitting of a measured current waveform to the numerical current waveform to correctly calibrate the model for the particular plasma focus machine. This crucial process provides a reliable and rigorous method to determine the ever so important pinch current. The thermodynamics and radiation properties of the resulting plasma are then reliably determined. This paper provides an overview of the recently published scaling laws for neutrons and neon SXR yield for plasma focus machines.

For neutron yield:

$Y_n = 3.2\text{x}10^{11} I_{pinch}^{4.5}$; $Y_n = 1.8\text{x}10^{10} I_{peak}^{3.8}$; I_{peak} (0.3 to 5.7), I_{pinch} (0.2 to 2.4) in MA.
$Y_n \sim E_0^{2.0}$ at tens of kJ to $Y_n \sim E_0^{0.84}$ at MJ level (up to 25MJ).

For neon soft x-rays:

$Y_{sxr} = 8.3\text{x}10^3 I_{pinch}^{3.6}$; $Y_{sxr} = 6\text{x}10^2 I_{peak}^{3.2}$; I_{peak} (0.1 to 2.4), I_{pinch} (0.07 to1.3) in MA.
$Y_{sxr} \sim E_0^{1.6}$ (kJ range) to $Y_{sxr} \sim E_0^{0.8}$ (towards MJ).

1. Introduction

Plasma focus machines of various energies are increasingly being studied as sources of neutrons and soft x-rays. Even a simple machine such as the UNU ICTP PFF 3 kJ machine consistently produces 10^8 neutrons when operated in deuterium [1]. Plasma focus machines operated in neon have also been studied as intense sources of soft x-rays with potential applications [2]-[4]. Whilst many recent experiments have concentrated efforts on low energy devices[2]-[4] with a view of operating these as repetitively pulsed sources, other experiments have looked at x-ray pulses from larger plasma focus devices [5], [6] extending to the MJ regime. Numerical experiments simulating x-ray pulses from plasma focus devices are also gaining more interest in the public domain. For example, the Institute of Plasma Focus Studies [7] conducted a recent international Internet Workshop on Plasma Focus Numerical Experiments [8], at which it was demonstrated that the Lee model code [9] not only computes realistic focus pinch parameters, but also absolute values of soft x-ray yield Y_{sxr} which are consistent with those measured experimentally. A comparison was made for the case of the NX2 machine [4], showing good agreement between computed and measured Y_{sxr} as a function of P_0 [8], [10]. This gives confidence that the Lee model code gives realistic results in the computation of Y_{sxr}.

In this paper, we show the comprehensive range of numerical experiments conducted to derive scaling laws on neutron yield Y_n [11], [12] and neon Y_{sxr}, in terms of E_0, peak discharge current I_{peak} and peak focus pinch current I_{pinch} obtained from studies carried out over bank energies varying from 0.2 kJ to 25 MJ for optimised machine parameters and operating parameters. It is worth mentioning that the scaling laws in terms I_{pinch} and I_{peak} have also been obtained for numerical experiments using the Lee model code fitted with the actual machine parameters and operating parameters and the difference from that obtained for the optimised conditions are within the order of 0.1 in the scaling laws power factor for neutrons and no **difference** for neon SXR yield.

We also wish to point out that the distinction of I_{pinch} from I_{peak} is of basic importance [13]-[15]. The scaling with I_{pinch} is the more fundamental and robust one; since obviously there are situations (no pinching or poor pinching however optimized) where I_{peak} may be large but Y_n is zero or small; whereas the scaling with I_{pinch} is

certainly more consistent with all situations. In these works the primary importance of I_{pinch} for scaling plasma focus properties including neutron yield Y_n, has been firmly established [11]-[15].

2. The Lee Model Code

The Lee model code couples the electrical circuit with plasma focus dynamics, thermodynamics and radiation, enabling realistic simulation of all gross focus properties. The basic model, described in 1984 [16] was successfully used to assist several projects [17]-[19]. Radiation-coupled dynamics was included in the five-phase code leading to numerical experiments on radiation cooling [20]. The vital role of a finite small disturbance speed discussed by Potter in a Z-pinch situation [21] was incorporated together with real gas thermodynamics and radiation-yield terms. Before this 'communication delay effect' was incorporated, the model consistently over-estimated the radial speeds. This is serious from the point of view of neutron yields. A factor of two in shock speeds gives a factor of four in temperatures leading to a difference in fusion cross-sections of ~1000 at the range of temperatures we are dealing with. This version of the code assisted other research projects [22]-[27] and was web-published in 2000 [28] and 2005 [29]. Plasma self-absorption was included in 2007 [27] improving SXR yield simulation. The code has been used extensively in several machines including UNU/ICTP PFF [1], [17], [22], [23], [25]-[27], [30], [31], NX2 [24], [27], [32], NX1 [3], [32] and adapted for the Filippov-type plasma focus DENA [33]. A recent development is the inclusion of the neutron yield Y_{n} using a beam–target mechanism [11], [12], [14], [15], [34], incorporated in recent versions [9] of the code (versions later than RADPFV5.13), resulting in realistic Y_{n} scaling with I_{pinch} [11], [12]. The versatility and utility of the model is demonstrated in its clear distinction of I_{pinch} from I_{peak} [13] and the recent uncovering of a plasma focus pinch current limitation effect [14], [15]. The description, theory, code and a broad range of results of this 'Universal Plasma Focus Laboratory Facility' is available for download from [9].

A brief description of the code is given below. The five phases are summarised as follows:

1) Axial Phase: Described by a snowplow model with an equation of motion coupled to a circuit equation. The equation of motion incorporates the axial phase model parameters: mass and current factors f_m and f_c respectively. The mass swept-up factor f_m accounts for not only the porosity of the current sheet but also for the inclination of the moving current sheet–shock front structure and all other unspecified effects which have effects equivalent to increasing or reducing the amount of mass in the moving structure– during the axial phase. The current factor f_c accounts for the fraction of current effectively flowing in the moving structure (due to all effects such as current shedding at or near the back-wall and current sheet inclination). This defines the fraction of current effectively driving the structure during the axial phase.

2) Radial Inward Shock Phase: Described by four coupled equations using an elongating slug model. The first equation computes the radial inward shock speed from the driving magnetic pressure. The second equation computes the axial elongation speed of the column. The third equation computes the speed of the current sheath, also called the magnetic piston, allowing the current sheath to separate from the shock front by applying an adiabatic approximation. The fourth is the circuit equation. Thermodynamic effects due to ionization and excitation are incorporated into these equations, these effects being important for gases other than hydrogen and deuterium. Temperature and number densities are computed during this phase. A communication delay between shock front and current sheath due to the finite small disturbance speed is crucially implemented in this phase. The model parameters, radial phase mass swept-up and current factors f_{mr} and f_{cr} are incorporated in all three radial phases. The mass swept-up factor f_{mr} accounts for all mechanisms which have effects equivalent to increasing or reducing the amount of mass in the moving slug during the radial phase. The current factor f_{cr} accounts for the fraction of current effectively flowing in the moving piston forming the back of the slug (due to all effects). This defines the fraction of current effectively driving the radial slug.

3) Radial Reflected Shock (RS) Phase: When the shock front hits the axis, because the focus plasma is collisional, a reflected shock develops which moves radially outwards, whilst the radial current sheath piston continues to move inwards. Four coupled equations are also used to describe this phase, these being for the reflected shock moving radially outwards, the piston moving radially inwards, the elongation of the annular column and the circuit. The same model parameters f_{mr} and f_{cr} are used as in the previous radial phase. The plasma temperature behind the RS undergoes a jump by a factor nearly two.

4) Slow Compression (Quiescent) or Pinch Phase: When the out-going reflected shock hits the in-going piston the compression enters a radiative phase in which for gases such as neon, radiation emission may actually enhance the compression, where we have included energy loss/gain terms from Joule heating and radiation losses into the piston equation of motion. Three coupled equations describe this phase; these being the piston radial motion equation, the pinch column elongation equation and the circuit equation, incorporating the same model parameters as in the previous two phases. Thermodynamic effects are incorporated into this phase. The duration of this slow compression phase is set as the time of transit of small disturbances across the pinched plasma column. The computation of this phase is terminated at the end of this duration.

5) Expanded Column Phase: To simulate the current trace beyond this point, we allow the column to suddenly attain the radius of the anode, and use the expanded column inductance for further integration. In this final phase the snowplow model is used, and two coupled equations are used; similar to the axial phase above. This phase is not considered important as it occurs after the focus pinch.

a. Computation of Neutron yield

The neutron yield is computed using a phenomenological beam-target neutron generating mechanism described recently by Gribkov et al [34] and adapted to yield the following equation. A beam of fast deuteron ions is produced by diode action in a thin layer close to the anode, with plasma disruptions generating the necessary high voltages. The beam interacts with the hot dense plasma of the focus pinch column to produce the fusion neutrons. The beam-target yield is derived [11], [12], [14],[28] as:

$$Y_{b\text{-}t} = C_n \, n_i \, I_{pinch}^{\,2} z_p^{\,2} (\ln (b/r_p)) \sigma / U^{0.5} \tag{1}$$

where n_i is the ion density, b is the cathode radius, r_p is the radius of the plasma pinch with length z_p, σ the cross-section of the D-D fusion reaction, n- branch [35] and U, the beam energy. C_n is treated as a calibration constant combining various constants in the derivation process.

The D-D cross-section is sensitive to the beam energy in the range 15-150 kV; so it is necessary to use the appropriate range of beam energy to compute σ. The code computes induced voltages (due to current motion inductive effects) V_{max} of the order of only 15-50 kV. However it is known, from experiments that the ion energy responsible for the beam-target neutrons is in the range 50-150 keV [34], and for smaller lower-voltage machines the relevant energy could be lower at 30-60 keV [31]. Thus in line with experimental observations the D-D cross section σ is reasonably obtained by using $U = 3V_{max}$. This fit was tested by using U equal to various multiples of V_{max}. A reasonably good fit of the computed neutron yields to the measured published neutron yields at energy levels from sub-kJ to near MJ was obtained when the multiple of 3 was used; with poor agreement for most of the data points when for example a multiple of 1 or 2 or 4 or 5 was used. The model uses a value of C_n=2.7x10^7 obtained by calibrating the yield [9], [13]-[14] at an experimental point of 0.5 MA.

The thermonuclear component is also computed in every case and it is found that this component is negligible when compared with the beam-target component.

b. Computation of Neon SXR yield

We note that the transition from Phase 4 to Phase 5 is observed in laboratory measurements to occur in an extremely short time with plasma/current disruptions resulting in localized regions of high densities and temperatures. These localized regions are not modelled in the code, which consequently computes only an average uniform density, and an average uniform temperature which are considerably lower than measured peak density and temperature. However, because the 4 model parameters are obtained by fitting the computed total current waveform to the measured total current waveform, the model incorporates the energy and mass balances equivalent, at least in the gross sense, to all the processes which are not even specifically modelled. Hence the computed gross features such as speeds and trajectories and integrated soft x-ray yields have been extensively tested in numerical experiments for several machines and are found to be comparable with measured values.

In the code[9], neon line radiation Q_L is calculated as follows:

$$\frac{dQ_L}{dt} = -4.6x10^{-31} n_i^{\,2} Z Z_n^4 \left(\pi r_p^2\right) z_f / T \tag{2}$$

where for the temperatures of interest in our experiments we take the SXR yield $Y_{sxr} = Q_L$. Z_n is the atomic number.

Hence the SXR energy generated within the plasma pinch depends on the properties: number density n_i, effective charge number Z, pinch radius r_p, pinch length z_f and temperature T. It also depends on the pinch duration since in our code the Q_L is obtained by integrating over the pinch duration.

This generated energy is then reduced by the plasma self-absorption which depends primarily on density and temperature; the reduced quantity of energy is then emitted as the SXR yield. These effects are included in the modelling by computing volumetric plasma self-absorption factor A derived from the photonic excitation number M which is a function of Z_n, n_i, Z and T. However, in our range of operation, the numerical experiments show that the self absorption is not significant. It was first pointed out by Liu Mahe [23] that a temperature around 300 eV is optimum for SXR production. Shan Bing's subsequent work [24] and our experience through numerical experiments suggest that around 2×10^6 K (below 200 eV) or even a little lower could be better. Hence unlike the case of neutron scaling, for SXR scaling there is an optimum small range of temperatures (T windows) to operate.

3. Numerical Experiments

The Lee code is configured to work as any plasma focus by inputting the bank parameters, L_0, C_0 and stray circuit resistance r_0; the tube parameters b, a and z_0 and operational parameters V_0 and P_0 and the fill gas. The standard practice is to fit the computed total current waveform to an experimentally measured total current waveform[11], [13]-[15], [28]-[29] using the four model parameters representing the mass swept-up factor f_m, the plasma current factor f_c for the axial phase and factors f_{mr} and f_{cr} for the radial phases.

From experience it is known that the current trace of the focus is one of the best indicators of gross performance. The axial and radial phase dynamics and the crucial energy transfer into the focus pinch are among the important information that is quickly apparent from the current trace.

The exact time profile of the total current trace is governed by the bank parameters, by the focus tube geometry and the operational parameters. It also depends on the fraction of mass swept-up and the fraction of sheath current and the variation of these fractions through the axial and radial phases. These parameters determine the axial and radial dynamics, specifically the axial and radial speeds which in turn affect the profile and magnitudes of the discharge current. The detailed profile of the discharge current during the pinch phase also reflects the Joule heating and radiative yields. At the end of the pinch phase the total current profile also reflects the sudden transition of the current flow from a constricted pinch to a large column flow. Thus the discharge current powers all dynamic, electrodynamic, thermodynamic and radiation processes in the various phases of the plasma focus. Conversely all the dynamic, electrodynamic, thermodynamic and radiation processes in the various phases of the plasma focus affect the discharge current. It is then no exaggeration to say that the discharge current waveform contains information on all the dynamic, electrodynamic, thermodynamic and radiation processes that occur in the various phases of the plasma focus. This explains the importance attached to matching the computed current trace to the measured current trace in the procedure adopted by the Lee model code.

a. Scaling laws for neutrons from numerical experiments over a range of energies from 10kJ to 25 MJ

We apply the Lee model code to the MJ machine PF1000 over a range of C_0 to study the neutrons emitted by PF1000-like bank energies from 10kJ to 25 MJ.

A measured current trace of the PF1000 with $C_0 = 1332$ μF, operated at 27 kV, 3.5 torr deuterium, has been published [34], with cathode/anode radii $b = 16$ cm, $a = 11.55$ cm and anode length $z_0 = 60$ cm. In the numerical experiments we fitted external (or static) inductance $L_0 = 33.5$ nH and stray resistance $r_0 = 6.1$ mΩ (damping factor $RESF = r_0/(L_0/C_0)^{0.5} = 1.22$). The fitted model parameters are: $f_m = 0.13$, $f_c = 0.7$, $f_{mr} = 0.35$ and $f_{cr} = 0.65$. The computed current trace [11], [15] agrees very well with the measured trace through all the phases, axial and radial, right down to the bottom of the current dip indicating the end of the pinch phase as shown in Fig.1.

This agreement confirms the model parameters for the PF1000. Once the model parameters have been fitted to a machine for a given gas, these model parameters may be used with some degree of confidence when operating parameters such as the voltage are varied [9]. With no measured current waveforms available for the higher

megajoule numerical experiments, it is reasonable to keep the model parameters that we have got from the PF1000 fitting.

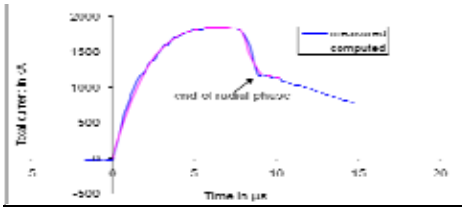

Fig 1. Current fitting computed current to measured current traces to obtain fitted parameters $f_m = 0.13$, $f_c = 0.7$, $f_{mr} = 0.35$ and $f_{cr} = 0.65$.

The optimum pressure for this series of numerical experiments is 10 torr and the ratio $c=b/a$ is retained at 1.39. For each C_0, anode length z_0 is varied to find the optimum. For each z_0, anode radius a_0 is varied so that the end axial speed is 10 cm/μs. The numerical experiments were carried out for C_0 ranging from 14 μF to 39960 μF corresponding to energies from 8.5 kJ to 24 MJ [12].

For this series of experiments we find that the Y_n scaling changes from $Y_n \sim E_0^{2.0}$ at tens of kJ to $Y_n \sim E_0^{0.84}$ at the highest energies (up to 25MJ) investigated in this series. This is shown in Fig 2.

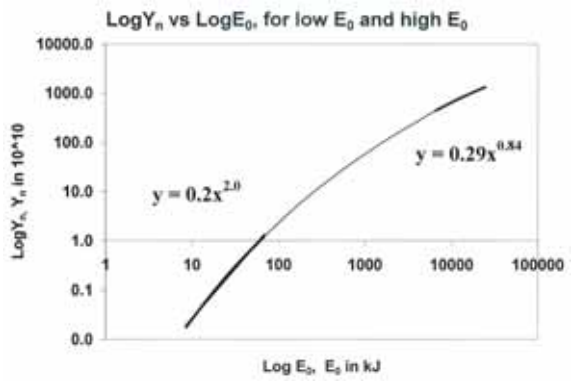

Fig 2. Y_n plotted as a function of E_0 in log-log scale, showing Y_n scaling changes from $Y_n \sim E_0^{2.0}$ at tens of kJ to $Y_n \sim E_0^{0.84}$ at the highest energies (up to 25MJ).

The scaling of Y_n with I_{peak} and I_{pinch} over the whole range of energies investigated up to 25 MJ (Fig. 3) is as follows:

$$Y_n = 3.2\text{x}10^{11} I_{pinch}^{4.5} \quad \text{and}$$

$$Y_n = 1.8\text{x}10^{10} I_{peak}^{3.8}$$

where I_{peak} ranges from 0.3 MA to 5.7 MA and I_{pinch} ranges from 0.2 MA to 2.4 MA.

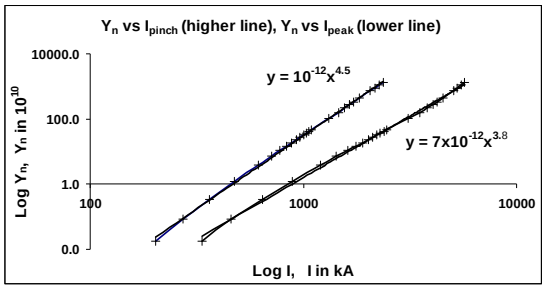

Fig. 3. Log(Y_n) scaling with Log(I_{peak}) and Log(I_{pinch}), for the range of energies investigated, up to 25 MJ

This compares to an earlier study carried out on several machines with published current traces and Y_n yield measurements, operating conditions and machine parameters including the PF400, UNU/ICTP PFF, the NX2 and Poseidon providing a slightly higher scaling laws: $Y_n \sim I_{pinch}^{4.7}$ and $Y_n \sim I_{peak}^{3.9}$. The slightly higher value of the scaling is because those machines fitted are of mixed '*c*' mixed bank parameters, mixed model parameters and currents generally below 1MA and voltages generally below the 35 kV [11].

b. Scaling laws for neon SXR from numerical experiments over a range of energies from 0.2 kJ to 1 MJ

We next use the Lee model code to carry out a series of numerical experiments over the energy range 0.2 kJ to 1 MJ [35]. In this case we apply it to a proposed modern fast plasma focus machine with optimised values for c the ratio of the outer to inner electrode radius and L_0 obtained from our numerical experiments.

The following parameters are kept constant : (i) the ratio $c=b/a$ (kept at 1.5, which is practically optimum according to our preliminary numerical trials; (ii) the operating voltage V_0 (kept at 20 kV); (iii) static inductance L_0 (kept at 30 nH, which is already low enough to reach the I_{pinch} limitation regime [13], [14] over most of the range of E_0 we are covering) and; (iv) the ratio of stray resistance to surge impedance *RESF* (kept at 0.1, representing a higher performance modern capacitor bank). The model parameters [8]-[14] f_m, f_c, f_{mr}, f_{cr} are also kept at fixed values 0.06, 0.7, 0.16 and 0.7. We choose the model parameters are they represent the average values from the range of machines that we have studied.

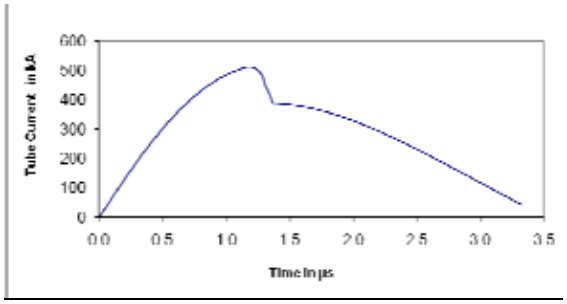

Fig 4. Computed total curent versus time for L_0= 30 nH and V_0= 20 kV, C_0= 30 uF, *RESF* = 0.1, c = 1.5 and model parameters f_m, f_c, f_{mr}, f_{cr} are fixed at 0.06, 0.7, 0.16 and 0.7 for optimised a = 2.285cm and z_0= 5.2 cm.

The storage energy E_0 is varied by changing the capacitance C_0. Parameters that are varied are operating pressure P_0, anode length z_0 and anode radius a. Parametric variation at each E_0 follows the order; P_0, z_0 and a until all realistic combinations of P_0, z_0 and a are investigated. At each E_0, the optimum combination of P_0, z_0 and a is found that produces the biggest Y_{sxr}. In other words at each E_0, a P_0 is fixed, a z_0 is chosen and a is varied until the largest Y_{sxr} is found. Then keeping the same values of E_0 and P_0, another z_0 is chosen and a is varied until the largest Y_{sxr} is found. This procedure is repeated until for that E_0 and P_0, the optimum combination of z_0 and a is found. Then keeping the same value of E_0, another P_0 is selected. The procedure for parametric variation of z_0 and a as described above is then carried out for this E_0 and new P_0 until the optimum combination of z_0 and a is found. This procedure is repeated until for a fixed value of E_0, the optimum combination of P_0, z_0 and a is found.

The procedure is then repeated with a new value of E_0. In this manner after systematically carrying out some 2000 runs, the optimized runs for various energies are tabulated in Table 1. From the data of Table 1, we plot Y_{sxr} against E_0 as shown in Fig 5.

Table 1. Optimised configuration found for each E_0. Optimisation carried out with *RESF* = 0.1, c = 1.5, L_0 = *30 nH and* V_0 = *20 kV and model parameters* f_m, f_c, f_{mr}, f_{cr} *are fixed at 0.06, 0.7, 0.16 and 0.7 respectively. The* v_a, v_s and v_p are the peak axial, radial shock and radial piston speeds respectively.

E_0 (kJ)	C_0 (μF)	a (cm)	z_0 (cm)	P_0 (Torr)	I_{peak} (kA)	I_{pinch} (kA)	v_a (cm/μs)	v_s (cm/μs)	v_p (cm/μs)	Y_{sxr} (J)
0.2	1	0.58	0.5	4.0	100	68	5.6	22.5	14.9	0.44
1	5	1.18	1.5	4.0	224	143	6.6	23.3	15.1	7.5
2	10	1.52	2.1	4.0	300	186	6.8	23.6	15.2	20
6	30	2.29	5.2	4.2	512	294	8.1	24.5	15.6	98
10	50	2.79	7.5	4.0	642	356	8.7	24.6	15.7	190
20	100	3.50	13	4.0	861	456	9.6	24.6	16.0	470

40	200	4.55	20	3.5	1109	565	10.3	24.7	16.2	1000
100	500	6.21	42	3.0	1477	727	11.2	24.8	16.4	2700
200	1000	7.42	63	3.0	1778	876	11.4	24.8	16.5	5300
400	2000	8.70	98	3.0	2079	1036	11.4	24.9	16.5	9400
500	2500	9.10	105	2.9	2157	1086	11.5	25.1	16.7	11000
1000	5000	10.2	160	3.0	2428	1261	11.4	25.2	16.7	18000

We then plot Y_{sxr} against I_{peak} and I_{pinch} and obtain SXR yield scales as $Y_{sxr} \sim I_{pinch}^{3.6}$ and $Y_{sxr} \sim I_{peak}^{3.2}$. The I_{pinch} scaling has less scatter than the I_{peak} scaling. We next subject the scaling to further test when the fixed parameters *RESF*, c, L_0 and V_0 and model parameters f_m, f_c, f_{mr}, f_{cr} are varied. We add in the results of some numerical experiments using the parameters of several existing plasma focus devices including the UNU/ICTP PFF (*RESF* = 0.2, c = 3.4, L_0 = 110 nH and V_0 = 14 kV with fitted model parameters f_m = 0.05, f_c = 0.7, f_{mr} = 0.2, f_{cr} = 0.8)[7]-[9], [23], the NX2 (*RESF* = 0.1, c = 2.2, L_0 = 20 nH and V_0 = 11 kV with fitted model parameters f_m = 0.10, f_c = 0.7, f_{mr} = 0.12, f_{cr} = 0.68)[7]-[10], [24] and PF1000 (*RESF* = 0.1, c = 1.39, L_0 = 33 nH and V_0 = 27 kV with fitted model parameters f_m = 0.1, f_c = 0.7, f_{mr} = 0.15, f_{cr} = 0.7) [7]-[9], [14]. These new data points (white data points in Fig. 6) contain wide ranges of c, V_0, L_0 and model parameters. The resulting Y_{sxr} versus I_{pinch} log-log curve remains a straight line, with the scaling index 3.6 unchanged and with no more scatter than before. However the resulting Y_{sxr} versus I_{peak} curve now exhibits considerably larger scatter and the scaling index has changed.

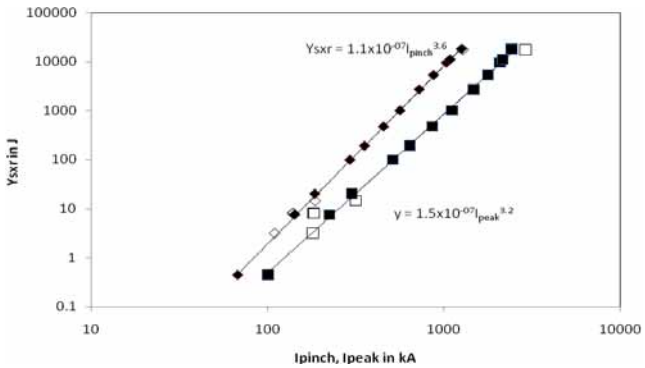

Fig 6. Y_{sxr} is plotted as a function of I_{pinch} and I_{peak}. The parameters kept constant for the black data points are: *RESF* = 0.1, c = 1.5, L_0 = 30nH and V_0 = 20 kV and model parameters f_m, f_c, f_{mr}, f_{cr} at 0.06, 0.7, 0.16 and 0.7 respectively. The white data points are for specific machines which have different values for the parameters c, L_0 and V_0.

We would like to highlight that the consistent behaviour of I_{pinch} in maintaining the scaling of $Y_{sxr} \sim I_{pinch}^{3.6}$ with less scatter than the $Y_{sxr} \sim I_{peak}^{3.2}$ scaling particularly when mixed-parameters cases are included, strongly support the conclusion that I_{pinch} scaling is the more universal and robust one. Similarly conclusions on the importance of I_{pinch} in plasma focus performance and scaling laws have been reported [11]-[15].

It may also be worthy of note that our comprehensively surveyed numerical experiments for Mather configurations in the range of energies 0.2 kJ to 1 MJ produce an I_{pinch} scaling rule for Y_{sxr} not compatible with Gates' rule [37]. However it is remarkable that our I_{pinch} scaling index of 3.6, obtained through a set of comprehensive numerical experiments over a range of 0.2 kJ to 1 MJ, on Mather-type devices is within the range of 3.5-4 postulated on the basis of sparse experimental data, (basically just two machines one at 5 kJ and the other at 0.9 MJ), by Filippov [6], for Filippov configurations in the range of energies 5 kJ to 1 MJ.

It must be pointed out that the results represent scaling for comparison with baseline plasma focus devices that have been optimized in terms of electrode dimensions. It must also be emphasized that the scaling with I_{pinch} works well even when there are some variations in the actual device from L_0 = 30 nH, V_0 = 20 kV and c = 1.5. However there may be many other parameters which can change which could lead to a further enhancement of x-ray yield.

Conclusion

Numerical experiments carried out using the universal plasma focus laboratory facility based on the Lee model code gives reliable scaling laws for neutrons production and neon SXR yields for plasma focus machines. The scaling laws obtained:

For neutron yield:

$Y_n = 3.2\text{x}10^{11} I_{pinch}^{4.5}$; $Y_n = 1.8\text{x}10^{10} I_{peak}^{3.8}$; I_{peak} (0.3 to 5.7), I_{pinch} (0.2 to 2.4) in MA.
$Y_n \sim E_0^{2.0}$ at tens of kJ to $Y_n \sim E_0^{0.84}$ at MJ level (up to 25MJ).

For neon soft x-rays:

$Y_{sxr} = 8.3\text{x}10^{3} I_{pinch}^{3.6}$; $Y_{sxr} = 6\text{x}10^{2} I_{peak}^{3.2}$; I_{peak} (0.1 to 2.4), I_{pinch} (0.07 to1.3) in MA.
$Y_{sxr} \sim E_0^{1.6}$ (kJ range) to $Y_{sxr} \sim E_0^{0.8}$ (towards MJ).

These laws provide useful references and facilitate the understanding of present plasma focus machines. More importantly, these scaling laws are also useful for design considerations of new plasma focus machines particularly if they are intended to operate as optimized neutron or neon SXR sources.

Acknowledgement

The authors acknowledge the contributions of Paul Lee and Rajdeep Singh Rawat to various parts of this paper.

References

[1] S Lee, "Twelve Years of UNU/ICTP PFF—A Review," IC/ 98/ 231 Abdus Salam ICTP, Miramare, Trieste; 1998, pp.5-34. ICTP Open Access Archive http://eprints.ictp.it/31/.
[2] Kato Y and Be S H 1986 *Appl. Phys. Lett.* **48** 686
[3] E P Bogolyubov, V D Bochkov, V A Veretennikov, L T Vekhoreva, V A Gribkov, A V Dubrovskii, Yu P Ivanov, A I Isakov, O N Krokhin, P Lee, S Lee, V Ya Nikulin, A Serban, P V Silin, X Feng and G X Zhang, "A powerful soft x-ray source for x-ray lithography based on plasma focusing" 1998 *Phys. Scripta.,* vol. 57, 1998, pp. 488-494.
[4] Lee S, Lee P, Zhang G, Feng X, Gribkov V A, Mahe L, Serban A, and Wong T K S 1998 IEEE Trans. Plasma Sci. **26** 1119
[5] Filippov N V, Filippova T I, Karakin M A, Krauz V I, Tykshaev V P, Vinogradov V P, Bakulin Y P, Timofeev V V, Zinchenko V F, Brzosko J R, Brzosko J S, IEEE Trans Plasma Sci. 24, 1215 – 1223, 1996
[6] Filippov N V, Filippova T I, Khutoretskaia I V, Mialton V V and Vinogradov V P," Megajoule scale plasma focus as efficient X-ray source," Physics Letters A Vol 211, Issue 3, 168-171, 1996
[7] Institute for Plasma Focus Studies http://www.plasmafocus.net
[8] Internet Workshop on Plasma Focus Numerical Experiments (IPFS-IBC1) 14 April-19 May 2008 http://www.plasmafocus.net/IPFS/Papers/IWPCAkeynote2ResultsofInternet-basedWorkshop.doc
[9] Lee S Radiative Dense Plasma Focus Computation Package: RADPF http://www.intimal.edu.my/school/fas/UFLF/File1RADPF.htm http://www.plasmafocus.net/IPFS/modelpackage/File1RADPF.htm
[10] Lee S, Rawat R S, Lee P and Saw S H. "Soft x-ray yield from NX2 plasma focus- correlation with plasma pinch parameters" (to be published)
[11] S Lee and S H Saw, "Neutron scaling laws from numerical experiments," J Fusion Energy 27, 2008, pp. 292-295.
[12] S Lee, "Current and neutron scaling for megajoule plasma focus machine," Plasma Phys. Control. Fusion 50, 2008, 105005, (14pp).

[13] S Lee, S H Saw, P C K Lee, R S Rawat and H Schmidt, "Computing plasma focus pinch current from total current measurement," Appl. Phys. Lett. 92 , 2008, 111501.
[14] S Lee and S H Saw, "Pinch current limitation effect in plasma focus," Appl. Phys. Lett. 92, 2008, 021503.
[15] S Lee, P Lee, S H Saw and R S Rawat, "Numerical experiments on plasma focus pinch current limitation," Plasma Phys. Control. Fusion 50, 2008, 065012 (8pp).
[16] S Lee, "Plasma focus model yielding trajectory and structure" in *Radiations in Plasmas*, ed B McNamara (Singapore: World Scientific Publishing Co, ISBN 9971-966-37-9) vol. II, 1984, pp. 978–987
[17] S Lee S et al, "A simple facility for the teaching of plasma dynamics and plasma nuclear fusion," Am. J. Phys. 56, 1988, pp. 62-68.
[18] T Y Tou, S Lee and K H Kwek, "Non perturbing plasma focus measurements in the run-down phase," IEEE Trans. Plasma Sci. 17, 1989, pp. 311-315.
[19] S Lee, "A sequential plasma focus," IEEE Trans. Plasma Sci., vol. 19, no. 12, 1991, pp. 912-919.
[20] Jalil bin Ali, "Development and Studies of a small Plasma Focus," PhD thesis, Universiti Teknologi Malaysia, Malaysia, 1990.
[21] D E Potter, "The formation of high density z-pinches," Nucl. Fus., vol. 18, pp. 813-823, 1978.
[22] S Lee and A Serban A, "Dimensions and lifetime of the plasma focus pinch," IEEE Trans. Plasma Sci., vol. 24, no.3, 1996, pp. 1101-1105.
[23] Liu Mahe, "Soft X-rays from compact plasma focus," PhD thesis, NIE, Nanyang Technological University, Singapore, 2006. ICTP Open Access Archive: http://eprints.ictp.it/327/.
[24] S Bing, "Plasma dynamics and x-ray emission of the plasma focus," PhD Thesis, NIE, Nanyang Technological University, Singapore, 2000. ICTP Open Access Archive: http://eprints.ictp.it/99/.
[25] A Serban and S Lee, "Experiments on speed-enhanced neutron yield from a small plasma focus," J Plasma Physics, vol. 60 part 1, 1998, pp. 3-15.
[26] M H Liu, X P Feng, S V Springham and S Lee "Soft x-ray measurement in a small plasma focus operated in neon," IEEE Trans. Plasma Sci. 26, 1998, pp. 135–140.
[27] D Wong, P Lee, T Zhang, A Patran, T L Tan, R S Rawat and S Lee, "An improved radiative plasma focus model calibrated for neon-filled NX2 using a tapered anode," Plasma Sources Sci. Technol. 16, 2007, pp. 116-123.
[28] S Lee. (2000–2007). http://ckplee.myplace.nie.edu.sg/plasmaphysics/.
[29] S Lee. (2005). ICTP Open Access Archive: http://eprints.ictp.it/85/.
[30] M A Mohammadi, S Sobhanian, C S Wong, S Lee, P Lee and R S Rawat , "The effect of anode shape on neon soft x-ray emissions and current sheath configuration in plasma focus device," J. Phys. D: Appl.Phys. 42, 2009, 045203 (10pp).
[31] S V Springham, S Lee and M S Rafique, "Correlated deuteron energy spectra and neutron yield for a 3 kJ plasma focus," Plasma Phys. Control. Fusion, vol. 42, 2000, pp. 1023-1032.
[32] S Lee, P Lee, G Zhang, X Feng, V A Gribkov, M Liu, A Serban and T Wong "High rep rate high performance plasma focus as a powerful radiation source" IEEE Trans. Plasma Sci., vol. 26, no. 4, 1998, pp. 1119-1126.
[33] V Siahpoush, M A Tafreshi, S Sobhanian and S Khorram, "Adaptation of Sing Lee's model to the Filippov type plasma focus geometry*,"* Plasma Phys. Control. Fusion 47, 2005, pp. 1065-1072.
[34] V A Gribkov, A Banaszak, B Bienkowska, A V Dubrovsky, I Ivanova-Stanik, L Jakubowski, L Karpinski, R A Miklaszewski, M Paduch, M J Sadowski, M Scholz, A Szydlowski and K Tomaszewski, "Plasma dynamics in the PF-1000 device under full-scale energy storage: II. Fast electron and ion characteristics versus neutron emission parameters and gun optimization perspectives," J. Phys. D: Appl. Phys. 40, 2007, pp. 3592-3607.
[35] Huba J D 2006 Plasma Formulary page 44
[36] S Lee, S H Saw, P Lee and R S Rawat, "Numerical experiments on plasma focus neon soft x-ray scaling", (to be published).
[37] D C Gates 1978 Proceedings of the IInd Int Conference on Energy Storage, Compression and Switching, Venice, 2, 3239 (Plenum Press, New York, 1983).

FUSION ENERGY AND THE PLASMA FOCUS

Sing Lee*

Institute for Plasma Focus Studies, 32, Oakpark Drive, Chadstone VIC3148, Australia
INTI University College, 71800 Nilai, Malaysia
Nanyang Technological University, National Institute of Education, Singapore 637616

Abstract

[1] An introduction is given to plasmas and fusion energy. A brief look into the past and future of Tokamak development is taken. It appears inevitable that fusion reactors will provide one of the solutions to civilization's need for increasing energy resources; although the technological scale of presently envisaged nuclear reactors makes the adoption of the technology cumbersome to manage.

[2] Alternative simpler schemes have been suggested. One of the most promising is based on pulsed high density compressions by large currents pinch effects. Among these is the plasma focus, a device which even in a table-top form produces significant radiation emissions including nuclear fusion neutrons, from the extremely hot compressed plasma. Early hopes were based on experimental results that predicted output fusion energy scales as the square of input energy, predicting breakeven at tens of megajoules (MJ), a much smaller scale than Tokamak installations. These hopes were quickly dimmed as neutron saturation effects were observed at a relatively low MJ level. Recently, numerical experiments have shown that simple circuit effects, overlooked in earlier intense scrutiny of complex non-linear effects, lead to a current saturation tendency, which is the primary factor for the neutron saturation. With the cause identified, further numerical experiments are expected to suggest a simple solution to add current, thus overcoming the saturation. This paper acts as the platform to launch the idea of beyond-saturation plasma focus machines, which is expected to enhance the prospects of plasma focus fusion energy research.

Keywords: Fusion energy, tokamak, plasma focus

1. Introduction

Nuclear fusion is the process that powers the stars. The study of plasma physics has led to technological developments which point to the possibility of the use of the fusion process to develop a new, clean and limitless energy source. At the forefront of the efforts to harness this process are Tokamak machines. Technical requirements to harness nuclear fusion include high temperatures, sufficient gas fuel densities and containment times which appear to be attainable in the next generation of Tokamaks. Other programmes to develop nuclear fusion reactors involve inertial methods, including laser implosions and plasma pinch (fast compression) devices such as the plasma focus.

1.1. Plasma and plasma characteristics

Plasmas form the fourth state of matter, the other three states being solid, liquid and gases. When matter is heated to very high temperatures, some of the atoms in the matter become ionized when electrons are ejected from the atoms. When sufficient ionization is attained, the matter is in an electrically conducting gaseous state which is known as the plasma state. A plasma interacts with electric and magnetic fields. The electrons and ions in a plasma may be controlled by electric and magnetic fields. A plasma has higher energy density (per unit mass) than matter in the other three states. A constituent particle in a gas at room temperature may have several hundredths of eV (electron-volt) of energy whilst a plasma, even a 'cold' plasma may have energies of several

* E-mail: leesing@optusnet.com.au

eV's (in this context: 1 eV=11,400K). A 'hot' plasma may have temperatures exceeding keV's. More than 99% of matter in the universe, including the stars, exists in the plasma state.

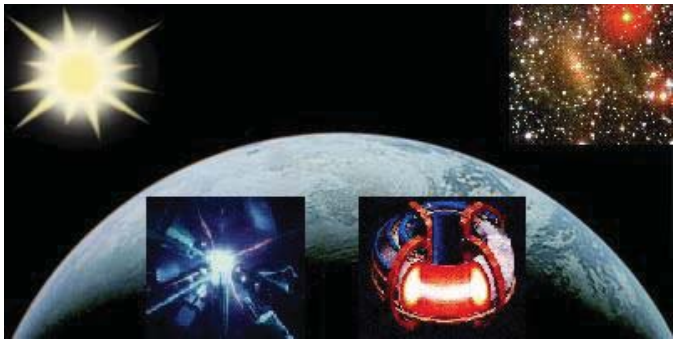

Figure 1. Natural fusion reactors and experimental fusion reactors on earth (credits: Figs 1 -11 are taken from some websites in the reference list [1-6])

1.2. Applications of plasmas

Plasmas have advantageous properties including high energy densities and ability to be precisely controlled by electric and magnetic fields. These properties lead to many applications [7] including surface processing, cleaning, etching, deposit of advanced materials including diamond-like and harder-than-diamond materials, materials related to nanotechnology, environmental applications such as waste disposal, high-temperature chemistry, MHD converters, thrusters, radiation sources for microelectronics lithography and micromachining, medical applications such as diagnostics, cleaning instrumentation and light sources for spectroscopy. The most important application is nuclear fusion energy.

2. Nuclear fusion energy

Plasma nuclear fusion promises a new limitless source of energy [1-6], essential for the continuing progress of human civilization. Mankind now stands at a dividing point in human history; 200 years ago the earth was under-populated (less than 1 billion population consuming little energy per head) with abundant resources of energy; 100 years from now, the earth will be overcrowded (25 billion population with voracious hunger for energy (assuming population doubling time of 45 years or 1.6% per year), with little energy resources left. Rate of growth will slow down amidst intensifying energy-caused conflicts unless a new large-scale source is found.

Plasma nuclear fusion is based on the following nuclear reaction:

$$ {}_1H^2 + {}_1H^3 \longrightarrow {}_2H^4 + {}_0n^1 $$

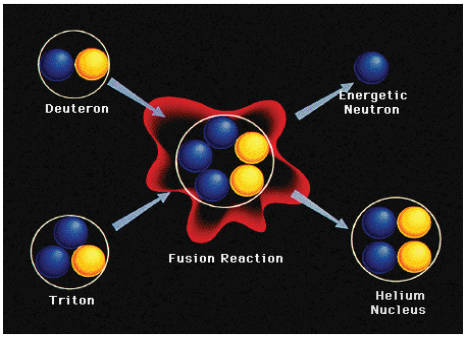

Figure 2. Deuterium-Tritium fusion

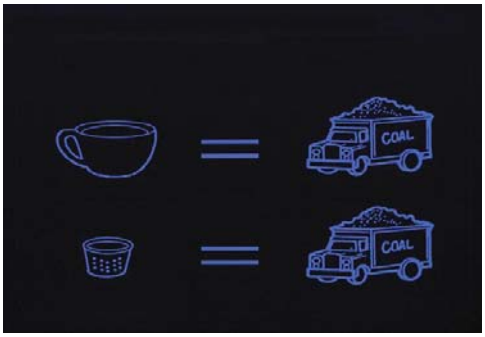

Figure 3. 1 thimble of heavy water extracted from 50 cups of water undergoing nuclear fusion produces energy equivalent to a truck of coal

The fusing of a deuteron (deuterium nucleus) with a triton (tritium nucleus), see Fig 2, to form a helium nucleus with the liberation of a neutron which carries with it the excess energy of the reaction, this excess energy coming from mass-energy conversion, since the reactons (deuteron nucleus and the tritium nucleus) have more mass than

the reaction products (the helium nucleus and the neutron); a clear demonstration of Einstein's $E=mc^2$. In the stars fusion reactions are responsible for the continuing shining of the universe. On earth the power of nuclear fusion has been demonstrated by the hydrogen bomb.

The plan of fusion scientists is to harness this same power in a controlled fashion in nuclear fusion reactors. The fuel for such reactors is practically limitless. 1 part in 6000 of sea water is heavy water (D_2O). This heavy water will act as the basic fuel for the nuclear fusion reactors and will last the most voracious usage of mankind for millions of years.

3. Conditions required for nuclear reactors

Thermalised. plasmas need to be at a high enough temperature for collisions to be able to overcome the Coulomb repulsive barrier. The ideal ignition temperature for D-T fusion is 4 keV. The other requirements are a high enough density contained for a sufficient period of time. Technological targets are set at: Temperature >10 keV (100 million K) and a density-containment time product $nt>10^{21}m^{-3}$-sec [6]. Attempts to fulfill the nt criterion appear to have settled down broadly into two approaches:

$n=10^{20}$ m^{-3}, with confinement time t=10 second (low density, long lived plasmas, contained by magnetic fields) and
$n=10^{31}$ m^{-3}, with confinement time $t=10^{-10}$ second (super-high density, inertially compressed pulsed plasmas, with confinement time provided by inertia).

The nt criterion together with the requirement for a high enough ignition temperature give a combined fusion product of: $ntT>10^{22}m^{-2}$-sec-keV.

On the the other hand, both the requirements of high temperature and confinement in stars are provided by gravitational forces.

4. Tokamak

A Tokamak[1-6] may be described as a doughnut shaped plasma vessel in which electric currents are used for heating the plasma and magnetic fields are used to contain the plasma away from the walls. The magnetic fields need special configurations for stability over the period of containment. A schematic is shown in Fig. 4 with a cut-away section showing the plasma in the vessel. The transformer core and the field coils necessary to confine and position the plasma are shown schematically in the next Fig 5.

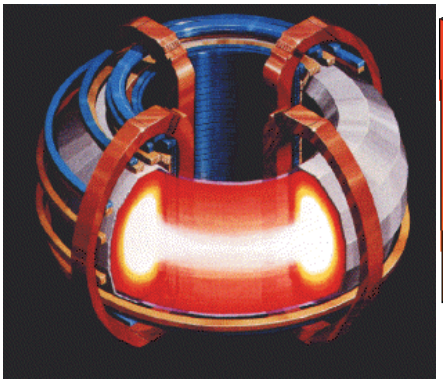

Figure 4. Tokamak vessel

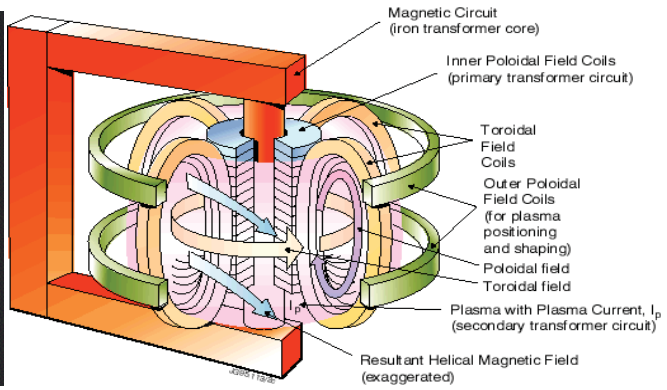

Figure 5. Magnetic fields for confining Tokamak Plasmas

The Joint European Torus (JET) sited at Culham, UK, is the world's largest nuclear fusion research facility [3]. Its structure and a worker inside the toroidal vessel are shown in the next figures 6 & 7.

Progress in Tokamak research is depicted in the Fig.8, which shows that the fusion product ntT has increased 10 million times in the 51 years of Tokamak research since 1958 [6]. The required fusion temperature of >10 keV has been achieved in several Tokamaks including JET (EU), JT-60 (Japan), TFTR (US) and DIII D (US). Fusion confinement ($ntT=10^{22}m^{-2}$-sec-keV for Q=1 breakeven; here Q is the ratio of output fusion energy/input energy)

is only one step away. Notably JET has already achieved Q=0.6 before year 2000.

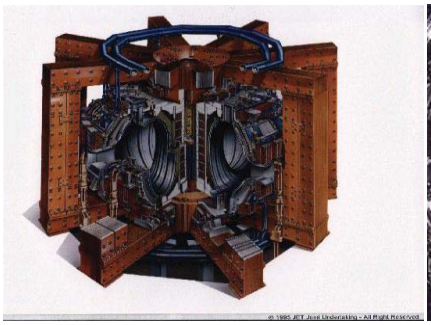

Figure 6. Struture of JET

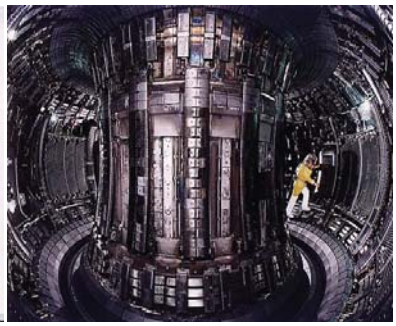

Figure 7. A worker inside the JET chamber

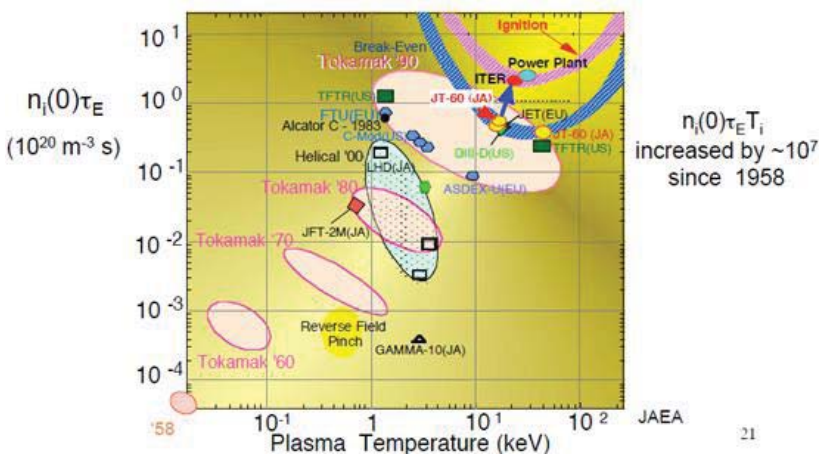

Figure 8. Illustrating fusion progress in 51 years. Break-even is only 1 step away

Moreover from all the experiments, cutting through all the difficulties in plasma physics and engineering technology, the energy confinement time is known to scale as some functions of plasma current I_p. Major radius R, minor radius 'a' and toroidal magnetic field B. The scaling law may be expressed generally as
$t \sim I_p^{\square} R^{\square} a^{\square} B^{\square}$ with the indices all positive. To achieve a sufficiently high ntT the scaling indicates increase in I_p, R, a and B.

4.1 International thermonuclear experimental reactor- ITER and beyond

In 1985 at the Geneva Superpower Summit, Reagan (USA) and Gorbachev (Soviet Union) agreed on a project [4,6] to develop a new, cleaner, sustainable source of energy-fusion energy. ITER was born. The initial signatories: former Soviet Union, USA, European union (via EURATOM) and Japan were joined by P R China and Republic of Korea in 2003 and India in 2005. The ITER Agreement was signed in November 2006. ITER construction has started in Cadarache, France with first plasma planned for 2018 and D-T experiments for 2022 and beyond.

Figure 9. The structure of ITER, and the site at Cadarache in France

ITER aims to demonstrate that it is possible to produce commercial energy from fusion with a scientific goal of Q> 10; ie to deliver 10 times the power it consumes; e.g. using 50 MW of input power to start and sustain the plasma, ITER will produce 500 MW of power from nuclear fusion over the cycle of the experiment.

Beyond ITER will be DEMO (early 2030's). This will be a demonstration fusion power plant which will feed power into electricity grid as early as 2040.

More advanced Tokamak designs include FIRE (Fusion Ignition Research Experiment) a design more compact than JET yet with a design Q=10 [2,6]. A 1 GW Tokamak ARIES has already been designed.

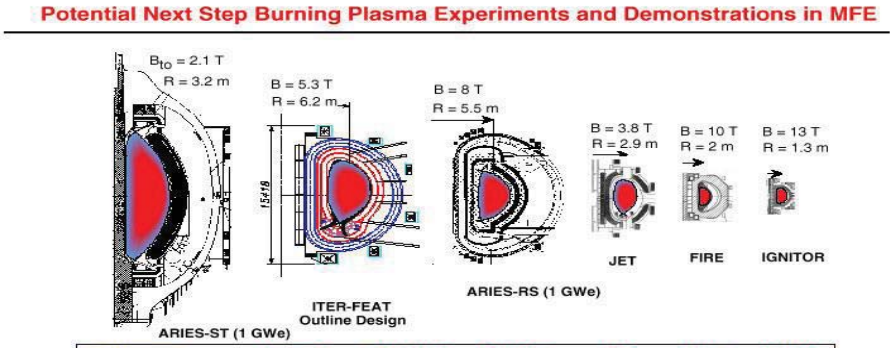

Cost Drivers	ARIES-ST	ITER-FEAT	ARIES-RS	JET	FIRE	IGNITOR
Plasma Volume (m^3)	810	837	350	95	18	11
Plasma Surface (m^2)	580	678	440	150	60	36
Plasma Current (MA)	28	15	11	4	6.5	12
Magnet Energy (GJ)	29	50	85	2	5	5
Fusion Power (MW)	3000	500	2200	16	200	100
Burn Time (s), inductive	steady	300	steady*	1	20	5

* assumes non-inductive current drive

Figure 10. Comparing plasma cross-sections of planned machines with JET

Some comparative data showing plasma cross-sections is shown in Fig 10, showing the technological advantages of the more advanced yet compact designs.

5. Inertial confinement

The other approach is to use pulsed super high density [8]. The super high density may be achieved by beaming powerful pulsed lasers from all directions onto D-T pellets (typically 0.1 mm radius). The radiation pressure exerted on the surface of the pellet together with the blow-off of hot surface material cause compression of the pellet to super dense conditions which may be 1000 times the density of water. Under these hot and dense conditions, the fuel fusion-ignites. The thermonuclear fusion spreads rapidly through the super-compressed fuel. This is depicted in Fig. 11. The whole process takes place in the sub nanosecond range.

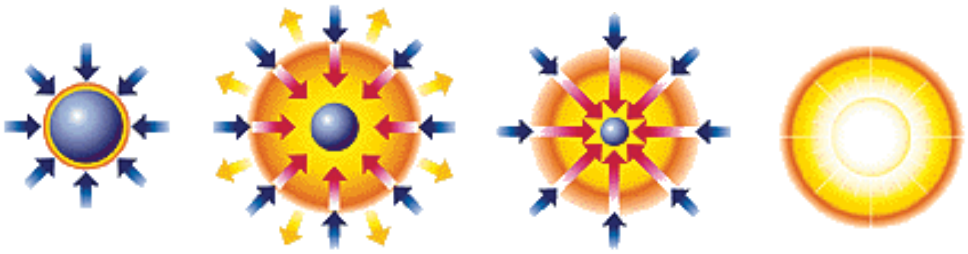

Figure. 11. Radiation induced super dense implosions leading to fusion burn

6. Pinches and the plasma focus

There is a view that whereas Tokamaks and laser implosions will likely be the devices to succeed in the efforts to harness nuclear fusion, these are huge programmes which will take extraordinary amounts of combined international resources and cooperation on a scale never before attempted.. Ongoing research on other devices

such as pinches has shown that these are able to produce nuclear fusion even in devices of much smaller scales [9].

An electrical discharge between two electrodes produces an azimuthal magnetic field which interacts with the column of current, giving rise to a self-compression force which tends to constrict (or pinch) the column. In order to 'pinch', or hold together a column of gas at atmospheric density and temperature of 1 million K, a large pressure has to be exerted by the pinching magnetic field. An electric current of hundreds of kiloAmperes is required for a column of 1mm radius. Moreover the dynamic process requires that the current rises rapidly, typically in under 0.1 microsecond, in order to have a sufficiently hot and dense pinch. Such a pinch is known as a super-fast pinch; and requires special megaAmpere fast-rise (ns) pulsed-lines. These lines may be powered by capacitor banks, and suffer the disadvantage of conversion losses, and high cost of the special technology pulse-shaping line, in addition to the capacitor bank.

A superior method of producing super-dense and super-hot pinch is to use the plasma focus. Not only does this device produce higher densities and temperatures, moreover its method of operation does away with the extra layer of technology required by the expensive and inefficient pulse-shaping line. A simple capacitor discharge is sufficient to power the plasma focus shown in Fig 12. Fig 13 shows shadowgraphs [10] of the plasma focus pinching process.

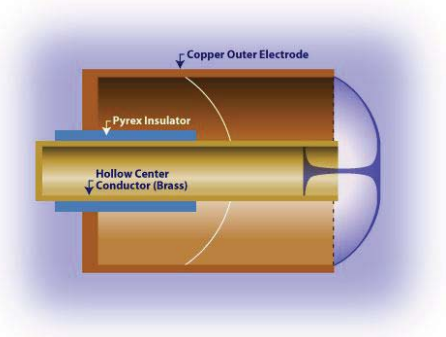

Figure 12. Dense plasma focus device. Image from Glenn Millam. Source: Focus Fusion Society

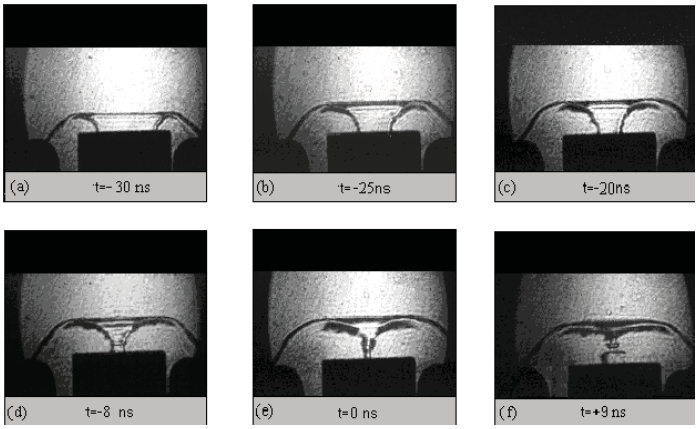

Figure 13. Shadowgraphic sequence showing formation of the plasma focus pinch

6.1. Scaling the plasma focus and neutron saturation

The plasma focus has shown great potential for developing into a fusion reactor. The plasma focus uses a first stage to match the risetime of a simple capacitor discharge, hus allowing the pinching stage to take place at peak current. Besides powerful bursts of x-rays, ion beams, REB's and EM radiation, this simple mechanism has increased its fusion efficiency so that even a simple table top device is able to demonstrate significant nuclear fusion [9].

The plasma focus offers scalability as it has the same energy density per unit mass across the whole range of very small to very big devices, due to its requirements of the same speed factor $(I/a)/p^{0.5}$ over the whole range of devices. The radiation yield is also predictable because of its scaling laws [11].

Its multiple radiations and beams enable it to be an excellent source for soft x-ray micro-lithography, micro-machining, materials processing, nanotechnology materials and a nuclear fusion source for energy [12-17].

Early experiments show that the fusion neutron yield is $Y_n \sim E_0^2$, i.e. proportional to the square of input energy [18]; so that break-even could be expected at several tens of MJ. However it was quickly shown that as E_0 approaches just 1 MJ (see Fig. 14) , the expected increase in neutron yield reduced and there appeared to be a tendency for the neutron yield to saturate [19]. The question now being asked: Is there a fundamental reason for neutron saturation [20] or is it just that the large plasma focus devices are not being properly operated.

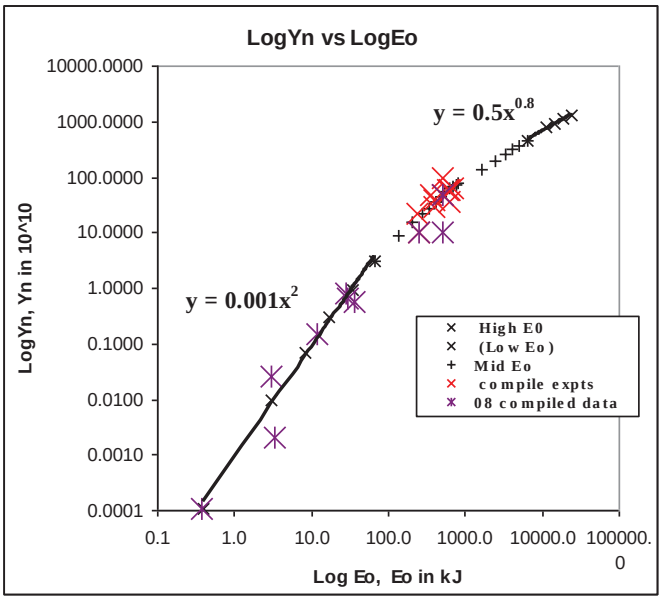

Figure 14. Illustrating neutron saturation observed in measurements and in numerical experiments. The small black crosses are from numerical experiments. The large coloured crosses are from experiments. The straight line at low energies is $Y_n \sim E_0^2$

6.2. Identifying the cause of neutron saturation

Extensive numerical experiments were carried out in the last 18 months using the Lee model code [21]; extending from very small plasma focus devices to the largest existing in the world to fix the base and reference lines for these experiments [22-25]. Then the numerical studies were extended [26] to devices as large as 25 MJ. The results show very clearly that neutron saturation is caused by a 'motor' effect. As mentioned earlier, all plasma focus are run at the same energy densities which means the same speeds. These give rise to the same 'dynamic resistances' which is of the order of 5 mOhm for every plasma focus, be it a 50 J device or one a million times larger at 50 MJ. Thus, operating the plasma focus at capacitor voltages 10-30 kV and with bank inductance around 20-40 nH, as all plasma focus are operated at, will lead to a situation where as bank capacitance is increased to 1000 uF, the bank surge (or short-circuit) impedance decreases to the level of 5 mOhm. At this point, which is around 0.5 MJ, the generator impedance is of the order of the load impedance (predominantly the dynamic resistance mentioned above). Further increase in bank energy by increasing capacitance leads to generator impedance reducing below the level of the load impedance, For example at 5 MJ, the capacitor bank surge impedance has dropped below 2 mOhm. Above 0.5 MJ and as bank energy gets bigger and bigger, the circuit current is more and more dominated by the constant dynamic resistance. At 30 kV, the current then tends towards an asymptotic value of 6 MA. This current saturation leads to neutron saturation [27].

6.3. Operating the plasma focus beyond neutron saturation- Ultra high voltage and current-steps

Now that we have identified the cause of the neutron saturation we may suggest a remedy to reach beyond saturation. There is nothing we can do about the dynamic resistance. It is there and is needed to provide the drive for the plasma. It cannot be reduced. What we need to do is to increase the voltage. For example if we use 300 kV capacitor banks instead of 30 kV, we will move the current saturation asymptotic value to 60MA. Thus

plasma focus will have to move into a brave new world of high voltages. Technically there is already a precedence in the German SPEED II [28], a plasma focus designed to operate at 300 kV using Marx, parallel charging, series discharge technique. SPEED II was not tested as extensively as it could have been and is now operating at reduced voltages in Chile. The Marx bank used in SPEED II has a large generator impedance of 50 mOhm, which is then the dominant impedance during the axial phase, and itself limits the current to 6 MA. 300 kV banks with low impedance of the order of 5 mOhm will be more efficient in this situation and may deliver more current up to 30 MA into the plasma focus. The bank energy would be of the order of 2 MJ. Moving up to 1 MV may deliver currents up to 100 MA at tens of MJ.

Results of numerical experiments summarized in Fig 15 illustrate the diminishing fusion gain of increasingly larger plasma focus devices. Fig 16 shows dramatic improvement when ultra high voltage is used.

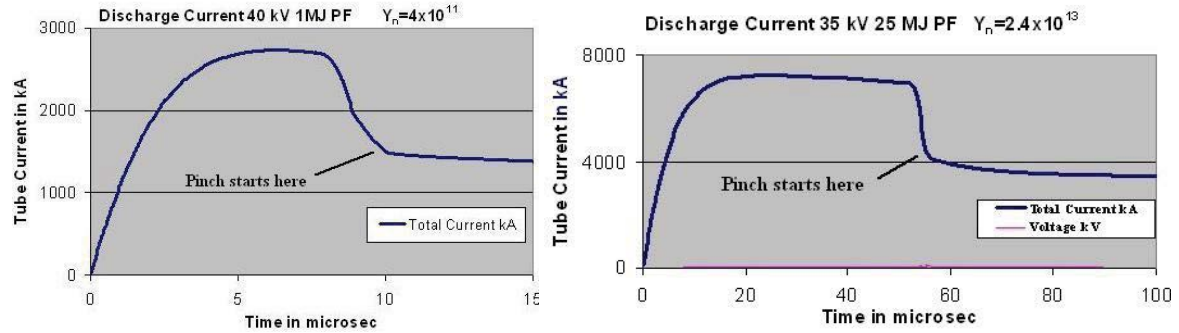

Figure 15. Comparing discharge current amplitudes and neutron yields as bank energy E_0 increases at constant voltage. There is fall away from the ideal scaling law of $Y_n \sim E_0^2$ (numerical experiments at IPFS & INTI UC May 2009, The 1 MJ PF of Fig 15 agrees with measurements at the ICDMP on PF1000)

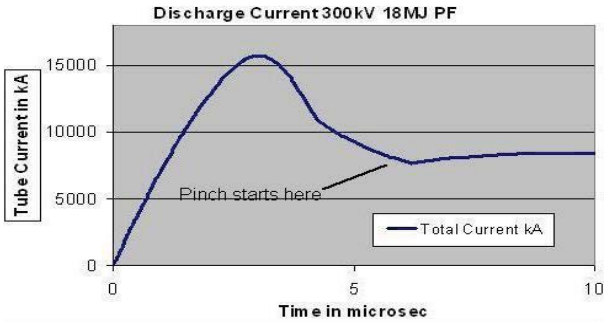

Figure 16. Discharge current reaches much larger values for less E_0 when operated at higher voltage. The neutron yield for this shot is computed as $4x10^{14}$ (numerical experiment at IPFS & UNTI UC, May 2009)

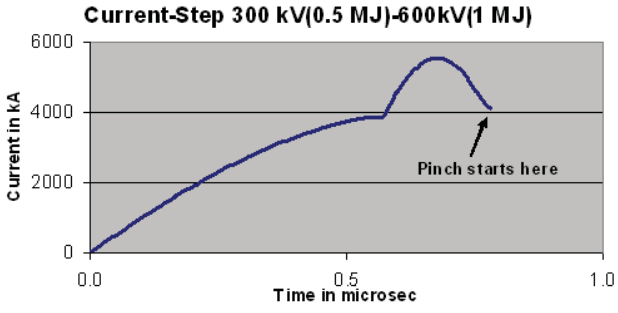

Figure 17. A current step can push the current value up at the crucial moment when the large pinch 'dynamic resistance' tends to drop the current (numerical experiment at IPFS & INTI UC, July 2009)

Other techniques could be used to increase the current. During the radial phase, in particular, there is a sharp drop in current due to the sharp increase in dynamic resistance. By the time the radial implosion reaches the dense pinch phase the current has dropped by as much as 30-50% for the biggest devices. This drop in current occurs at the time when the current is most crucial, being needed to drive the pinch compression. A current-step would be very usefully applied at this time (see Fig 17 which is the latest numerical experiment carried out at IPFS) . At the University of Malaya we had experimented with such current steps in the '80s [29,30]. This

technology is feasible. With the combination of low-impedance, high-voltage drivers and current-stepping technology, plasma focus would move into new regimes and once again regain momentum in the quest for fusion energy.

6.4. Plasma focus fusion reactor energy cycle

A schematic of a plasma focus fusion reactor may be as shown in the final figure.

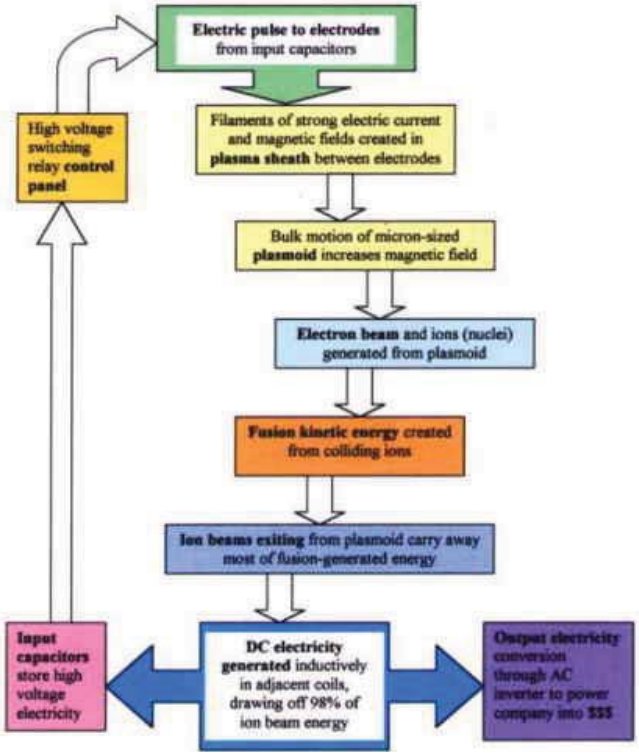

Figure 18. Illustrating the Plasma Focus Fusion Reactor Cycle (from Focus Fusion Society)

7. Conclusion

Tokamak-based nuclear fusion programmes are moving steadily towards harnessing plasma nuclear energy to provide clean, limitless energy for the continuing progress of civilization. Other smaller scale plasma fusion experiments will also have a role to play in this scientific and technological development, the most challenging and rewarding in the history of Mankind. In particular numerical experiments currently under intensive investigations are pointing the way to plasma focus research to go beyond present neutron saturation regimes; thus to regain momentum for this class of devices in the quest for fusion energy.

Acknowledgement

The author thanks for the support of The Scientific and Technical Research Council of Turkey (TUBITAK) within the programme of foreign scientist support.

References:

[1] http://fusion.gat.com
[2] http://fire.pppl.gov
[3] http://www.jet.efda.org
[4] http://www.iter.org
[5] http://www.fusion.org.uk
[6] Meade, Dale. “50 Years of Fusion Research”, PPPL Colloquium, April 1, 2009, Princeton, NJ 08543 http://fire.pppl.gov/meade_PPPL_colloq_040109.pdf

[7] Lee, S and Gribkov, Vladimir A. "Cooperation with Small Countries in Plasma Science and Attempts to Apply to Industrial Needs", ICTP/IAEA Workshop on Plasma Diagnostics and Industrial Applications of Plasmas, October 2000, ICTP Trieste. http://eprints.ictp.it/101/
[8] http://www.hiper-laser.org
[9] S. Lee, T. Y. Tou, S. P. Moo, M. A. Eissa, A. V. Gholap, K. H. Kwek, S. Mulyodrono, A. J. Smith, S. Suryadi, W. Usada, and M. Zakaullah, "A simple facility for the teaching of plasma dynamics and plasma nuclear fusion," *Amer. J. Phys.*, vol. 56, no. 1, pp. 62–68, Jan. 1988.
[10] S. Lee, in *Twelve Years of UNU/ICTP PFF—A Review*. Trieste, Italy: Abdus Salam ICTP, 1998, pp. 5–34. IC/ 98/ 231, ICTP Open Access Archive. [Online]. Available: http://eprints.ictp.it/31/
[11] S. Lee and A. Serban, "Dimensions and lifetime of the plasma focus pinch," IEEE Trans. Plasma Sci., vol. 24, no. 3, pp. 1101–1105, Jun. 1996. http://eprints.ictp.it/42/
[12] M Favre, S Lee, SP Moo, CS Wong X-ray emission in a small plasma focus operating with H2-Ar mixtures. Plasma Sources Science and Technology, 1992
[13] E P Bogolyubov, V D Bochkov, V A Veretennikov, L T Vekhoreva, V A Gribkov, A V Dubrovskii, Yu P Ivanov, A I Isakov, O N Krokhin, P Lee, S Lee, V Ya Nikulin, A Serban, P V Silin, X Feng and G X Zhang ,"A Powerful Soft X-ray Source for X-ray Lithography Based on Plasma Focusing", Physica Scripta, (1998), 57 488-494
[14] S.V. Springham, S. Lee, and M.S. Rafique, "Correlated deuteron energy spectra and neutron yield for a 3 kJ plasma focus," Plasma Phys. Control. Fusion, vol. 42, no. 10, pp. 1023–1032, Oct. 2000.
[15] S V Springham, TL Tan, P Lee, M Zakaullah, S Lee "Spectral study of the electron beam emitted from a 3 kJ plasma focus" PLASMA SOURCES SCIENCE AND TECHNOLOGY, 2005 14, 549-560
[16] A. Serban and S. Lee, "Experiments on speed-enhanced neutron yield from a small plasma focus," J. Plasma Phys., vol. 60, 3–15, Aug. 1998.
[17] LY Soh, P Lee, X Shuyan, S Lee, RS Rawat, Shadowgraphic studies of DLC film deposition process in dense plasma focus device, IEEE Transactions on Plasma Science, 2004, 32, 448- 455
[18] Rapp H. " Measurements referring to plasma focus scaling laws" 1973 Phys Lett A 43A 420-422
[19] Herold H, Jerzykiewicz A, Sadowski M, Schmidt H (1989) Comparative analysis of large plasma focus riments performed at IPF, Stuttgart, and IPJ, Swierk. Nucl Fusion 29 1255–1260
[20] M. Scholz, Report at the ICDMP Meeting, ICDMP, Warsaw, Poland, November2007
[21] Lee S Radiative Dense Plasma Focus Computation Package: RADPF http://www.intimal.edu.my/school/fas/UFLF/
http://www.plasmafocus.net/IPFS/modelpackage/File1RADPF.htm
[22] S. Lee and S. H. Saw, "Neutron scaling laws from numerical experiments," *J. Fusion Energy*, vol. 27, no. 4, pp. 292–295, Dec. 2008.
[23] S. Lee and S. H. Saw, "Pinch current limitation effect in plasma focus," *Appl. Phys. Lett.*, vol. 92, no. 2, p. 021 503, Jan. 2008.
[24] S. Lee, P. Lee, S. H. Saw, and R. S. Rawat, "Numerical experiments on plasma focus pinch current limitation," *Plasma Phys. Control. Fusion*, vol. 50, no. 6, Jun. 2008. 065 012 (8pp).
[25] S. Lee, S. H. Saw, P. C. K. Lee, R. S. Rawat, and H. Schmidt, "Computing plasma focus pinch current from total current measurement," *Appl. Phys.Lett.*, vol. 92, no. 11, p. 111 501, Mar. 2008.
[26] S. Lee, "Current and neutron scaling for megajoule plasma focus machines," *Plasma Phys. Control. Fusion*, vol. 50, no. 10, p. 105 005 (14pp), Oct. 2008.
[27] S Lee "Diagnostics and Insights from Current waveform and Modelling of Plasma Focus" Keynote address presented at the International Workshop on Plasma Diagnostics and Applications, Singapore 2-3 July 2009 http://www.plasmafocus.net/IPFS/Papers/keynoteaddressIWPDA09.doc
[28] G Decker, W Kies, R Nadolny, P Röwekamp, F Schmitz, G Ziethen, K N Koshelev, Yu V Sidelnikov Observations of soft x-ray production in the speed 2 plasma focus 1996 Plasma Sources Sci. Technol. 5 112-118
[29] S.H. Saw, 1991 Experimental studies of a current-stepped pinch PhD Thesis Universiti Malaya
[30] S. Lee, 1984, 'A current-stepping technique to enhance pinch compression' J Phys D: Appl. Phys., 17, 733

Fusion Energy and the Plasma Focus

S Lee

Institute for Plasma Focus Studies

INTI University College, Malaysia

Nanyang Technological University Singapore

Tubav Conferences: Nuclear & Renewable Energy Sources

Ankara, Turkey, 28 & 29 September 2009

Outline of Talk

- **Introduction: Plasma & plasma characteristics**
- **The fusion process**
- **Tokamaks-early days to ITER & beyond**
- **Alternative fusion programs**
- **Plasma Focus**
  - **Early scaling laws**
  - **Neutron saturation**
  - **Cause of neutron saturation**
  - **Beyond saturation**

Conclusion:

STARS:-

Nature's Plasma Fusion Reactors

Tokamak-planned nuclear fusion reactor

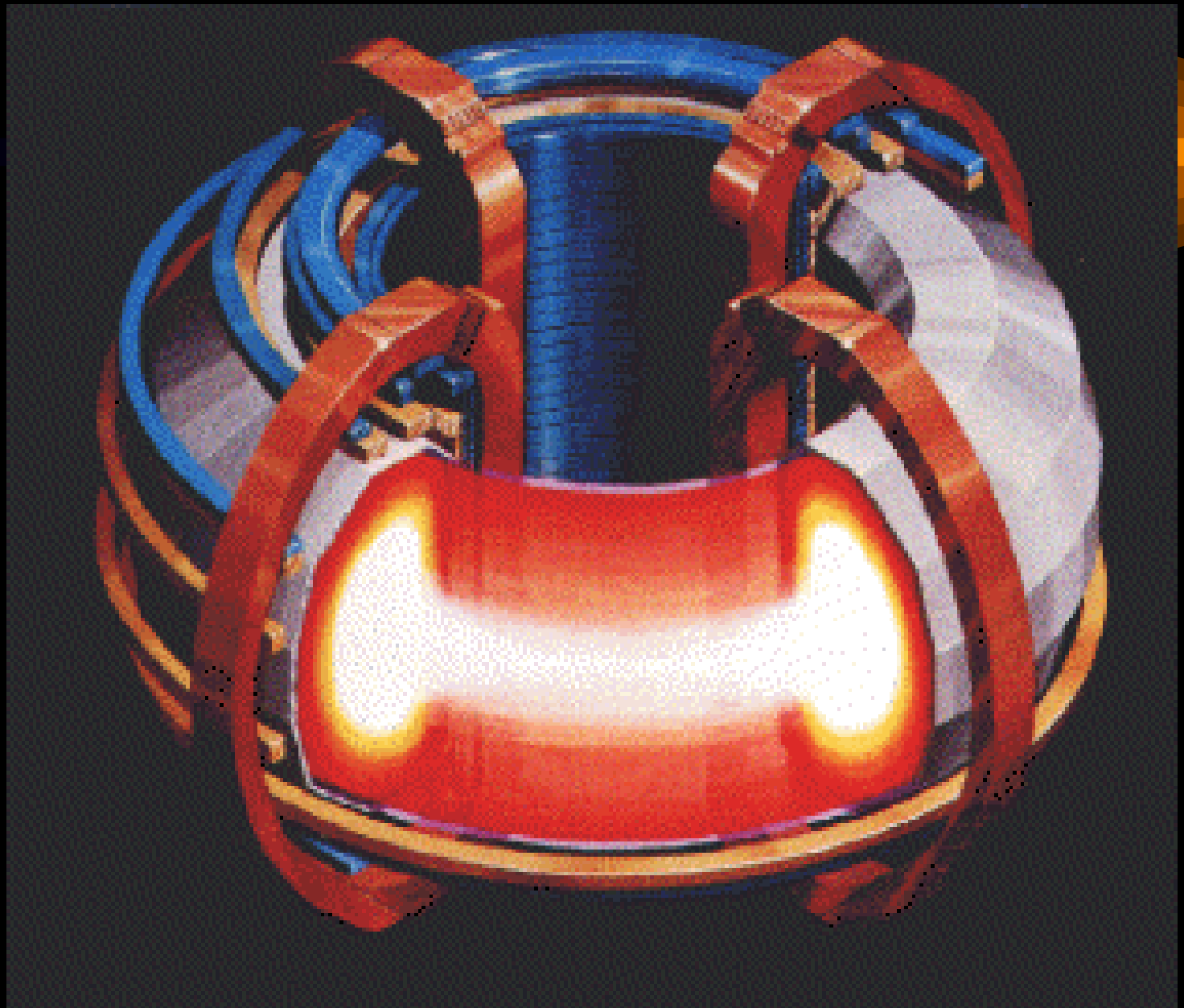

Natural Fusion Reactors vs Fusion Experiments on Earth

Plasma Physics:

- **Introductory: What is a Plasma?**
- **Characteristics & high energy density**

Introductory: What is a ***Plasma?***

Matter heated to high temperatures becomes a Plasma

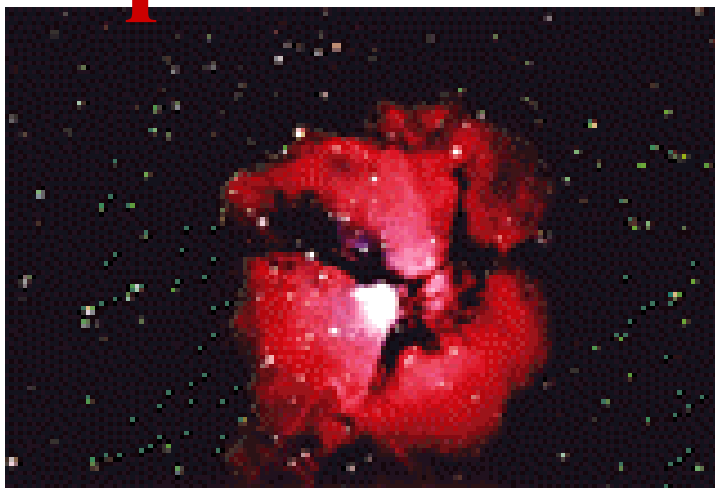

Four States of Matter

SOLID **LIQUID** **GAS** **PLASMA**

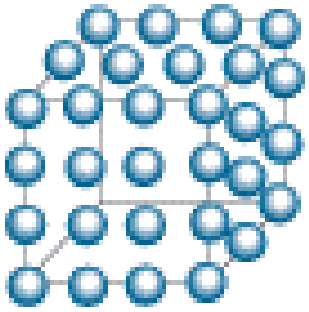

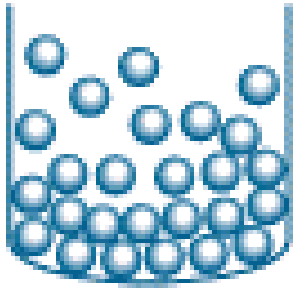

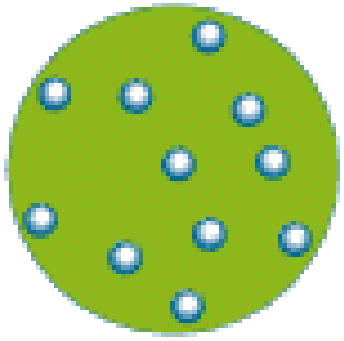

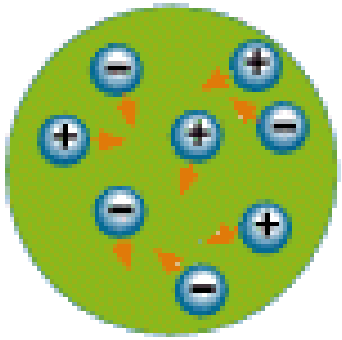

Characteristics of Plasma State

- **Presence of electrons and ions**
- **Electrically conducting**
- **Interaction with electric & magnetic fields**
- **Control of ions & electrons: applications**
- **High energy densities/selective particle energies**

-Cold plasmas: several eV's; (1eV~10^4K)

-Hot plasmas: keV's ; (1keV~10^7K)

- **Most of matter in Universe is in the Plasma State (e.g. the STARS)**

Major technological applications

- **Surface processing, cleaning, etching, deposition**
- **Advanced materials, diamond/CN films**
- **Environmental e.g.waste/water treatment**
- **High temperature chemistry**
- **MHD-converters, thrusters, high power switches**
- **Radiation sources: Microelectronics lithography**
- **Medical: diagnostics, cleaning, instrumentation**
- **Light sources, spectroscopic analysis, FP displays**
- **Fusion Energy**

The Singular, arguably Most Important Future Technological Contribution, essential to Continuing Progress of Human Civilization:-

A NEW LIMITLESS SOURCE OF ENERGY

Scenario: World Population stabilizes at 10 billion; consuming energy at 2/3 US 1985 per capita rate

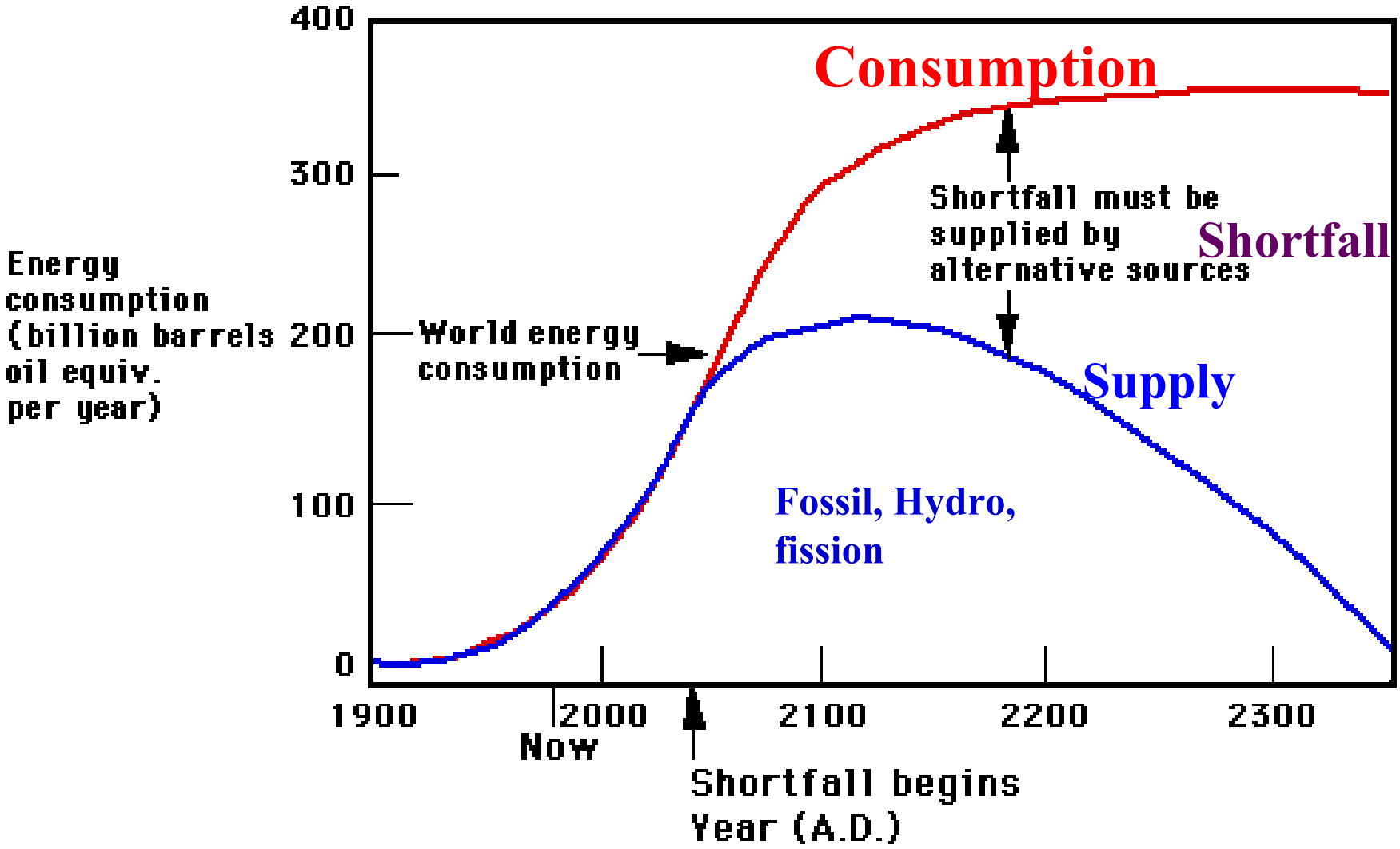

Plasma Fusion (CTR) & the Future of Human Civilization

A new source of abundant (limitless) energy is needed for the continued progress of human civilization.

Mankind now stands at a dividing point in human history:

- **200 years ago, the Earth was under-populated with abundant energy resources**
- **100 years from now, the Earth will be over-crowded, with no energy resources left**

Without a new abundant source of energy

Human civilization cannot continue to flourish.

Only 1 good possibility:

Fusion (CTR) Energy from Plasma Reactors

The fusion process

Collisions in a Plasma

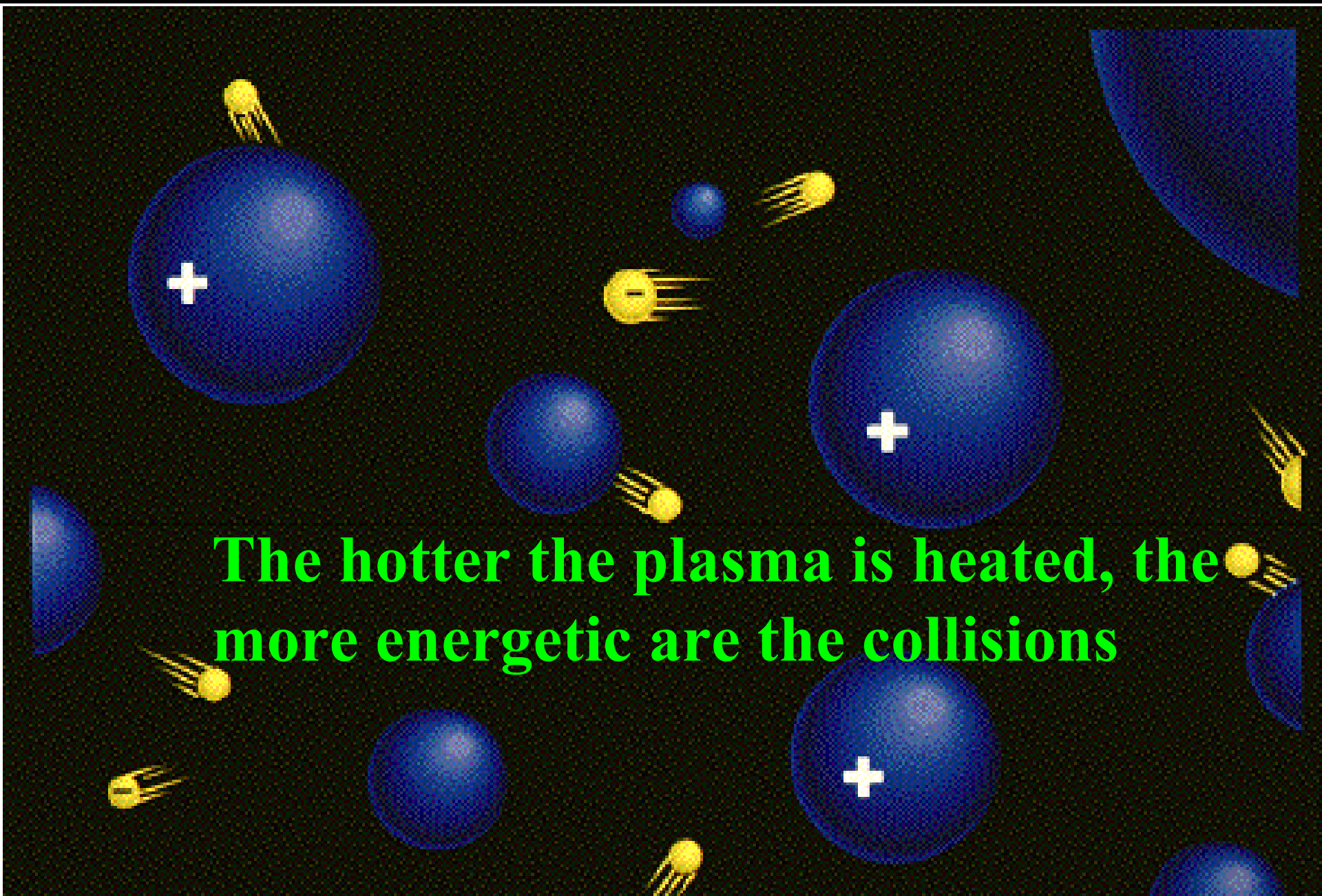

Nuclear Fusion

If a Collision is sufficiently energetic, nuclear fusion will occur

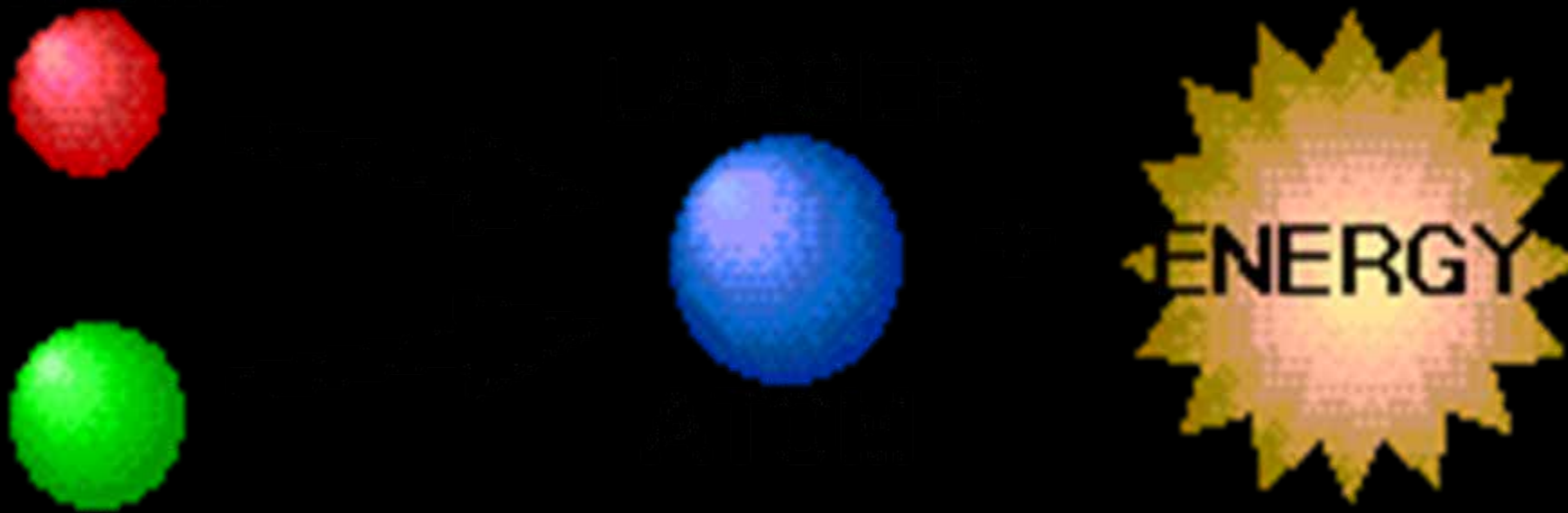

Isotopes of hydrogen- Fuel of Fusion

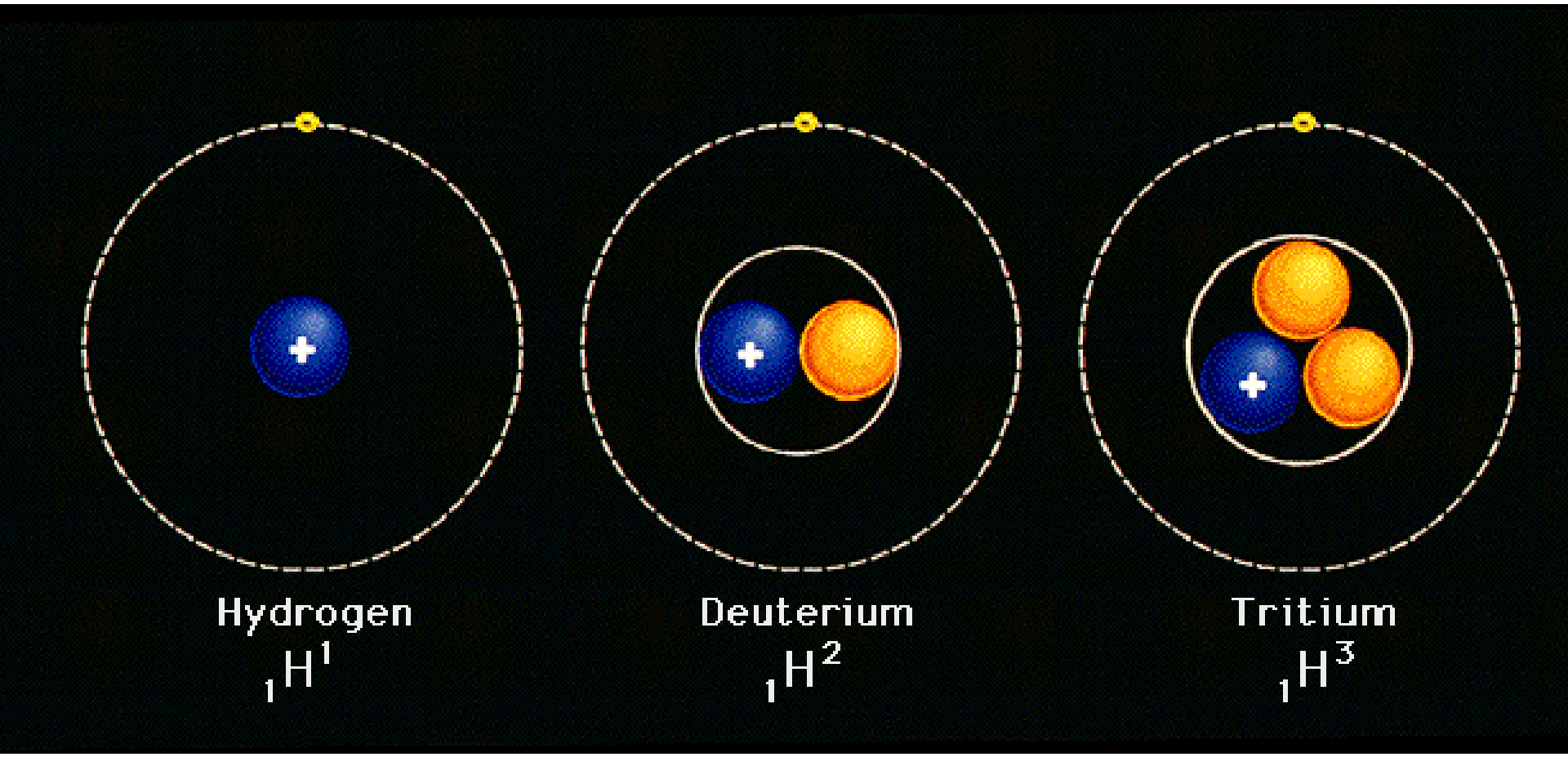

Release of energy in Fusion

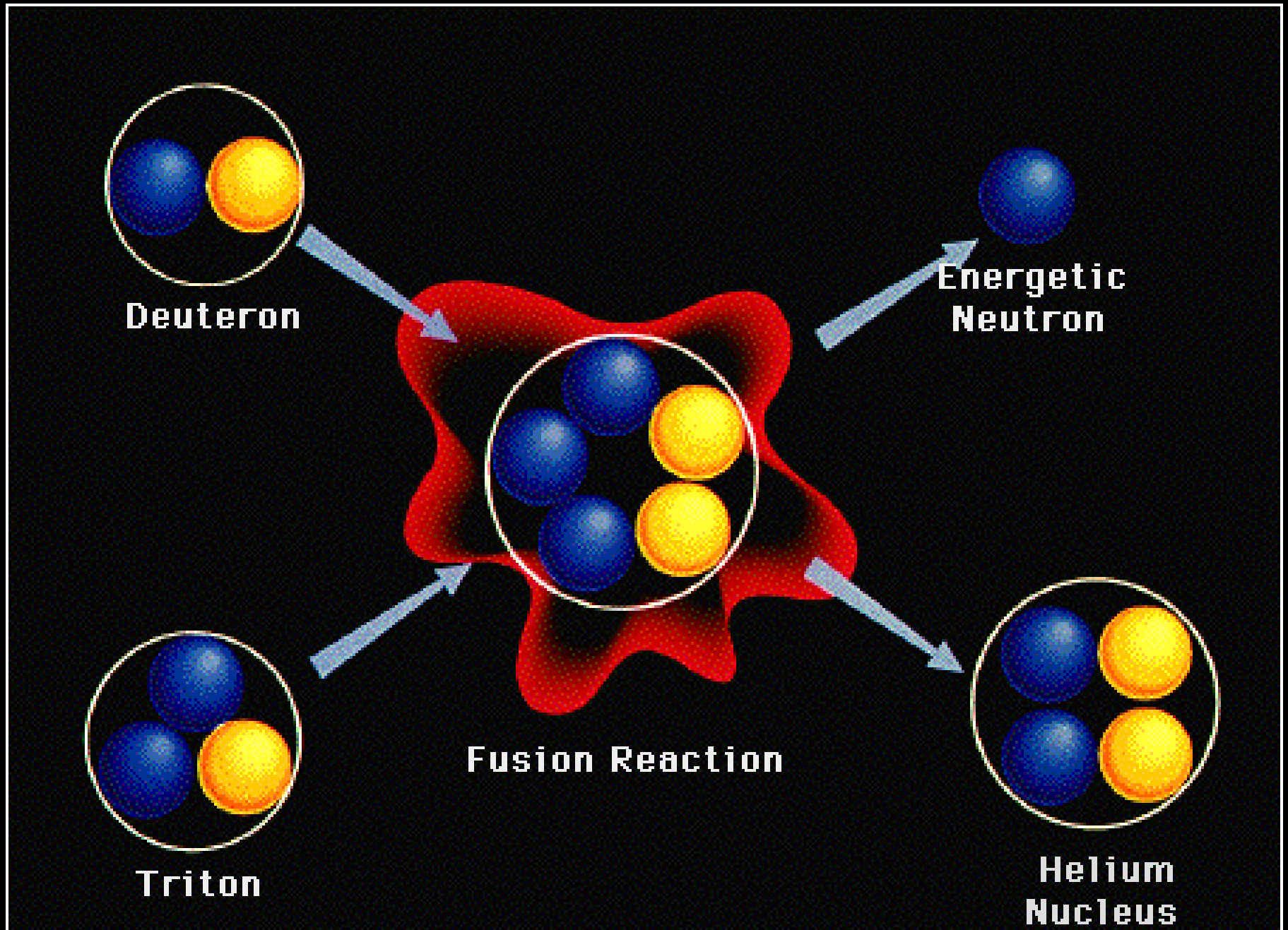

Conversion of mass into Energy

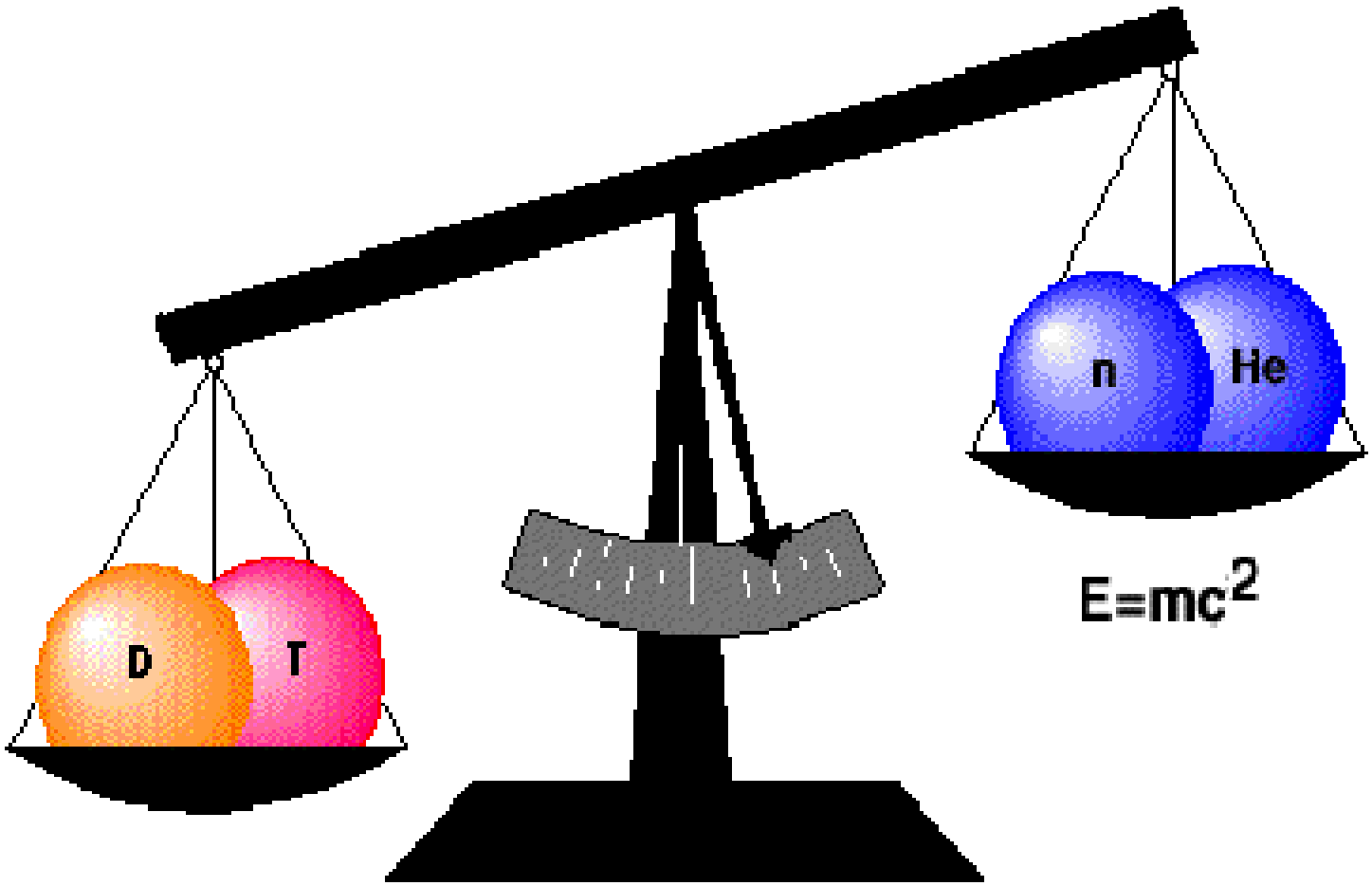

Fusion Energy Equivalent

50 cups water

=

- **1 thimble heavy water, extracted from 50 cups of water**

=

Summary of Conditions

Technological Targets:

- **T> 100 million K (10keV)**
- **nt>10^{21} m^{-3}-sec**

Two approaches:

n=10^{20} m^{-3}, confined t=10s
(low density, long-lived plasma) or :

n=10^{31} m^{-3}, confined 10^{-10}s
(super-high density, pulsed plasma)

Combined: ntT>$10^{22}$$m^{-3}$-sec-keV

Containing the Hot Plasma

Long-lived low-density Confinement

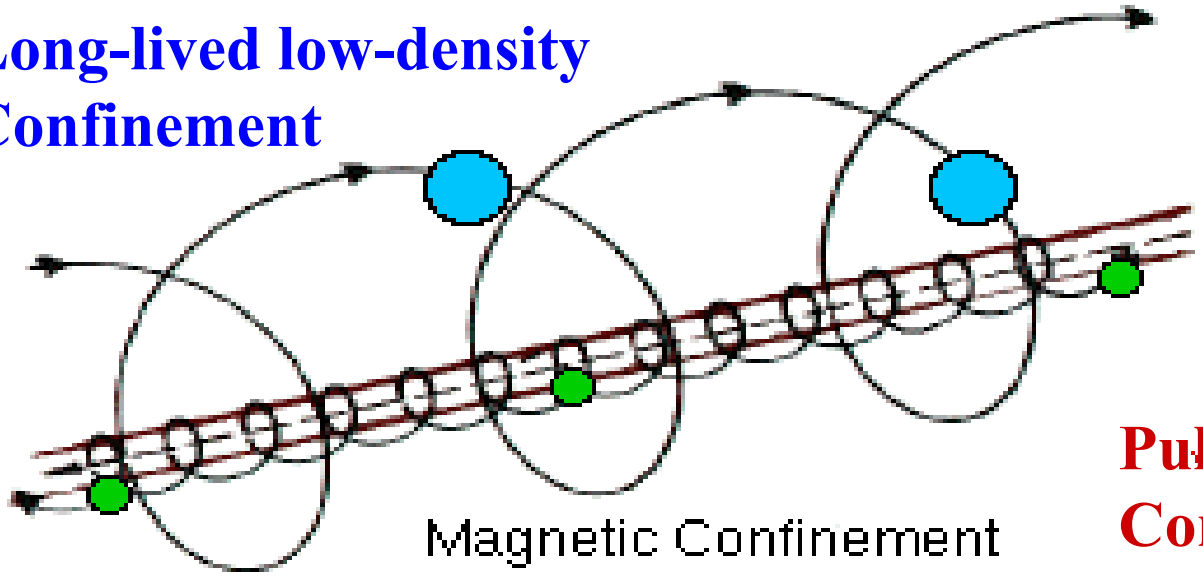

Magnetic Confinement

Pulsed High Density Confinement

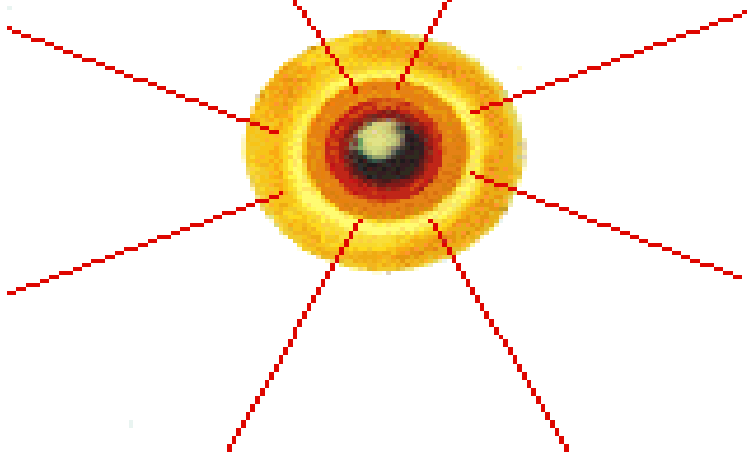

Inertial Confinement Using Lasers

Continuous Confinement

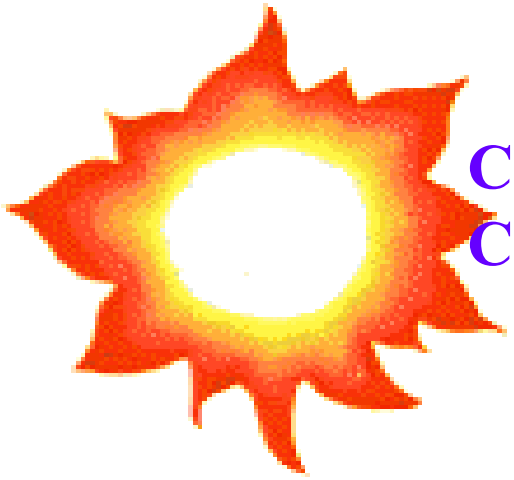

Gravitational Confinement in the Sun and Stars

Low Density, Long-lived Approach (Magnetic Compression)

Tokamak

- **Electric currents for heating**
- **Magnetic fields in special configuration for stability**

Schematic of Tokamak

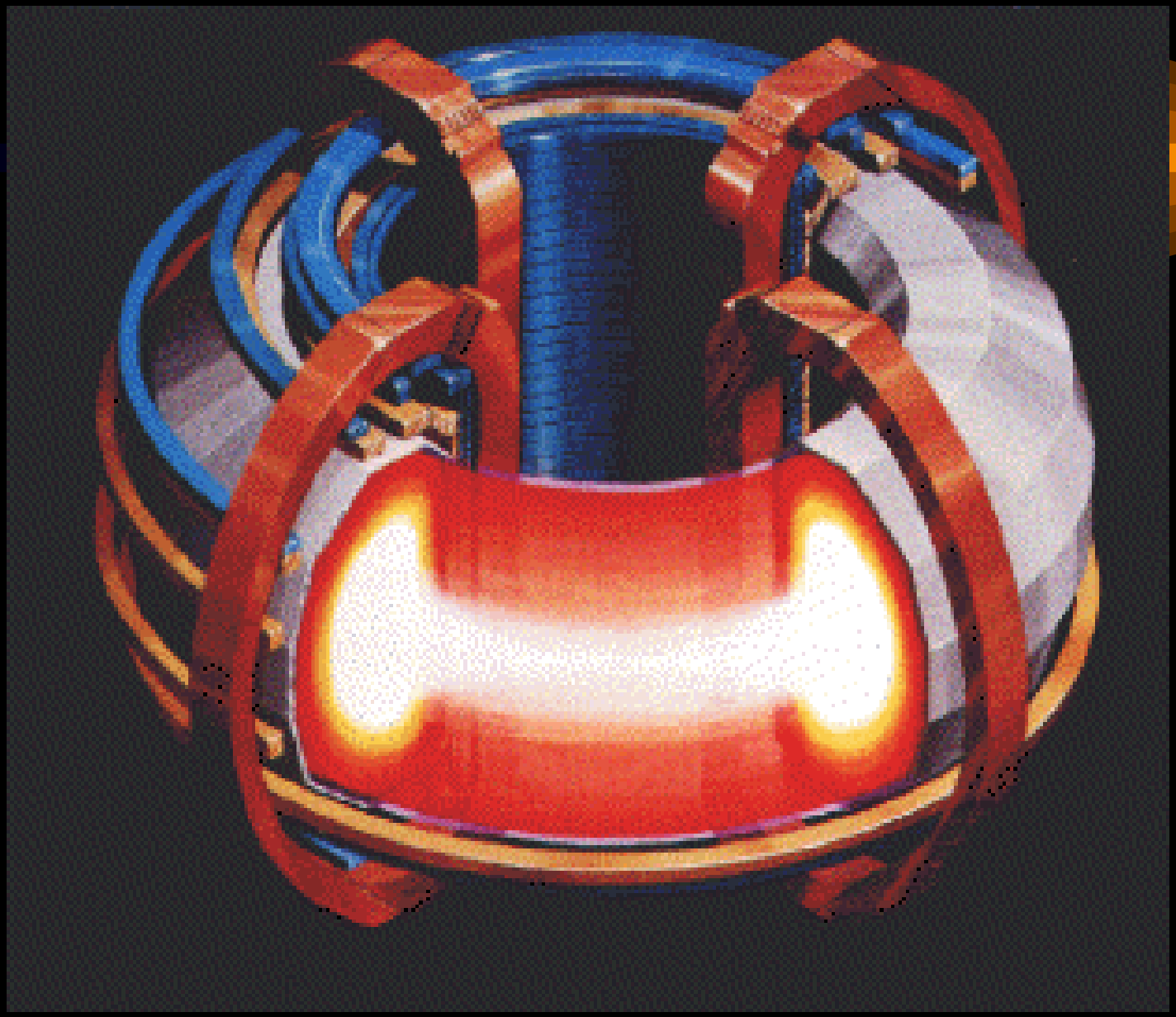

Magnetic Yoke to induce Plasma Current

Field Coils to Produce suitable Magnetic Field Configuration

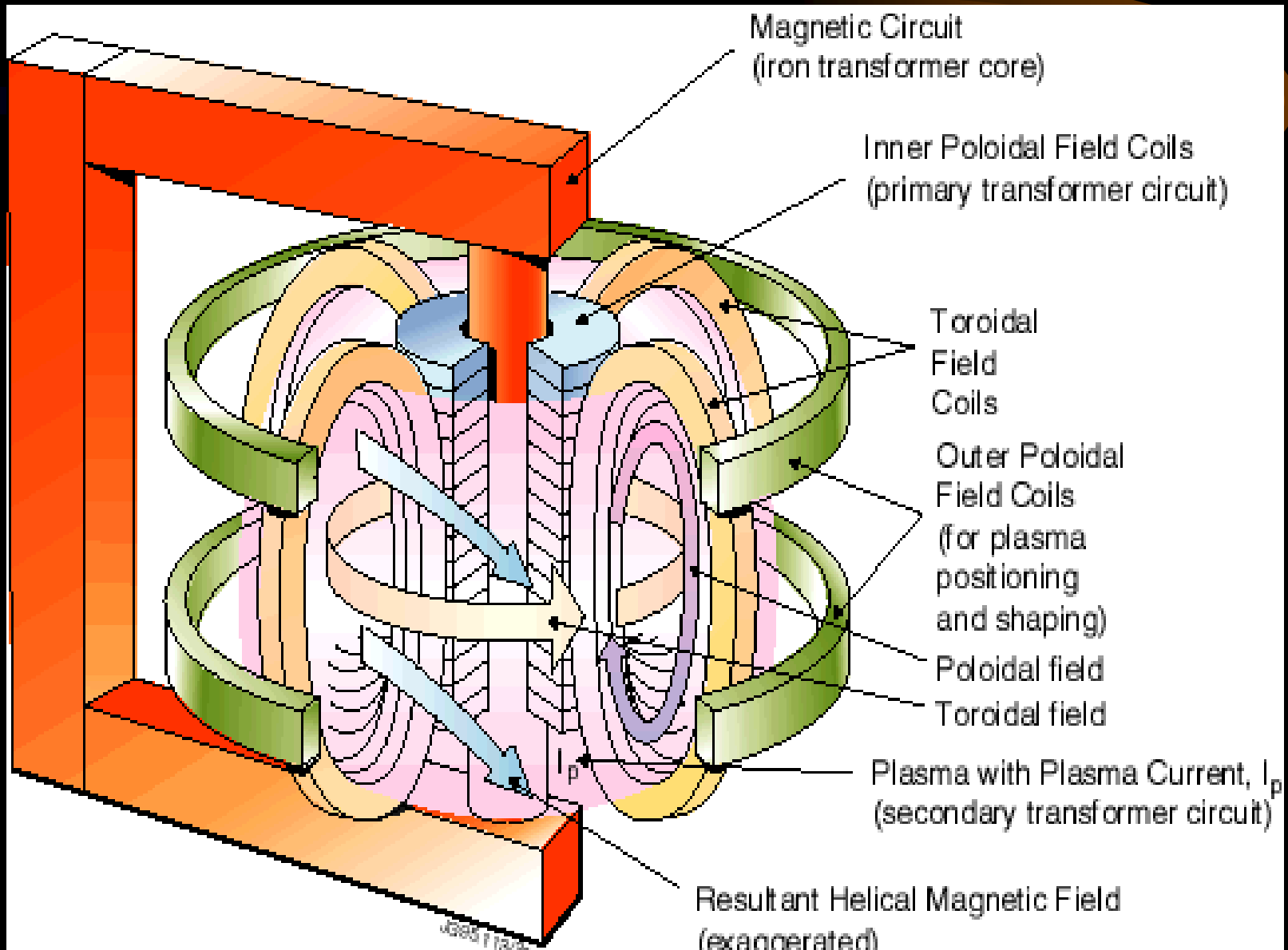

JET (Joint European Torus)

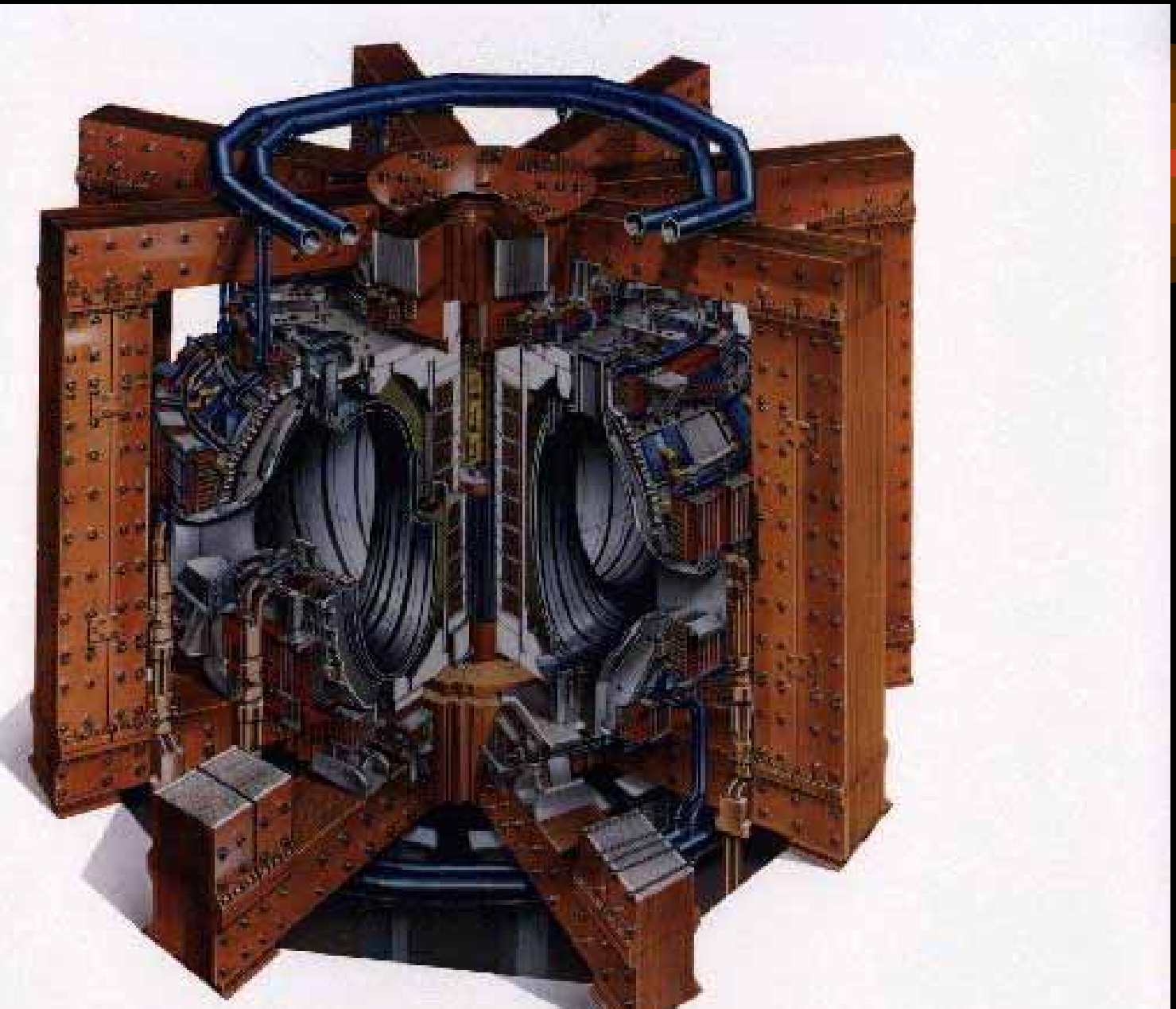

Project successfully completed January 2000

Inside JET

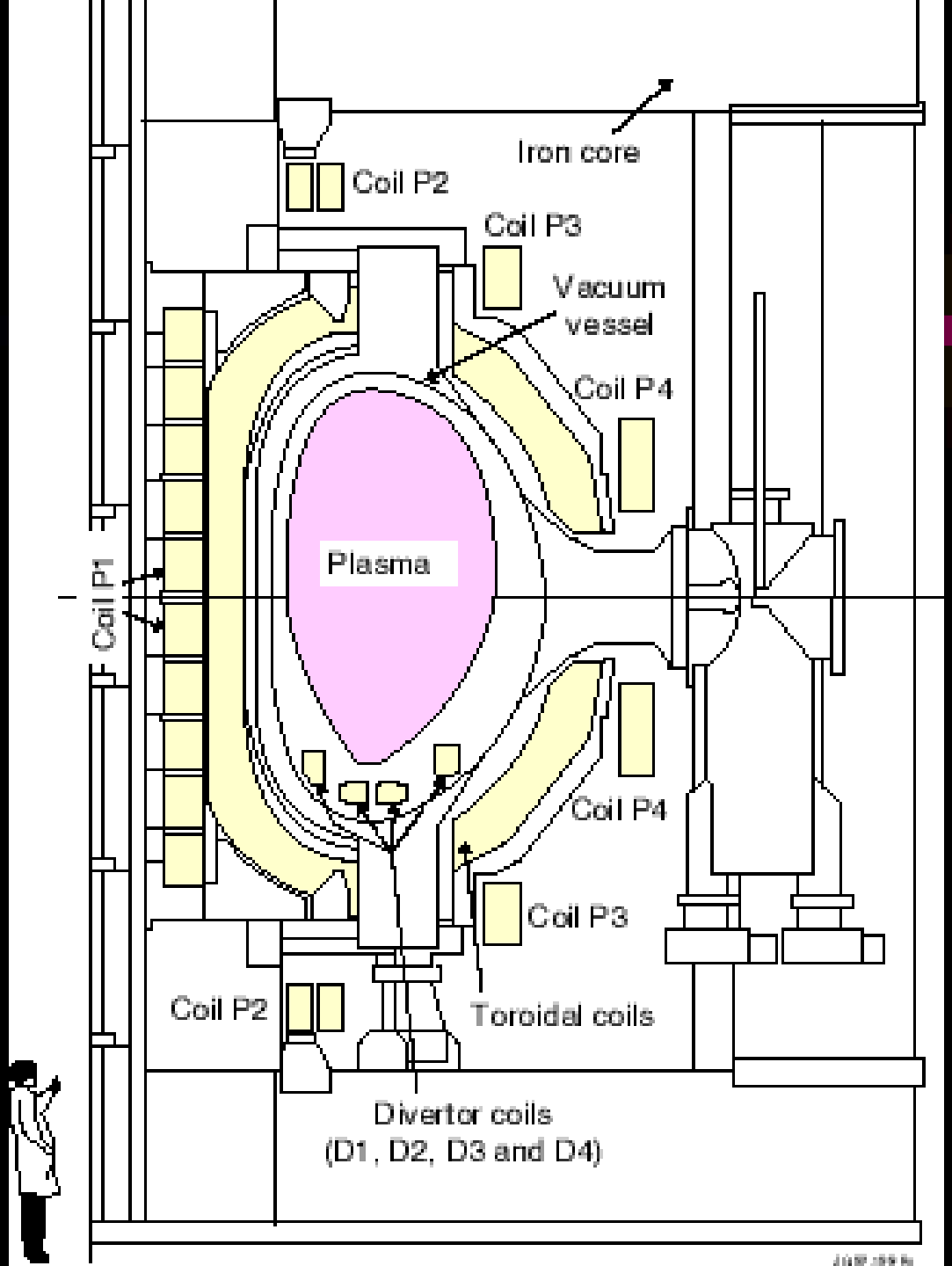

JET X-Section

Energy confinement time t scales as some functions of:

- **Plasma current I_p**
- **Major Radius R**
- **Minor radius 'a'**
- **Toroidal Magnetic Field B**

scaling law: $t \sim I_p^{\alpha} R^{\beta} a^{\gamma} B^{\lambda}$

indices $\alpha,\beta,\gamma,\lambda$ all positive

To achieve sufficient value of ntT requires:

scaling of present generation of Tokamaks upwards in terms of:

I_p, R, 'a' and B.

Fusion Temperature attained
Fusion confinement one step away

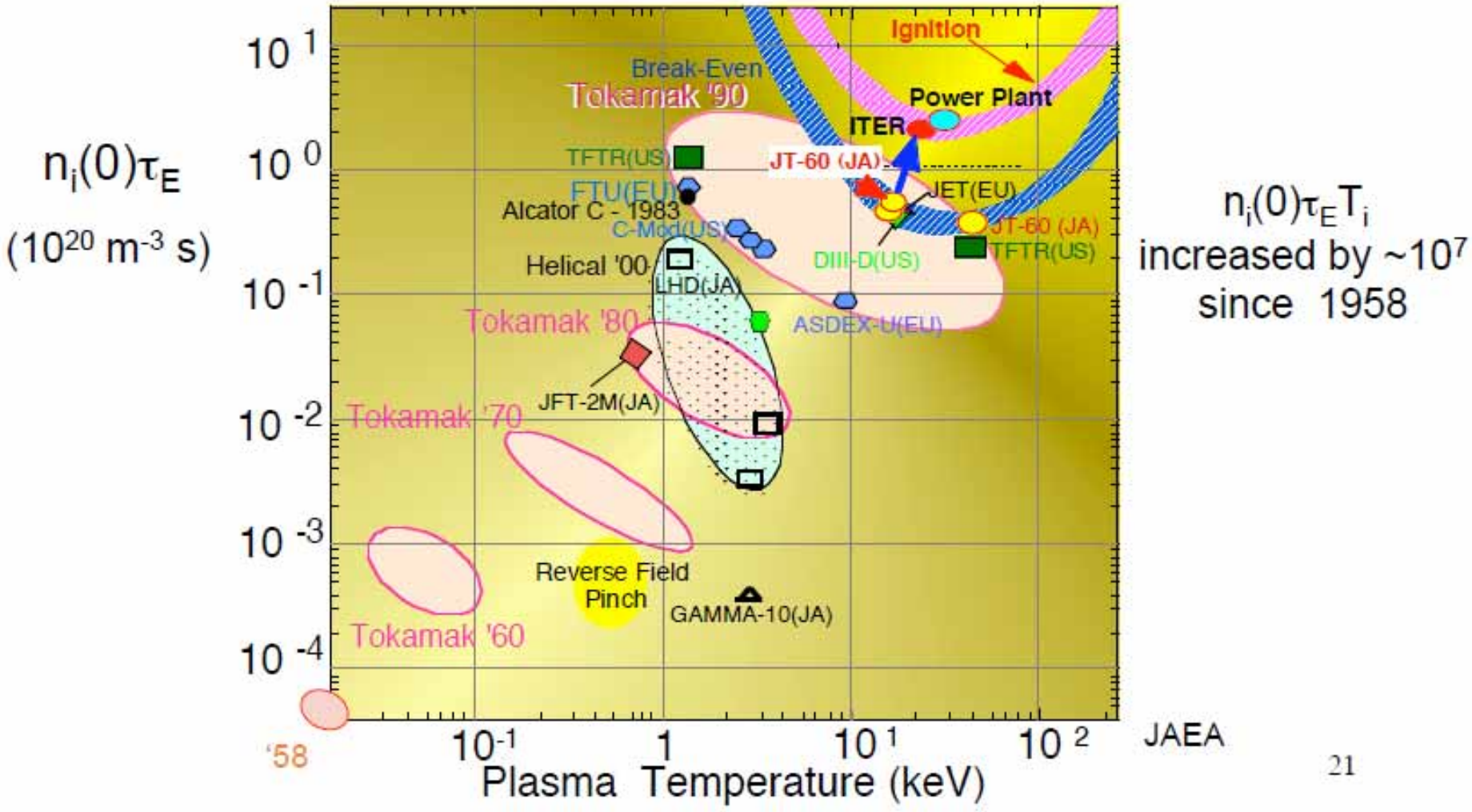

International Collaboration to develop Nuclear Fusion Energy-ITER

- 1985- Geneva Superpower Summit:
- Reagan (US) & Gorbachev (Soviet Union) agreed on project to develop new cleaner, sustainable source of energy- Fusion energy
- ITER project was born
- Initial signatories: former Soviet Union, USA, European Union (via EURATOM) & Japan
- Joined by P R China & R Korea in 2003 & India 2005
- ITER Agreement- signed in November 2006

ITER (International Thermonuclear Experimental Reactor)

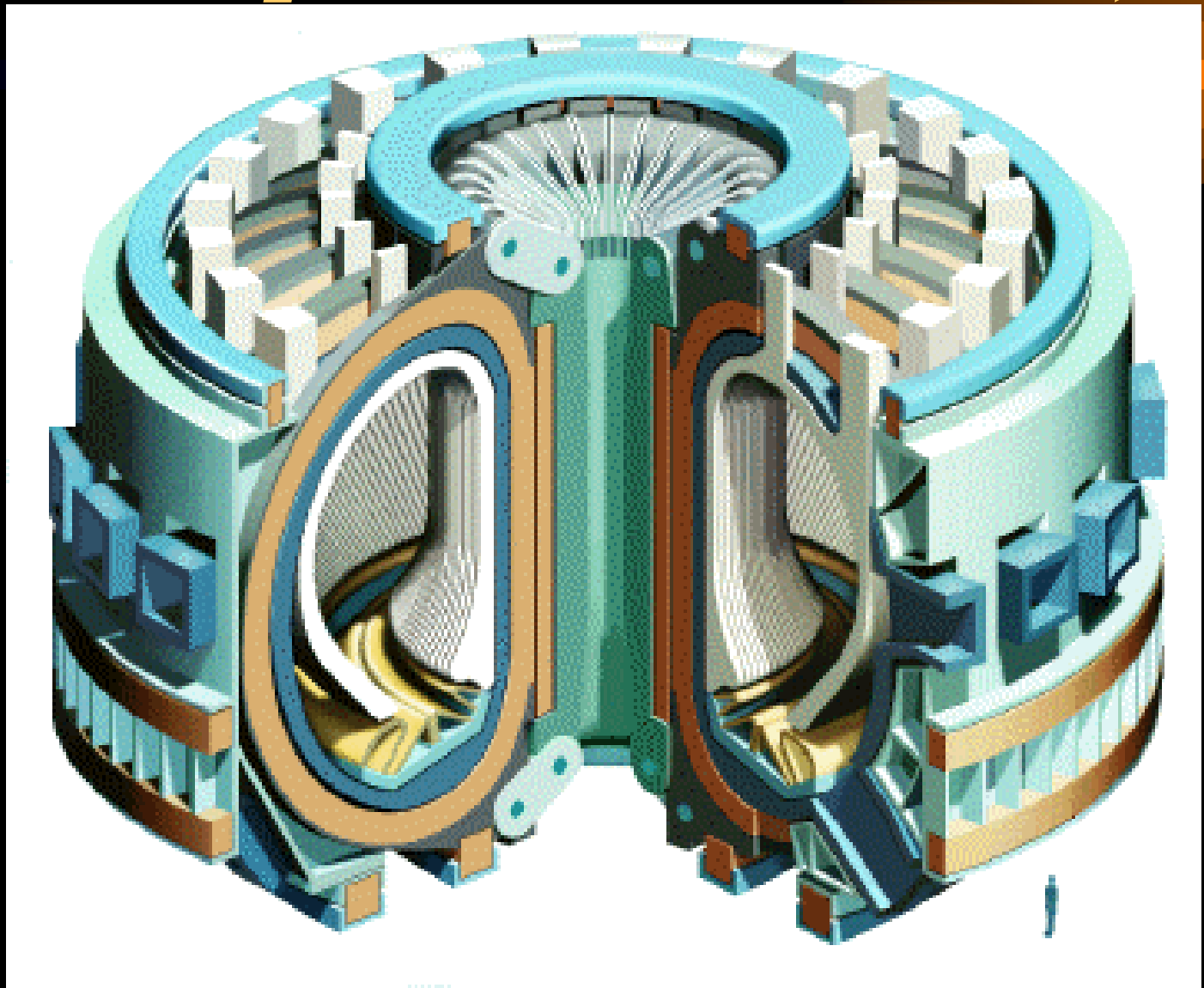

ITER Construction has now started in Cadarache, France

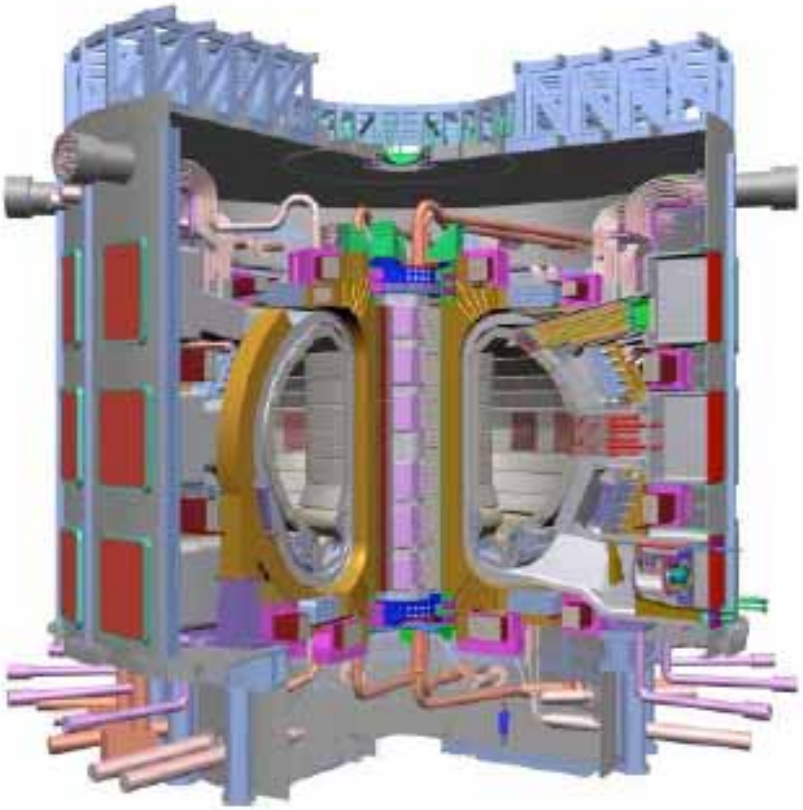

Reactor scale

ITER Site Under Construction

First plasma planned 2018

First D-T planned 2022

Q>10 and Beyond

ITER : to demonstrate: possible to produce commercial energy from fusion.

Q= ratio of fusion power to input power.

Q ≥ 10 represents the scientific goal of ITER :

to deliver 10x the power it consumes.

From 50 MW input power to 500 MW of fusion power - first fusion experiment to produce net energy.

Beyond ITER will be DEMO (early 2030's), demonstration fusion power plant which will put fusion power into the grid as early as 2040

FIRE: Incorporates Many Advanced Features

FIRE Incorporates Advanced Tokamak Innovations

AT Features

- DN divertor
- strong shaping
- very low ripple
- internal coils
- space for wall stabilizers
- inside pellet injection
- large access ports

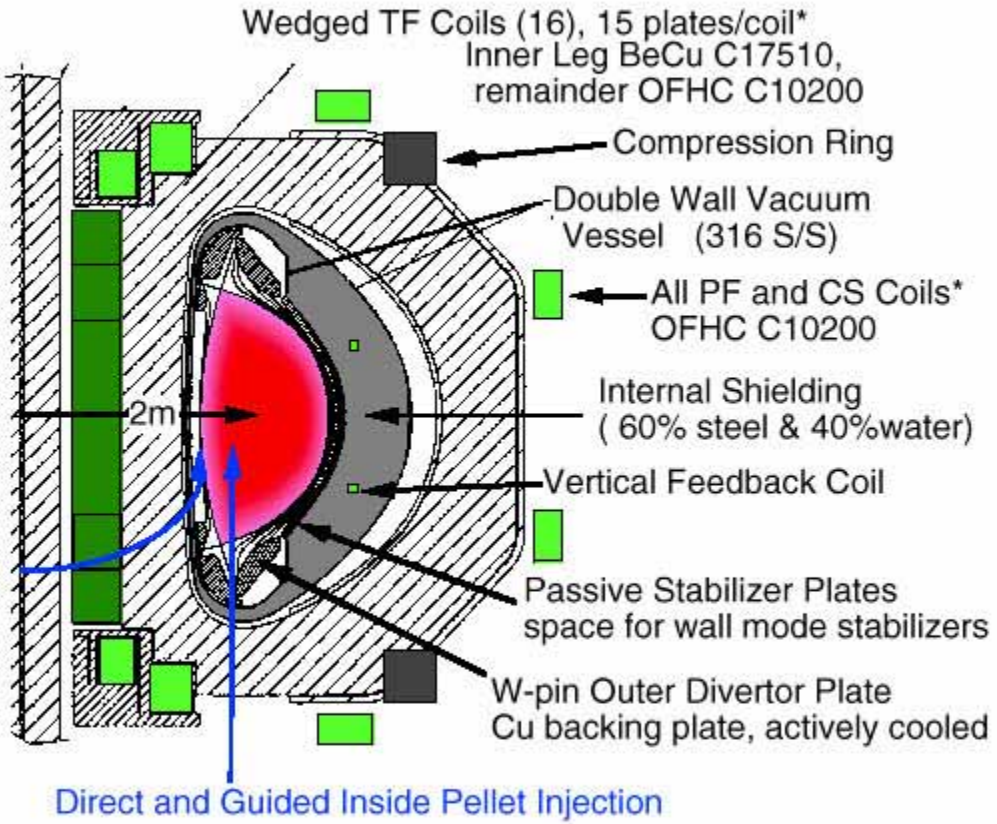

*Coil systems cooled to 77 °K prior to pulse, rising to 373 °K by end of pulse.

Potential Next Step Fusion Burning Experiments

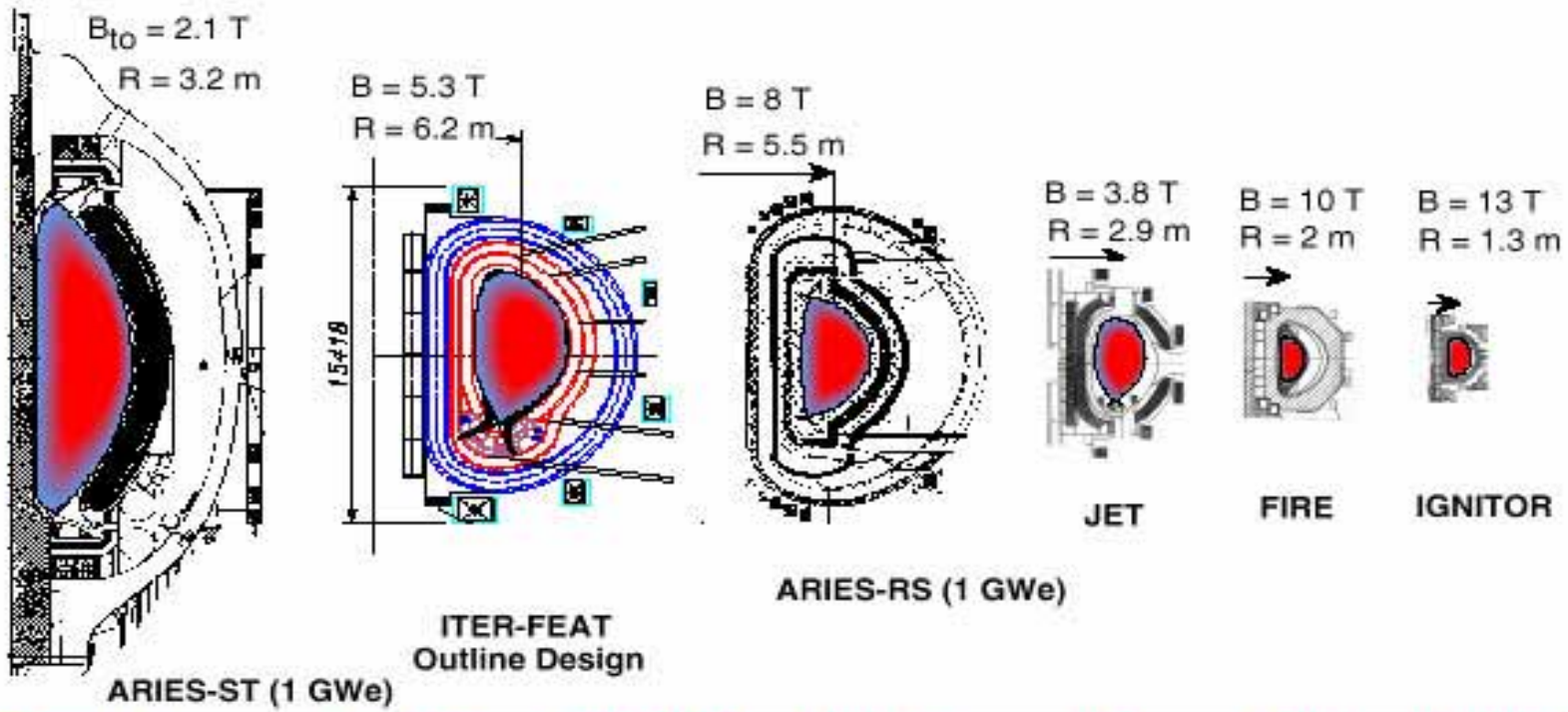

Cost Drivers	ARIES-ST	ITER-FEAT	ARIES-RS	JET	FIRE	IGNITOR
Plasma Volume (m^3)	810	837	350	95	18	11
Plasma Surface (m^2)	580	678	440	150	60	36
Plasma Current (MA)	28	15	11	4	6.5	12
Magnet Energy (GJ)	29	50	85	2	5	5
Fusion Power (MW)	3000	500	2200	16	200	100
Burn Time (s), inductive	steady	300	steady*	1	20	5

* assumes non-inductive current drive

The other approach: Pulsed Super-high Density (Inertial Compression)

- Radiation Compression

Pulsed Fusion: Radiation Compression

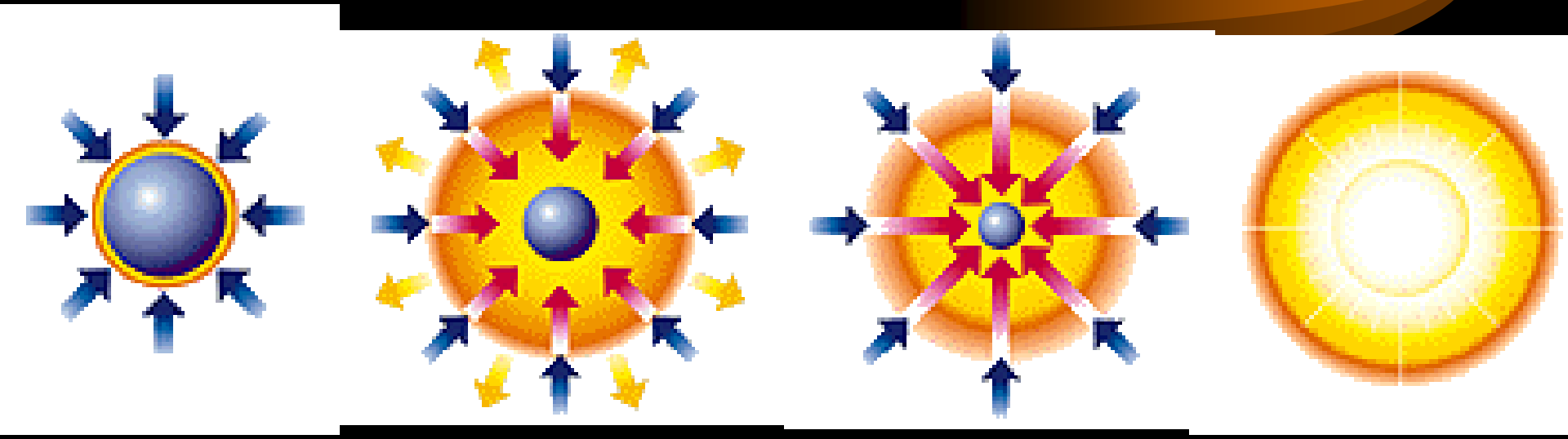

Radiation Pressure

e.g. powerful lasers beamed from all directions onto D-T pellet (0.1mm radius)

Compression:

fuel is compressed by rocket-like blow-off of hot surface material

Ignition:

density of fuel core reaches 1000 times density of water & ignites at 100 million K

Burn:

Thermonuclear fusion spreads rapidly through super-compressed fuel yielding many times input energy

Cross-sectional view of the KOYO-F fast ignition reactor (Norimatsu et al.)

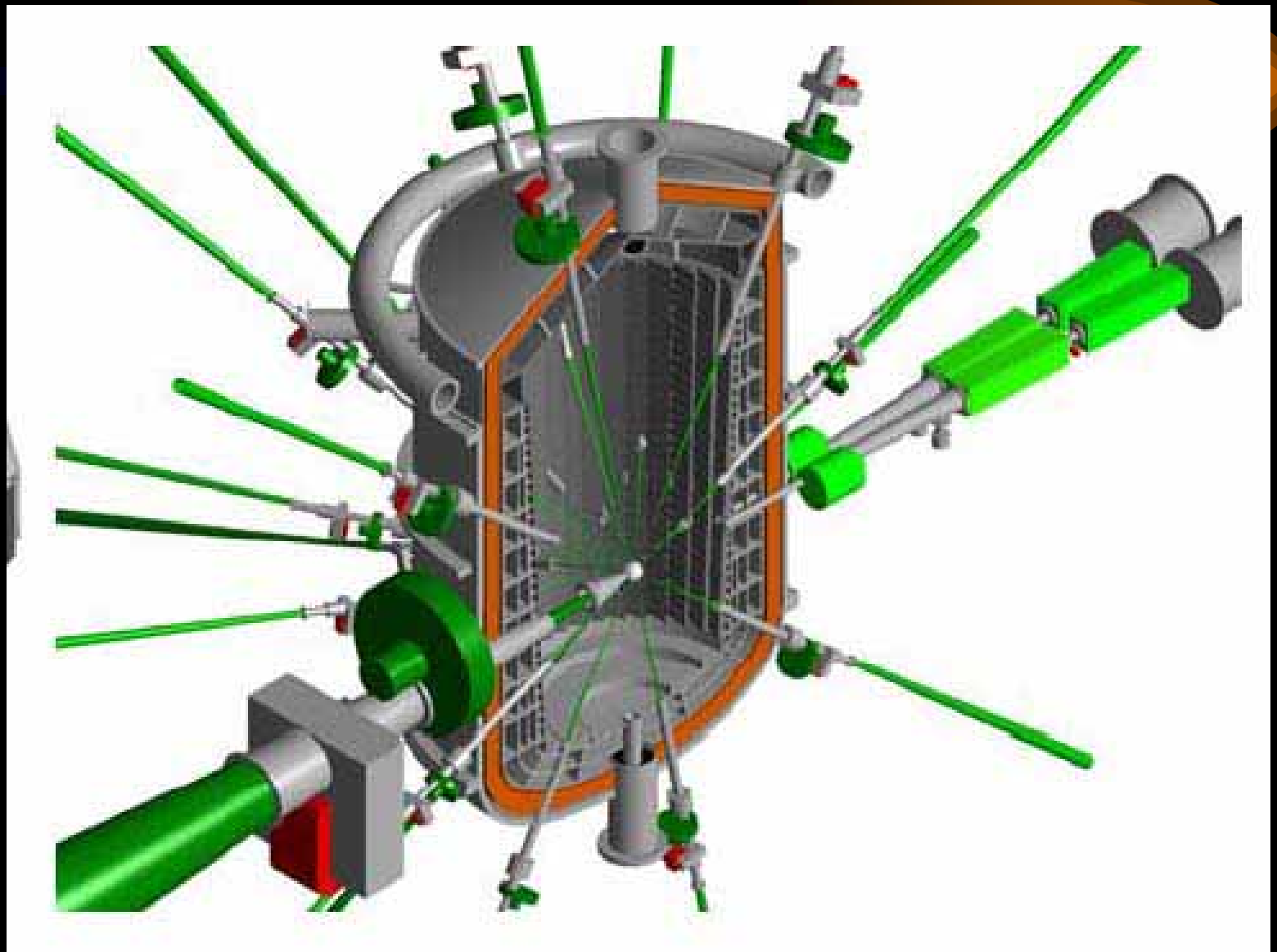

Large scale Fusion Experiments

- **Tokamaks: Low density, long confinement plasmas**
- **Laser Implosions: Super-dense, sub-nanosecond plasmas**

Smaller scale Fusion Experiments

Pinches: Dense, microsecond plasmas

Introduction

- **Plasma Focus (PF)-**
  - **remarkably copious source of multiple radiation: x-rays, fast electrons, ions and plasma stream**
  - **Fusion neutrons demonstrated even in table top devices**
  - **same energy density at storage energy levels of 0.1-1000 kJ; hence scalability of neutrons**

Superior method for dense pinches

- **The PF produces suitable densities and temperatures.**

- **A simple capacitor discharge is sufficient to power the plasma focus.**

THE PLASMA FOCUS (PF)

- **The PF is divided into two sections**.
- **Pre-pinch (axial) section**: Delays the pinch until the capacitor discharge current approaches peak value.
- **The pinch starts & occurs at top of the current pulse**.

The Plasma Dynamics in Focus

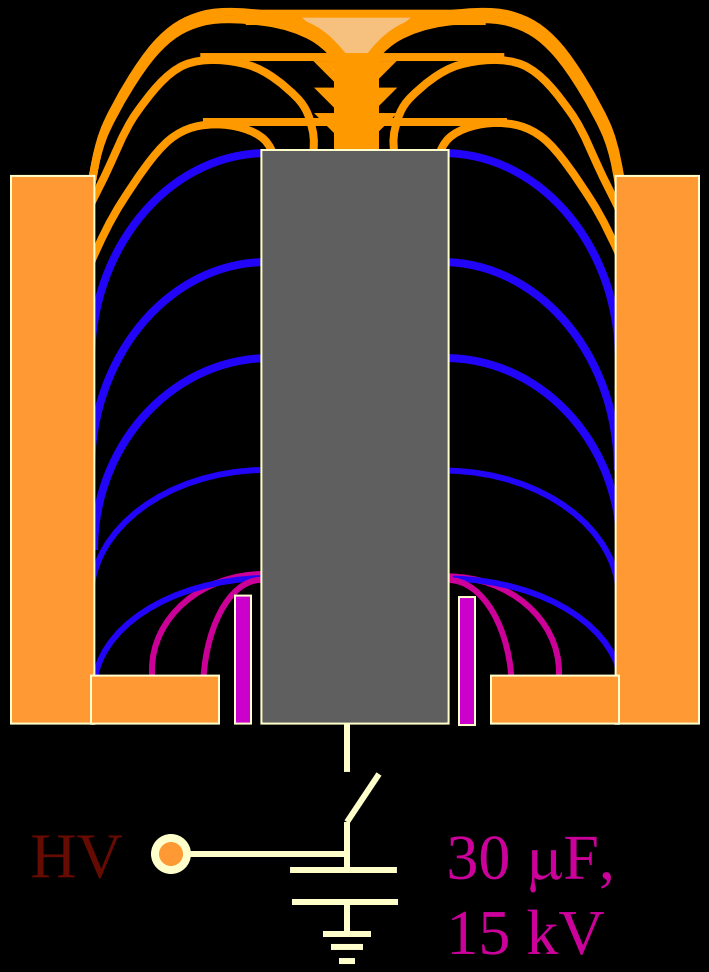

Radial Phase

Axial Accelaration Phase

Inverse Pinch Phase

Radial Compression (Pinch) Phase of the Plasma Focus

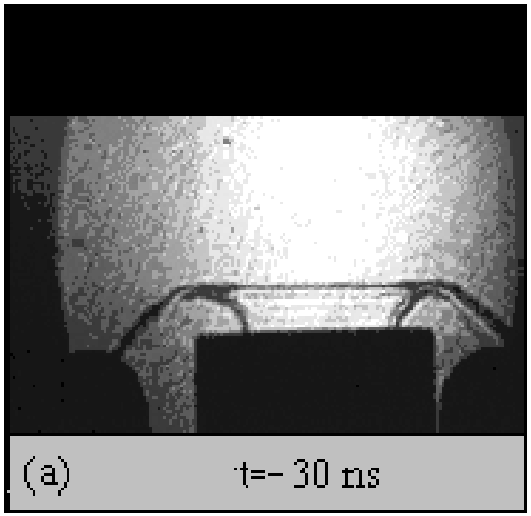

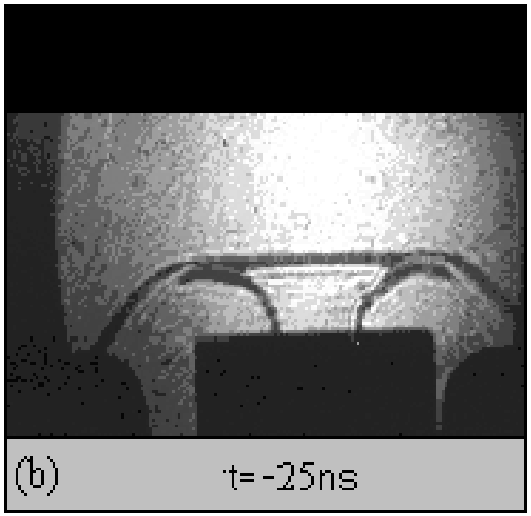

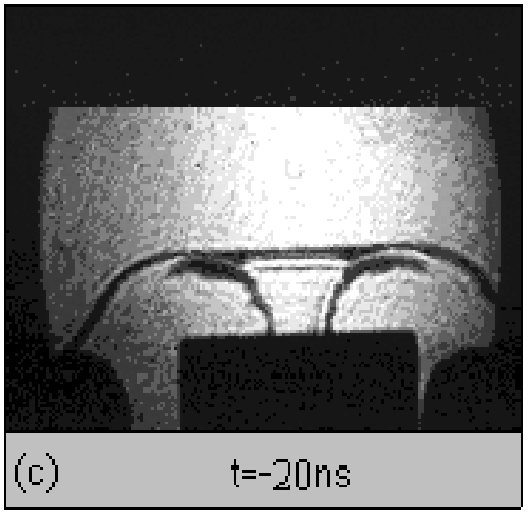

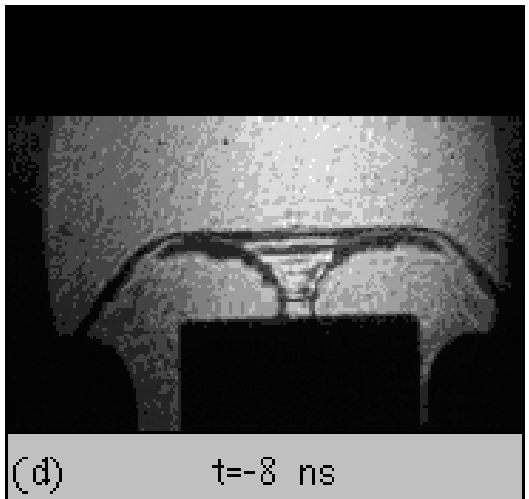

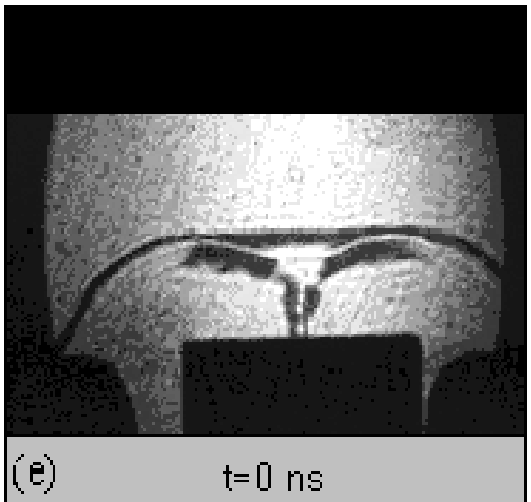

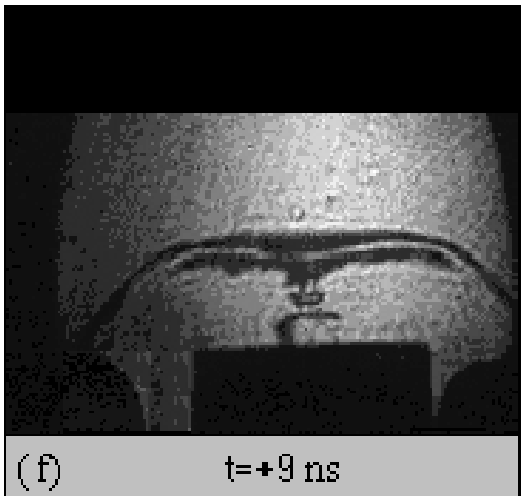

High Power Radiation from PF

- **powerful bursts of x-rays, ion beams, REB's, & EM radiation (>10 gigaW)**
- **Intense radiation burst, extremely high powers**
- **E.g. SXR emission peaks at 10^9 W over ns**
- **In deuterium, fusion neutrons also emitted**

Same Energy Density in small and big PF devices leads to:

- Scalability
  - constant speed factor, $[(I/a)/\rho^{1/2}]$ for all machines, big or small lead to same plasma energy density

- from 0.1 to 1000 kJ of storage energy
  - predictable yield of radiation

One of most exciting properties of plasma focus is its neutron yield Y_n

- **Early experiments show: $Y_n \sim E_0^2$**
- **Prospect was raised in those early research years that, breakeven could be attained at several tens of MJ .**
- **However quickly shown that as E_0 approaches 1 MJ, a neutron saturation effect was observed; Y_n does not increase as much as expected, as E_0 was progressively raised towards 1 MJ.**
- **Question: Is there a fundamental reason for Y_n saturation?**

Chart from M Scholz (November 2007 ICDMP)

Scaling

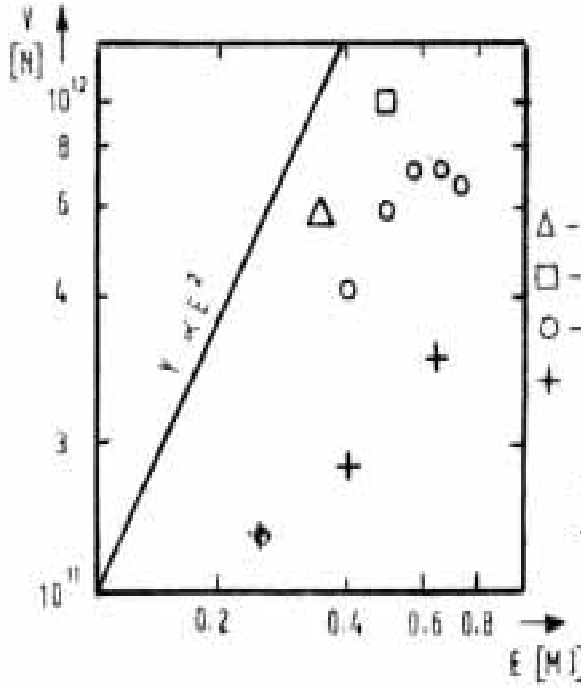

$$\frac{1}{2}(L+L_0)I^2 \cong \gamma E$$

$$L \cong L_0$$

$$Y_n \propto E^2$$

$$I^2 \propto E$$

Frascati (Program Euroatom), $E_b = 1MJ$; $U_b = 50\ kV$;

Y_n 'saturation' observed in numerical experiments (small black crosses) compared to measurements on various machines (larger coloured crosses) -IPFS

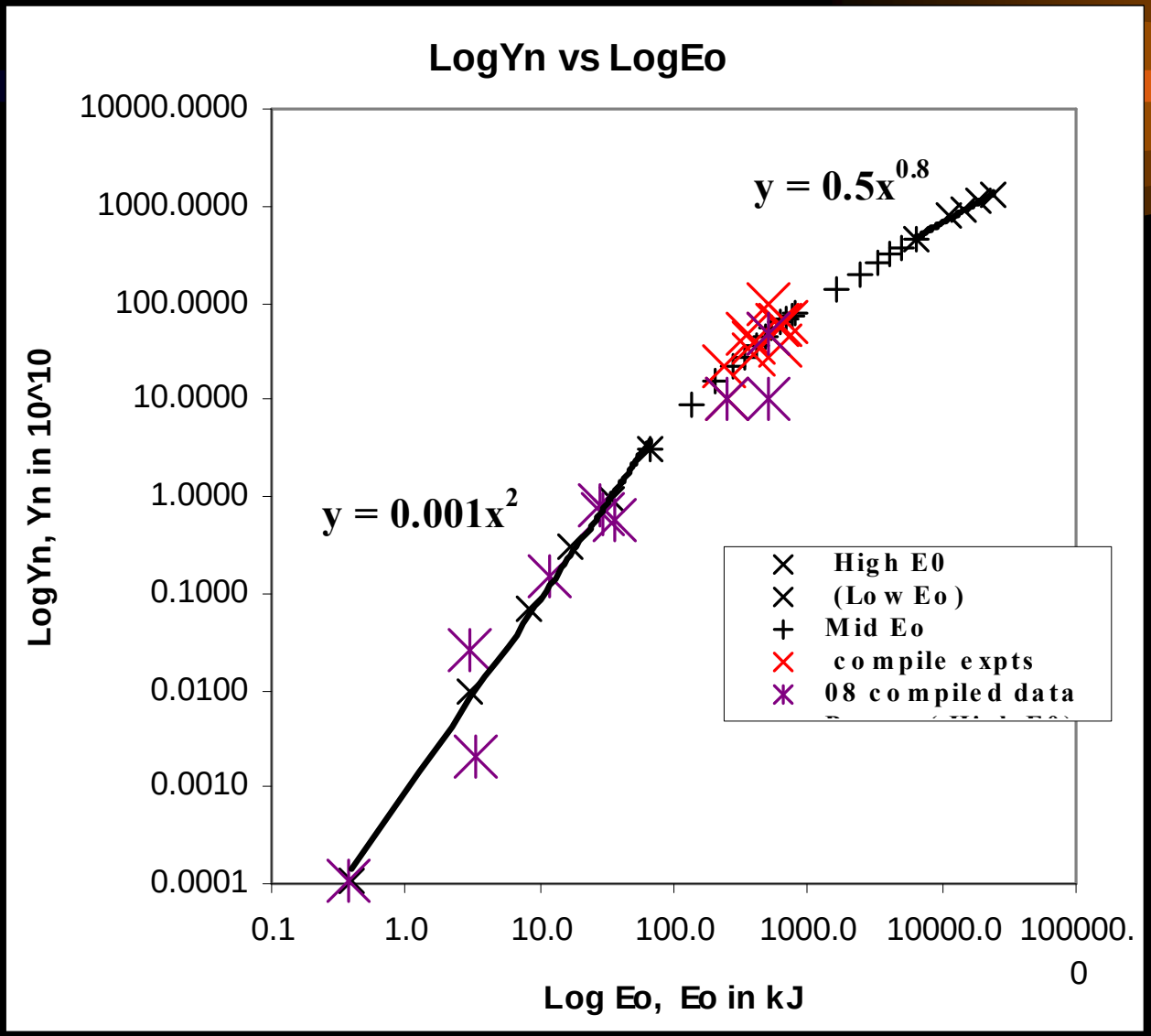

Comparing generator impedance & Dynamic Resistance DR_0 of small & large plasma focus- before I_{peak}

PF	$Z_0 = (L_0/C_0)^{1/2}$	Axial DR_0	Axial dominance	I_{peak}
Small	100 mΩ	7 mΩ	Z_0	~ V_0/Z_0
Large	1 mΩ	7 mΩ	DR_0	~V_0/DR_0

As E_0 is increased by increasing C_0, with voltage kept around tens of kV, Z_0 continues to decrease and I_{peak} tends towards asymptotic value of V_0/DR_0

Confirming I_{peak} saturation is due to constancy of DR_0

I_{peak} vs E_0 from DR_0 analysis compared to model simulation

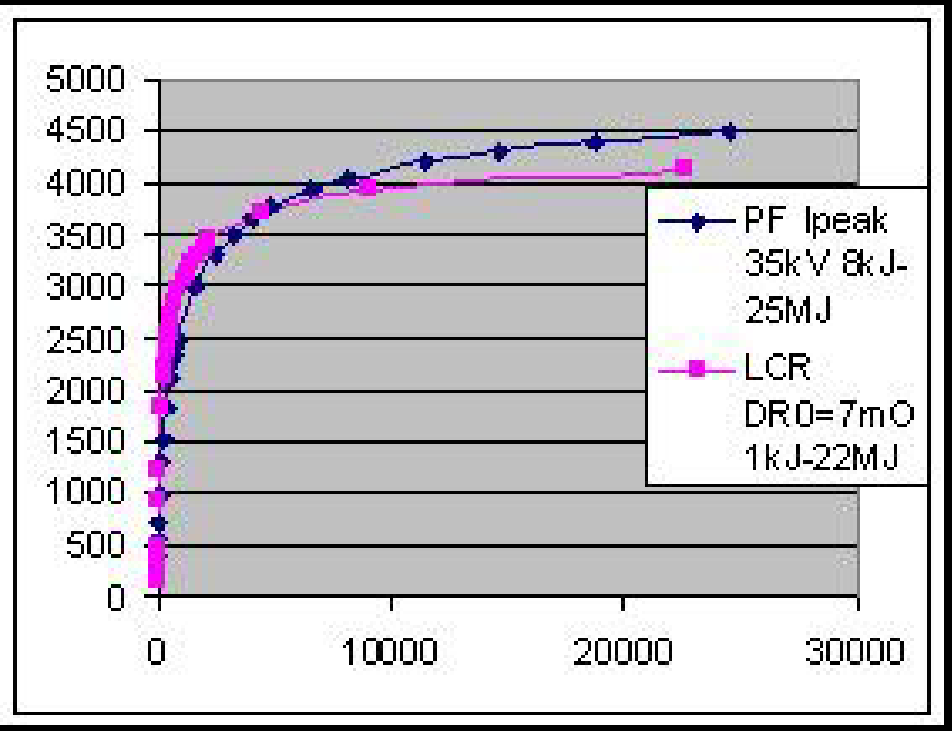

Model simulation gives higher I_{peak} due to a 'current overshoot effect' which lifts the value of I_{peak} before the axial DR_0 fully sets in

I_{peak} vs E_0 on log-log scale DR_0 analysis

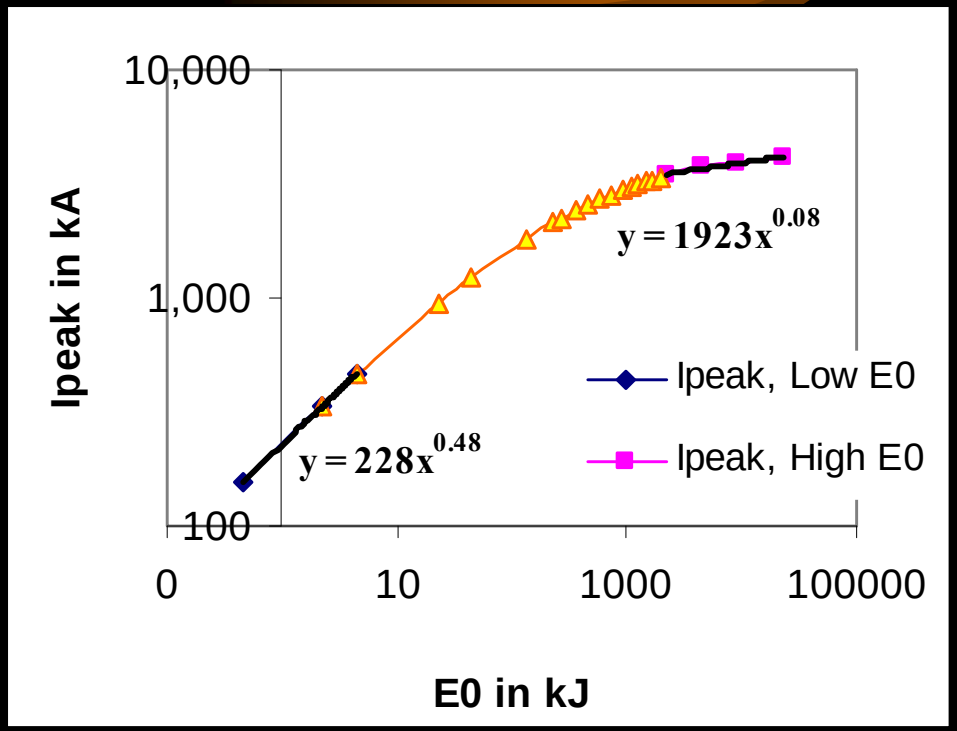

Confirming that I_{peak} scaling tends to saturate before 1 MJ

At IPFS, we have shown that: constancy of DR_0 leads to current 'saturation' as E_0 is increased by increasing C_0. Tendency to saturate occurs before 1 MJ

From both numerical experiments as well as from accumulated laboratory data:

- $\mathbf{Y_n \sim I_{pinch}^{4.5}}$
- $\mathbf{Y_n \sim I_{peak}^{3.8}}$

Hence the 'saturation' of I_{peak} leads to saturation of neutron yield Y_n

Insight- neutron saturation

- **A major factor for ‘neutron saturation’ is simply: Axial Phase Dynamic Resistance**

Conclusions and Discussion

Beyond saturation?

Possible ways to improve Y_n:

- **Increase operating voltage. Eg SPEED II uses Marx technology: 300kV, driver impedance 60 mΩ. With E_0 of under 200 kJ, the system was designed to give I_{peak} of 5 MA and I_{pinch} just over 2 MA.**
- **Extend to 1MV-with low bank impedance- would increase I_{peak} to 100 MA; at several tens of MJ. I_{pinch} could be 40 MA**
- **Y_n enhancing methods such as doping deuterium with low % of krypton.**
- **Further increase in I_{pinch} by fast current-injection near the start of radial phase. This could be achieved with charged particle beams or by circuit manipulation such as current-stepping. This model is ideally suited for testing circuit manipulation schemes.**

Ongoing IPFS numerical experiments of Multi-MJ, High voltage MJ and Current-step Plasma Focus

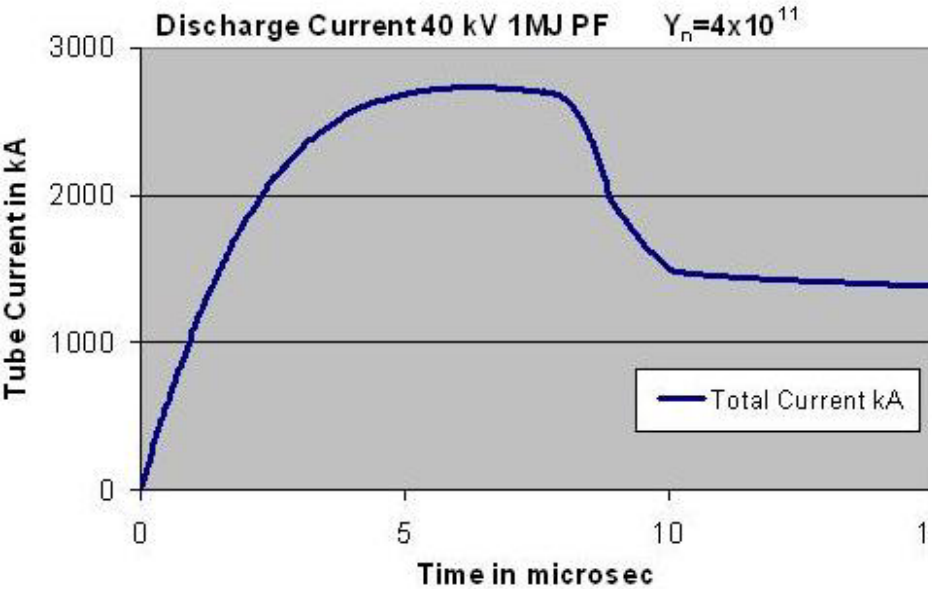

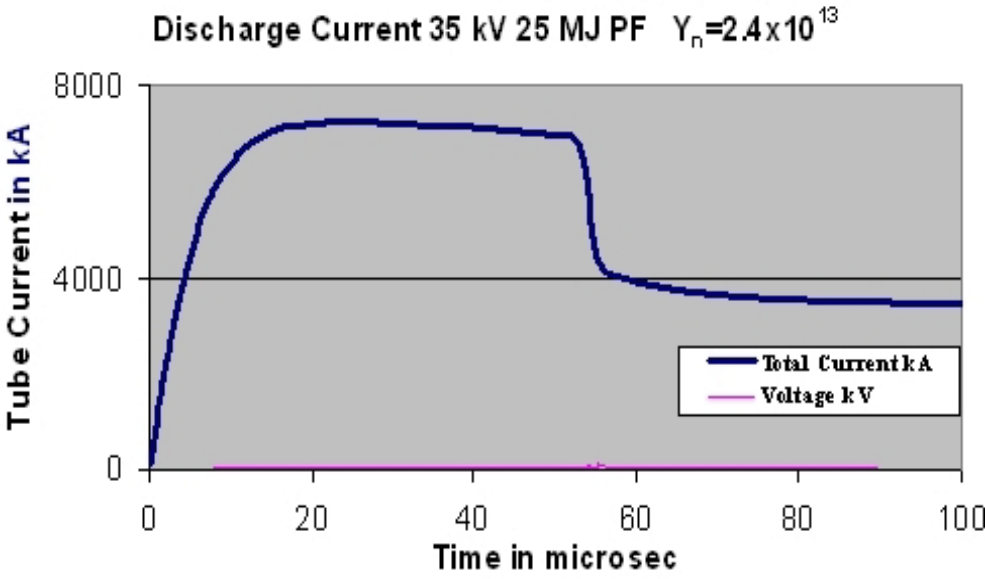

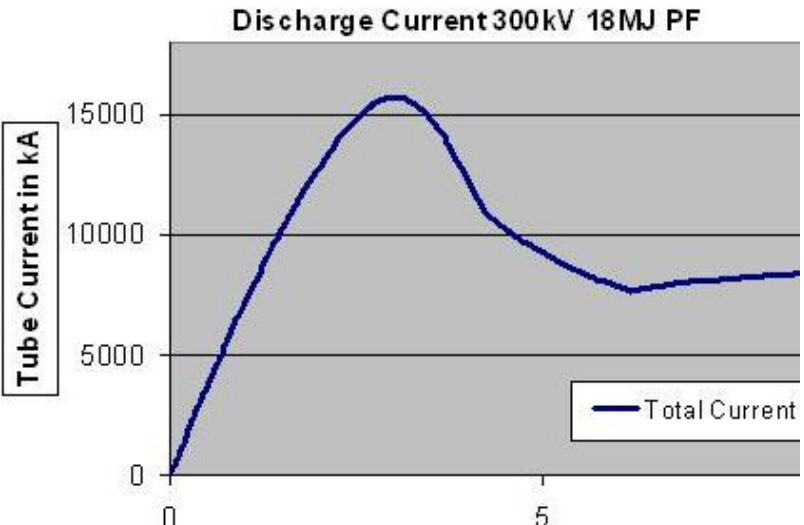

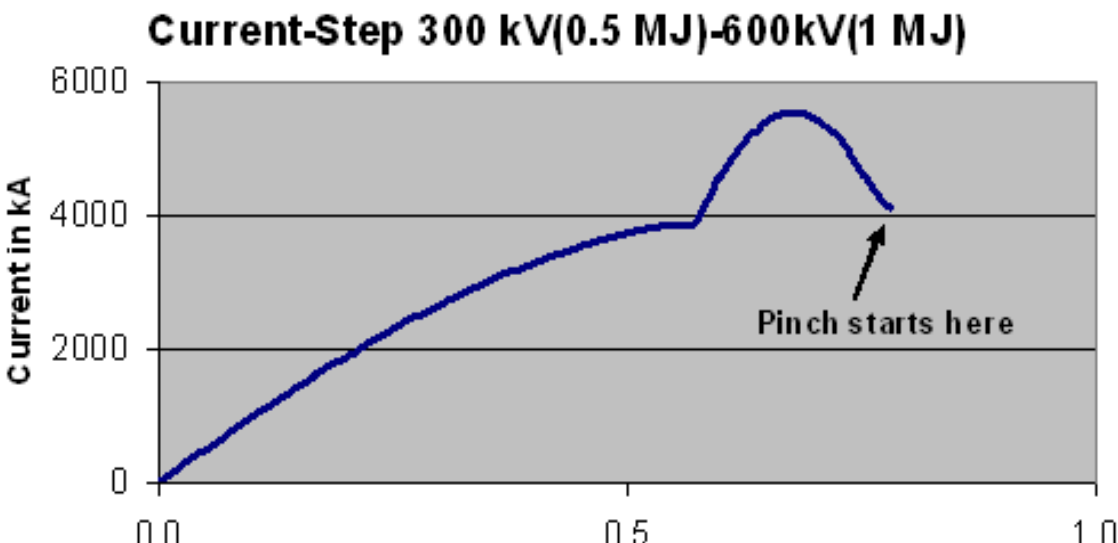

Conclusion:

- **Tokamak programme is moving steadily towards harnessing nuclear fusion energy as a limitless clean energy source for the continuing progress of civilisation**

- **Alternative and smaller scale experiments will also play a role in this most challenging technological development**

THANK YOU *Appreciation to the following web-sites:*

- **http://fusion.gat.com**
- **http://chandra.harvard.edu**
- **http://fire.pppl.gov**
- **http://www.jet.efda.org**
- **http://www.iter.org**
- **http://www.fusion.org.uk**
- **http://www-jt60.naka.jaeri.go.jp**
- **http://www.hiper-laser.org/**
- **http://www.intimal.edu.my/school/fas/UFLF**
- **http://www.plasmafocus.net**

SCALING THE PLASMA FOCUS FOR FUSION ENERGY CONSIDERATIONS

Sor Heoh Saw[1,3] and Sing Lee[1,2,3]

[1]INTI University College, 71800 Nilai, Malaysia
[2]NSSE, National Institute of Education, Nanyang Technological University, Singapore 637616
[3]Institute for Plasma Focus Studies, 32 Oakpark Drive, Chadstone, VIC 3148, Australia

Abstract

Using the Lee model code for dense plasma focus, series of numerical experiments were systematically carried out to determine: the scaling of bank energies with total current and focus pinch current; the scaling of neutron yields with energies and currents; and the possible extension for operation in D-D with extension to D-T. The numerical experiments were carried out over a range of bank energies from 8 kJ extending up to 24 MJ on the PF1000 and a proposed less damped modern bank. It also includes a study on the effects of increasing bank energies by increasing bank charging voltage and capacitance of the bank for a practical optimum plasma focus machine. The results provide convincing data to show that it is possible to scale up the plasma focus machine for D-D neutron yield of 10^{13} per shot and 10^{15} neutrons per shot when it is converted to operate in D-T.

Keywords: Dense plasma focus, neutrons source, focus pinch current, fusion energy

1. Introduction

Plasma focus machines can consistently produce considerable amounts of neutrons. The scalability of the device to fusion reactor conditions remains an area of research[1]. Even a simple machine such as the UNU ICTP PFF 3 kJ machine consistently produces 10^8 neutrons when operated in deuterium [2]. A big machine such as the PF1000 typically produces 10^{11} neutrons per shot[3]. Gribkov et al [4] had pointed out that $Y_n = 10^{13}$ in Deuterium is a desired landmark to achieve in a plasma focus device; from the point of view of possible exploitation as a powerful source of *fusion* neutrons for testing of prospective materials for the first wall components and construction elements in magnetic confinement fusion and, especially, in inertial confinement fusion reactors. Converting such a plasma focus yield to operation in D-T, with $Y_n = 10^{15}$ could produce, during a one-year run, an overall fluence of the order of 0.1–1.0 dpa for such testing purposes, at a very low cost relative to other methods currently being considered. We now examine the requirements to reach this landmark.

This paper presents the results from series of numerical experiments systematically carry out using the Lee model code [5] to investigate the scalability of the plasma focus to achieve $Y_n = 10^{13}$ D-D yield . Preceding to it is to determine the scaling laws between bank energies and peak total current and peak pinch current; and between Y_n and peak total current and peak pinch current[6-9].

2. The Lee model code

2.1. Description of the model

The Lee model code couples the electrical circuit with plasma focus dynamics, thermodynamics and radiation, enabling realistic simulation of all gross focus properties. The basic model, described in 1984 [10] was successfully used to assist several projects [11]-[13]. Radiation-coupled dynamics was included in the five-phase code leading to numerical experiments on radiation cooling [14]. The vital role of a finite small disturbance speed discussed by Potter in a Z-pinch situation [15] was incorporated together with real gas thermodynamics and radiation-yield terms. Before this 'communication delay effect' was incorporated, the model consistently over-estimated the radial speeds. This is serious from the point of view of neutron yields. A factor of 2 in shock speeds gives a factor of 4 in temperatures leading to a difference in fusion cross-sections of ~1000 at the range of

temperatures we are dealing with. This version of the code assisted other research projects [16]-[18], [19]-[21] and was web-published in 2000[22] and 2005[23]. Plasma self-absorption was included in 2007[21] improving SXR yield simulation. The code has been used extensively in several machines including UNU/ICTP PFF [2], [11],[16],[17],[19],[20], [24],[25], NX2[18], [21], [26], NX1[26], [27] and adapted for the Filippov-type plasma focus DENA [28]. A recent development is the inclusion of the neutron yield, Y_n, using a beam–target mechanism [3],[6]-[8],[29], incorporated in recent versions [5] of the code (versions later than RADPFV5.13), resulting in realistic Y_n scaling with I_{pinch}[7], [8]. The versatility and utility of the model is demonstrated in its clear distinction of I_{pinch} from I_{peak} [30] and the recent uncovering of a plasma focus pinch current limitation effect [6],[29]. The description, theory, code and a broad range of results of this 'Universal Plasma Focus Laboratory Facility' are available for download from [5].

2.2. A brief description of the code

The five phases are summarised as follows:

1) Axial phase: Described by a snowplow model with an equation of motion coupled to a circuit equation. The equation of motion incorporates the axial phase model parameters: mass and current factors f_m and f_c respectively. The mass swept-up factor f_m accounts for not only the porosity of the current sheet but also for the inclination of the moving current sheet- shock front structure and all other unspecified effects which have effects equivalent to increasing or reducing the amount of mass in the moving structure, during the axial phase. The current factor, f_c , accounts for the fraction of current effectively flowing in the moving structure (due to all effects such as current shedding at or near the back-wall and current sheet inclination). This defines the fraction of current effectively driving the structure, during the axial phase.

2) Radial inward shock phase: Described by four coupled equations using an elongating slug model. The first equation computes the radial inward shock speed from the driving magnetic pressure. The second equation computes the axial elongation speed of the column. The third equation computes the speed of the current sheath, also called the magnetic piston, allowing the current sheath to separate from the shock front by applying an adiabatic approximation. The fourth is the circuit equation. Thermodynamic effects due to ionization and excitation are incorporated into these equations, these effects being important for gases other than hydrogen and deuterium. Temperature and number densities are computed during this phase. A communication delay between shock front and current sheath due to the finite small disturbance speed is crucially implemented in this phase. The model parameters, radial phase mass swept-up and current factors, f_{mr} and f_{cr} , are incorporated in all three radial phases. The mass swept-up factor f_{mr} accounts for all mechanisms which have effects equivalent to increasing or reducing the amount of mass in the moving slug, during the radial phase. The current factor, f_{cr} , accounts for the fraction of current effectively flowing in the moving piston forming the back of the slug (due to all effects). This defines the fraction of current effectively driving the radial slug.

3) Radial reflected shock (RS) phase: When the shock front hits the axis, because the focus plasma is collisional, a reflected shock develops which moves radially outwards, whilst the radial current-sheath piston continues to move inwards. Four coupled equations are also used to describe this phase, these being for the reflected shock moving radially outwards, the piston moving radially inwards, the elongation of the annular column and the circuit. The same model parameters, f_{mr} and f_{cr} , are used as in the previous radial phase. The plasma temperature behind the RS undergoes a jump by a factor approximately two.

4) Slow compression (quiescent) or pinch phase: When the out-going RS hits the in-coming piston the compression enters a radiative phase in which for gases such as neon, radiation emission may actually enhance the compression where we have included energy loss/gain terms from Joule heating and radiation losses into the piston equation of motion. Three coupled equations describe this phase; these being the piston radial motion equation, the pinch column elongation equation and the circuit equation, incorporating the same model parameters as in the previous two phases. Thermodynamic effects are incorporated into this phase. The duration of this slow compression phase is set as the time of transit of small disturbances across the pinched plasma column. The computation of this phase is terminated at the end of this duration.

5) Expanded column phase: To simulate the current trace beyond this point, we allow the column to suddenly attain the radius of the anode and use the expanded column inductance for further integration. In this final phase the snowplow model is used, and two coupled equations are used; similar to the axial phase aforementioned. This phase is not considered important as it occurs after the focus pinch.

2.3. Computation of neutron yield

The neutron yield is computed using a phenomenological beam-target neutron generating mechanism described recently by Gribkov et al [3] and adapted to yield the following equation. A beam of fast deuteron ions is produced by diode action in a thin layer close to the anode, with plasma disruptions generating the necessary high voltages. The beam interacts with the hot dense plasma of the focus pinch column to produce the fusion neutrons. The beam-target yield is derived [6] as:

$$Y_{b\text{-}t}= C_n\, n_i I_{pinch}^{2} z_p^{2} (\ln(b/r_p))\sigma / U^{0.5} \quad (1)$$

where n_i is the ion density, b is the cathode radius, r_p is the radius of the plasma pinch with length z_p, σ the cross-section of the D-D fusion reaction, n- branch[31] and U, the beam energy. C_n is treated as a calibration constant combining various constants in the derivation process.

The D-D cross-section is sensitive to the beam energy in the range 15-150 kV; so it is necessary to use the appropriate range of beam energy to compute σ. The code computes induced voltages (due to current motion inductive effects) V_{max} of the order of only 15-50 kV. However it is known, from experiments that the ion energy responsible for the beam-target neutrons is in the range 50-150 keV [3], and for smaller lower-voltage machines the relevant energy could be lower at 30-60keV[1]. Thus in line with experimental observations the D-D cross section σ is reasonably obtained by using $U= 3V_{max}$. This fit was tested by using U equal to various multiples of V_{max}. A reasonably good fit of the computed neutron yields to the measured published neutron yields at energy levels from sub-kJ to near MJ was obtained when the multiple of 3 was used; with poor agreement for most of the data points when for example a multiple of 1 or 2 or 4 or 5 was used. The model uses a value of $C_n = 2.7 \times 10^7$ obtained by calibrating the yield [5], [6] at an experimental point of 0.5 MA.

The thermonuclear component is also computed in every case and it is found that this component is negligible when compared with the beam-target component.

3. Procedures for numerical experimetns

The Lee model code is configured to work as any plasma focus by inputting the bank parameters, L_0, C_0 and stray circuit resistance r_0; the tube parameters b, a and z_0 and operational parameters V_0 and P_0 and the fill gas. The standard practice is to fit the computed total current waveform to an experimentally measured total current waveform [5]-[8], [23], [24], [29], [30] using four model parameters representing the mass swept-up factor f_m, the plasma current factor f_c for the axial phase and factors f_{mr} and f_{cr} for the radial phases.

From experience it is known that the current trace of the focus is one of the best indicators of gross performance. The axial and radial phase dynamics and the crucial energy transfer into the focus pinch are among the important information that is quickly apparent from the current trace.

The exact time profile of the total current trace is governed by the bank parameters, by the focus tube geometry and the operational parameters. It also depends on the fraction of mass swept-up and the fraction of sheath current and the variation of these fractions through the axial and radial phases. These parameters determine the axial and radial dynamics, specifically the axial and radial speeds which in turn affect the profile and magnitudes of the discharge current. The detailed profile of the discharge current during the pinch phase also reflects the Joule heating and radiative yields. At the end of the pinch phase the total current profile also reflects the sudden transition of the current flow from a constricted pinch to a large column flow. Thus the discharge current powers all dynamic, electrodynamic, thermodynamic and radiation processes in the various phases of the plasma focus. Conversely all the dynamic, electrodynamic, thermodynamic and radiation processes in the various phases of the plasma focus affect the discharge current. It is then no exaggeration to say that the discharge current waveform contains information on all the dynamic, electrodynamic, thermodynamic and radiation processes that occurs in the various phases of the plasma focus. This explains the importance attached to matching the computed current trace to the measured current trace in the procedure adopted by the Lee model code.

For this series of experiments we configure the Lee model code using a published current trace measured from the PF1000 with C_0 = 1332 μF, operated at 27 kV, 3.5 torr deuterium, with cathode/anode radii b = 16 cm, a = 11.55 cm and anode length z_0 = 60 cm[3]. In the numerical experiments we fitted external (or static) inductance L_0= 33.5 nH and stray resistance r_0 = 6.1 mΩ (damping factor RESF= stray resistance/$(L_0/C_0)^{0.5}$=1.22). The fitted model parameters are: f_m = 0.13, f_c = 0.7, f_{mr} = 0.35 and f_{cr}=0.65. Figure 1 shows the computed current trace [5], [6], [29] agrees very well with the measured trace through all the phases, axial and radial, right down to the

bottom of the current dip indicating the end of the pinch phase. This agreement confirms the model parameters for the PF1000. Once the model parameters have been fitted to a machine for a given gas, these model parameters may be used with some degree of confidence when operating parameters such as the voltage are varied [5]. With no measured current waveform available for the higher megajoule numerical experiments, it is reasonable to keep the model parameters that we have got from the PF1000 fitting.

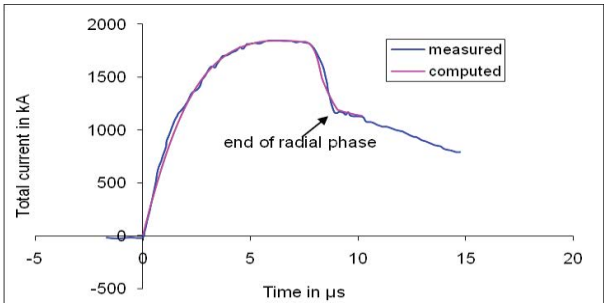

Figure 1. Current fitting computed current to measured current traces to obtain fitted parameters $f_m = 0.13$, $f_c = 0.7$, $f_{mr} = 0.35$ and $f_{cr}=0.65$.

3.1. Determining the scaling laws for neutrons from numerical experiments over a range of energies from 8.5 kJ to 24.5 MJ

Using the model parameters determined in the above for PF1000, we run the first series of numerical experiments on PF1000 at V_0 = 35kV, P_0 =10 Torr, L_0=33.5nH, RESF=1.22 and the c=b/a=1.39 for varying bank energies from 8.5 kJ to 24.5 MJ. This series of numerical experiments is operated at optimum pressure of 10 torr deuterium, and the ratio b/c retained at 1.39.

The numerical experiments were carried out for C_0 ranging from 14 µF to 39960 µF corresponding to energies from 8.5 kJ to 24.5 MJ. For each C_0, we parametrically varied z_0 and then *'a'* to find the optimum combination of z_0 and *'a'* for each given C_0 corresponding to an end axial speed of about 10 cm/µs. The optimum combinations for each C_0 and with the peak total current, peak pinch current and neutron yield computed for the range of bank energies from 8.5 kJ to 24.5 MJ are tabulated in Table 1.

Table 1. Numerical experiments to find the scaling of I_{peak}, I_{pinch} and Y_n with C_0

E_0	**C_0**	**A**	**z_0**	**I_{peak}**	**I_{pinch}**	**Y_n**
kJ	uF	Cm	Cm	kA	kA	10^{10}
24476	39960	23.55	500.0	5678	2368	1320
18765	30636	22.80	400.0	5479	2267	1094
14685	23976	21.90	350.0	5268	2165	906
11422	18648	21.00	300.0	5046	2062	737
6527	10656	18.73	220.0	4506	1827	438
4895	7992	17.66	160.0	4229	1721	329
4079	6660	16.88	140.0	4043	1650	273
3263	5328	15.90	120.0	3812	1563	215
2448	3996	14.53	86.6	3510	1461	159
1632	2664	12.69	65.0	3101	1316	102
816	1332	9.95	45.0	2458	1086	45.4
748	1221	9.62	42.0	2383	1059	40.9
680	1110	9.18	38.0	2295	1032	36.3
612	999	8.82	36.0	2208	1000	31.8
544	888	8.47	35.0	2116	965	27.3
476	777	8.05	33.0	2012	926	22.9
408	666	7.60	31.0	1898	882	18.6
340	555	7.04	28.0	1766	833	14.5
272	444	6.38	24.0	1613	778	10.8
204	333	5.59	20.0	1425	706	7.1
136	222	4.74	17.0	1205	613	3.8
68	111	3.47	12.0	888	476	1.21

34	56	2.48	8.0	644	363	0.346
17	28	1.72	5.0	457	272	0.085
8.5	14	1.28	4.0	335	202	0.017

The results show no saturation of the peak total current and peak pinch current as the energies of the bank is increased except for a lesser degree of corresponding increased in the currents.

Figure 2 shows the computed I_{peak} as a function of C_0, from the numerical experiments which show no saturation; although there is a scaling shift from $I_{peak} \sim E_0^{0.47}$ to $I_{peak} \sim E_0^{0.22}$ which is seen when plotted on log-log scale (see Figure 3).

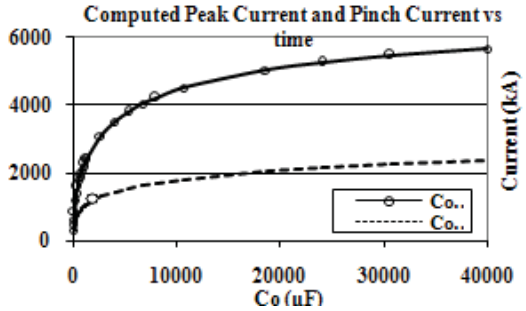

Figure 2. I_{peak} (top trace) computed from numerical experiments as a function of C_0. Also shown is the $_{pinch}$ curve (lower trace). The single point at the 2 MA level is an experimental PF1000 point.

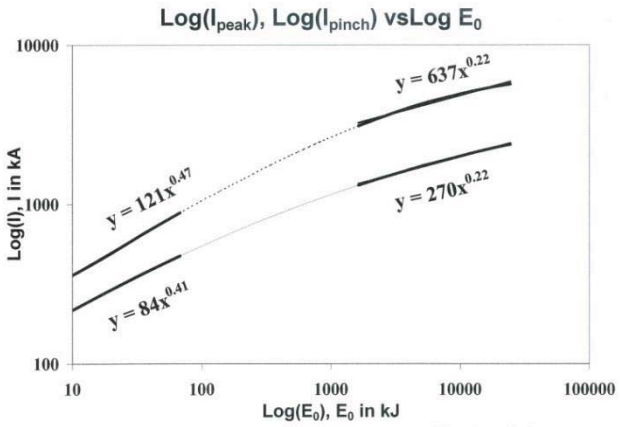

Figure 3. Log I_{peak} (top curve) and Log I_{pinch} vs Log E_0, showing no saturation for E_0 up to 24.5 MJ

Similarly, the I_{pinch} scaling with E_0 slows down from $I_{pinch} \sim E_0^{0.41}$ to $I_{pinch} \sim E_0^{0.22}$ (see Figure 3), but again no saturation. We would like to emphasize that the findings in earlier papers [6], [7], [29], [30] concluded that it is the I_{pinch} scaling, rather than I_{peak} which directly affects the neutron yield scaling.

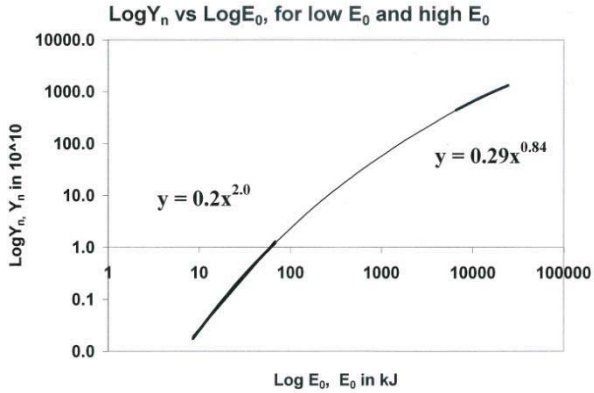

Figure 4. Y_n plotted as a function of E_0 in log-log scale, showing no saturation of neutron yield up to 24.5 MJ, the highest energy investigated.

For this series of experiments we find that the Y_n scaling decreases from $Y_n \sim E_0^{2.0}$ at tens of kJ to $Y_n \sim E_0^{0.84}$ at the highest energies (up to 24.5MJ). This is shown in Figure 4.

Because of the way Y_n versus E_0 scaling slows down at the megajoule level and the corresponding way I_{peak} and I_{pinch} scaling with E_0 also slow down, the scaling of Y_n with I_{peak} and I_{pinch} over the whole range of energies investigated up to 24.5 MJ (Figure 5) are as follows:

$Y_n=3.2\text{x}10^{11}I_{pinch}^{4.5}$; $Y_n=1.8\text{x}10^{10}I_{peak}^{3.8}$ where I_{pinch} (0.2 to 2.4) and I_{peak} (0.3 to 5.7) are in MA.

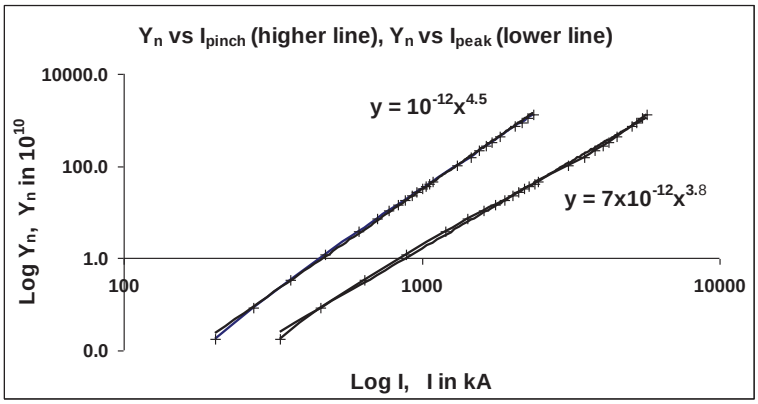

Figure 5. Log(Y_n) scaling with Log(I_{peak}) and Log(I_{pinch}), for the range of energies investigated, up to 24.5 MJ

In the above series of numerical experiments we have shown that as the bank energies of the plasma focus increases from 10kJ to 25MJ:

$I_{peak} \sim E_0^{x}$ where x=0.47 at tens of kJ and x=0.22 at the highest energies (up to 24.5MJ)
$I_{pinch} \sim E_0^{x}$ where x=0.41 at tens of kJ and x=0.22 at the highest energies (up to 24.5MJ)
$Y_n \sim E_0^{x}$, where x=2.0 at tens of kJ and x=0.84 at the highest energies (up to 24.5MJ)

Y_n does not saturate with increasing E_0 at the megajoule level and the resultant scaling laws for Y_n in relation to the total peak current, I_{peak} and the total pinch current I_{pinch} are:

$Y_n=3.2\text{x}10^{11}I_{pinch}^{4.5}$ where I_{pinch} (0.2 to 2.4) in MA; and
$Y_n=1.8\text{x}10^{10}I_{peak}^{3.8}$ where I_{peak} (0.3 to 5.7) in MA

This first series of numerical experiments show that it is possible to scale up the plasma focus machine to fusion reactor conditions to yield 10^{13} D-D neutrons at 2.5 MeV. This is achieved at bank energy E_0=18.7 MJ with I_{peak}= 5.5 MA and I_{pinch}=2.3 MA, corresponding to the focus anode length z_0=4 m and anode radius a=22.8 cm and cathode radius b=31.7 cm.

3.2. Investigating the effect of RESF on Y_n yield

The PF1000 has an unusually high damping factor represented by RESF=1.22. As it is practically possible for a modern capacitor bank system to be very much less damped with RESF=0.12, we proceed to run the second series of numerical experiments with RESF changed to 0.12. Again for each C_0, we parametrically varied z_0 and then *'a'* to find the optimum combination of z_0 and *'a'* for each given C_0 corresponding to an end axial speed of about 10 cm/μs. The optimum combinations for each C_0 and with the peak total current, peak pinch current and neutron yield computed for the range of bank energies from 68kJ to 24.5 MJ are tabulated in Table 2. Figure 6 shows the summary of the results.

Table 2. Numerical experiments with less resistive bank of RESF=0.12

E_0	C_0	A	z_0	I_{peak}	I_{pinch}	Y_n
kJ	uF	cm	cm	kA	kA	10^{10}
24476	39960	28.25	450.0	6774	2720	2255
18765	30636	27.44	430.0	6612	2622	1968
14685	23976	27.01	350.0	6488	2541	1711
11421	18646	26.34	300.0	6327	2449	1460

8159	13320	25.26	260.0	6077	2314	1157
6527	10656	24.62	210.0	5909	2236	974
4895	7992	23.61	160.0	5663	2130	777
4079	6660	22.83	140.0	5487	2060	668
3263	5328	21.72	110.0	5252	1976	558
2448	3996	20.36	93.0	4948	1866	437
1632	2664	18.40	75.0	4512	1711	303
816	1332	14.74	47.0	3726	1466	154
748	1221	14.26	44.0	3623	1436	140
680	1110	13.90	43.0	3528	1402	127
612	999	13.46	41.0	3419	1366	113
476	777	12.42	37.0	3161	1280	85.72
340	555	10.61	28.0	2763	1175	58.43
204	333	8.81	22.0	2312	1025	32.30
136	222	7.33	17.0	1954	913	19.46
68	111	5.45	12.0	1472	735	7.64

These results show that using a less resistive modern bank, RESF=0.12 reduces the E_0 required to reach $Y_n=10^{13}$ in Deuterium to some 8MJ with corresponding I_{peak}=6 MA, I_{pinch}= 2.3 MA, the focus length z_0=2.6 m, anode radius a=25.3 cm and cathode radius b=35.2 cm as compared to19 MJ with corresponding I_{peak}= 5.5 MA, I_{pinch}=2.3 MA, the focus length z_0=4 m, anode radius a=22.8 cm and cathode radius b=31.7 cm for the earlier heavily damped bank with RESF=1.22.

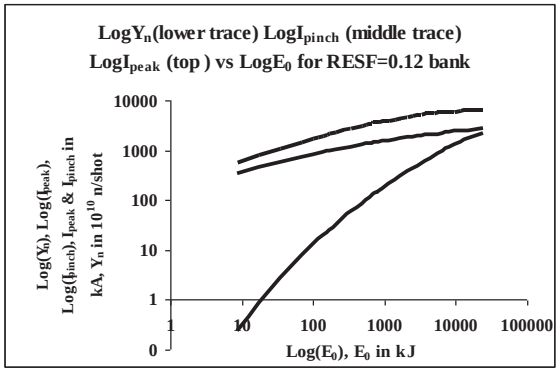

Figure 6. Log-log plots of Y_n (lower trace), I_{pinch} (middle trace) and I_{peak} (top trace) versus E_0 for a high performance bank up to 25 MJ; computed from numerical experiments

3.3. Investigating the effect on Y_n as operating voltage is increased from 35 kV to 90 kV, at C_0 = 777 µF

We run a third series of numerical experiments for a practical optimum configuration [8] with c=b/a=1.39, L_0=36 nH, P_0=10 Torr and C_0=777 uF, and vary V_0 from 35 kV to 90 kV. The results are summarized in Table 3 and plotted in Figure 7 in log-log scale.

Table 3. Numerical experiments on effect of increasing V_0, at fixed C_0 of 777 µF

V_0	E_0	B	a	z_0	I_{peak}	I_{pinch}	Y_n
kV	kJ	cm	cm	cm	kA	kA	10^{10}
90	3147	39.92	27.65	25	7580	2483	1228
70	1904	31.14	22.40	30	5955	2091	631
50	971	23.44	16.86	35	4365	1652	246
35	476	16.69	12.01	37	3074	1286	88

Figure 7 shows that $Y_n \sim V_0^{2.8}$ over the range of voltages examined from 35-90kV. Looking at this scaling, it may at first sight be tempting to think in terms of increasing the voltage further. However it is then necessary to look more closely at that prospect.

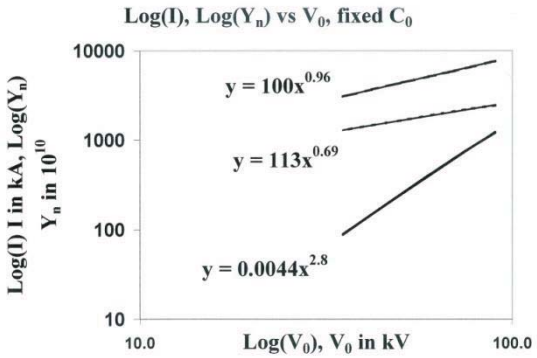

Figure 7. Scaling of currents and Y_n as functions of operating voltage V_0.

Top curve:Log(I_{peak}), middle curve: Log(I_{pinch}) and bottom curve: Log(Y_n).

An examination of the computed results shows that the computed effective beam energy [6], [7], [29] for 90kV is already at the 330 keV level. Looking at data for the D-D cross-section [31] as a function of beam energy, it is seen that above 300 keV, the rise in D-D fusion cross-section is very slow. Hence we wish to highlight that there is little advantage operating above 90kV. In fact the situation is actually disadvantageous to increase operating voltage if one considers changing to D-T operation. The D-T fusion cross-section [31] has already peaked at 120 keV; and operating at 90 kV with the beam energy at 330 keV, the beam energy is already too high; the D-T cross-section having dropped by a factor around 3.6 from its peak. It seems then that from this point of view there is no advantage to operate a plasma focus at higher than 90 kV. For conversion to D-T operation it would probably be better to operate at a lower voltage. It would then be necessary to increase C_0 until 10^{15} D-T neutrons is reached.

3.4. Investigating operation at 90 kV, varying E_0 by varying C_0; at 10 Torr, L_0=36 nH, and b/a=1.39; RESF=0.12

We consider the effect of operating at 90kV. We run the fourth series of numerical experiments at 90 kV with increasing E_0 (by increasing C_0) to obtain the energy required to reach $Y_n=10^{13}$ D-D neutrons per shot. At each C_0, z_0 is varied whilst adjusting 'a' for an end axial speed of 10 cm/us. The optimum z_0 is thus found for each C_0 . Results are shown in Figure 8. Again at this higher voltage, no saturation is found for I_{peak}, I_{pinch} or Y_n. At 90 kV the results show that the E_0 required for $Y_n=10^{13}$ D-D fusion neutrons per shot is reduced further to 3MJ, with C_0= 777 μF as shown in the following Figure 8. The values of I_{peak} and I_{pinch} are respectively 7.6 and 2.5 MA. Furthermore at 90 kV with the highest value of C_0 investigated as 39960 μF, the storage energy is 162 MJ. At that storage energy, optimized Y_n is 4.5×10^{14} D-D neutrons/shot with I_{peak}=17.3 MA and I_{pinch}=5.7 MA.

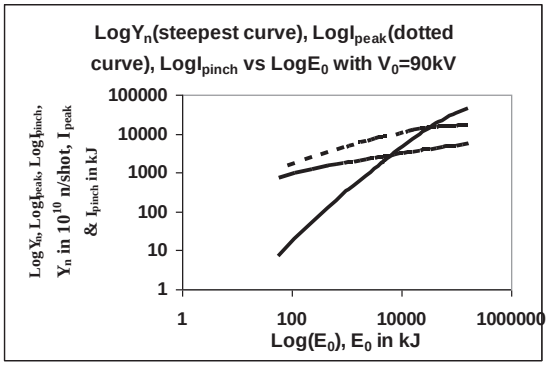

Figure 8. Numerical experiments at 90 kV, varying C_0, to obtain scaling of I_{peak}, I_{pinch} and Y_n with E_0. Log(Y_n): steepest curve; Log(I_{peak}): dotted curve; Log(I_{pinch}): other curve. Y_n in units of 10^{10} D-D neutrons/shot; I_{peak} and I_{pinch} in kA.

4. Conclusions

This paper finds that it is possible to scale up the focus to fusion conditions. In the first series of numerical experiments we have shown that as the bank energies of the plasma focus increases from 10kJ to 25MJ:

$I_{peak} \sim E_0^{\,x}$ where x=4.7 at tens of kJ and x=0.22 at the highest energies (up to 25MJ)
$I_{pinch} \sim E_0^{\,x}$ where x=4.1 at tens of kJ and x=0.22 at the highest energies (up to 25MJ)
$Y_n \sim E_0^{\,x}$, where x=2.0 at tens of kJ and x=0.84 at the highest energies (up to 25MJ)

Y_n does not saturate with increasing E_0 at the megajoule level and the resultant scaling laws for Y_n in relation to the total peak current, I_{peak} and the total pinch current I_{pinch} are:

$$Y_n = 3.2 \times 10^{11} I_{pinch}^{\,4.5} \text{ where } I_{pinch} \text{ (0.2 to 2.4) in MA; and}$$
$$Y_n = 1.8 \times 10^{10} I_{peak}^{\,3.8} \text{ where } I_{peak} \text{ (0.3 to 5.7) in MA}$$

To scale up from a PF1000-like capacitor bank requires close to 19 MJ to reach a target D-D neutron yield of 10^{13} per shot. The energy requirement can be reduced to 8 MJ using a modern capacitor bank with typical lower damping operating at typical voltage of 35 KV. By increasing the operational voltage to 90kV, the energy requirement is further reduced to 3 MJ. Because of the high effective beam energy already at 90 kV, there is little advantage to operate at voltages above 90 kV for D-D neutron yield; from this point of view.

References

[1] M G Haines in *Laser and Plasma Technology*, edited by S Lee, B C Tan, C S Wong, A C Chew (World Scientific, Singapore, 1985), pp 560-585.
[2] S Lee, "Twelve Years of UNU/ICTP PFF—A Review," IC/ 98/ 231 Abdus Salam ICTP, Miramare, Trieste; 1998, pp.5-34. ICTP Open Access Archive http://eprints.ictp.it/31/.
[3] V A Gribkov, A Banaszak, B Bienkowska, A V Dubrovsky, I Ivanova-Stanik, L Jakubowski, L Karpinski, R A Miklaszewski, M Paduch, M J Sadowski, M Scholz, A Szydlowski and K Tomaszewski, "Plasma dynamics in the PF-1000 device under full-scale energy storage: II. Fast electron and ion characteristics versus neutron emission parameters and gun optimization perspectives," J. Phys. D: Appl. Phys. 40, 2007, pp. 3592-3607.
[4] Gribkov V A et al, "Plasma dynamics in PF-1000 device under full-scale energy storage: I. Pinch dynamics, shock wave diffraction, and inertial electrode," J Phys. D: Appl. Phys. 40, 2007, pp 1977-1989.
[5] Lee S Radiative Dense Plasma Focus Computation Package: RADPF
http://www.intimal.edu.my/school/fas/UFLF/File1RADPF.htm
http://www.plasmafocus.net/IPFS/modelpackage/File1RADPF.htm
[6] S Lee and S H Saw, "Pinch current limitation effect in plasma focus," Appl. Phys. Lett. 92, 2008, 021503.
[7] S Lee and S H Saw, "Neutron scaling laws from numerical experiments," J Fusion Energy 27, 2008, pp. 292-295.
[8] S Lee, "Current and neutron scaling for megajoule plasma focus machine," Plasma Phys. Control. Fusion 50, 2008, 105005, (14pp).
[9] S Lee, S H Saw, L Soto, SV Springham, S P Moo, "Numerical experiments on plasma focus neutron yield versus pressure compared with laboratory experiments," Plasma Physics and Controlled Fusion 51,2009,075006 (11p).
[10] S Lee, "Plasma focus model yielding trajectory and structure" in *Radiations in Plasmas*, ed B McNamara (Singapore: World Scientific Publishing Co, ISBN 9971-966-37-9) vol. II, 1984, pp. 978–987
[11] S Lee S et al, "A simple facility for the teaching of plasma dynamics and plasma nuclear fusion," Am. J. Phys. 56, 1988, pp. 62-68.
[12] T Y Tou, S Lee and K H Kwek, "Non perturbing plasma focus measurements in the run-down phase," IEEE Trans. Plasma Sci. 17, 1989, pp. 311-315.
[13] S Lee, "A sequential plasma focus," IEEE Trans. Plasma Sci., vol. 19, no. 12, 1991, pp. 912-919.
[14] Jalil bin Ali, "Development and Studies of a small Plasma Focus," PhD thesis, Universiti Teknologi Malaysia, Malaysia, 1990.
[15] D E Potter, "The formation of high-density z-pinches,"Nucl. Fusion, vol 18 pp813-823, 1978.
[16] S Lee and A Serban A, "Dimensions and lifetime of the plasma focus pinch," IEEE Trans. Plasma Sci., vol. 24, no.3, 1996, pp. 1101-1105.
[17] Liu Mahe, "Soft X-rays from compact plasma focus," PhD thesis, NIE, Nanyang Technological University, Singapore, 2006. ICTP Open Access Archive: http://eprints.ictp.it/327/.

[18] S Bing, "Plasma dynamics and x-ray emission of the plasma focus," PhD Thesis, NIE, Nanyang Technological University, Singapore, 2000. ICTP Open Access Archive: http://eprints.ictp.it/99/.
[19] A Serban and S Lee, "Experiments on speed-enhanced neutron yield from a small plasma focus," J Plasma Physics, vol. 60 part 1, 1998, pp. 3-15.
[20] M H Liu, X P Feng, S V Springham and S Lee, "Soft x-ray measurement in a small plasma focus operated in neon," IEEE Trans. Plasma Sci. 26, 1998, pp. 135-140.
[21] D Wong, P Lee, T Zhang, A Patran, T L Tan, R S Rawat and S Lee, "An improved radiative plasma focus model calibrated for neon-filled NX2 using a tapered anode," Plasma Sources Sci. Technol. 16, 2007, pp. 116-123.
[22] S Lee. (2000–2007). http://ckplee.myplace.nie.edu.sg/plasmaphysics/.
[23] S Lee. (2005). ICTP Open Access Archive: http://eprints.ictp.it/85/.
[24] S V Springham, S Lee and M S Rafique, "Correlated deuteron energy spectra and neutron yield for a 3 kJ plasma focus," Plasma Phys. Control. Fusion, vol 24, 2000 pp 1023-1032
[25] M A Mohammadi, S Sobhanian, C S Wong, S Lee, P Lee and R S Rawat , "The effect of anode shape on neon soft x-ray emissions and current sheath configuration in plasma focus device," J. Phys. D: Appl.Phys. 42, 2009, 045203 (10pp).
[26] Lee S, Lee P, Zhang G, Feng X, Gribkov V A, Mahe L, Serban A, and Wong T K S 1998 IEEE Trans. Plasma Sci. **26** 1119
[27] E P Bogolyubov, V D Bochkov, V A Veretennikov, L T Vekhoreva, V A Gribkov, A V Dubrovskii, Yu P Ivanov, A I Isakov, O N Krokhin, P Lee, S Lee, V Ya Nikulin, A Serban, P V Silin, X Feng and G X Zhang, "A powerful soft x-ray source for x-ray lithography based on plasma focusing" 1998 *Phys. Scripta.,* vol. 57, 1998, pp. 488-494.
[28] V Siahpoush, M A Tafreshi, S Sobhanian and S Khorram, "Adaptation of Sing Lee's model to the Filippov type plasma focus geometry*,"* Plasma Phys. Control. Fusion 47, 2005, pp. 1065-1072.
[29] S Lee, P Lee, S H Saw and R S Rawat, "Numerical experiments on plasma focus pinch current limitation," Plasma Phys. Control. Fusion 50, 2008, 065012 (8pp).
[30] S Lee, S H Saw, P C K Lee, R S Rawat and H Schmidt, "Computing plasma focus pinch current from total current measurement," Appl. Phys. Lett. 92 , 2008, 111501
[31] Huba J D 2006 Plasma Formulary pg44
[32] Sadowski M J and Scholz M 2002 Nukloenika 47 31-7
[33] Gribkov V A 2003 Private Communication

Latest Trends in Plasma Focus Fusion Studies

S Lee & S H Saw

Institute for Plasma Focus Studies

INTI University College, Malaysia

Turkish Atomic Energy Authority, Saraykoy Nuclear Research Training Center Ankara 1 October 2009- 2.30 pm

Plan of Talk

- Present generation of Plasma Focus devices
- Experimental results
- Failure of Scaling Laws
- Beyond saturation Numerical Expts
- Development of next generation devices also requires next generation measurements-Scholz ICDMP

When matter is heated to high temperatures:

- It ionizes and becomes a plasma; emitting radiation
- Emission spectrum depends on temperature (T) and the atomic species
- Generally, the higher T and density n, the more intense the radiation
- Depending on heating mechanisms, beams of ions and electrons may also be emitted
- In Deuterium, nuclear fusion may take place, if n & T are high enough; neutrons are also emitted.
- Typically T> several million K; & compressed n: above atmospheric density.

One method: electrical discharge through gases.

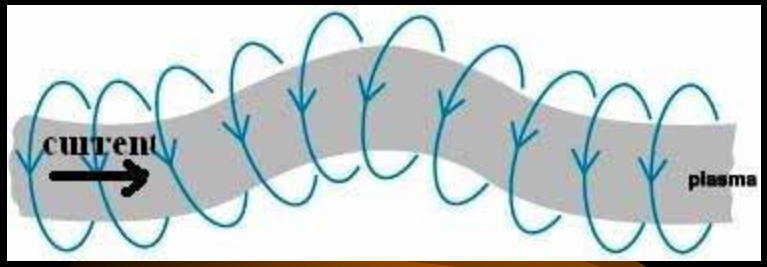

- **Heated gas expands**, lowering the density; making it difficult to heat further.
- **Necessary to compress** whilst heating, to achieve sufficiently intense conditions.
- **Electrical discharge between two electrodes** produces azimuthal magnetic field which interacts with column of current; giving rise to a **self compression** force which tends to constrict (or **pinch**) the column.
- To **'pinch'** a column of gas to atmospheric density at T~ 1 million K, a rather large pressure has to be exerted by the pinching magnetic field.
- Electric current **of hundreds of kA** required, even for column of radius of say 1mm.
- **Dynamic pinching** process requires current to rise very rapidly, typically in under **0.1 microsec** in order to have a sufficiently hot and dense pinch.
- **Super-fast, super-dense pinch; requires special MA fast-rise (nanosec) pulsed-lines**; **Disadvantages**: conversion losses and cost of the high technology pulse-shaping line, additional to the capacitor.

Superior method for super-dense-hot pinch: plasma focus (PF)

- The PF produces superior densities and temperatures.
- 2-Phase mechanism of plasma production does away with the extra layer of technology required by the expensive and inefficient pulse-shaping line.
- **A simple capacitor discharge is sufficient to power the plasma focus.**

THE PLASMA FOCUS

- **The PF is divided into two sections.**
- **Pre-pinch (axial) section: Delays the pinch until the capacitor discharge approaches maximum current.**
- **The pinch starts & occurs at top of the current pulse.**
- **Equivalent to driving the pinch with a super-fast rising current; without necessitating the fast line technology.**
- **The intensity which is achieved is superior to even the super fast pinch.**

Two Phases of the Plasma Focus

Axial Phase

Radial Phase

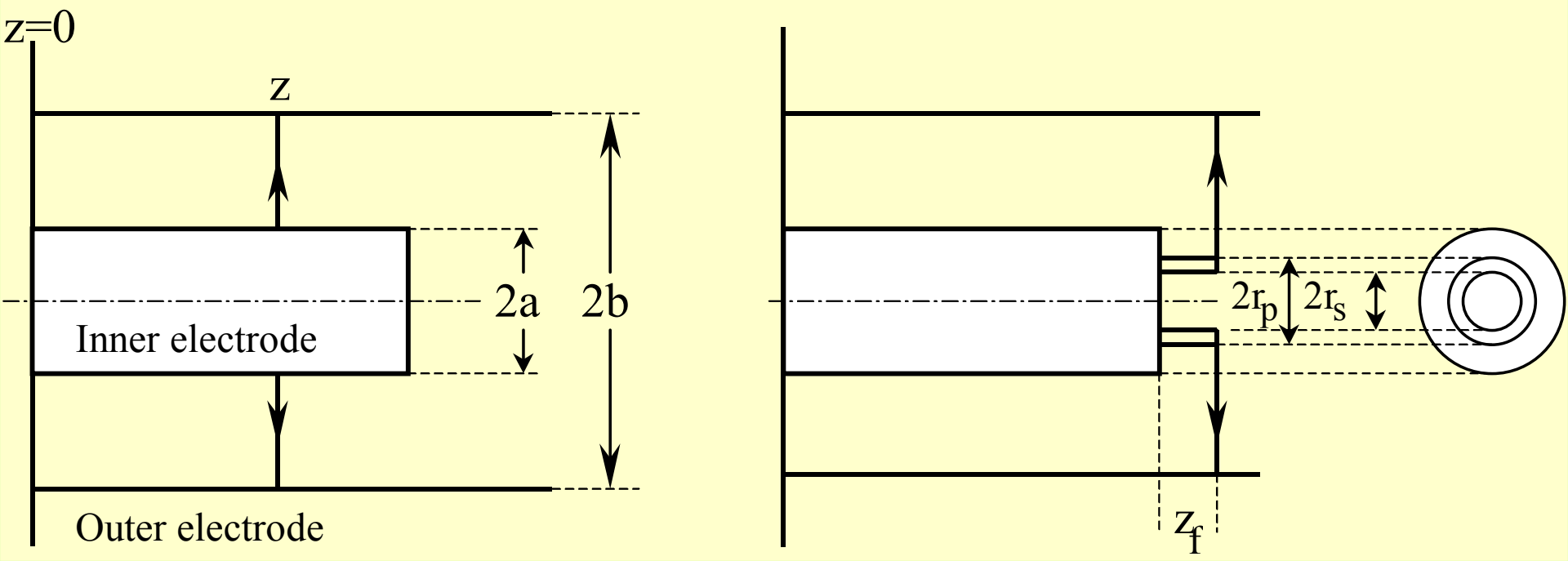

Radial Compression (Pinch) Phase of the Plasma Focus

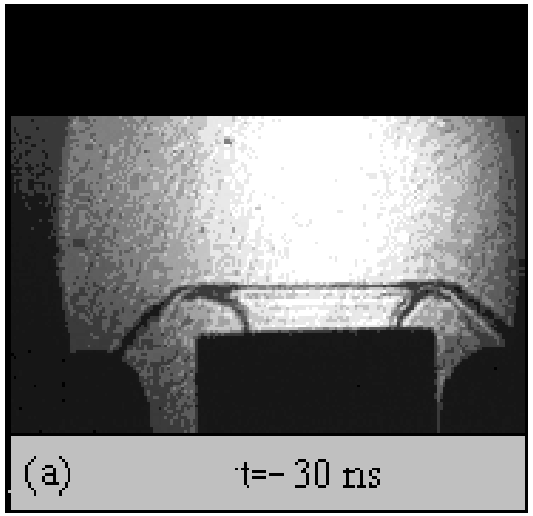

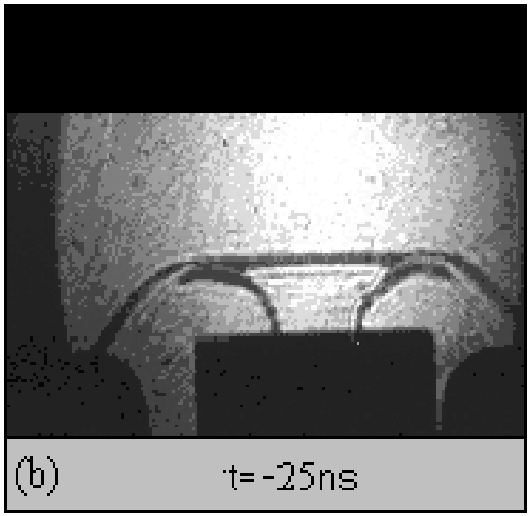

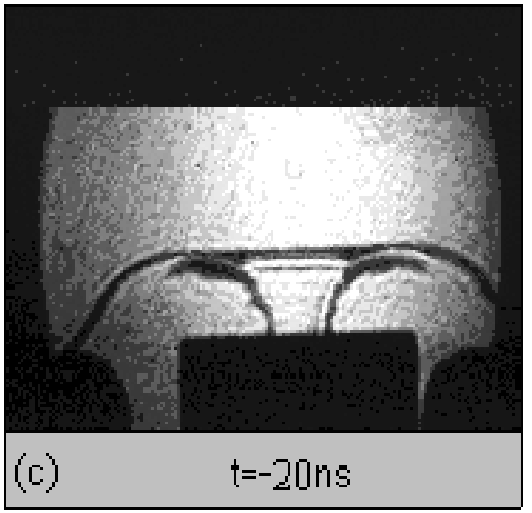

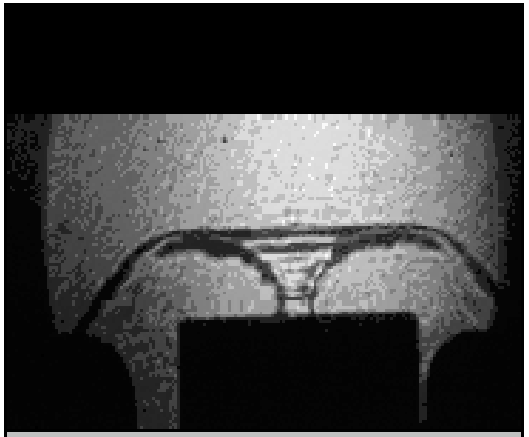

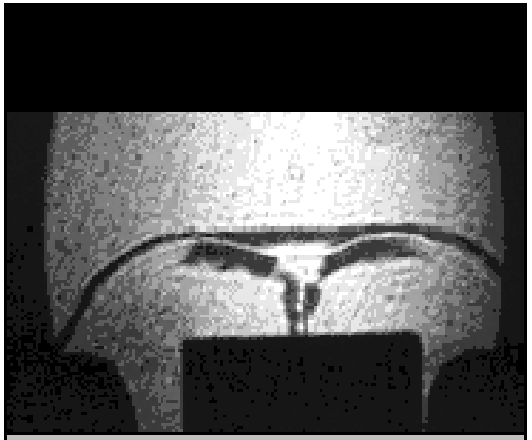

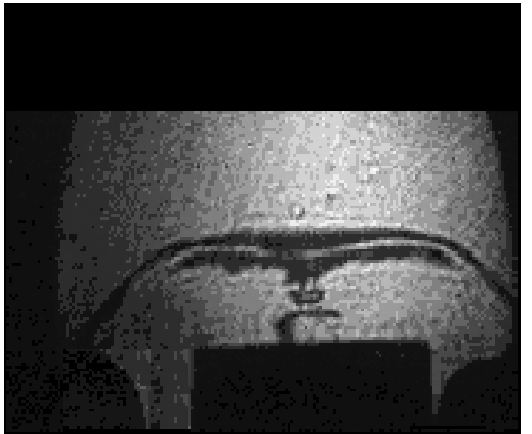

Plasma Focus Devices in Singapore

The UNU/ICTP PFF

(UnitedNationsUniversity/International Centre for Theoretical Physics Plasma Focus Facility)

- 15 kV, 3kJ
- **single-shot**, portable; 170kA
- 3J SXR per shot (neon)
- 10^8 neutrons/ shot (in D_2)
- 10^{16} neutrons/s (estimated)

(This device is also in operation in Malaysia, Thailand, India, Pakistan, Egypt, Zimbabwe)

NX2-Plasma SXR Source

- **NX2**
- 11.5kV, 2 kJ
- **16 shots /sec**; 400 kA
- 20J SXR/shot (neon)
- 10^9 neutrons/shot (est)

Small PF, high rep rate for materials interrogation applications

- Pulsed neutron source, 'fast miniature plasma focus (PF) device‘- first step in develoopment
- Neutron yield 10^6 neutrons/shot ~80 kA, 2 mbar.
- Strong pinching action, hard x-rays followed by a neutron pulse;
- measured by 3He proportional counter, NE102A plastic scintillator and CR-39 SSNTDs).
- 0.2 m × 0.2 m × 0.5 m ~25 kg.

300J portable (25 kg); 10^6 neutrons per shot fusion device

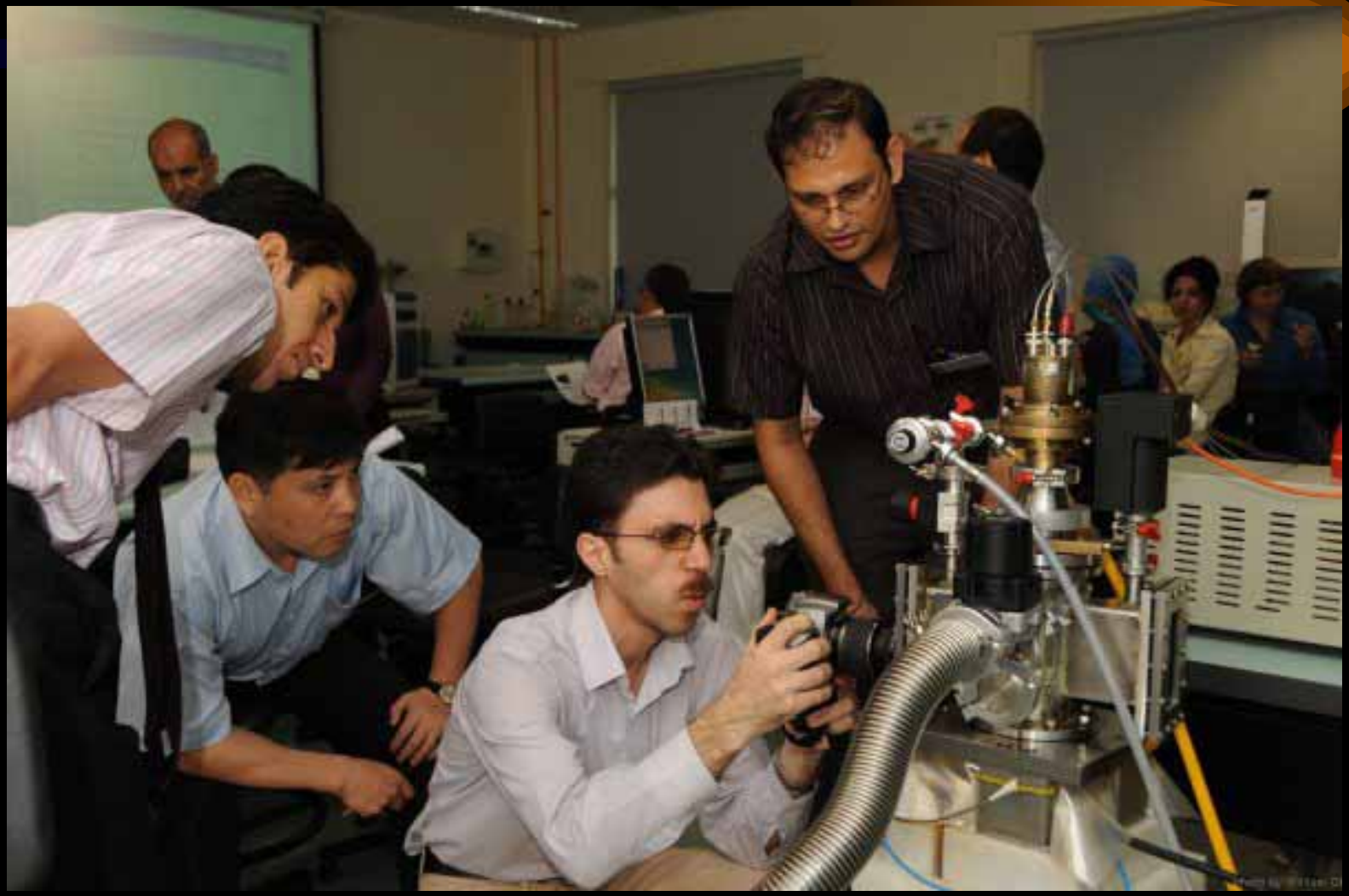

High Power Radiation from PF

- **Powerful bursts of x-rays, ion beams, REB's, & EM radiation (>10 gigaW)**
- **Intense radiation burst, extremely high powers**
- **E.g. SXR emission peaks at 10^9 W over ns**
- **In deuterium, fusion neutrons also emitted**

Introduction

PF: independently discovered by N.Filippov and J.Mather in the mid 50s – early 60s.

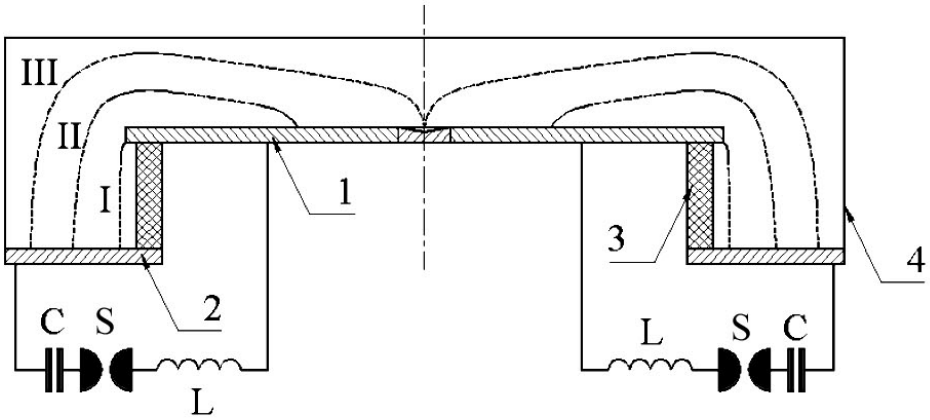

Filippov-type

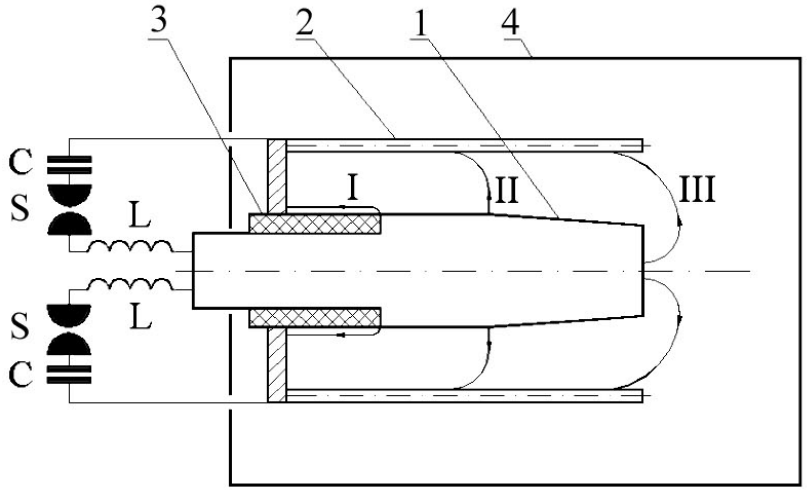

Mather-type

1 – anode, 2 – cathode, 3 – insulator, 4 – vacuum chamber, C – power supply, L – external inductance, S – spark gap. I – break-down phase; II – run-down phase; III – dense plasma focus phase

Modern Status

Now PF facilities (small to big) operate in Poland (PF-1000 and PF-6 in IPPLM, PF-360), Argentina, China, Chile, Great Britain, India, Iran, Japan, Mexico, Korea, Malaysia, Pakistan, Romania, Singapore, Thailand, Turkey, USA, Zimbabwe etc.

This direction is also traditional for Russia: Kurchatov Institute (PFE, 180 kJ and biggest in the world facility PF-3, 2.8 MJ), Lebedev Institute ("Tulip", PF-4), MEPhI, Sarov, ITEF (PF-10)-

from V.I. Krauz

1997 ICDMP (International Centre for Dense Magnetised Plasmas) Warsaw-now operates one of biggest plasma focus in the world, the PF1000

Apparatus

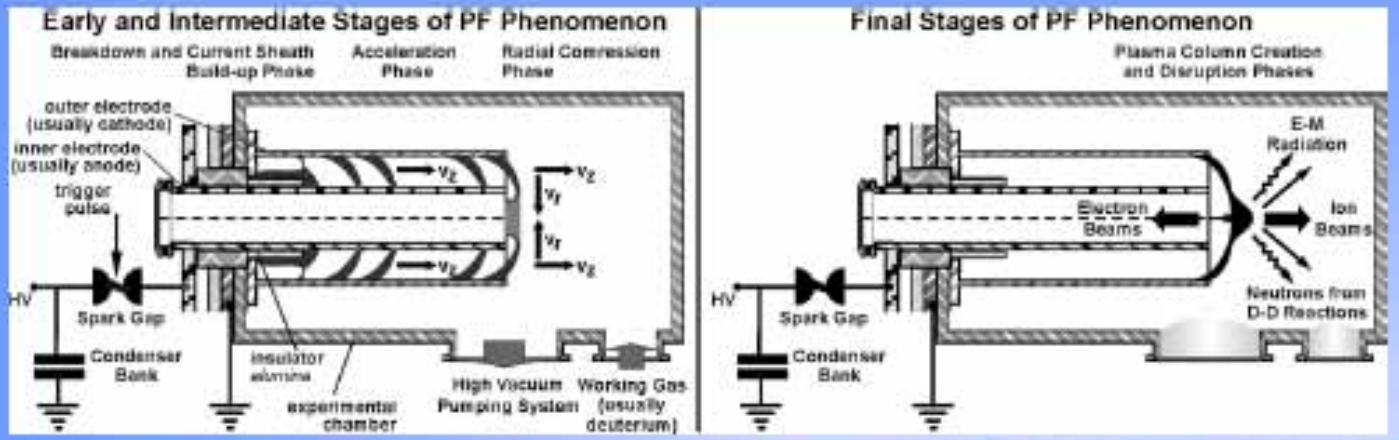

Institute of Plasma Physics and Laser Microfusion
Warsaw, Poland

PF-1000, IPPLM, Warsaw

Charging voltage - U_0 = 20 - 40 kV,
Bank capacitance - C_0 = 1.332 mF,
Bank energy - E_0 = 266 - 1064 kJ,
Nominal inductance - L_0 = 15 nH,
Quarter discharge time - T/4 = 6 μs,
Short-circuit current – I_{SC} = 12 MA,
Characteristic resistance - R_0 = 2.6 mΩ,

Vacuum chamber ~ 3.8 m^3
∅= 1.4 m, L = 2.5 m
Anode diameter is 226 mm
Cathode diameter is 400 mm
Cathode consists of 24 rods (32 mm in diameter)
Anode length is 560 mm
Insulator length is 113 mm

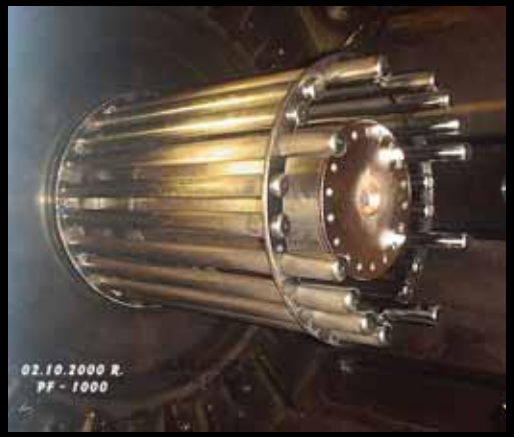

Main goal – studies on neutron production at high energy input

Measurements of Current and Voltage

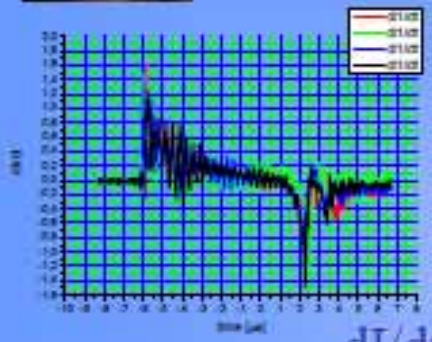

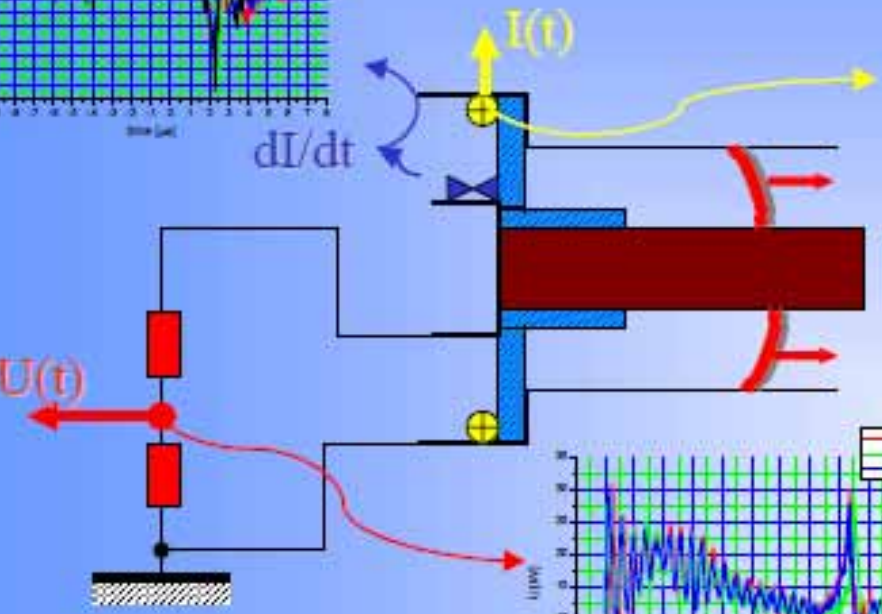

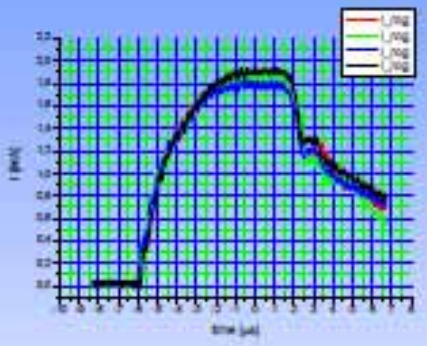

U_b= 27 kV, E_b= 480 kJ,

p = 3,5 Torr

$Y = 5 \cdot 10^{10} - 3 \cdot 10^{11}$

Institute of Plasma Physics and Laser Microfusion
Warsaw, Poland

An interesting trend-Numerical Experiments using Lee model code to benchmark Diagnostics

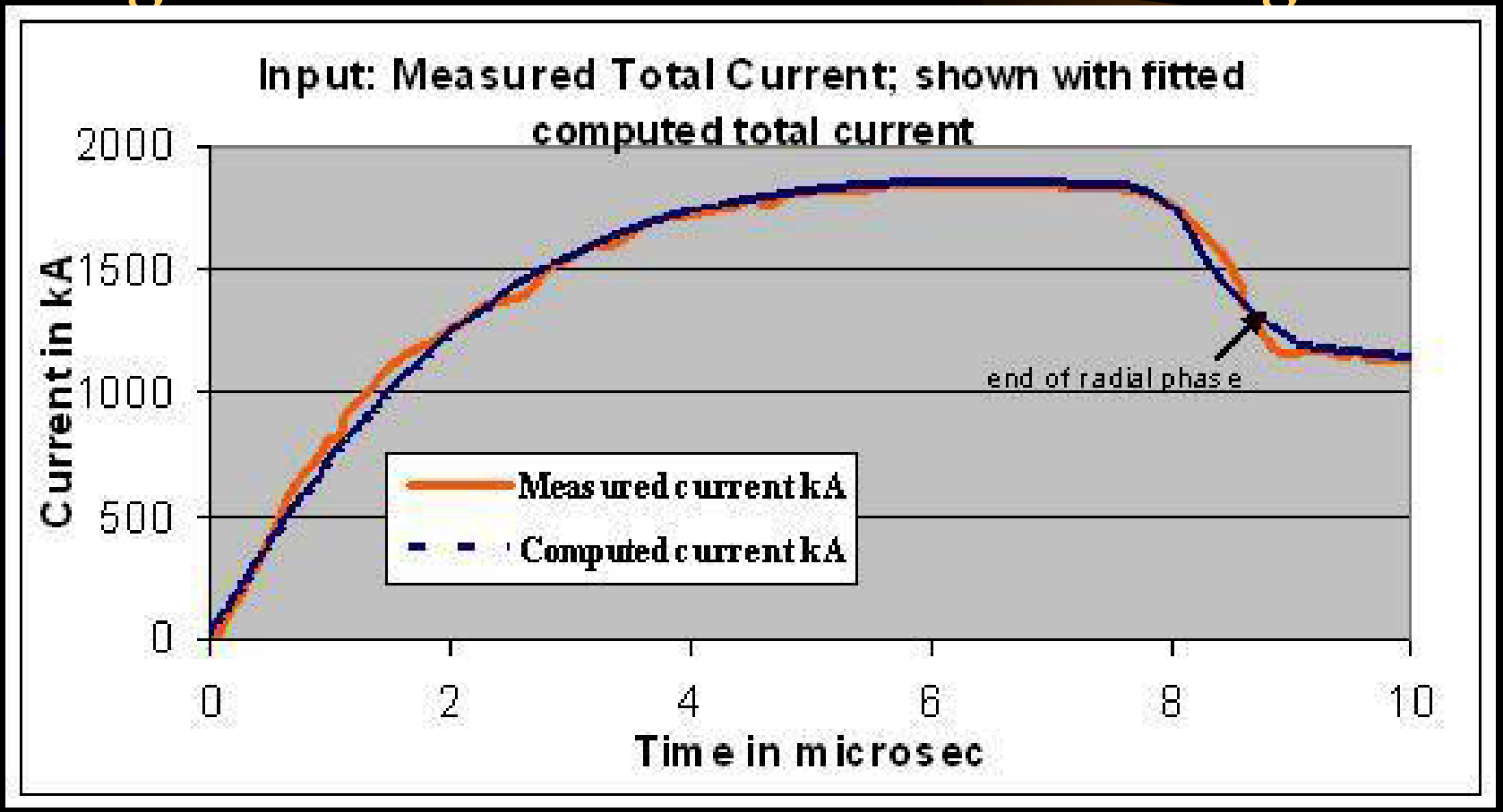

Once the computed current trace is fitted to the Measured Current, the numerical experiment and the laboratory experiment are mass and energy compatible; & computed properties are realistic. Model is an Universal Numerical Machine

Computed Properties of the PF1000: Currents, tube voltage, trajectories, speeds, energy distributions, temperatures, densities, SXR power and neutron yield

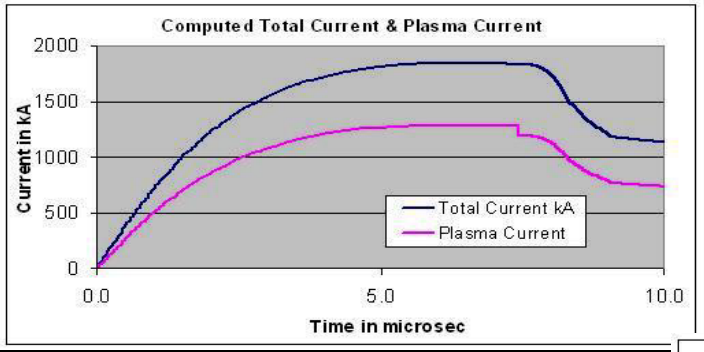

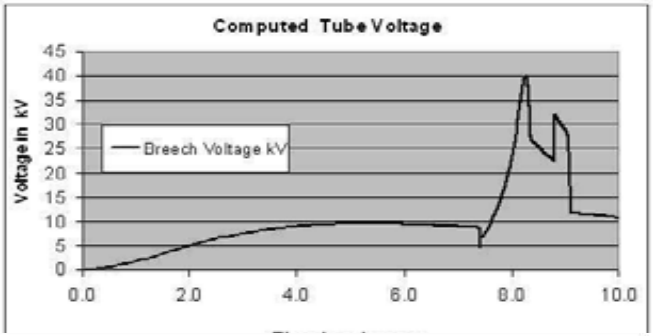

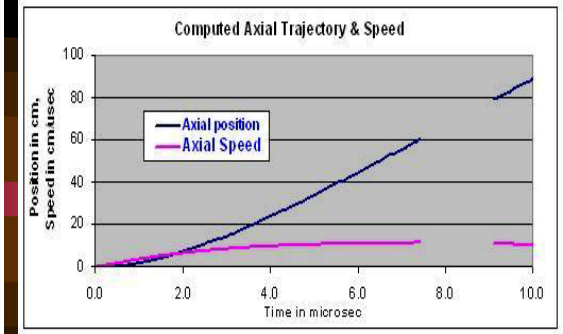

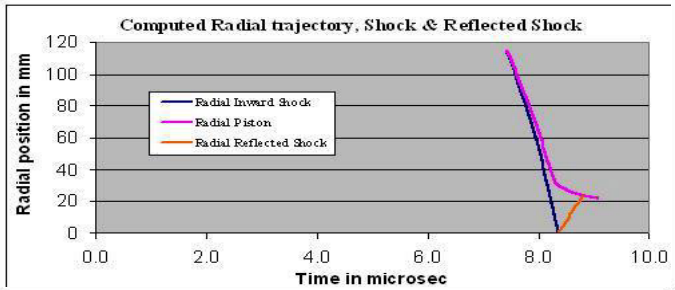

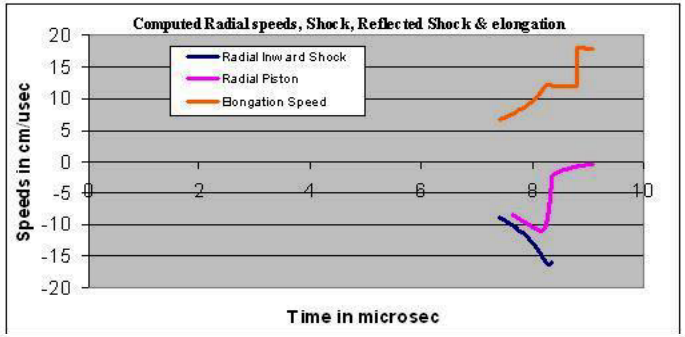

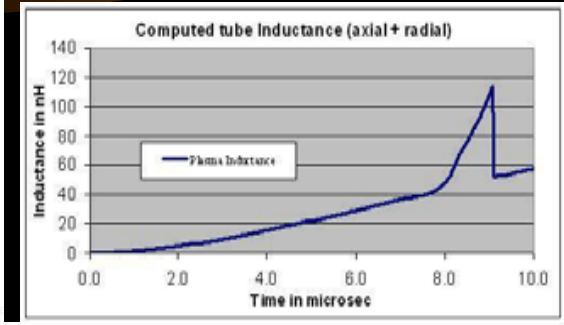

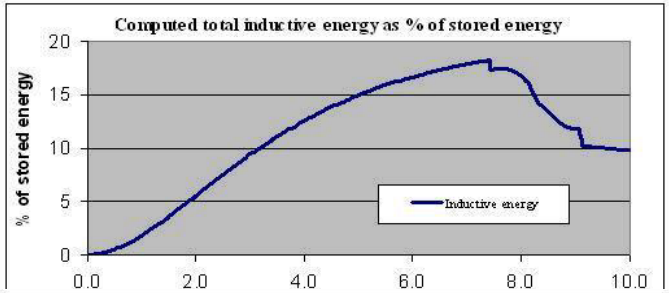

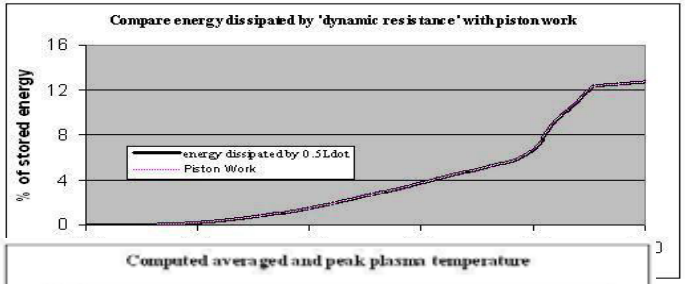

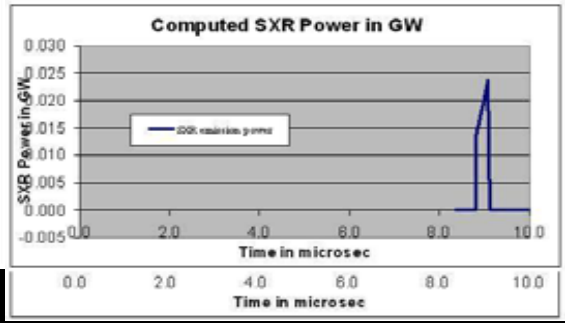

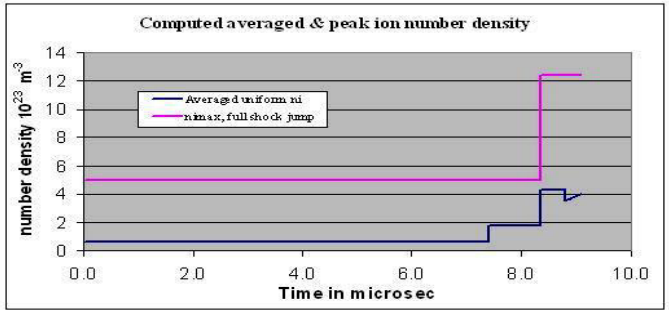

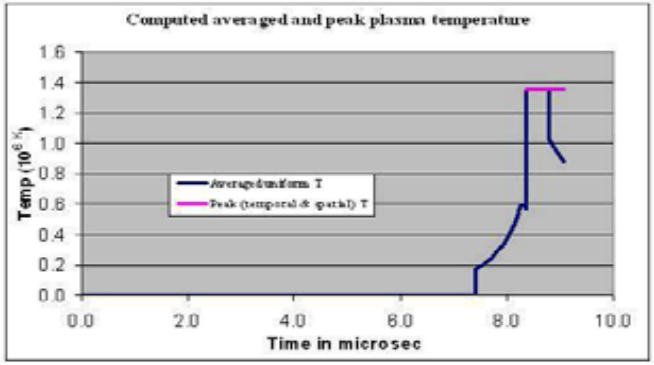

Correlation of neutron signals with frames

(first neutron pulse)

-50 ns -30 ns -10 ns 0 ns 10 ns 30 ns 50 ns

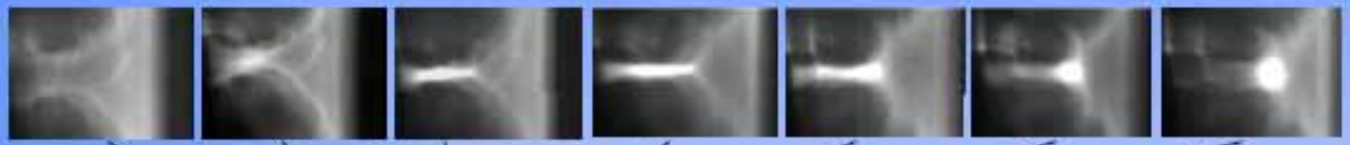

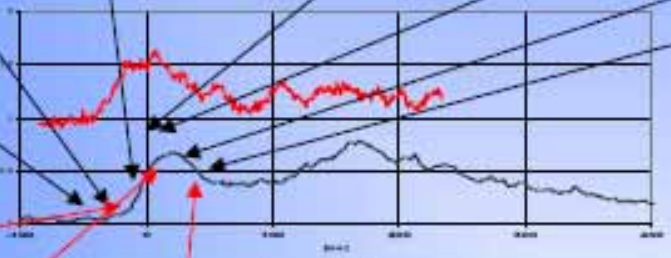

-20 ns -10 ns 30 ns

-30 ns 0 ns

Institute of Plasma Physics and Laser Microfusion
Warsaw, Poland

Visible frames – exposure time 1 ns, window 589 nm

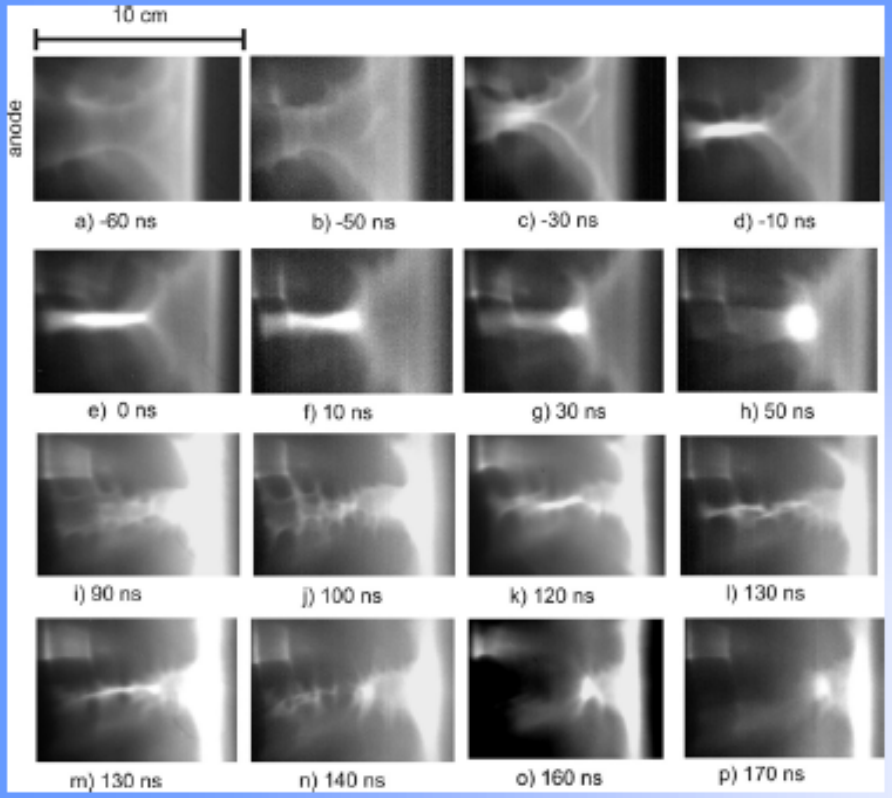

a-d *implosion 2x10^{5}m/s*
e *minimum radius t=0*
c-g *intense light - dense plasma, dense spherical structure*
g-p *instabilities*
j-m *second pinch*
m-n *second explosion*
m-p *second dense structure*

Institute of Plasma Physics and Laser Microfusion
Warsaw, Poland

XUV frames – exposure time 2 ns, window 200-300 eV+above 600 eV

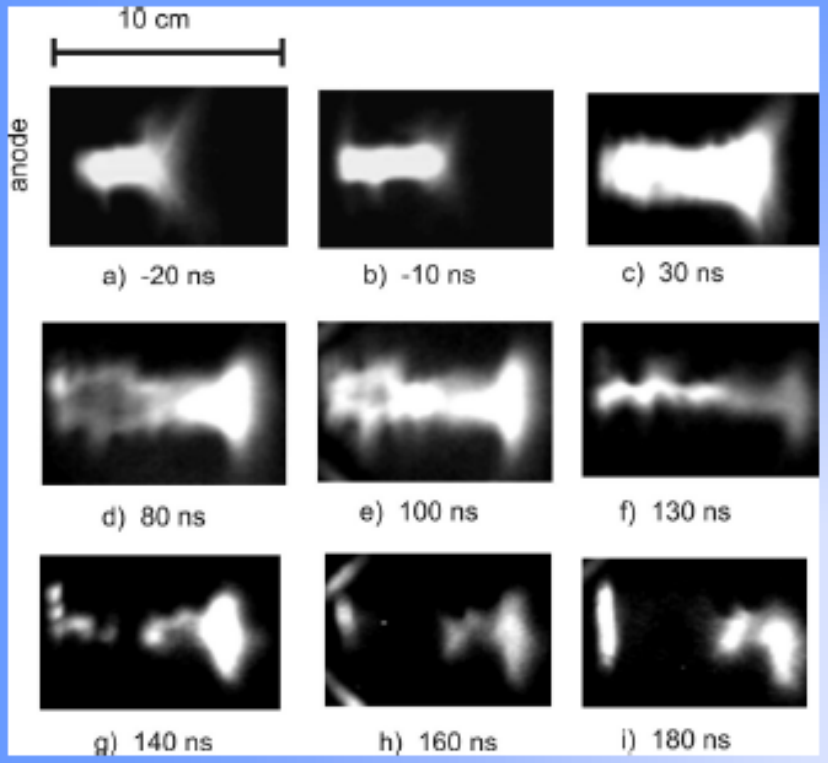

a-c *pinch o 1-2 cm;*
d *– first expansion*
e-f *- second pinch*
g-i *explosion, dense structure*
dense spherical structure

RUSSIAN RESEARCH CENTRE KURCHATOV INSTITUTE

Plasma Focus PF-3

- Filippov's-type
- Anode Diameter = 1 m
- Chamber Diameter=2,5 m
- Cathode - 48 rods; diameter = 115 cm
  Distance between anode and upper = 10 cm
- Height of the insulator = 14 cm
- Maximal energy (C_{max}=9,2 mF, V_{max}=25 kV) is 2,8 MJ
- Short-circuit current =19 MA
- Current on the load - up to 4 MA at 1MJ

Main direction of activity - Search of new ways of PF performance and applications.

E.g. use PF as a driver for magnetic compression of liners

PF-3 Experimental Setup- with plasma producing substances

Experiments with various plasma-producing substances & various filling gases were recently the main content of activities at the PF-3 facility

Vacuum lock developed for delivery of liners to compression zone.

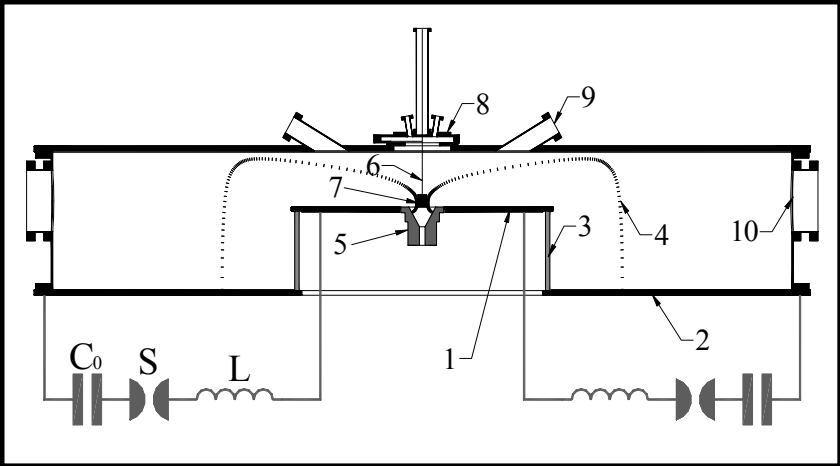

1 – anode; 2 – cathode; 3 – insulator; 4 – plasma current sheath; 5 – anode insertion; 6 – suspension ware; 7 – liner; 8 – loading unit with a vacuum lock; 9, 10 – diagnostics ports;

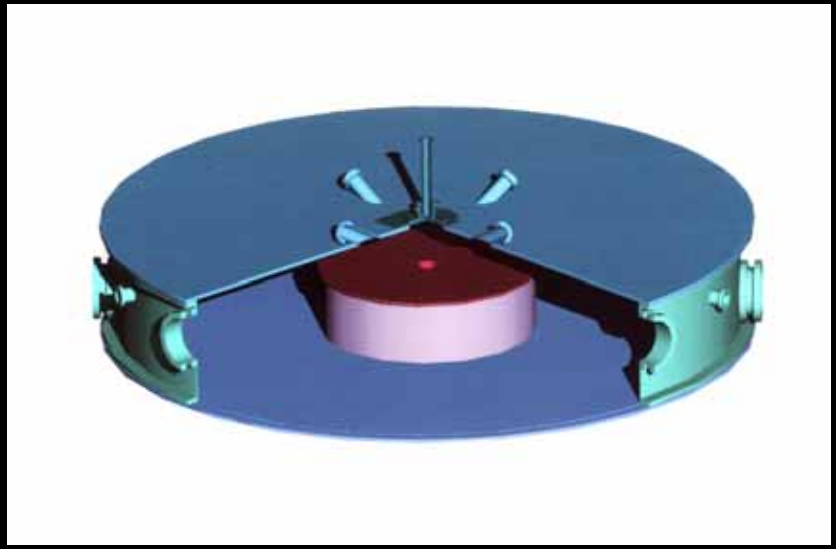

PF discharge chamber

Plasma focus as a driver for magnetic compression of liners

Some combined schemes are discussed for production of laboratory soft X-ray sources, where PF is used as inductive storage and the current sheath realizes energy transport to the load located at the system axis.

Due to spatial-temporal current peaking it is possible to achieve current rise rate on the load $\dot{I} \sim I\,(V_r / \delta) \sim 10^{14}$ A/s at $I \sim 3$ MA, $\delta \sim 1$ cm & $V_r \sim 3 \cdot 10^7$ cm/c

The prospects of such an approach has been shown first in the Polish-Russian experiment on the foam liner compression at PF-1000 facility:

M.Scholz, L.Karpinski, W.Stepniewski, A.V.Branitski, M.V.Fedulov, S.F.Medovstchikov, S.L.Nedoseev, V.P.Smirnov, M.V.Zurin, A.Szydlowski, Phys.Lett., A 262 (1999), 453-456

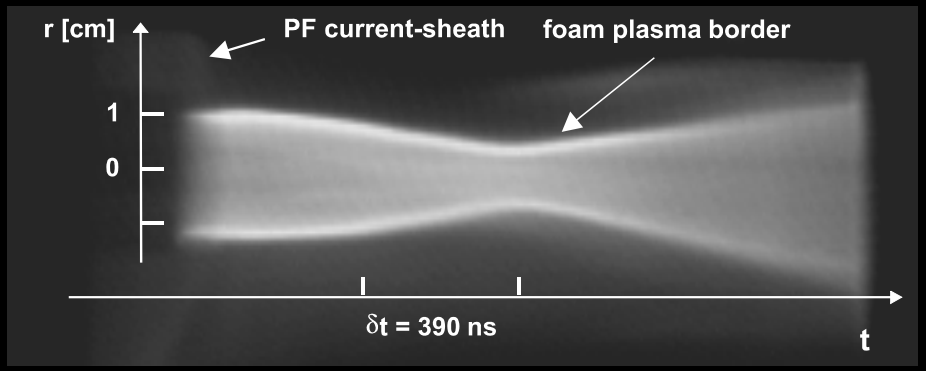

<u>Main problem</u>: the efficiency of the energy transfer to the load

Experiments with liners

Long radial compression duration (~ 10μs) : preliminary heating of the target and, subsequently, acceleration of the initially – condensed material into plasma state is attained.

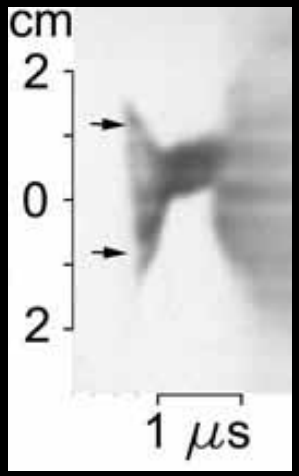

foam liner
0.3 mg/cm
I_p = 1.2 MA

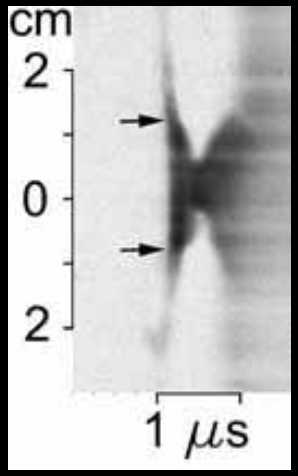

foam liner
0.3 mg/cm
I_p = 2.5 MA

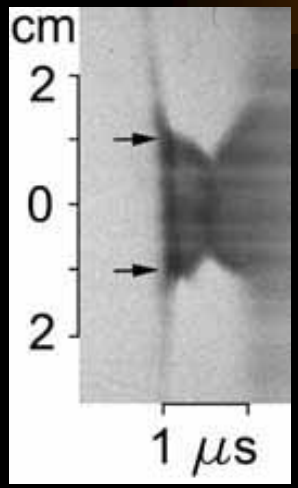

foam liner
1.0 mg/cm
I_p = 2.5 MA

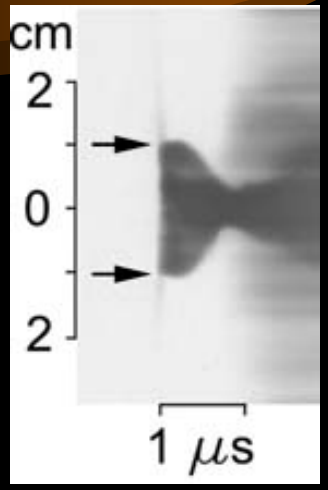

wire array
0.66 mg/cm
I_p = 1.2 MA

Diameter of the foam liner at the moment of the contact with the sheath exceeds the initial diameter – pre-heating by the sheath radiation Therefore, PF discharge can effectively control process of liner evaporation and ionisation by changing the gas and the liner parameters; thus assists in overcoming "cold start" problem.

Experimental set-up — Dust Target

Dust target produced at system axis as a freely-falling flow of fine-dispersed (2 - 50 μm) powder of Al_2O_3

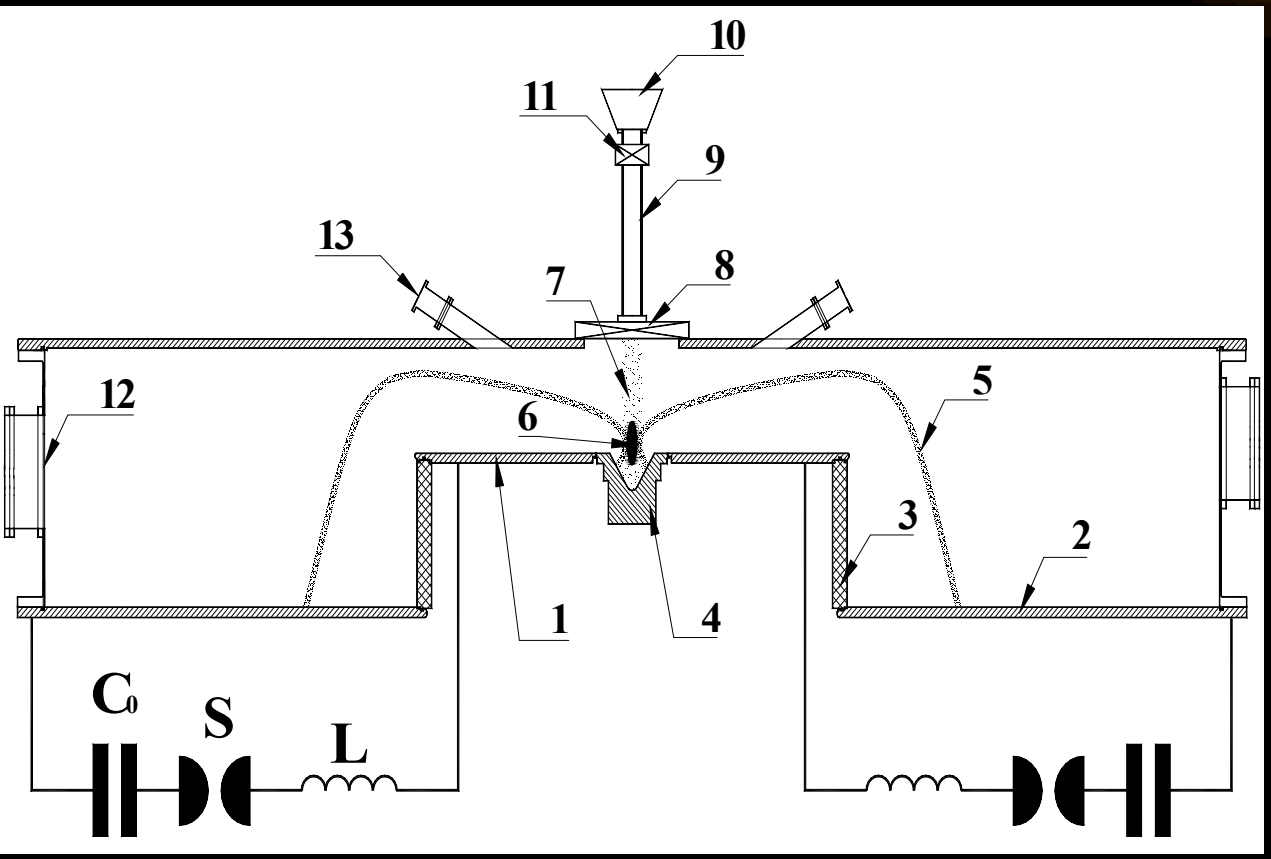

1 – anode; 2 – cathode; 3 – insulator; 4 – central anode insert; 5 – plasma-current sheath; 6 – pinch; 7 – dust column; 8 – vacuum lock; 9 – shaping drifting tube; 10 – tank with powder; 11 – electromagnet; 12, 13 – diagnostic ports

KPF-4 ("PHOENIX"), SPhTI, Sukhum

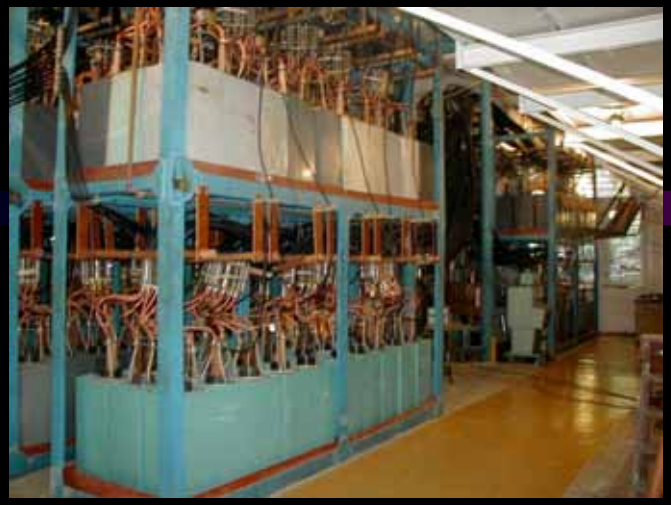

Capacitive storage (left) and discharge chamber with current collector (right)

W_{max}= 1.8 MJ, V_{max}=50 kV, discharge system – Mather-type

outer electrode – 300 mm diameter (36 cooper rods, 10 mm in diameter)

inner electrode (anode) – 182 mm diameter, 326 mm in length

insulator – alumina, 128 mm in diameter, 50-100 mm in length

Discharge dynamics has been studied at energy supply up to 700 kJ and discharge currents 3-3.5 MA

***Main goal** – development of powerful neutron and X-ray source for applications.*

(E.A.Andreeshchev, D.A.Voitenko, V.I.Krauz, A.I.Markolia, Yu.V.Matveev, N.G.Reshetnyak, E.Yu.Khautiev, 33 Zvenigorod Conf. on Plasma Phys. and Nuclear Fus., February 13-17, 2006, Zvenigorod, Russia)

Plasma-wall interaction simulation for thermonuclear reactor experiments

- D-plasma jets (1 keV) and fast ion beams (50-150keV) generated in the PF was used to bombard low-activated austenitic steel 25Cr12Mn20W and ferrite steel 10Cr9W positioned in cathode part of PF chamber. PF beam conditions was suitable for reactor first wall material testing, during the PF short burst.
- ERDA (Elastic Recoil Detection Analysis) was used to trace D scattering profile within irradiated samples

Some conclusions of plasma-wall interaction using PF

- When power flux density of irradiation was 10^6-10^8 W/cm2. ion implantation to irradiating material surface layer is observed
- When power flux density increases to 10^9 W/cm2 , so-called ‘broken-implantation” takes place
- Ion diffusion velocity of implanted deuterium through both interfaces-’layer-bulk material’ and ‘layer-gas phase’ for Fe-based alloys were estimated.

Plasma Focus Technology: PFMA-1, Plasma Focus for Medical Applications, the first prototype of a PF device for 18-F production, a 150 kJ (350 μF @ 30 kV) Mather-type Plasma Focus operated at 1 Hz repetition frequency that could breed ~ 1 Ci of F^{18} in 2 hours.

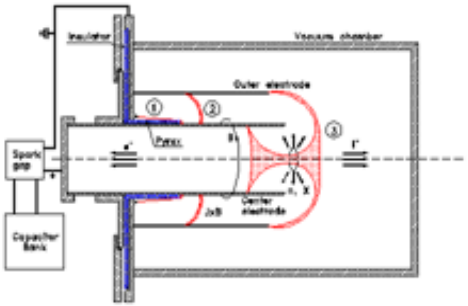

Mather type PF scheme

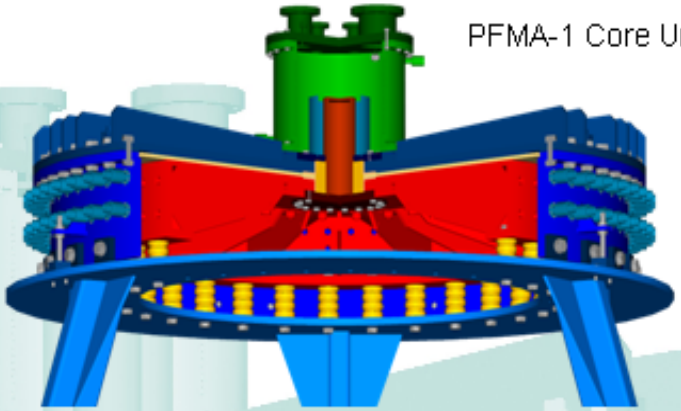

PFMA-1 Core Unit

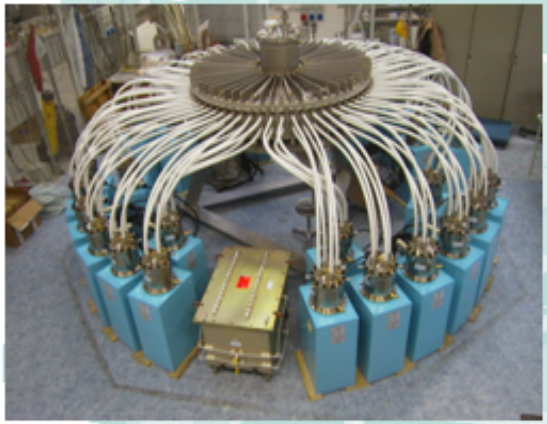

PFMA-1

UNIVERSITY OF BOLOGNA

ABO PROJECT 2010

azienda Ulss 12 veneziana

UNIVERSITY OF FERRARA

Presented by A.Tartari, University of Ferrara

International Collaboration

- Plasma Focus
  - is a very cost effective experimental set-up
  - Multitude of physical phenomena
  - Many applications
- PF is used successfully as facilities for scientific collaboration
  - Asian African Association for Plasma Training
  - International Centre for Dense Magnetised Plasmas

UNU/ICTP Training Programmes

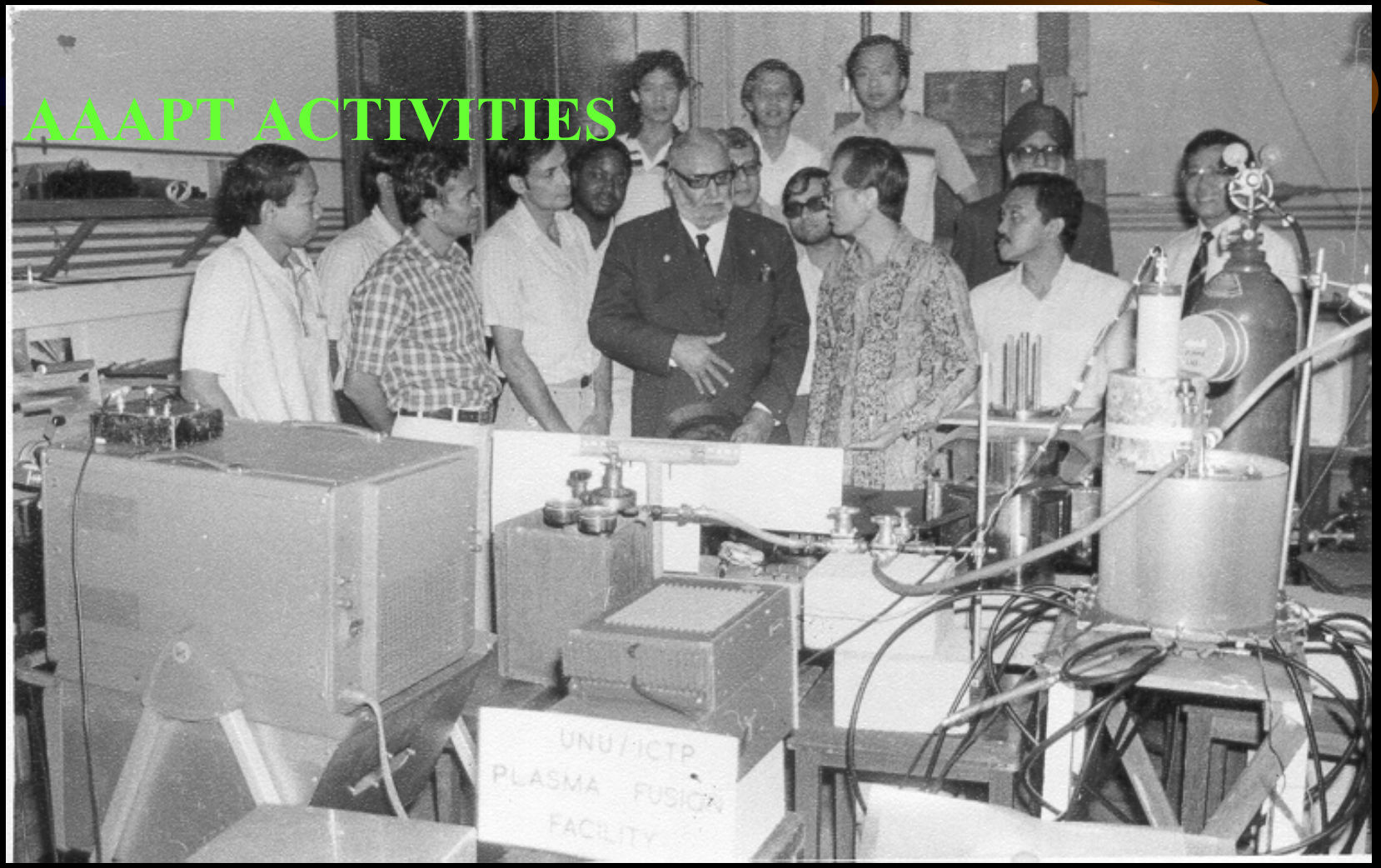

Abdus Salam with UNU Plasma Focus Trainees, Kuala Lumpur, 1986

IAEA Co-ordinated Research Programme

IAEA Co-ordinated Research Project "Dense Magnetized Plasma" joins 12 institutions from 8 countries: Poland, Russia, Italy, Singapore, China, Estonia, Romania, Republic of Korea.

The main directions of applications developed are:

-radiation material science;

-proton emission tomography;

-X-ray lithography;

-radiation enzymology;

-radiation medicine, etc;

(*Proceedings of the 2nd IAEA Co-ordination Meeting of the Co-ordinated Research Project on Dense Magnetized Plasma, 1-3 June 2005, Kudowa Zdroj, Poland,* ***Nukleonika 2006; 51(1))***

Neutron Scaling:
from optimism up to disappointment

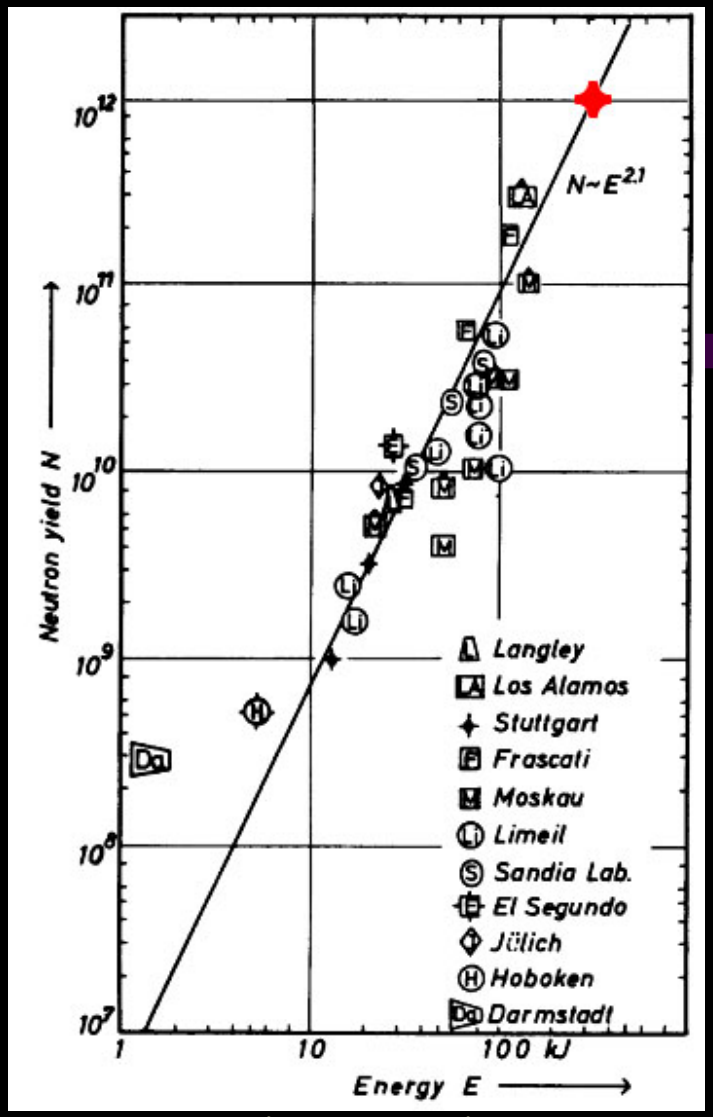

Neutron yields N against energy E, assembled by H.Rapp

(Michel L., Schonbach K.H., Fisher H. Appl. Phys. Lett.- 1974.-V.24, N2.-P.57-59)

- Essential progress was achieved in the early 2-3 decades in the understanding physical processes in PF.
- One of the most important achievement was empirical scaling for neutron output: $N \sim E^2$ or $N \sim I^4$
- All attempts to reach 10^{13} D-D neutrons expected for 1 MJ were failed
- The best result achieved till now is $\sim 10^{12}$ at W~500 kJ (Los-Alamos, Limeil, Frascati)
- As a result PF activities were shut down in many countries – leaders in fusion researches

Chart from M Scholz (November 2007 ICDMP)

Scaling

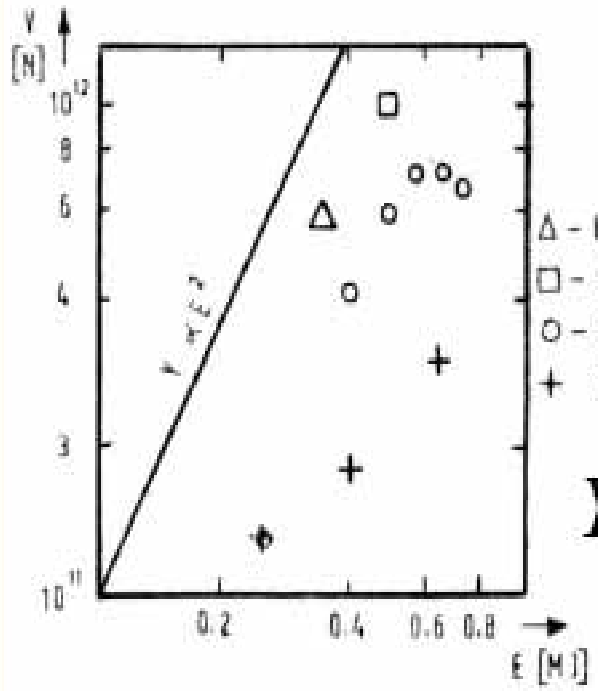

$$\frac{1}{2}(L + L_0)I^2 \cong \gamma E$$

$$L \cong L_0$$

$$Y_n \propto E^2$$

$$I^2 \propto E$$

Frascati (Program Euroatom), $E_b = 1MJ$; $U_b = 50$ kV;

Illustrating Y_n 'saturation' observed in numerical experiments (solid line) compared to measurements on various machines (small squares)

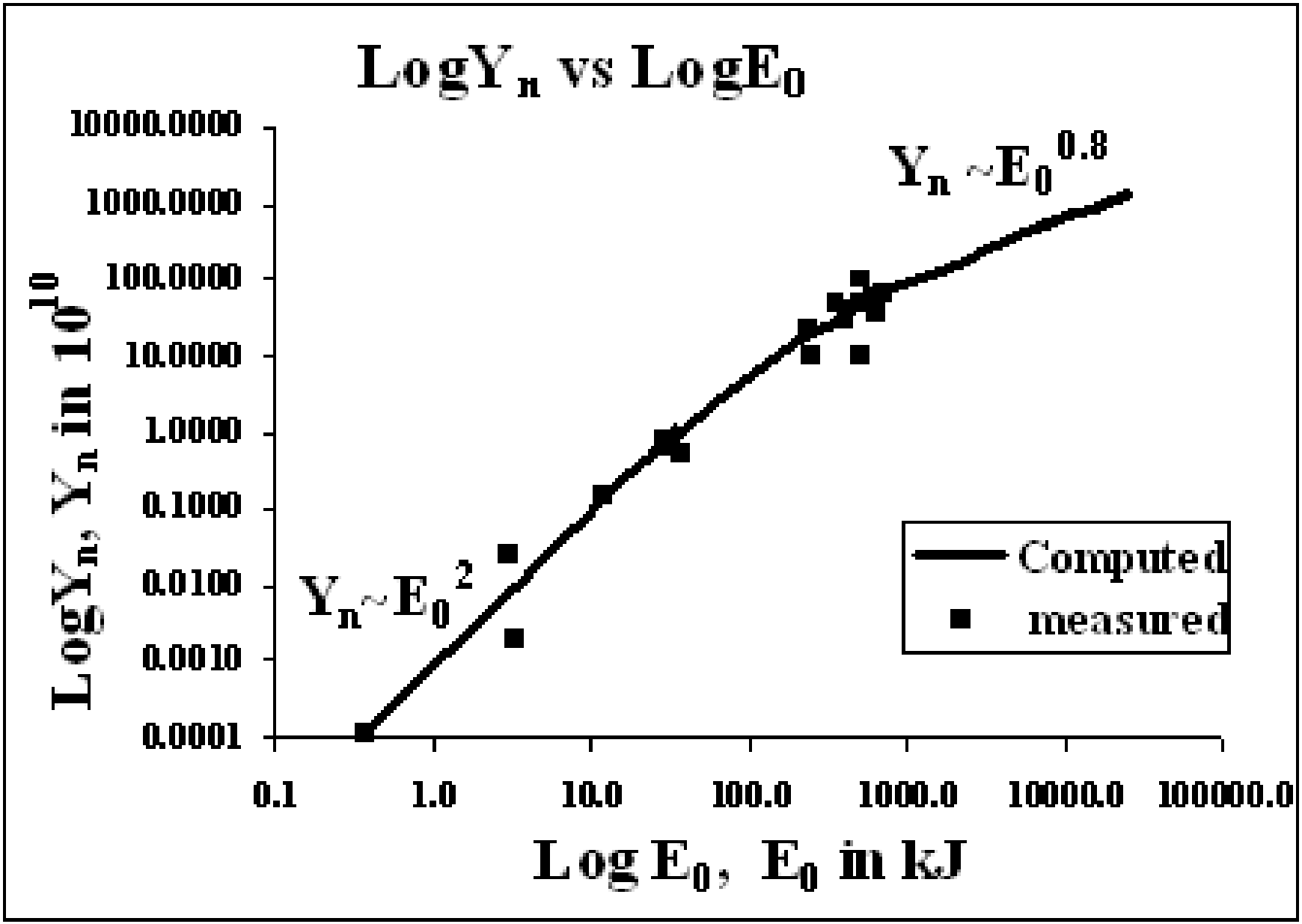

Comparing I_{total} for small & large plasma focus

- **Small PF-400J; 0.4kJ 28 kV 6.6 Torr D2**
- **Large PF1000 (0.5 MJ) 27 kV 3.5 Torr D2**

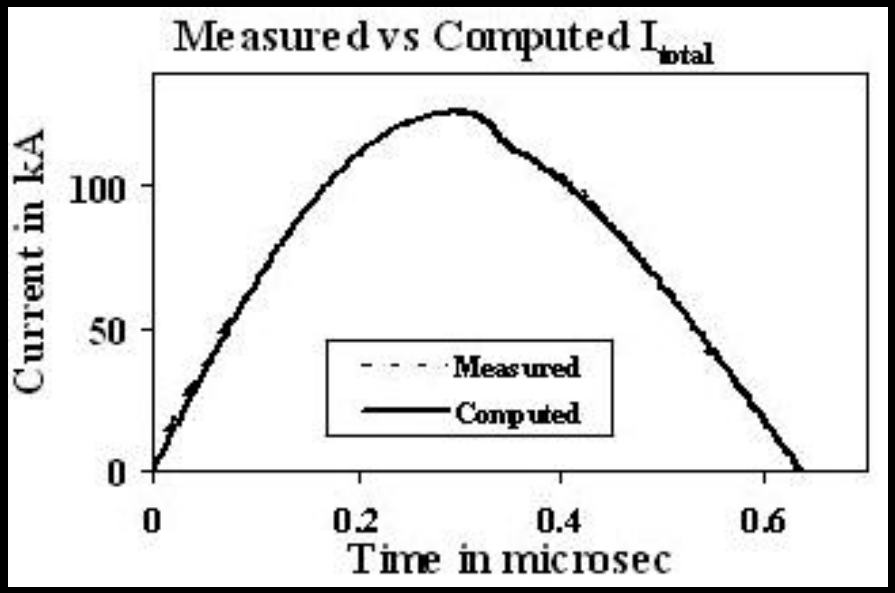

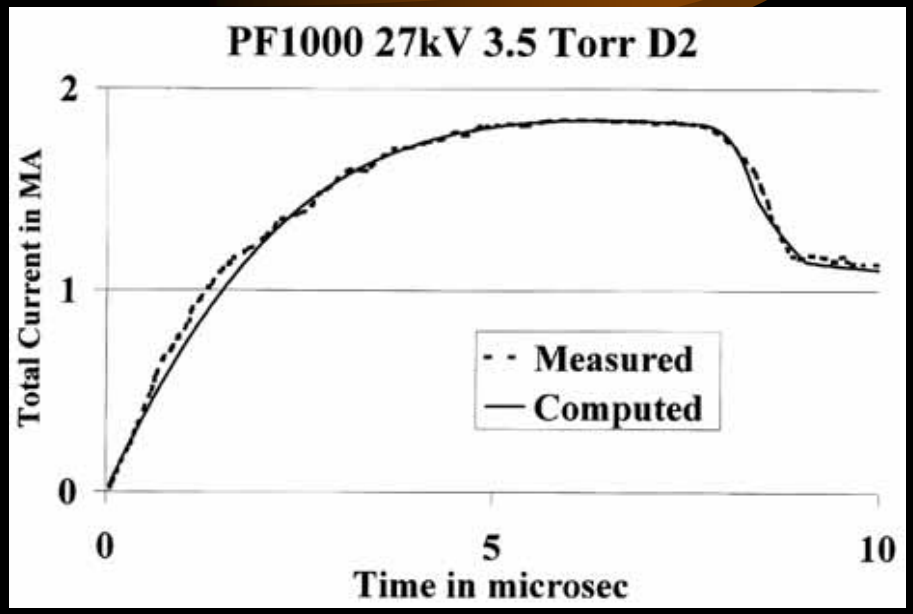

~300ns risetime; ~ 20ns current dip of <5%

End axial speed: 10cm/us

~8 us risetime; ~2 us current dip of 35%

End axial speed: 10cm/us

Y_n saturation trend already observed in numerical experiments

- **The deterioration of the Y_n scaling observed in numerical experiments agree generally with the measured data on Y_n yield of large experiments**
- **What is the physical basis of this scaling deterioration?**

Comparing generator impedance & Dynamic Resistance of small & large plasma focus- before I_{peak}

PF	$Z_0 = (L_0/C_0)^{1/2}$	Axial DR_0	Axial dominance	I_{peak}
Small	100 mΩ	7 mΩ	Z_0	~ V_0/Z_0
Large	1 mΩ	7 mΩ	DR_0	~V_0/DR_0

As E_0 is increased by increasing C_0, with voltage kept around tens of kV, Z_0 continues to decrease and I_{peak} tends towards asymptotic value of V_0/DR_0

Illustrating the dominance of DR_0 as E_0 increases,

V_0=30kV, L_0=30nH; $Z_{total}=1.1Z_0+DR_0$

E_0	C_0	Z_0	DR_0	Z_{total}	$I_{peak} = V_0/Z_{total}$	I_{peak} from L-C-R	
kJ	uF	mΩ	mΩ	mΩ	kA	kA	
0.45	1	173	7	197	152	156	
4.5	10	55	7	67	447	464	
45	100	17	7	26	1156	1234	
135	300	10	7	18	1676	1819	
450	1000	5.5	7	12.9	2321	2554	
1080	2400	3.5	7	10.8	2781	3070	
4500	10000	1.7	7	8.8	3407	3722	
45000	100000	0.55	7	7.6	4209	4250	

Confirming I_{peak} saturation is due to constancy of DR_0

I_{peak} vs E_0 from DR_0 analysis compared to model simulation

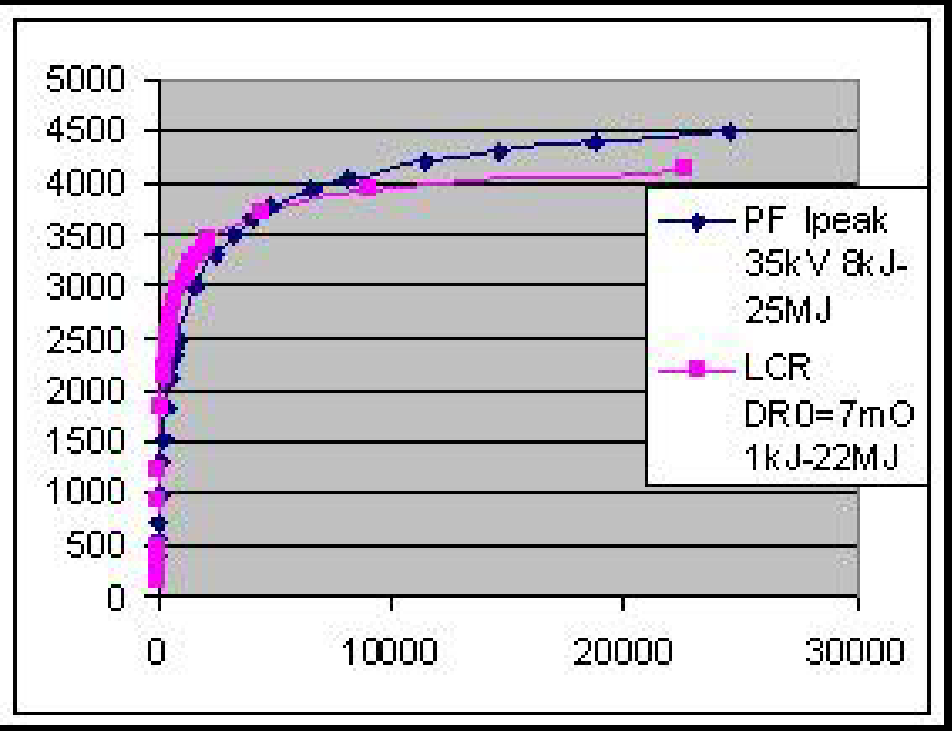

Model simulation gives higher I_{peak} due to a 'current overshoot effect' which lifts the value of I_{peak} before the axial DR_0 fully sets in

I_{peak} vs E_0 on log-log scale DR_0 analysis

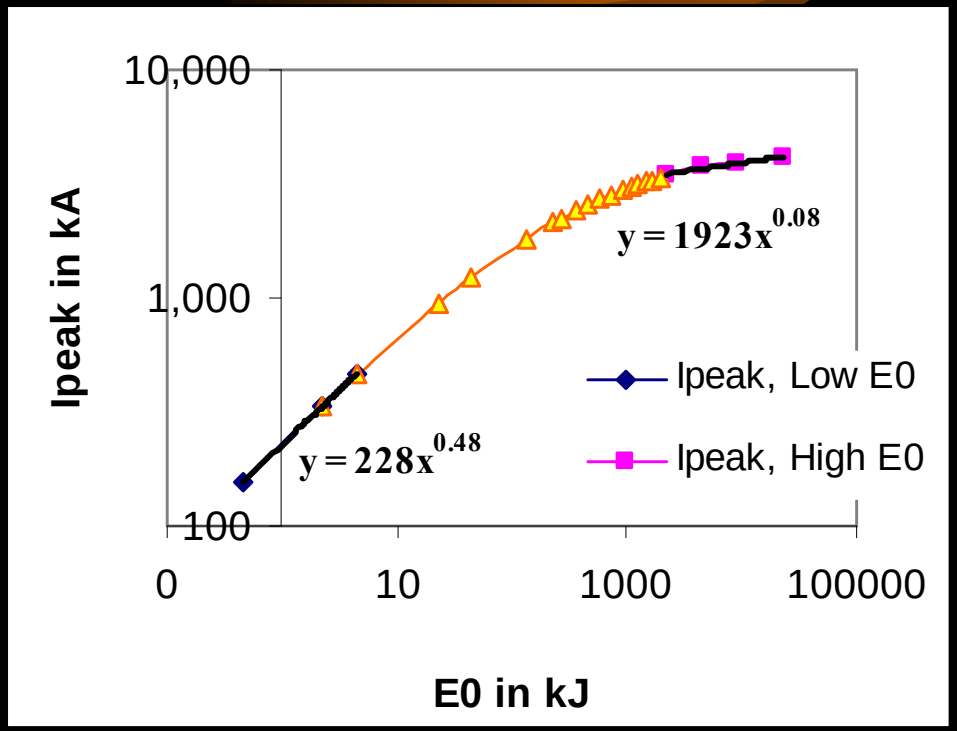

Confirming that I_{peak} scaling tends to saturate before 1 MJ

We have shown that: constancy of DR_0 leads to current 'saturation' as E_0 is increased by increasing C_0. Tendency to saturate occurs before 1 MJ

From both numerical experiments as well as from accumulated laboratory data

- $\mathbf{Y_n \sim I_{pinch}^{4.5}}$
- $\mathbf{Y_n \sim I_{peak}^{3.8}}$

Hence the 'saturation' of I_{peak} leads to saturation of neutron yield Y_n

Insight- neutron saturation

- **A major factor for ‘neutron saturation’ is simply: Axial Phase Dynamic Resistance**

Beyond saturation?

Possible ways to improve Y_n:

- **Increase operating voltage. Eg SPEED II uses Marx technology: 300kV, driver impedance 60 mΩ. With E_0 of under 200 kJ, the system was designed to give I_{peak} of 5 MA and I_{pinch} just over 2 MA.**
- **Extend to 1MV-with low bank impedance- would increase I_{peak} to 100 MA; at several tens of MJ. I_{pinch} could be 40 MA**
- **Y_n enhancing methods such as doping deuterium with low % of krypton.**
- **Further increase in I_{pinch} by fast current-injection near the start of radial phase. This could be achieved with charged particle beams or by circuit manipulation such as current-stepping. This model is ideally suited for testing circuit manipulation schemes.**

Ongoing IPFS numerical experiments of Multi-MJ, High voltage MJ and Current-step Plasma Focus
IPFS & INTI UC September 2009

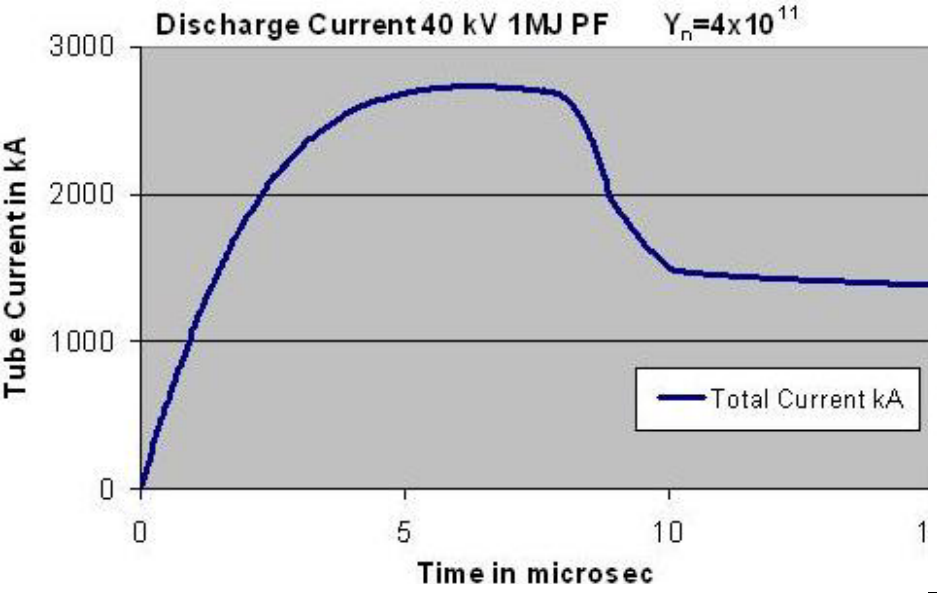

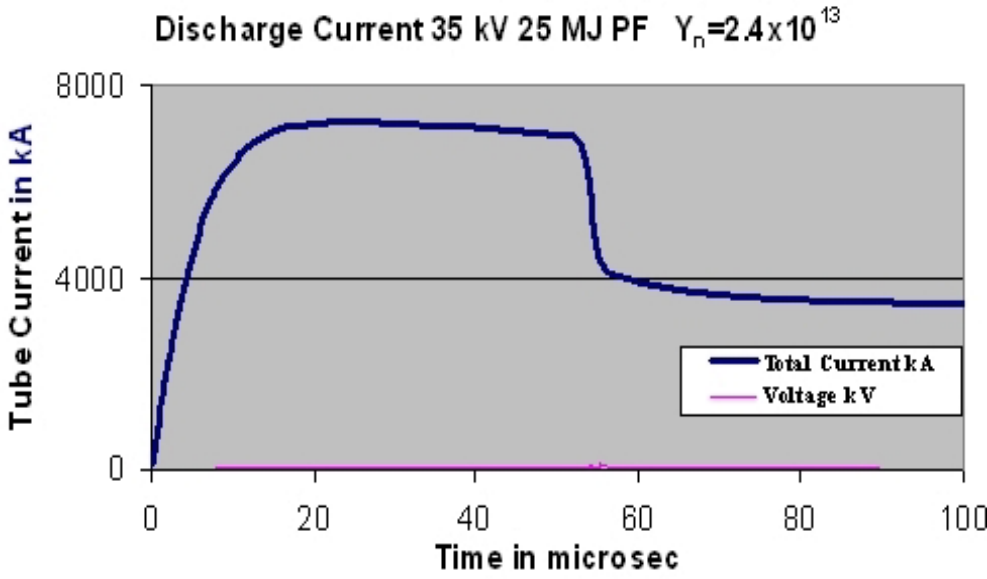

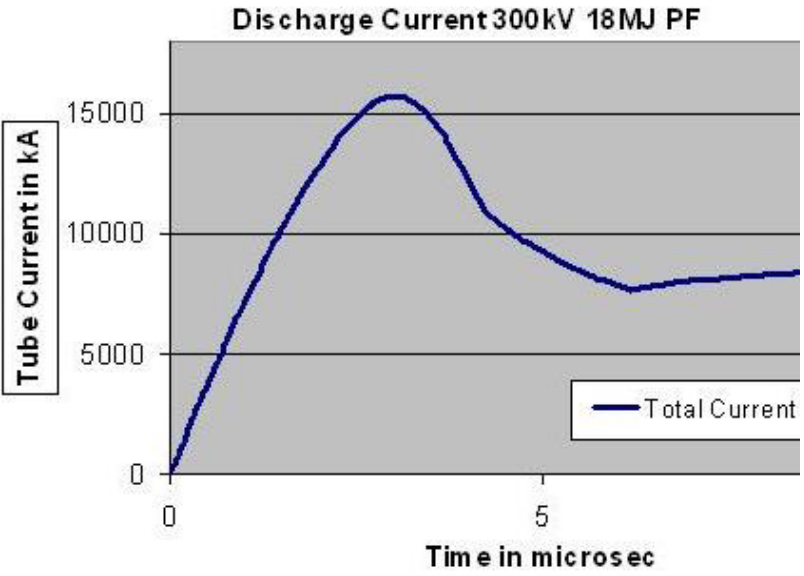

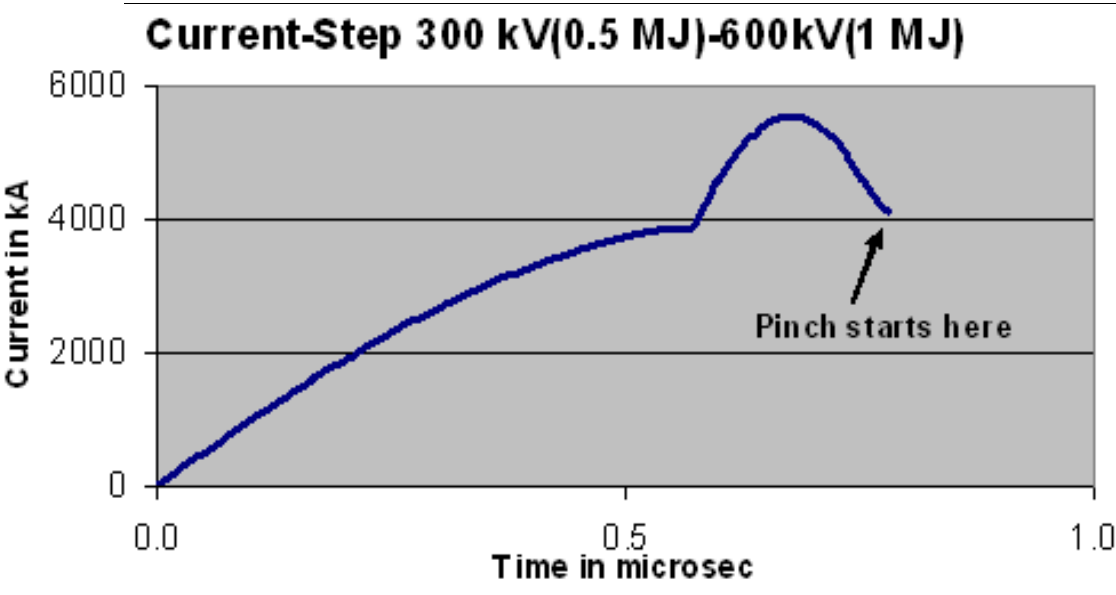

Improvement to Diagnostics-another key to plasma focus fusion studies

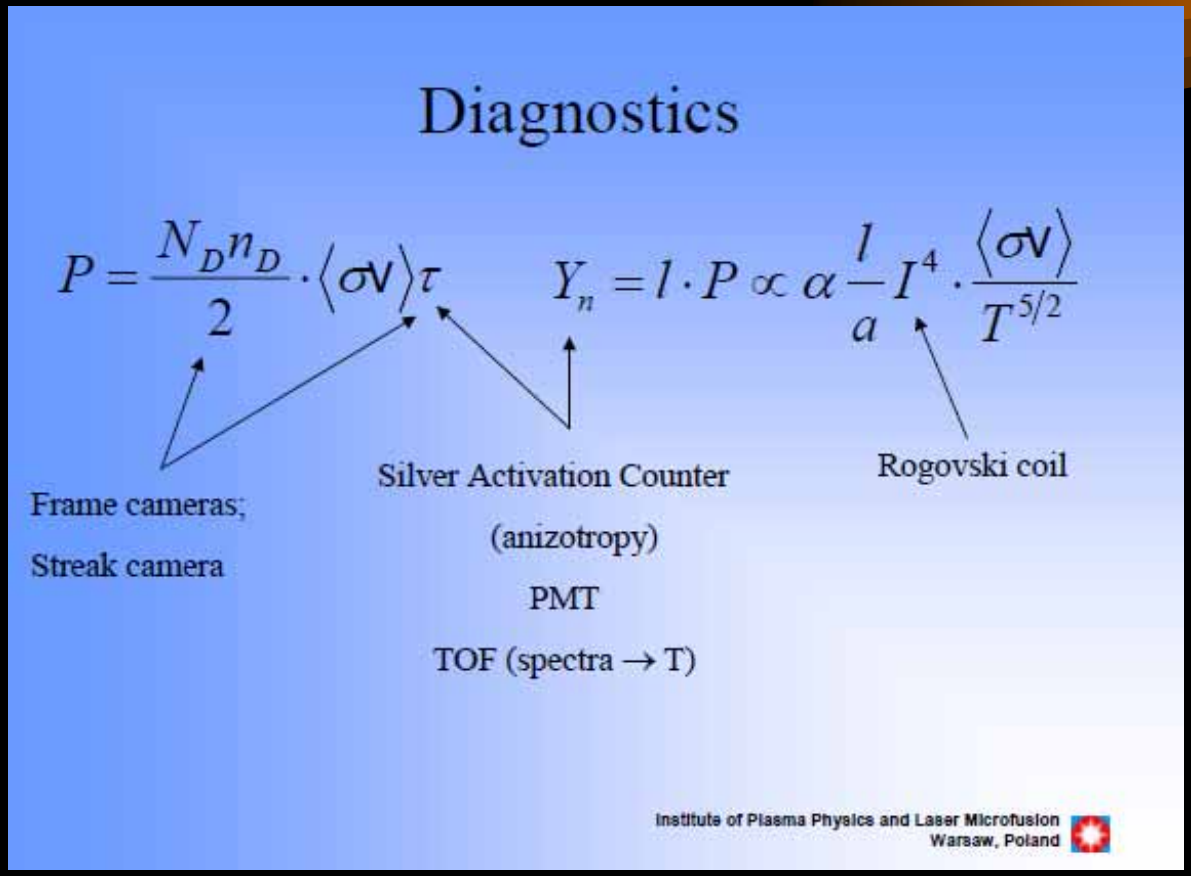

Compression, Pinch & Post-pinch

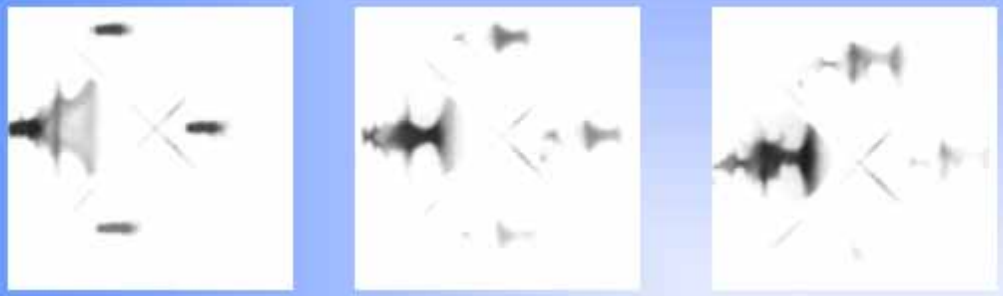

XUV frames – exposure time 2 ns, window 200-300 eV+above 600 eV

Institute of Plasma Physics and Laser Microfusion
Warsaw, Poland

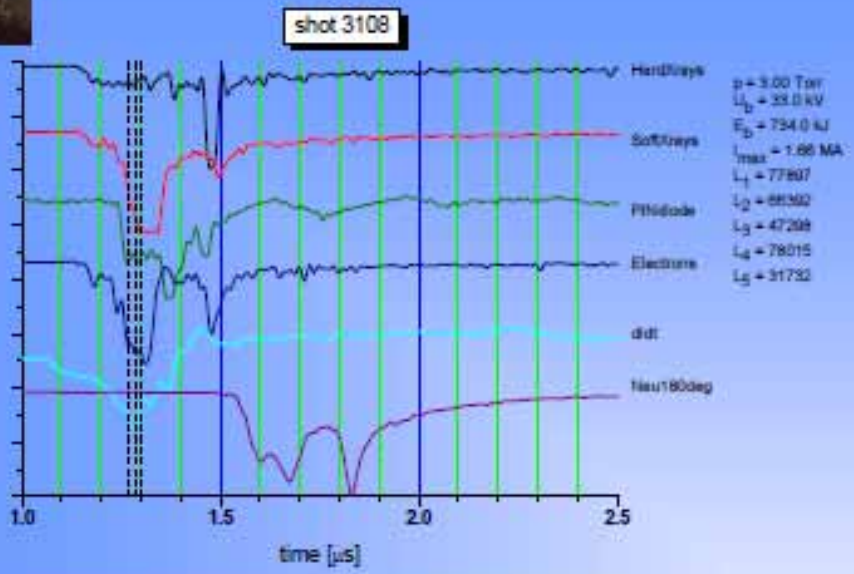

1.269 μs

1.289 μs

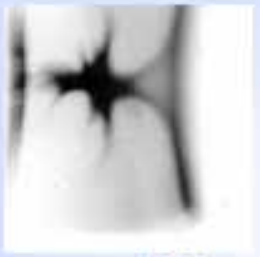

1.299 μs

Institute of Plasma Physics and Laser Microfusion
Warsaw, Poland

Visible streak-camera

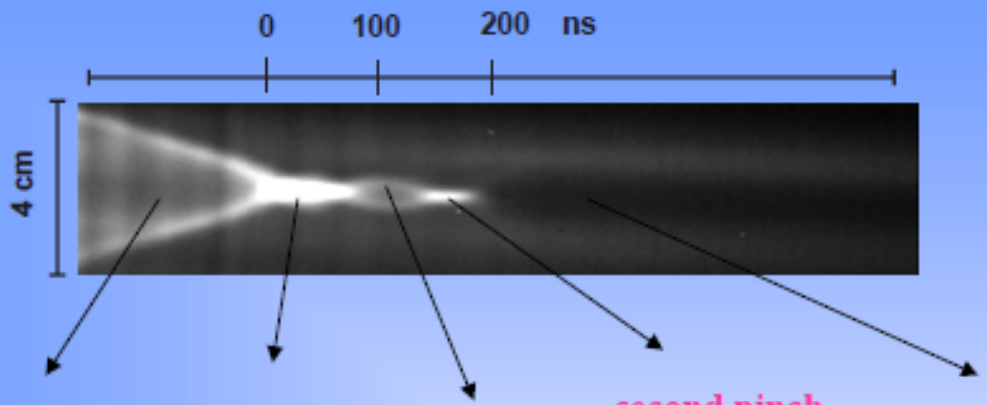

implosion of the current sheath

first pinch

development of instabilities

second pinch

explosion

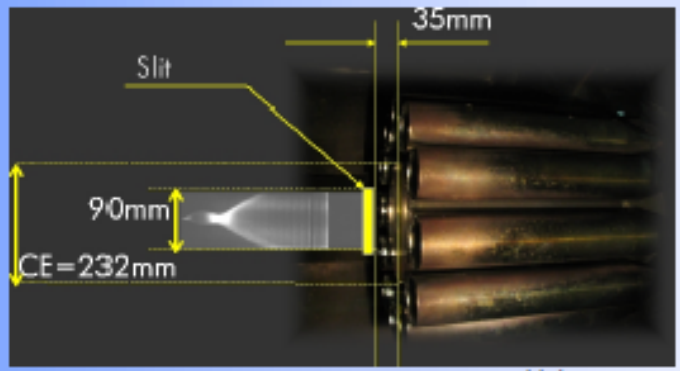

Institute of Plasma Physics and Laser Microfusion
Warsaw, Poland

Correlation of neutron signals with frames

(first neutron pulse)

-50 ns -30 ns -10 ns 0 ns 10 ns 30 ns 50 ns

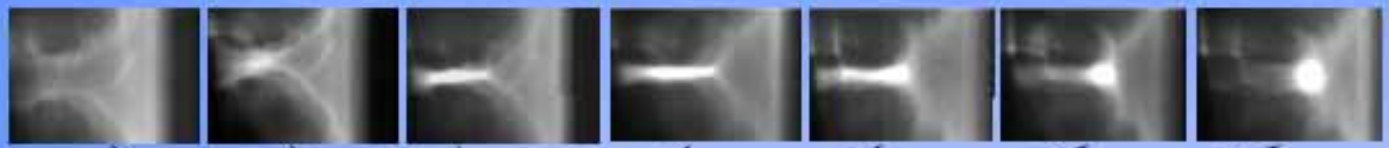

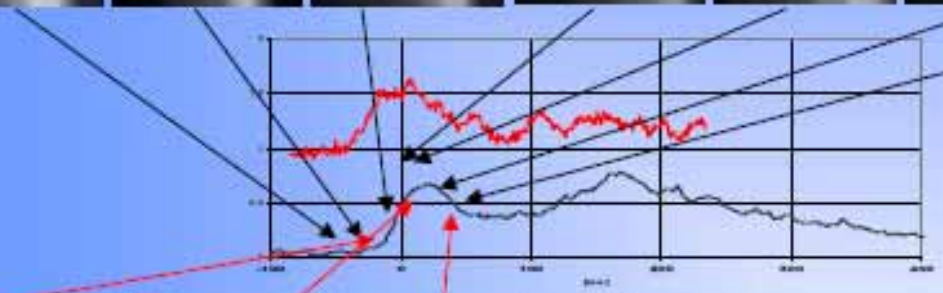

-20 ns -10 ns 30 ns -30 ns 0 ns

XUV frames – exposure time 2 ns, window 200-300 eV+above 600 eV

t_2-t_1=10ns

Question for future

- Determination of parameters of the dense plasma structure in the head of the pinch
- role of outflow
- role of disipation procesess of magnetic field energy into a pinch plasma
- nature of neutron generation

Correct neutron measurements

Measurements of a current flowing in a pinch

Diagnostics

$$P = \frac{N_D n_D}{4} \cdot \langle \sigma v \rangle \tau$$

$$Y_n = l \cdot P \propto \alpha \frac{l}{a} I^4 \cdot \frac{\langle \sigma v \rangle}{T^{5/2}}$$

Interferometry !!;

Streak camera

Activation Measurements

(anizotropy !!)

Method of calibration!

PMT

TOF (spectra)

Current probes

Soft X-ray Measurements

(D+Ar or D+Kr)

Interferometry for PF-1000

Mach-Zenhder

Laser output specyfication

Max. Pulse energy, mJ

At 1053 nm	1000
At 527 nm	450
At 351 nm	320
At 263 nm	160

16 frames, 60 ns between frames

Pulse duration at 1053 nm (FWHM) < 1 ns

Optical pulse jitter +/-1 ns

Beam divergence at 1053 nm (ful angle @ 1/e2) < 0.25 mrad

Beam diametr 12 mm

Institute of Plasma Physics and Laser Microfusion
Warsaw, Poland

Cut view of MCNP geometry of PF-1000 facility.

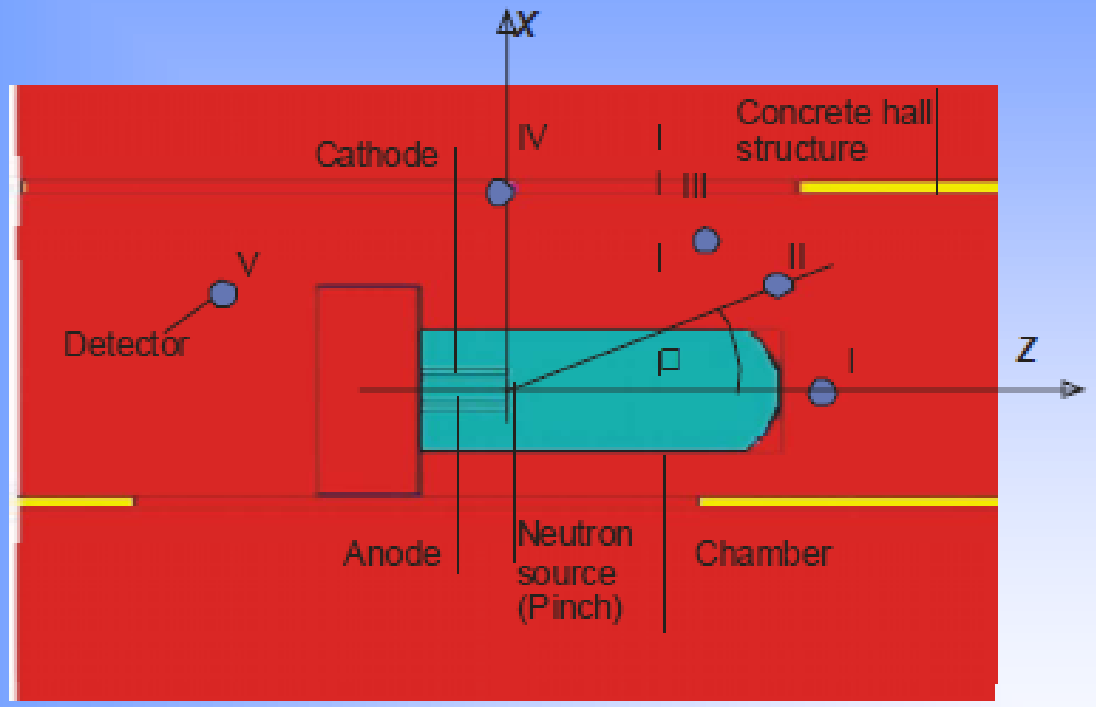

Procedure of calibration

1. $\langle \sigma\Phi \rangle = \frac{A_0}{(a\psi)M(N_A/A)\eta(1-e^{-\lambda t})}$

Calibration source with defined S

$$S = \frac{\langle \sigma(E)\Phi(E) \rangle_{exp}}{K_{exp}}, \left[\frac{n}{s}\right]$$

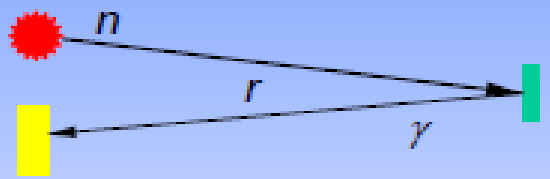

2. MCNP modelling including:

defined calibration source;

all masses surrounding the source;

defined samples

$$S = \frac{\langle \sigma(E)\Phi(E) \rangle_{cal}}{K_{cal}}, \left[\frac{n}{s}\right]$$

3. MCNP modelling including:

DD neutron source (plasma) Y_n;

all masses surrounding the source;

defined samples

$$Y_n = \frac{\langle \sigma(E)\Phi(E) \rangle_{DD}}{K_{DD}}, \left[\frac{n}{s}\right]$$

Institute of Plasma Physics and Laser Microfusion
Warsaw, Poland

Neutron Activation Diagnostic

New Foil Project

1.Selection of an appropriate set of neutron activation foils, depending on the anticipated measurement conditions.

Reaction	Eγ [keV]	Maxyline En. Effic (C19 cal)	Daughter $T_{1/2}$	$\sigma_{2.45}$ [barn]	Parent abundance ratio (Θ)	Sensitive for thermal neutrons (S_{th})	Relative mass ratios				
$^{27}Al\ (n,\gamma)\ ^{28}Al$	1778(1)	$0.8 \cdot 10^{-3}$	2.2 m	0.4	1	Yes	20%	37%	18%	22%	27%
$^{27}Al\ (n,p)\ ^{27}Mg$	844(0.718), 1014	$1.6 \cdot 10^{-3}$	9.5 m	1.5E-5	1	No					
$^{180}Hf\ (n,n')\ ^{180m}Hf$	216, 332(0.941), 443, 501	$4.4 \cdot 10^{-3}$	5.5 h	2.7	0.3508	No	20%	0%	18%	0%	28%
$^{180}Hf\ (n,\gamma)\ ^{181}Hf$	133, 346, 482(0.805)	$2.9 \cdot 10^{-3}$	42.4 d	0.03	0.3508	Yes					
$^{111}Cd\ (n,n')\ ^{111m}Cd$	151, 245(0.94)	$8.2 \cdot 10^{-3}$	48.5 m	1.76	0.128	No					
$^{116}Cd\ (n,\gamma)\ ^{117}Cd$	273(0.279), 344, 1303	$5.5 \cdot 10^{-3}$	2.5 h	*0.01*	0.0749	Yes	36%	0%	33%	40%	48%
	1066, 1997(0.282)	$0.6 \cdot 10^{-3}$	3.4 h	*0.01*		Yes					
$^{89}Y\ (n,n')\ ^{89m}Y$	909(0.9916)	$1.4 \cdot 10^{-3}$	16.7 s	1.12	1	No	24%	43%	21%	28%	0%
$^{77}Se\ (n,n')\ ^{77m}Se$	162(0.53)	$8.5 \cdot 10^{-3}$	17.36 s	1.87	0.763	No	0%	8%	4%	5%	0%
$^{79}Br\ (n,n')\ ^{79m}Br$	207.2(0.76)	$7.4 \cdot 10^{-3}$	4.86 s	1.82	0.5068	No	0%	12%	6%	7%	0%

Institute of Plasma Physics and Laser Microfusion
Warsaw, Poland

Neutron Activation Diagnostic

New Foil Project

2.*New germanium detector provides the increasing high energy resolution and high efficiency measurement of the full energy peaks for multi-elements sample.*

To use IPPLM's HPGe detector (35% 'effectivnes', coaxial, pre-calibrated)

3.*Fast neutron spectrum unfolding method using activation measurements. The method is based on the procedure of minimize following functional:*

$$J_x[\varphi(E)] = \int_0^\infty [\varphi(E) - \varphi_0(E)]^2 \cdot \sigma_x^{\,2}(E) \cdot dE$$

for given reaction type – x, where $\varphi_0(E)$ is a first step approximation of the spectrum, which was obtained from another procedure (e.g. MCNP modelling, TOF)

Plasma Focus Advanced Fuel Fusion

- **Business Plan for the Focus Fusion 2 MW Electricity Generation Facility Development**

- **Lawrenceville Plasma Physics**
  9 Tower Place
  Lawrenceville, NJ 08648
  609-406-7857

- **Eric J. Lerner**
  Project Director
  elerner@igc.org

- **Version 6**

- **This document is prepared for information purposes only. It is not intended nor to be construed as a solicitation for stock purchase.**

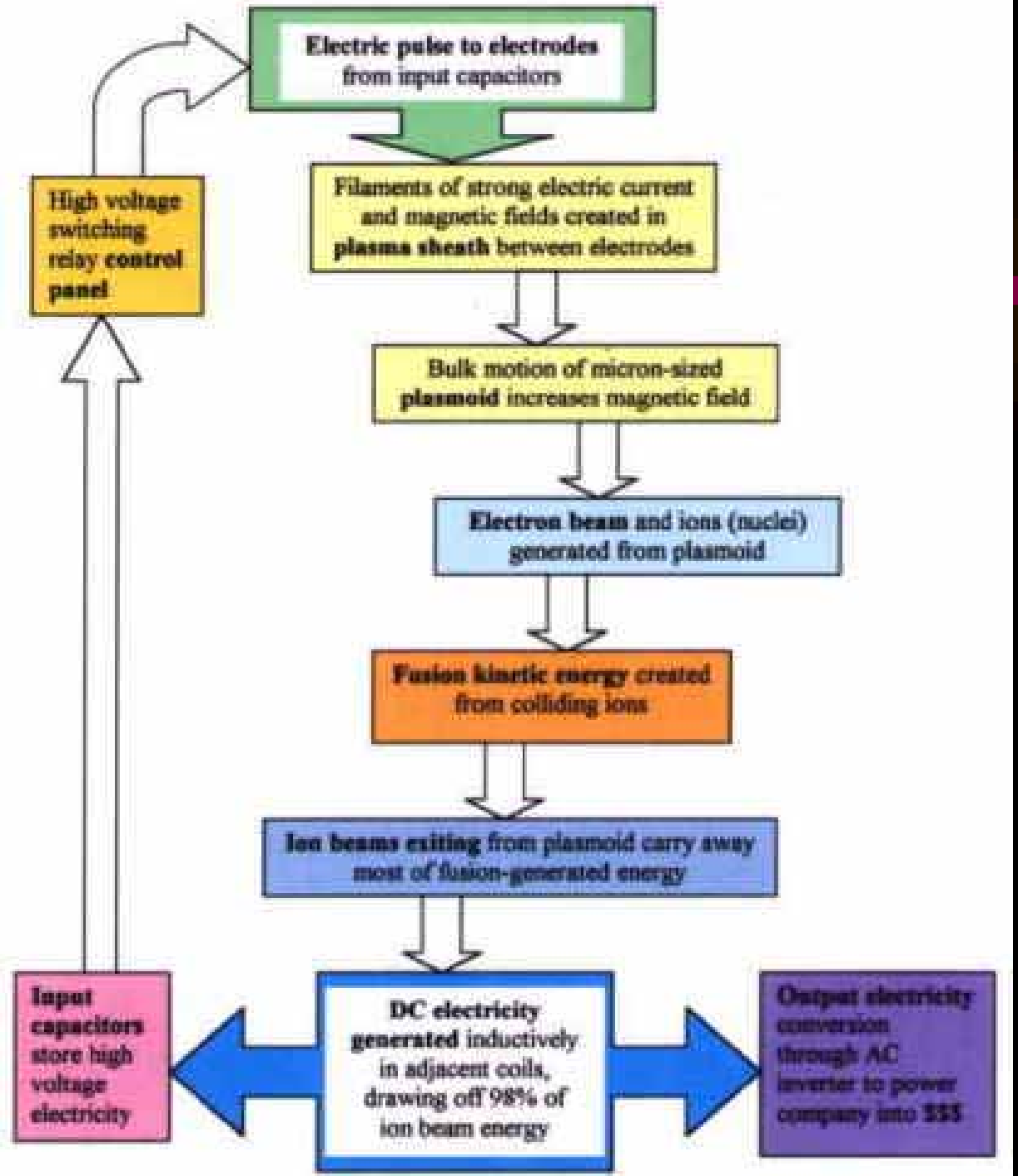

Energy Flow Schematic-Focus Fusion-Lerner

2 MW FOCUS FUSION PROTOTYPE GENERATOR

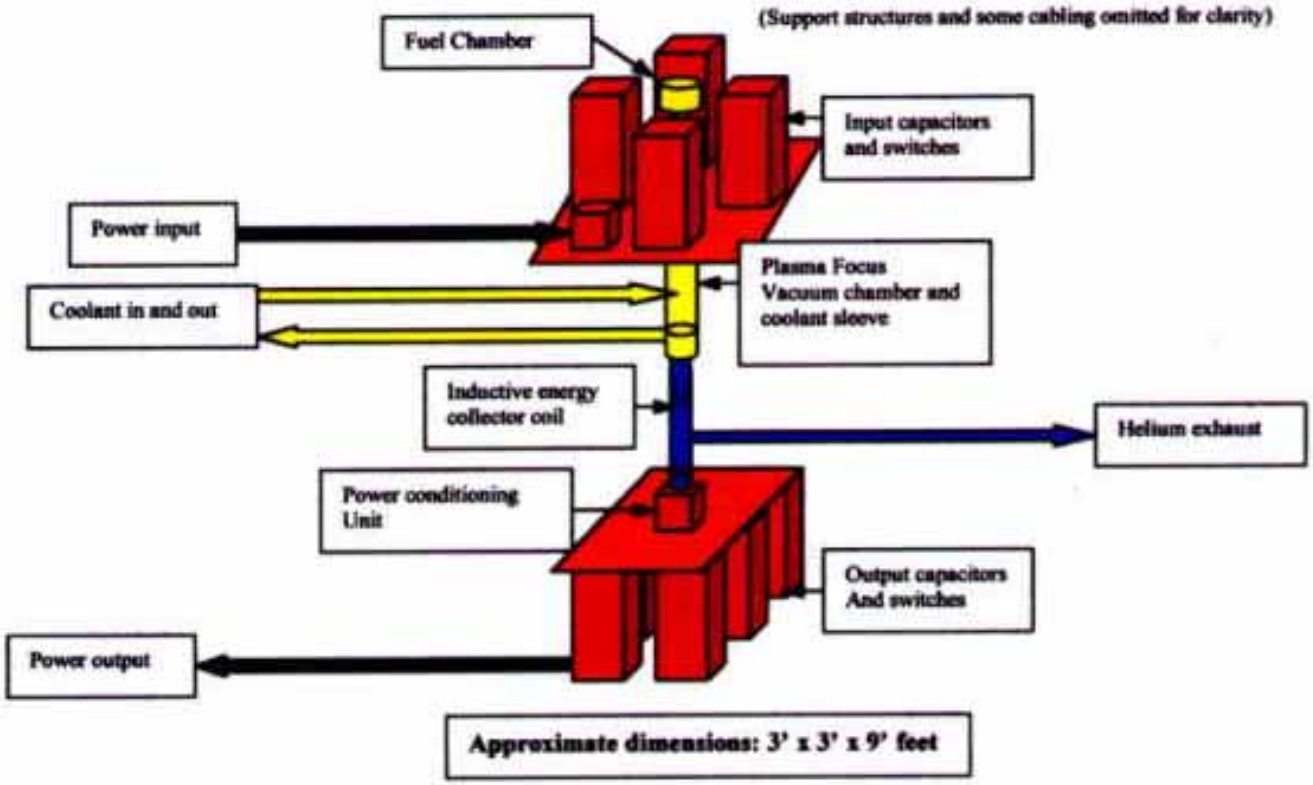

Plasma Focus Generator #1

Eric Lerner Feb., 2003

Conclusions and Discussion

Latest Trends of Plasma Focus Fusion Studies

- **Based on 45 years of research with small and large devices.**
- **Laboratory and more recently numerical experiments provide insight into Y_n scaling laws, as functions of I_{pinch}, I_{peak} and E_0.**
- **These numerical experiments show tendency towards Y_n saturation, in agreement with laboratory experiments**
- **Latest results indicate breakthrough in concept is imminent; new directions: ultra high voltage and current steps**

Energy Gain from Thermonuclear Fusion

S Lee & S H Saw

Institute for Plasma Focus Studies

INTI University College, Malaysia

Turkish Science Research Foundation Ankara 1 October 2009 -6 pm

Content

- Thermonuclear fusion reactions
- Energy gain per D-T reaction; per gm seawater
- Cross sections vs beam energies & temperatures
- IIT, ntT criteria
- Progress up to 2009
- ITER, DEMO
- Other schemes: Inertial, Pinches

STARS:-

Nature's Plasma Fusion Reactors

Tokamak-planned nuclear fusion reactor

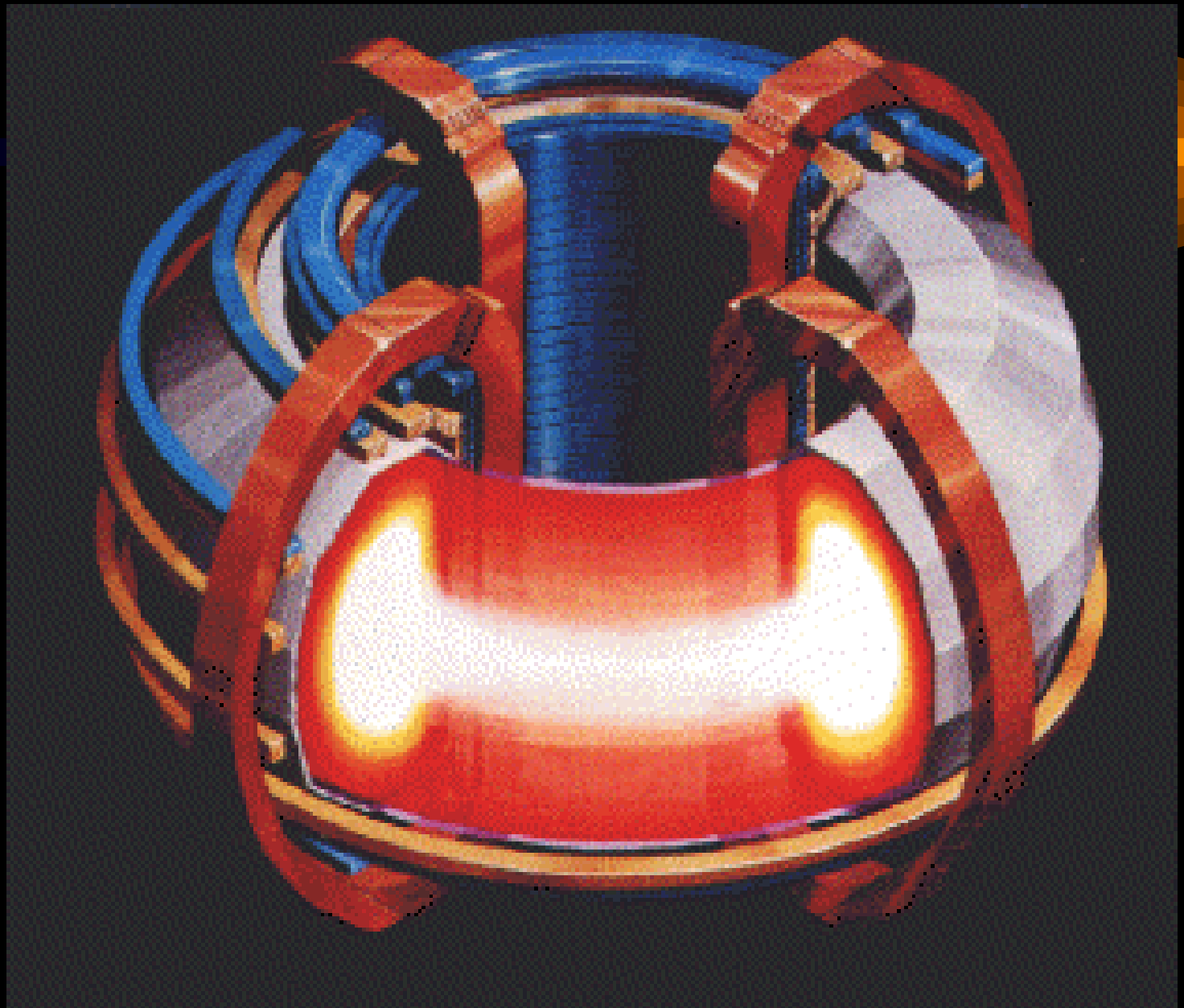

Natural Fusion Reactors vs Fusion Experiments on Earth

Introductory: What is a ***Plasma?***

Matter heated to high temperatures becomes a Plasma

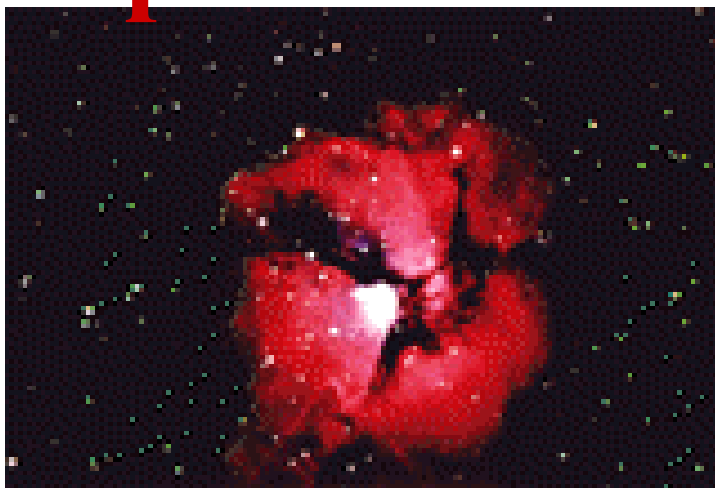

Four States of Matter

SOLID **LIQUID** **GAS** **PLASMA**

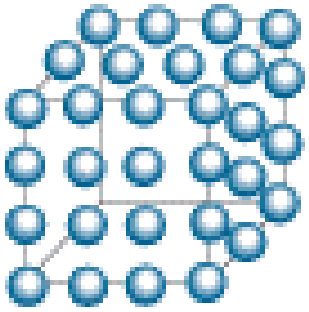

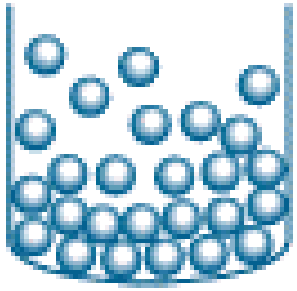

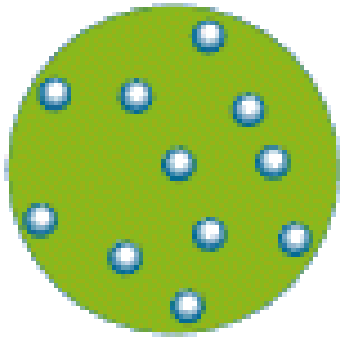

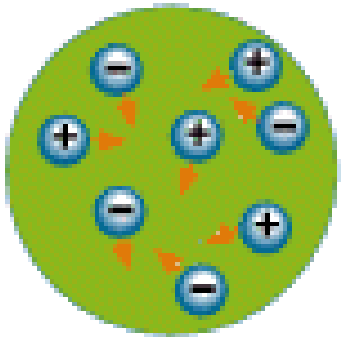

Characteristics of Plasma State

- **Presence of electrons and ions**
- **Electrically conducting**
- **Interaction with electric & magnetic fields**
- **Control of ions & electrons: applications**
- **High energy densities/selective particle energies**

-Cold plasmas: several eV's; (1eV~10^4K)

-Hot plasmas: keV's ; (1keV~10^7K)

- **Most of matter in Universe is in the Plasma State (e.g. the STARS)**

Major technological applications

- **Surface processing, cleaning, etching, deposition**
- **Advanced materials, diamond/CN films**
- **Environmental e.g.waste/water treatment**
- **High temperature chemistry**
- **MHD-converters, thrusters, high power switches**
- **Radiation sources: Microelectronics lithography**
- **Medical: diagnostics, cleaning, instrumentation**
- **Light sources, spectroscopic analysis, FP displays**
- **Fusion Energy**

The Singular, arguably Most Important Future Technological Contribution, essential to Continuing Progress of Human Civilization:-

A NEW LIMITLESS SOURCE OF ENERGY

Scenario: World Population stabilizes at 10 billion; consuming energy at 2/3 US 1985 per capita rate

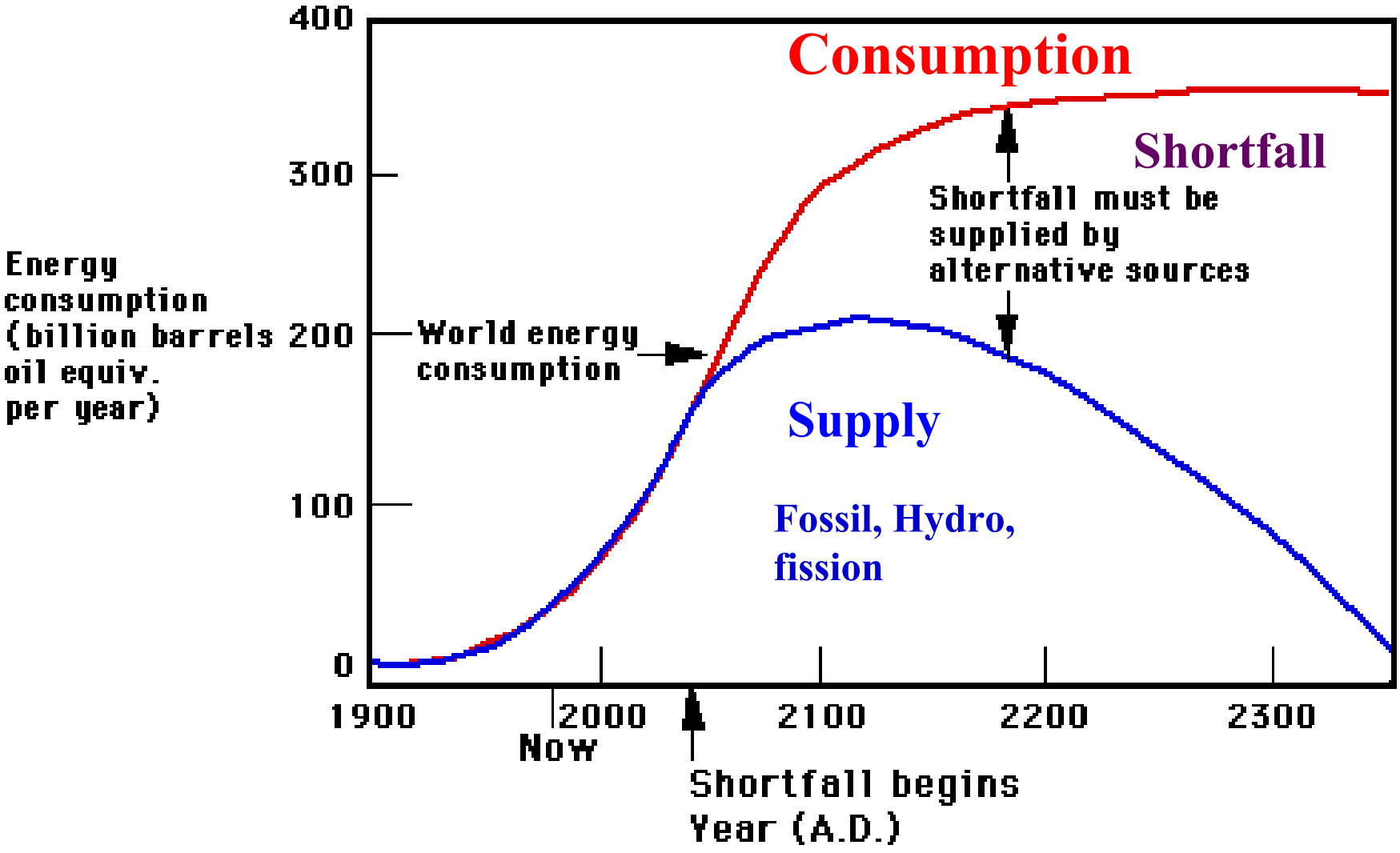

Plasma Fusion (CTR) & the Future of Human Civilization

A new source of abundant (limitless) energy is needed for the continued progress of human civilization.

Mankind now stands at a dividing point in human history:

- **200 years ago, the Earth was under-populated with abundant energy resources**
- **100 years from now, the Earth will be over-crowded, with no energy resources left**

Without a new abundant source of energy

Human civilization cannot continue to flourish.

Only 1 good possibility:

Fusion (CTR) Energy from Plasma Reactors

Collisions in a Plasma

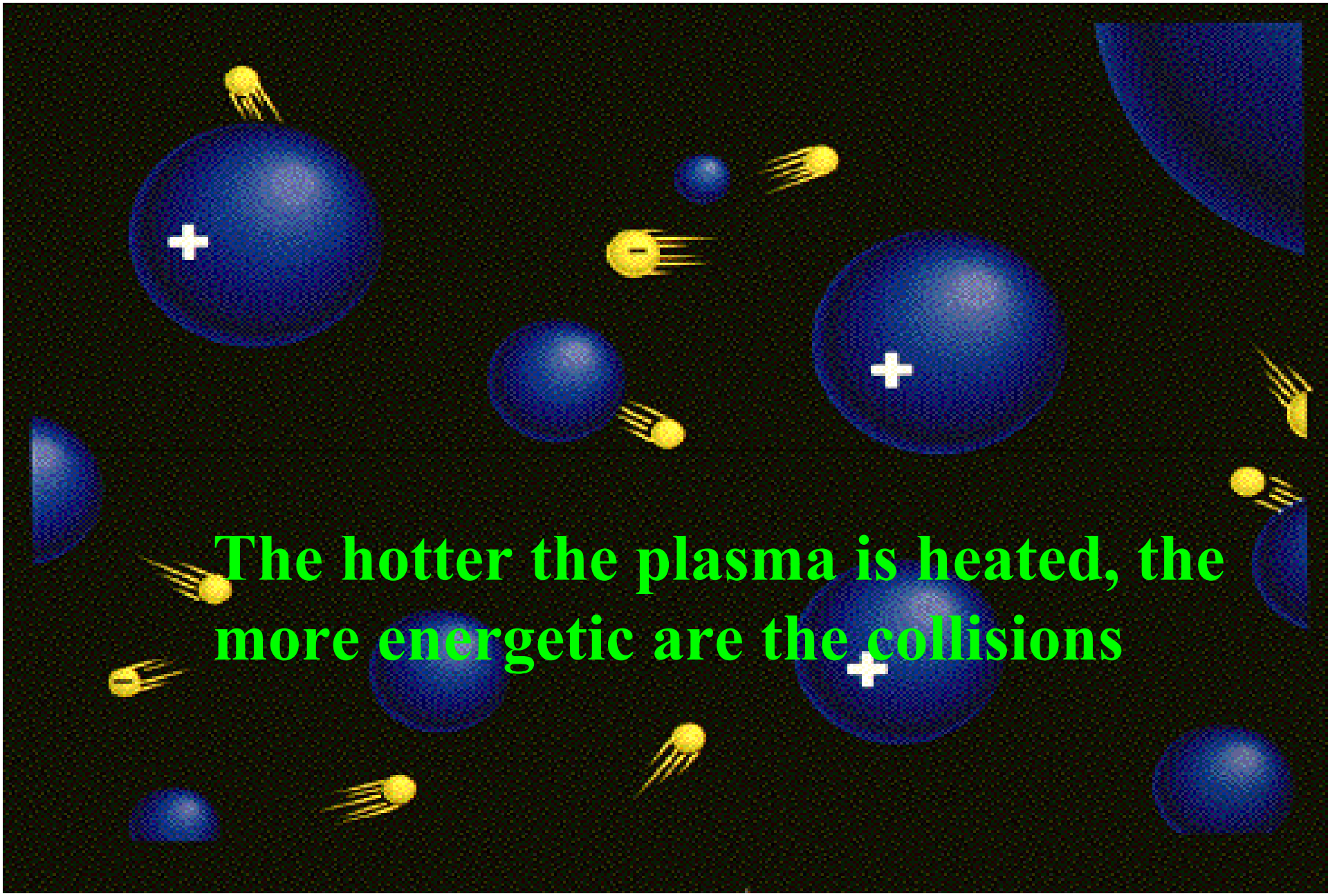

Nuclear Fusion

If a Collision is sufficiently energetic, nuclear fusion will occur

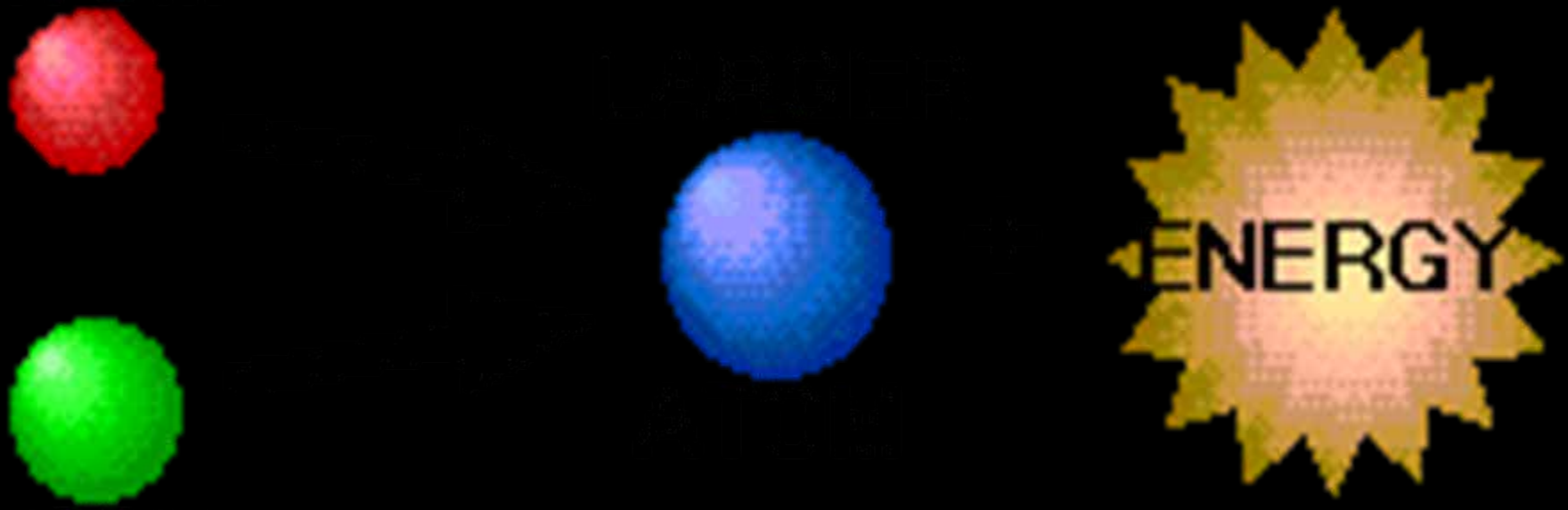

Isotopes of hydrogen- Fuel of Fusion

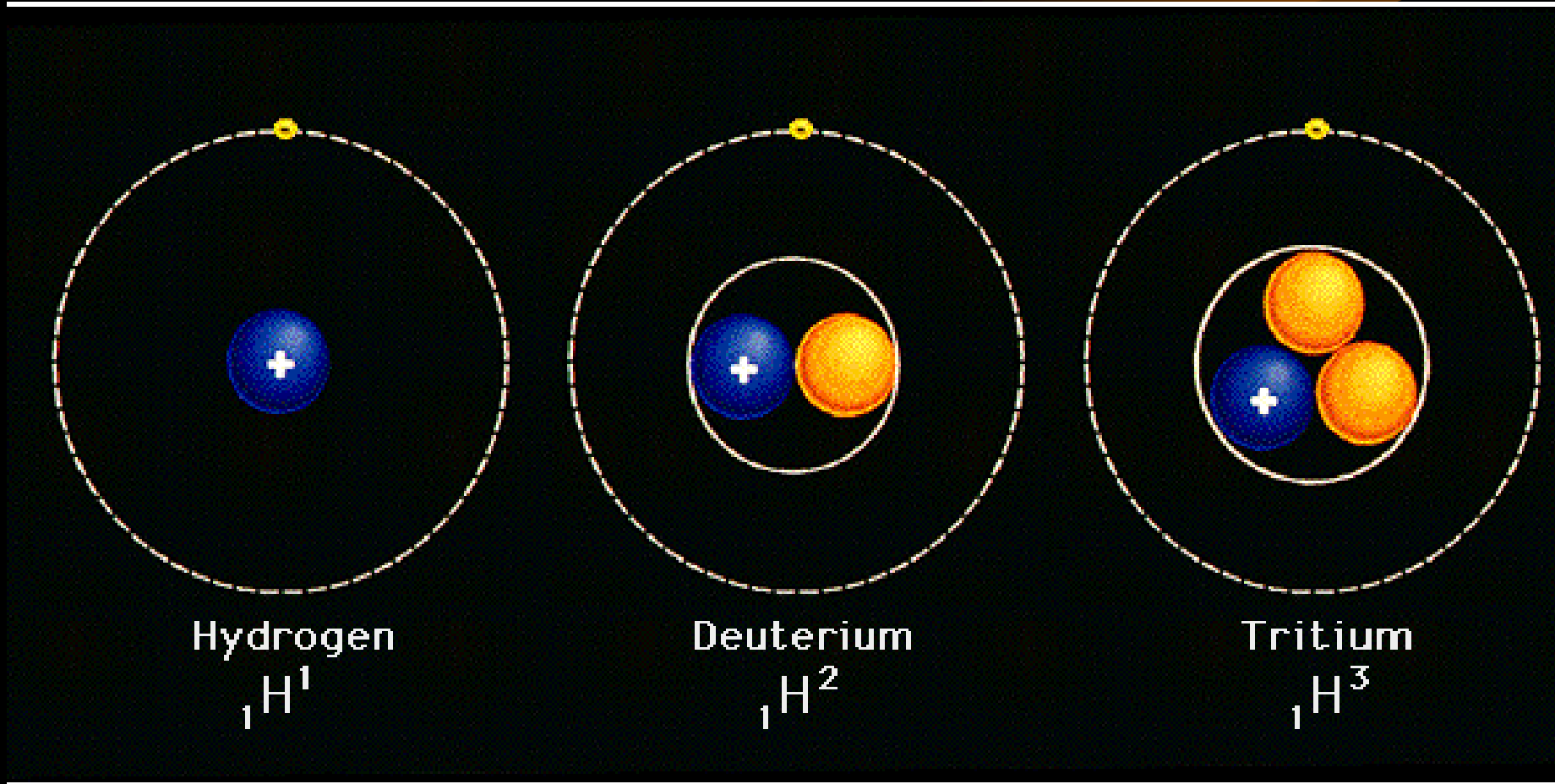

Release of energy in Fusion

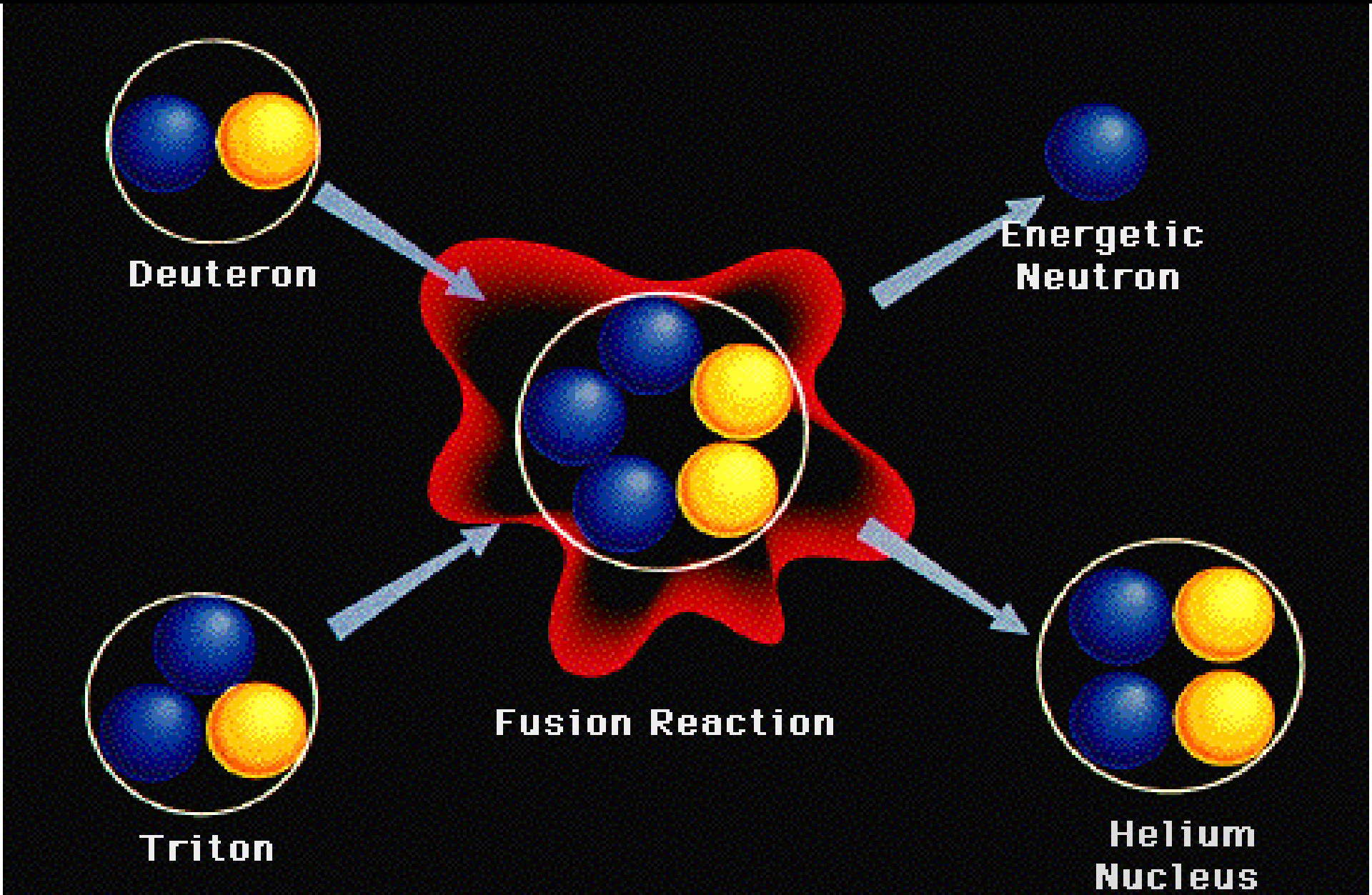

Conversion of mass into Energy

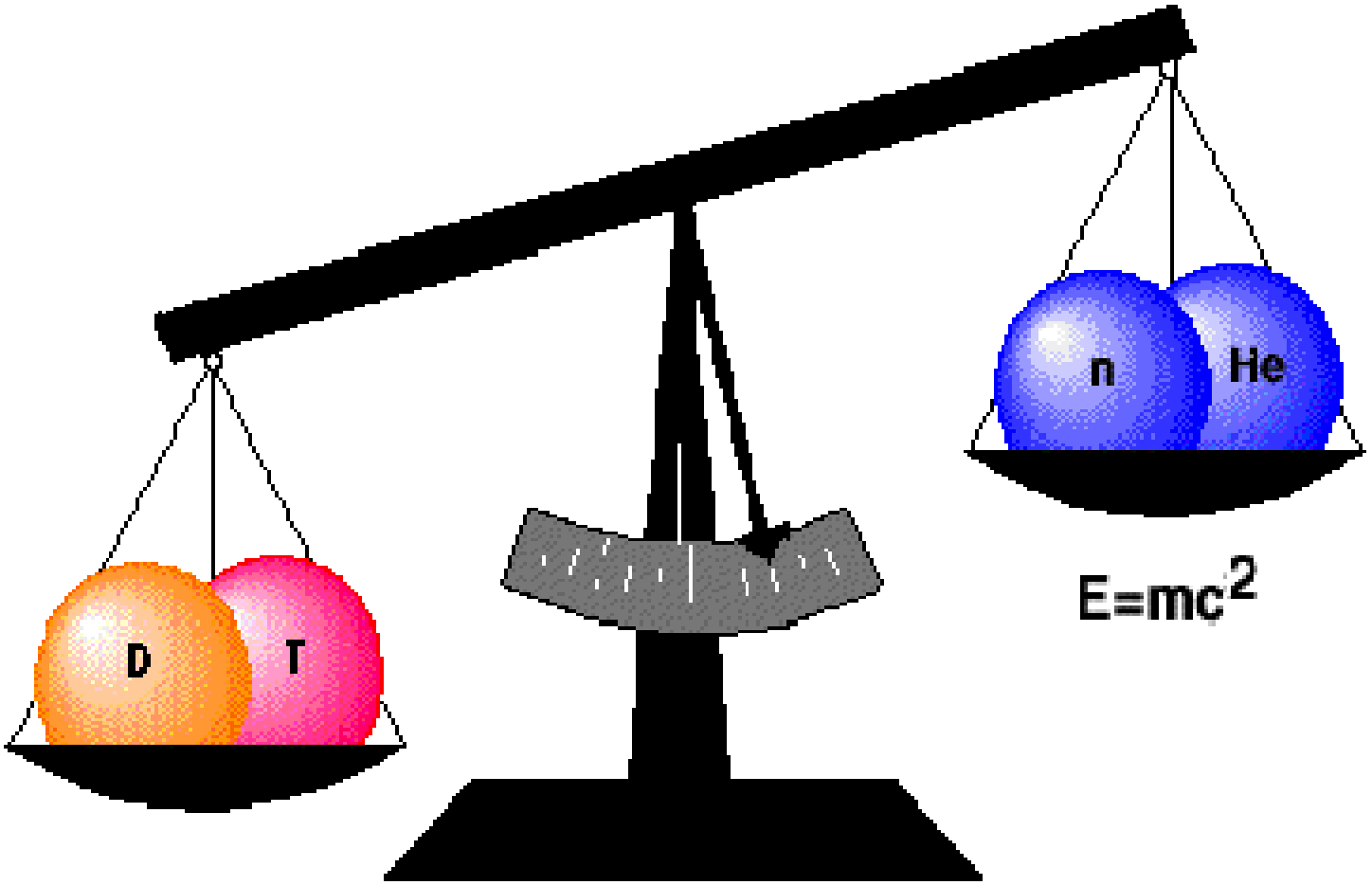

Fusion Energy Equivalent

50 cups water

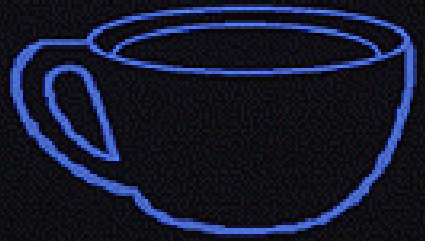

=

- **1 thimble heavy water, extracted from 50 cups of water**

=

Fusion Energy Equivalent

- One litre of water contains 30mg of deuterium. If fully burned in fusion reactions, the energy output would be equivalent to 300 litres of gasoline.
- Equivalent to filling the Atlantic and Pacific oceans 300 times with gasoline.
- Would satisfy the entire world's energy needs for millions of years.
- Fusion can also produce hydrogen which may be useful for transportation.

Energy-Demand and Supply: 3% demand scenario

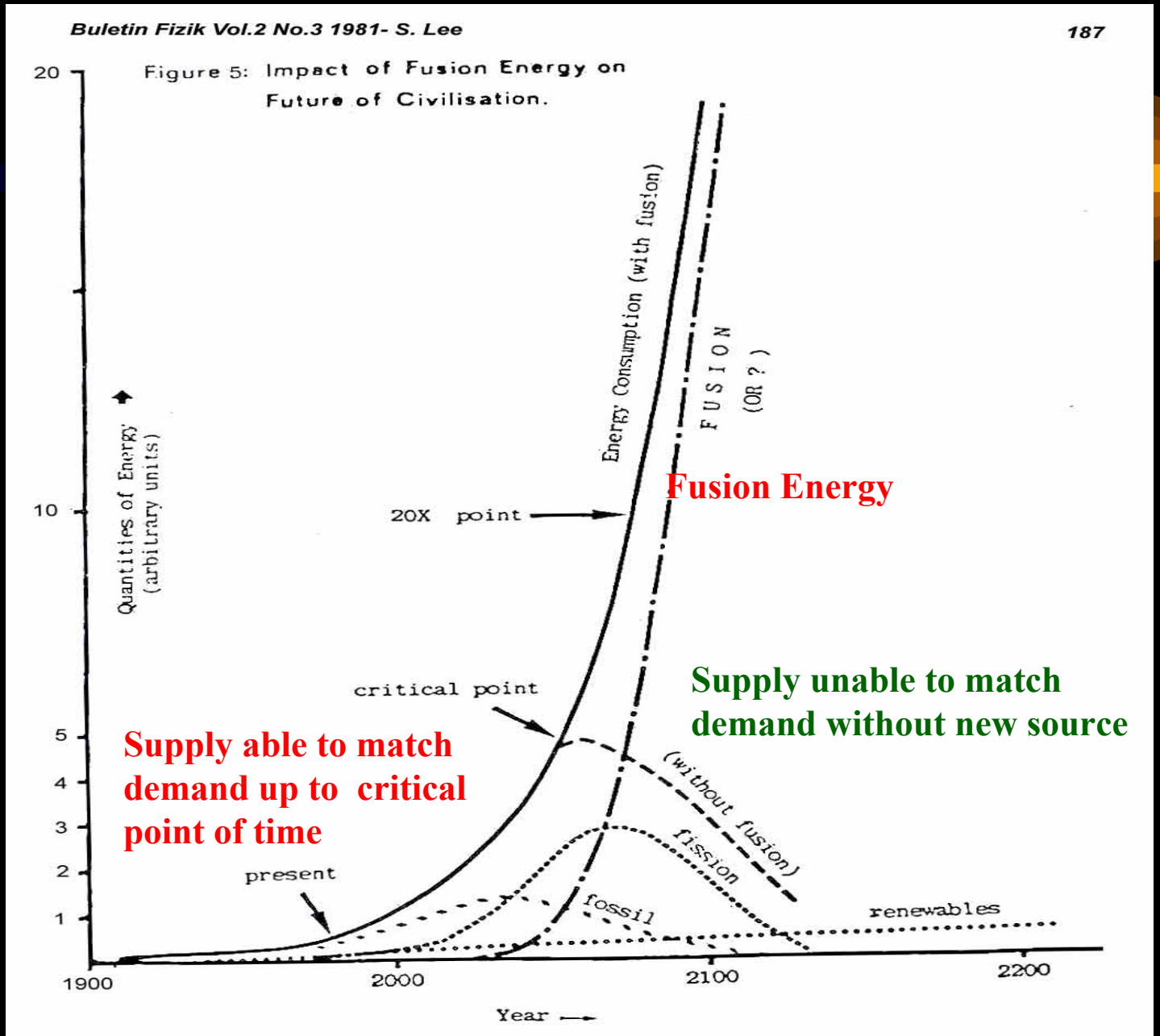

1Q=10^{18} BTU~10^{21}J
estimates: various sources (conservative)

World consumption per year:

1860: 0.02Q

1960: 0.1 Q

1980: 0.2 Q

2005: 0.5Q

Doubling every 20-30 years into the future (depending on scenario)

1Q=10^{18} BTU~10^{21}J
World reserves: -H R Hulme

- Coal: 100Q
- Oil: 10Q
- Natural gas: 1 Q
- Fission: 100Q
- Low grade ore for fission (economic?): 10^7 Q
- D-T fusion (Li breeding): 100Q
- D-T fusion (low grade Li economic?): 10^7 Q
- Fusion deuterium> 10^{10} Q

Cross sections for D-T, D-D reactions- 1 barn=10^{-24} cm^2;1 keV~10^7K

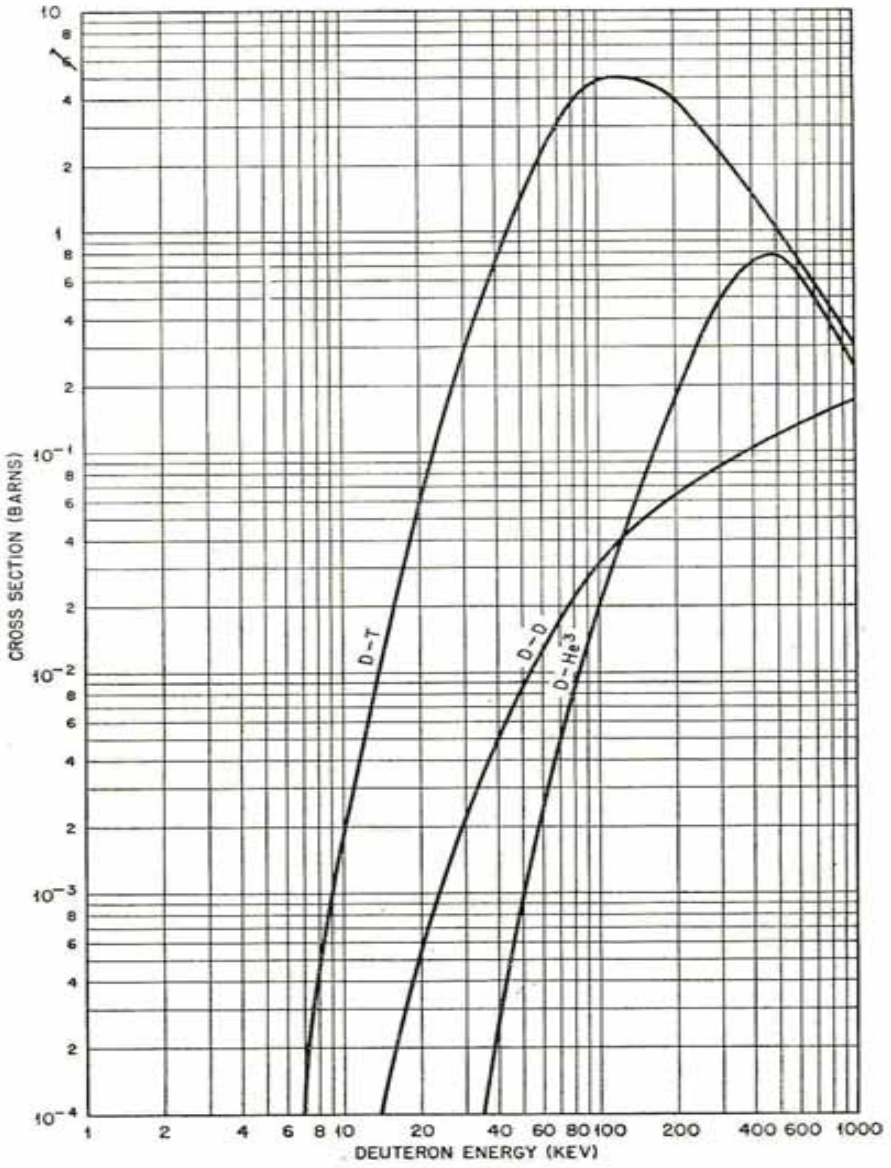

FIG 2.3. Cross sections for D-T, D-D (total), and D-He^3 reactions.

Thermalised <σv> parameter for D-T, D-D Plasmas

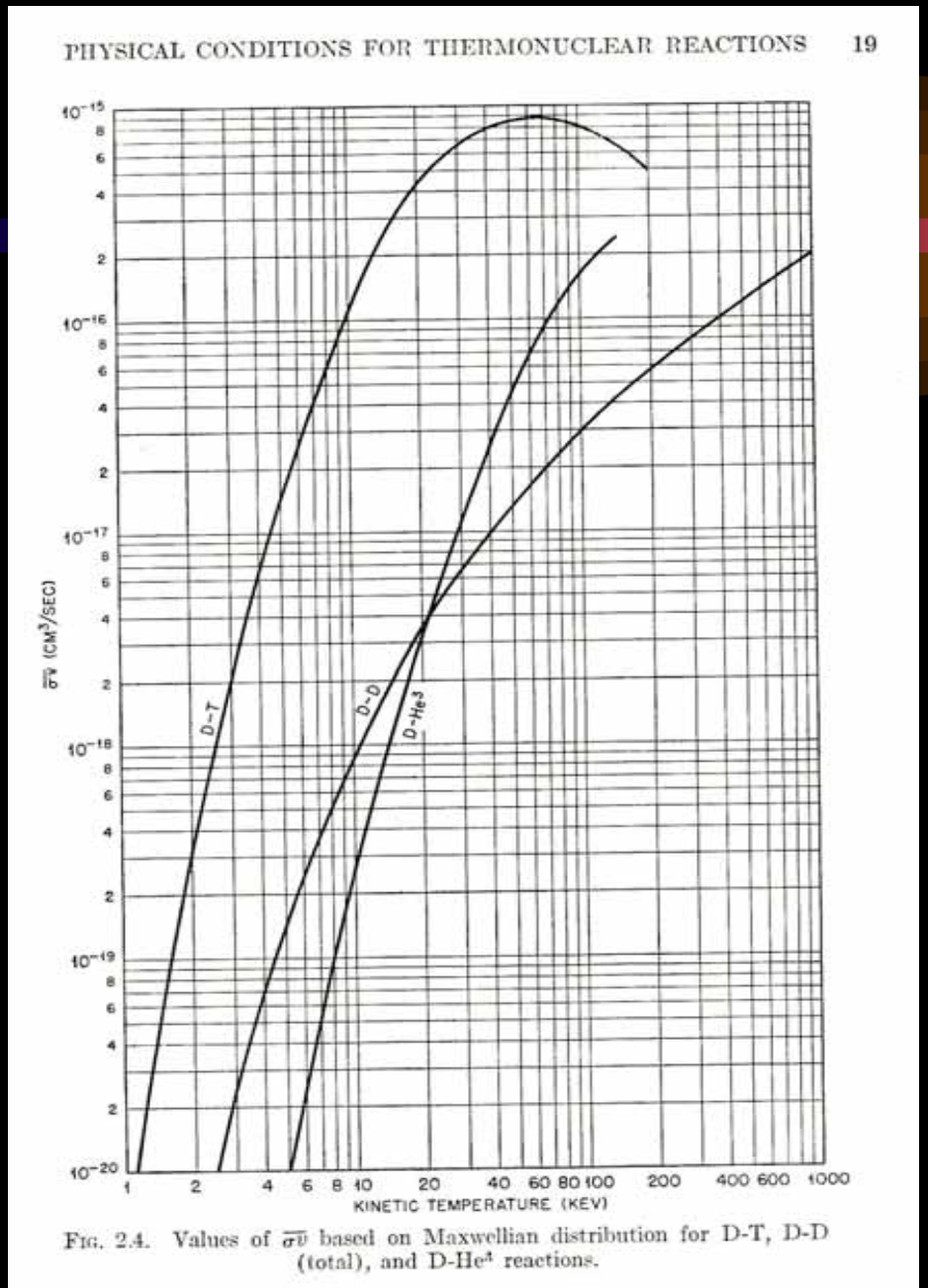

FIG. 2.4. Values of $\overline{\sigma v}$ based on Maxwellian distribution for D-T, D-D (total), and D-He^3 reactions.

Power densities for D-T, D-D reactions and Bremsstrahlung defining Ideal Ignition Temperatures- for 10^{15} nuclei cm^{-3}

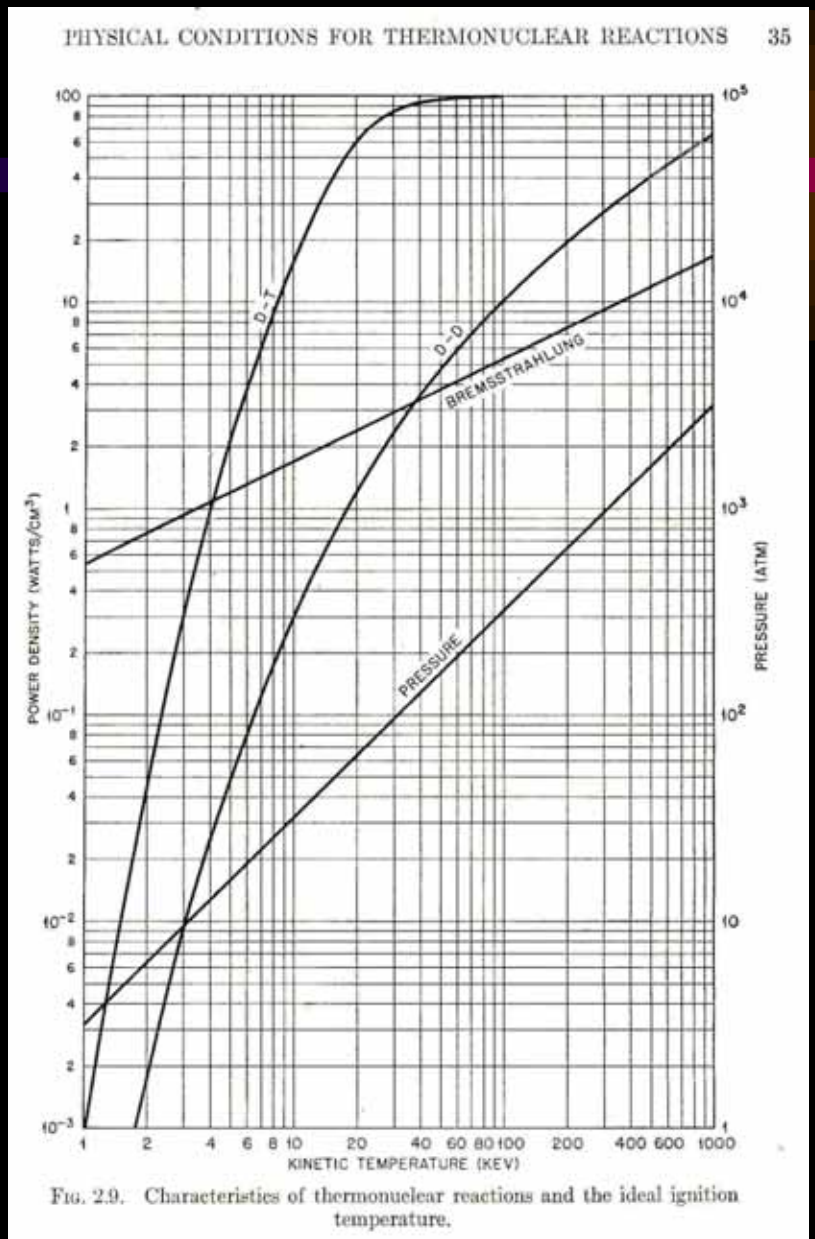

FIG. 2.9. Characteristics of thermonuclear reactions and the ideal ignition temperature.

Mean free paths and mean free times in fusion plasmas

- These have also to be considered, as at the high temperatures, the speeds of the reactons are high and mfp of thousands of kms are typical before a fusion reaction takes place.
- Such considerations show that at 10 keV, the plasma lifetime (containment time) has to be of the order of 1 sec for a density of 10^{21} m^{-3}

Summary of Conditions

Technological Targets:

- **T> 100 million K (10keV)**
- **nt>10^{21} m^{-3}-sec**

Two approaches:

n=10^{20} m^{-3}, confined t=10s
(low density, long-lived plasma) or :

n=10^{31} m^{-3}, confined 10^{-10}s
(super-high density, pulsed plasma)

Combined: ntT>$10^{22}$$m^{-3}$-sec-keV

Containing the Hot Plasma

Long-lived low-density Confinement

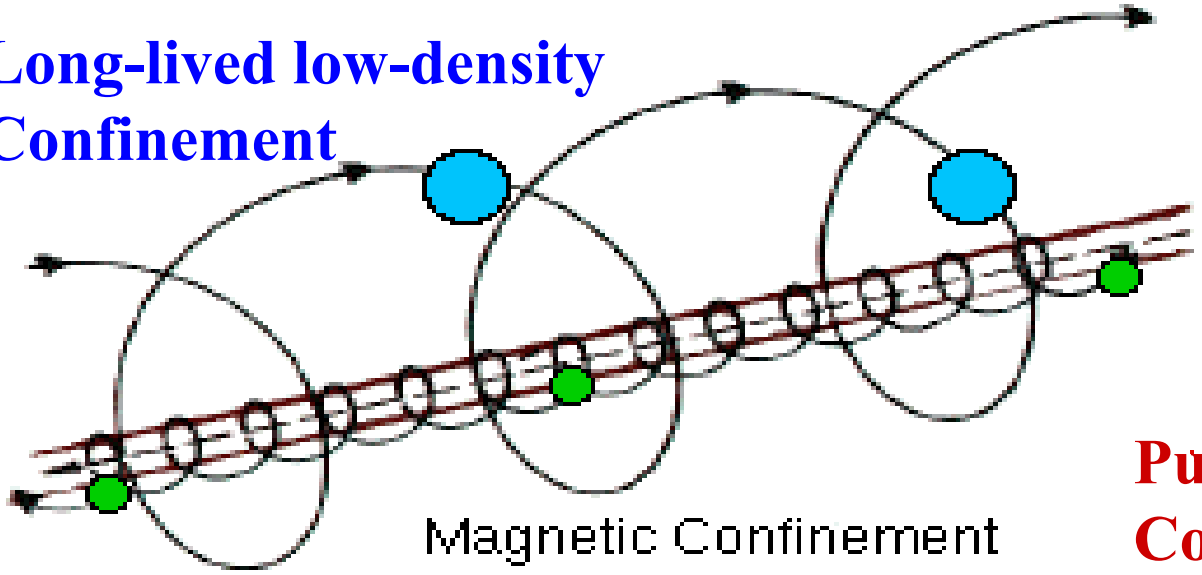

Magnetic Confinement

Pulsed High Density Confinement

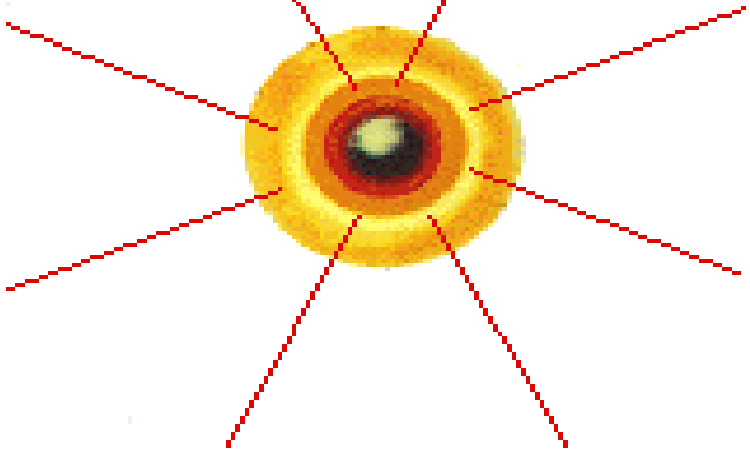

Inertial Confinement Using Lasers

Continuous Confinement

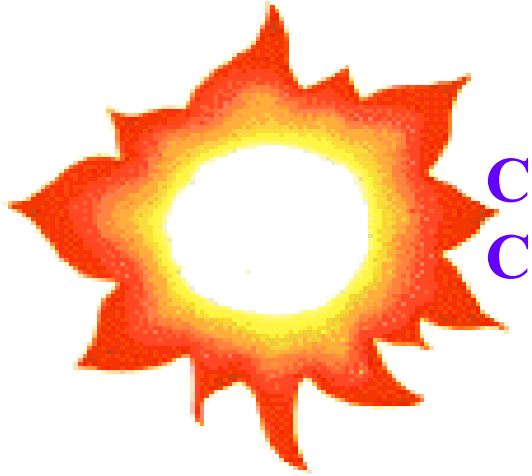

Gravitational Confinement in the Sun and Stars

Low Density, Long-lived Approach (Magnetic Compression)

Tokamak

- **Electric currents for heating**
- **Magnetic fields in special configuration for stability**

Schematic of Tokamak

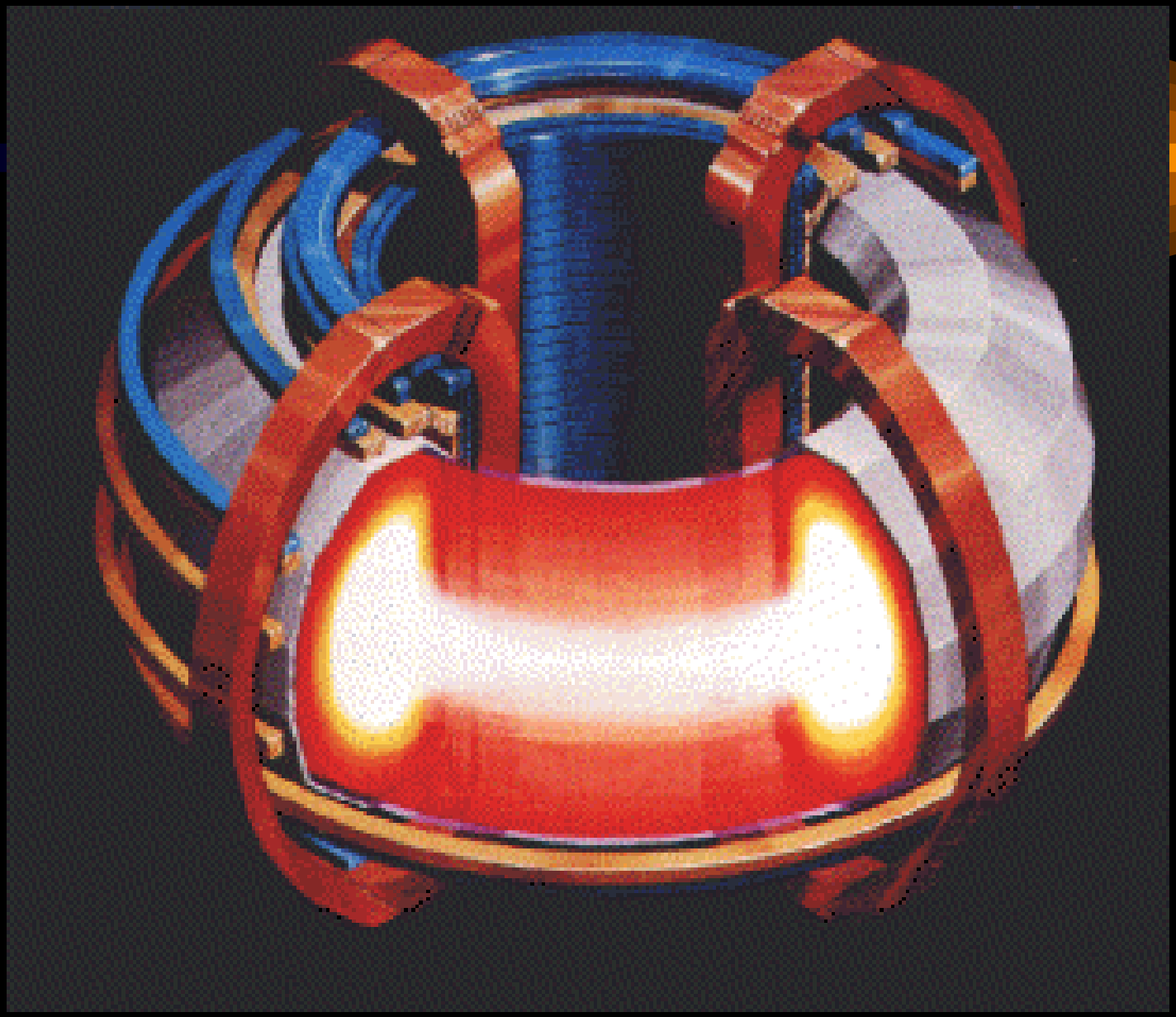

Magnetic Yoke to induce Plasma Current

Field Coils to Produce suitable Magnetic Field Configuration

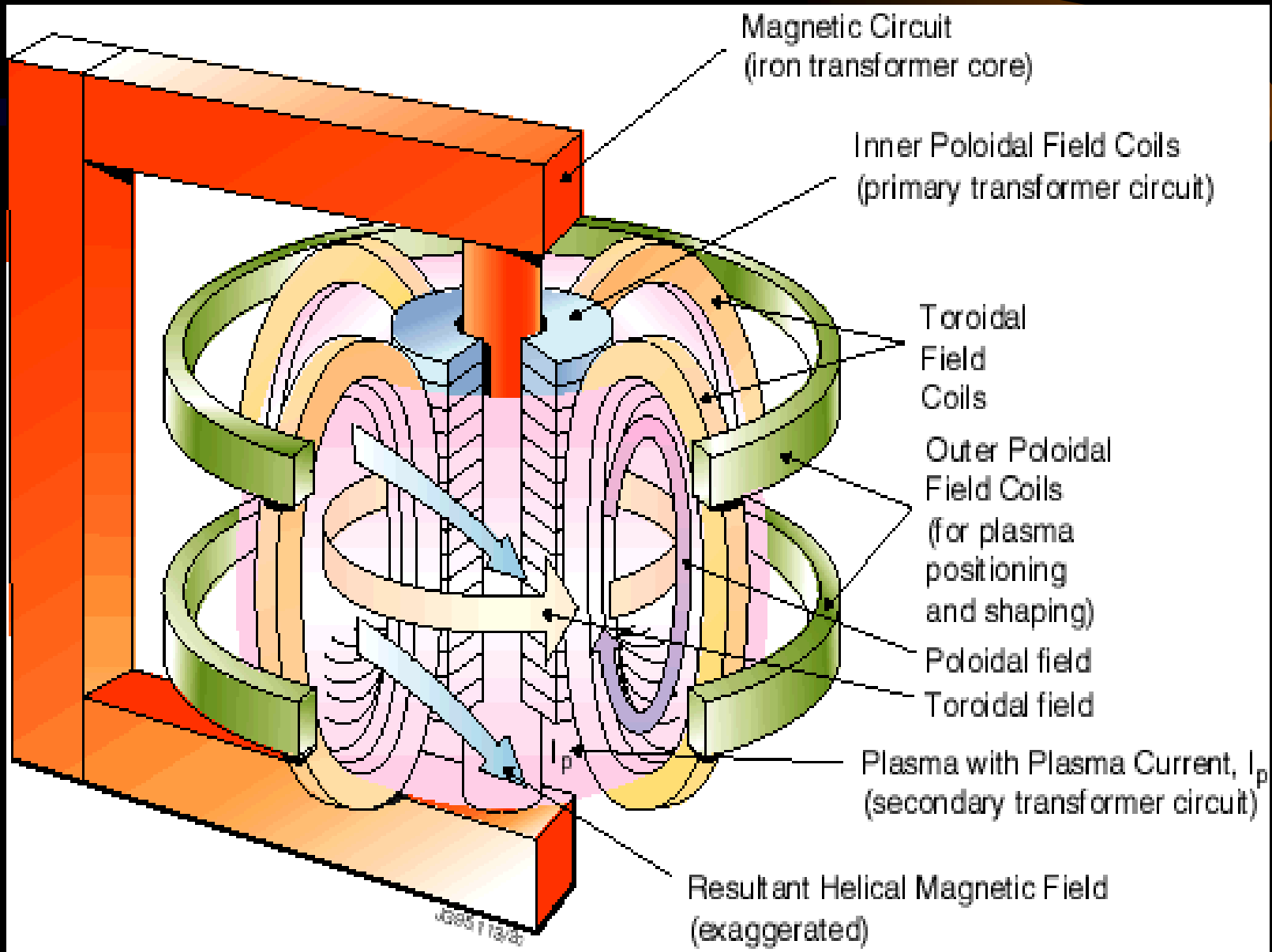

JET (Joint European Torus)

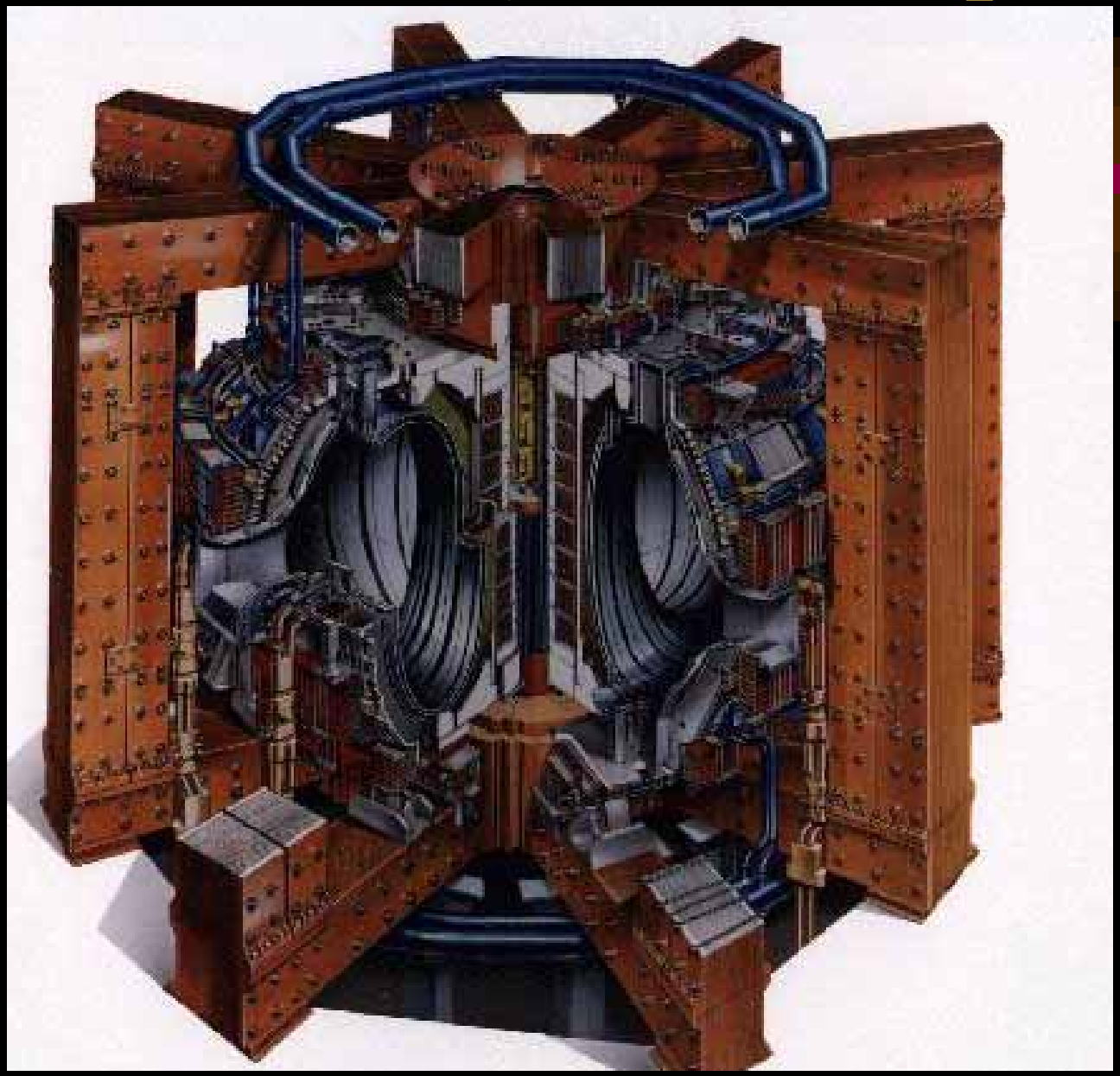

- **Project successfully completed January 2000**

Inside JET

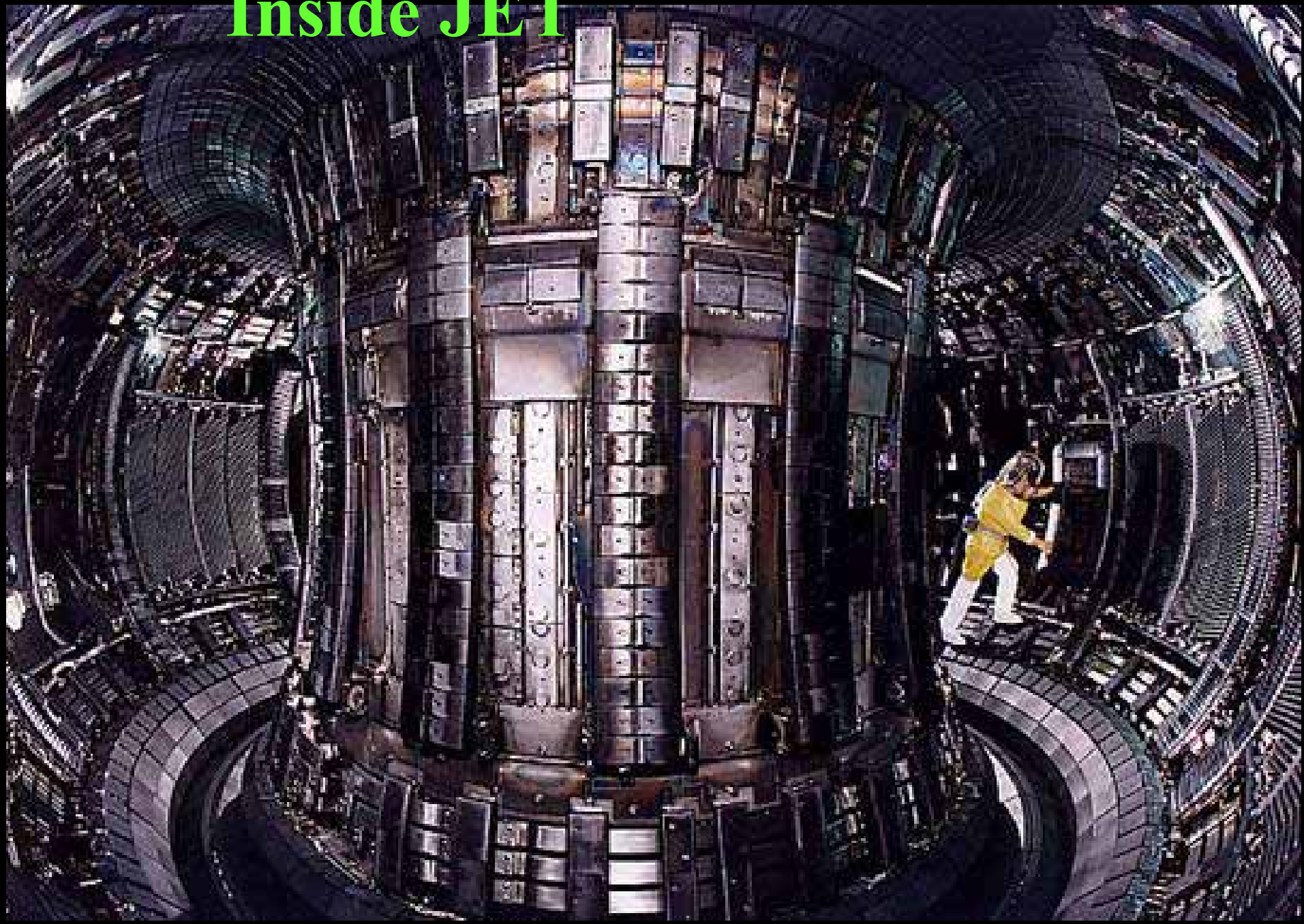

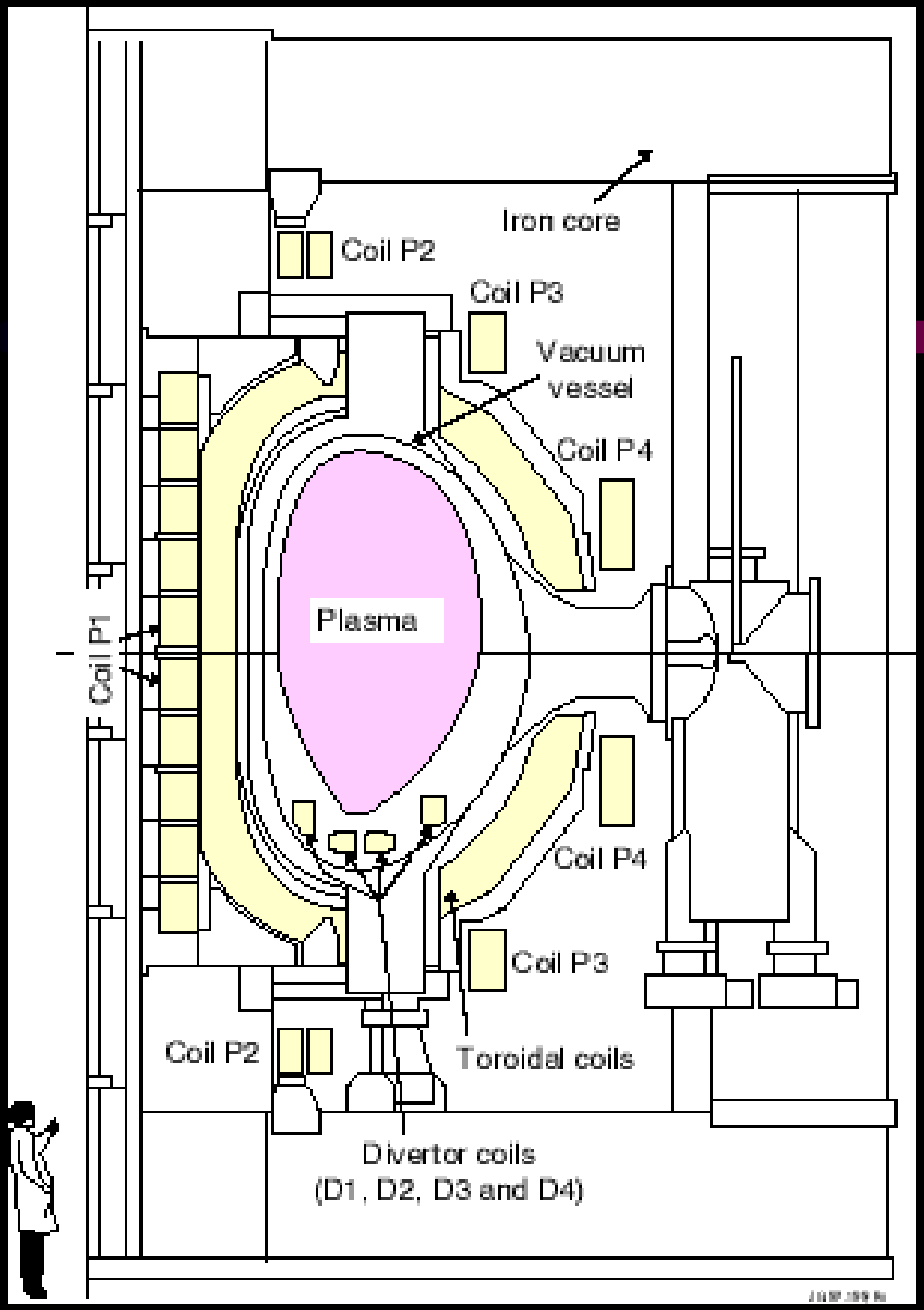

JET X-Section

Energy confinement time t scales as some functions of:

- **Plasma current I_p**
- **Major Radius R**
- **Minor radius 'a'**
- **Toroidal Magnetic Field B**

scaling law: $t \sim I_p^{\alpha} R^{\beta} a^{\gamma} B^{\lambda}$

indices $\alpha,\beta,\gamma,\lambda$ are all positive

To achieve sufficient value of ntT requires:

scaling of present generation of Tokamaks upwards in terms of:

I_p, R, 'a' and B.

Fusion Temperature attained
Fusion confinement one step away

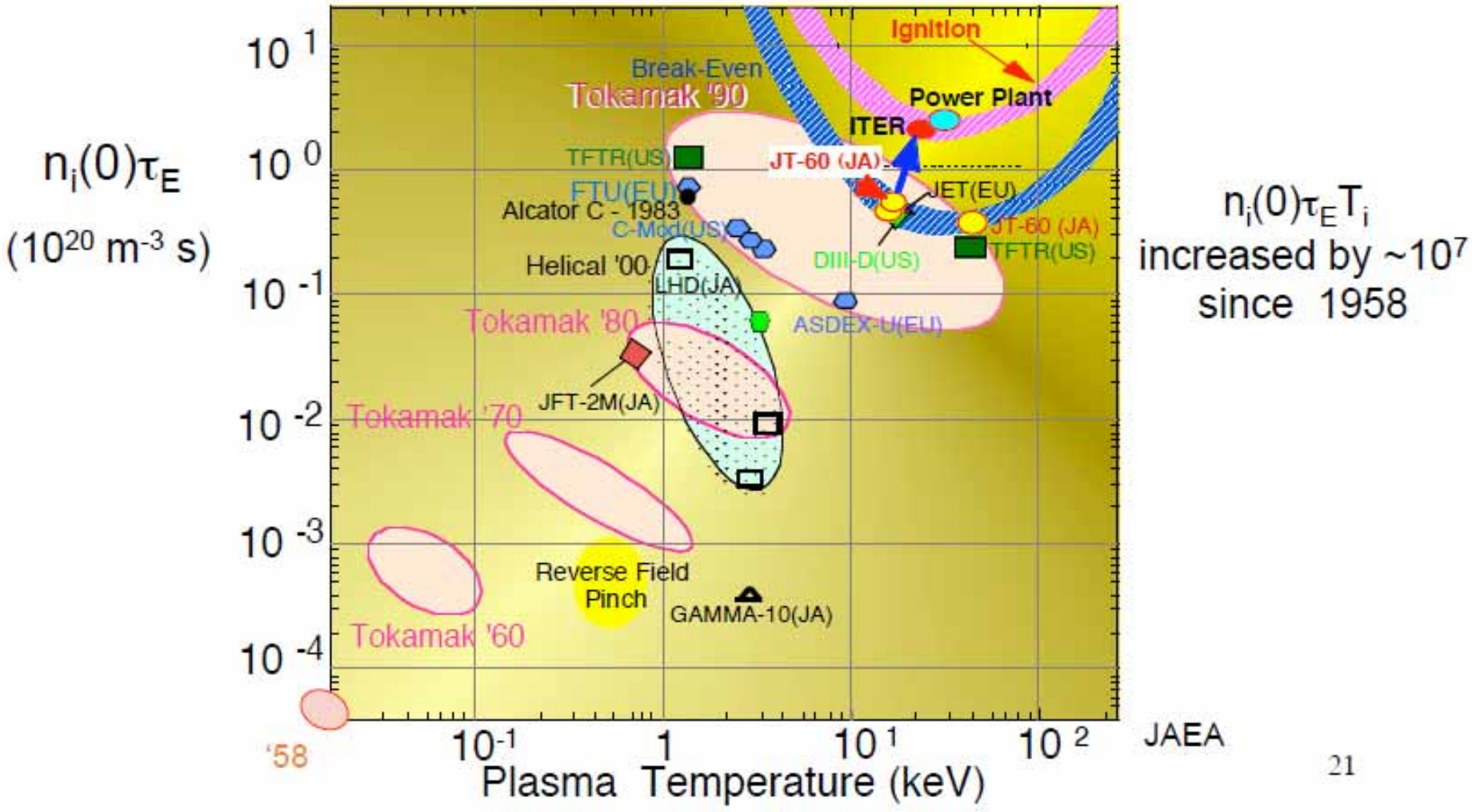

International Collaboration to develop Nuclear Fusion Energy-ITER

- 1985- Geneva Superpower Summit:
- Reagan (US) & Gorbachev (Soviet Union) agreed on project to develop new cleaner, sustainable source of energy- Fusion energy
- ITER project was born
- Initial signatories: former Soviet Union, USA, European Union (via EURATOM) & Japan
- Joined by P R China & R Korea in 2003 & India 2005
- ITER Agreement- signed in November 2006

ITER (International Thermonuclear Experimental Reactor)

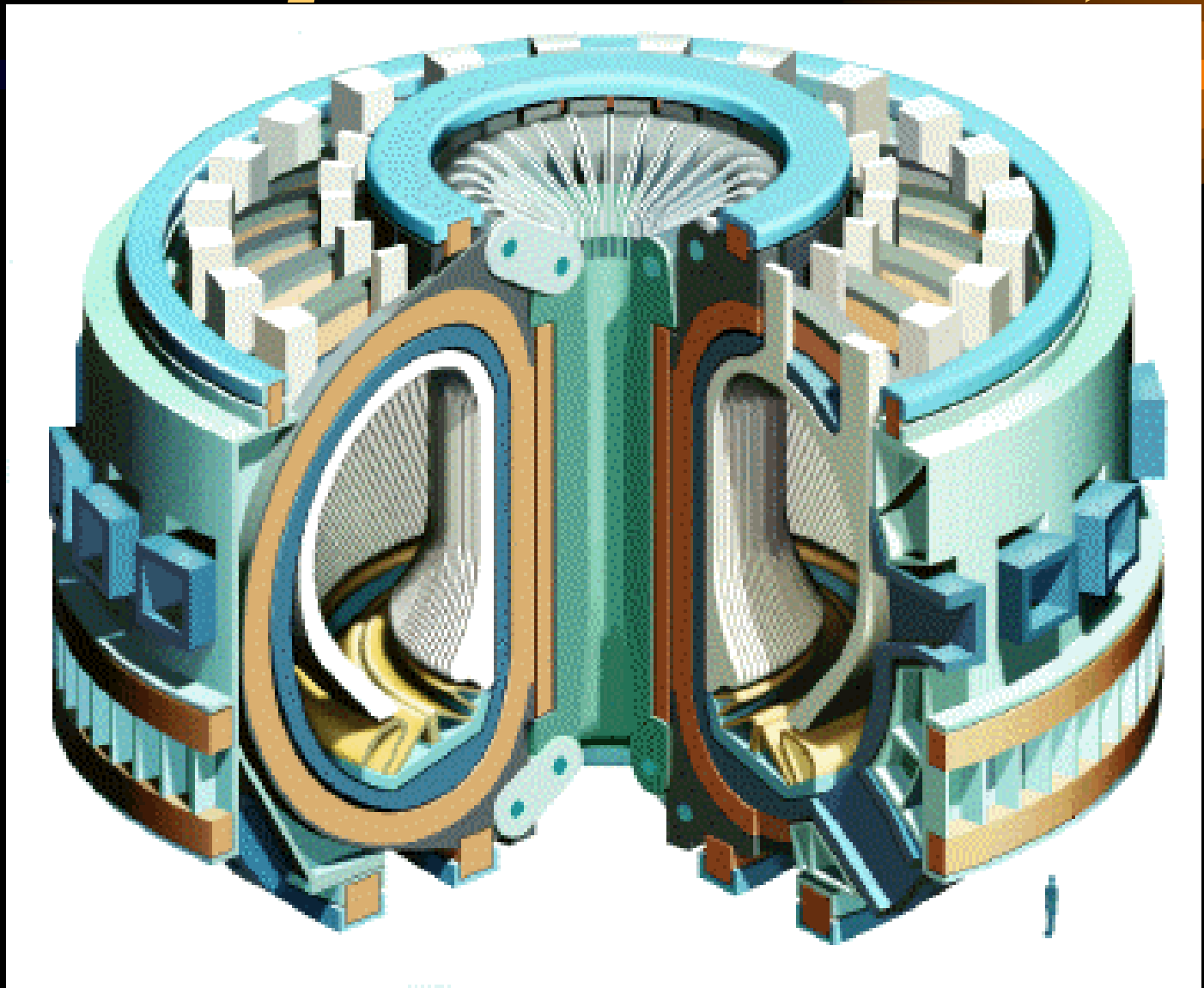

ITER Construction has now started in Cadarache, France

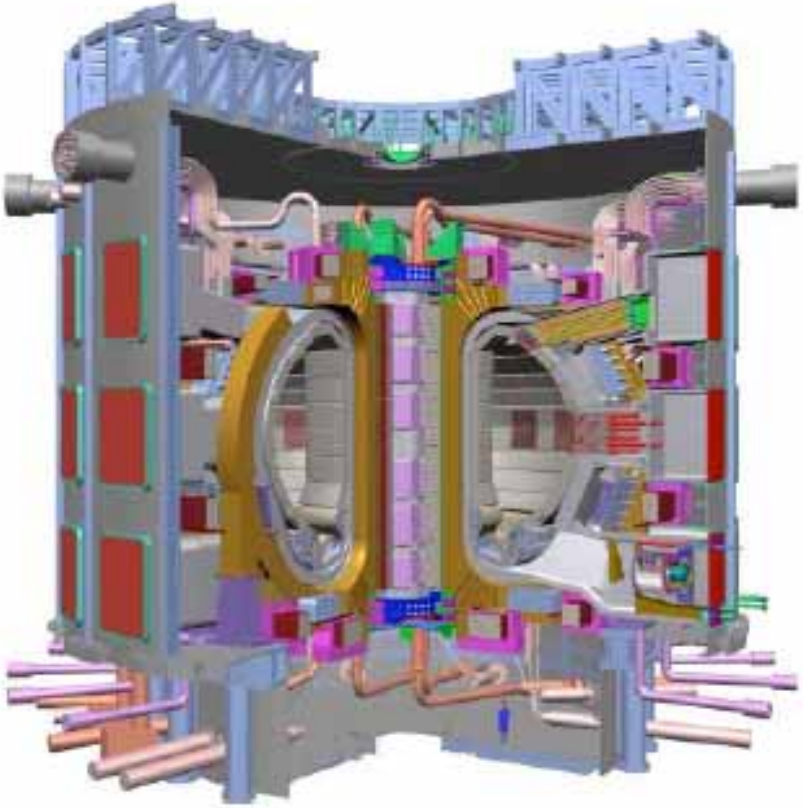

Reactor scale

ITER Site Under Construction

First plasma planned 2018

First D-T planned 2022

Q>10 and Beyond

ITER : to demonstrate: possible to produce commercial energy from fusion.

Q= ratio of fusion power to input power.

Q ≥ 10 represents the scientific goal of ITER :

to deliver 10x the power it consumes.

From 50 MW input power to 500 MW of fusion power - first fusion experiment to produce net energy.

Beyond ITER will be DEMO (early 2030's), demonstration fusion power plant which will put fusion power into the grid as early as 2040

FIRE: Incorporates Many Advanced Features

FIRE Incorporates Advanced Tokamak Innovations

AT Features

- DN divertor
- strong shaping
- very low ripple
- internal coils
- space for wall stabilizers
- inside pellet injection
- large access ports

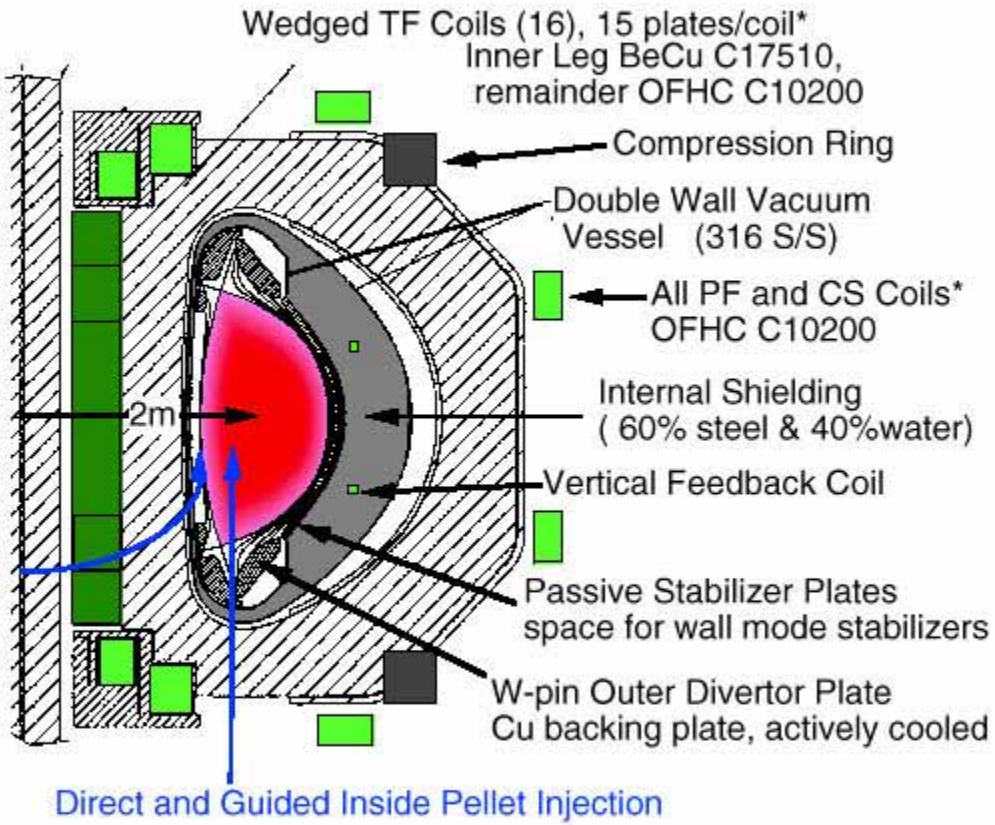

*Coil systems cooled to 77 °K prior to pulse, rising to 373 °K by end of pulse.

FIRE Cross/Persp- 5/25/99-8/DOE

Potential Next Step Fusion Burning Experiments

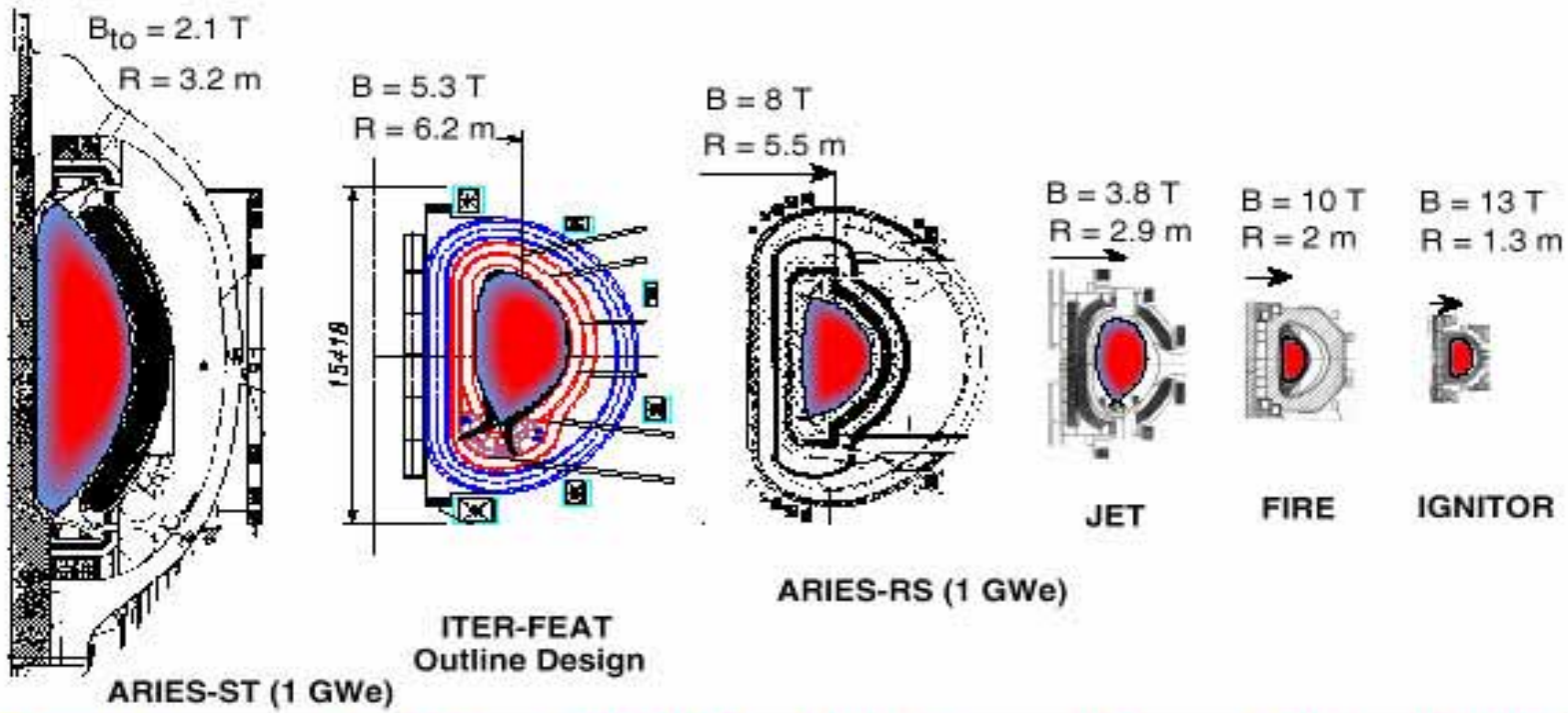

Cost Drivers	ARIES-ST	ITER-FEAT	ARIES-RS	JET	FIRE	IGNITOR
Plasma Volume (m^3)	810	837	350	95	18	11
Plasma Surface (m^2)	580	678	440	150	60	36
Plasma Current (MA)	28	15	11	4	6.5	12
Magnet Energy (GJ)	29	50	85	2	5	5
Fusion Power (MW)	3000	500	2200	16	200	100
Burn Time (s), inductive	steady	300	steady*	1	20	5

* assumes non-inductive current drive

The other approach: Pulsed Super-high Density (Inertial Compression)

- Radiation Compression

Pulsed Fusion: Radiation Compression

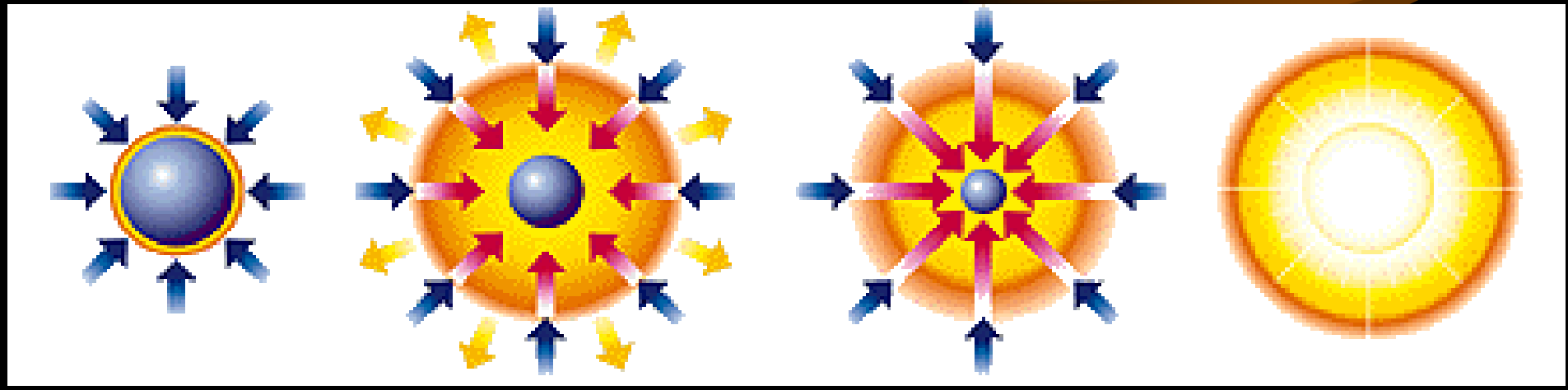

Radiation Pressure

e.g. powerful lasers beamed from all directions onto D-T pellet (0.1mm radius)

Compression:

fuel is compressed by rocket-like blow-off of hot surface material

Ignition:

density of fuel core reaches 1000 times density of water & ignites at 100 million K

Burn:

Thermonuclear fusion spreads rapidly through super-compressed fuel yielding many times input energy

Cross-sectional view of the KOYO-F fast ignition reactor (Norimatsu et al.)

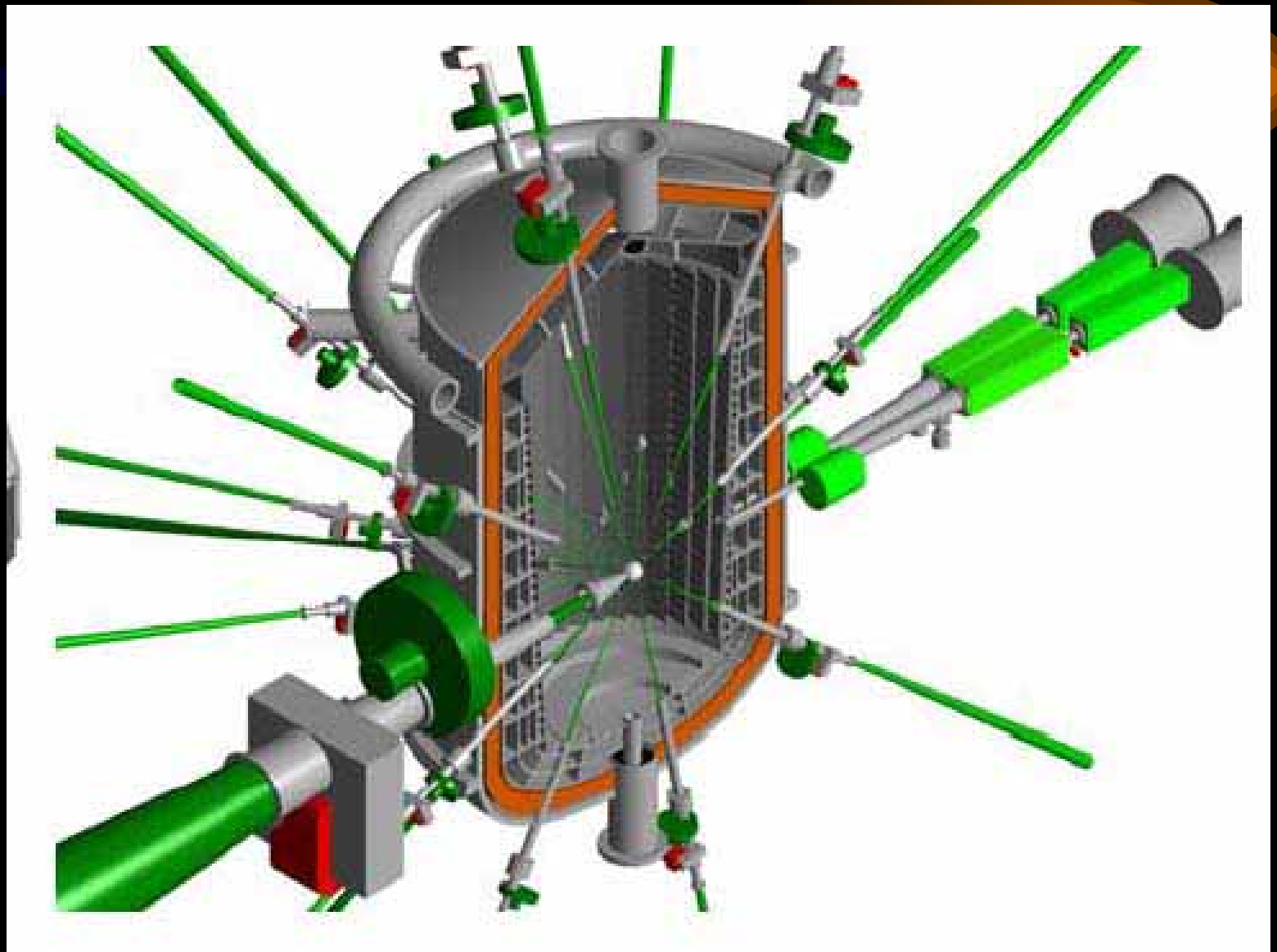

Large scale Fusion Experiments

- **Tokamaks: Low density, long confinement plasmas**
- **Laser Implosions: Super-dense, sub-nanosecond plasmas**

Smaller scale Fusion Experiments

Pinches: Dense, microsecond plasmas

Introduction

- **Plasma Focus (PF)-**
  - **remarkably copious source of multiple radiation: x-rays, fast electrons, ions and plasma stream**
  - **Fusion neutrons demonstrated even in table top devices**
  - **same energy density at storage energy levels of 0.1-1000 kJ; hence scalability of neutrons**

Superior method for dense pinches

- **The PF produces suitable densities and temperatures.**

- **A simple capacitor discharge is sufficient to power the plasma focus.**

THE PLASMA FOCUS (PF)

- **The PF is divided into two sections**.
- **Pre-pinch (axial) section**: Delays the pinch until the capacitor discharge current approaches peak value.
- **The pinch starts & occurs at top of the current pulse**.

The Plasma Dynamics in Focus

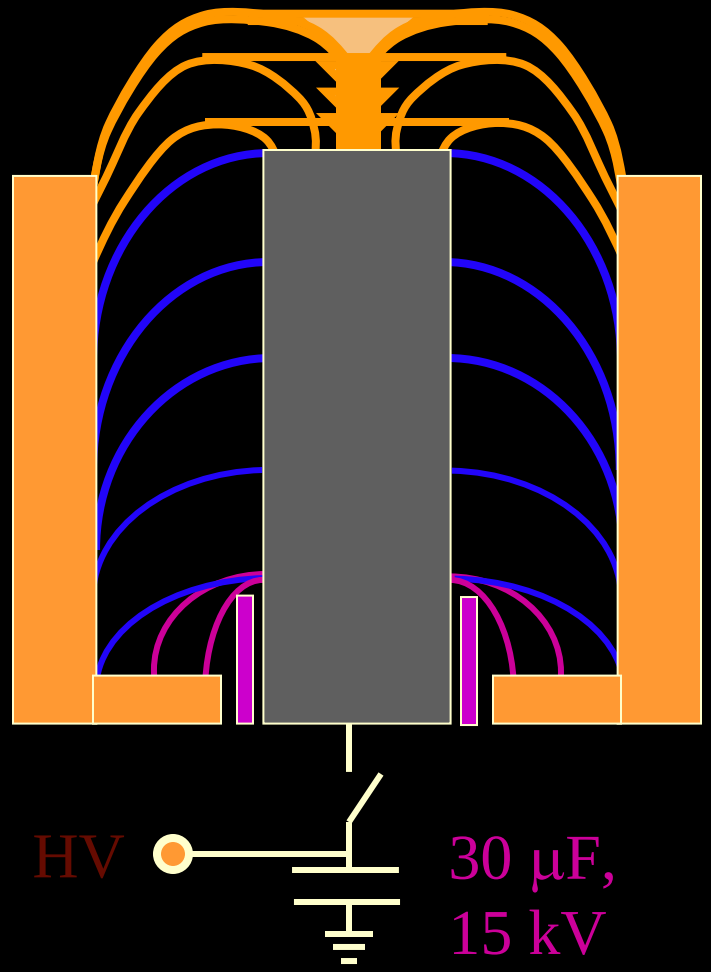

Radial Phase

Axial Accelaration Phase

Inverse Pinch Phase

Radial Compression (Pinch) Phase of the Plasma Focus

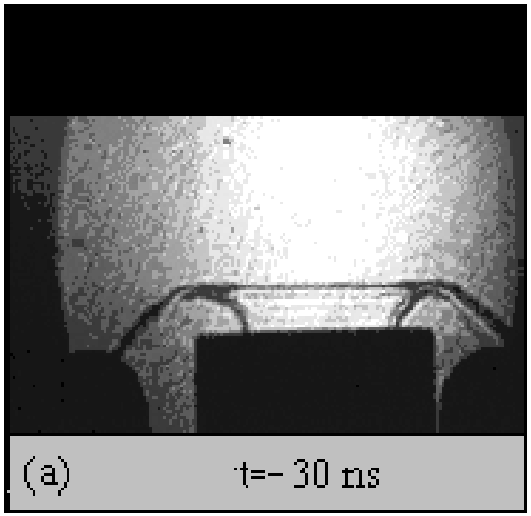

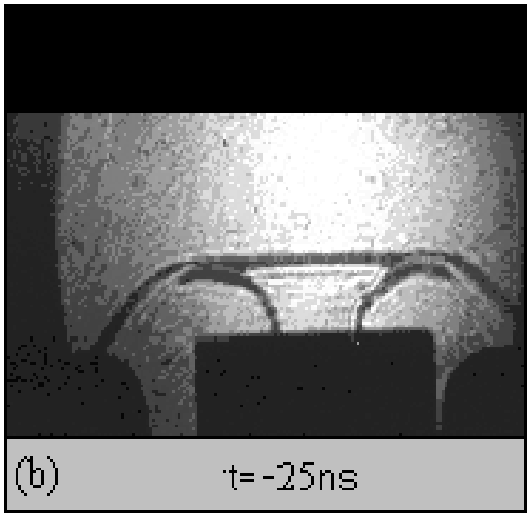

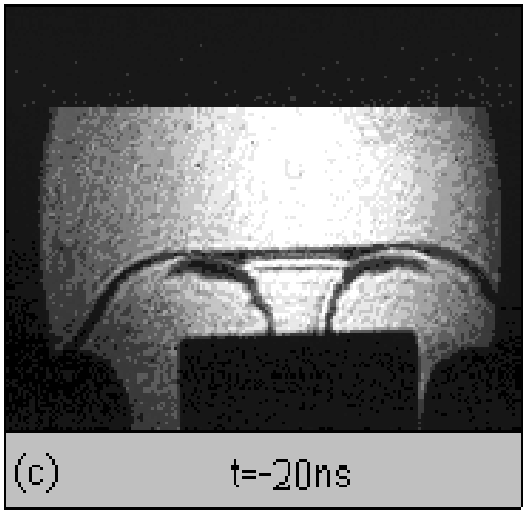

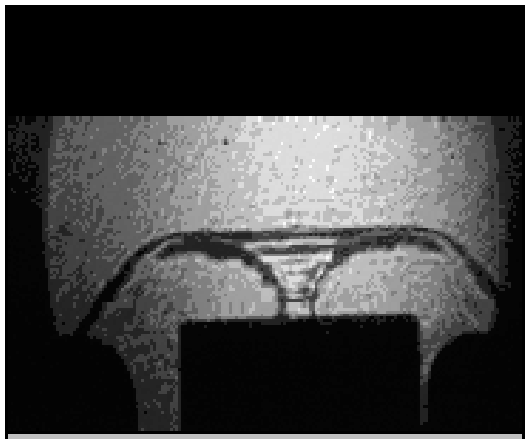

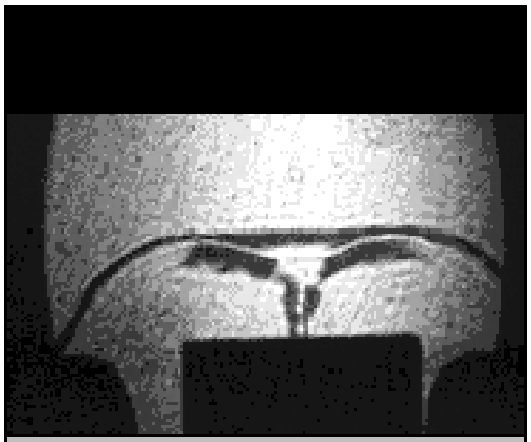

High Power Radiation from PF

- **powerful bursts of x-rays, ion beams, REB's, & EM radiation (>10 gigaW)**
- **Intense radiation burst, extremely high powers**
- **E.g. SXR emission peaks at 10^9 W over ns**
- **In deuterium, fusion neutrons also emitted**

Same Energy Density in small and big PF devices leads to:

- Scalability
  - constant speed factor, $[(I/a)/\rho^{1/2}]$ for all machines, big or small lead to same plasma energy density

- from 0.1 to 1000 kJ of storage energy
  - predictable yield of radiation

One of most exciting properties of plasma focus is its neutron yield Y_n

- **Early experiments show: $Y_n \sim E_0^2$**
- **Prospect was raised in those early research years that, breakeven could be attained at several tens of MJ .**
- **However quickly shown that as E_0 approaches 1 MJ, a neutron saturation effect was observed; Y_n does not increase as much as expected, as E_0 was progressively raised towards 1 MJ.**
- **Question: Is there a fundamental reason for Y_n saturation?**

Chart from M Scholz (November 2007 ICDMP)

Scaling

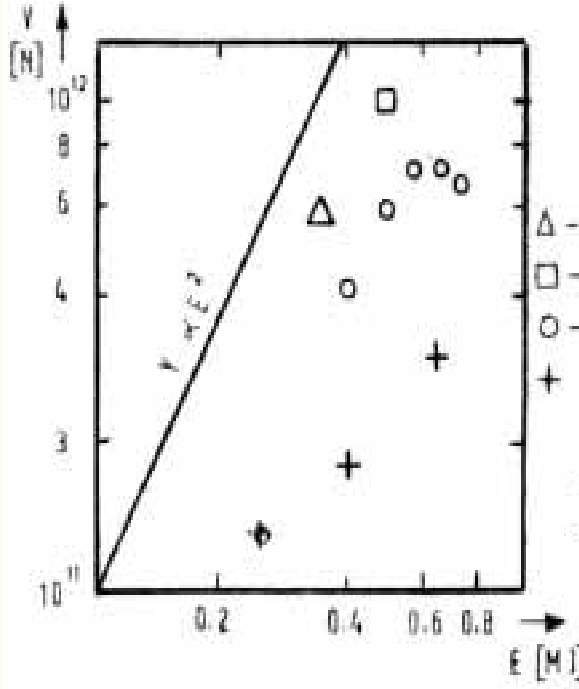

$$\frac{1}{2}(L+L_0)I^2 \cong \gamma E$$

$$L \cong L_0$$

$$Y_n \propto E^2$$

$$I^2 \propto E$$

Frascati (Program Euroatom), $E_b = 1MJ$; $U_b = 50\ kV$;

Y_n 'saturation' observed in numerical experiments (solid line) compared to measurements on various machines (small squares) -IPFS

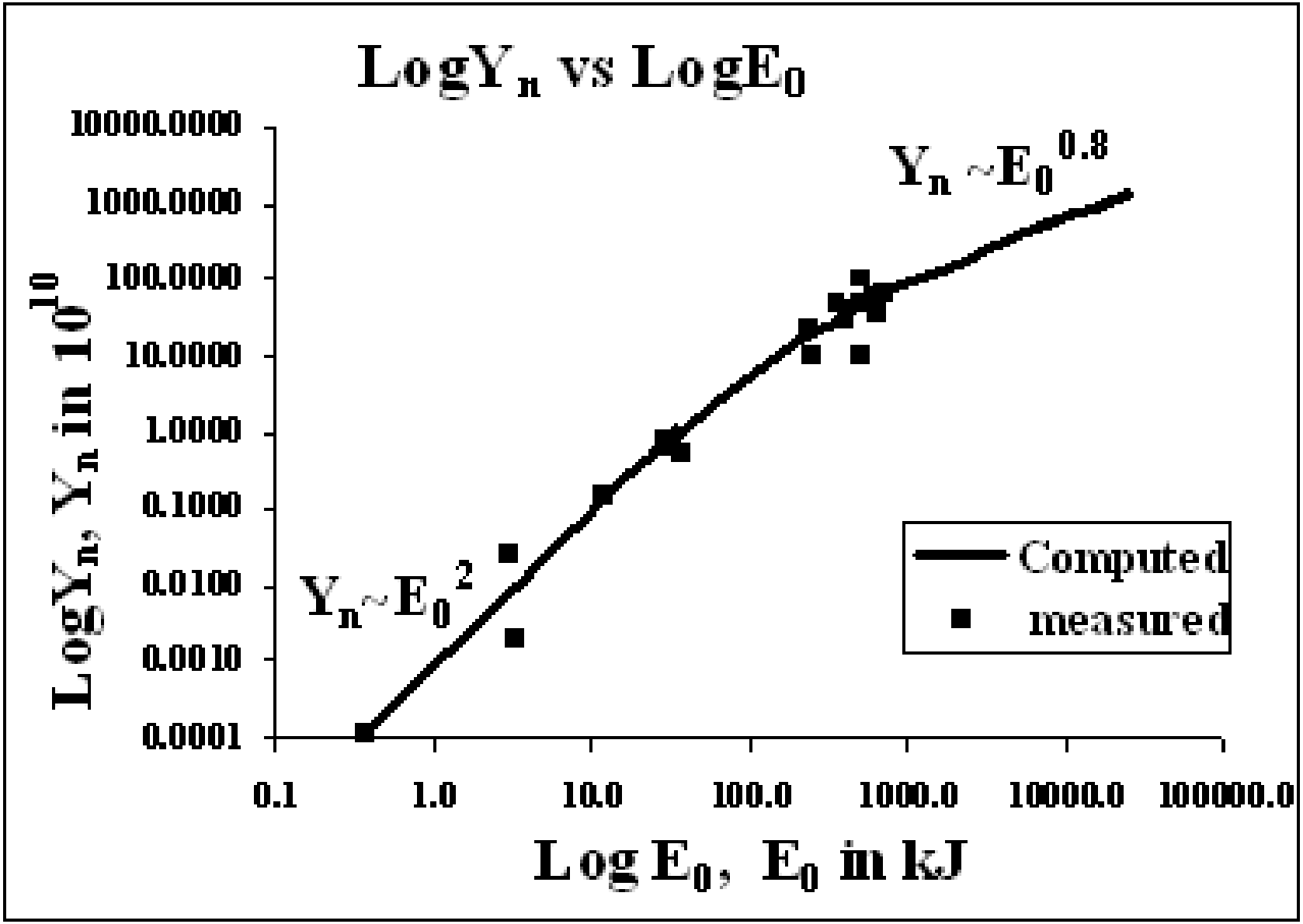

Comparing generator impedance & Dynamic Resistance DR_0 of small & large plasma focus- before I_{peak}

PF	$Z_0 = (L_0/C_0)^{1/2}$	Axial DR_0	Axial dominance	I_{peak}
Small	100 mΩ	7 mΩ	Z_0	~ V_0/Z_0
Large	1 mΩ	7 mΩ	DR_0	~V_0/DR_0

As E_0 is increased by increasing C_0, with voltage kept around tens of kV, Z_0 continues to decrease and I_{peak} tends towards asymptotic value of V_0/DR_0

Confirming I_{peak} saturation is due to constancy of DR_0

I_{peak} vs E_0 from DR_0 analysis compared to model simulation

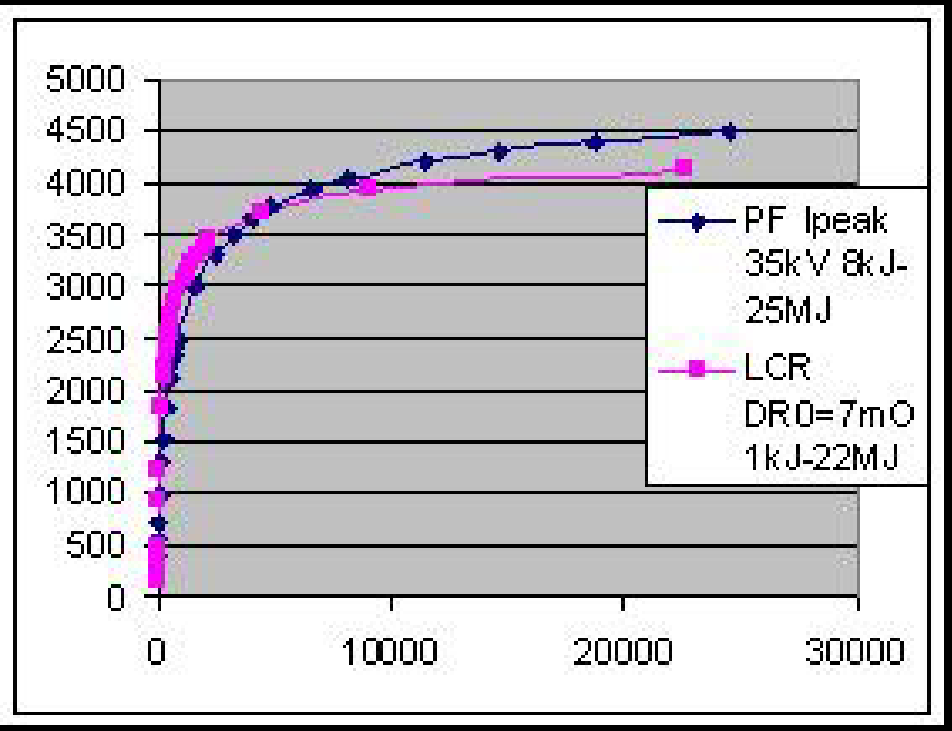

Model simulation gives higher I_{peak} due to a 'current overshoot effect' which lifts the value of I_{peak} before the axial DR_0 fully sets in

I_{peak} vs E_0 on log-log scale DR_0 analysis

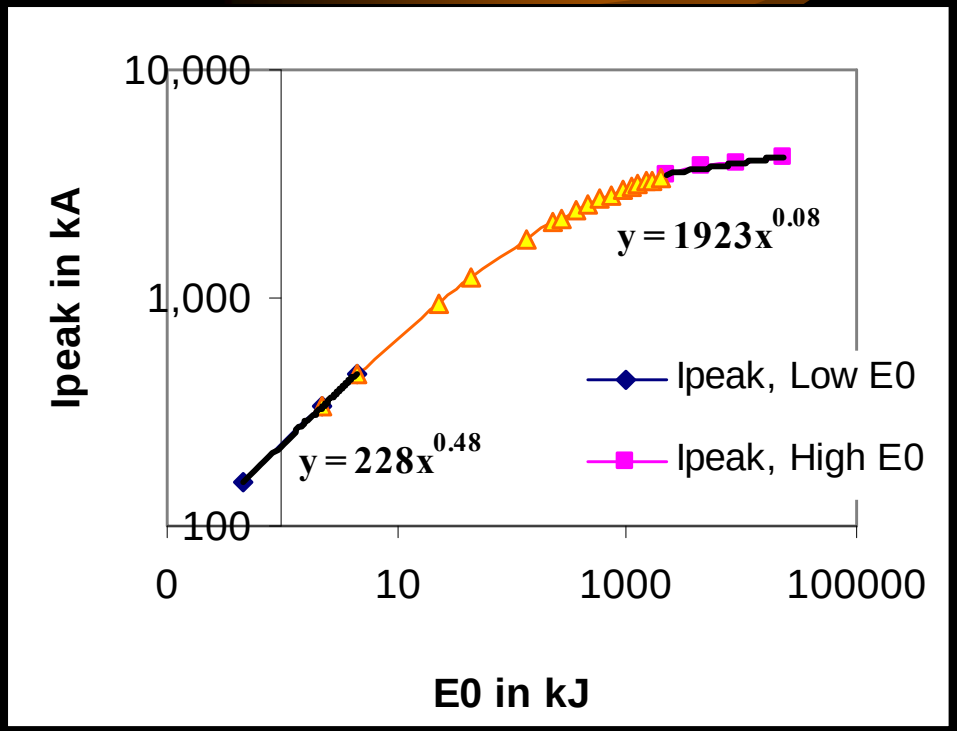

Confirming that I_{peak} scaling tends to saturate before 1 MJ

At IPFS, we have shown that: constancy of DR_0 leads to current 'saturation' as E_0 is increased by increasing C_0. Tendency to saturate occurs before 1 MJ

From both numerical experiments as well as from accumulated laboratory data:

- $\mathbf{Y_n \sim I_{pinch}^{4.5}}$
- $\mathbf{Y_n \sim I_{peak}^{3.8}}$

Hence the 'saturation' of I_{peak} leads to saturation of neutron yield Y_n

Insight- neutron saturation

- **A major factor for ‘neutron saturation’ is simply: Axial Phase Dynamic Resistance**

Conclusions and Discussion

Beyond saturation?

Possible ways to improve Y_n:

- **Increase operating voltage. Eg SPEED II uses Marx technology: 300kV, driver impedance 60 mΩ. With E_0 of under 200 kJ, the system was designed to give I_{peak} of 5 MA and I_{pinch} just over 2 MA.**
- **Extend to 1MV-with low bank impedance- would increase I_{peak} to 100 MA; at several tens of MJ. I_{pinch} could be 40 MA**
- **Y_n enhancing methods such as doping deuterium with low % of krypton.**
- **Further increase in I_{pinch} by fast current-injection near the start of radial phase. This could be achieved with charged particle beams or by circuit manipulation such as current-stepping. This model is ideally suited for testing circuit manipulation schemes.**

Ongoing IPFS numerical experiments of Multi-MJ, High voltage MJ and Current-step Plasma Focus

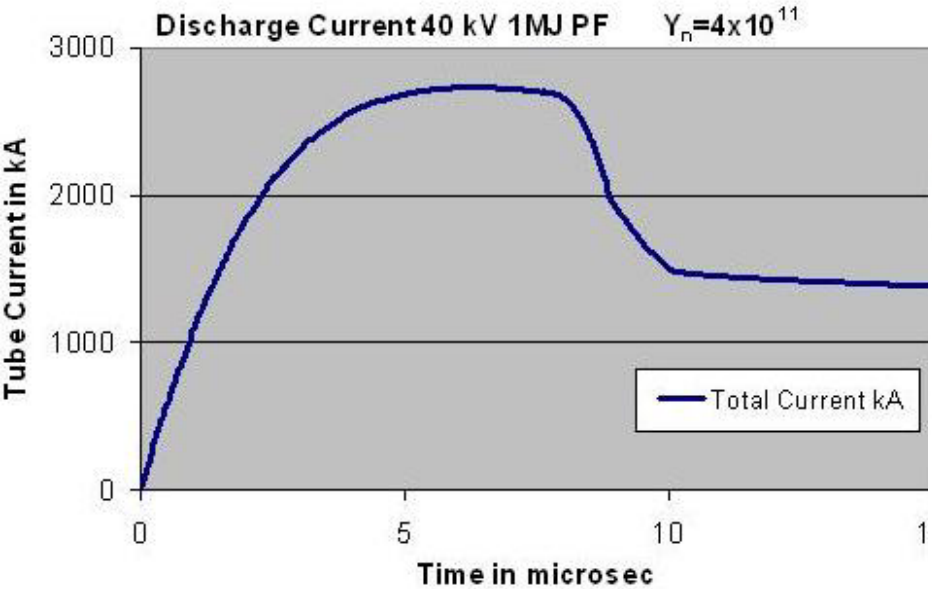

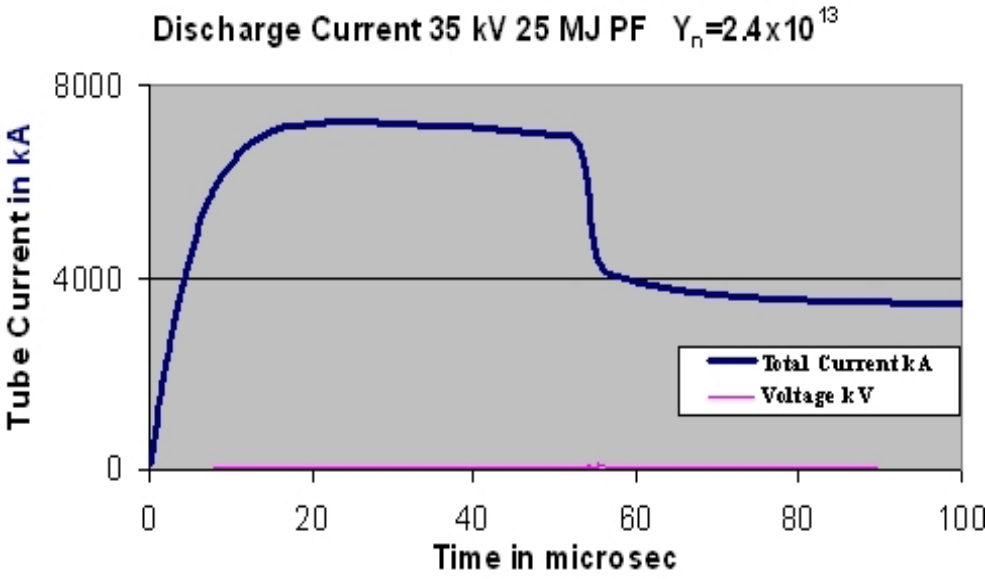

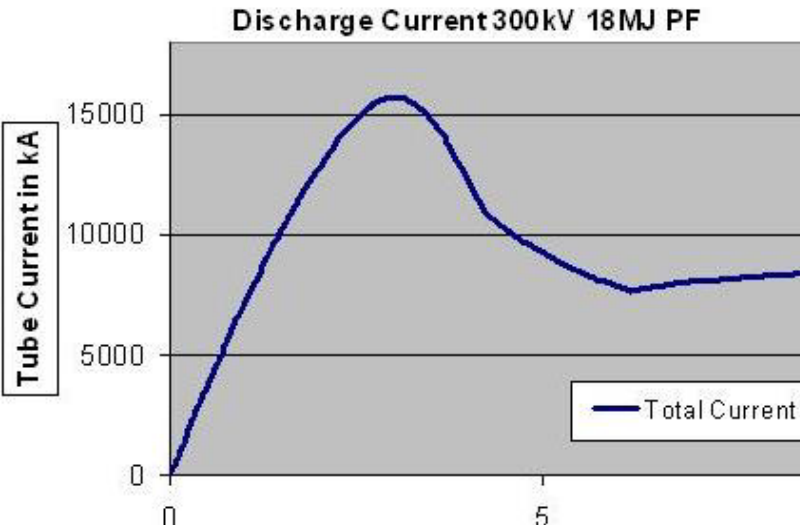

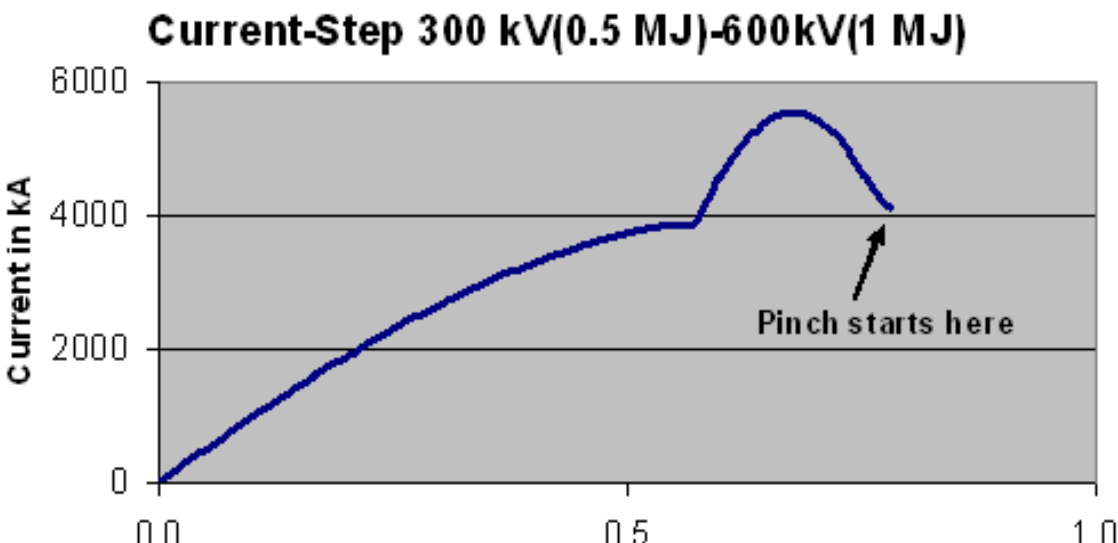

Conclusion:

- **Tokamak programme is moving steadily towards harnessing nuclear fusion energy as a limitless clean energy source for the continuing progress of civilisation**

- **Alternative and smaller scale experiments will also play a role in this most challenging technological development**

THANK YOU

Appreciation to the following web-sites:

- **http://fusion.gat.com**
- **http://chandra.harvard.edu**
- **http://fire.pppl.gov**
- **http://www.jet.efda.org**
- **http://www.iter.org**
- **http://www.fusion.org.uk**
- **http://www-jt60.naka.jaeri.go.jp**
- **http://www.hiper-laser.org/**
- **http://www.intimal.edu.my/school/fas/UFLF**
- **http://www.plasmafocus.net**

Plasma Focus Fusion Devices

S Lee & S H Saw

Institute for Plasma Focus Studies

INTI University College, Malaysia

Gazi University Technical Education Faculty, Ankara

2 October 2009 10 am

Plan of Talk

- **Description of PF fusion devices- from small to big**
- **Experiments and results**
- **Numerical Experiments confirm deterioration of scaling laws**
- **New ideas needed- beyond present saturation.**

When matter is heated to high temperatures:

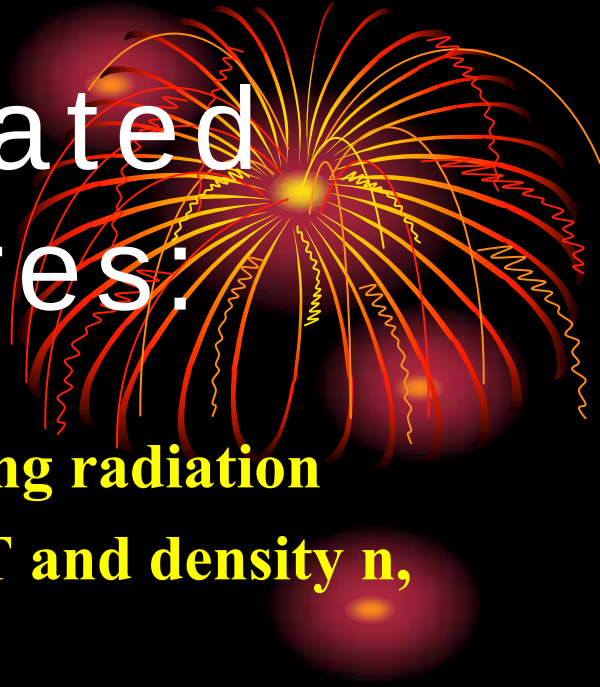

- **It ionizes and becomes a plasma; emitting radiation**
- **Generally, the higher the temperature T and density n, the more intense the radiation**
- **Depending on heating mechanisms, beams of ions and electrons may also be emitted**
- **In Deuterium, nuclear fusion may take place, if n & T are high enough; neutrons are also emitted.**
- **Typically T> several million K; & compressed n: above atmospheric density.**

One method: electrical discharge through gases.

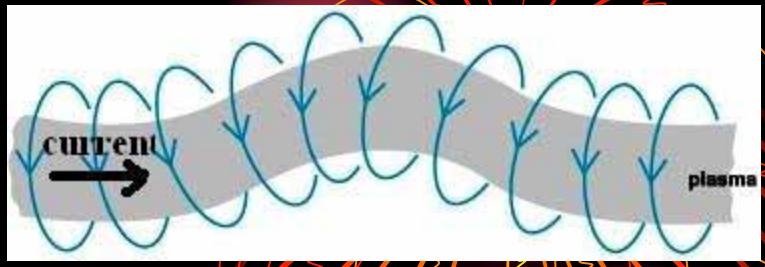

- Heated gas expands, lowering the density; making it difficult to heat further.
- Necessary to compress whilst heating, to achieve sufficiently intense conditions.
- Electrical discharge between two electrodes produces azimuthal magnetic field which interacts with column of current; giving rise to a self compression force which tends to constrict (or pinch) the column.
- To ‘pinch’ a column of gas to atmospheric density at T~ 1 million K, a rather large pressure has to be exerted by the pinching magnetic field.
- Electric current of hundreds of kA required, even for column of radius of say 1mm.
- Dynamic pinching process requires current to rise very rapidly, typically in under 0.1 microsec in order to have a sufficiently hot and dense pinch.
- Super fast, super dense pinch requires special MA fast

Superior method for super-dense-hot pinch: plasma focus (PF)

- **The PF produces superior densities and temperatures.**
- **2-Phase mechanism of plasma production does away with the extra layer of technology required by the expensive and inefficient pulse-shaping line.**
- **A simple capacitor discharge is sufficient to power the plasma focus.**

THE PLASMA FOCUS

- **The PF is divided into two sections.**
- **Pre-pinch (axial) section: Delays the pinch until the capacitor discharge approaches maximum current.**
- **The pinch starts & occurs at top of the current pulse.**
- **Equivalent to driving the pinch with a super-fast rising current; without necessitating the fast line technology.**
- **The intensity which is achieved is superior to even the super fast pinch.**

Two Phases of the Plasma Focus

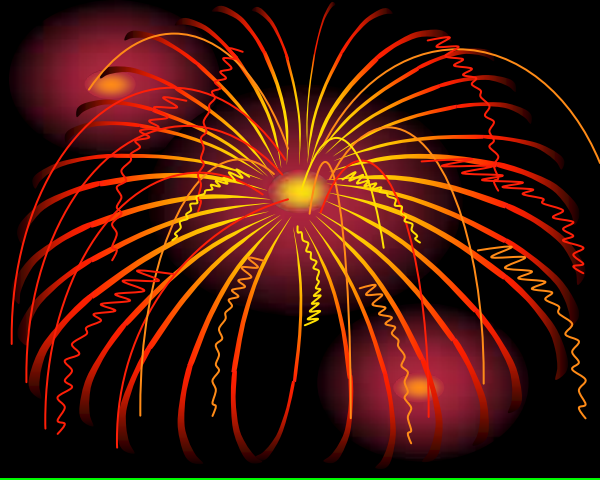

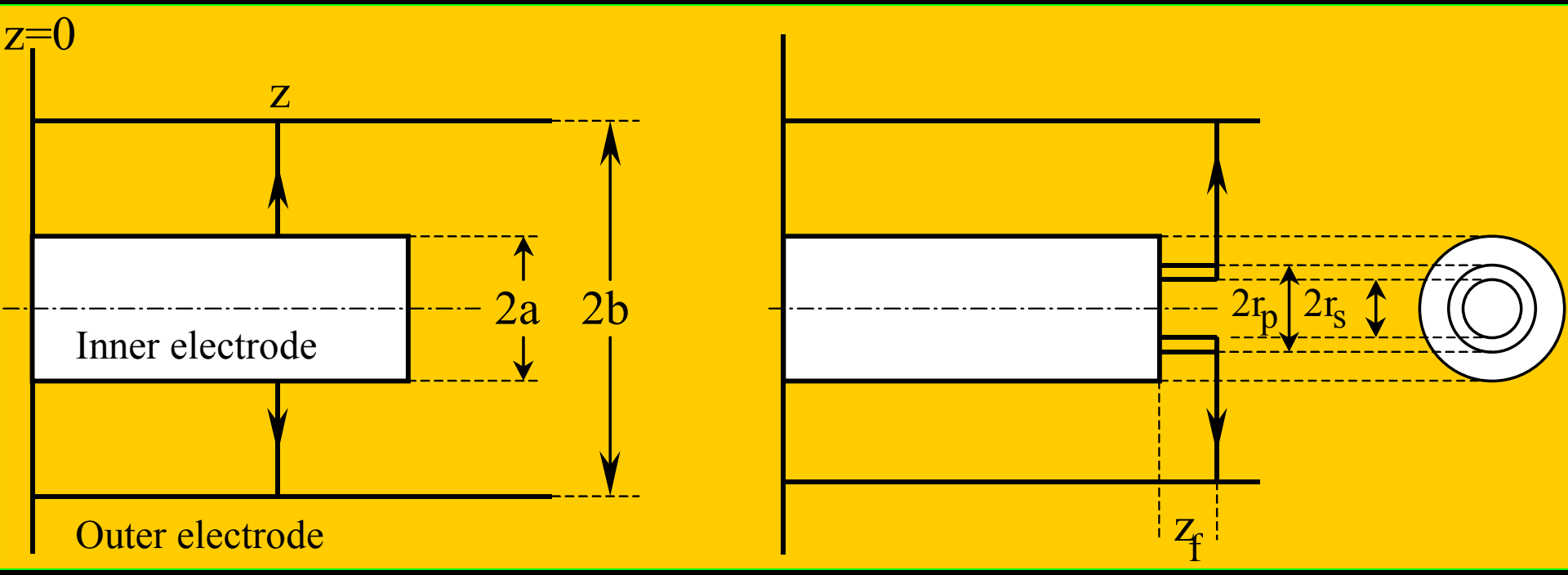

Radial Compression (Pinch) Phase of the Plasma Focus

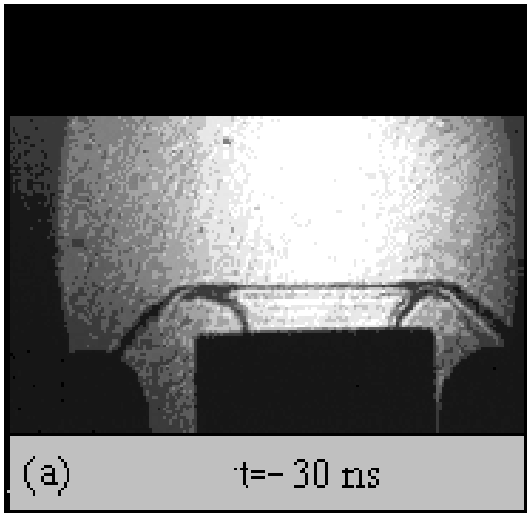

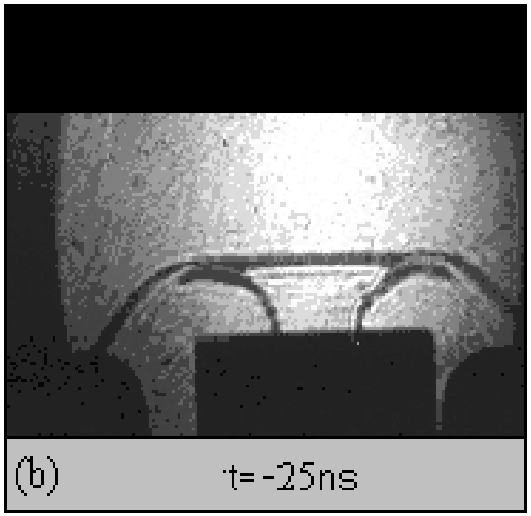

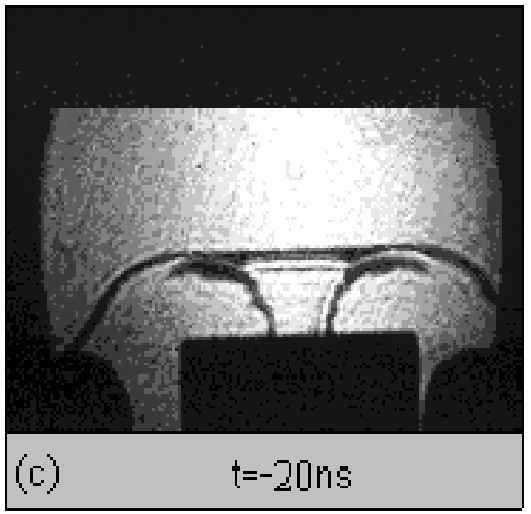

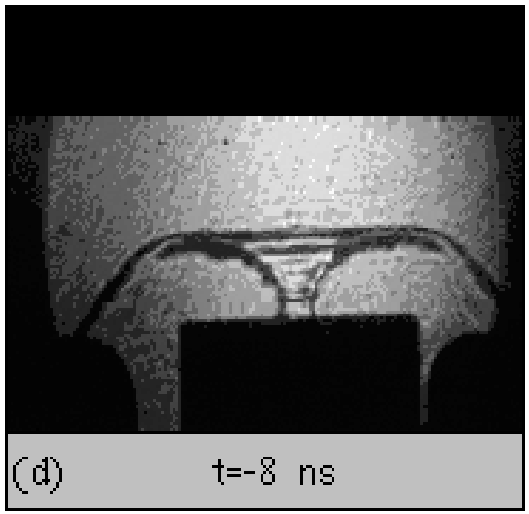

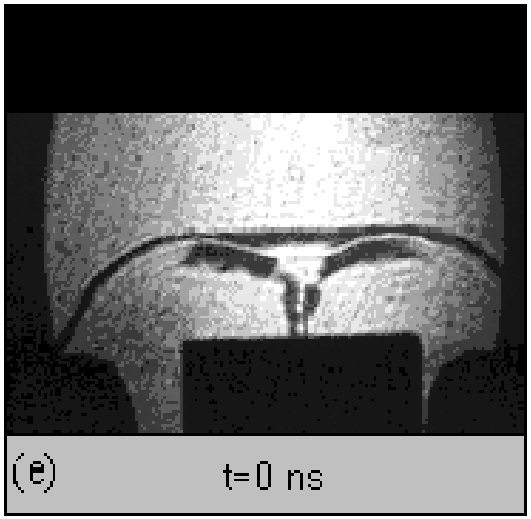

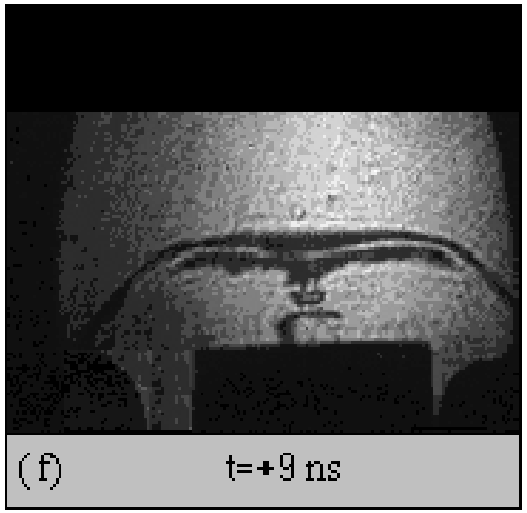

The Plasma Dynamics in Focus

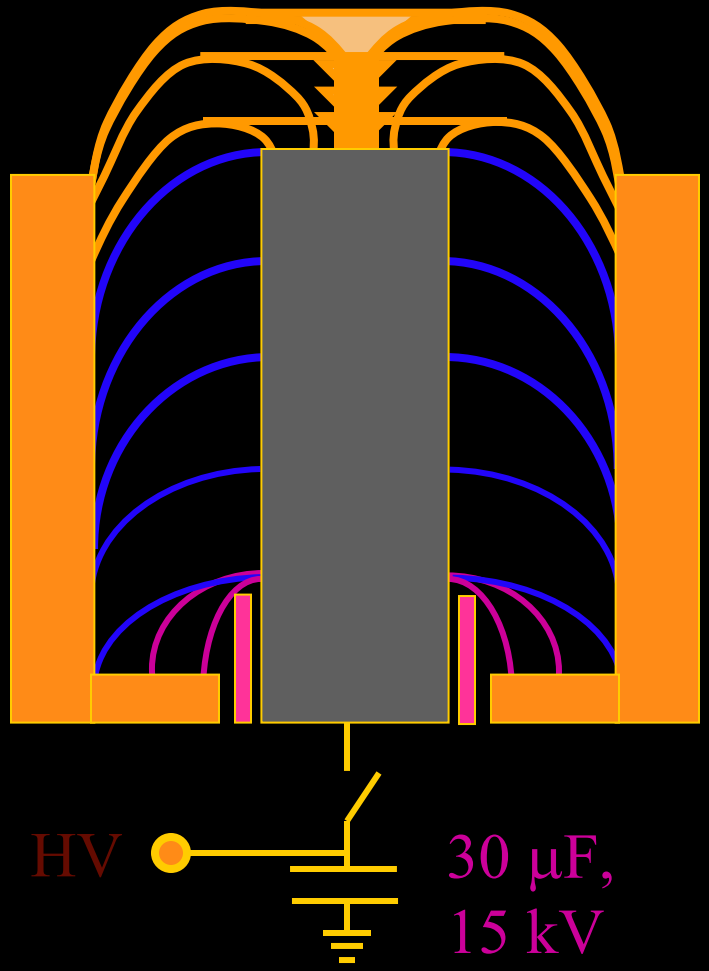

Radial Phase

Axial Acceleration Phase

Inverse Pinch Phase

Plasma Focus Devices in Singapore

The UNU/ICTP PFF

(UnitedNationsUniversity/International Centre for Theoretical Physics Plasma Focus Facility)

- 15 kV, 3kJ
- single-shot, portable; 170kA
- 3J SXR per shot (neon)
- 10^8 neutrons/ shot (in D_2)
- 10^{16} neutrons/s (estimated)

(This device is also in operation in Malaysia, Thailand, India, Pakistan, Egypt, Zimbabwe)

NX2- Plasma SXR Source

- 11.5kV, 2 kJ
- 16 shots /sec; 400 kA
- 20J SXR/shot (neon)
- 10^9 neutrons/shot

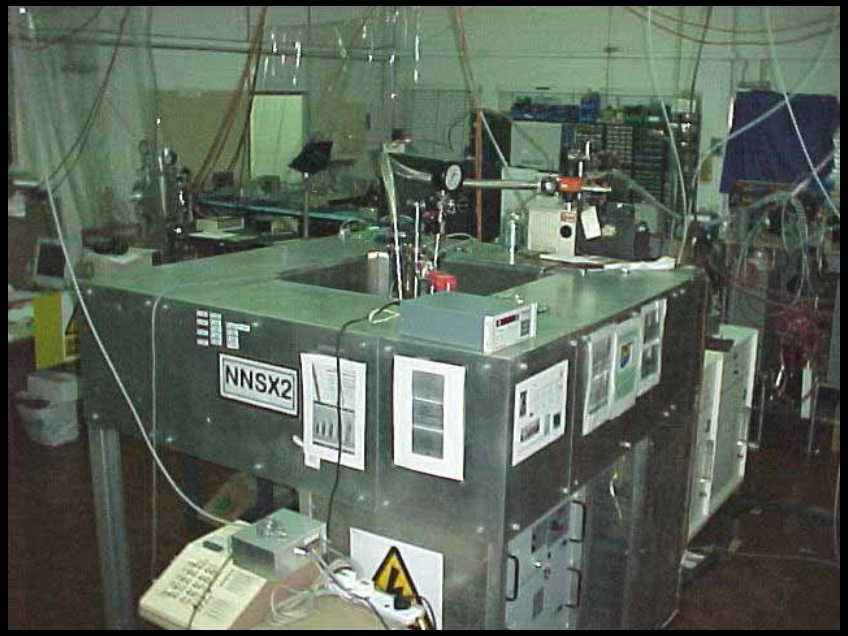

300J PF:
(2.4 µF, $T/4$ ~ 400 ns, 15 kV, 270 J, total mass ~25 kg)
neutron yield: (1.2±0.2) × 10^6 neutrons/shot at ~80 kA peak current;
compact, portable, quasi-continuous pulsed neutron fusion source, a 'fast miniature plasma focus device'

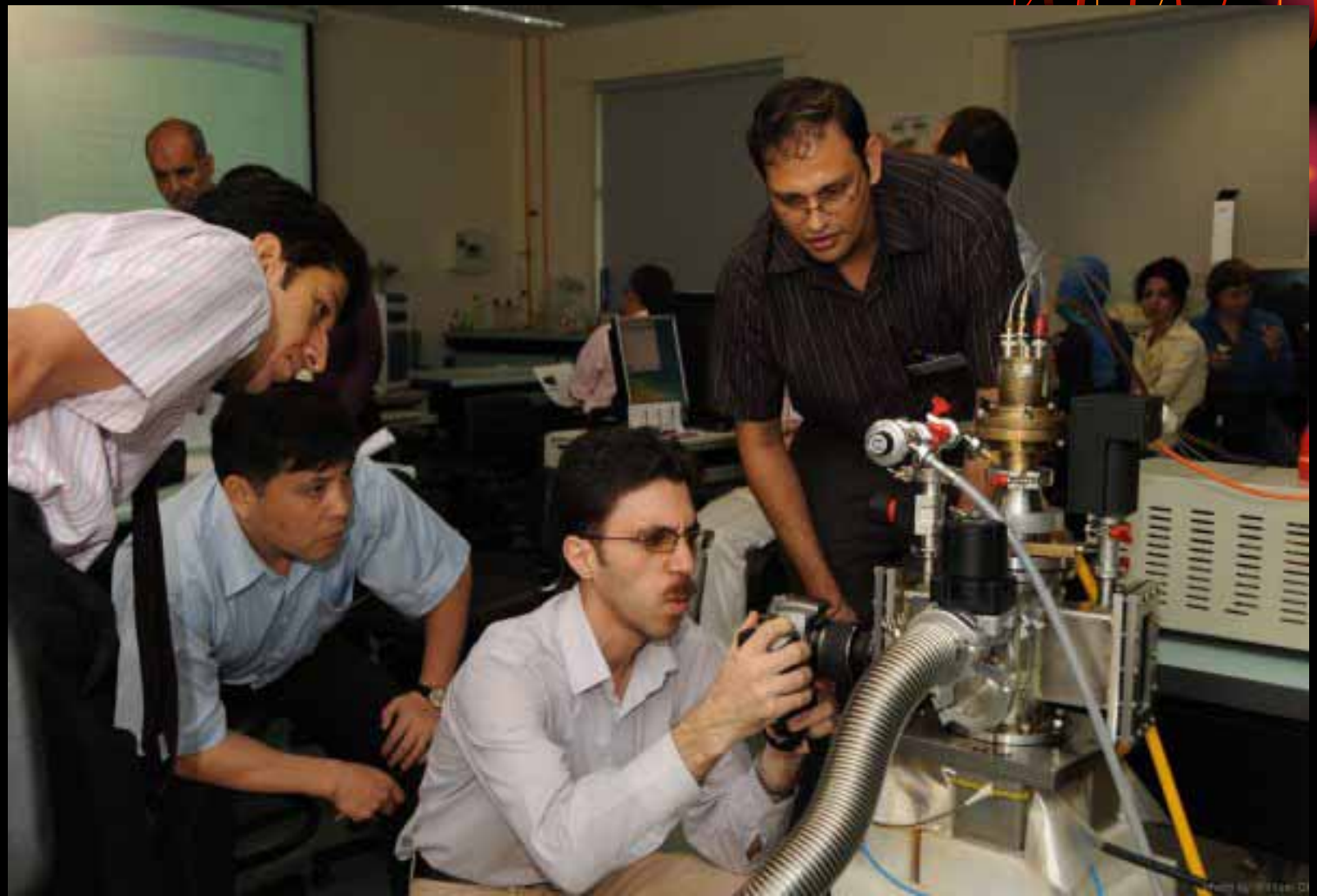

High Power Radiation from PF

- **powerful bursts of x-rays, ion beams, REB's, & EM radiation (>10 gigaW)**
- **Intense radiation burst, extremely high powers**
- **E.g. SXR emission peaks at 10^9 W over ns**
- **In deuterium, fusion neutrons also emitted**

Applications (non-fusion)

SXR Lithography

- **As linewidths in microelectronics reduces towards 0.1 microns, SXR Lithography is set to replace optical lithography.**

- **Baseline requirements, point SXR source**
  - **less than 1 mm source diameter**
  - **wavelength range of 0.8-1.4 nm**
  - **from industrial throughput considerations, output powers in excess of 1 kW (into 4p)**

SXR lithography using NX2

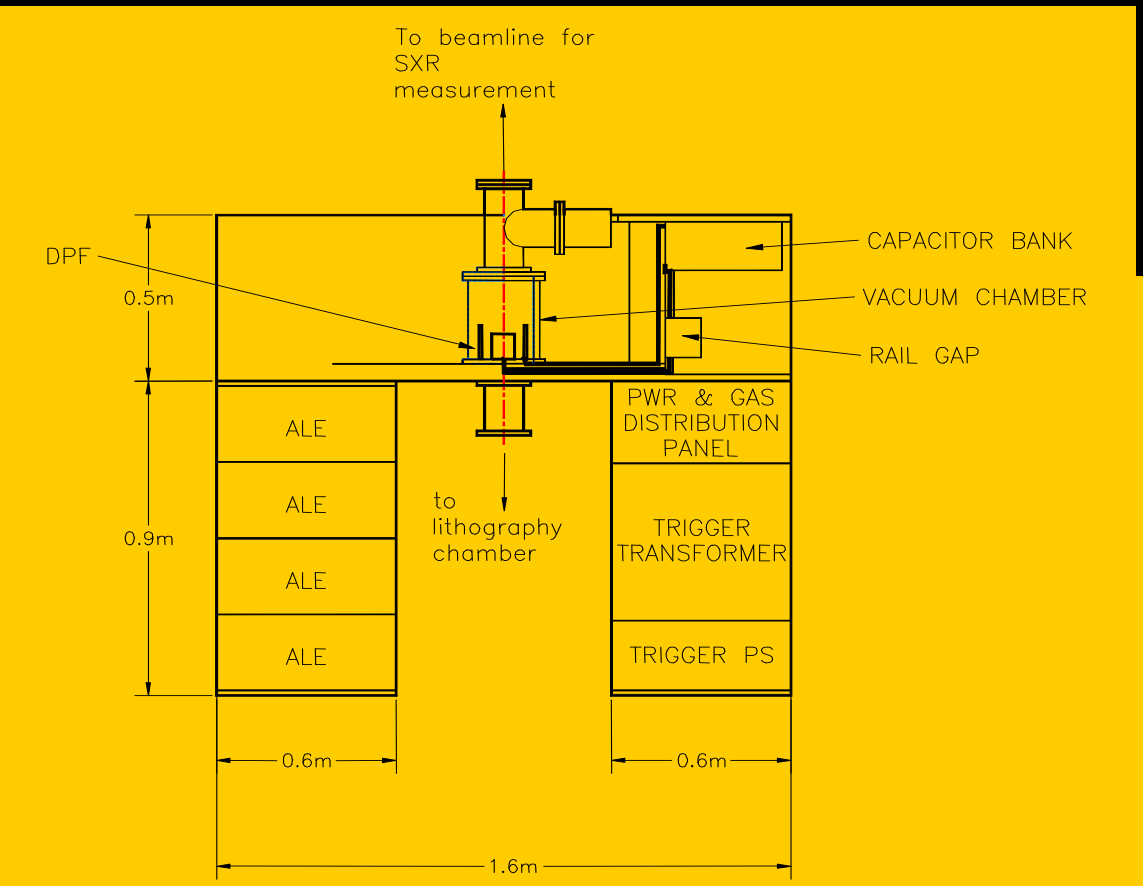

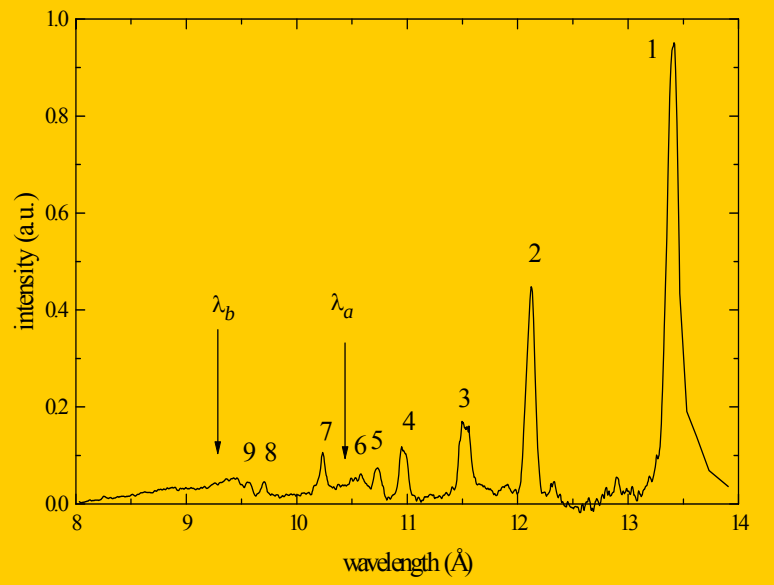

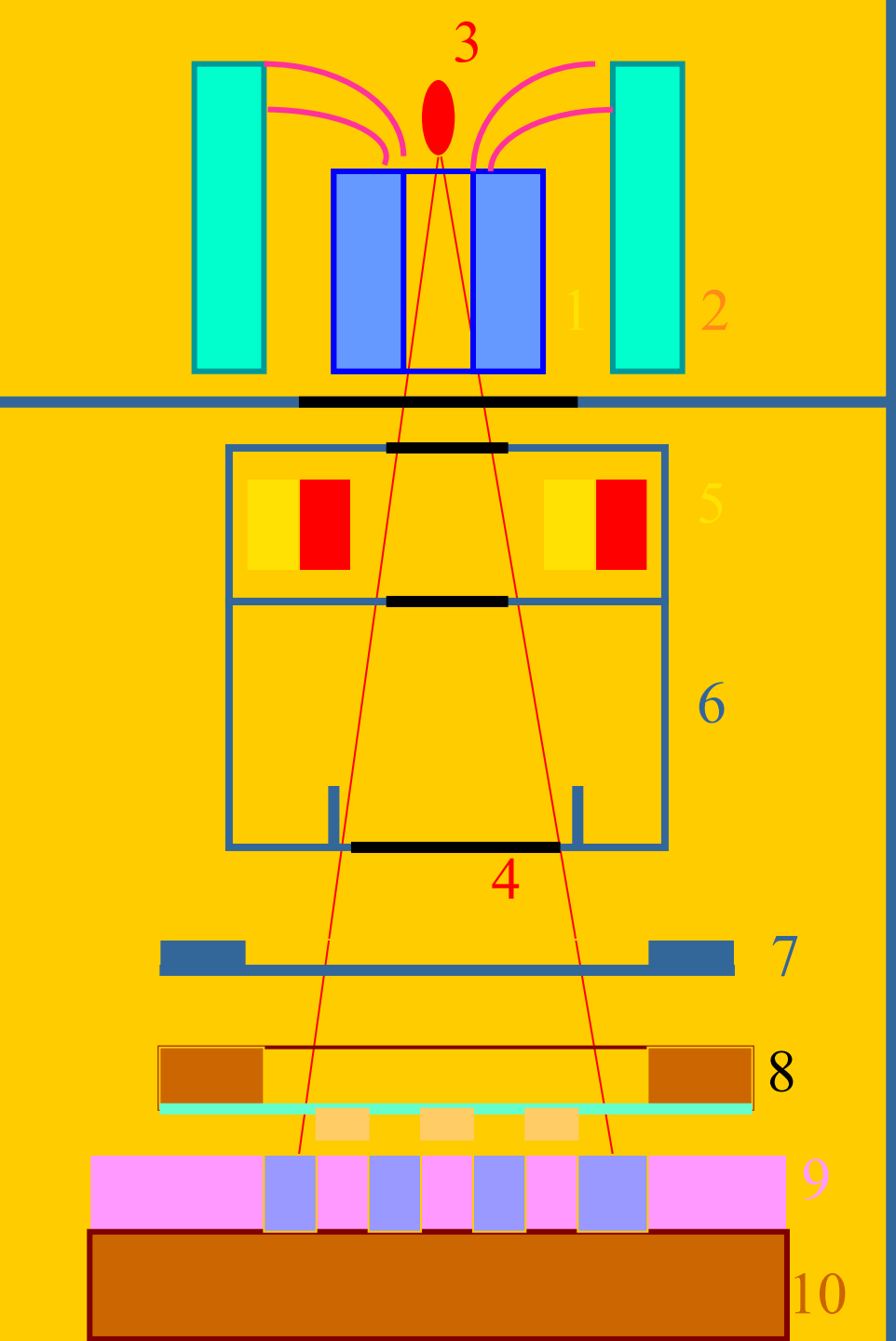

PF SXR Schematic for Microlithography

- 1 - anode
- 2 - cathode
- 3 - SXR point source
- 4 - x-rays
- 5 - electron beam deflection magnets
- 6 - shock wave shield
- 7 - Be window
- 8 - x-ray mask
- 9 - x-ray resist
- 10 - substrate

Lines transferred using NX2 SXR

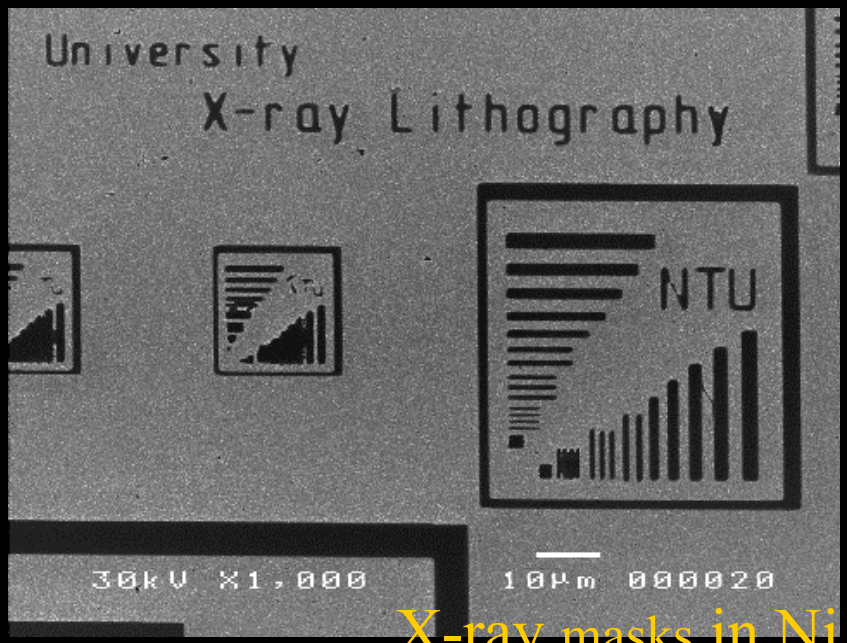

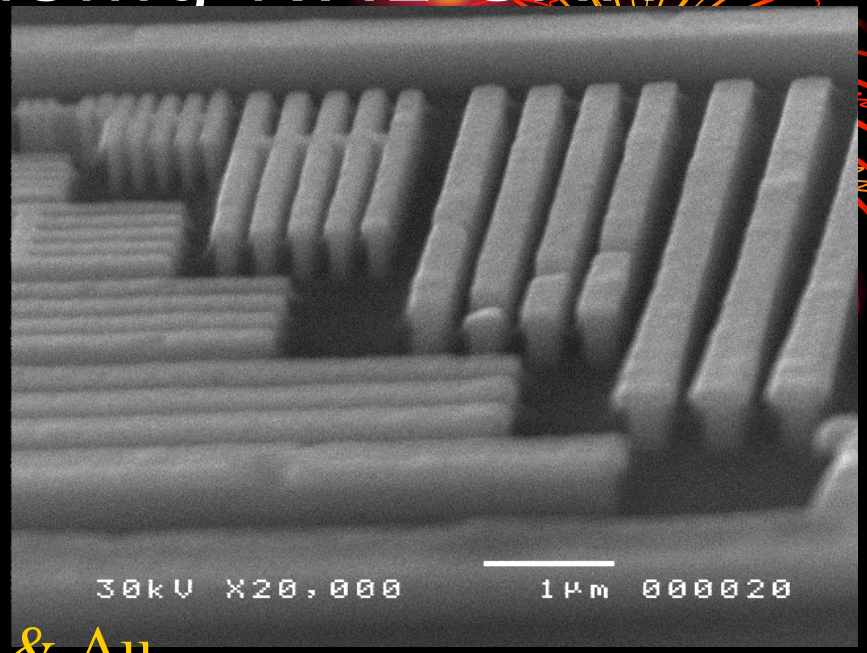

X-ray masks in Ni & Au

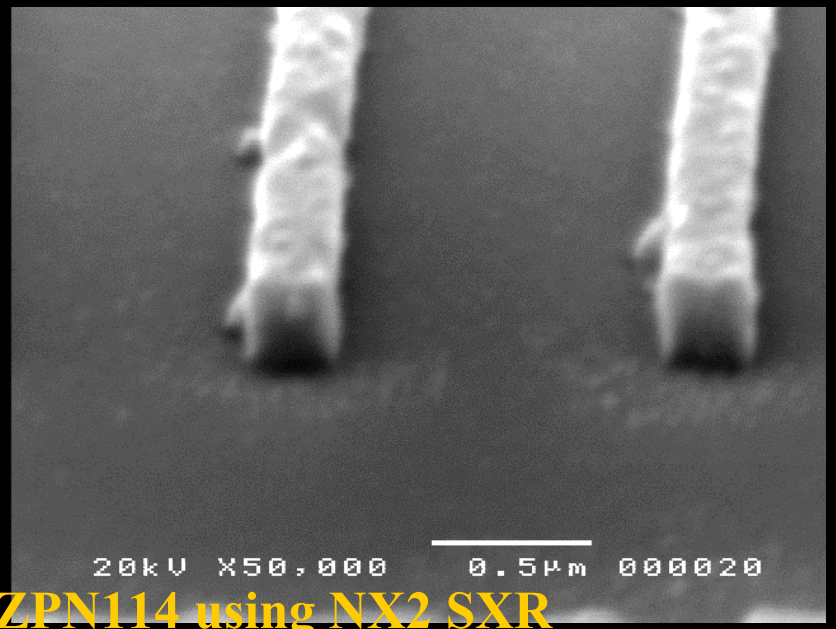

SEM Pictures of transfers in AZPN114 using NX2 SXR

X-ray Micromachining

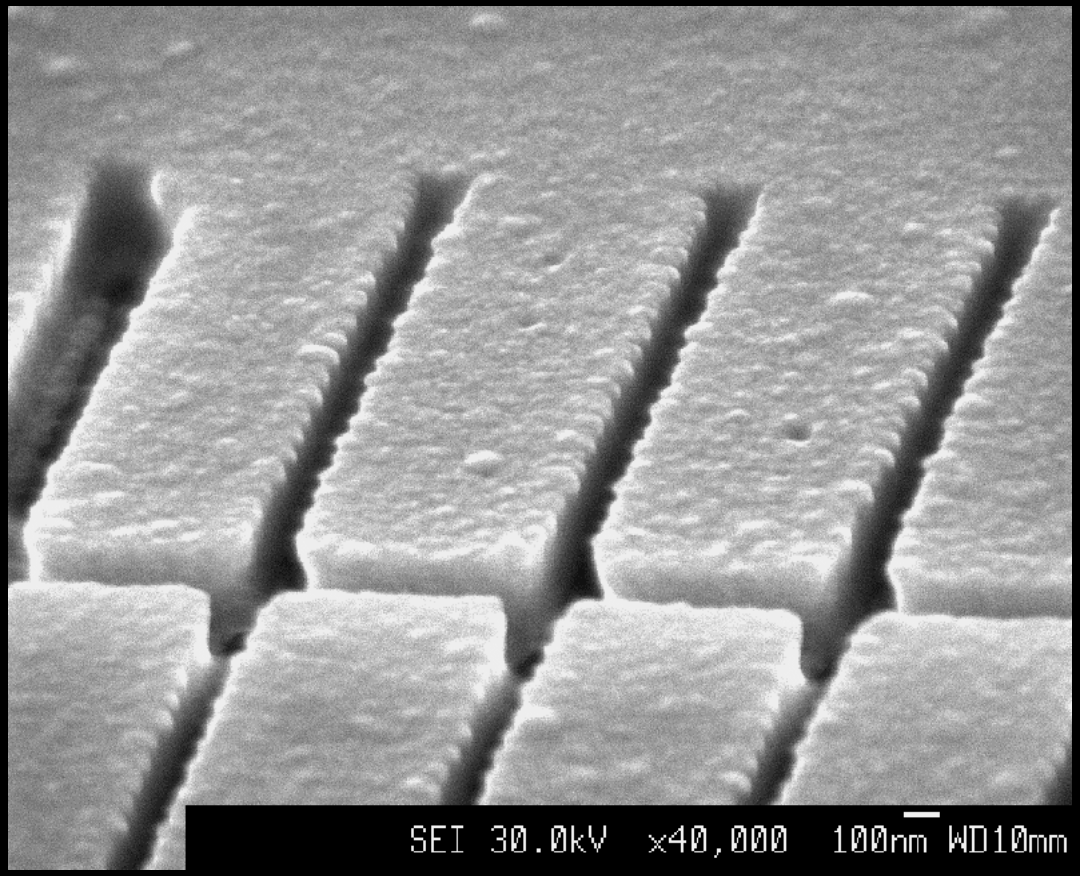

Other Applications –non fusion

Materials modification using Plasma Focus Ion Beam

For plasma processing of thin film materials on different substrates with different phase changes.

Other Applications

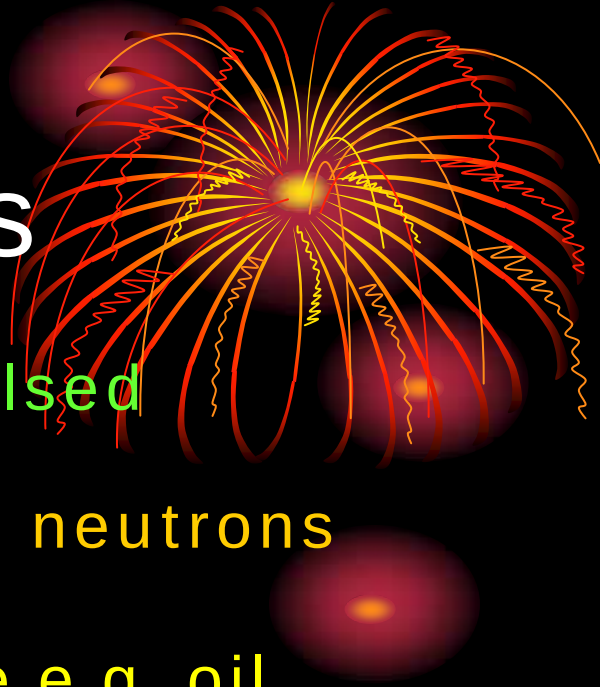

- Studies on Radiation safety & pulsed neutron activation
- Baggage inspection using pulsed neutrons
- Plasma propulsion
- Pulsed neutron source for on-site e.g. oil well inspection
- High speed imaging using combined x-rays & neutrons
- Broad-spectrum, improved contrast x-ray tomography
- Simulation of radiation from nuclear explosion

Important general results from Decades of research

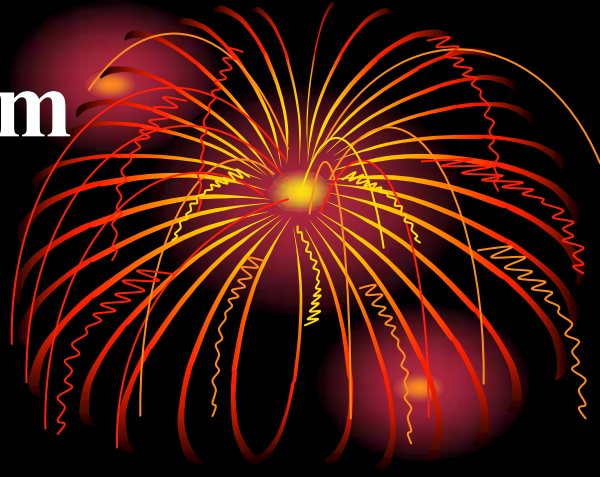

measuring all aspects of the plasma focus:

-imaging for dynamics

-interferometry for densities

-spectroscopy for temperatures

-neutrons, radiation yields, MeV particles

Result: commonly accepted picture today that mechanisms within the focus pinch :

- micro- & MHD instabilities

-acceleration by turbulence

- 'anomalous' plasma resistance

are important to plasma focus behaviour, and

neutron yields are non-thermonuclear in origin

Summarised in: Bernard A, Bruzzone H, Choi P, Chuaqui H, Gribkov V, Herrera J, Hirano K, Krejci A, Lee S, Luo C 1998 "Scientific status of plasma focus research" J Moscow Physical Society 8 93-170

Most important general property of the Plasma Focus

Energy density constancy

The smallest sub-kJ plasma focus and the largest MJ plasma focus have practically:

- the same energy density (per unit mass)

- the same temperatures,

- the same speeds.

Plasma volumes & lifetimes; increase with anode radius 'a'

pinch radius ~a

pinch length ~a

pinch lifetime ~a

radius a~ current I

Derived from model scaling, based on observation of constancy of speed factor across plasma focus devices

One of most exciting properties of plasma focus is its neutron yield Y_n

- **Early experiments show: $Y_n \sim E_0^2$**
- **Prospect was raised in those early research years that, breakeven could be attained at ~100 MJ.**
- **However quickly shown that as E_0 approaches 1 MJ, a neutron saturation effect was observed; in other words, Y_n does not increase much more as E_0 was progressively raised above several hundred kJ**
- **Question: Is there a fundamental reason for Y_n saturation?**
- **In Part 2 of this paper we will identify one simple fundamental factor for Y_n saturation; after we discuss the use of modelling for providing reference points for diagnostics.**

Modern Status

Now PF facilities (small to big) operate in Poland (PF-1000 and PF-6 in IPPLM, PF-360), Argentina, China, Chile, Great Britain, India, Iran, Japan, Mexico, Korea, Malaysia, Pakistan, Romania, Singapore, Thailand, Turkey, USA, Zimbabwe etc.

This direction is also traditional for Russia: Kurchatov Institute (PFE, 180 kJ and biggest in the world facility PF-3, 2.8 MJ), Lebedev Institute (“Tulip”, PF-4), MEPhI, Sarov, ITEF (PF-10)-

1997 ICDMP (International Centre for Dense Magnetised Plasmas) Warsaw-now operates one of biggest plasma focus in the world, the PF1000

PF 1000 ICDMP Poland-M Scholz

Apparatus

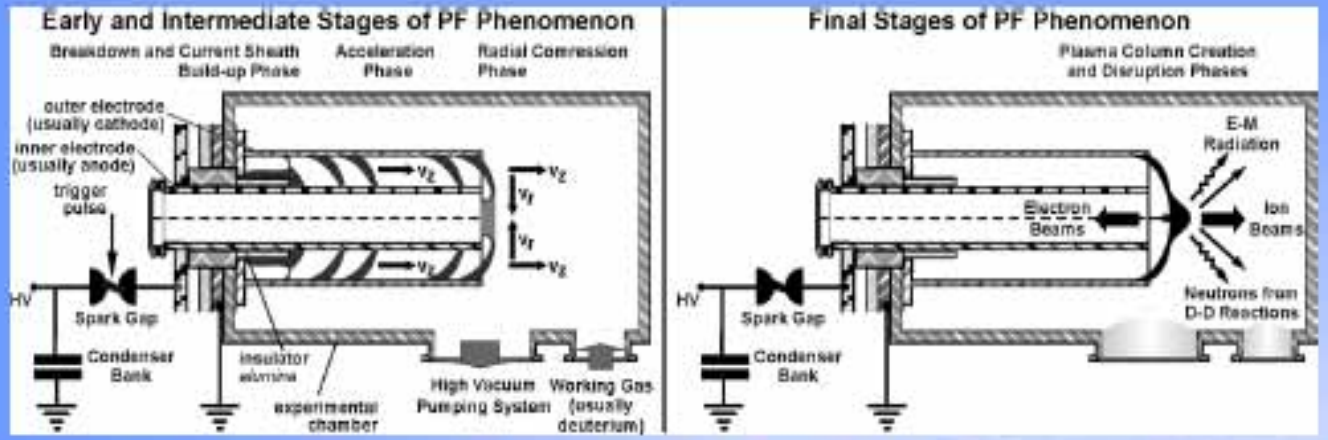

Institute of Plasma Physics and Laser Microfusion
Warsaw, Poland

PF-1000, IPPLM, Warsaw

Charging voltage - U_0 = 20 - 40 kV,
Bank capacitance - C_0 = 1.332 mF,
Bank energy - E_0 = 266 - 1064 kJ,
Nominal inductance - L_0 = 15 nH,
Quarter discharge time - T/4 = 6 μs,
Short-circuit current – I_{SC} = 12 MA,
Characteristic resistance - R_0 = 2.6 mΩ,

Vacuum chamber – 3.8 m^3
∅= 1.4 m, L = 2.5 m
Anode diameter is 226 mm
Cathode diameter is 400 mm
Cathode consists of 24 rods (32 mm in diameter)
Anode length is 560 mm
Insulator length is 113 mm

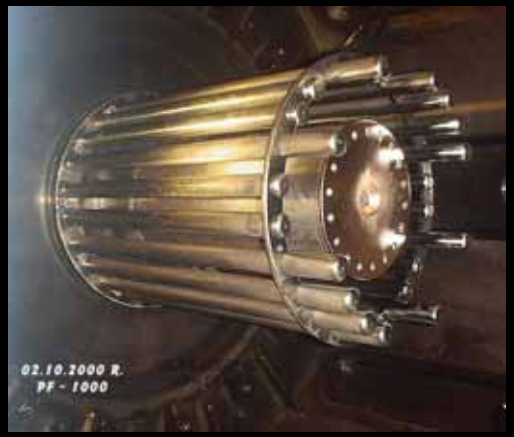

Main goal – studies on neutron production at high energy input

Presented by M.Scholz,
IPPLM

Measurements of Current and Voltage

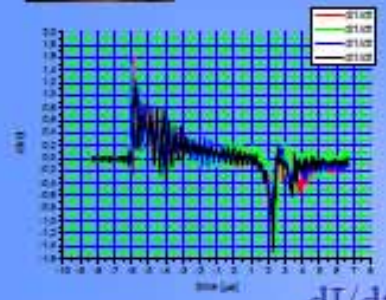

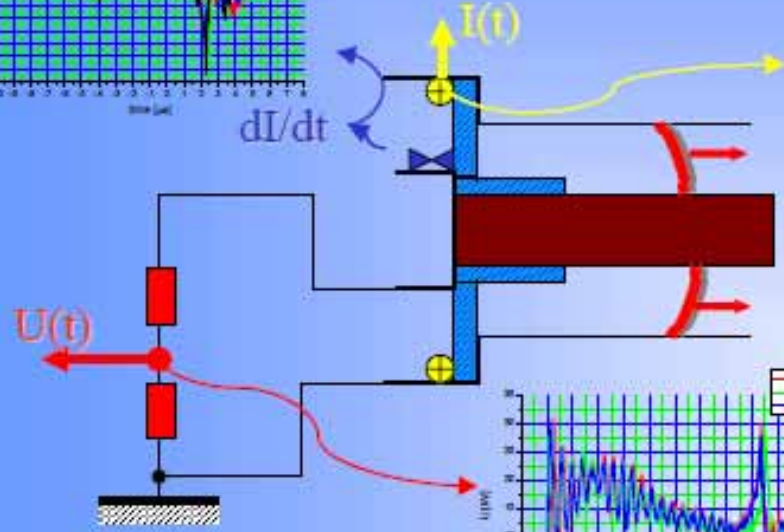

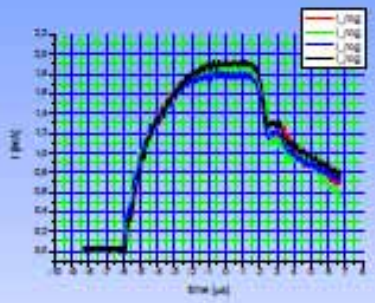

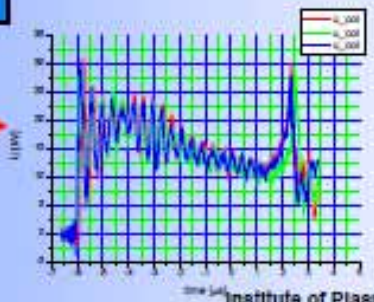

U_b= 27 kV, E_b= 480 kJ,

p = 3,5 Torr

Y = $5 \cdot 10^{10}$ - $3 \cdot 10^{11}$

Institute of Plasma Physics and Laser Microfusion
Warsaw, Poland

An interesting trend-Numerical Experiments using Lee model code to benchmark Diagnostics

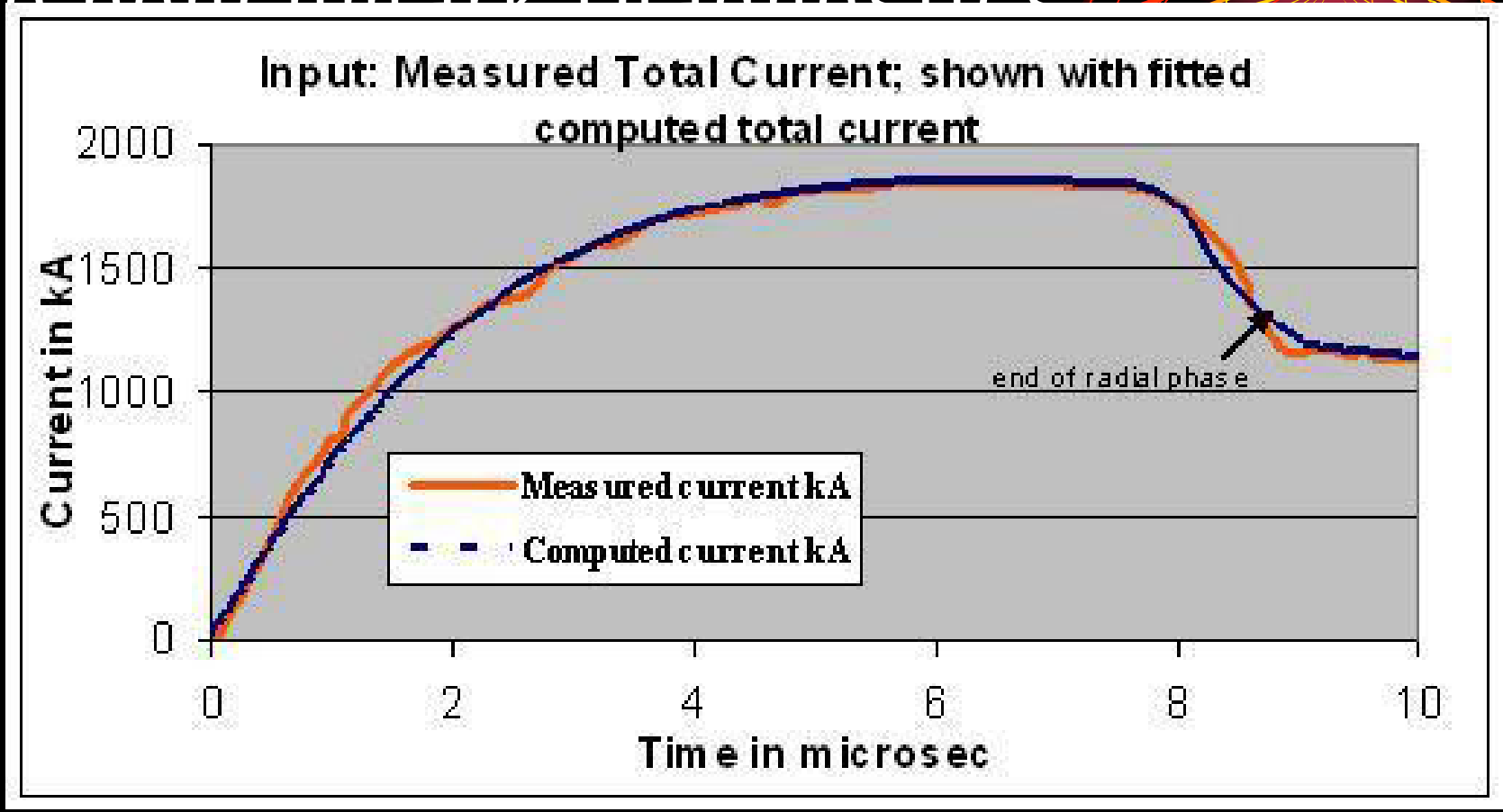

Once the computed current trace is fitted to the Measured Current, the numerical experiment and the laboratory experiment are mass and energy compatible; & computed properties are realistic. Model is an Universal Numerical Machine

Computed Properties of the PF1000: Currents, tube voltage, trajectories, speeds, energy distributions, temperatures, densities, SXR power and neutron yield

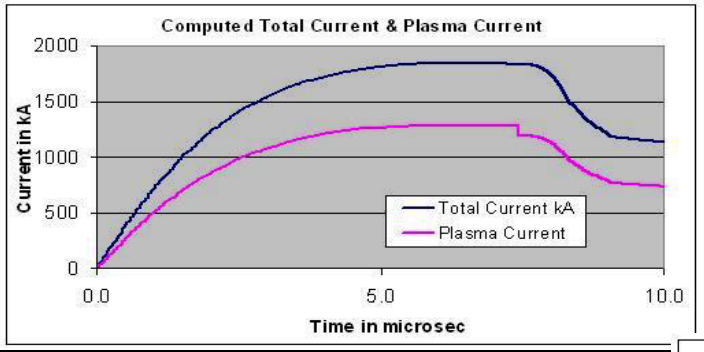

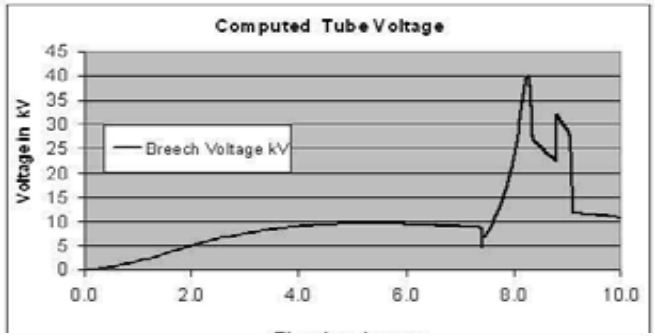

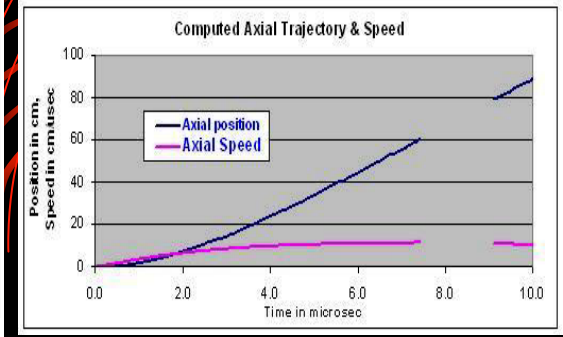

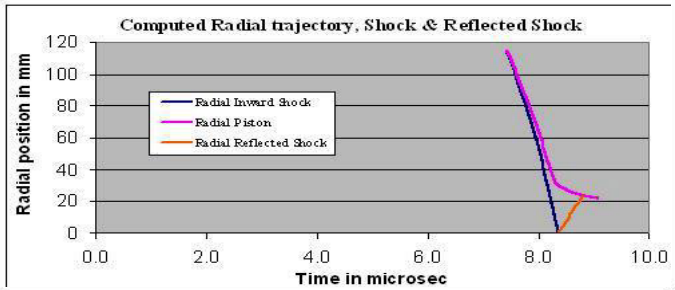

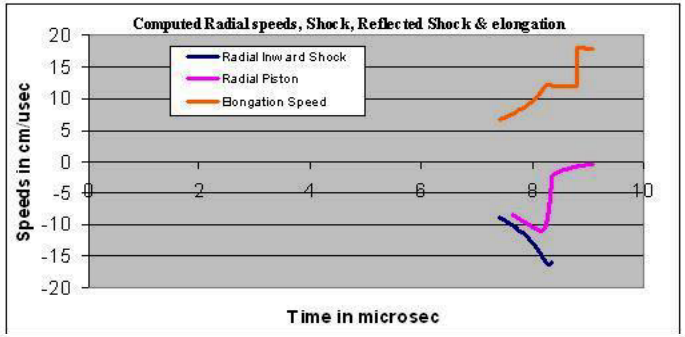

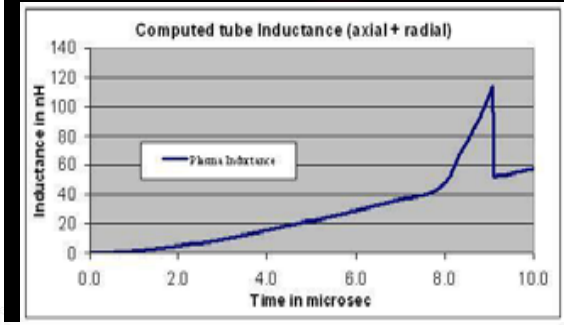

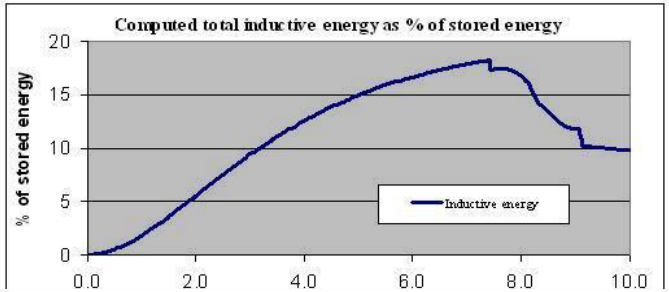

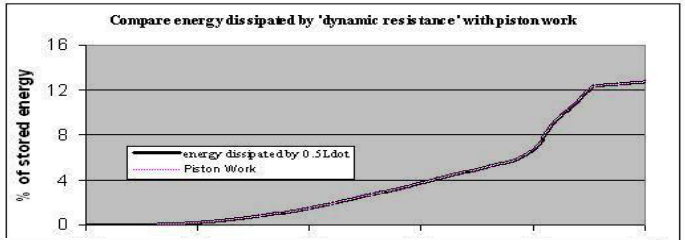

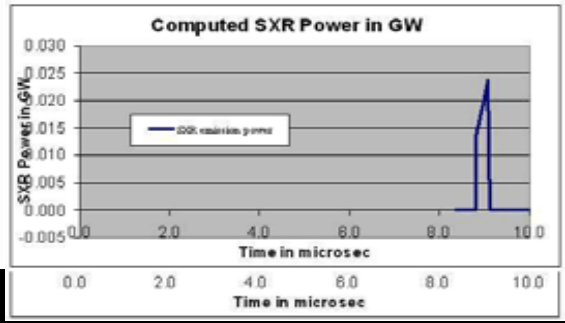

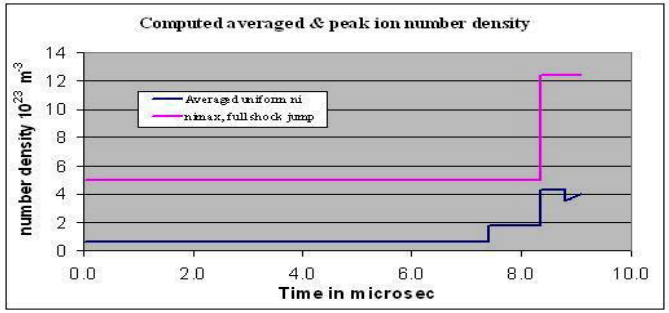

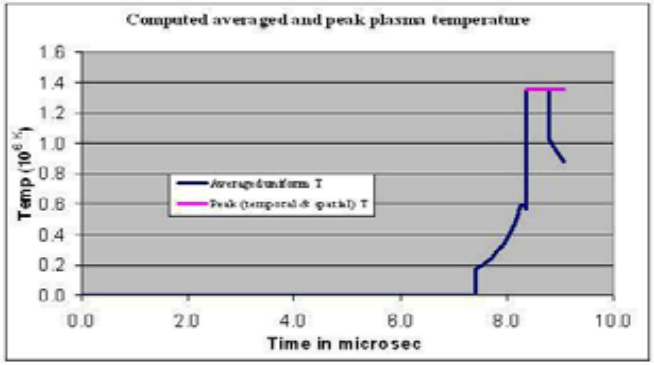

Correlation of neutron signals with frames

(first neutron pulse)

-50 ns -30 ns -10 ns 0 ns 10 ns 30 ns 50 ns

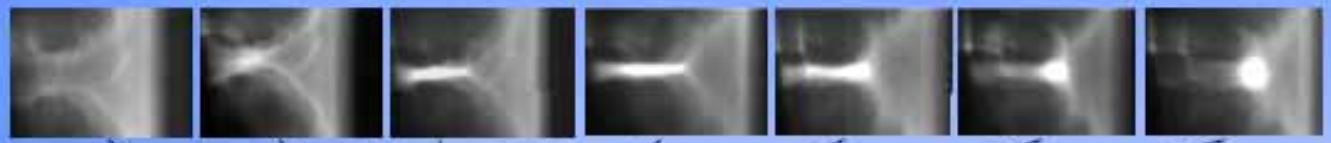

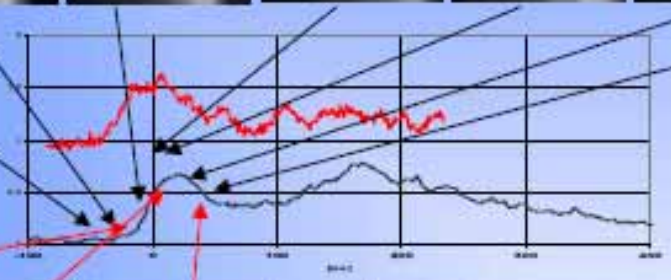

hard x-rays

neutron signal

-20 ns -10 ns 30 ns

-30 ns 0 ns

Institute of Plasma Physics and Laser Microfusion
Warsaw, Poland

RUSSIAN RESEARCH CENTRE KURCHATOV INSTITUTE

Plasma Focus PF-3

- Filippov's-type
- Anode Diameter = 1 m
- Chamber Diameter=2,5 m
- Cathode - 48 rods; diameter = 115 cm Distance between anode and upper = 10 cm
- Height of the insulator = 14 cm
- Maximal energy (C_{max}=9,2 mF, V_{max}=25 kV) is 2,8 MJ
- Short-circuit current =19 MA
- Current on the load - up to 4 MA at 1MJ

Main direction of activity - Search of new ways of PF performance and applications.

E.g. use PF as a driver for magnetic compression of liners

PF-3 Experimental Setup- with plasma producing substances

Experiments with various plasma-producing substances & various filling gases were recently the main content of activities at the PF-3 facility

Vacuum lock developed for delivery of liners to compression zone.

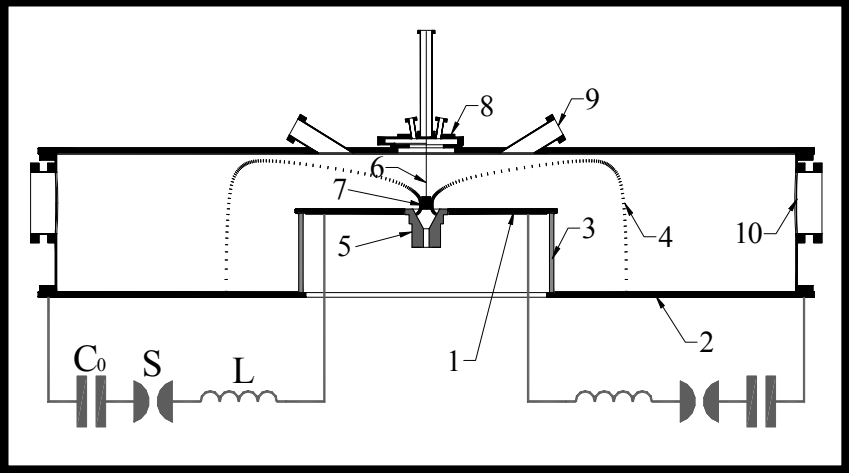

1 – anode; 2 – cathode; 3 – insulator; 4 – plasma current sheath; 5 – anode insertion; 6 – suspension ware; 7 – liner; 8 – loading unit with a vacuum lock; 9, 10 – diagnostics ports;

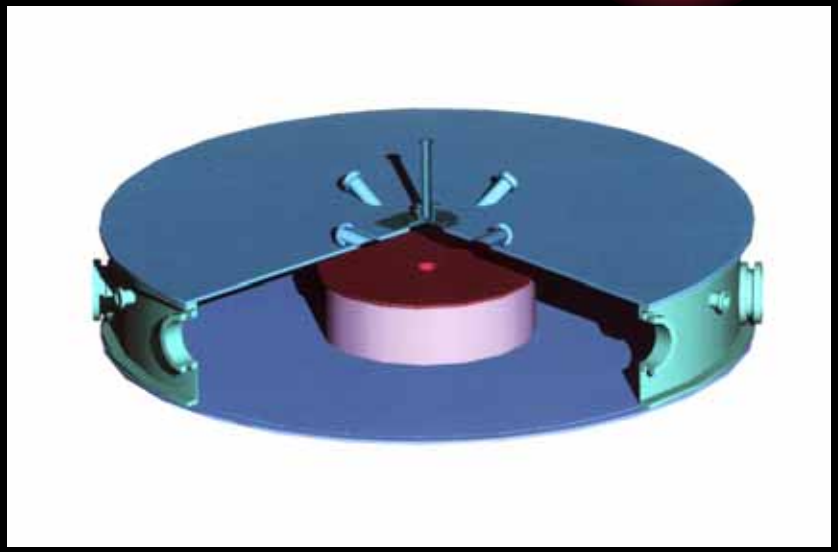

PF discharge chamber

Experimental set-up – Dust Target

Dust target produced at system axis as a freely-falling flow of fine-dispersed (2 - 50 μm) powder of Al_2O_3

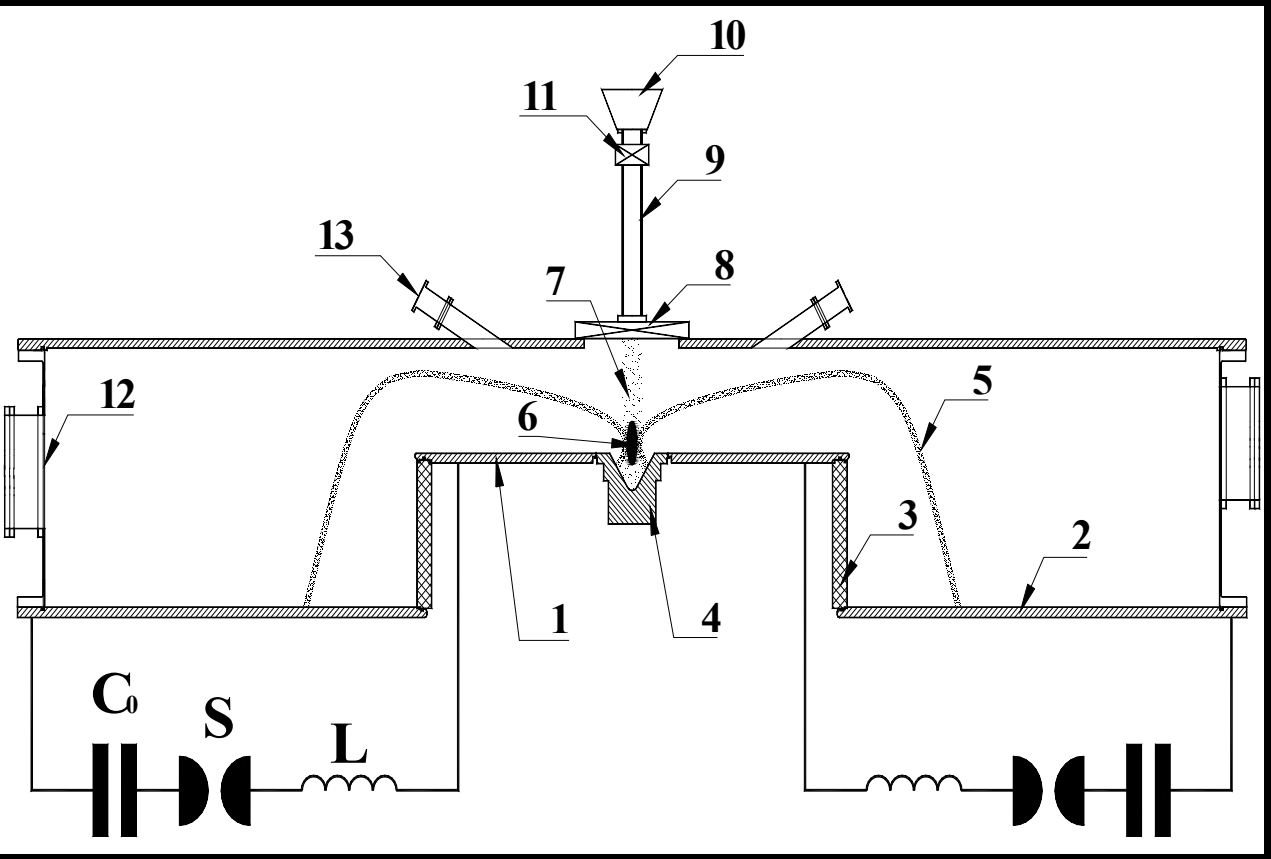

1 – anode; 2 – cathode; 3 – insulator; 4 – central anode insert; 5 – plasma-current sheath; 6 – pinch; 7 – dust column; 8 – vacuum lock; 9 – shaping drifting tube; 10 – tank with powder; 11 – electromagnet; 12, 13 – diagnostic ports

Frame Camera Pictures of Pinch Formation

Frame exposure – 12 ns, time delay between frames – 150 ns

Discharge in neon without dust

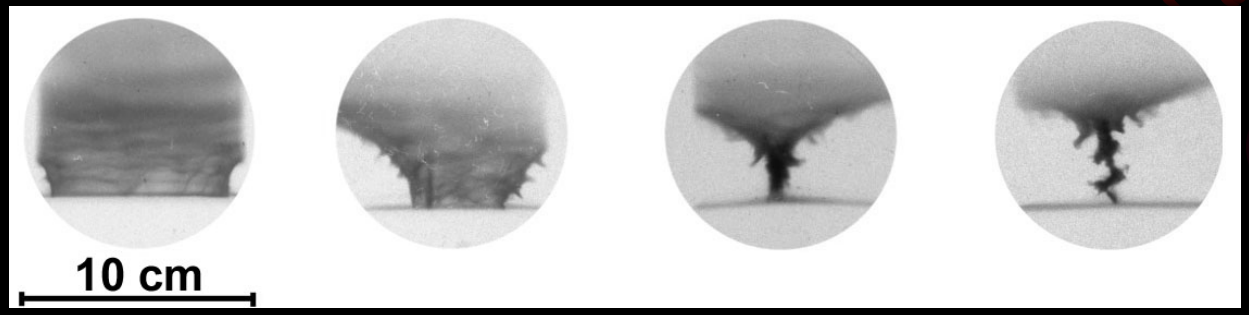

-300 ns -150ns 0 ns 150 ns

Discharge in neon with dust

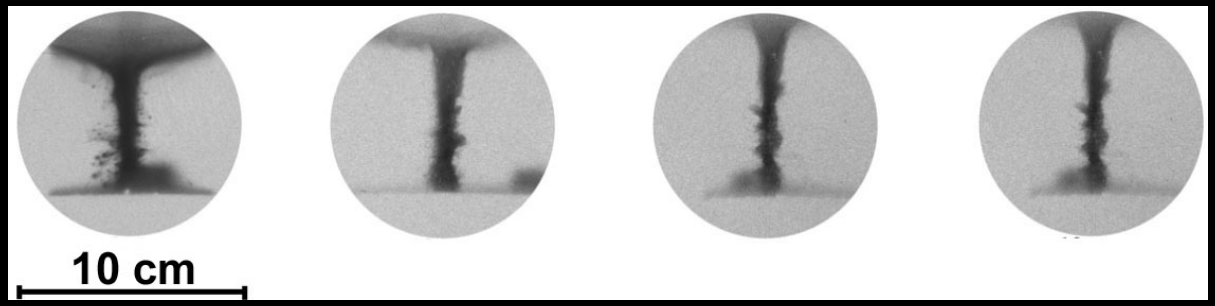

500 ns 650 ns 800 ns 950 ns

KPF-4 (“PHOENIX”), SPhTI, Sukhum

Yu .V.Matveev

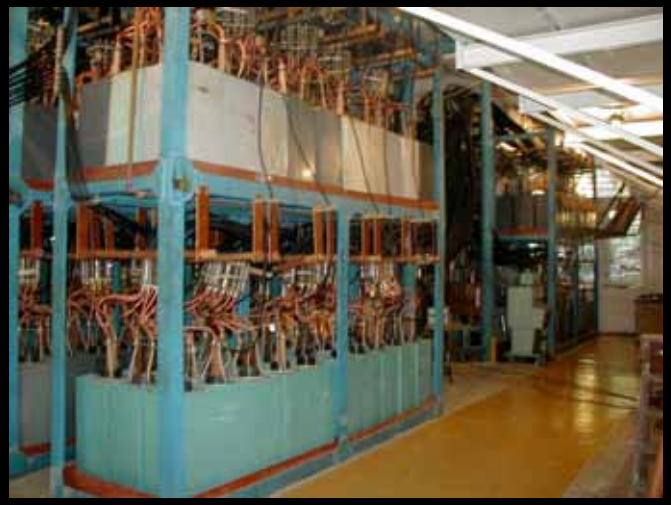

Capacitive storage (left) & chamber with current collector (right)

W_{max}= 1.8 MJ, V_{max}=50 kV, Mather-type

outer electrode – 300 mm in diameter (36 cooper rods, 10 mm in diameter)
inner electrode (anode) – 182 mm in diameter, 326 mm in length
insulator – alumina, 128 mm in diameter, 50-100 mm in length
Discharge dynamics studied up to 700 kJ and discharge currents 3-3.5 MA
Main goal – development of powerful neutron and X-ray source for applications.

(E.A.Andreeshchev, D.A.Voitenko, V.I.Krauz, A.I.Markolia, Yu.V.Matveev, N.G.Reshetnyak, E.Yu.Khautiev, 33 Zvenigorod Conf. on Plasma Phys. and Nuclear Fus., February 13-17, 2006, Zvenigorod, Russia)

Plasma Focus for medical application programme (PFMA_1)

This program is developed in Italy in cooperation of Ferrara and Bologna Universities

Today's status is:

- Preliminary campaign with a relatively small Plasma Focus device (7 kJ, 17 kV, 600 kA maximum) confirmed the feasibility of short-live radioisotopes: ~ 1 μCi/shot of ^{13}N, ^{15}O, ^{17}F is achieved.
  (E. Angeli, A. Tartari, M. Frignani, D. Mostacci, F. Rocchi, M. Sumini, Applied Radiation and Isotopes 63 (2005) 545–551)

- 150 kJ machine (350 μF, 30 kV, 3 MA) is just completely assembled and a preliminary test campaign will be starting soon

Presented by A.Tartari,
University of Ferrara

Plasma Focus Technology: PFMA-1, Plasma Focus for Medical Applications, the first prototype of a PF device for 18-F production, a 150 kJ (350 μF @ 30 kV) Mather-type Plasma Focus operated at 1 Hz repetition frequency that could breed ~ 1 Ci of F^{18} in 2 hours.

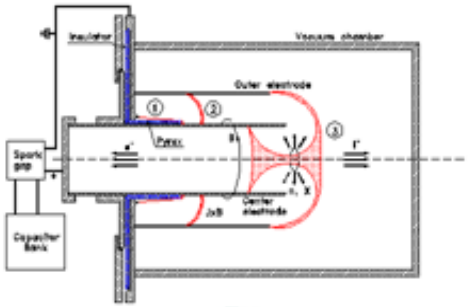

Mather type PF scheme

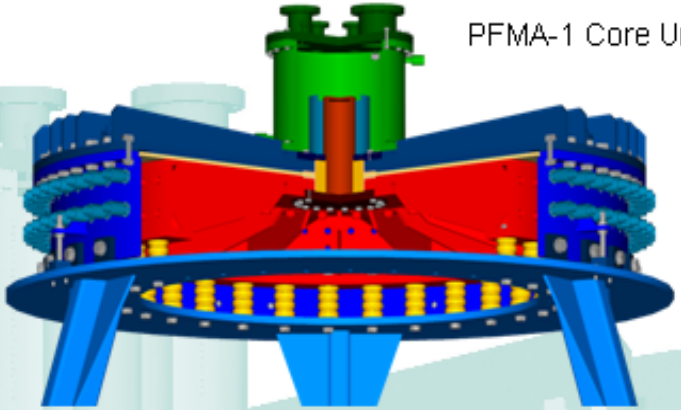

PFMA-1 Core Unit

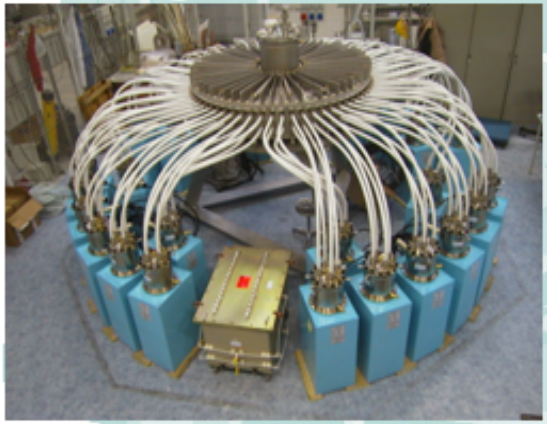

PFMA-1

UNIVERSITY OF BOLOGNA

ABO PROJECT 2010

azienda Ulss 12 veneziana

UNIVERSITY OF FERRARA

Presented by A.Tartari,
University of Ferrara

International Collaboration

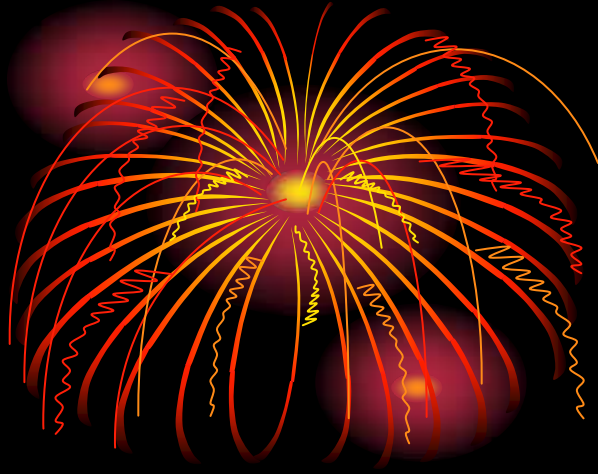

- Plasma Focus
  - is a very cost effective experimental set-up
  - Multitude of physical phenomena
  - Many applications
- PF is used successfully as facilities for scientific collaboration
  - Asian African Association for Plasma Training
  - International Centre for Dense Magnetised Plasmas

UNU/ICTP Training Programmes

Abdus Salam with UNU Plasma Focus Trainees, Kuala Lumpur, 1986

IAEA Co-ordinated Research Programme

IAEA Co-ordinated Research Project “Dense Magnetized Plasma” joints 12 institutions from 8 countries: Poland, Russia, Italy, Singapore, China, Estonia, Romania, Republic of Korea.

The main directions of applications developed are:

-radiation material science;

-proton emission tomography;

-X-ray lithography;

-radiation enzymology;

-radiation medicine, etc;

(*Proceedings of the 2nd IAEA Co-ordination Meeting of the Co-ordinated Research Project on Dense Magnetized Plasma, 1-3 June 2005, Kudowa Zdroj, Poland, Nukleonika 2006; 51(1))*

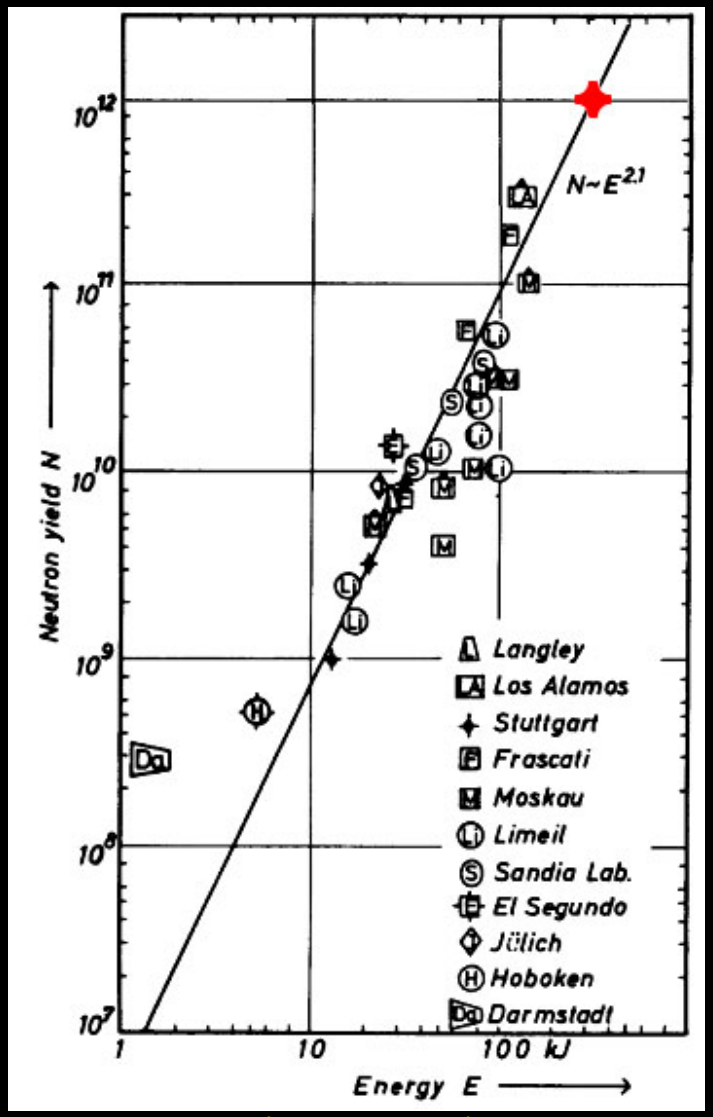

Neutron yields N against energy E, assembled by H.Rapp

(Michel L., Schonbach K.H., Fisher H. Appl. Phys. Lett.- 1974.-V.24, N2.-P.57-59)

Neutron Scaling:

from optimism to disappointment-V. I. Krauz

- empirical scaling for neutron output: $N \sim E^2$ or $N \sim I^4$
- However All attempts to reach 10^{13} D-D neutrons expected for 1 MJ failed
- The best result achieved till now is ~ 10^{12} at W~500 kJ (Los-Alamos, Limeil, Frascati)
- As a result PF activities were shut down in many countries – leaders in fusion researches

Insight from modelling-Scaling Laws

Numerical experiments using the Lee model code have been carried out systematically over wide ranges of energy; optimizing pressure, anode length and radius, to obtain scaling laws:

Neutron yield, Y_n:

- $Y_n = 3.2 \times 10^{11} I_{pinch}^{4.5}$ I_{pinch} in MA (0.2 to 2.4 MA)
- $Y_n = 1.8 \times 10^{10} I_{peak}^{3.8}$ I_{peak} in MA (0.3 to 5.7 MA))
- $Y_n \sim E_0^{2.0}$ at tens of kJ to $Y_n \sim E_0^{0.84}$ at MJ level (up to 25MJ).

For neon soft x-rays:

- $Y_{sxr} = 8.3 \times 10^3 \times I_{pinch}^{3.6}$; I_{pinch} in MA (0.07 to1.3 MA)
- $Y_{sxr} = 600 \times I_{peak}^{3.2}$; I_{peak} in MA (0.1 to 2.4 MA),.
- $Y_{sxr} \sim E_0^{1.6}$ (kJ range) to $Y_{sxr} \sim E_0^{0.8}$ (towards MJ).

Our experience: the laws scaling yield with I_{pinch} are robust and more reliable than the others.

Insight into Neutron saturation

- Recently discussed by M. Scholz among others. Following Scholz we show a chart depicting the deterioration of the neutron scaling as E_0 increases; compared with the expected $Y_n \sim E_0^2$ scaling shown by lower energy experiments. This chart depicts the idea of Y_n saturation. Note that the capacitor banks all operate at several tens of kV and the increase of E_0 is essentially through increase of C_0.

Chart from M Scholz (November 2007 ICDMP)

Scaling

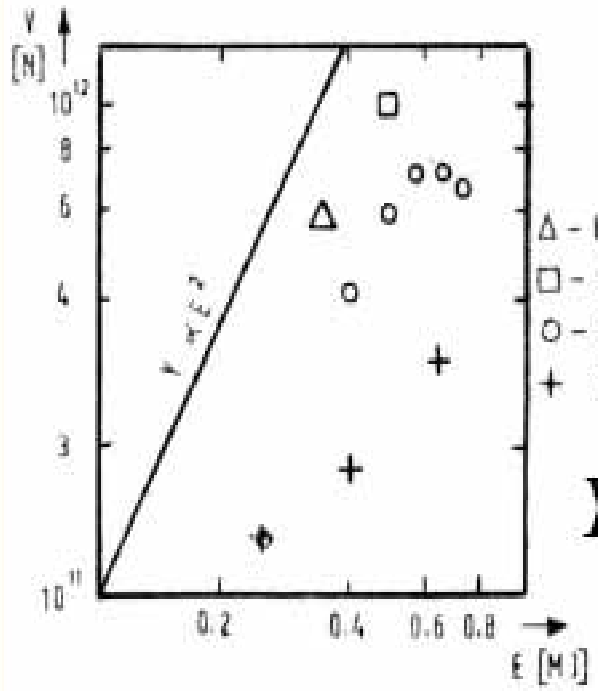

$$\frac{1}{2}(L+L_0)I^2 \cong \gamma E$$

$$L \cong L_0$$

$$Y_n \propto E^2$$

$$I^2 \propto E$$

Frascati (Program Euroatom), $E_b = 1MJ$; $U_b = 50$ kV;

Institute of Plasma Physics and Laser Microfusion
Warsaw, Poland

Illustrating Y_n 'saturation' observed in numerical experiments (line) compared to measurements on various machines (small squares)

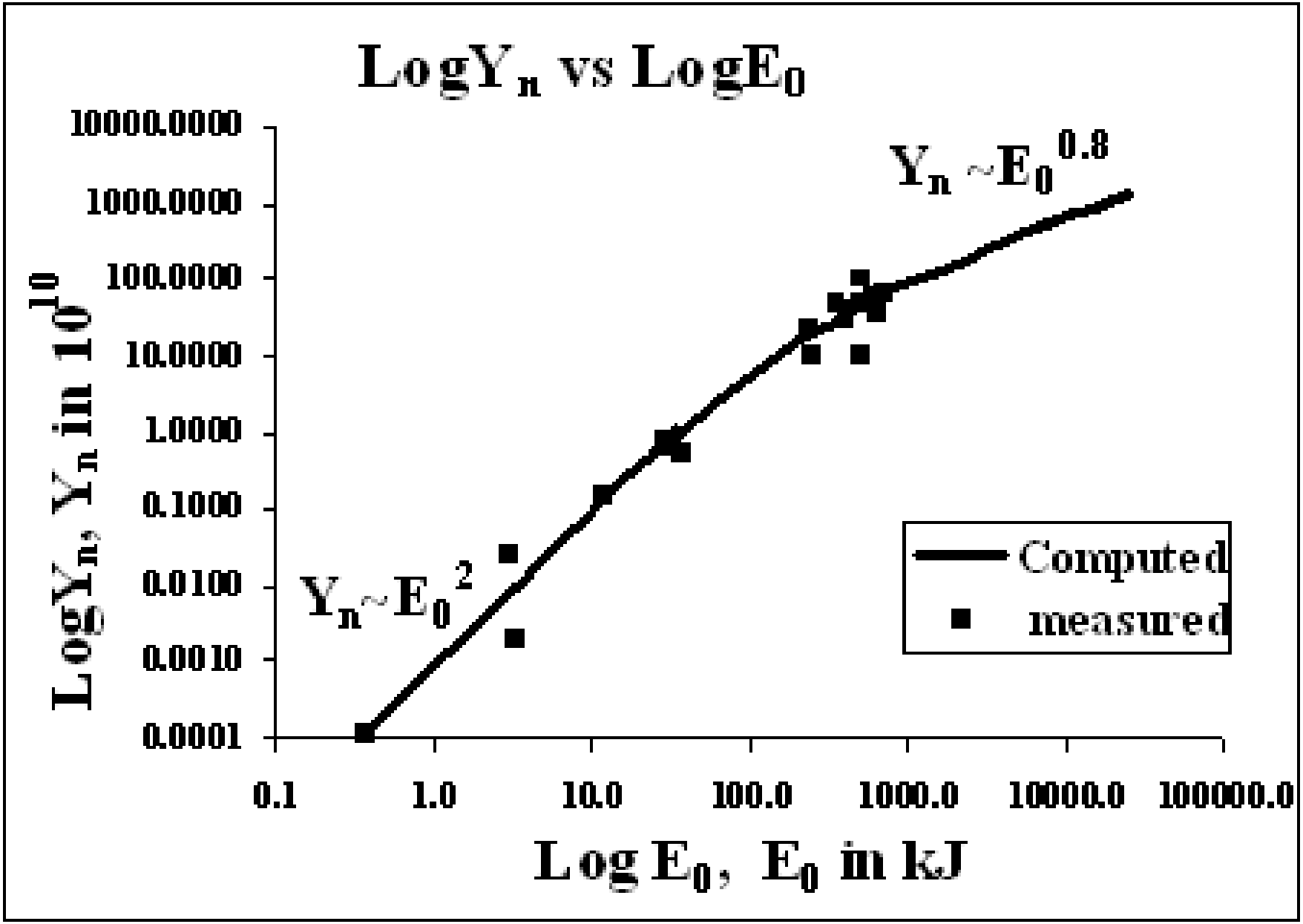

Y_n saturation trend already observed in numerical experiments

- The deterioration of the Y_n scaling observed in numerical experiments agree generally with the measured data on Y_n yield of large experiments
- What is the physical basis of this scaling deterioration?

Comparing I_{total} for small & large plasma focus

- **Small PF-400J; 0.4kJ 28 kV 6.6 Torr D2**
- **Large PF1000 (0.5 MJ) 27 kV 3.5 Torr D2**

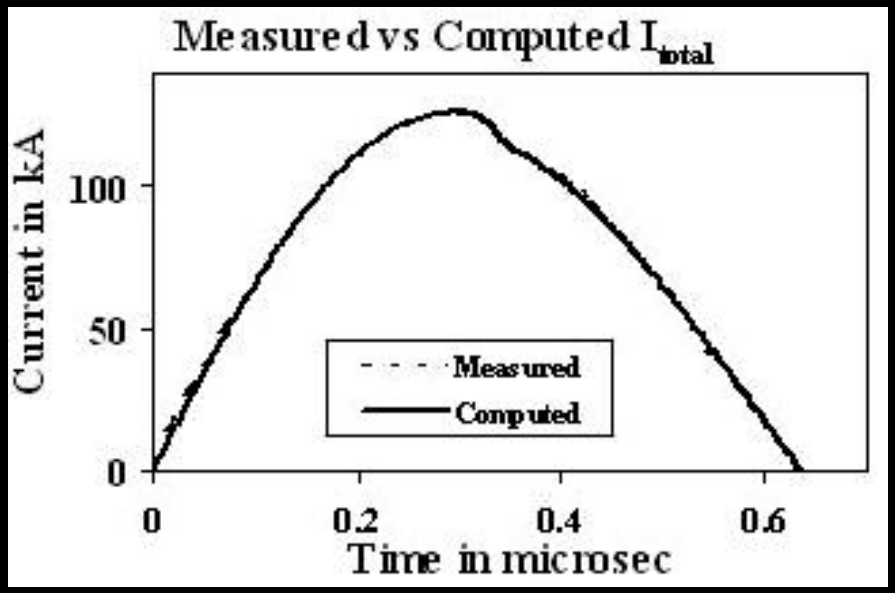

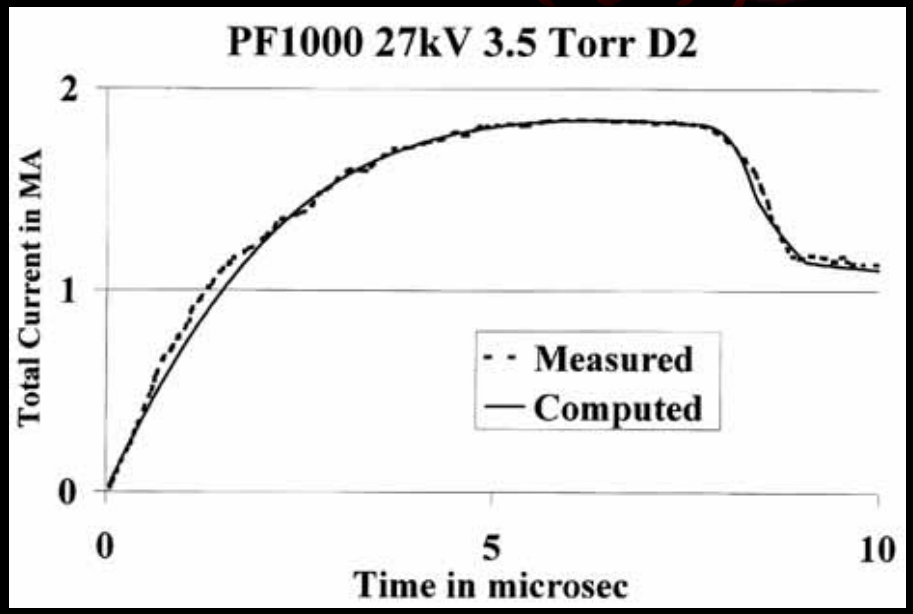

~300ns risetime; ~ 20ns current dip of <5%

End axial speed: 10cm/us

~8 us risetime; ~2 us current dip of 35%

End axial speed: 10cm/us

Comparing generator impedance & Dynamic Resistance of small & large plasma focus- before I_{peak}

PF	$Z_0 = (L_0/C_0)^{1/2}$	Axial DR_0	Axial dominance	
Small	100 mΩ	7 mΩ	Z_0	~ V_0/Z_0
Large	1 mΩ	7 mΩ	DR_0	~V_0/DR_0

As E_0 is increased by increasing C_0, with voltage kept around tens of kV, Z_0 continues to decrease and I_{peak} tends towards asymptotic value of V_0/DR_0

Illustrating the dominance of DR_0 as E_0 increases,

V_0=30kV, L_0=30nH; $Z_{total}=1.1Z_0+DR_0$

	C_0	Z_0	DR_0	Z_{total}	$I_{peak} = V_0/Z_{total}$	I_{peak} from L-C-R	
	uF				kA	kA	
	1	173	7	197	152	156	
4.5	10	55	7	67	447	464	
45	100	17	7	26	1156	1234	
135	300	10	7	18	1676	1819	
450	1000	5.5	7	12.9	2321	2554	
1080	2400	3.5	7	10.8	2781	3070	
4500	10000	1.7	7	8.8	3407	3722	
45000	100000	0.55	7	7.6	4209	4250	

Confirming I_{peak} saturation is due to constancy of DR_0

I_{peak} vs E_0 from DR_0 analysis compared to model simulation

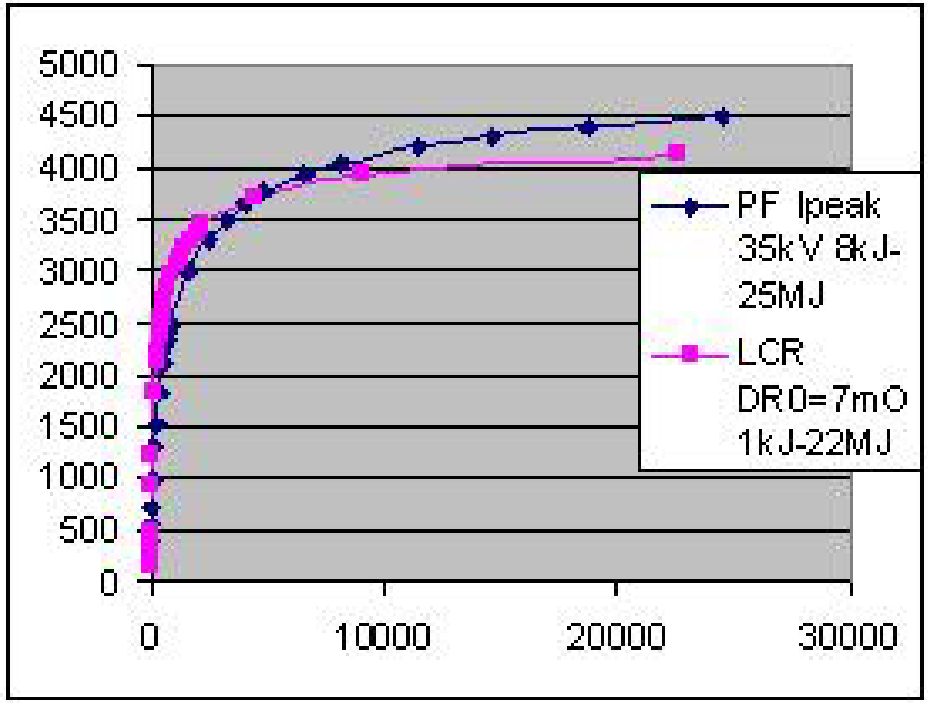

I_{peak} vs E_0 on log-log scale DR_0 analysis

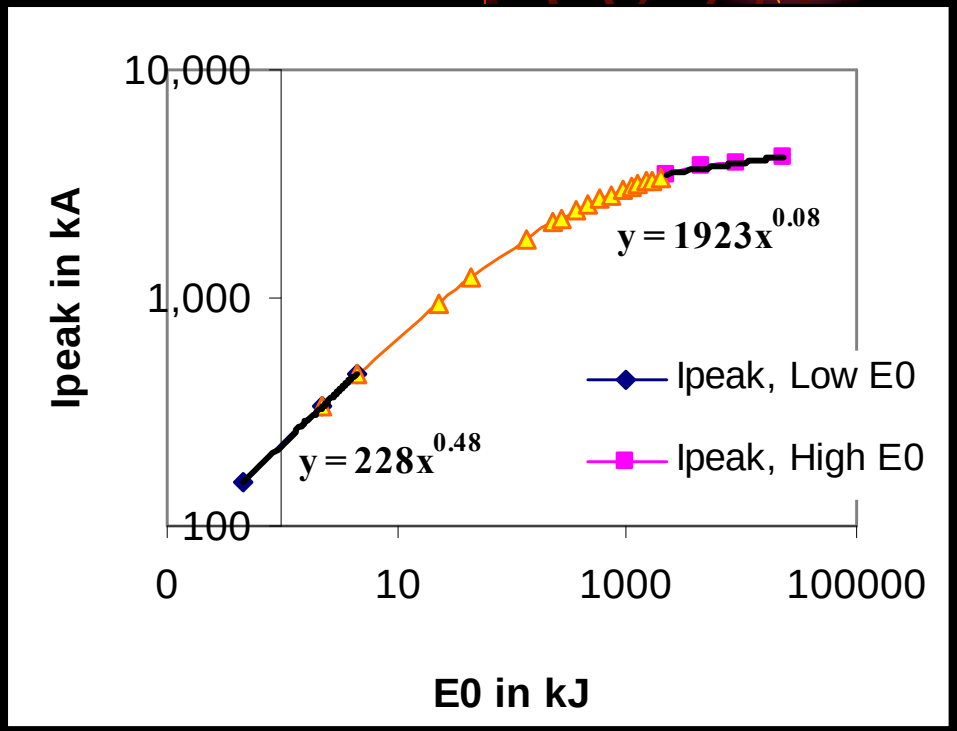

Model simulation gives higher I_{peak} due to a 'current overshoot effect' which lifts the value of I_{peak} before the axial DR_0 fully sets in

Confirming that I_{peak} scaling tends to saturate before 1 MJ

We have shown that: constancy of DR_0 leads to current 'saturation' as E_0 is increased by increasing C_0. Tendency to saturate occurs before 1 MJ

From both numerical experiments as well as from accumulated laboratory data

- $Y_n \sim I_{pinch}^{4.5}$
- $Y_n \sim I_{peak}^{3.8}$

Hence the 'saturation' of I_{peak} leads to saturation of neutron yield Y_n

Illustrating Y_n 'saturation' observed in numerical experiments (small black crosses) compared to measurements on various machines (larger coloured crosses)

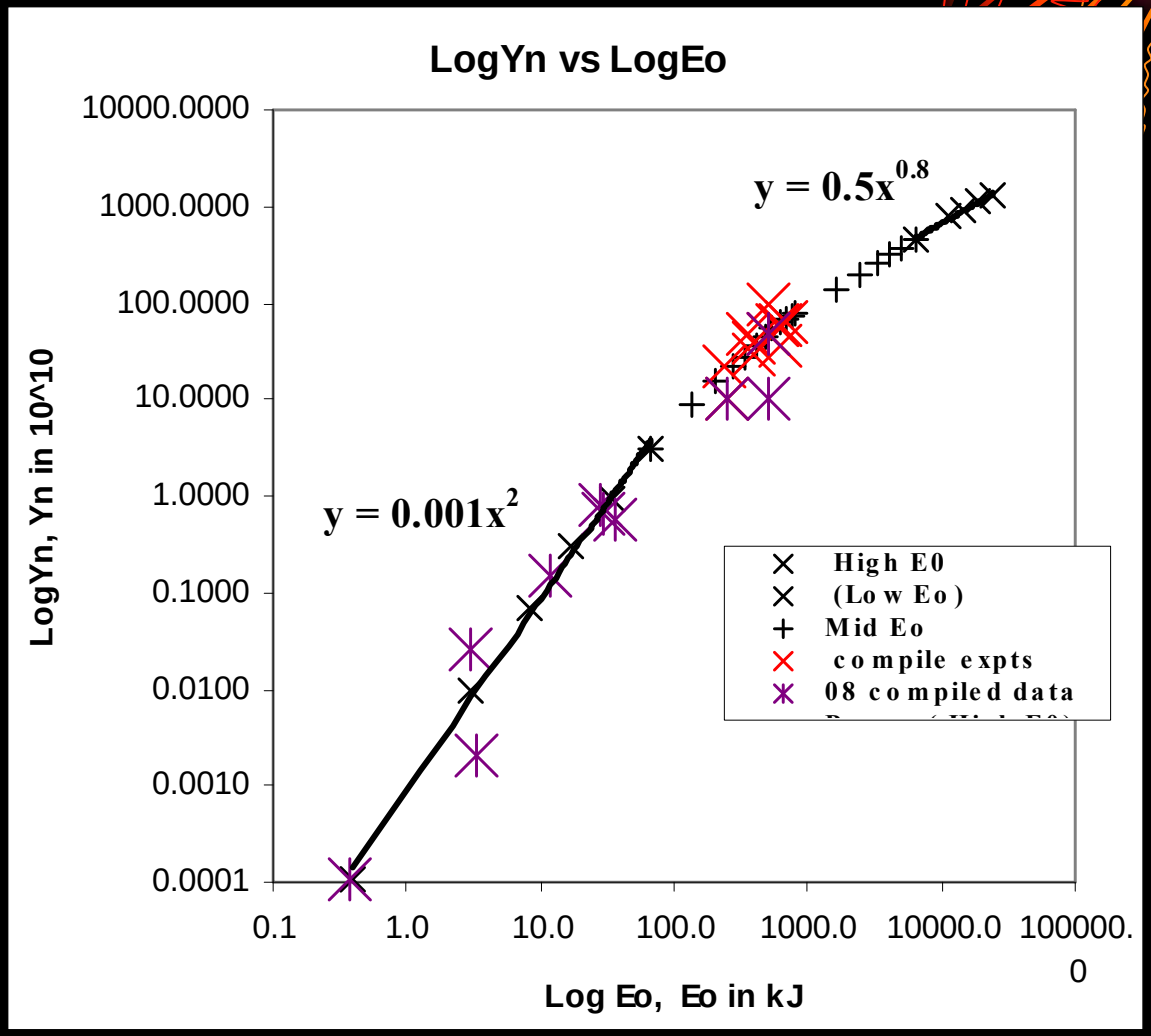

Insight- neutron saturation

- **A major factor for ‘neutron saturation’ is simply: Axial Phase Dynamic Resistance**

Conclusions and Discussion

Diagnostics and scaling laws

- Reference points for plasma focus diagnostics are provided by the model, giving realistic time histories of dynamics, energies, plasma properties and Y_{sxr}; also Y_n.
- Systematic numerical experiments then provide insight into Y_n and Y_{sxr} scaling laws, as functions of I_{pinch}, I_{peak} and E_0.
- These numerical experiments show tendency towards Y_n saturation, in agreement with laboratory experiments

Conclusions and Discussion

Y_n saturation due to DR_0

- **Insight: Identification of a major factor contributing to Y_n saturation. It is current saturation due to DR_0. Nukulin & Polukhin [2007 paper] had discussed current saturation based on a wrong assumption of z_0 proportional to C_0. If their assumption were correct, reducing z_0 would overcome the current saturation. Unfortunately the causal mechanism is not length z_0, but speed dz/dt, more specifically DR_0.**

- **The same effect is expected to cause the saturation of other current –dependent radiation yields such as Y_{sxr}.**

Conclusions and Discussion

Beyond saturation?

Possible ways to improve Y_n:

- **Increase operating voltage. Eg SPEED II uses Marx technology: 300kV, driver impedance 60 mΩ. With E_0 of under 200 kJ, the system was designed to give I_{peak} of 5 MA and I_{pinch} just over 2 MA.**
- **Extend to 1MV?- would increase I_{peak} to 15 MA and I_{pinch} to 6 MA. Or multiple Blumleins at 1 MV, in parallel, could provide driver impedance matching radial phase DR, resulting in fast rise I_{peak} of 10 MA with 5 MA I_{pinch}. [at several MJ]**
- **Y_n enhancing methods such as doping deuterium with low % of krypton.**
- **Further increase in I_{pinch} by fast current-injection near the start of radial phase. This could be achieved with charged particle beams or by circuit manipulation such as current-stepping. This model is ideally suited for testing circuit manipulation schemes.**

Ongoing IPFS numerical experiments of Multi-MJ, High voltage MJ and Current-step Plasma Focus
IPFS & INTI UC September 2009

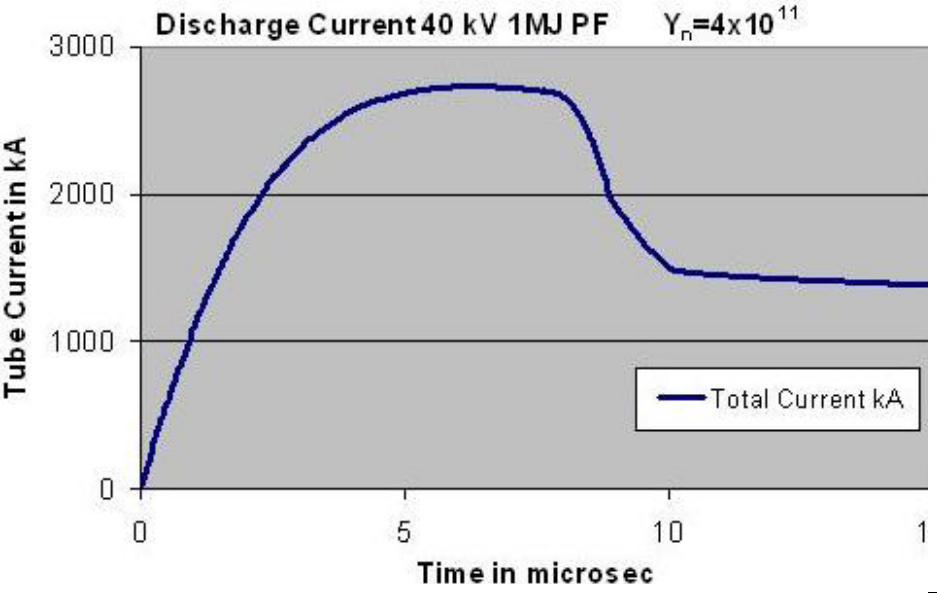

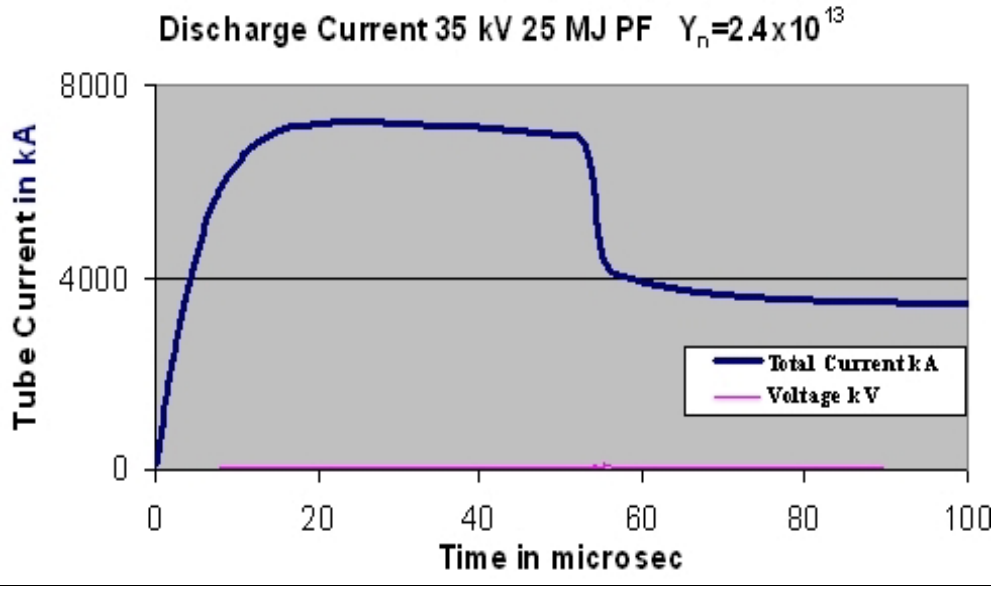

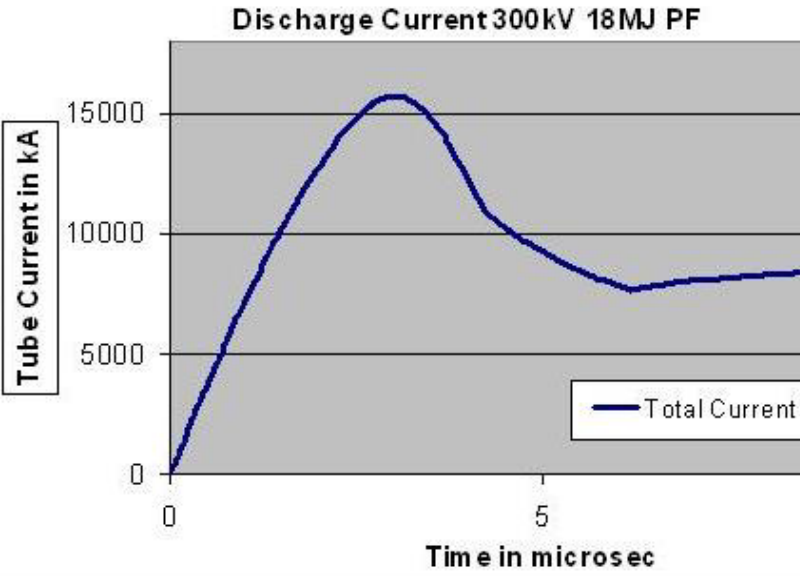

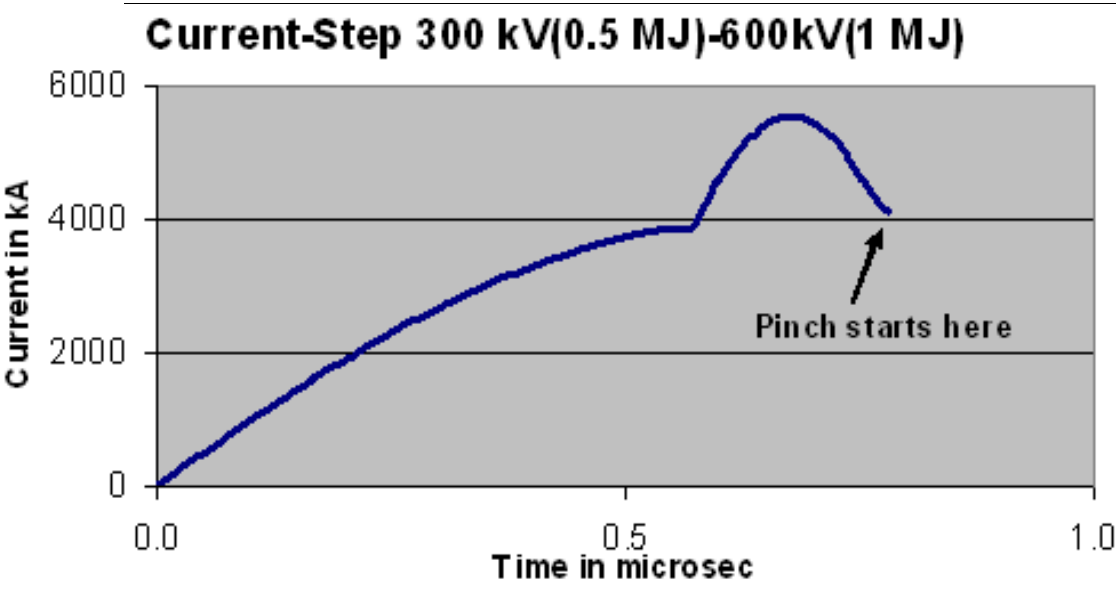

Appreciation to the following :

- **V. I Krauz**
- **Marek Scholz**
- **Yu .V.Matveev**

Plasma Fusion Energy Technology

S Lee[1,2,3] & S H Saw[2,1]

[1]Institute for Plasma Focus Studies

[2]INTI University College, Malaysia

[3]Nanyang Technological University/NIE Singapore

International Conference on Recent and Emerging Advanced Technologies in Engineering

iCREATE 2009, 23 & 24 November 2009, Kuala Lumpur Malaysia

Outline of Talk

- **Introduction: The energy crisis**
- **Nuclear Fusion Technology & energy**
- **Tokamaks-early days to ITER & beyond**
- **Alternative fusion programs**
- **Plasma Focus technology into the future**
- **Conclusion**

STARS:-

Nature's Plasma Fusion Reactors

Tokamak-planned nuclear fusion reactor

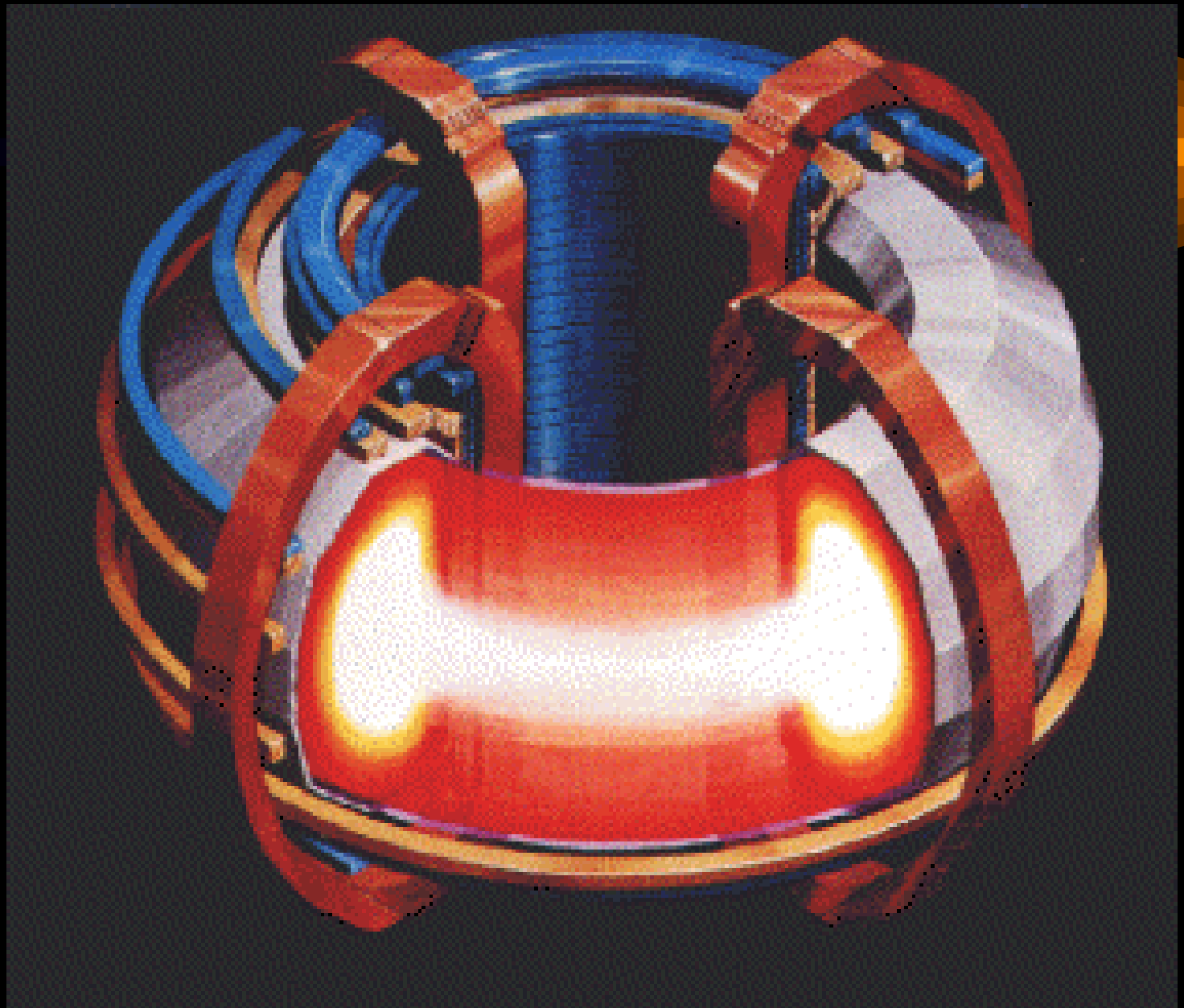

Natural Fusion Reactors vs Fusion Experiments on Earth

Plasma Physics:

- **Introductory: What is a Plasma?**
- **Characteristics & high energy density**

Introductory: What is a ***Plasma?***

Matter heated to high temperatures becomes a Plasma

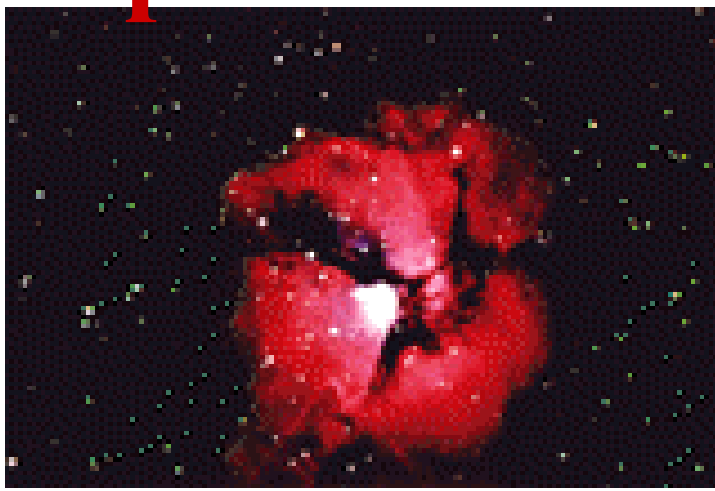

Four States of Matter

SOLID **LIQUID** **GAS** **PLASMA**

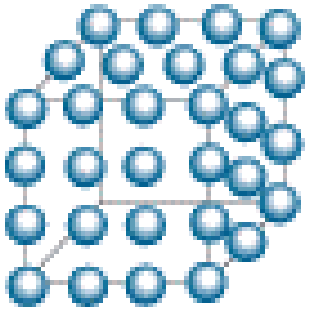

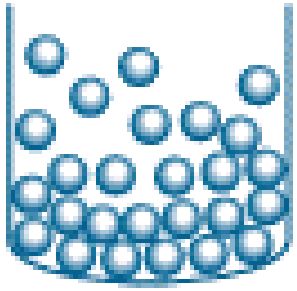

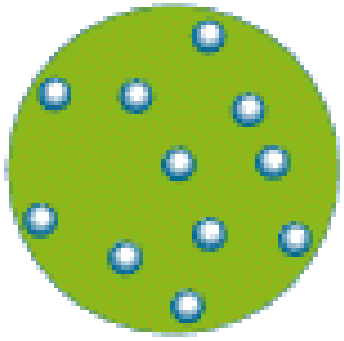

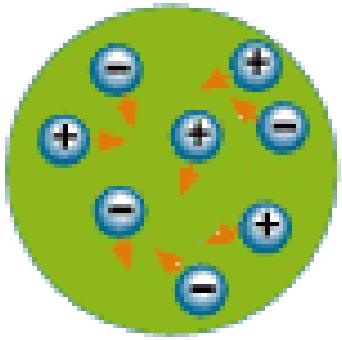

Characteristics of Plasma State

- **Presence of electrons and ions**
- **Electrically conducting**
- **Interaction with electric & magnetic fields**
- **Control of ions & electrons: applications**
- **High energy densities/selective particle energies**

-Cold plasmas: several eV's; (1eV~10^4K)

-Hot plasmas: keV's ; (1keV~10^7K)

- **Most of matter in Universe is in the Plasma State (e.g. the STARS)**

Major technological applications

- **Surface processing, cleaning, etching, deposition**
- **Advanced materials, diamond/CN films**
- **Environmental e.g.waste/water treatment**
- **High temperature chemistry**
- **MHD-converters, thrusters, high power switches**
- **Radiation sources: Microelectronics lithography**
- **Medical: diagnostics, cleaning, instrumentation**
- **Light sources, spectroscopic analysis, FP displays**
- **Fusion Energy**

The Singular, arguably Most Important Future Technological Contribution, essential to Continuing Progress of Human Civilization:-

A NEW LIMITLESS SOURCE OF ENERGY

Scenario: World Population stabilizes at 10 billion; consuming energy at 2/3 US 1985 per capita rate

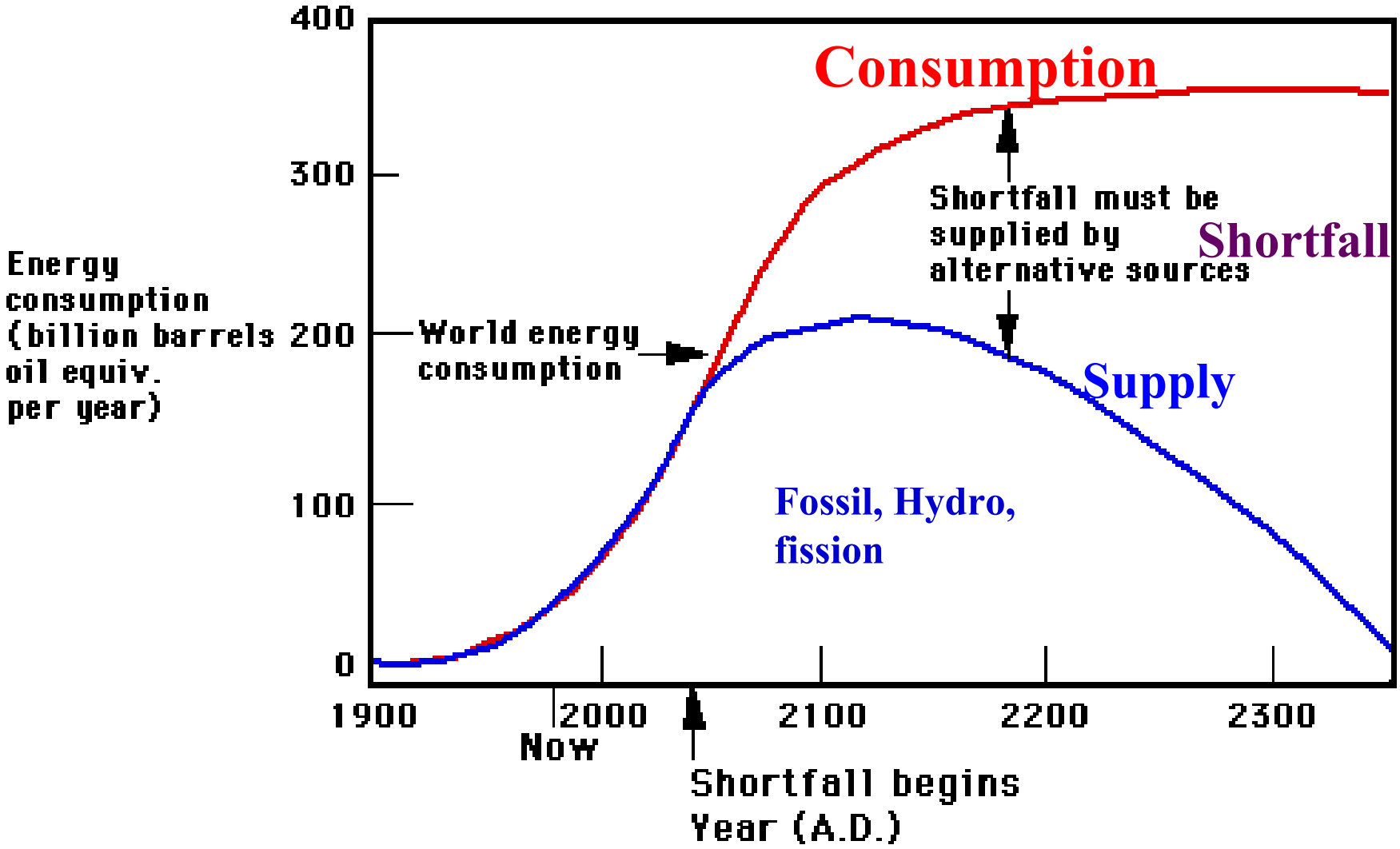

Plasma Fusion & the Future of Human Civilization

A new source of abundant (limitless) energy is needed for the continued progress of human civilization.

Mankind now stands at a dividing point in human history:

- **200 years ago, the Earth was under-populated with abundant energy resources**
- **100 years from now, the Earth will be over-crowded, with no energy resources left**

Without a new abundant source of energy

Human civilization cannot continue to flourish.

Only 1 good possibility:

Fusion Energy from Plasma Reactors

The Fusion Process

Collisions in a Plasma

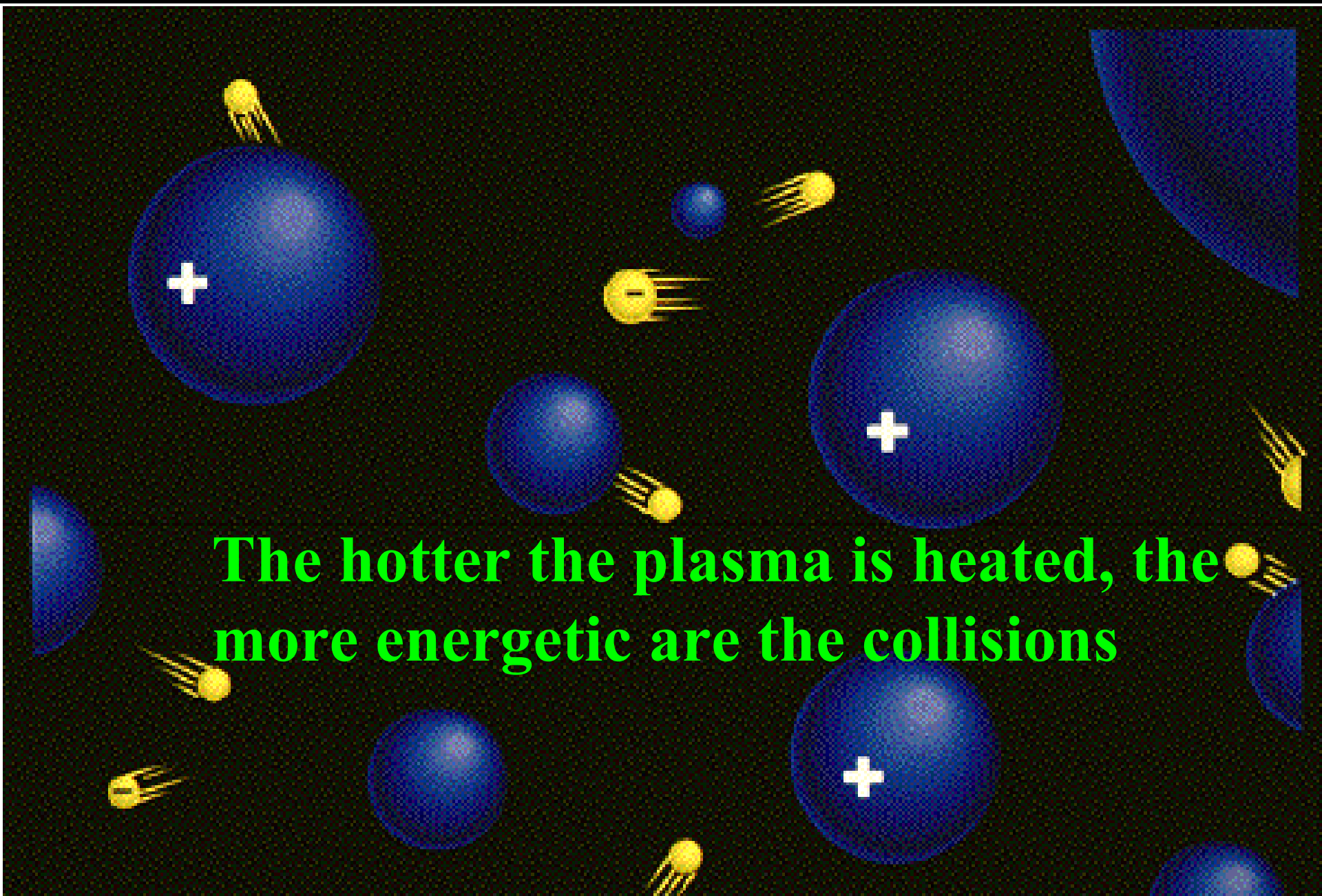

Nuclear Fusion

If a Collision is sufficiently energetic, nuclear fusion will occur

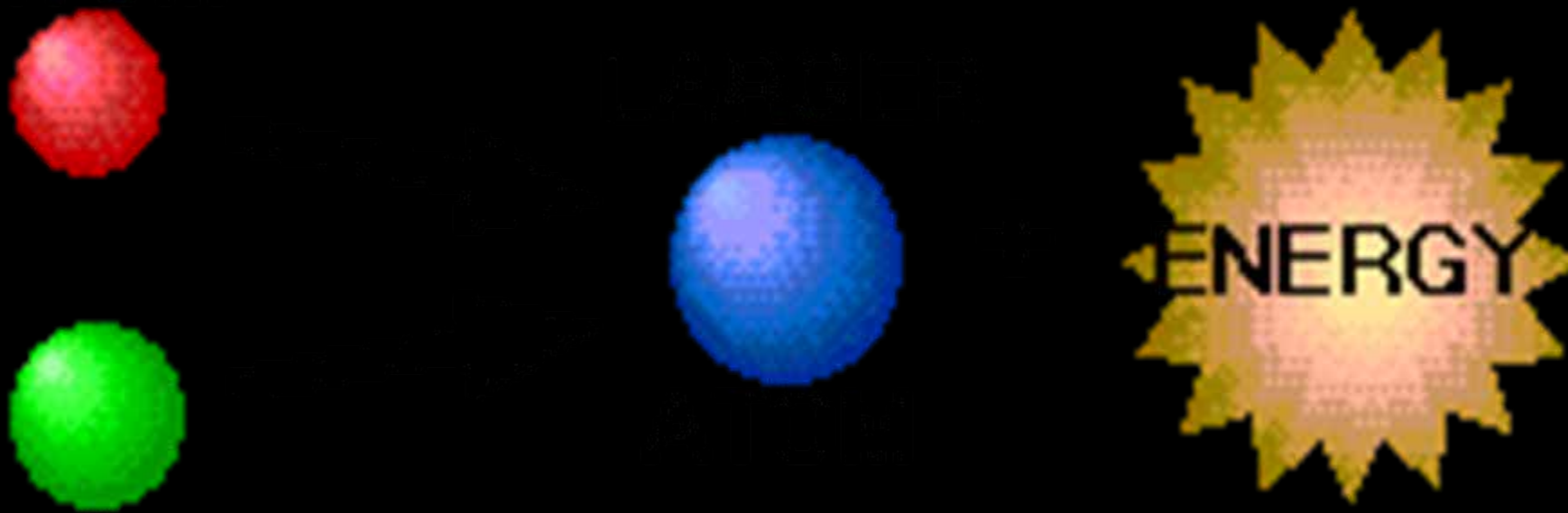

Isotopes of hydrogen- Fuel of Fusion

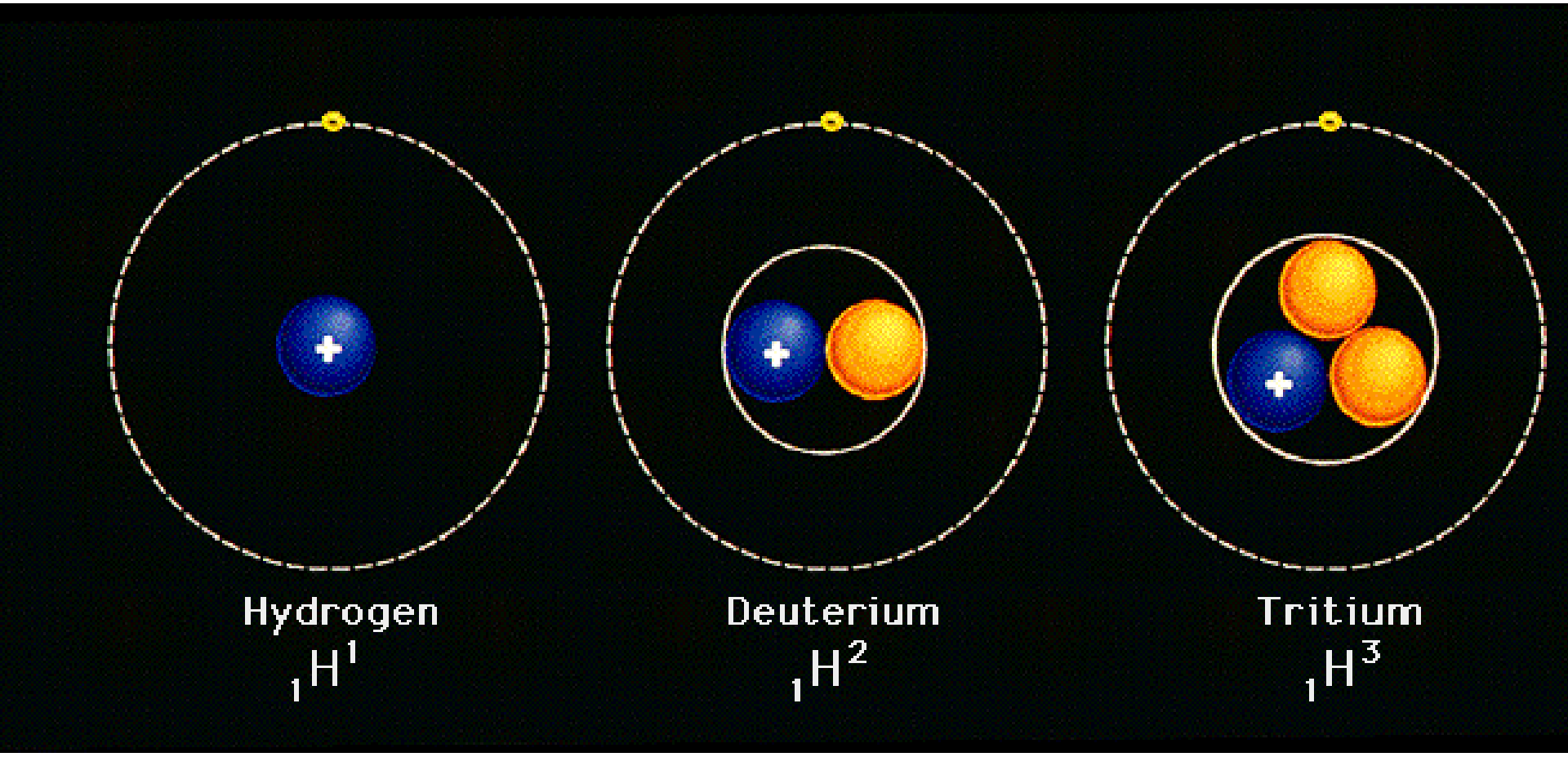

Release of energy in Fusion

$$_1H^2 + {}_1H^3 \longrightarrow {}_2He^4 + {}_0n^1 + 17.6\ MeV$$

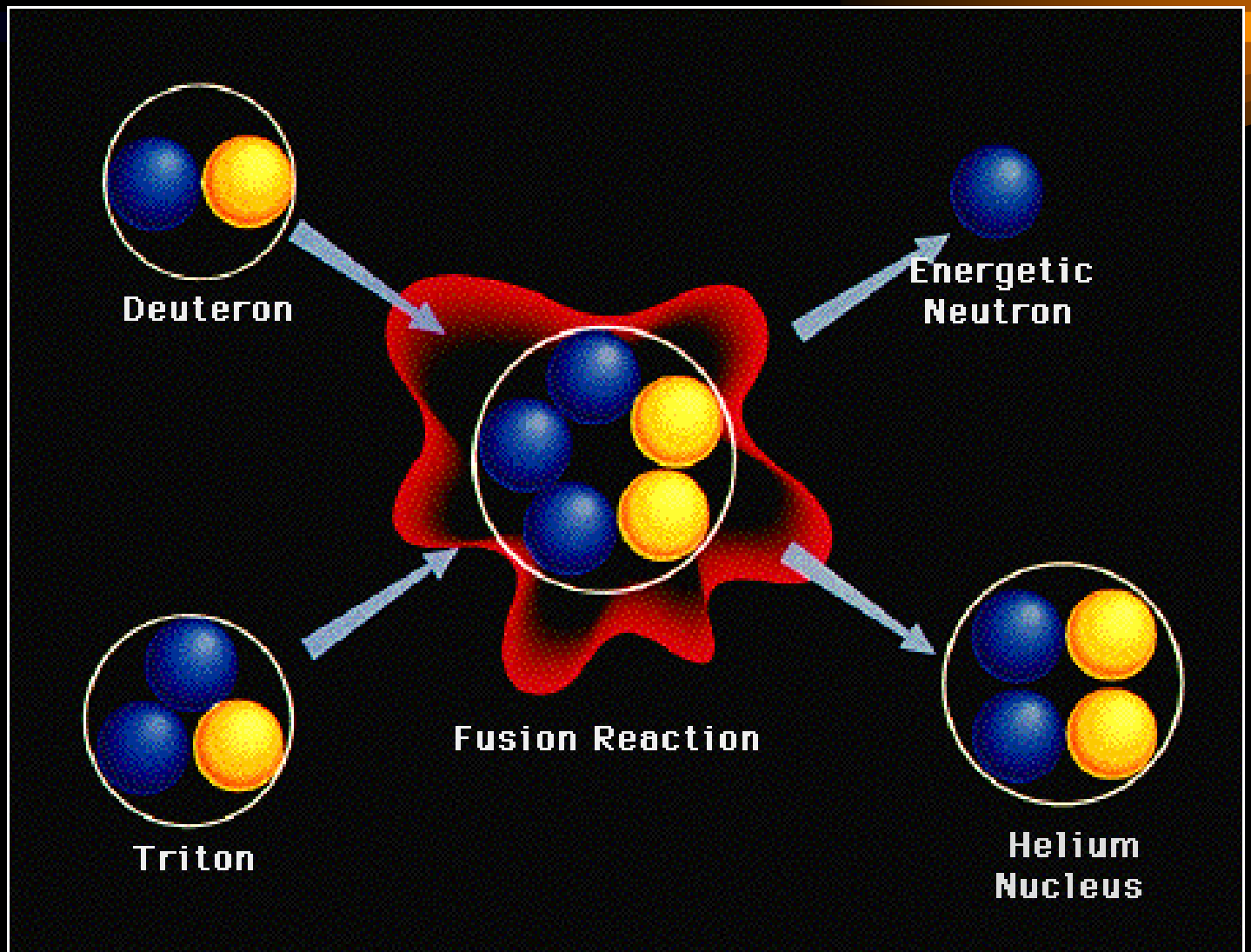

Conversion of mass into Energy

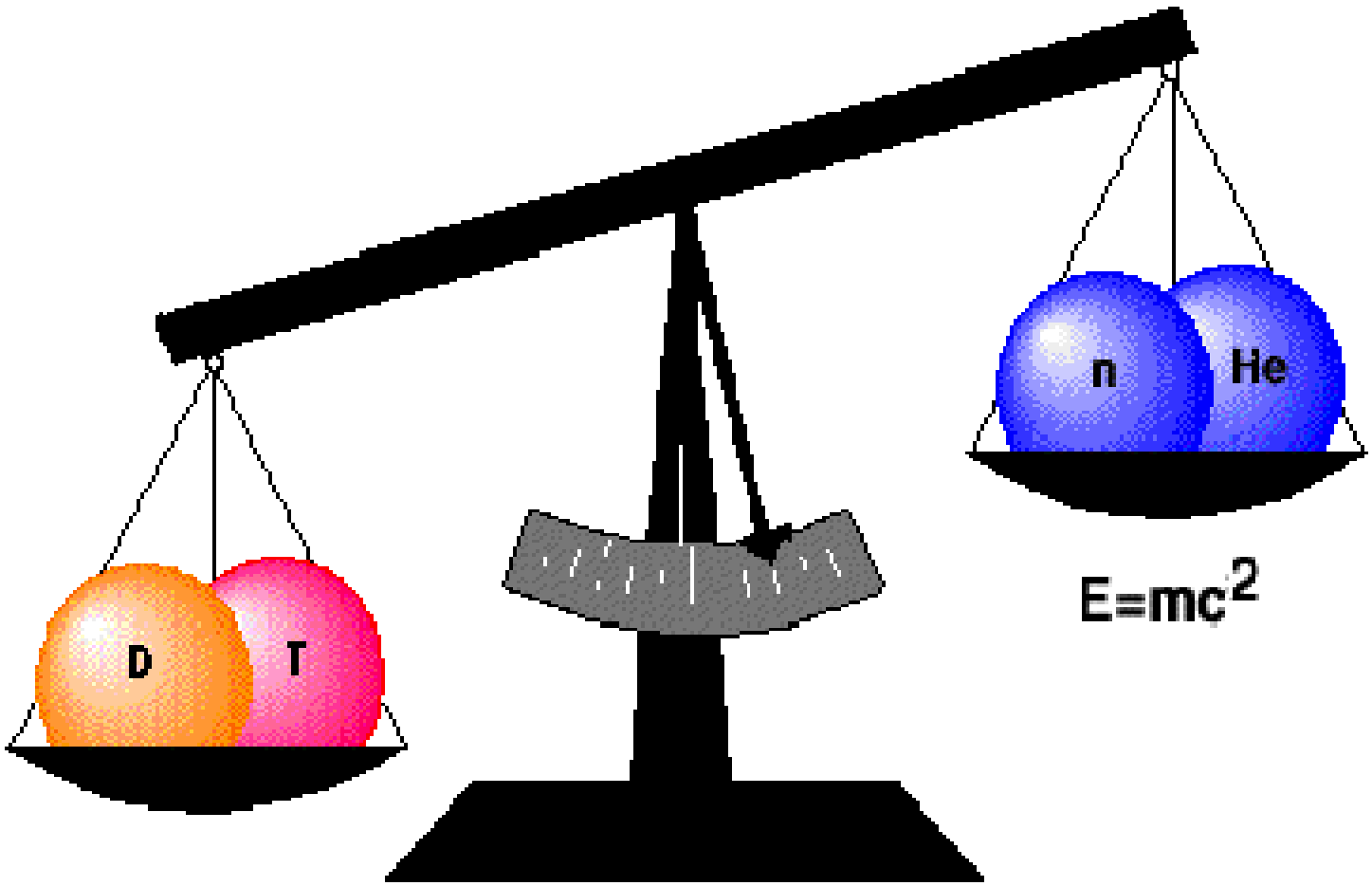

Fusion Energy Equivalent

50 cups water

=

- **1 thimble heavy water, extracted from 50 cups of water**

=

Summary of Conditions

Technological Targets:

- **T> 100 million K (10keV)**
- **nt>10^{21} m^{-3}-sec**

Two approaches:

n=10^{20} m^{-3}, confined t=10s
(low density, long-lived plasma) or :

n=10^{31} m^{-3}, confined 10^{-10}s
(super-high density, pulsed plasma)

Combined: ntT>$10^{22}$$m^{-3}$-sec-keV

Containing the Hot Plasma

Long-lived low-density Confinement

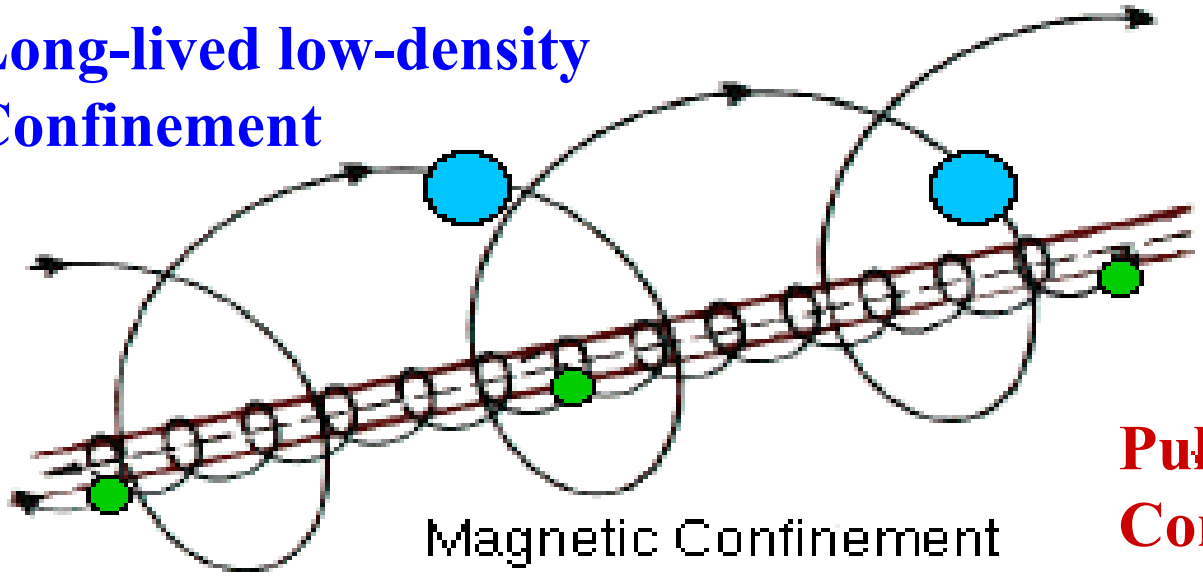

Magnetic Confinement

Pulsed High Density Confinement

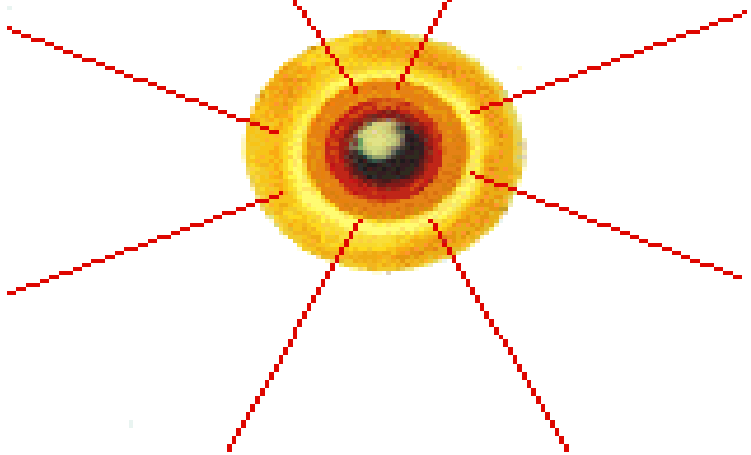

Inertial Confinement Using Lasers

Continuous Confinement

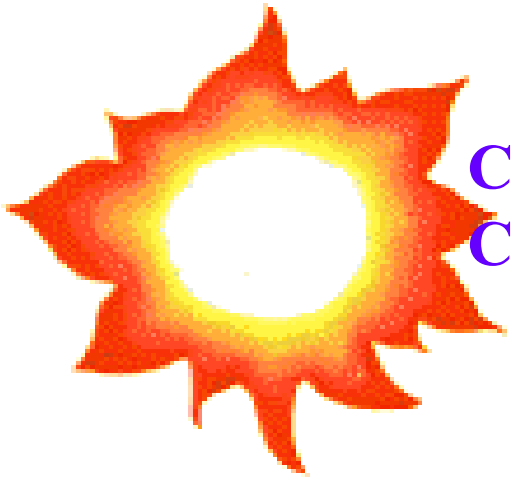

Gravitational Confinement in the Sun and Stars

Low Density, Long-lived Approach (Magnetic Compression)

Tokamak

- **Electric currents for heating**
- **Magnetic fields in special configuration for stability**

Schematic of Tokamak

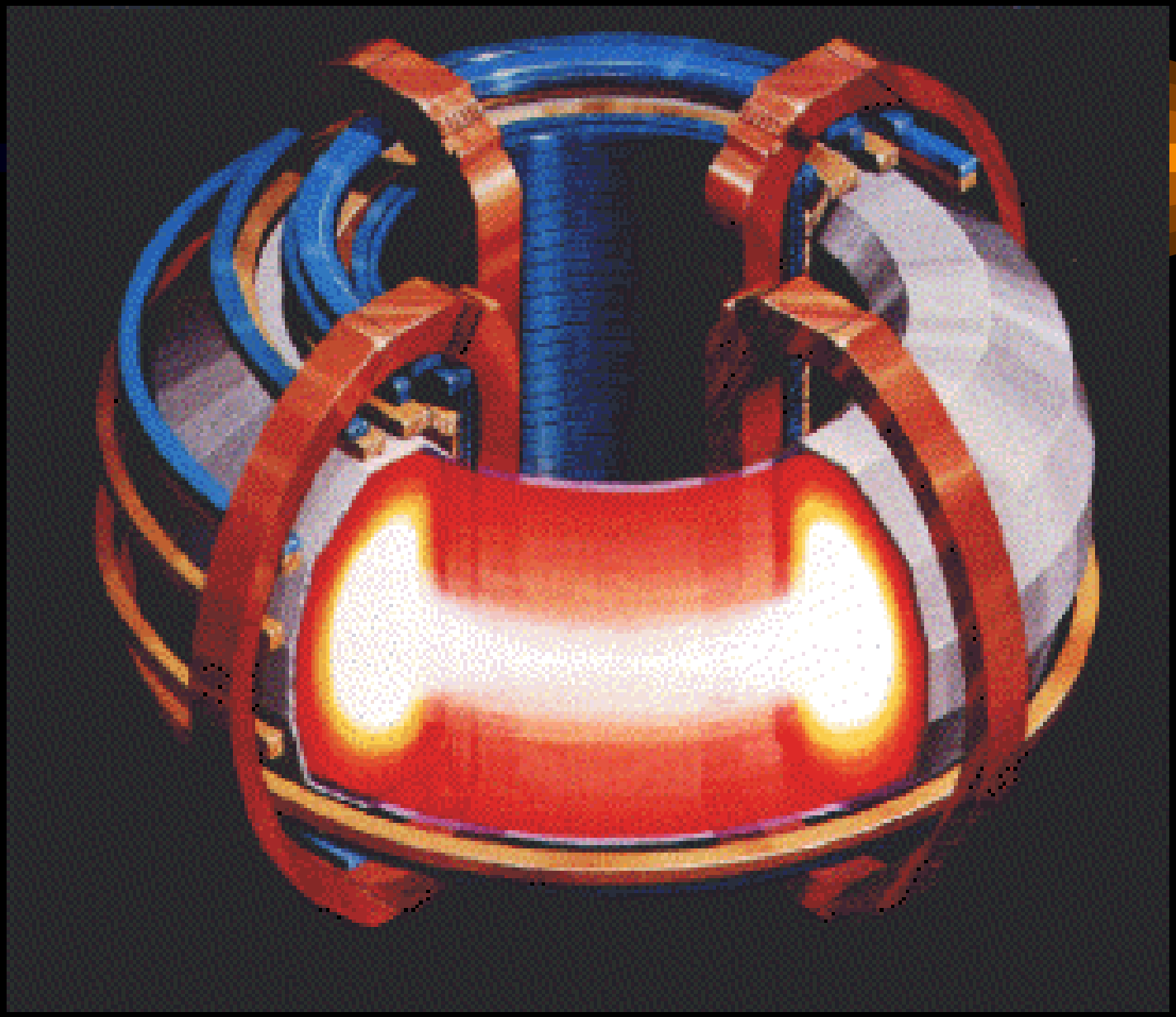

Magnetic Yoke to induce Plasma Current

Field Coils to Produce suitable Magnetic Field Configuration

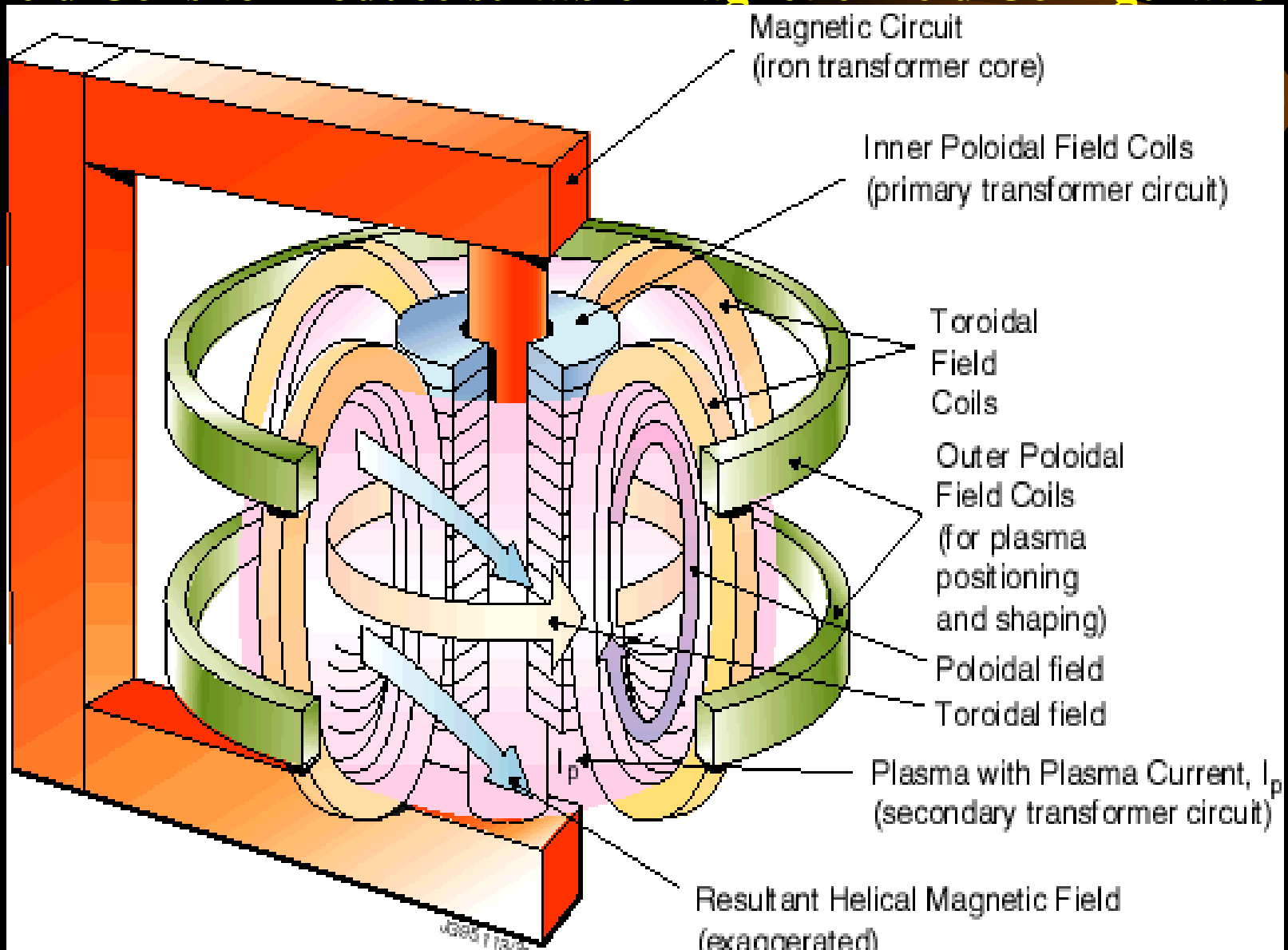

JET (Joint European Torus)

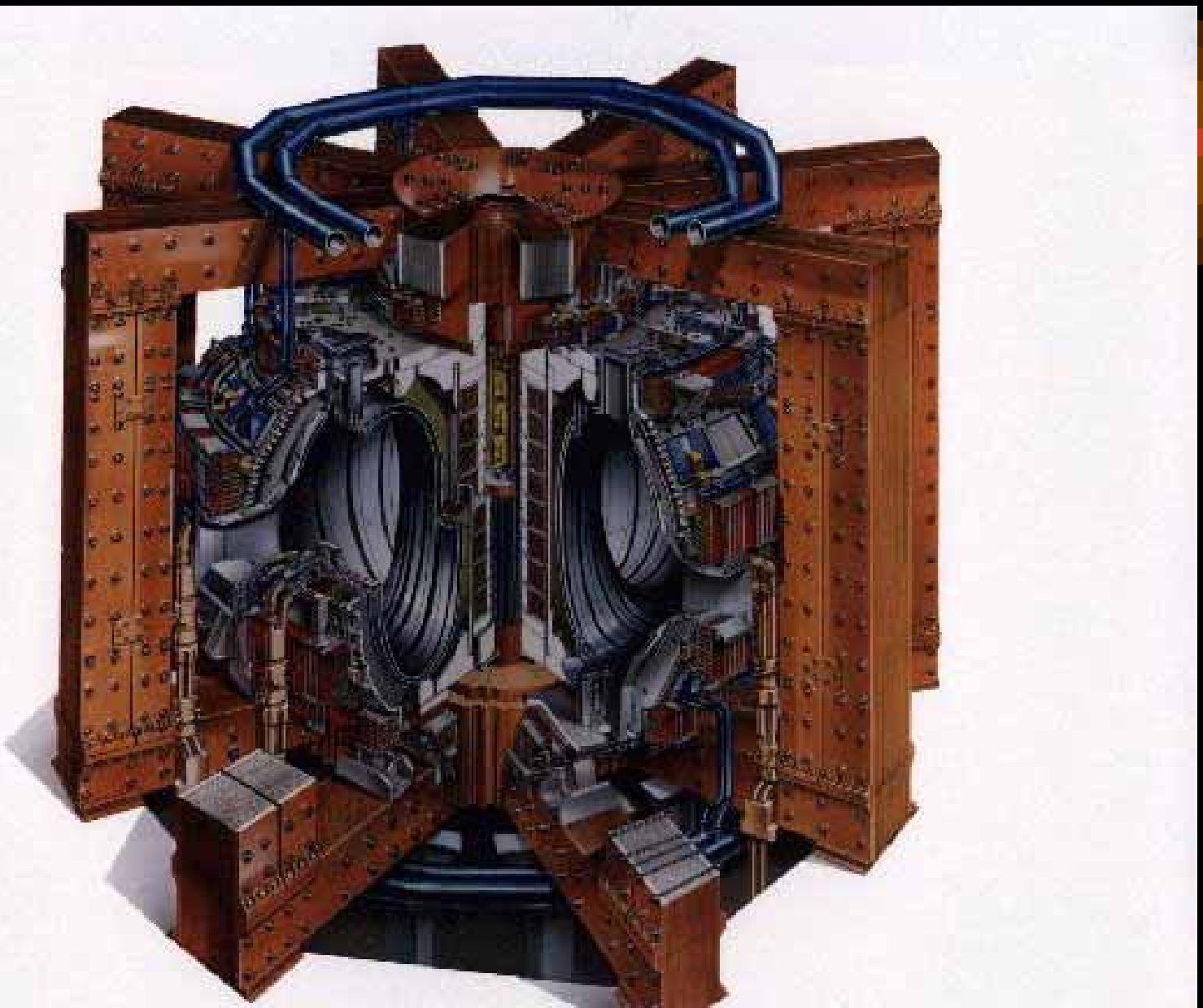

Project successfully completed January 2000

Inside JET

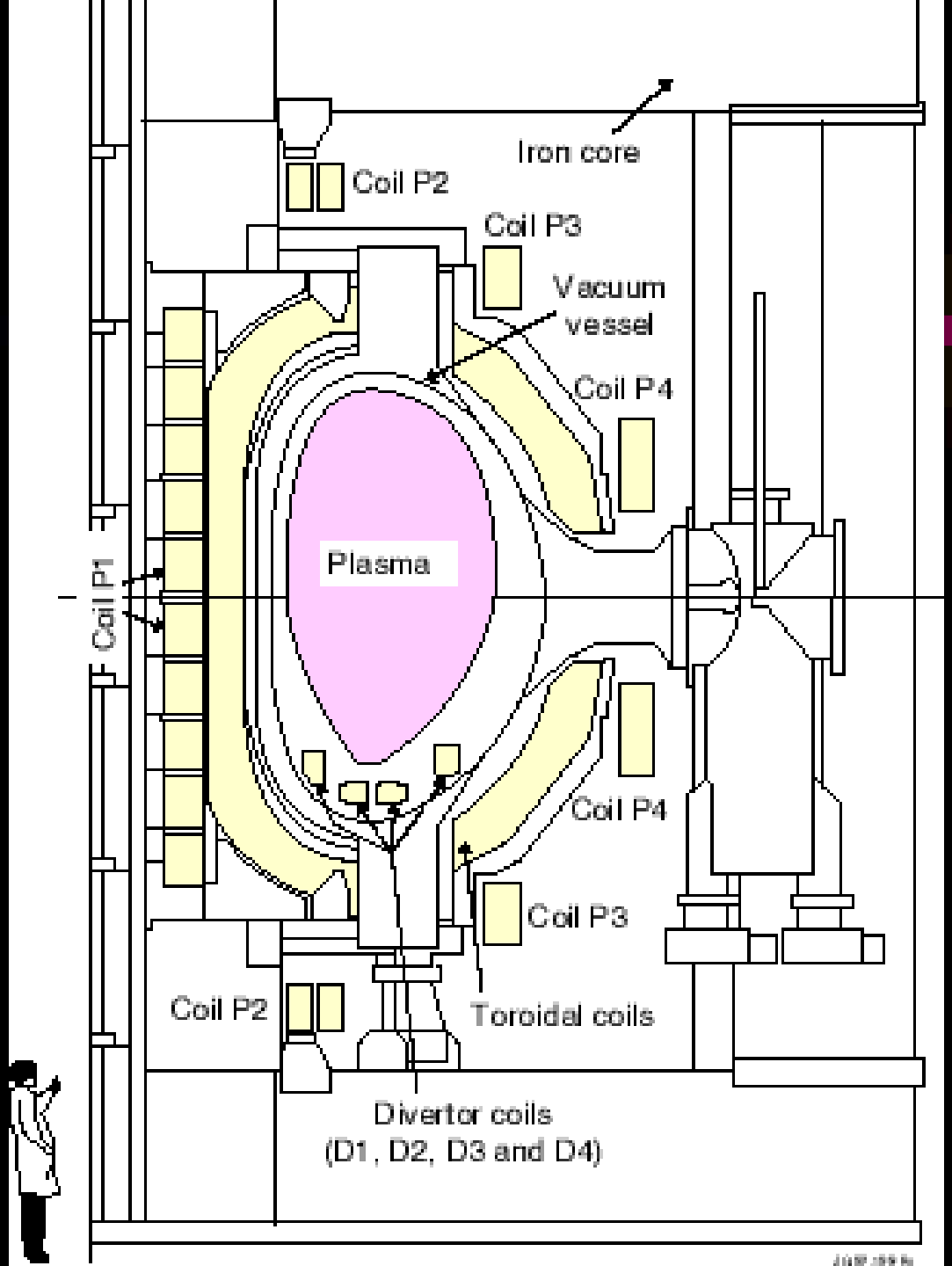

JET X-Section

Energy confinement time t scales as some functions of:

- **Plasma current I_p**
- **Major Radius R**
- **Minor radius 'a'**
- **Toroidal Magnetic Field B**

scaling law: $t \sim I_p^{\alpha} R^{\beta} a^{\gamma} B^{\lambda}$

indices $\alpha,\beta,\gamma,\lambda$ all positive

To achieve sufficient value of ntT requires:

scaling of present generation of Tokamaks upwards in terms of:

I_p, R, 'a' and B.

Fusion Temperature attained
Fusion confinement one step away

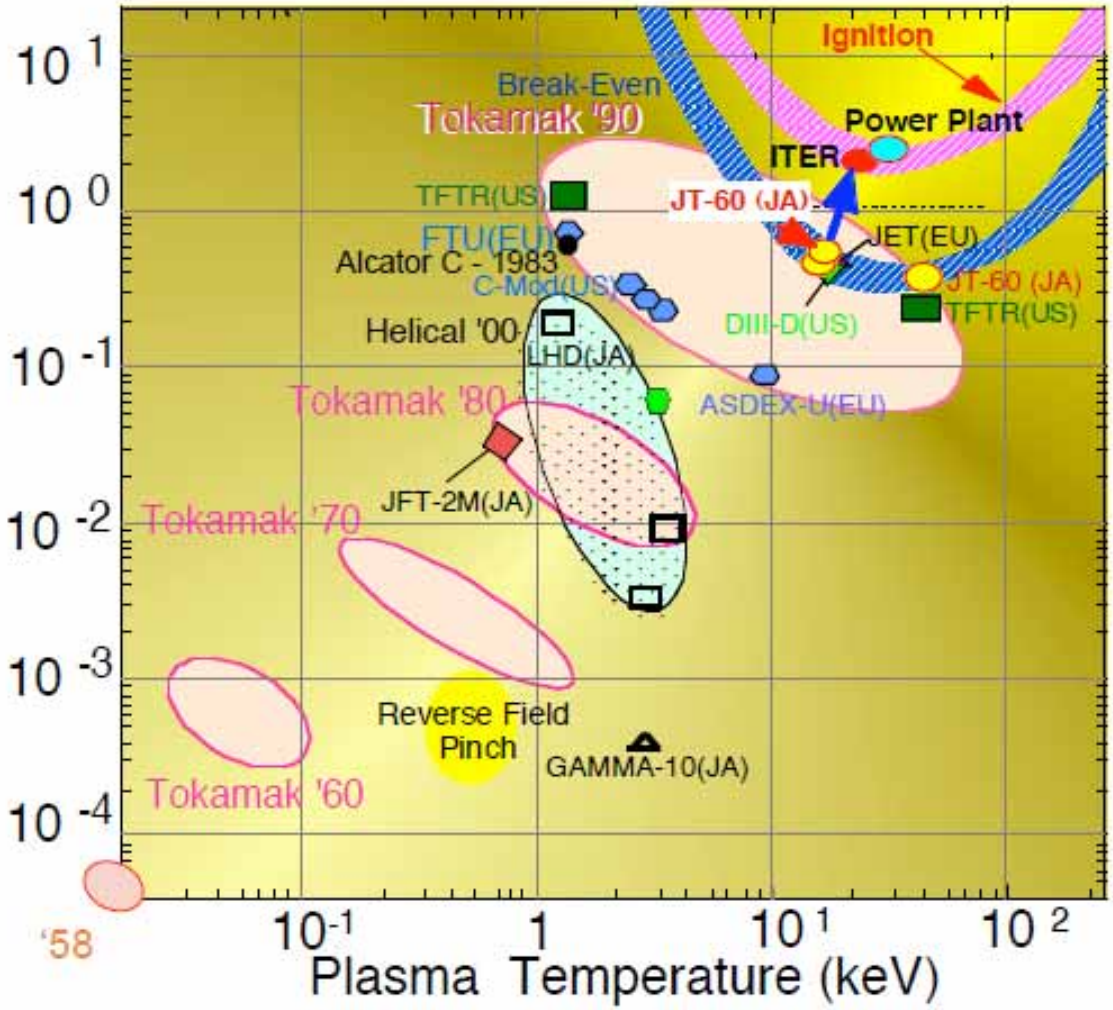

$n_i(0)\tau_E$

$(10^{20}\ m^{-3}\ s)$

$n_i(0)\tau_E T_i$ increased by ~10^7 since 1958

Needs x10 to reach ITER

Needs another 2x to reach Power Plant

JAEA

International Collaboration to develop Nuclear Fusion Energy-ITER

- 1985- Geneva Superpower Summit:
- Reagan (US) & Gorbachev (Soviet Union) agreed on project to develop new cleaner, sustainable source of energy- Fusion energy
- ITER project was born
- Initial signatories: former Soviet Union, USA, European Union (via EURATOM) & Japan
- Joined by P R China & R Korea in 2003 & India 2005
- ITER Agreement- signed in November 2006

ITER (International Thermonuclear Experimental Reactor)

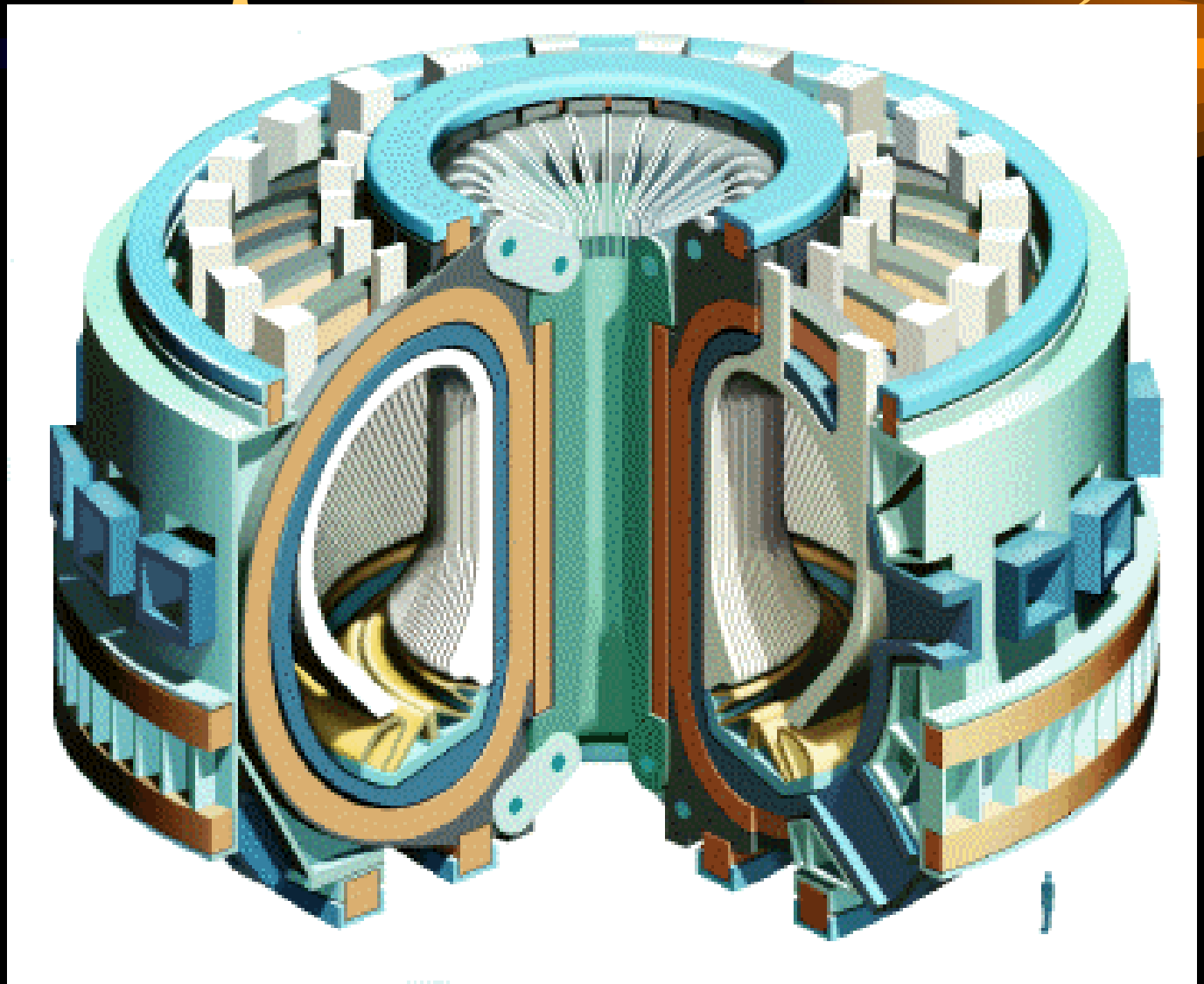

ITER A more detailed drawing

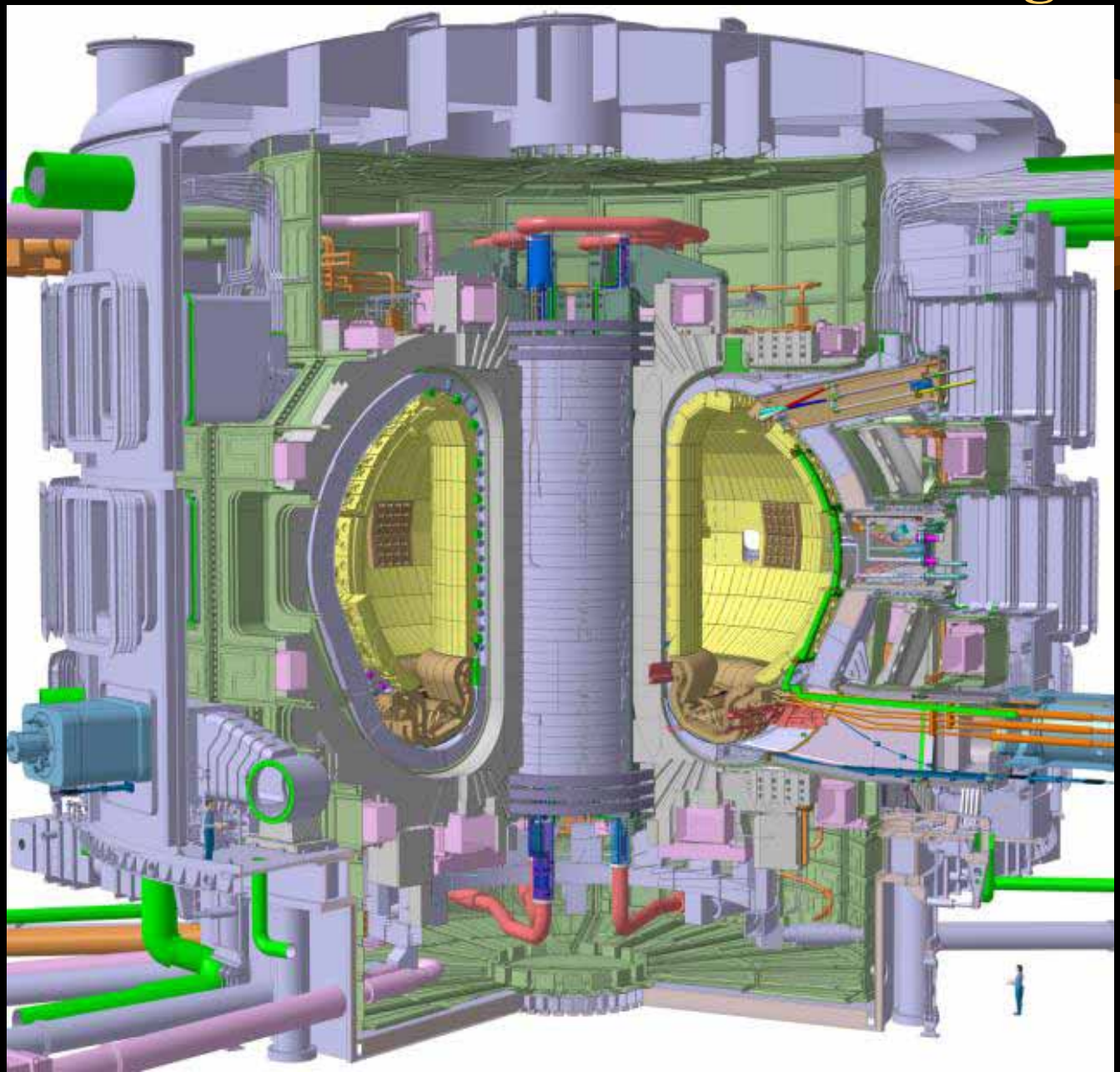

Systems:

Magnets: Ten thousand tons of magnets: 18 extremely powerful superconducting Toroidal Field & 6 Poloidal Field coils; a Central Solenoid, and a set of Correction coils: magnetically confine, shape and control the plasma inside the toroidal chamber

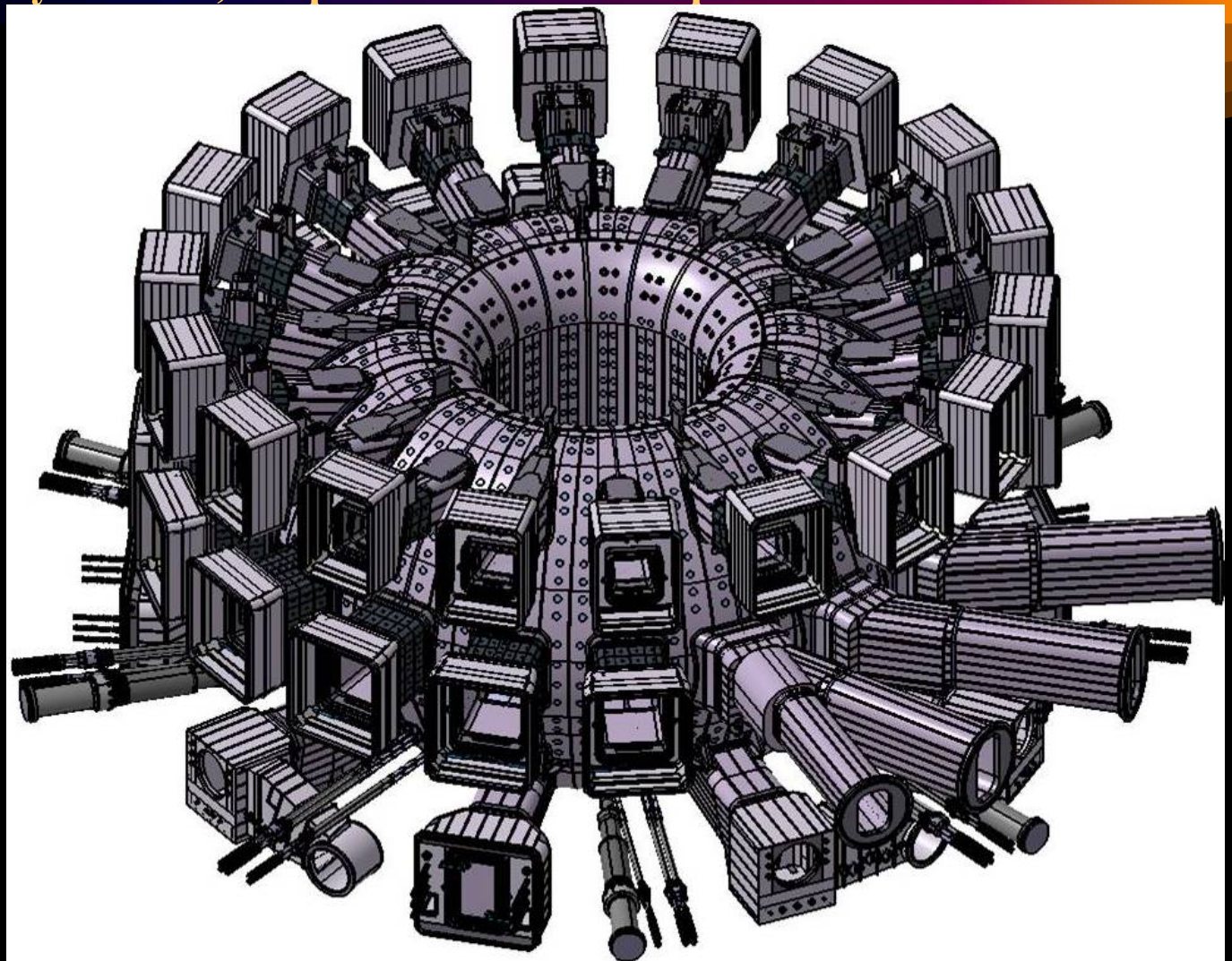

Vacuum & Cryogenics

Vacuum vessel: Volume=1400 m^3

Surrounding Cryostat vacuum jacket (not shown): Volume=8500 m^3;

Total vacuum volume~10,000 m^3

Largest vacuum volumes ever built; use mechanical & cryogenic pumps

Vacuum vessel is double-walled with water flowing between the walls

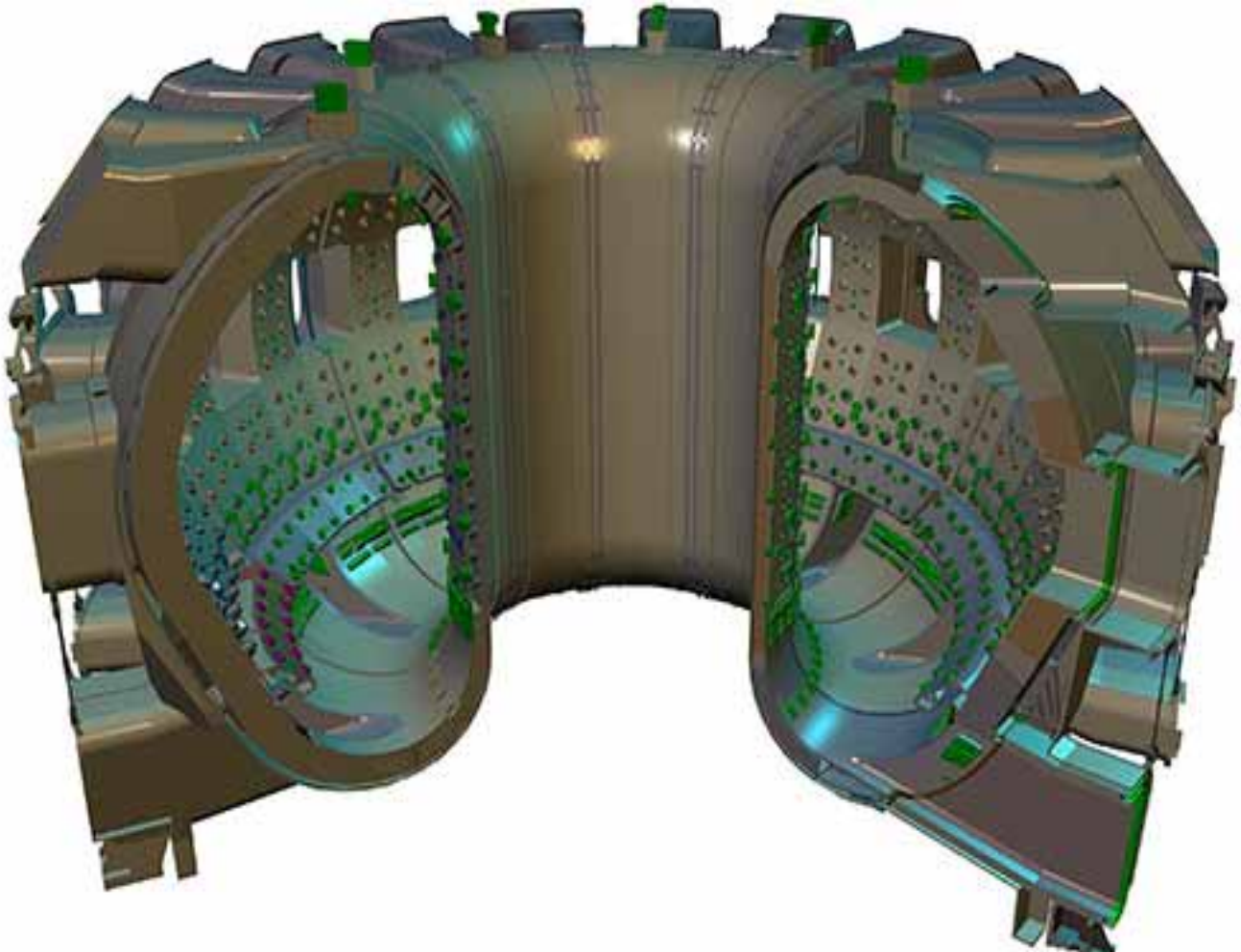

Associated with the vacuum vessel, advanced technological features include the following:

- **The Blanket: covers the interior surfaces of the Vacuum Vessel,**
  provides shielding to the Vessel and the superconducting Magnets from the heat and neutron fluxes of the fusion reaction.
  The neutrons are slowed down in the blanket, their K.E. is transformed into heat energy and collected by coolants. This energy will be used for electrical power production. One of the most critical and technically challenging components:
  together with the divertor it directly faces the hot plasma.

- ***Tritium breeding modules-in the first wall behind the front cover of the blanmket***
  Breeding modules will be used to test materials for Tritium Breeding. A future fusion power plant will be required to breed all of its own Tritium.

- ***The Divertor***
  The Divertor is situated along the bottom of the Vacuum Vessel,
  its function is to extract heat and Helium ash — the products of the fusion reaction — and other impurities from the plasma, in effect acting like a giant exhaust pipe.
  It will comprise two main parts: a supporting structure made primarily from stainless steel and the plasma facing component, weighing about 700 tons. The plasma facing component will be made of Tungsten, a high-refractory material.

BLANKET: *covers the interior surfaces of the Vacuum Vessel, provides shielding to the vessel & the superconducting magnets from the heat and neutron flux of the fusion reaction*
Modular wall: 440 segments each 1x1.5m weighing 5 tons; surface facing the plasma is plated with Berylium

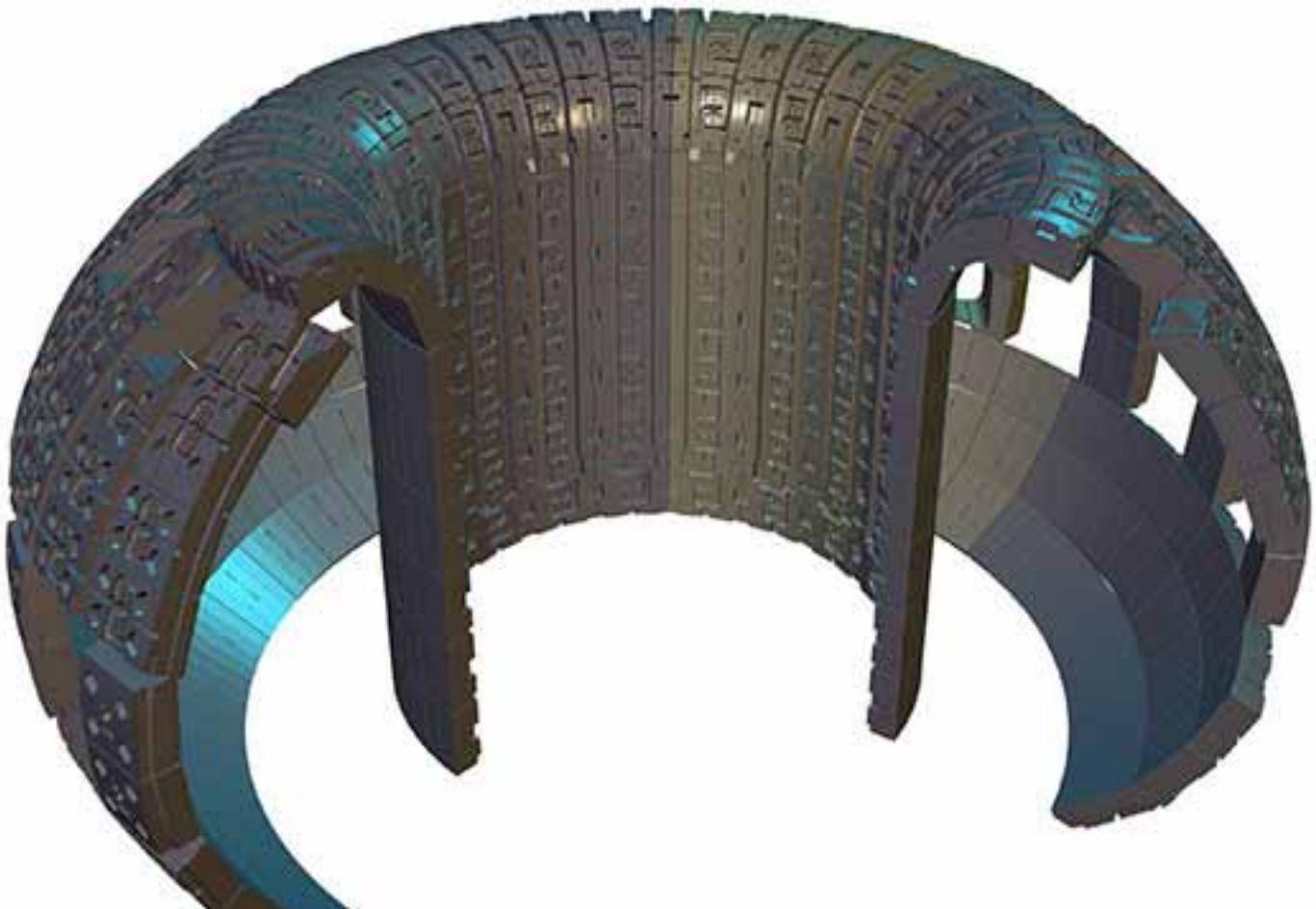

Divertor: Is placed at bottom of the vacuum chamber
To remove waste gases from the D-T reaction;
and to recover the heat from this waste gas.
The surface temperature of the divertor goes up to 3000 C;
surface cover will be composite carbon or tungsten

An extensive diagnostic system (50 individual systems) installed to provide t measurements: control, evaluate & optimize plasma performance. Include measurements of temperature, density, impurity concentration, and particle &energy confinement times.

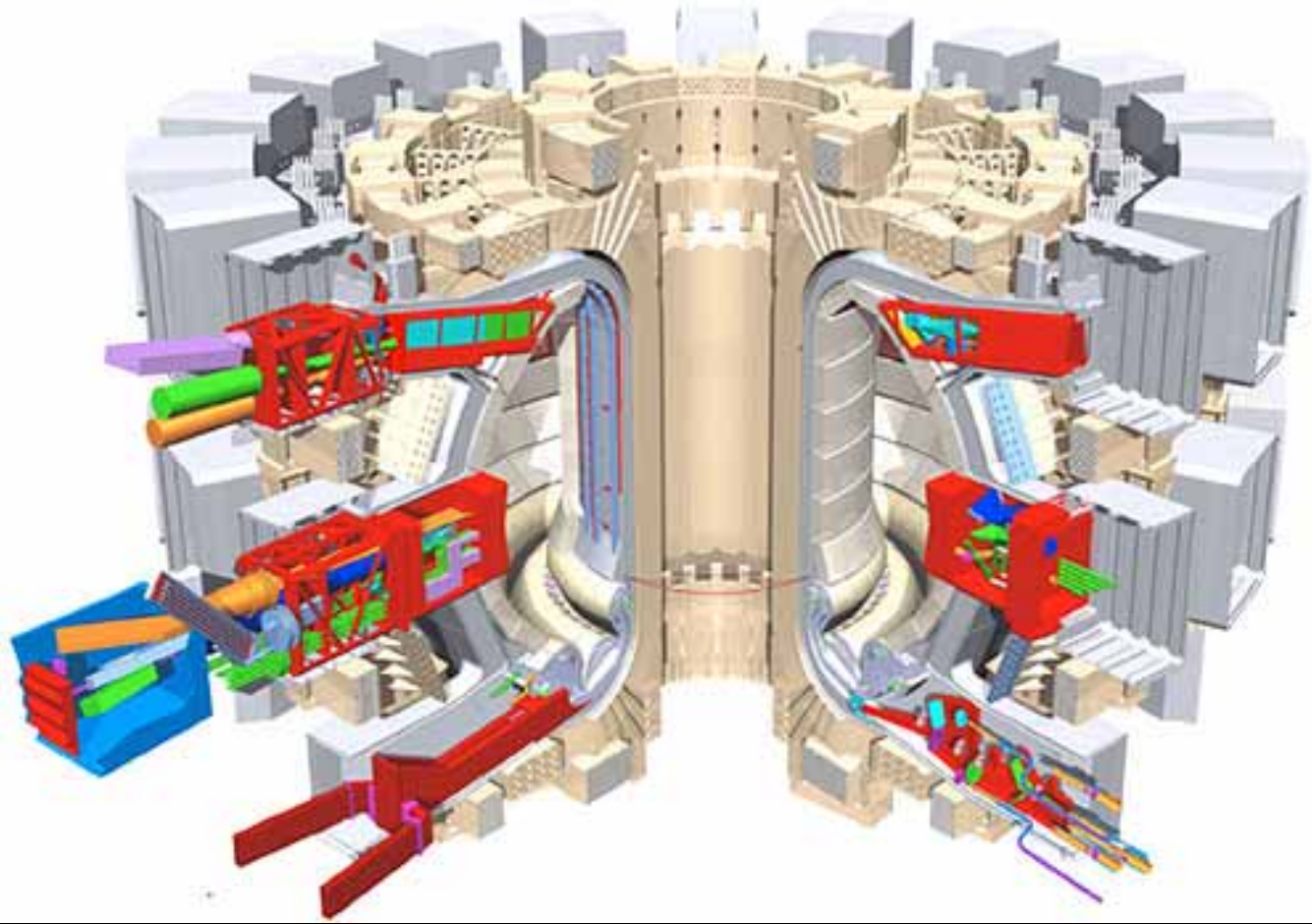

Cryostat: Large stainless steel structure surrounding the vacuum vessel & superconducting magnets, providing a supercooled vacuum jacket.
Double wall, space between filled with pressurised He, as a thermal barrier.
This is a huge structure: 31m tall x 37m wide; with openings for access to vacuum chamber, cooling systems, magnets, blanket and divertor

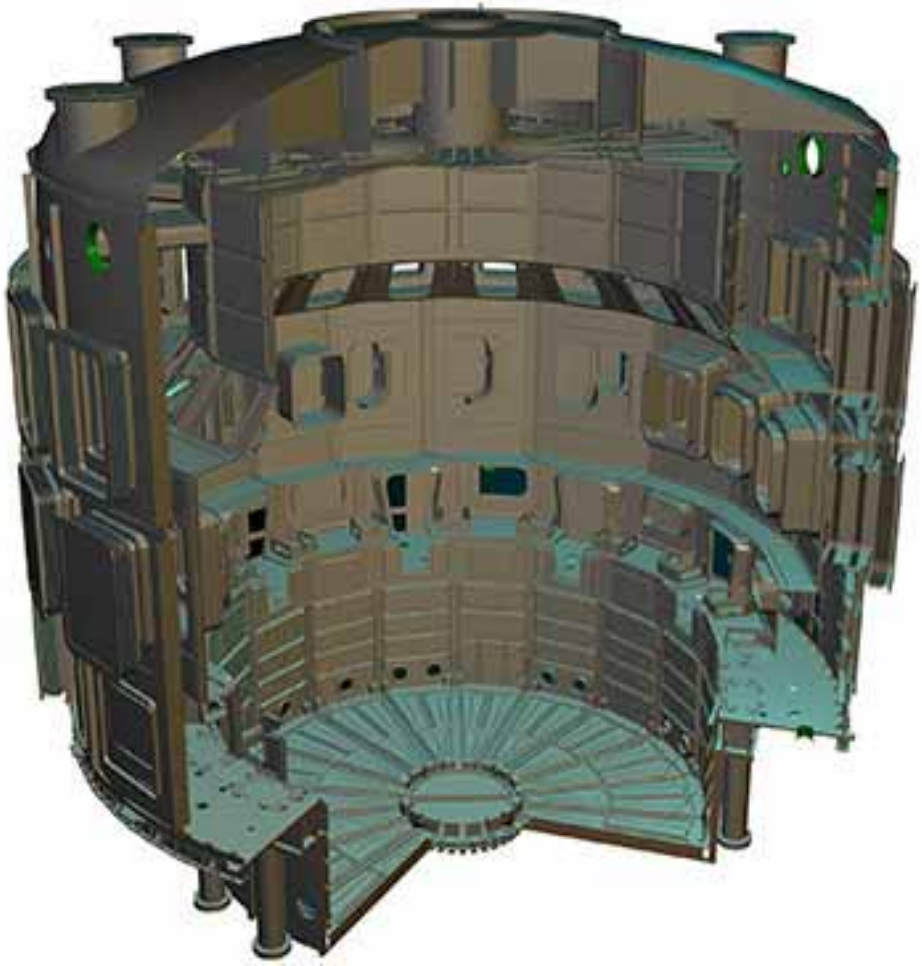

Plasma Heating

- **The temperatures inside the ITER Tokamak must reach 150 million C —**

  ten times hotter than the Sun's core- & be sustained in a controlled way in order to extract energy.

The plasma in the vacuum vessel is produced and heated by a current induced by transformer action using a central solenoid (inner poloidal) coil, as primary of a transformer; the toroidal plasma current forms the secondary of the transformer

Then 3 sources of external heating are used to provide the input heating power of 50 MW required to bring the plasma to the necessary temperature.

1. neutral beam injection

2. ion cyclotron heating &

3. electron cyclotron heating.

A "burning plasma" is achieved –in which the energy of the Helium from the fusion reaction is enough to maintain the plasma temperature. The external heating is then switched off. The plasma fusion burn continues.

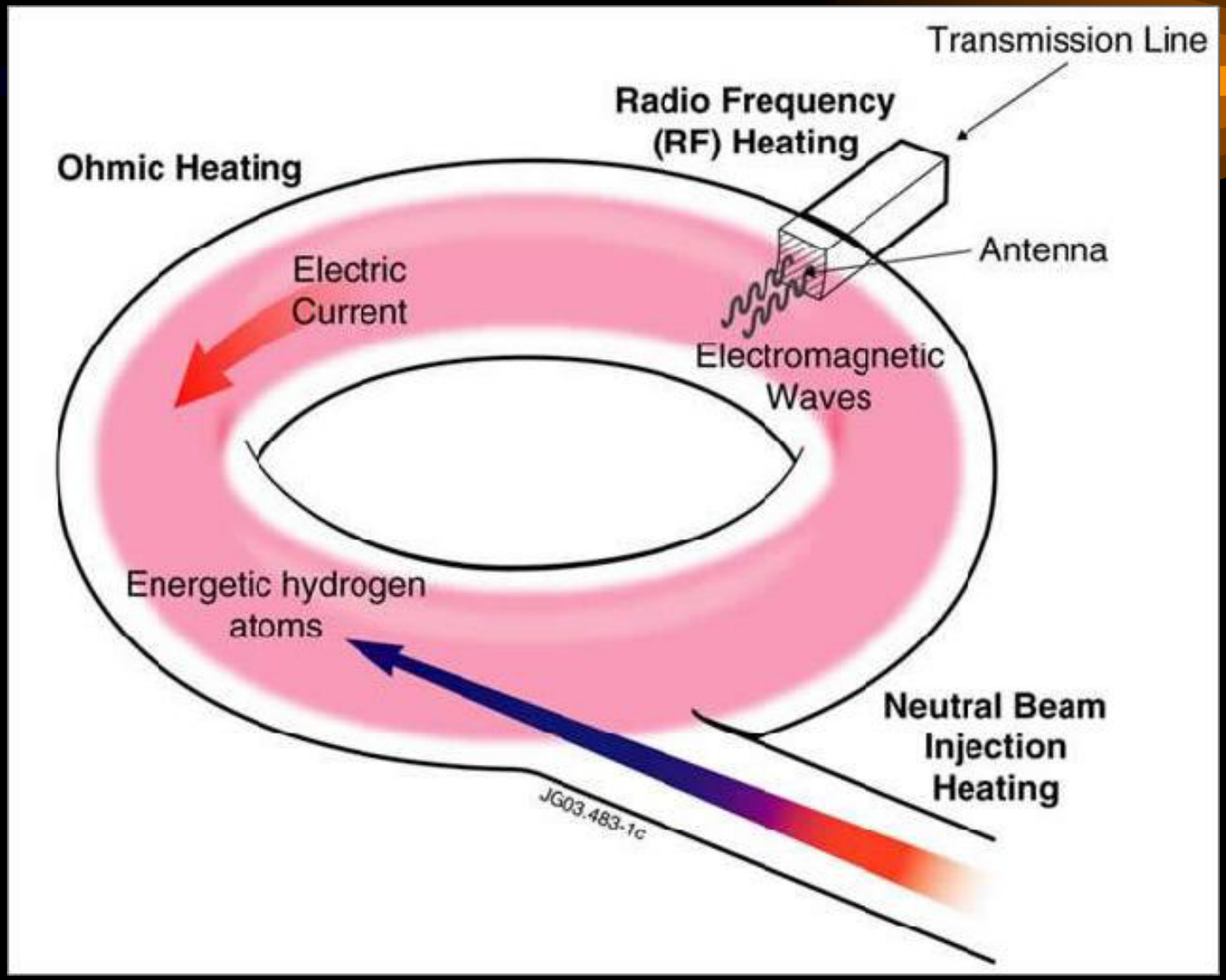

Cooling and heat Transfer

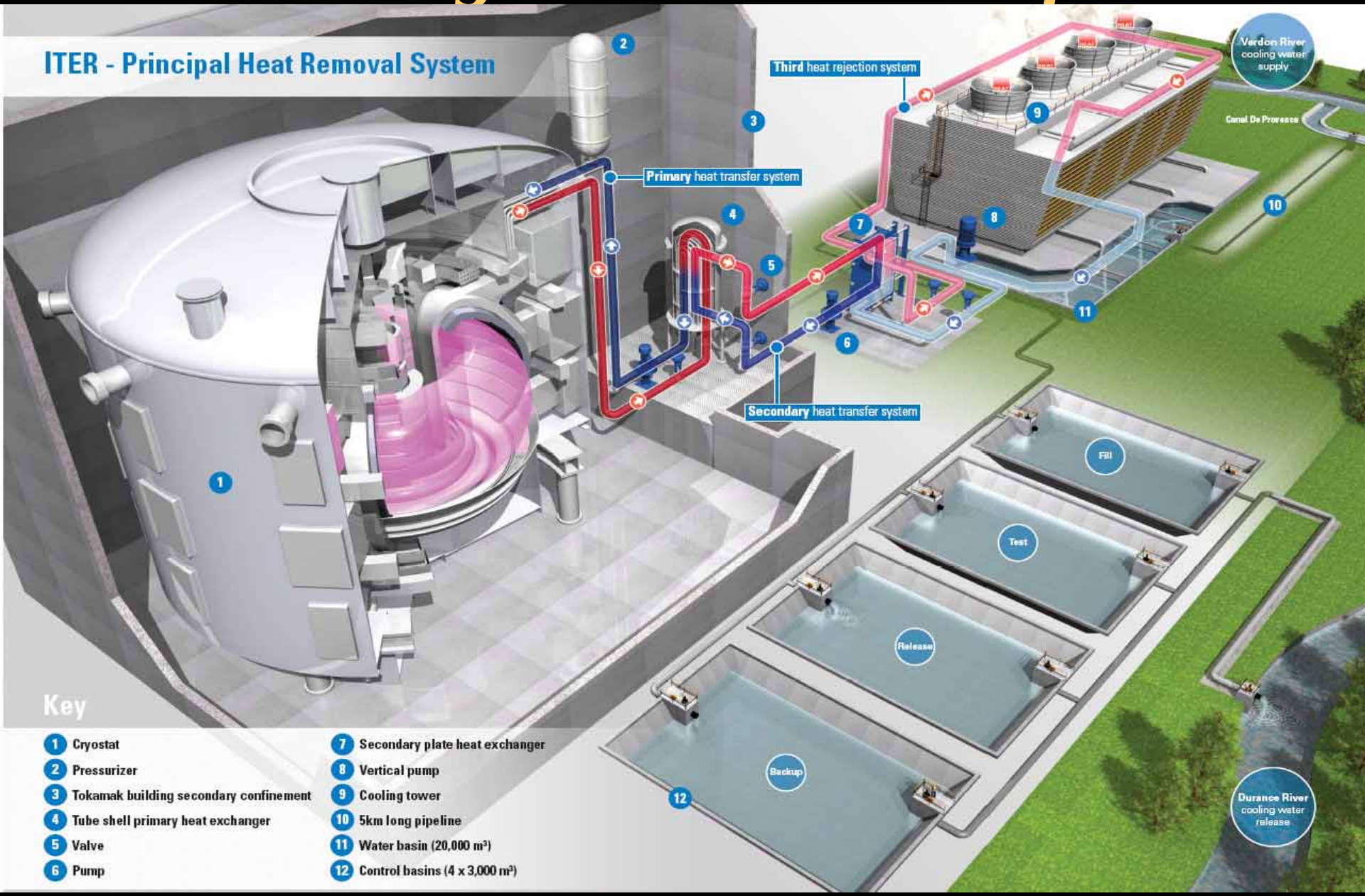

ITER Construction has now started in Cadarache, France

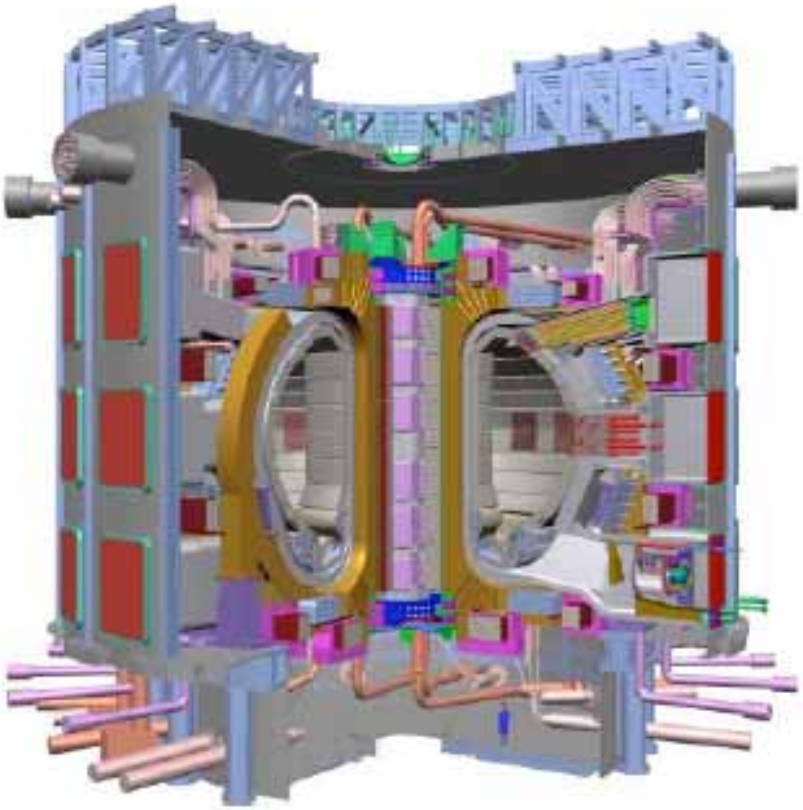

Reactor scale

ITER Site Under Construction

First plasma planned 2018

First D-T planned 2022

Q>10 and Beyond

ITER : to demonstrate: possible to produce commercial energy from fusion.

Q= ratio of fusion power to input power.

Q ≥ 10 represents the scientific goal of ITER :

to deliver 10x the power it consumes.

From 50 MW input power to 500 MW of fusion power - first fusion experiment to produce net energy.

Beyond ITER will be DEMO (early 2030's), demonstration fusion power plant which will put fusion power into the grid as early as 2040

FIRE: Incorporates Many Advanced Features

FIRE Incorporates Advanced Tokamak Innovations

AT Features

- DN divertor
- strong shaping
- very low ripple
- internal coils
- space for wall stabilizers
- inside pellet injection
- large access ports

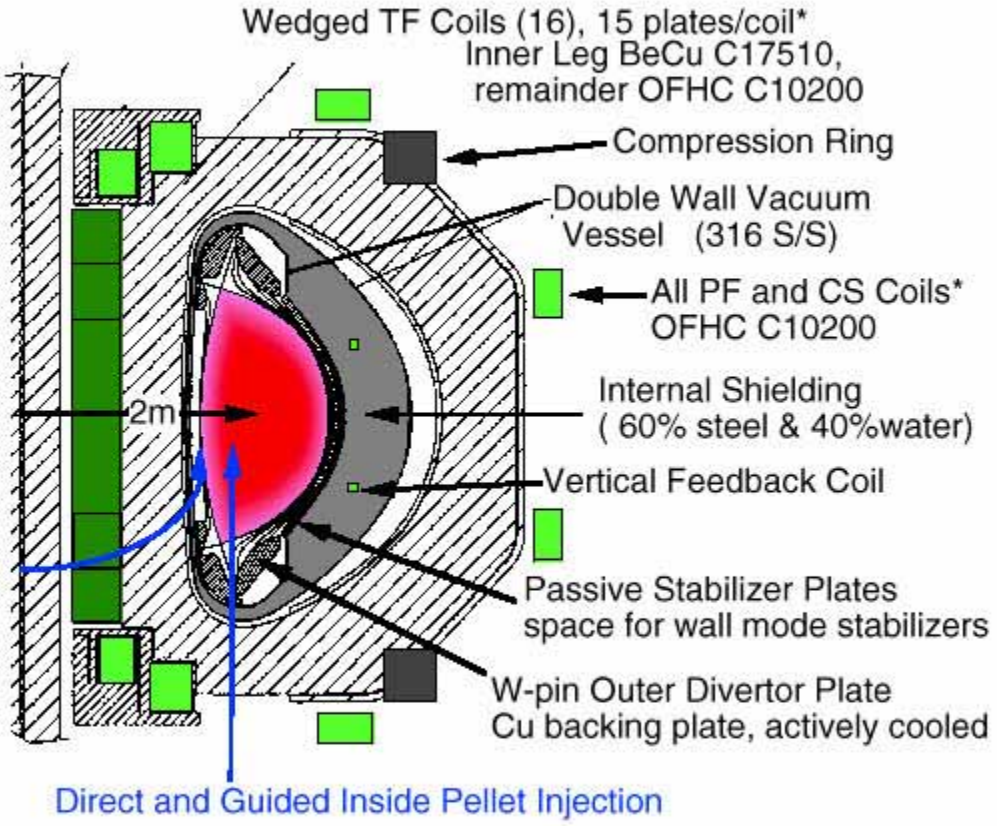

*Coil systems cooled to 77 °K prior to pulse, rising to 373 °K by end of pulse.

Potential Next Step Fusion Burning Experiments

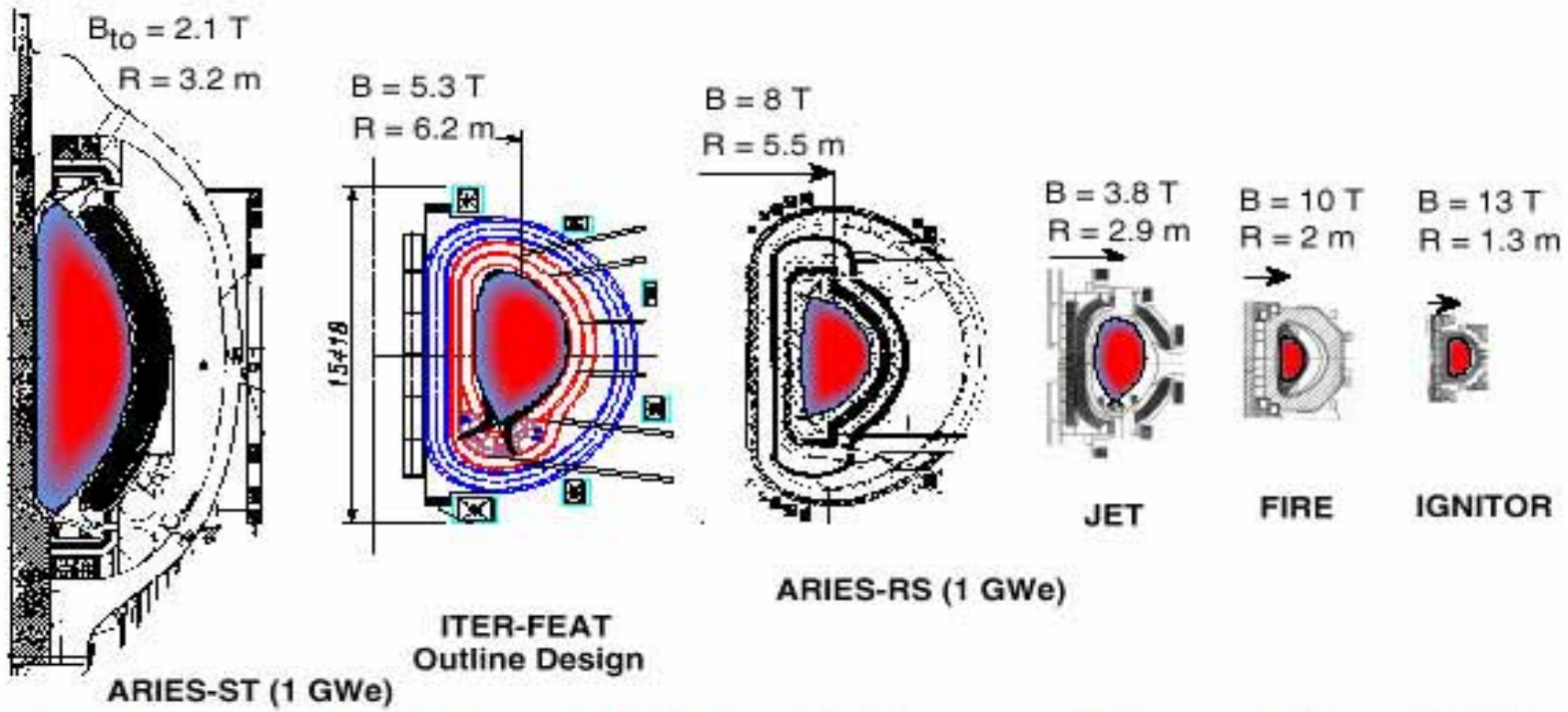

Cost Drivers	ARIES-ST	ITER-FEAT	ARIES-RS	JET	FIRE	IGNITOR
Plasma Volume (m^3)	810	837	350	95	18	11
Plasma Surface (m^2)	580	678	440	150	60	36
Plasma Current (MA)	28	15	11	4	6.5	12
Magnet Energy (GJ)	29	50	85	2	5	5
Fusion Power (MW)	3000	500	2200	16	200	100
Burn Time (s), inductive	steady	300	steady*	1	20	5

* assumes non-inductive current drive

The other approach: Pulsed Super-high Density (Inertial Compression)

- Radiation Compression

Pulsed Fusion: Radiation Compression

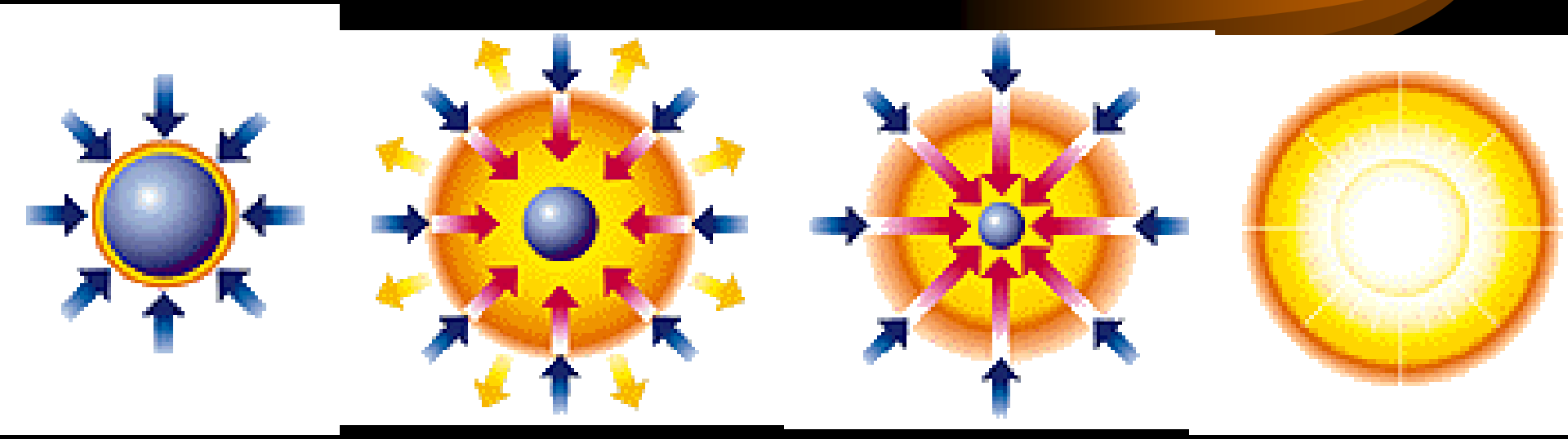

Radiation Pressure

e.g. powerful lasers beamed from all directions onto D-T pellet (0.1mm radius)

Compression:

fuel is compressed by rocket-like blow-off of hot surface material

Ignition:

density of fuel core reaches 1000 times density of water & ignites at 100 million K

Burn:

Thermonuclear fusion spreads rapidly through super-compressed fuel yielding many times input energy

Cross-sectional view of the KOYO-F fast ignition reactor (Norimatsu et al.)

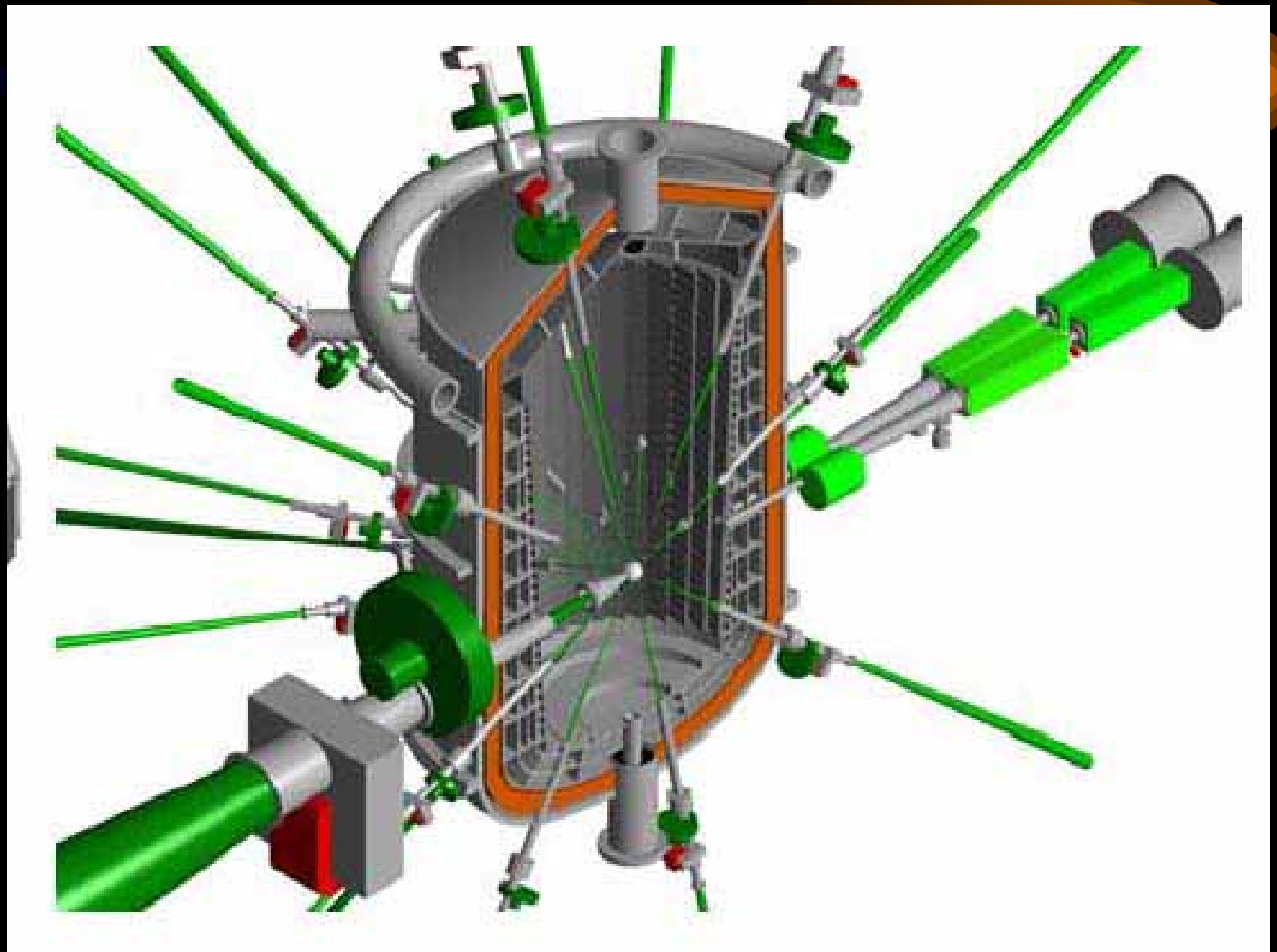

Large scale Fusion Experiments

- **Tokamaks: Low density, long confinement plasmas**
- **Laser Implosions: Super-dense, sub-nanosecond plasmas**

Smaller scale Fusion Experiments

- **Pinches: Dense, microsecond plasmas**
- **Plasma Focus (PF) An advanced pinch system**

Superior method for dense pinches

- **The Plasma Focus produces exceptional densities and temperatures.**
- **A simple capacitor discharge is sufficient to power the plasma focus.**

- **Plasma Focus (PF)-**
  - **remarkably copious source of multiple radiation: x-rays, fast electrons, ions and plasma stream**
  - **Fusion neutrons demonstrated even in table top devices**
  - **same energy density at storage energy levels of 0.1-1000 kJ; hence scalability of neutrons**

THE PLASMA FOCUS (PF)

- **The PF is divided into two sections**.
- **Pre-pinch (axial) section**: Delays the pinch until the capacitor discharge current approaches peak value.
- **The pinch starts & occurs at top of the current pulse**.

The Plasma Dynamics in Focus

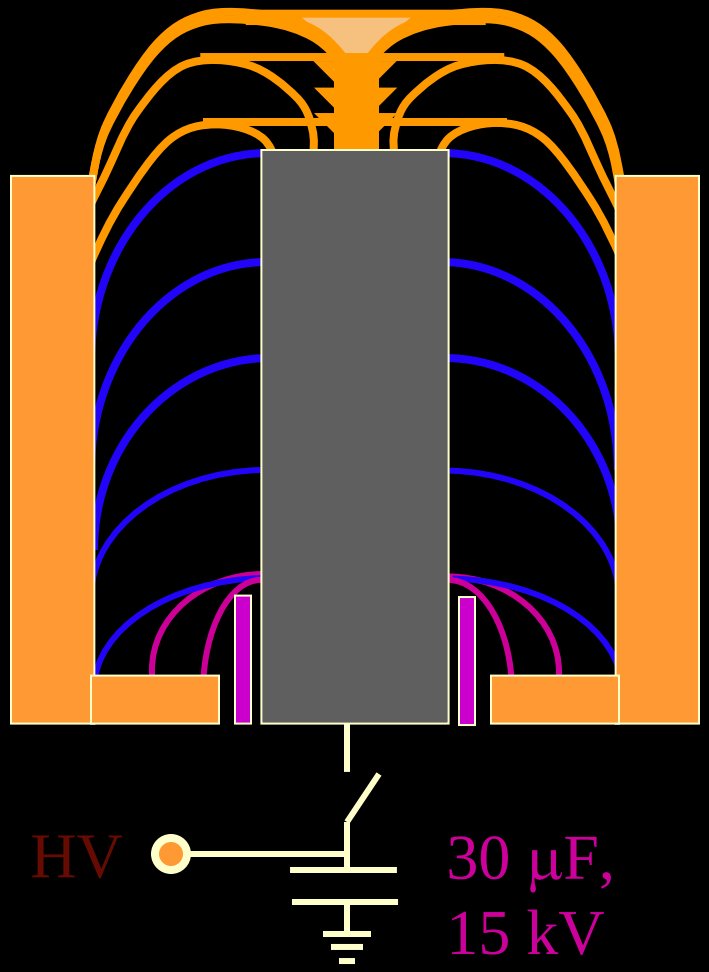

Radial Phase

Axial Accelaration Phase

Inverse Pinch Phase

Radial Compression (Pinch) Phase of the Plasma Focus

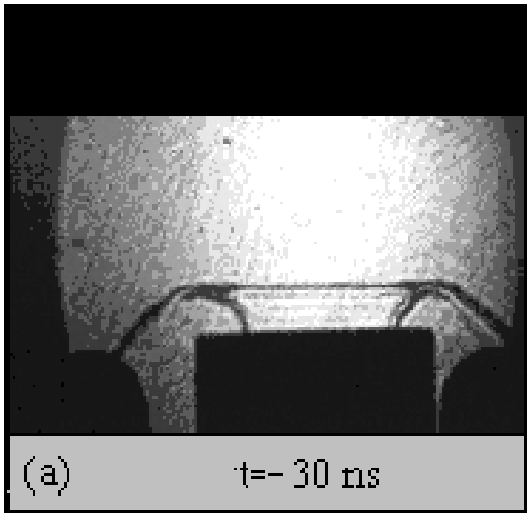

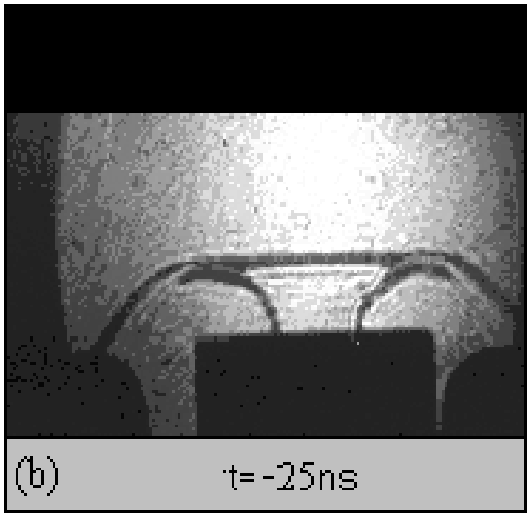

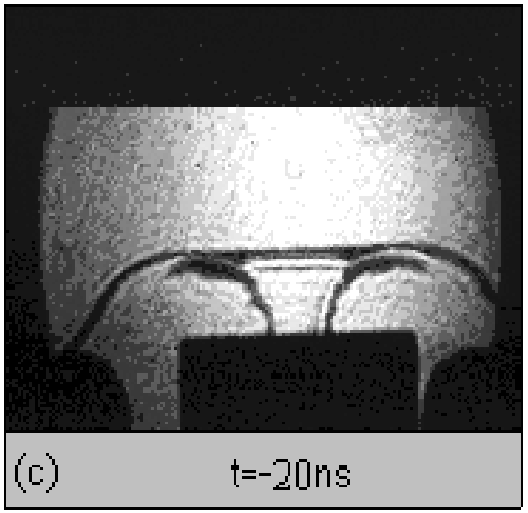

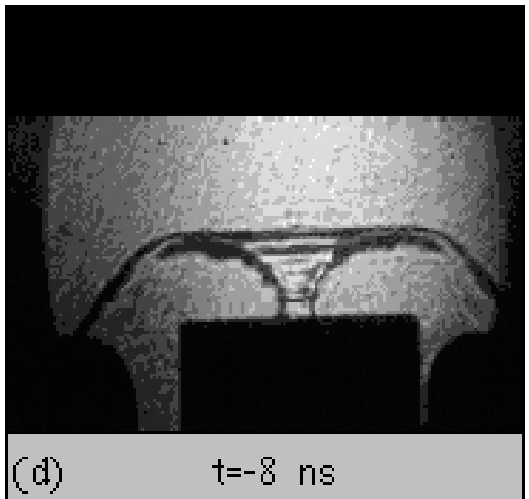

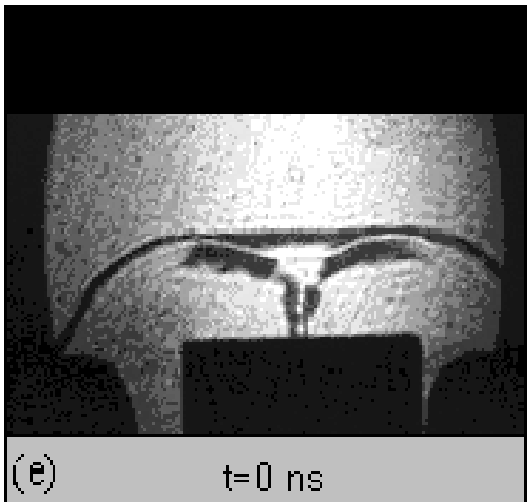

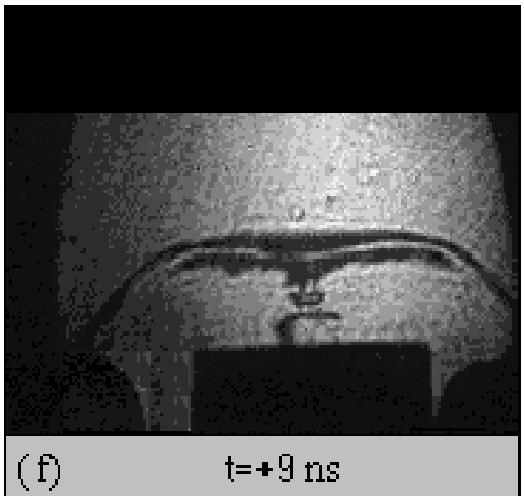

High Power Radiation from PF

- **powerful bursts of x-rays, ion beams, REB's, & EM radiation (>10 gigaW)**
- **Intense radiation burst, extremely high powers**
- **E.g. SXR emission peaks at 10^9 W over ns**
- **In deuterium, fusion neutrons also emitted**

300J portable (25 kg); 10^6 neutrons per shot fusion device-at NTU-NIE

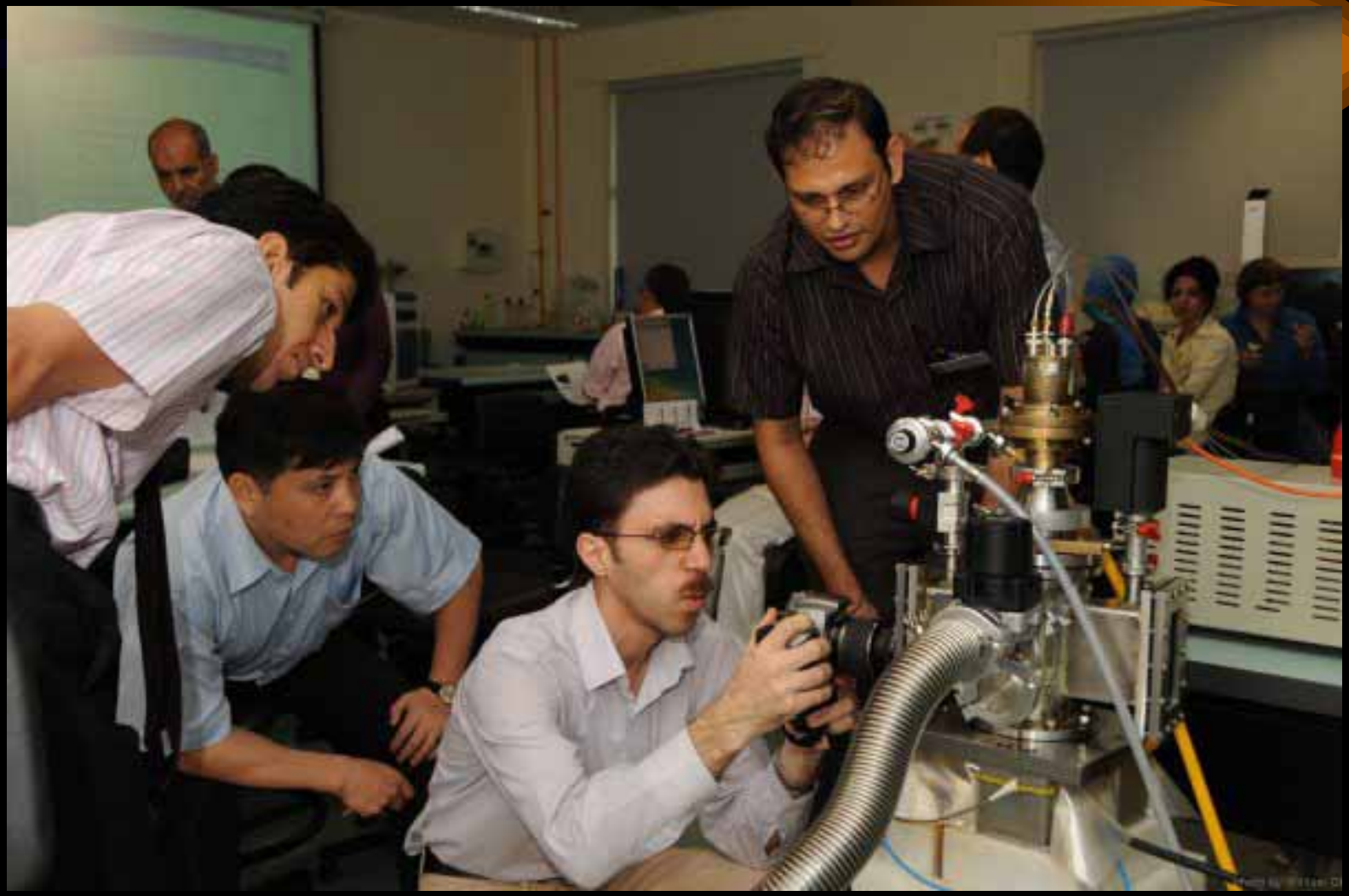

INTI UC Centre for Plasma Research -Plasma Focus & Pulse Power Laboratory

23 June 2009 - First test shot of INTI-PF

10 kV
2 Torr Neon

Current: 120 kA

Temperature: 2 million ^{o}C

Soft x-ray burst: 100 Megawatt- 10 ns

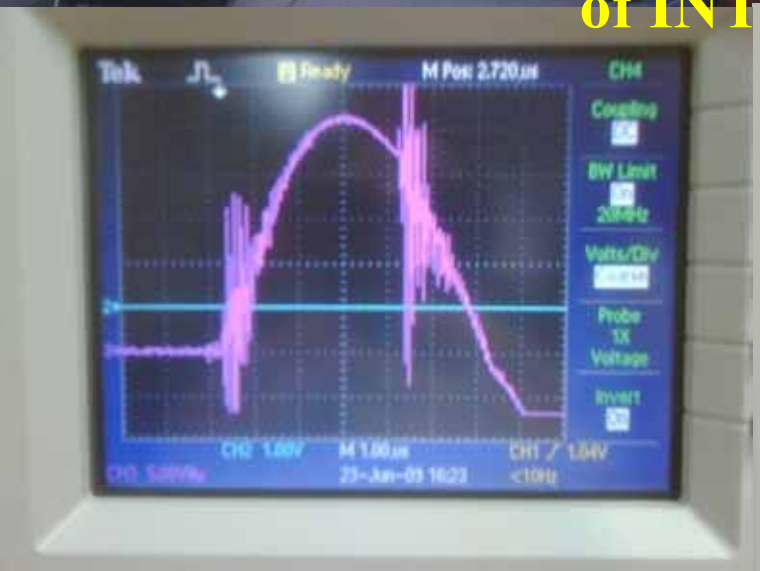

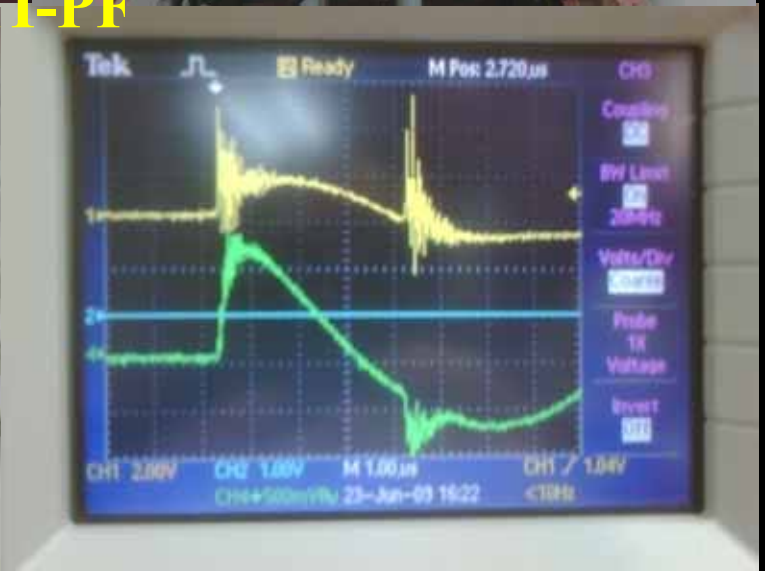

1997 ICDMP (International Centre for Dense Magnetised Plasmas) Warsaw-now operates one of biggest plasma focus in the world, the PF1000

Same Energy Density in small and big PF devices leads to:

- Scalability
  - constant speed factor, $[(I/a)/\rho^{1/2}]$ for all machines, big or small lead to same plasma energy density

- from 0.1 to 1000 kJ of storage energy
  - predictable yield of radiation

Consideration of nτT parameter for different plasmas: (comparative)

- **For a thermonuclear burning plasma in all cases need T=10 keV**
- **Hence to get the required nτT of 10^{22} m^{-3}-s-keV we need nτ of 10^{21} m^{-3}-s.**
- **This requirement of nτ= 10^{21} m^{-3}-s can be achieved as follows:**

	n (m^{-3})	τ (sec)
Tokamak	10^{21}	1
Plasma focus	10^{27}	10^{-6}
Laser implosion	10^{31}	10^{-10}

- **However note that plasma focus neutrons are known to be not produced from a thermonuclear plasma; so this situation of nτT does not really apply.**

For the PF the scaling needs to be pushed in a different direction using the consideration of a beam-target mechanism. This is what we are doing in the global scaling slide where Y_n is found as a scaling of E_0.

One of most exciting properties of plasma focus is its neutron yield Y_n

- **Early experiments show: $Y_n \sim E_0^2$**
- **Prospect was raised in those early research years that, breakeven could be attained at several tens of MJ .**
- **However quickly shown that as E_0 approaches 1 MJ, a neutron saturation effect was observed; Y_n does not increase as much as expected, as E_0 was progressively raised towards 1 MJ.**
- **Question: Is there a fundamental reason for Y_n saturation?**

Chart from M Scholz (November 2007 ICDMP) purported to show neutron saturation

Scaling

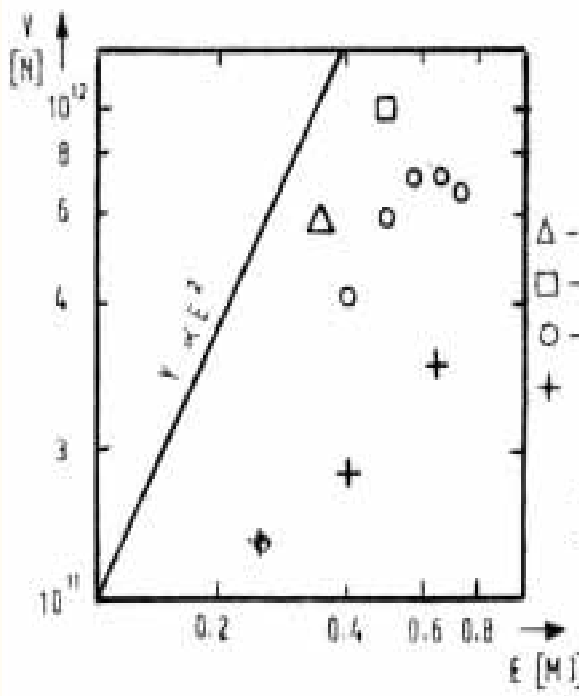

$$\frac{1}{2}(L+L_0)I^2 \equiv \gamma E$$

$$L \equiv L_0$$

$$Y_n \propto E^2$$

$$I^2 \propto E$$

Frascati (Program Euroatom), E_b = 1MJ; U_b= 50 kV;

Institute of Plasma Physics and Laser Microfusion
Warsaw, Poland

Global Scaling Law

Scaling deterioration observed in numerical experiments (small black crosses) compared to measurements on various machines (larger coloured crosses) Neutron 'saturation' is more accurately portrayed as a scaling deterioration-Conclusion of IPFS-INTI UC research

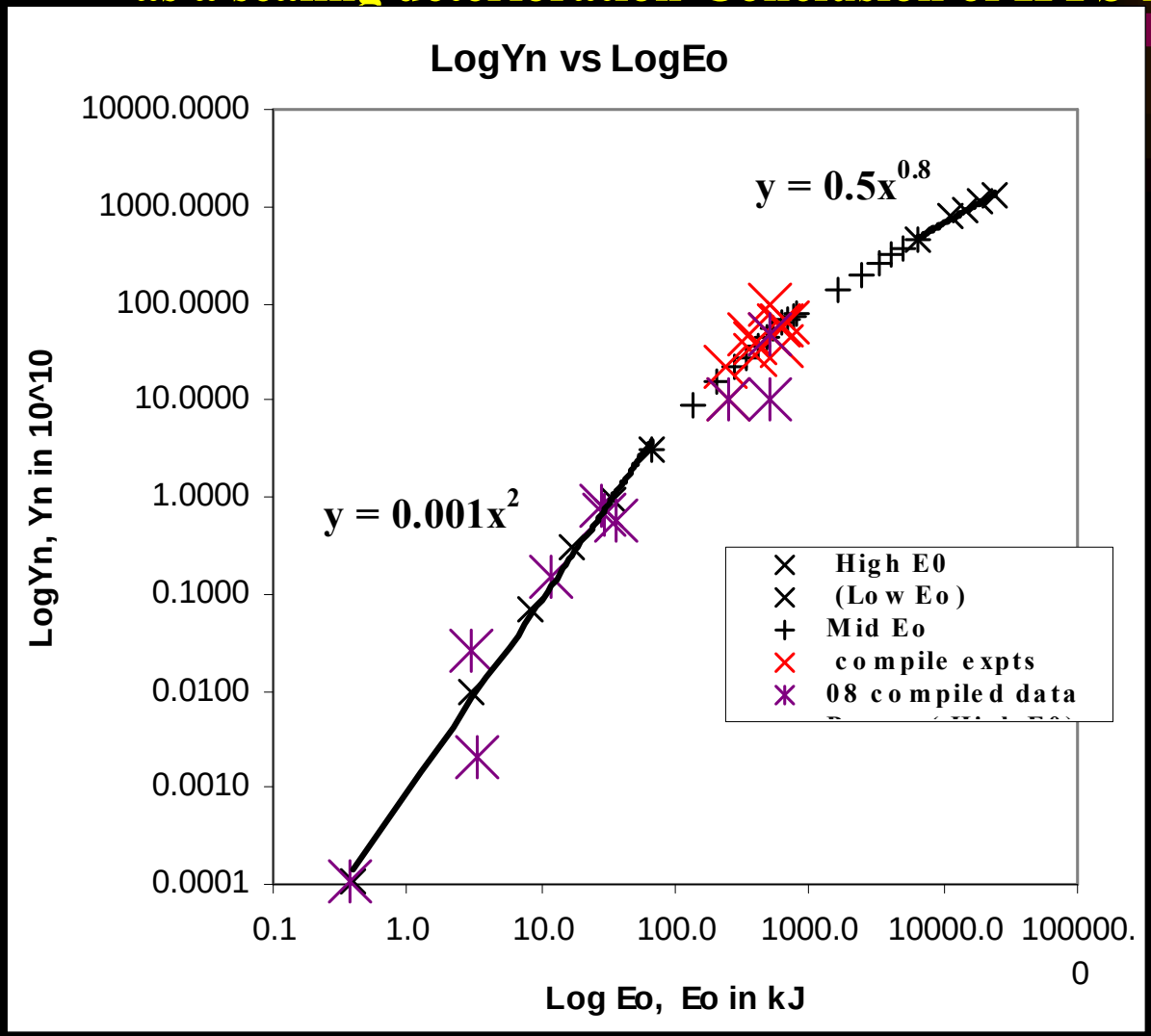

- **S Lee & S H Saw**, J Fusion Energy, 27 292-295 (2008)
- **S Lee**, Plasma Phys. Control. Fusion, 50 (2008) 105005
- **S H Saw & S Lee**. Scaling the plasma focus for fusion energy. Nuclear & Renewable Energy Sources Ankara, Turkey, 28 & 29 September 2009.
- S Lee Appl Phys Lett 95, 151503 (2009)

Plasma Focus
Axial and Radial Phases

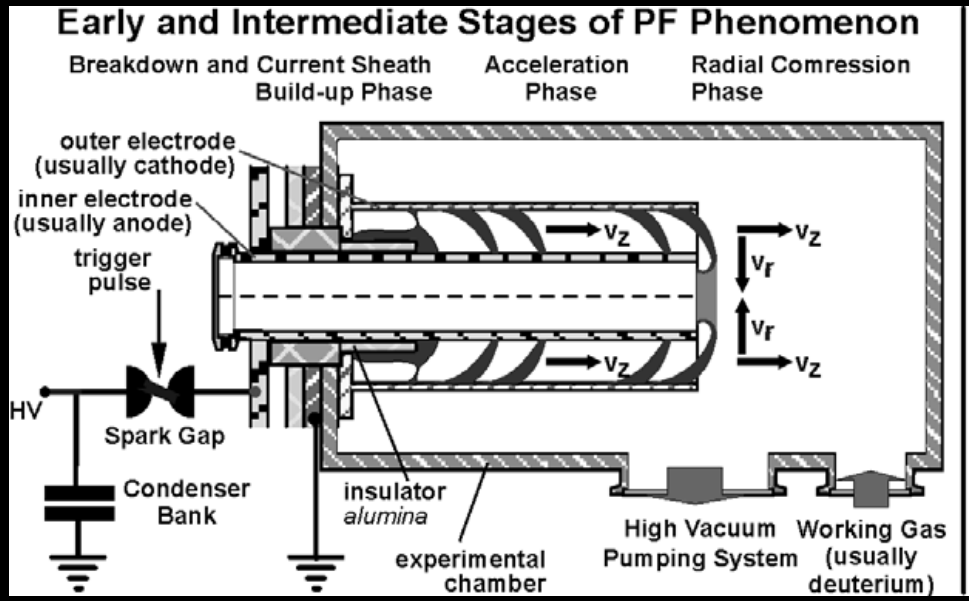

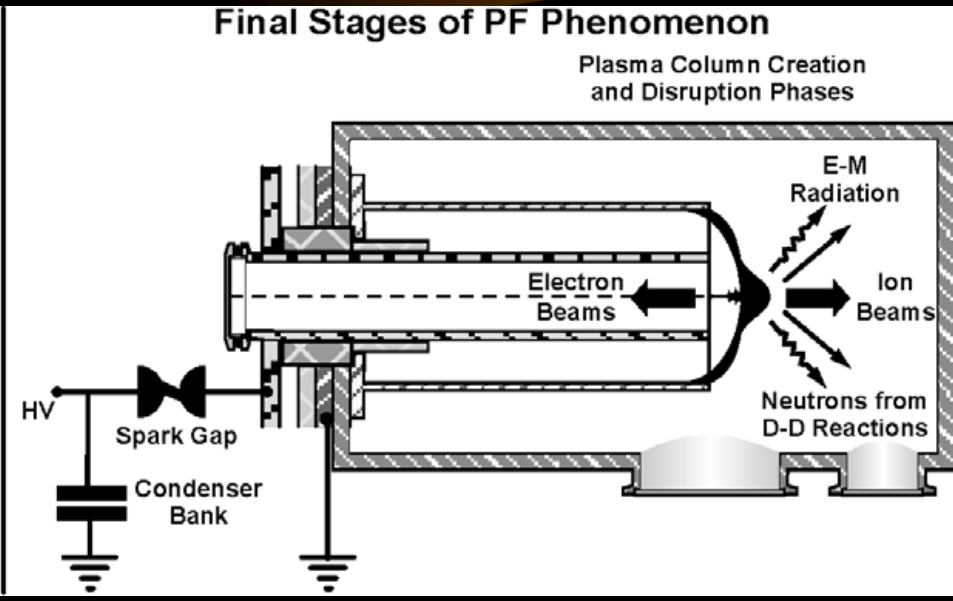

Schematic of Plasma Focus Axial Phase

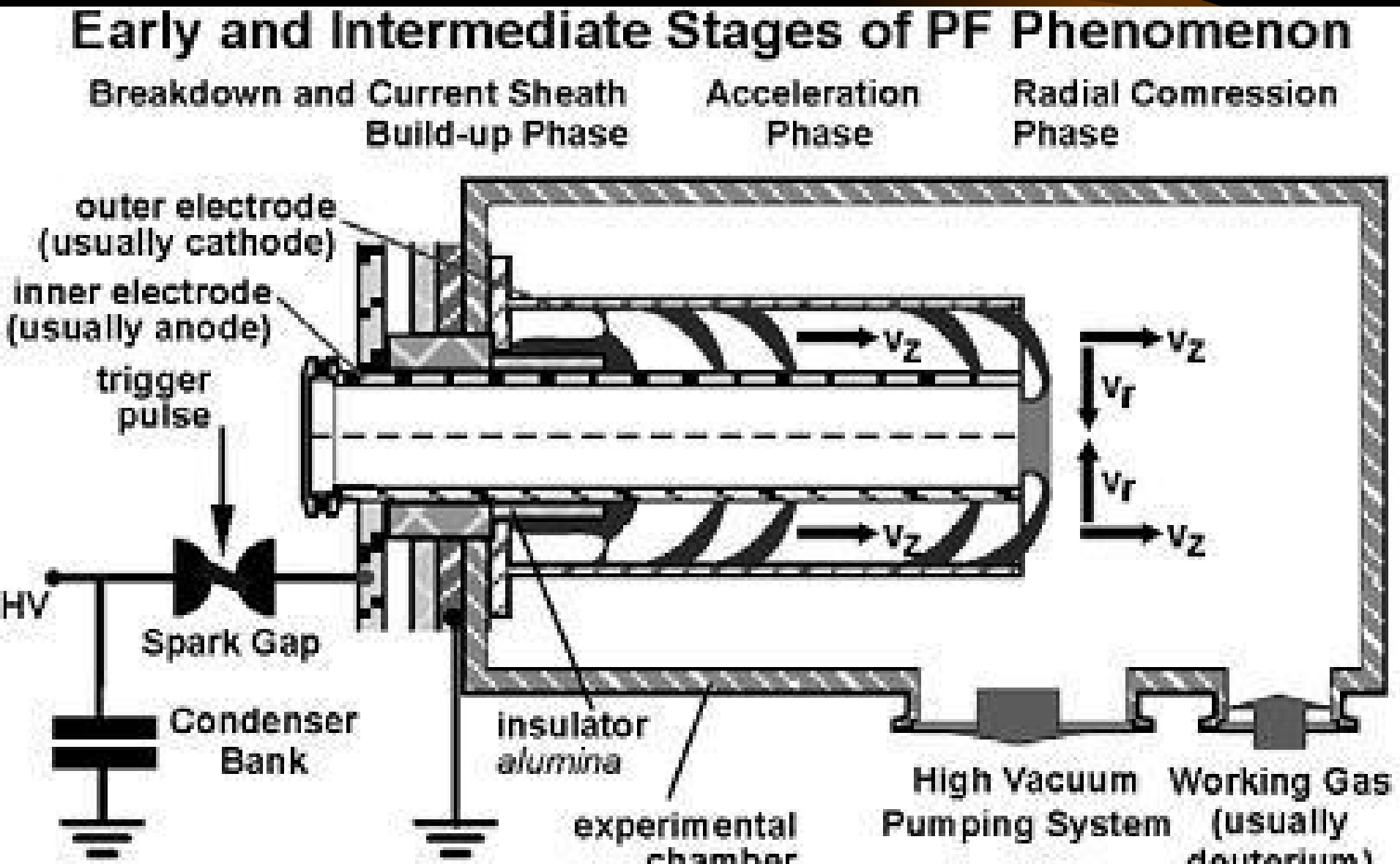

Circuit representation of Axial Phase of Plasma Focus (consider just the outside mesh only)

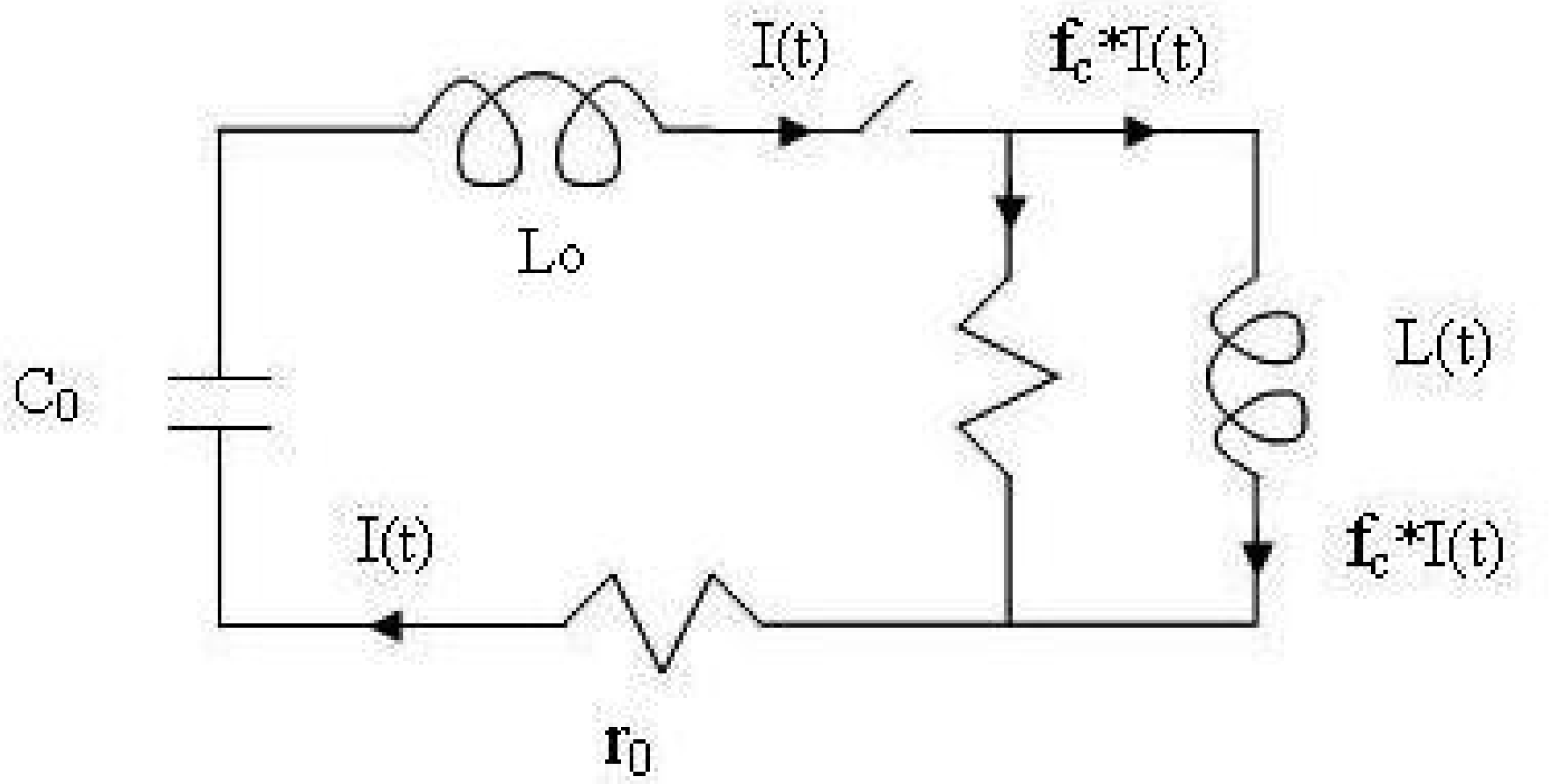

Comparing generator impedance & Dynamic Resistance DR_0 of small & large plasma focus- before I_{peak}

PF	$Z_0 = (L_0/C_0)^{1/2}$	Axial DR_0	Axial dominance	I_{peak}
Small	100 mΩ	7 mΩ	Z_0	~ V_0/Z_0
Large	1 mΩ	7 mΩ	DR_0	~V_0/DR_0

As E_0 is increased by increasing C_0, with voltage kept around tens of kV, Z_0 continues to decrease and I_{peak} tends towards asymptotic value of V_0/DR_0

Confirming I_{peak} saturation is due to constancy of DR_0

I_{peak} vs E_0 from DR_0 analysis compared to model simulation

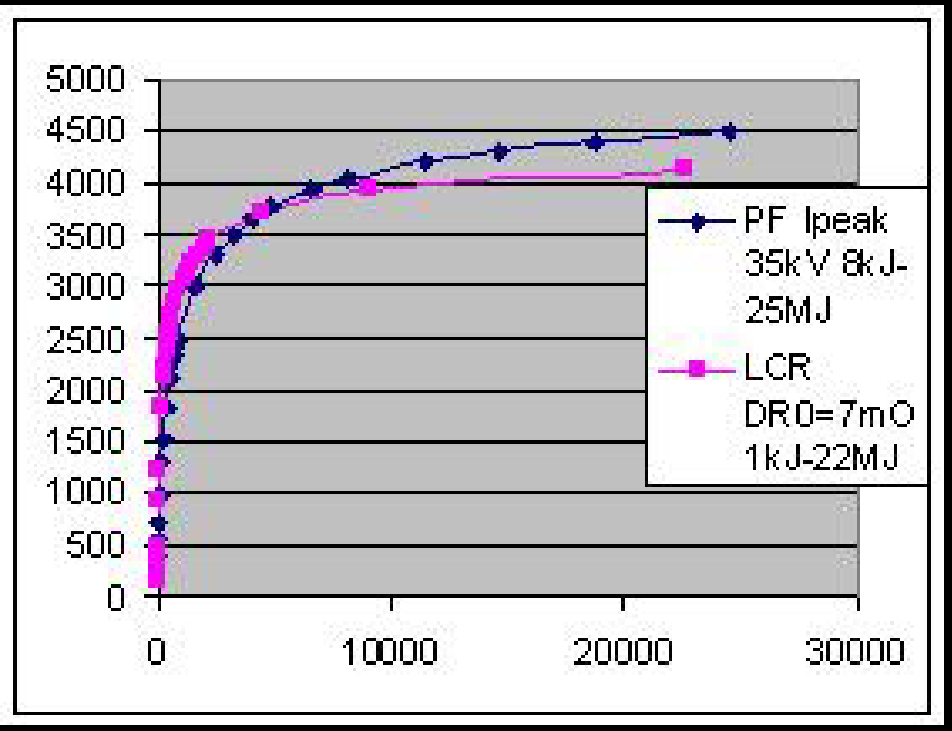

Model simulation gives higher I_{peak} due to a 'current overshoot effect' which lifts the value of I_{peak} before the axial DR_0 fully sets in

I_{peak} vs E_0 on log-log scale DR_0 analysis

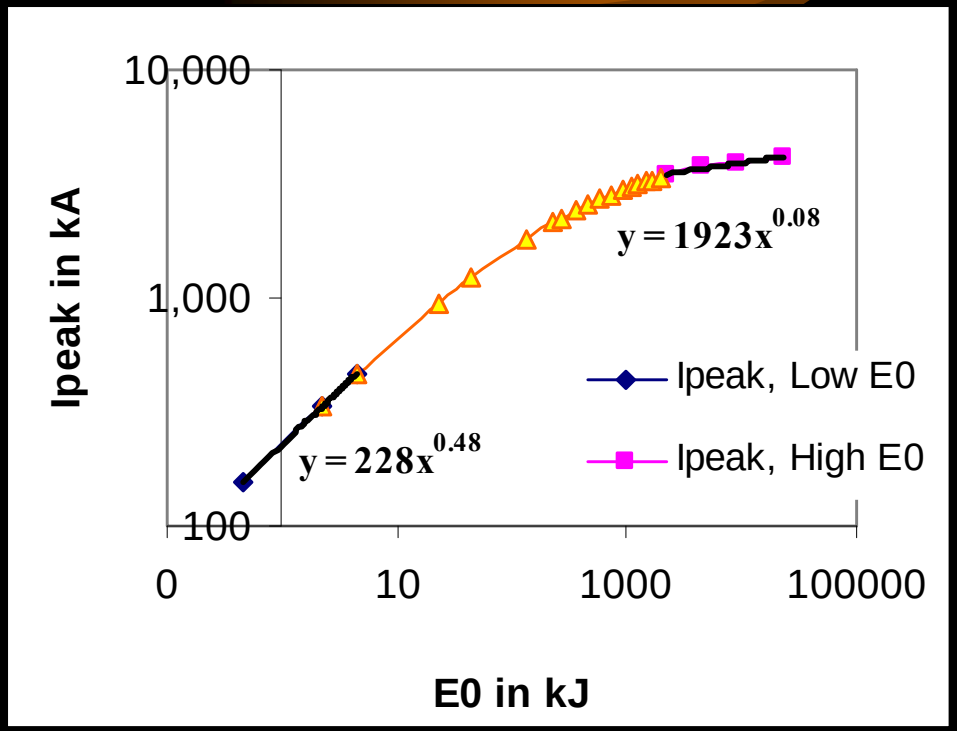

Confirming that I_{peak} scaling tends to saturate before 1 MJ

IPFS-INTI UC Project: we have shown that: constancy of DR_0 leads to current 'saturation' as E_0 is increased by increasing C_0. Tendency to saturate occurs before 1 MJ

From both numerical experiments as well as from accumulated laboratory data:

- $\mathbf{Y_n \sim I_{pinch}^{4.5}}$
- $\mathbf{Y_n \sim I_{peak}^{3.8}}$

Hence the 'saturation' of I_{peak} leads to 'saturation' of neutron yield Y_n

Insight into neutron 'saturation'

- **A fundamental factor for 'neutron saturation' is simply: Axial Phase Dynamic Resistance**

Beyond saturation?-to stimulate the development of Plasma Focus for fusion Energy

Possible ways to improve Y_n:

- **Increase operating voltage. Eg SPEED II uses Marx technology: 300kV, driver impedance 60 mΩ. With E_0 of under 200 kJ, the system was designed to give I_{peak} of 5 MA and I_{pinch} just over 2 MA.**
- **Extend to 1MV-with low bank impedance- would increase I_{peak} to 100 MA; at several tens of MJ. I_{pinch} could be 40 MA**
- **Y_n enhancing methods such as doping deuterium with low % of krypton.**
- **Further increase in I_{pinch} by fast current-injection near the start of radial phase. This could be achieved with charged particle beams or by circuit manipulation such as current-stepping. This model is ideally suited for testing circuit manipulation schemes.**
- **Technology of ultra-high voltages, and multiple circuits have to mastered.**

Ongoing IPFS-INTI UC numerical experiments of Multi-MJ, High voltage MJ and Current-step Plasma Focus

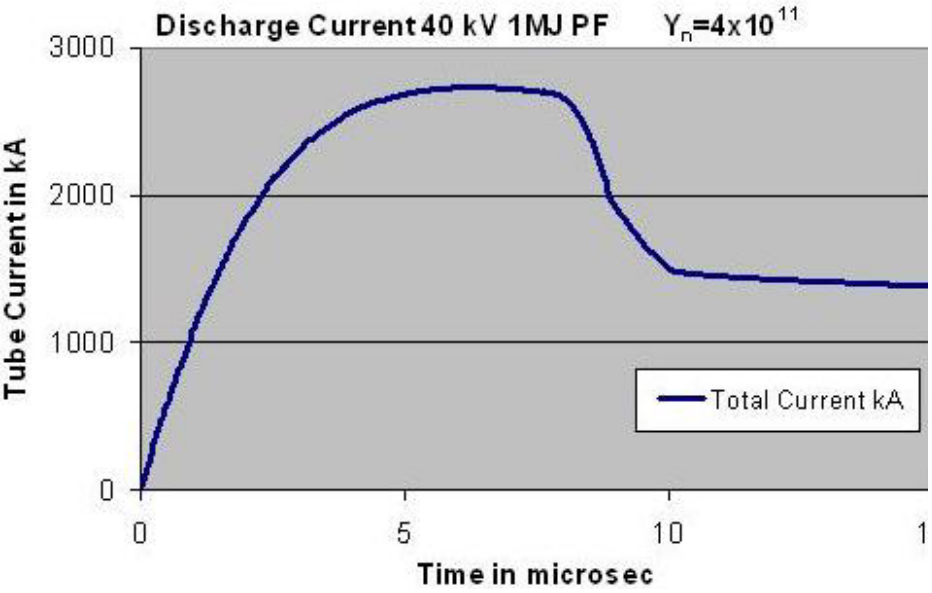

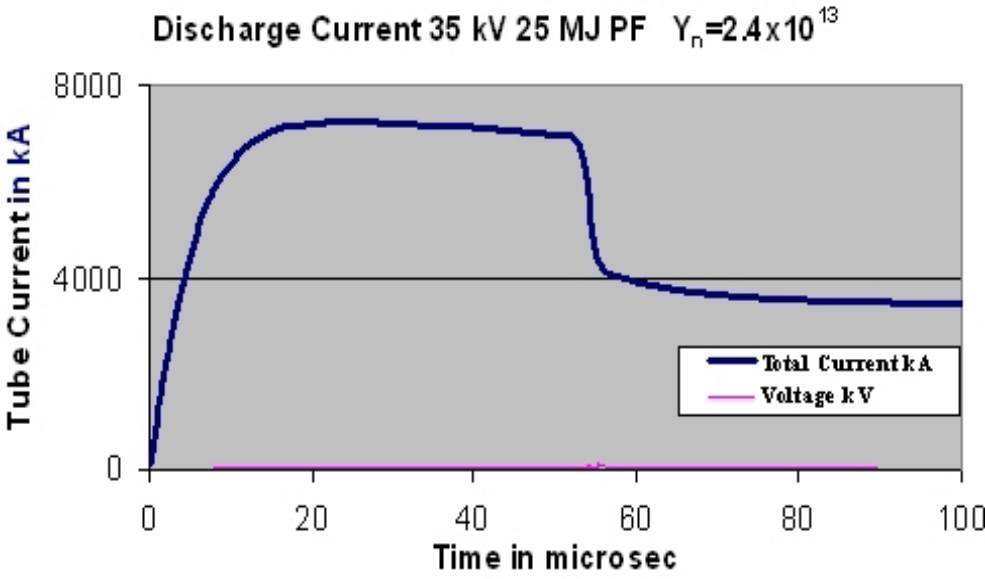

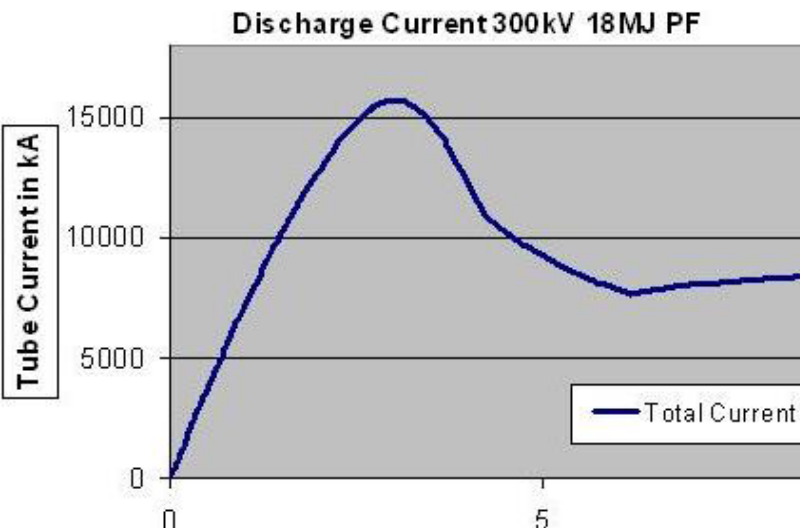

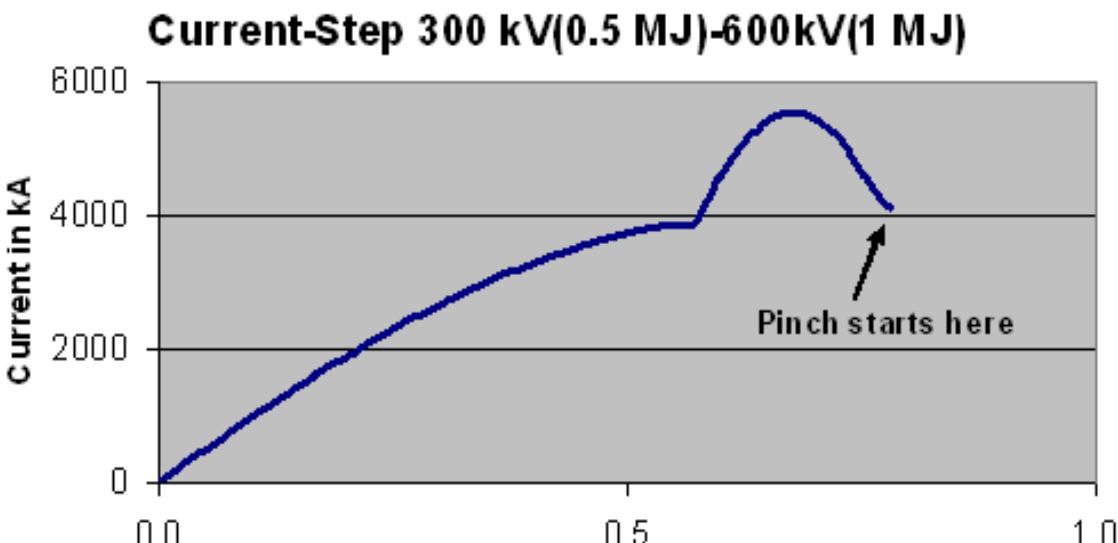

This latest research breakthrough by the IPFS-INTI UC team will enable the plasma focus to go to beyond saturation regimes. The plasma focus could then become a viable nuclear fusion energy scheme.

Conclusions

- **Tokamak programme is moving steadily towards harnessing nuclear fusion energy as a limitless clean energy source for the continuing progress of civilisation**

- **Alternative and smaller scale experiments will also play a role in this most challenging technological development**

THANK YOU *Appreciation to the following web-sites:*

- **http://fusion.gat.com**
- **http://chandra.harvard.edu**
- **http://fire.pppl.gov**
- **http://www.jet.efda.org**
- **http://www.iter.org**
- **http://www.fusion.org.uk**
- **http://www-jt60.naka.jaeri.go.jp**
- **http://www.hiper-laser.org/**
- **http://www.intimal.edu.my/school/fas/UFLF**
- **http://www.plasmafocus.net**

The effect of anode shape on neon soft x-ray emissions and current sheath configuration in plasma focus device

2009 J. Phys. D: Appl. Phys. 42 045203

(http://iopscience.iop.org/0022-3727/42/4/045203)

IOP PUBLISHING JOURNAL OF PHYSICS D: APPLIED PHYSICS

J. Phys. D: Appl. Phys. **42** (2009) 045203 (10pp) doi:10.1088/0022-3727/42/4/045203

The effect of anode shape on neon soft x-ray emissions and current sheath configuration in plasma focus device

M A Mohammadi[1,2], S Sobhanian[1], C S Wong[3], S Lee[2], P Lee[2] and R S Rawat[2,4]

[1] Faculty of Physics, University of Tabriz, Tabriz, Iran
[2] Natural Sciences and Science Education, National Institute of Education, Nanyang Technological University, Singapore
[3] Plasma Research Laboratory, Physics Department, University of Malaya, Kuala Lumpur, Malaysia

E-mail: rajdeep.rawat@nie.edu.sg

Received 4 August 2008, in final form 10 November 2008
Published 15 January 2009
Online at stacks.iop.org/JPhysD/42/045203

Abstract

The effect of three different anode shapes, flat, tapered and hemispherical, on the x-ray emission characteristics of a neon filled UNU–ICTP plasma focus device is investigated. The current sheath dynamics, in the radial collapse phase, has been simultaneously interrogated using the laser shadowgraphy method to understand the variation in x-ray emission characteristics for anodes of different shapes used in the experiments. The maximum neon soft x-ray (SXR) yield for the flat anode is about 7.5 ± 0.4 J at 4 mbar, whereas for hemispherical and tapered anodes the neon SXR is almost halved with the optimum pressure shifting to a lower value of 3 mbar. The laser shadowgraphic images confirm that the reduction in the overall neon SXR yield is due to the reduced focused plasma column length for these anodes. The relative HXR yield was the highest for the hemispherical anode followed by the tapered and the flat anodes in that order. The shadowgraphic images and the voltage probe signals confirmed that for the hemispherical anode the multiple-pinch phenomenon was most commonly observed, which could be responsible for multiple HXR bursts for this anode with maximum HXR yields.

1. Introduction

Dense plasma focus (DPF) is essentially a pulsed electric gas discharge between coaxially arranged electrodes. DPF devices belong to the family of dynamic Z-pinches which are self-constricted plasma configurations. They were originally developed in the early 1960s independently in the former Soviet Union (Filippov type) [1] and the USA (Mather type) [2] with $D/H > 1$ and $D/H < 1$, respectively, where D and H are the diameter and the height of the anode, respectively. Recently, some investigations [3, 4] have been done on the development of small PF devices operating in the range of tens to hundreds of joules of capacitor bank energy instead of the kilojoule or megajoule range. The DPF devices are pulsed plasma generators with a relatively simple operating principle that makes use of a self-generated magnetic field, for compressing the plasma to very high densities ($\approx 10^{25}$–10^{26} m^{-3}) and high temperatures (1–2 keV). The DPF has been historically established as a fusion device due to the intense bursts of neutrons it produces when operated in deuterium. The DPF device, however, is not only a source of fusion neutrons [5] but also produces highly energetic ions [6], relativistic electrons [7] and an abundant amount of soft x-ray (SXR) and hard x-ray (HXR) [8–11].

An important part of the experimental studies on x-ray and particle emission from DPF is oriented to interesting applications such as contact microscopy, x-ray and electron beam lithography, x-ray radiography and micro-machining [12–18]. In these applications, it is important to be able to accurately monitor and measure the SXR yield or dosage. Typically, silicon PIN diodes, together with appropriate filters, have been employed as pulsed x-ray detectors [19, 20]. The PIN diode's inherent fast rise times, high quantum efficiency and excellent stability in intense radiation environments make

[4] Author to whom any correspondence should be addressed.

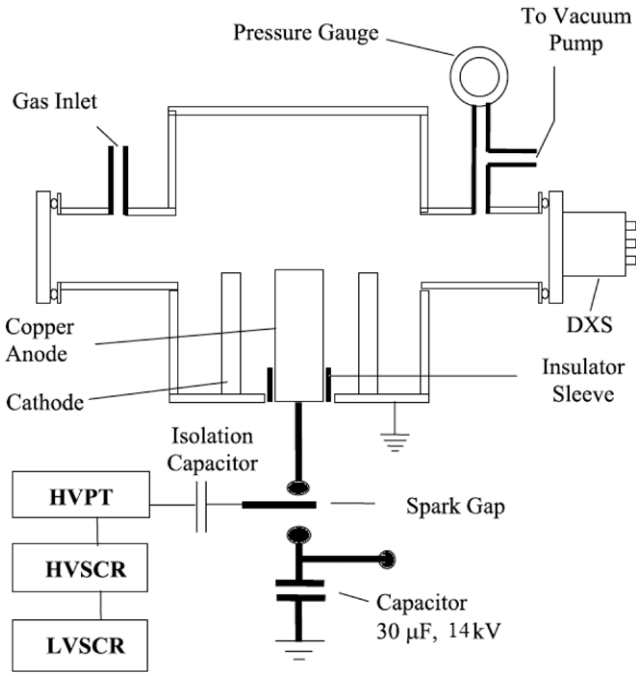

Figure 1. The two-dimensional view of the DPF device.

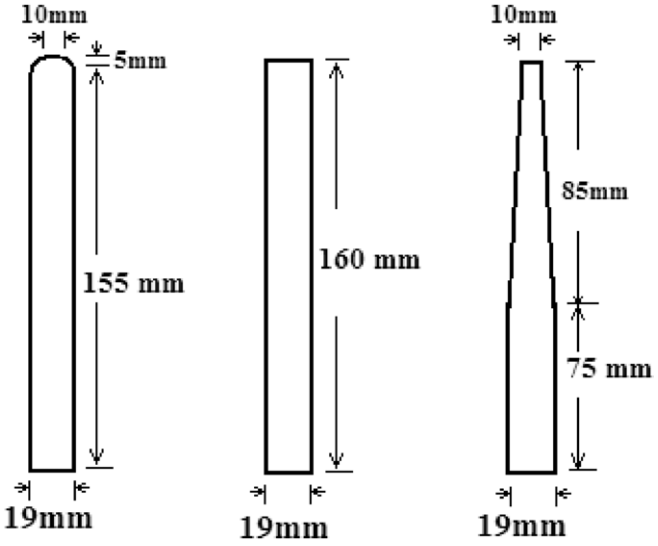

Figure 2. Configuration of anode shapes used in the experiment.

it well suited as x-ray detectors for pulsed plasma devices. In particular, the BPX65 type PIN diode has been commonly used. It has been used not only for measuring the SXR yield [15] but also to monitor the temporal characterization of x-ray emission [21, 22] and to determine the time-resolved plasma electron temperature [23]. The nanosecond N_2-laser shadowgraphy is used as an effective method of assessing plasma dynamics by providing a quick and comprehensive picture which would be difficult to obtain by other methods.

Previously, the effect of anode shape on argon x-ray energy and also on SXR energy from nitrogen and hydrogen plasmas was studied for Mather-type PF by Zakaullah *et al* [24] and Bhuyan *et al* [25]. In this paper, the effect of anode shape on the plasma focus neon SXR and also on the current sheath configuration in the radial collapse phase is investigated and reported. To the best of our knowledge, this is the first paper that reports the effect of anode shape on the current sheath configuration and dynamics by the laser shadowgraphy method to understand the radiation emission characteristic of a neon filled DPF device fitted with different anode shapes.

2. Experimental setup and diagnostics

We used the DPF device designated at the United Nations University–International Center for Theoretical Physics Plasma Focus Facility (UNU–ICTP PFF) [26]. The two-dimensional view of the DPF device is shown in figure 1. It is a Mather-type focus device, energized by a single 30 μF, 15 kV fast discharging capacitor, with maximum energy storage of 3.3 kJ. In our investigation, the device was operated at a charging voltage of 14 kV. The typical peak discharge current is about 170 kA. The electrode system consists of an anode and a cathode consisting of six copper rods arranged in a circle of 6.4 cm diameter concentric with the anode. A schematic of the different types of anodes used in this investigation is given in figure 2. The anode length in each case is 160 mm, measured from the cathode base plate. The diameters of the flat, hemispherical and tapered anodes in the radial phase are 19 mm, 10 mm and 10 mm, respectively. The insulator sleeve is made of Pyrex glass and the device is operated with neon as a working gas.

We performed shadowgraphy to study the symmetry and shape of the fast moving current sheath in the axial and radial collapse phases of the DPF device equipped with anodes of different shapes. The setup of the shadowgraphy system is shown in figure 3. It consists of (a) a 337.1 nm home-made TEA nitrogen laser as a source, (b) a telescopic arrangement of two lenses L1 and L2 to obtain the probing laser beam of 30 mm diameter, (c) an imaging system consisting of lenses L3 and L4 to obtain a proper magnification of the laser probing window on a CCD camera chip, (d) two narrow bandpass interference filters, centred at 340 nm, to cut off most of the unwanted plasma light, (e) a JETVIEW Jb-361 CCD (Charge Coupled Device) camera and (f) a video capture card, coupled to the CCD camera, operated using mgrab® programmed on the Linux® platform to record the shadowgraphs. The laser probing window of about 30 mm diameter was used to record the shadowgraphs of the plasma at various stages of plasma focus dynamics. In order to cut off most of the plasma light, an aperture stop of approximately 1 mm diameter was placed in the focal plane of lens L3. A delay unit was used in laser flash line to introduce a suitable delay to capture shadowgraphs at different time instants.

The voltage across the DPF was monitored by a voltage probe (resistive divider). The voltage probe signal with a laser pulse signal is shown in figure 4. The laser timing instant (t_l) of the shadowgraphs has been obtained using the laser pulse (captured using a BPX65 photodiode) and the voltage probe signals. The time t_l is the time difference between the first peak of the voltage probe signal ($t = 0$) and the laser flash time instant and it is marked in figure 4. It may be noted that

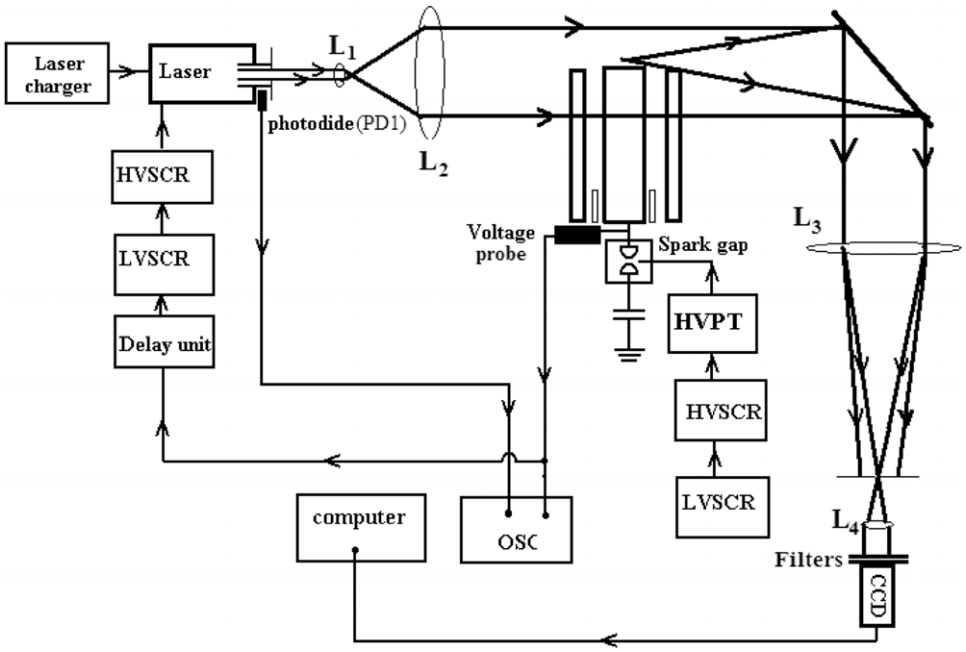

Figure 3. Shadowgraphic setup on the plasma focus with various subsystems.

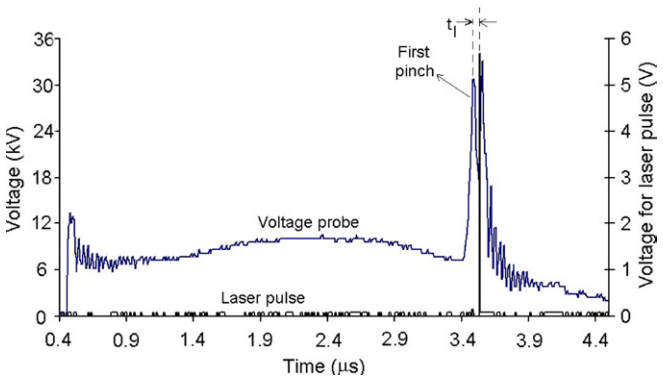

Figure 4. Typical voltage probe and laser pulse signals. (This figure is in colour only in the electronic version)

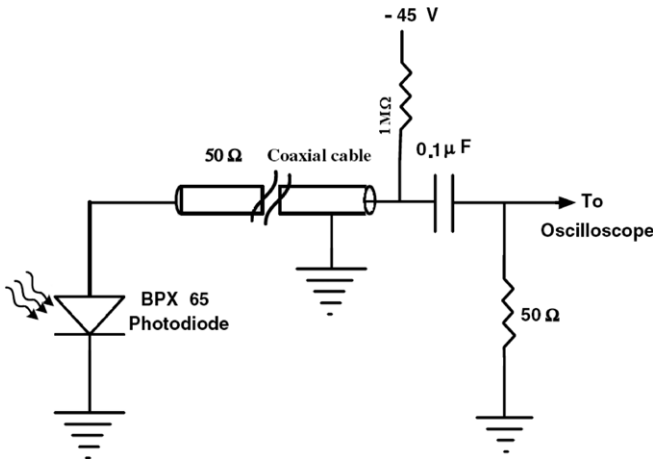

Figure 5. The BPX65 photodiode with bias circuit used in the experiment.

the uncertainty in the laser time instant, caused by the digitizing step size of the oscilloscope, is about 5 ns.

The diagnostic used to record the x-ray emissions in the DPF was a five channel diode x-ray spectrometer (DXS). The DXS provided information on the time evolution of x-rays in the DPF. The signals from DXS were also used to estimate the total radiated x-ray energy [26]. The five channel DXS assembly consisted mainly of an array of five windowless silicon p–i–n diodes (BPX65) covered with different x-ray filtration foils. The whole assembly was housed inside a small chamber. Individual bias voltage was provided by a regulated power supply having five output terminals each of −45 V. The BPX65 photodiode with the bias circuit is shown in figure 5. A four channel digital storage oscilloscope (5 GS s^{-1}, 1 GHz) was used to record x-ray signals. The attenuating filters used in four channels were 20 μm aluminium, 10 μm aluminium + 125 μm Mylar, 16 μm Co + 125 μm Mylar and 20 μm Ni. In our experiment we used two channels (covered with 20 μm Al and 10 μm Al + 125 μm Mylar) to calculate the SXR yield. The silicon diode sensitivity curves with these two filters for photons up to 10 keV energy are plotted in figure 6.

3. Experimental results

3.1. Neon x-ray emission results

For the measurement of the neon SXR yield, we used two filters which have overlapping sensitivities for the HXR region whereas their sensitivity for SXR is significantly different, as shown in figure 6. In plotting the sensitivity curve shown in figure 6, the characteristics of the BPX65 photodiode were taken into account. The radiation sensitive area, intrinsic silicon wafer thickness and dead layer thickness are 1 mm^2, 10 μm and 0.5 μm, respectively. Figure 6 shows that both DXS channels covered with 20 μm aluminium and 10 μm aluminium plus 125 μm Mylar filters transmit

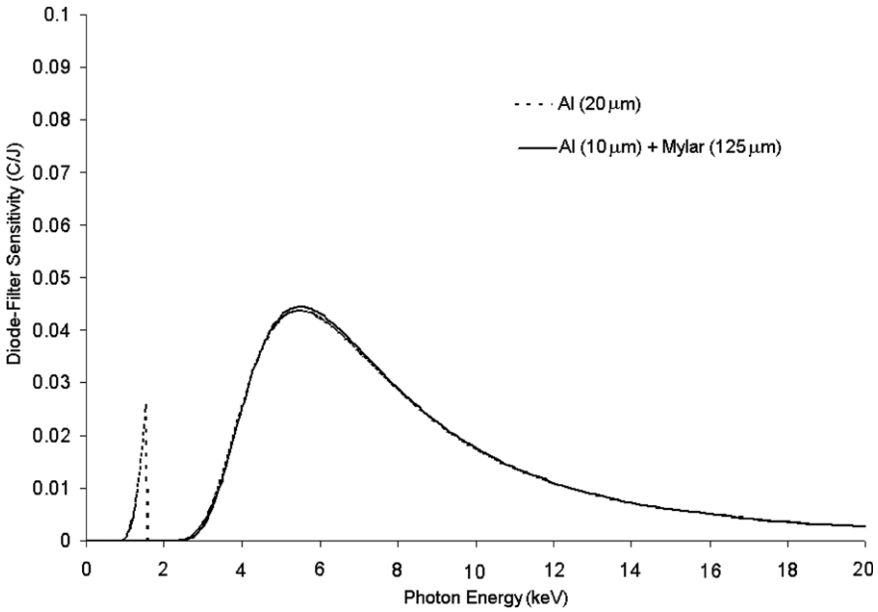

Figure 6. Transmission of 20 μm aluminium and 10 μm aluminium plus 125 μm Mylar filters used in the experiment.

HXRs, which are emitted mainly by electron bombardment of anode material. One may also note, from figure 6, that the thermal neon plasma, which radiates in the SXR range of 900–1550 eV [27], will not generate any signal on the DXS channel covered with 10 μm aluminium plus 125 μm Mylar filter. The oscilloscopic traces of x-ray signals for typical plasma focus shots are shown in figure 7. In these traces, x-ray signals for optimum pressure (in that pressure the yield of SXR is maximum) operation for each of the different anode shapes are provided. The SXR and HXR peaks (or their combinations) are identified in figure 7 on the basis of the difference in the area under the identified peaks as well by taking into account the estimated cross calibration factors of the PIN diodes involved in the recording of these signals: for the peak identified as SXR there is hardly any signal on the second channel, for the peak identified as HXR the area under the peaks on both channels is approximately the same and the peak identified as a mixture of SXR and HXR components has an area under the peak on channel 1 bigger than that under channel 2.

The flat anode, for optimized pressure, during the first pinch phase mostly radiates in the SXR regime corresponding to characteristic neon line emissions and hot neon plasma bremsstrahlung emissions. This is indicated by strong SXR peaks, S1 and S2, from the channel covered with a 20 μm aluminium filter in figure 7(*a*) and almost no signal on the other channel corresponding to S1 and a relatively weak HXR peak H1 corresponding to S2. It may, however, be noted that during the subsequent pinching the plasma focus mostly radiates HXRs as indicated by similar peaks, H2, H3 and H4, from the two channels of DXS. A careful analysis of figures 7(*b*) and (*c*) shows that for the plasma focus with tapered and hemispherical anode shapes, both SXRs and HXRs are emitted during all the pinch phases of plasma focus as indicated by relatively similar signal strengths on the two channels. This means that for HXR production the tapered and the hemispherical anodes are better while the flat anode is the best option for neon SXR emission.

For all the three anode configurations, we scanned the neon gas filling pressure and recorded fifteen shots for each of the selected pressure. For minimizing the effect of impurities we used a continuous flow of gas. The averages of the total SXR yields for three different anodes and different gas pressures are shown in figure 8. The maximum SXR energy is 7.5 ± 0.4 J for the flat anode, 4.0 ± 0.3 J for the tapered anode and 3.3 ± 0.2 J for the hemispherical anode.

3.2. Shadowgraphy results

The current sheath evolution in the radial collapse phase of the plasma focus device for three different anode shapes is shown in laser shadowgraphic sequences shown in figure 9. As seen from this figure, the current sheath shape and its thickness are affected by the anode shapes. It is clearly seen from these images that the length of the pinched plasma column is significantly reduced for the tapered and the hemispherical anodes as compared with the flat anode, which is a direct result of the reduced anode radii used for these two anodes. This fact is more obviously noticed in the set of shadowgraphs provided in figure 10. The shadowgraphs shown in figure 10 are taken at a time instant of 35 ns before maximum compression, i.e. final pinch plasma column formation. In these pictures, the space between the flat top of the current sheath and the anode tip is 3.7 mm, 2.5 mm and 1.3 mm for the flat, tapered and hemispherical anodes, respectively.

Another interesting observation is that of shadowgraphic imaging evidence of multiple pinches in figure 11, more so often for the hemispherical anode. One may argue that they do not actually show 'several pinches' but probably show only several consecutive current sheaths which may or may not produce several pinches. However, it can logically be concluded, as discussed in detail in section 4.2, that some of these shadow images taken for the hemispherical anode do provide shadowgraphic evidence of multiple-pinch observation in the plasma focus device.

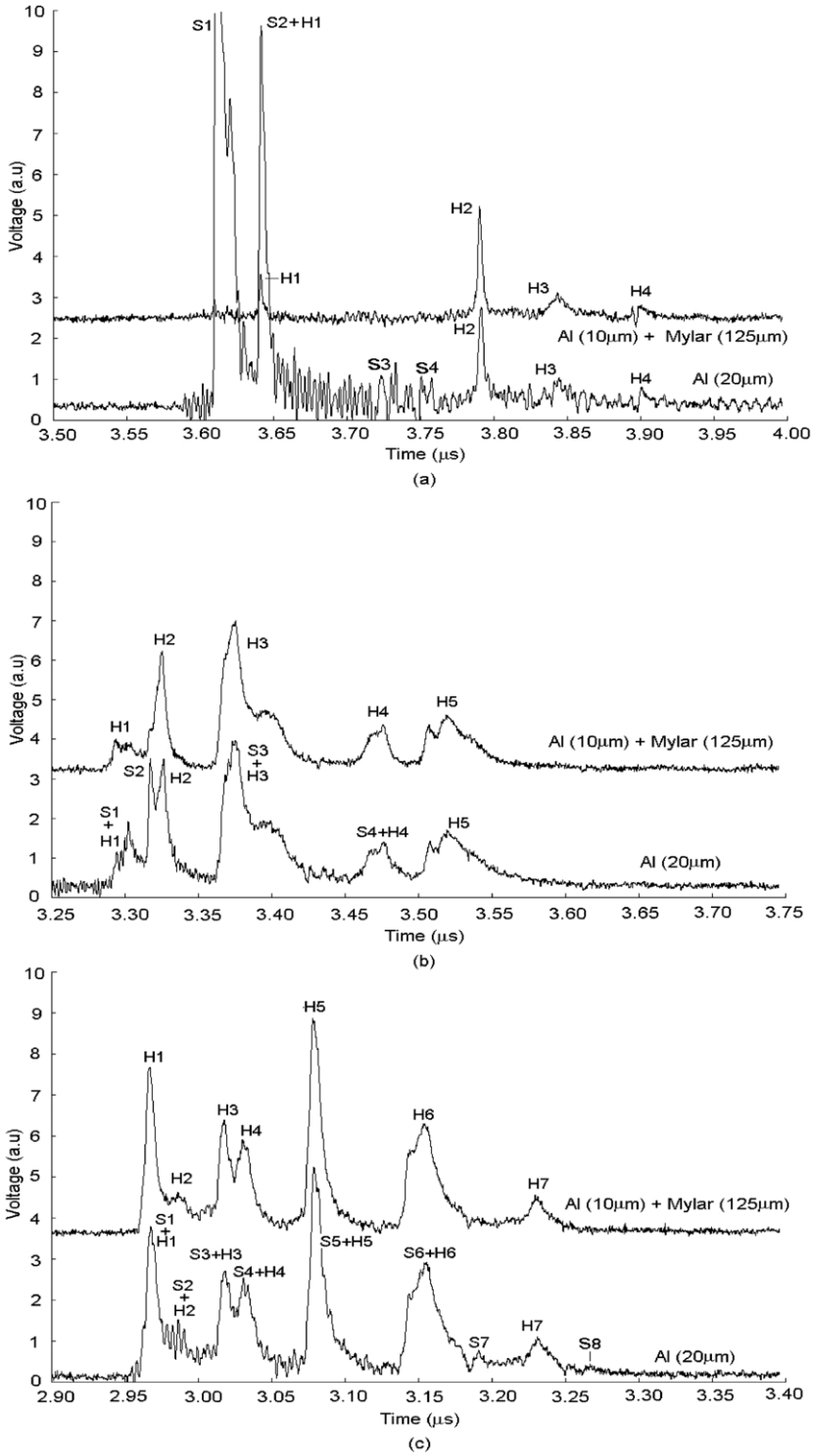

Figure 7. Typical waveforms of DXS signals at optimum pressure for (*a*) flat, (*b*) hemispherical and (*c*) tapered anode shapes.

4. Discussion

4.1. X-ray emission with anodes of different shapes

The reduction in the overall neon SXR yield for the tapered and the hemispherical anodes as compared with that of the flat anode, which is shown in figure 8, may be simply attributed to the reduction in the focused plasma column length for these anodes. The effective final anode radii for those geometries are approximately half of that of the flat anode. It is well known that the typical length and diameter of the pinch plasma column are directly related to the anode radius [28]. This argument is well supported by the shadowgraphic results, shown in figures 9 and 10, that the length of the pinched plasma column is significantly reduced for the tapered and the hemispherical anodes as compared with the flat anode due to reduced anode radii of these two anodes. Hence, the decrease in the radiating

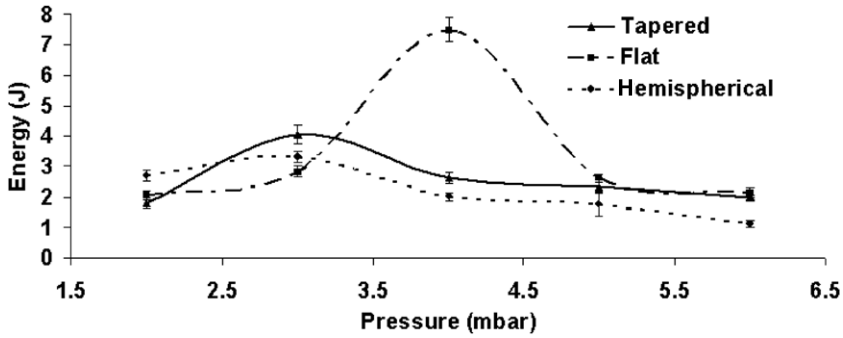

Figure 8. The neon SXR yield for different anode shapes at different gas pressures.

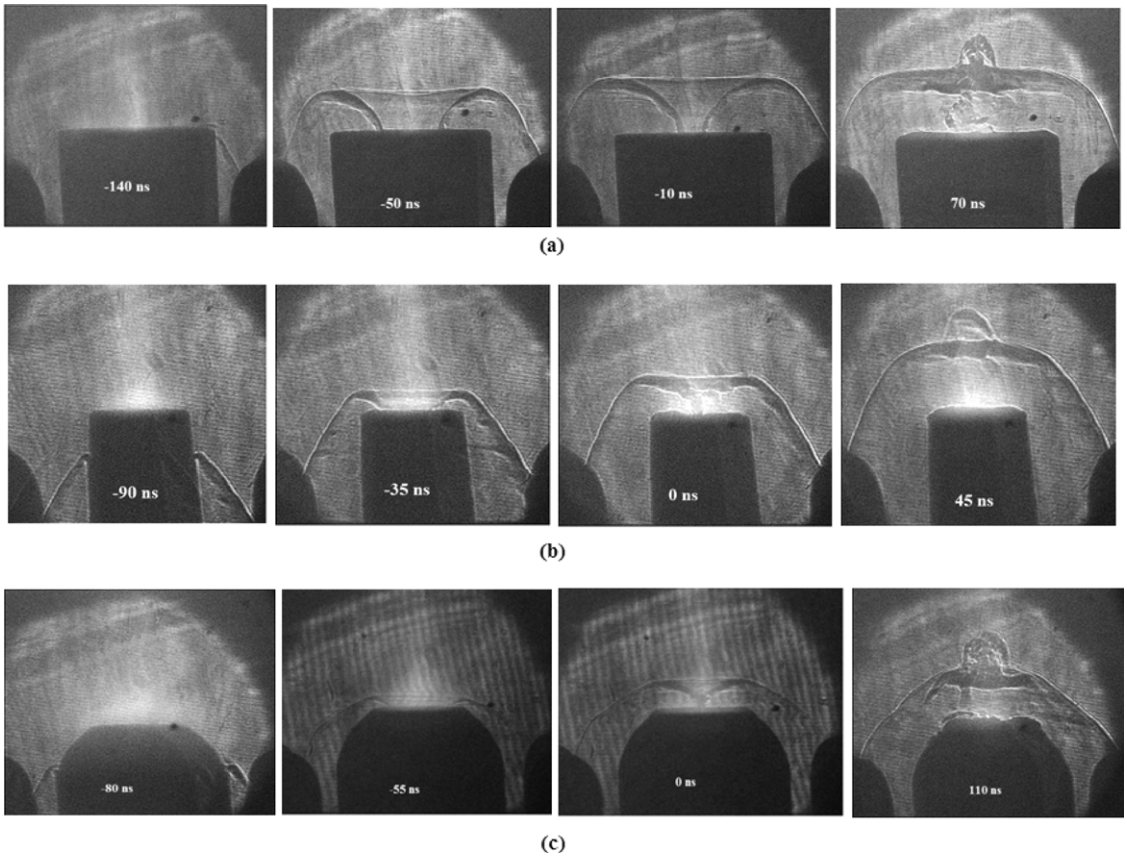

Figure 9. Shadowgraphs of current sheath dynamics in DPF of different anode shapes of (*a*) flat, (*b*) tapered and (*c*) hemispherical.

pinch plasma volume is responsible for the lowering of the neon SXR yield for the tapered and the spherical anodes used in this investigation as they have lower radii.

One of the effects of anode shape on neon SXR emission from the plasma focus, as seen in figure 8, is the shift in its optimum working pressure condition to lower pressures of 3 mbar for the tapered and the hemispherical anodes. For the UNU–ICTP machine with neon as a working gas, the optimum pressure is 4 mbar [21] for the flat anode. Experiments with the flat anode also confirm this pressure.

The quantity $I_0/(a\sqrt{\rho_0})$, defined as the speed factor [29] and directly related to the axial and radial speeds of current sheaths, is reported to have a consistent value of about $89 \pm 7\,\mathrm{kA\,cm^{-1}\,Torr^{-1/2}}$ for optimum neutron production for a wide range of plasma focus devices. The value of the speed factor for the SXR optimized pressure of 3 mbar for the tapered and the hemispherical anodes is significantly high at about $227\,\mathrm{kA\,cm^{-1}\,Torr^{-1/2}}$ due to reduced anode radius and lower optimized pressure, while for 4 mbar optimized pressure of the flat anode it is about $103\,\mathrm{kA\,cm^{-1}\,Torr^{-1/2}}$ which is close to the typical value. This is an interesting observation as we expect that probably the speed factor enhancement (or increased axial/radial speed) for the tapered and the hemispherical anodes due to almost halving of the anode radius will allow this device to be operated at a higher filling gas pressure. This is because almost similar speed factors will be obtained for two different anode configurations with (i) one having an anode of radius a and operated at an ambient gas density of ρ_0 and (ii) another having an anode of radius $a/2$ but operated at an ambient gas density of $4\rho_0$. As the anode length is kept the

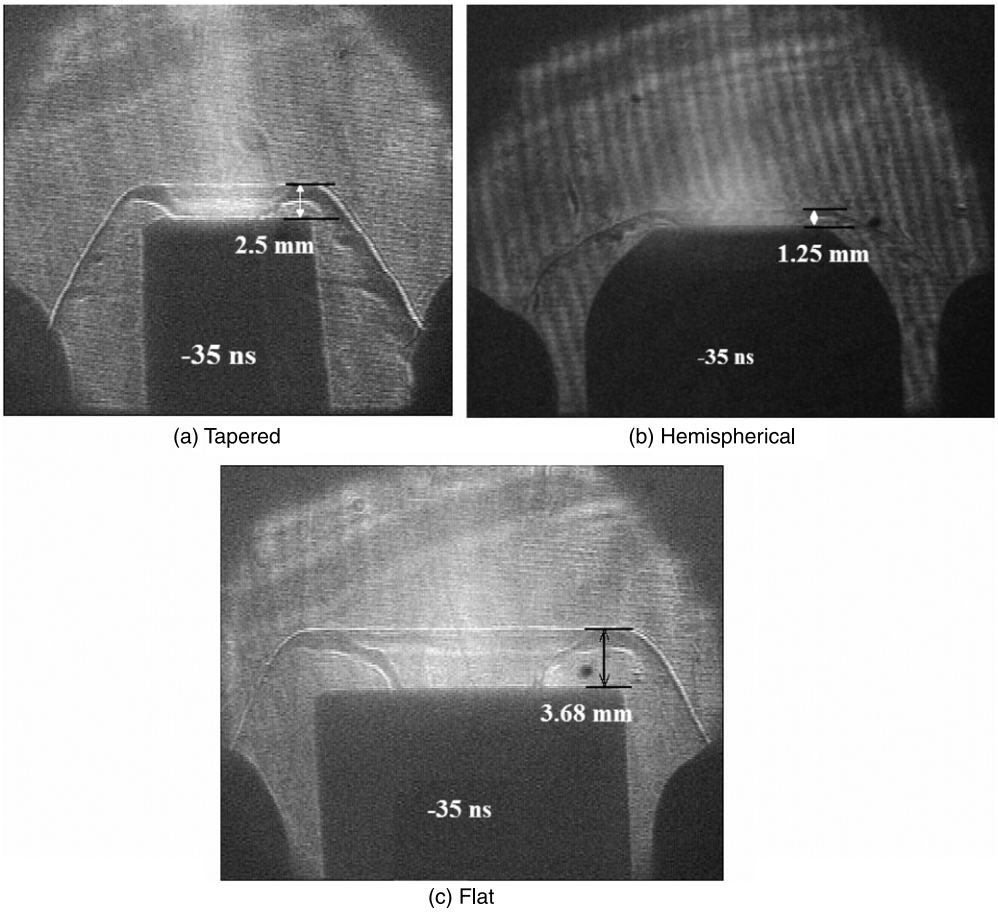

Figure 10. Typical shadowgraphic images for (*a*) tapered, (*b*) hemispherical and (*c*) flat anode shapes.

same and the second anode is tapered only over the last few centimetres of its length, the dynamic plasma inductance does not change significantly, especially for our UNU–ICTP device, as compared with the static inductance of the device which is about 110 nH. Hence the impedance and the peak discharge current do not change significantly. So, the enhancement of SXR emission will be expected if the optimized operation regime is shifted to a higher pressure. In the NX2 device, the change in anode shape from flat to tapered resulted in a high pressure operation regime with a significant increase in the neutron yield [30]. This investigation, however, reveals that this is not the case when it comes to SXR emission from the UNU–ICTP device and that too specifically for neon as the filling gas; the higher speed factor does not result in the shift in the SXR optimized regime towards higher neon operating pressures.

The observation and discussion in the preceding paragraph leads to the conclusion that for SXR emission from neon gas, the optimized speed factor values are different from that of neutron emission from deuterium. This is not unexpected, because to have a similar current sheath speed, an optimum neon pressure can be obtained by multiplying the optimum deuterium pressure by $\sqrt{M_{\mathrm{D}}/M_{\mathrm{Ne}}} = 1/\sqrt{5}$ (M_{D} and M_{Ne} are molar masses of deuterium and neon), i.e. about $\sqrt{5}$ times less as compared with that of deuterium optimum pressure. Knowing that the NX2 device for the tapered anode gives a maximum neutron yield at 20 mbar [30], the neon SXR maximum can be expected at about 9 mbar, while we got the maximum neon SXR yield at about 5–6 mbar [16]. Another important point to take note of is that the higher the current sheath speed during the radial collapse phase (i) the higher will be the pinch plasma temperature causing the increase in the thermonuclear component of neutron emission and (ii) the faster will be the changes in the pinch inductance resulting in hence a higher electric field and hence more efficient acceleration of deuterons resulting in increased beam–target component of the neutron yield. However, for the neon SXR emission the plasma temperature of about 200 eV is required for the maximum line radiation yield and it is for this reason that for the neon filled plasma focus operation the SXR emission starts during the early part of the radial collapse phase [31] and higher temperatures at higher speeds may reduce the neon line radiation emission efficiency. Hence, for optimized SXR operation we should not be comparing the speed factor value with 89 ± 7 kA cm^{-1} Torr$^{-1/2}$ reported for optimized neutron emission [29] but to some other value depending on the gas used in the machine.

Figure 12 shows the average number of x-ray peaks measured with a photodiode covered with 10 μm aluminium plus 125 μm Mylar. This is the number of HXR peaks. As is evident from figure 7, also discussed before, the plasma focus with tapered and hemispherical anodes emits both SXR and HXR in the compression and quiescent phases whereas the flat anode radiates mostly in the SXR range. Figure 12 also

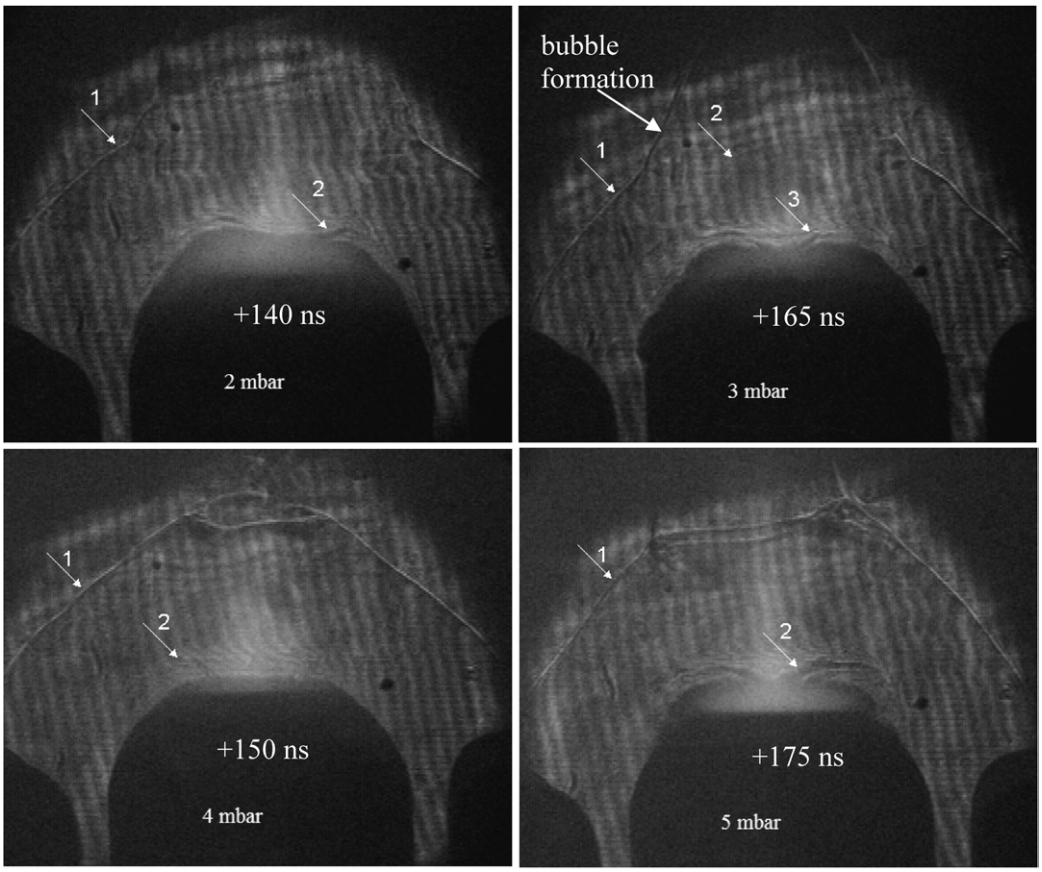

Figure 11. Some shadowgraphs showing the formation of multiple pinches.

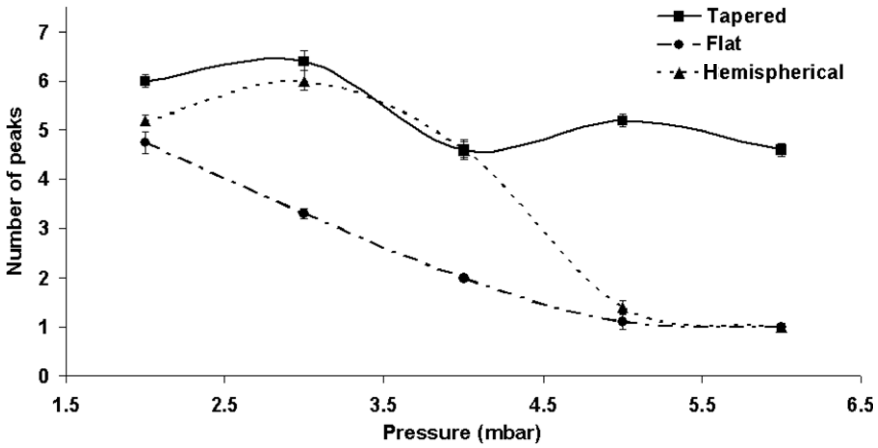

Figure 12. The number of x-ray peaks in photodiode signals.

emphasizes that the average number of HXR peaks produced by the tapered and the hemispherical anodes is much more than that for the flat anode in the optimum pressure regime of 3–4 mbar. At low pressure operation, they all essentially emit in the HXR regime.

The area under the curve of signal from the photodiode covered with aluminium (10 μm) + Mylar (125 μm) filter is proportional to the HXR emission yield which is shown in figure 13. From this figure one can note that the highest and the lowest HXR yields, at all neon operating pressures, are obtained for the hemispherical and the flat anodes, respectively. Another interesting feature to note is the continuous increase in HXR emission with the decreasing filling gas pressure, for all the anode shapes, which confirms that at smaller pressures the higher current sheath speeds make the plasma column more unstable and hence the instability accelerated electrons produce HXRs more efficiently.

4.2. Discussion on shadowgraphic observations

The shadow images shown in figure 10 are taken at similar time instants (−35 ns) before the final pinch column formation and

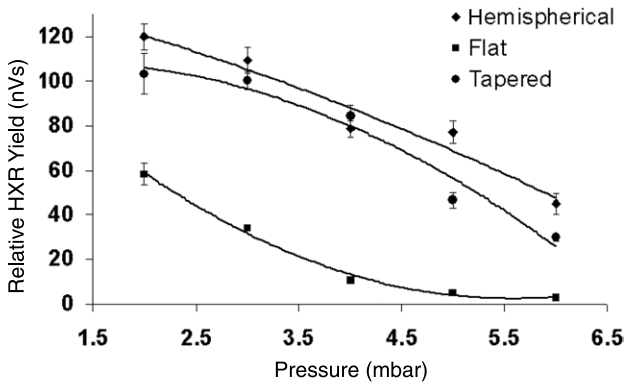

Figure 13. Relative HXR yields for different anode shapes.

hence it can be inferred from these images that the length of the pinch plasma column is the highest for the flat anode. Among the other two anodes, even though they have a similar final anode radius of 5 mm, the tapered anode will have a longer pinch column as compared with that of the hemispherical anode. The shadowgraphic results therefore suggest that the axial elongation of the current sheath, which controls the final pinch plasma column length, depends on the anode shape and hence contributes towards the different radiation yields from the anodes of different shapes.

As mentioned before, some of the shadow images shown in figure 11 do provide concrete evidence of multiple-pinch observation. For example, the shadow images captured at +165 and +175 ns, shown in figures 11(*b*) and (*d*), respectively, clearly show multiple pinching as the arrows labelled as '3' and '2' show the second pinch at the time instants of images as the sheath profile is similar to that of the pinching current sheath during the first pinch. The positive sign for the laser pulse time basically means that the images are captured at time instants after the first voltage probe peak, i.e. after the first pinch has already taken place. The arrow labelled as '1' points to the main current sheath whose central part, closer to the anode, participated in the first pinch earlier while the outer part, which is not disintegrated, is still in axial motion down the chamber. In fact, the shadow images shown in figures 11(*b*) and (*d*) clearly show the bubble formation on the frontal part of the current sheath marked by arrow '1', which is the evidence of strong focusing action during the first pinch (refer figure 6(*c*) of [32], figure 6(*b*) of [33] and last shadow images in figures 7(*a*), (*b*) and (*c*) of this paper). It has been reported that the $m = 0$ instabilities enhance the induced electric field which accelerates ions towards the top of the chamber which in turn cause an ionization front which soon overtakes the axial shock front (formed due to axial expansion of the current sheath) and develops into a bubble structure [34]. Hence, we can conclude that some of these shadow images, particularly the ones shown in figures 11(*b*) and (*d*), provide shadowgraphic evidence of multiple pinches with a bubble structure, on the current sheath labelled as arrow '1', indicating the previously occurring pinch and the second or third ongoing pinch of current sheath labelled as arrow '2' or '3'.

The formation of successive multiple pinches, observed in figure 10, can be explained in the following way: in the axial rundown phase, the snow plough efficiency of the current sheath is not 100% and hence this leaves back an atmosphere of low density neutral gas near the insulator sleeve. The first pinch/compression phase, indicated by the first peak in the voltage probe signal, is shown in shadowgraphs of figures 9 and 10. At this instant, another discharge on the insulator is produced and a second current sheath is produced which owing to the low density of gas in front of it moves much faster and collapses at the anode top as a second pinch/compression phase. This phenomenon can occur more than twice or thrice due to restrikes at the lower end of the electrodes generating multiple pinches. As the intensity of current as well as the non-plowed gas density is expected to decrease after each successive restrike, sheath formation, upward movement and compression, it becomes increasingly difficult to observe them shadowgraphically though the voltage probe signal will still show the spike corresponding to each pinching phase. Multiple-pinch column formation and their successive disintegration by instabilities may be responsible for successive energetic electrons and, thus, HXR generation in the plasma focus operating at low pressures or the plasma focus device with hemispherical and tapered anodes. The use of reduced anode radii for the tapered and the hemispherical anodes has resulted in higher speed factors for these anodes which probably brings in greater instability in the current sheath dynamics in the plasma focus device and hence in the multiple-pinch formation.

5. Conclusions

The change in the anode shape is found to affect the current sheath configuration and the x-ray emission characteristics of the neon filled UNU–ICTP plasma focus device. The maximum neon SXR yield for the flat anode is about 7.5 ± 0.4 J at 4 mbar and 4.0 ± 0.3 and 3.3 ± 0.2 J for the hemispherical and the tapered anodes, respectively, both at 3 mbar. The laser shadowgraphic images confirm that reduction in the overall neon SXR yield for the tapered and the hemispherical anodes can be attributed to the reduction in the focused plasma column length for these anodes as their radii were approximately half of that of the flat anode. It was also noticed that the relative yield of the HXR component was the highest for the hemispherical anode followed by the tapered and the flat anodes in that order. The shadowgraphic images and voltage probe signals confirmed that for the hemispherical anode the multiple-pinch phenomenon was most commonly observed which could be responsible for multiple HXR bursts for this anode with maximum HXR yields.

Acknowledgments

MAM acknowledges the Abdus Salam International Center for Theoretical Physics under the purview of the Asian African Association for Plasma Training (AAAPT) for financial support and the National Institute of Education, Nanyang Technological University, Singapore, for providing Non-Graduating Student status for six months to conduct research work at their Plasma Radiation Source Laboratory.

References

[1] Filippov N V, Filippova T I and Vinogradov V P 1962 *Nucl. Fusion Supl.* **2** 577
[2] Mather J W 1964 *Phys. Fluids* **S28**
[3] Soto L 2005 *Plasma Phys. Control. Fusion* **47** A361
[4] Verma R, Lee P, Springham S V, Tan T L, Krishnan M and Rawat R S 2008 *Appl. Phys. Lett.* **92** 011506
[5] Springham S V, Lee S and Rafique M S 2000 *Plasma Phys. Control. Fusion* **42** 1023
[6] Wong C S, Choi P, Leong W S and Singh J 2002 *Japan. J. Appl. Phys.* **41** 3943
[7] Patran A, Stoenescu D, Rawat R S, Springham S V, Tan T L, Tan L C, Rafique M S, Lee P and Lee S 2006 *J. Fusion Energy* **25** 57
[8] Zakaullah M, Alamgir A, Shafiq M, Sharif M and Waheed A 2002 *IEEE Trans. Plasma Sci.* **30** 2089
[9] Zakaullah M, Alamgir K, Shafiq M, Hassan S M, Sharif M, Hussain S and Waheed A 2002 *Plasma Sources Sci. Technol.* **11** 377
[10] Shafiq M, S Hussain, Waheed A and Zakaullah M 2003 *Plasma Sources Sci. Technol.* **12** 199
[11] Bhuyan H, Mohanty S R, Neagy N K, Bujarbarua S and Rout R K 2004 *J. Appl. Phys.* **95** 2975
[12] Lee S *et al* 2003 *Singap. J. Phys.* **173** 276
[13] Kato Y and Be S H 1986 *Appl. Phys. Lett.* **48** 686
[14] Gribkov V A, Srivastava A, Keat P L C, Kudryashov V and Lee S 2002 *IEEE Trans. Plasma Sci.* **30** 1331
[15] Beg F N, Ross I, Lorena A, Worley J F, Danger A E and Hanies M G 2000 *J. Appl. Phys.* **88** 3225
[16] Wong D, Patran A, Tan T L, Rawat R S and Lee P 2004 *IEEE Trans. Plasma Sci.* **32** 2227
[17] Hussain S, Shafiq M, Ahmad R, Waheed A and Zakaullah M 2005 *Plasma Sources Sci. Technol.* **14** 61
[18] Castillo F, Gamboa-deBuen I, Herrera J J E, Rangel J and Villalobos S 2008 *Appl. Phys. Lett.* **92** 051502
[19] Neff W, Eberle J, Holz R, Lebert R and Richter F 1989 *X-Ray Instrum.* **13** 1140
[20] Hussain S, Ahmad S, Khan M Z, Zakaullah M and Waheed A 2004 *J. Fusion Energy* **22** 195
[21] Rawat R S, Zhang T, Phua C B L, Then J X, Chandra K A, Lin X, Patran A and Lee P 2004 *Plasma Sources Sci. Technol.* **13** 569
[22] Silva P and Favre M 2002 *J. Phys. D: Appl. Phys.* **35** 2543
[23] Asif M and Ikram A 2004 *Plasma Sci. Technol.* **6** 2199
[24] Zakaullah M, Ahmad I, Omar A, Murtaza G and Beg M M 1996 *Plasma Sources Sci. Technol.* **5** 544
[25] Bhuyan H, Mohanty S R, Neog N K, Bujarbarua S and Rout R K 2004 *J. Appl. Phys.* **95** 2975
[26] Lee S, Tou T Y, Moo S P, Eissa M A, Gholap A V, Kwek K H, Mulyodrono S, Smith A J, Suryadi, Usada W and Zakaullah M 1988 *Am. J. Phys.* **56** 62
[27] Liu M, Feng X, Springham S V and Lee S 1998 *IEEE Trans. Plasma Sci.* **26** 135
[28] Lee S 1998 Scaling ot the plasma focus *Int. Workshop on Plasma Focus Research (PF98) (Kudowa, Poland, July 1998)* http://eprints.ictp.it/109/ (also in *First Conf. on Plasma Physics Applications, Int. Cooperation Bilateral Seminars* vol 34 2004 *Forschungszentrum Jülich Gmbh (Jülich, Germany)* pp 27–33)
[29] Lee S and Serban A 1996 *IEEE Trans. Plasma Sci.* **24** 1101
[30] Koh J M, Rawat R S, Patran A, Zhang T, Wong D, Springham S V, Tan T L, Lee S and Lee P 2005 *Plasma Sources Sci. Technol.* **14** 12
[31] Mohammadi M M, Verma R, Sobhanian S, Wong C S, Lee S, Springham S V, Tan T L, Lee P and Rawat R S 2007 *Plasma Sources Sci. Technol.* **16** 785
[32] Lee S, Alabraba M A, Gholap A V, Kumar S, Kwek K H, Nisar M, Rawat R S and Singh J 1990 *IEEE Trans. Plasma Sci.* **18** 1028
[33] Gupta R, Mohanty S R, Rawat R S and Srivastava M P 2000 *IEEE Trans. Plasma Sci.* **28** 1263
[34] Bernard A, Coudeville A, Jolas A, Launspach J and Mascureau J de 1975 *Phys. Fluids* **18** 180

Backward high energy ion beams from plasma focus

M. V. Roshan, P. Lee, S. Lee, A. Talebitaher, R. S. Rawat, and S. V. Springham
National Institute of Education, Nanyang Technological University, Singapore 637616, Singapore

(Received 11 May 2009; accepted 29 June 2009; published online 15 July 2009)

High energy neutrons, more than 2.45 MeV from deuteron-deuteron fusion reaction, have been measured in backward direction of plasma focus devices in many laboratories. However the experimental evidence for high energy deuterons responsible for such neutrons has not been reported so far. In this brief communication, backward high energy deuteron beam from NX2 plasma focus [M. V. Roshan *et al.*, Phys. Lett. A **373**, 851 (2009)] is reported, which was measured with a direct and unambiguous technique of nuclear activation. The relevant nuclear reaction for the target activation is $^{12}C(d,n)^{13}N$, which has a deuteron threshold energy of 328 keV.
 [DOI: 10.1063/1.3183715]

Plasma focus (PF) devices are essentially a form of Z pinch, with a characteristic feature of producing short lifetime plasma with high density and temperature.[1] The density and temperature remain relatively constant for PF devices in a wide range of energies from 1 kJ to 1 MJ.[2] It is an efficient source of D-D fusion neutrons of up to 10^{11} (Ref. 3) and high energy ions of a few MeV.[4] This is in spite of the fact that the charging voltage is one or two orders of magnitude less than the induced voltage in the pinch. Plasma focus devices have been extensively studied in a large number of laboratories; however, there is as yet no fully satisfactory explanation for the mechanism of ion beam acceleration and consequently neutron production.

Early observations of neutrons from pinched plasma devices were initially interpreted in terms of thermonuclear fusion. However it soon became clear that the observed neutron yields were much higher than the predictions of simple calculations based on plasma temperature, volume, and duration. Moreover, various experimental results from different plasma focus devices proved that most of the neutron yield could not come from thermonuclear fusion.[5] The evidence for their nonthermal origin came from observations of (i) neutron anisotropy (i.e., neutron fluence is higher in the axial direction), (ii) spread in neutron energies (away from 2.45 MeV as expected from thermonuclear fusion) and shape of the neutron spectra, and (iii) variation of mean neutron energy with direction.[6–9]

The experimental results of neutron production in plasma focus suggested that a substantial fraction of the neutrons are produced due to the axial acceleration of a comparatively small number of deuterons.[10] Based on experimental results, axial ion acceleration has been demonstrated by assuming a strong axial electric field.[11] However, the initial experiments showed that high energy ions are also generated in radial direction, and the angular distribution of deuterons with energies more than 328 keV was strongly forward peaked with anisotropy exceeding 10^2 (the ratio of deuterons yield in axial and radial directions).[12] Our experiments with NX2 plasma focus showed the anisotropy of high energy deuterons (more than 328 keV) in the range of 4–8.[13]

Ion acceleration mechanisms in the plasma focus device have been investigated assuming (i) particle motion in dynamically induced electromagnetic fields,[14] (ii) anomalous enhanced plasma resistivity,[15] (iii) rapid dynamic growth of sausage type pinch instability mode,[5] and (iv) fast magnetosonic shock wave produced during the pinch phase.[16] In the acceleration modeling, ions are considered mostly to be accelerated in forward direction although other directions are not excluded. Measurements of ion beam from NX2 plasma focus have employed a variety of techniques including nuclear activation of low-Z material,[17] activation yield ratio,[18] and magnetic spectrometer equipped with a Faraday cup (the results will be discussed in a future publication).

In this brief communication, we report ion beam measurements in the backward direction (more than 90°) of NX2 plasma focus using graphite activation. Nuclear activation is a direct and unambiguous diagnostic for deuteron measurements as graphite is activated by deuterons with threshold energy of 328 keV. Therefore, the activation is evidence of very high energy deuterons moving in backward direction. It is possible to rely on this simple method in the backward direction even where other methods like Faraday cups and magnetic spectrometer would fail for technical reasons.

The NX2 device is a high repetition rate small Mather-type plasma focus with a 27.6 μF capacitor bank coupled to the electrodes through four pseudospark switches.[19] The total system inductance is 26 nH. Throughout these experiments the NX2 was operated with 8 mbar deuterium gas and 12 kV charging voltage. Ion measurement is conducted with the activation of graphite target (20 mm in diameter) inserted on the anode tip. The schematic diagram of the experimental setup is shown in Fig. 1.

The interaction of high energy deuterons with the graphite target results in the production of nitrogen-13. The threshold energy for this reaction is 328 keV, although the cross section remains very small below 600 keV. The graphite activation is therefore caused by the high energy tail of the deuteron distribution. ^{13}N is a short-lived radioisotope, and decays with the half-life of 9.96 min and produces positron. The positrons slow down in the graphite and annihilate with electrons. Two oppositely directed 511 keV gamma rays are produced by each positron annihilation event. Bismuth ger-

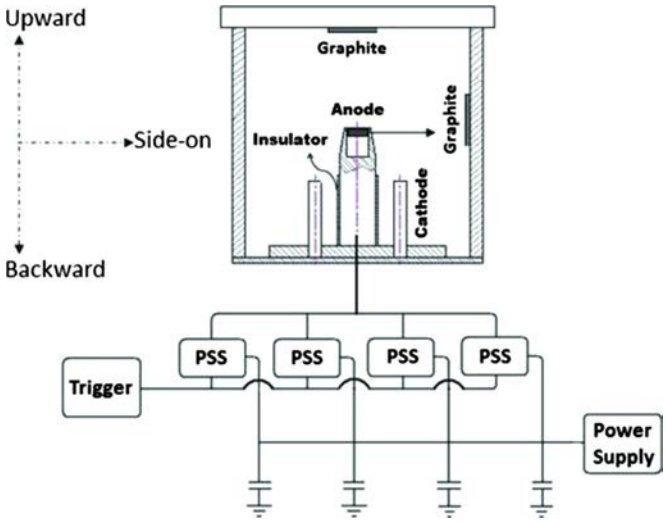

FIG. 1. (Color online) Schematic of NX2 plasma focus and the experimental setup. PSS stands for pseudospark switch.

manate (BGO) scintillation detector (with a radius of 3 in. and thickness of 1 in.) and multichannel analyzer (MCA) system are used to detect the 511 keV gamma rays. The efficiency of the BGO and MCA system for 511 keV annihilation gamma-ray measurement is obtained by Monte Carlo simulations with MCNPX.[20] Simulations show that the BGO system has an efficiency of 52% for detection of positron annihilation events, using an integration window from 400 to 600 keV.

The experiments comprise a sequence of 30 shots fired at 1 Hz repetition rate. NX2 chamber is filled with deuterium at 8 mbars, which is comparatively lower than the optimum pressure for neutron production (14 mbars). At low pressures, neutron yield decreases while the probability of high energy deuteron production is much higher.[17] The discharge voltage in these experiments is 12 kV. Results show significant activation of graphite by high energy deuterons in backward direction as it is shown in Fig. 2.

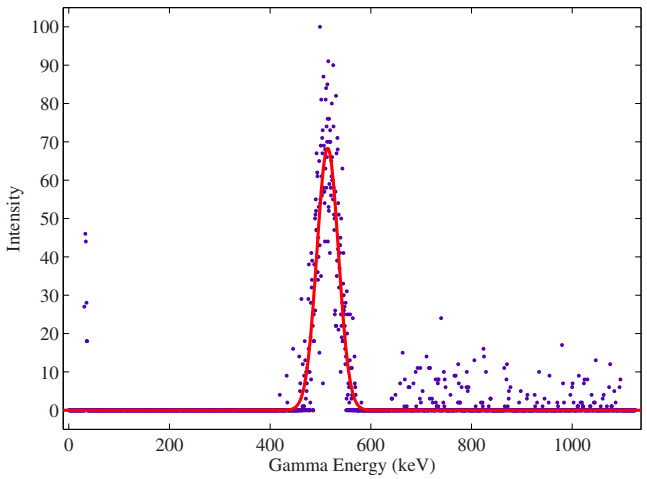

FIG. 2. (Color online) Typical background subtracted spectrum from graphite activation with high energy deuterons.

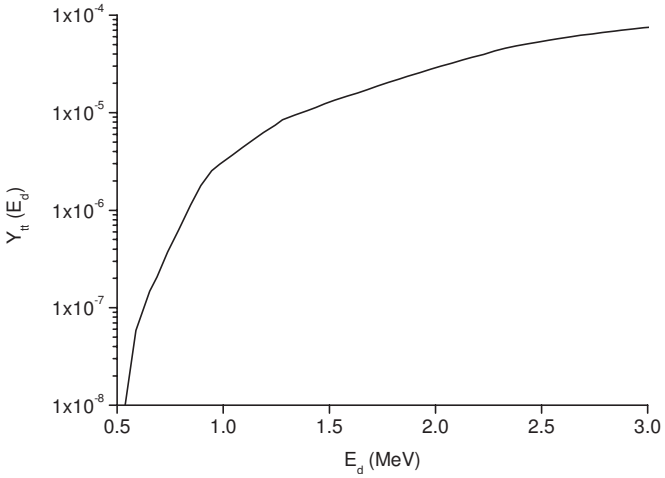

FIG. 3. Thick target yield for $^{12}C(d,n)^{13}N$ nuclear reaction.

The total number of ^{13}N nuclides produced in the target by deuteron bombardment can be obtained from

$$N_{13_N} = k\int_0^{E_{\max}} E_d^{-m} y_{tt}(E_d)dE, \tag{1}$$

where the deuteron energy distribution follows an empirical power law of the form $(dn_d/dE_d)=kE_d^{-m}$ (Ref. 21) and $y_{tt}(E_d)$ is the thick target yield

$$y_{tt}(E_d) = \int_0^R n\sigma(E)dx = n\int_0^{E_d} \frac{\sigma(E)}{|dE/dx|}dE, \tag{2}$$

where E_d is the incident energy of deuterons, $\sigma(E)$ is the reaction cross section, n is the target nuclei per cm^3, dE/dx is the stopping power, and R is deuterons range in the target. Figure 3 displays the calculated thick target yield as a function of deuteron energy.

The total number of ^{13}N nuclides obtained from 511 keV gamma-ray measurements with BGO and MCA system is estimated to be 5.7×10^4. The activation yield-ratio technique gives the value of m to be about 9.[18] The characteristic deuteron energy activating the graphite target is in the range of 650–750 keV. The value of k determined from Eq. (1) is 1.7×10^{10} MeV^{-1}, which gives 1.3×10^{11} *backward deuterons* per shot per steradian with energies higher than 500 keV. The backward deuterons are about one order of magnitude less than the forward ones.[13] For an $\sim E^{-9}$ spectrum, the distribution of ^{13}N yield with deuteron energy is shown in Fig. 4.

The graphite target in current experiments was drilled by electrons at the center (a hole with 0.9 mm depth and 1.5 mm radius) and most of the activated particles were sputtered. A plasma jet drills the target as well. Therefore, the activation in the target which is measured by the BGO and MCA system is much less than the real activation caused by high energy deuterons. Hence, the total number of ^{13}N nuclides produced by high energy deuteron activation of the graphite was underestimated.

Bernstein has reported high energy neutrons (more than 2.45 MeV) at 180°, so it was assumed that some high energy ions have high velocities in the backward direction.[14] How-

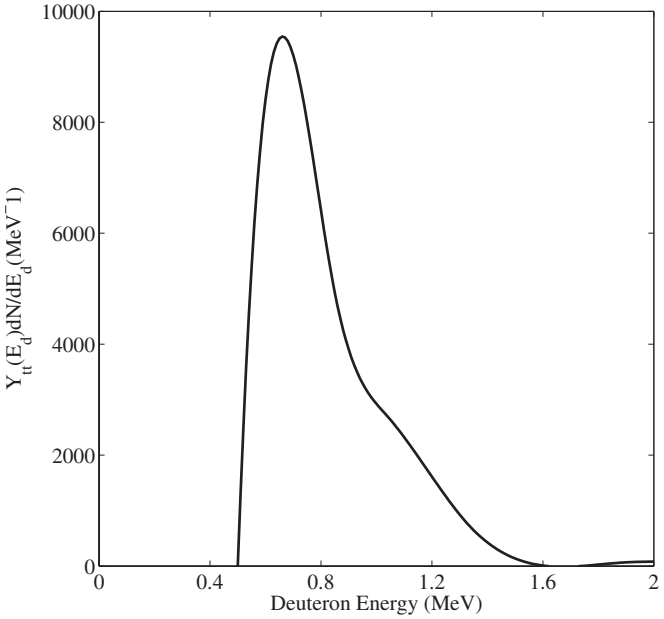

FIG. 4. Nitrogen-13 yield distribution for a deuteron spectrum of $dn_d/dE = kE^{-m}$ $(m=9)$.

ever, the experimentally measured high energy deuterons have not been reported so far, and our experiments could justify the backward high energy neutrons production.

Ion energy, velocity vector, and the mechanism in which they are accelerated, are required to be taken into account for ion acceleration in the pinch. If ions are upward directed and the acceleration is in the same direction, they are accelerated in upward with increasing curvature radius, because the magnetic field depends on the position as shown in Fig. 5.

The pinch current in NX2 plasma focus is about 200 kA and the pinch radius is 1 mm. The magnetic field in the pinch is estimated to be 40 T, which is maximum on the pinch surface and minimum on the axis. Deuterons with the energy $\leq$40 keV, have got the chance to gyrate within the pinch volume, and it is interesting to mention that vast majority of neutrons are produced from deuterons with the energy range of 30–60 keV.[22] However, the curvature radius for deuterons with higher energy is more than the pinch radius, which results in the deuterons to move in the upward direction. This is the case when we assume that deuterons are accelerated with any mechanism and the initial velocity vector is oriented in the upward.

With this assumption, which is considered by most of the authors, it is concluded that none of the deuterons (even with energies much less than the deuterons activating the graphite) are produced in nonaxial directions. So it is required to introduce a mechanism in which the deuterons can be accelerated in different directions. Currently we are working on the possible mechanisms for ion acceleration, including the acceleration in nonaxial directions, in order to clarify the idea based on the experimental measurements.

Comparing the current results with the one reported in Ref. 13, it is concluded that the acceleration of deuterons to very high energies occurs not only in one direction in plasma focus, a fact that is required to be considered in any experimental and theoretical investigation of the mechanism in which the ions are accelerated in the pinch plasma devices. It may also be concluded that the works which search to relate the neutron production to the thermonuclear mechanism, with anisotropy measurements, take into account that the present results strongly suggest that nonthermal mechanism is still dominant in plasma focus.

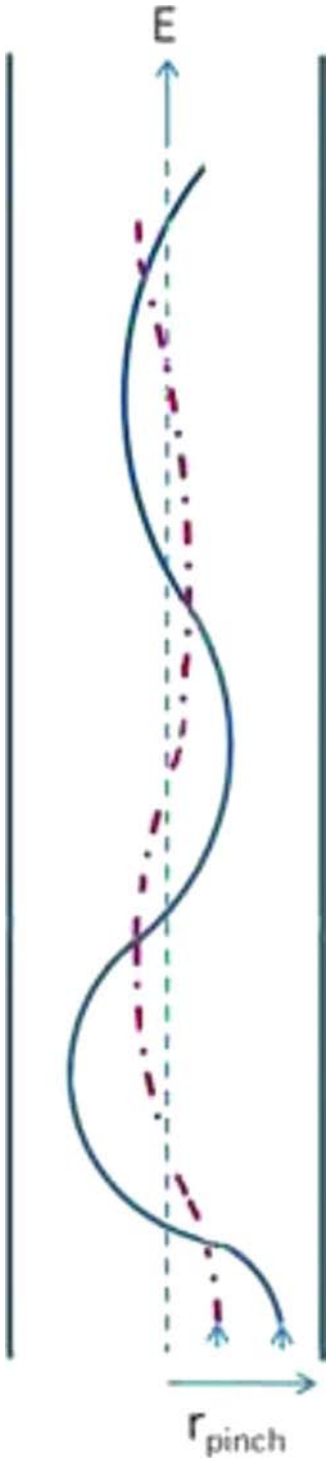

FIG. 5. (Color online) Conceptual drawing of ion trajectories in a constant electric field and magnetic field. Dashed line is the path for high energy ion and solid line for lower energy ion.

[1]J. W. Mather, Methods Exp. Phys. **9**, 187 (1971).
[2]L. Soto, Plasma Phys. Controlled Fusion **47**, A361 (2005).
[3]V. A. Gribkov, A. Banaszak, B. Bienkowska, A. V. Dubrovsky, I. Ivanova-Stanik, L. Jakubowski, L. Karpinski, R. A. Miklaszewski, M. Paduch, M. J. Sadowski, M. Scholz, A. Szydlowski, and K. Tomaszewski, J. Phys. D: Appl. Phys. **40**, 3592 (2007).
[4]L. Bertalot, H. Herold, U. Jager, A. Mozer, T. Oppenlander, M. Sadowski, and H. Schmidt, Phys. Lett. **79A**, 389 (1980).
[5]O. A. Anderson, W. R. Baker, S. A. Colgate, J. Ise, Jr., and R. V. Pyle, Phys. Rev. **110**, 1375 (1958).
[6]L. Michel, H. Schonbach, and H. Fischer, Appl. Phys. Lett. **24**, 57 (1974).
[7]F. N. Beg, K. Krushelnick, C. Gower, S. Tom, A. E. Dangor, A. Howard, T. Sumner, A. Bewick, V. Lebedenko, J. Dawson, D. Davidge, M. Joshi, and J. R. Gillespie, Appl. Phys. Lett. **80**, 3009 (2002).
[8]M. Milanese and J. Pouzo, Nucl. Fusion **18**, 533 (1978).
[9]F. Castillo, M. Milanese, R. Moroso, and J. Pouzo, J. Phys. D: Appl. Phys. **33**, 141 (2000).
[10]J. H. Lee, L. P. Shomo, M. D. Williams, and H. Hernabsdorfer, Phys. Fluids **14**, 2217 (1971).
[11]M. J. Bernstein, Phys. Fluids **13**, 2858 (1970).
[12]R. L. Gullickson and H. L. Sahlin, J. Appl. Phys. **49**, 1099 (1978).
[13]M. V. Roshan, R. S. Rawat, A. Talebitaher, P. Lee, and S. V. Springham, Phys. Plasmas **16**, 053301 (2009).
[14]M. J. Bernstein and G. G. Cosimar, Phys. Fluids **15**, 700 (1972).
[15]S. P. Gary, Phys. Fluids **17**, 2135 (1974).
[16]Y. Mizuguchi, J. I. Sakai, H. R. Yousefi, T. Haruki, and K. Masugatab, Phys. Plasmas **14**, 032704 (2007).
[17]M. V. Roshan, R. S. Rawat, A. Talebitaher, R. Verma, P. Lee, and S. V. Springham, "High energy deuterons emission in NX2 plasma focus," J. Plasma Fus. Res. Ser. (to be published).
[18]M. V. Roshan, S. V. Springham, A. Talebitaher, R. S. Rawat, and P. Lee, Phys. Lett. A **373**, 851 (2009).
[19]J. M. Koh, R. S. Rawat, A. Patran, T. Zhang, D. Wong, S. V. Springham, T. L. Tan, S. Lee, and P. Lee, Plasma Sources Sci. Technol. **14**, 12 (2005).
[20]L. S. Waters, G. W. McKinney, J. W. Durkee, M. L. Fensin, J. S. Hendricks, M. R. James, R. C. Johns, and D. B. Pelowitz, AIP Conf. Proc. **896**, 81 (2007).
[21]H. Kelly and A. Marquez, Plasma Phys. Controlled Fusion **38**, 1931 (1996).
[22]S. V. Springham, S. Lee, and M. S. Rafique, Plasma Phys. Controlled Fusion **42**, 1023 (2000).

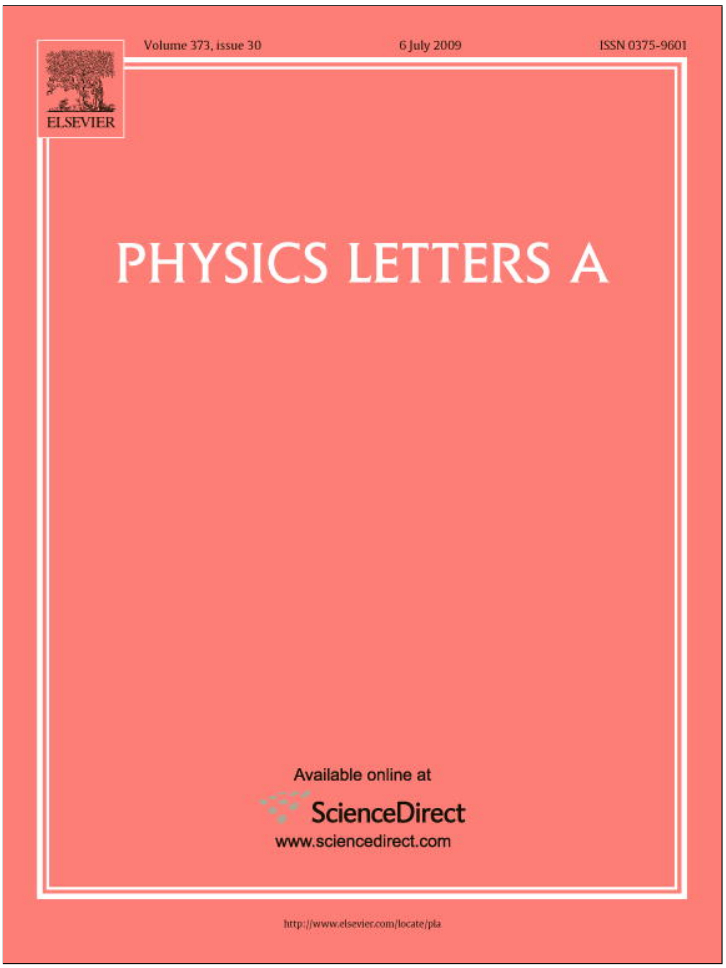

Physics Letters A 373 (2009) 2568–2571

Contents lists available at ScienceDirect

Physics Letters A

www.elsevier.com/locate/pla

Effect of cathode structure on neutron yield performance of a miniature plasma focus device

Rishi Verma [a,1], R.S. Rawat [a,*], P. Lee [a], S. Lee [a], S.V. Springham [a], T.L. Tan [a], M. Krishnan [b]

[a] NSSE, National Institute of Education, Nanyang Technological University, 1 Nanyang Walk, Singapore-637616, Singapore
[b] Alameda Applied Sciences Corporation, San Leandro, CA 94577, USA

ARTICLE INFO

Article history:
Received 19 February 2009
Received in revised form 4 May 2009
Accepted 15 May 2009
Available online 23 May 2009
Communicated by F. Porcelli

PACS:
52.58.Lq
29.25.Dz
82.80.Rt
85.60.Ha

Keywords:
Miniature plasma focus
Neutrons
Time of flight
Pinch current

ABSTRACT

In this Letter we report the effect of two different cathode structures – tubular and squirrel cage, on neutron output from a miniature plasma focus device. The squirrel cage cathode is typical of most DPF sources, with an outer, tubular envelope that serves as a vacuum housing, but does not carry current. The tubular cathode carries the return current and also serves as the vacuum envelope, thereby minimizing the size of the DPF head. The maximum average neutron yield of $(1.82 \pm 0.52) \times 10^5$ n/shot for the tubular cathode at 4 mbar was enhanced to $(1.15 \pm 0.2) \times 10^6$ n/shot with squirrel cage cathode at 6 mbar operation. These results are explained on the basis of a current sheath loading/mass choking effect. The penalty for using a non-transparent cathode negates the advantage of the smaller size of the DPF head.

A long-standing problem of plasma focus devices has been to elucidate the mechanism of neutron production and the correlation between various factors that influence the neutron yield. Over the past few decades various attempts have been made to enhance the neutron yield from deuterium plasma focus devices, for their probable use in fast-neutron activation analysis (FNAA) applications [1], by optimizing various parameters such as anode geometry [2], anode material [3], insulator sleeve material and length [4,5], centre electrode polarity [6], radioactivity assisted pre-ionization [7,8] and high-atomic number gas admixture concentration [9].

Recently many groups have reported the development of miniature plasma focus devices as portable neutron sources [10–15]. A potential limitation of such miniature sources is the fact that the neutron output tends to scale roughly as $(\text{current})^4$ or as $(\text{stored energy})^2$. Hence as one scales down to the sub-kilojoule range (with <100 kA currents) there is a premium on finding ways in which to increase the neutron output above the observed, unfavorable scaling criteria. Among these options is to vary the cathode geometry, which is the province of this Letter. The influence of cathode structure on neutron emission is an important issue since in the typical miniature plasma focus devices, the conventional bar/squirrel cage cathodes are replaced with tubular cathodes [10,11] that double as vacuum barriers and hence reduce the size of the DPF "head". However, the price for this miniaturization in term of its effects on neutron yield has not been investigated; hence in this Letter we describe the effect of conventional squirrel cage cathode structure as opposed to that of newly adopted tubular cathode structure on the neutron yield.

We present results from two different types of cathode geometries (whilst maintaining other operating conditions/parameters and varying only the pressure to optimize the neutron output) on neutron emission from newly developed fast miniature plasma focus device – FMPF-1 [9,10].

The capacitor bank of the FMPF-1 consists of four 0.6 μF, 30 kV capacitors in a compact layout. The detailed design and characterization of this device have been described elsewhere [10]. In the present arrangement, the optimized electrode assembly consists of a 15 mm long stainless steel hollow anode of composite geometry (tapered over the last 5 mm with diameter decreasing from 12 mm to 7 mm) and the cathode diameter is 30 mm. These electrode as-

* Corresponding author.
E-mail address: rajdeep.rawat@nie.edu.sg (R.S. Rawat).
[1] Also at: Pulsed Power Group, Institute for Plasma Research, Bhat, Gandhinagar, Gujarat 382428, India.

0375-9601/$ – see front matter
doi:10.1016/j.physleta.2009.05.025

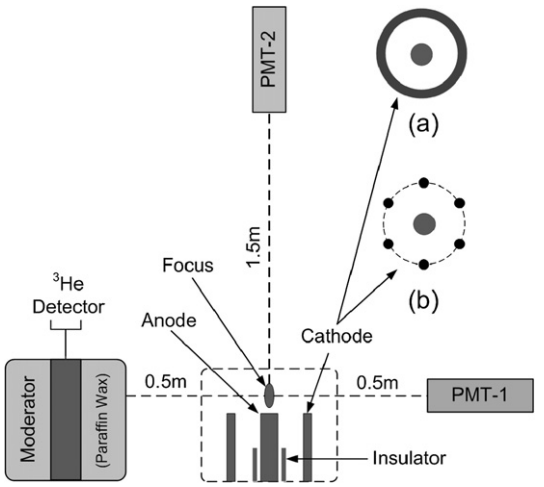

Fig. 1. Layout of time resolved and time integrated neutron diagnostic set-up.

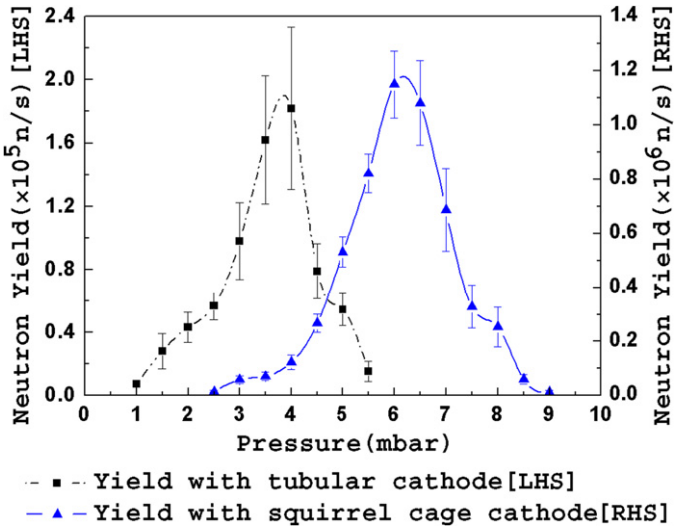

Fig. 2. Neutron yield versus D_2 filling gas pressure for tubular and squirrel cage cathode.

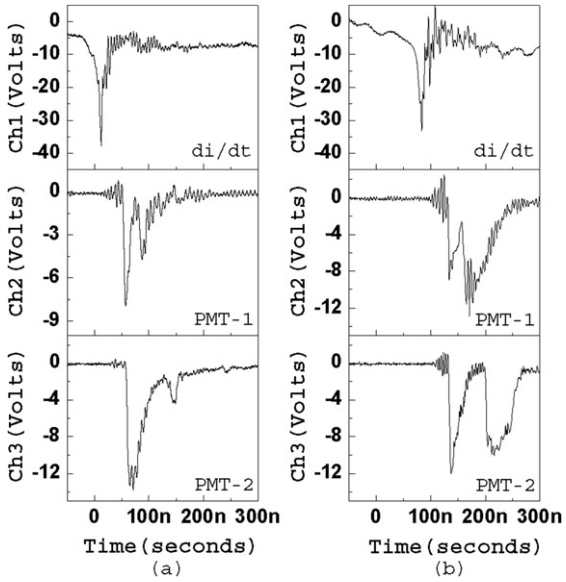

Fig. 3. Current derivative signal trace with HXR/neutron signal recorded with side-on (PMT-1) and end-on (PMT-2) scintillator-photomultiplier detector with (a) tubular cathode, (b) squirrel cage cathode.

sembly dimensions are improved over the dimensions mentioned in our previously published work [10] and they provide better neutron yields as discussed later.

A specially designed Rogowski coil (having response time <3 ns) was used for electrical diagnostics. To measure time integrated neutron yields, a high sensitivity ^{3}He detector arrangement has been used [10,16]. To acquire the time resolved history of emitted radiation, a 'dual time of flight' arrangement consisting of two identical scintillator photomultiplier detectors – PMT-1 and PMT-2 was used. Each of the scintillator photomultiplier detectors consists of an NE102A plastic scintillator (of thickness 40 mm and diameter of 50 mm) and photomultiplier tube EMI 9813B (biased at -1800 V and enclosed inside 1 cm thick Aluminum casing). The PMT-1 was placed radially (90°) at a distance of 0.5 m from the anode face, whereas PMT-2 was placed axially (0°) at a distance of 1.5 m from the anode face along the anode axis. A schematic drawing of this arrangement is shown in Fig. 1. In the insets images of the utilized tubular and squirrel cage cathode structures are shown as inset (a) and inset (b), respectively.

The effects of tubular and squirrel cage cathode geometries on neutron and hard X-ray (HXR) emissions for different fill pressures are investigated at the fixed stored energy of 230 J (with about 80 kA peak discharge current at 13.8 kV charging voltage). The results were obtained for averages of 20 shots for every choice of deuterium gas pressure. To reduce the effect of electrode particulate contamination on neutron output, the gas was refreshed after every five shots. A nominal pressure increase of ≈0.05 mbar was observed after each set of 5 shots.

Our experiments with two different cathode geometries have demonstrated that the final pinch characteristics and in particular, the emission of neutrons is strongly influenced by the cathode structure. The measured average neutron outputs for tubular and squirrel cage cathode geometries, for different D_2 filling gas pressures, are shown in Fig. 2. A remarkable enhancement in neutron yield was observed with squirrel cage cathode operation. The maximum average neutron output of $(1.82 \pm 0.52) \times 10^5$ and $(1.15 \pm 0.2) \times 10^6$ n/shot were measured for tubular and squirrel cage cathode geometries, respectively. It is also observed that the neutron yield peaked at the higher gas pressure 6 mbar for squirrel cage cathode while it peaked at 4 mbar for tubular cathode structure.

Time resolved information about the hard X-ray and neutron emission is obtained using the scintillator photomultiplier detectors PMT-1 and PMT-2 for tubular and squirrel cage cathodes. Those data are shown in Fig. 3 along with corresponding di/dt signals. The first peak in the PMT signals of these two figures (shown as Ch2 and Ch3), is of non-thermal, hard X-rays produced by the instability accelerated electron beam upon hitting the anode target. The second peak is confirmed to be that of neutrons, on the basis of time of flight estimates, assuming that the hard X-rays and neutrons are created at the same time in the pinch. Since the PMT-1 and PMT-2 were placed at a distance of 0.5 m (radially) and 1.5 m (axially), from and along the anode axis, subsequent registration of neutron pulses (i.e. second, delayed peak in the respective signals) at about 23 ± 2 ns and 66 ± 3 ns, respectively, after the emission of hard X-ray pulses confirms that the second peak is due to ≈2.45 MeV D–D neutrons. The relative time difference of 45 ± 3 ns, between the neutron pulses, recorded by the channels Ch2 and Ch3 also re-confirms the neutron pulse emission. The average duration of HXR and neutron pulses, estimated from the FWHM of the corresponding peaks and averaged over 20 shots, in the axial/radial direction are 18 ± 3 ns/12 ± 2 ns and 16 ± 3 ns/16 ± 2 ns, respectively, for tubular cathode operation (Fig. 3(a)), and 18 ± 2 ns/15 ± 2 ns and 46 ± 3 ns/45 ± 2 ns, respectively, for squirrel cage cathode opera-

tion (Fig. 3(b)). The ∼30 ns delay in the appearance of HXR peak (Ch2 and Ch3 trace in the respective figures) from the peak of the current derivative signal (Ch1 trace) is because of the inherent latency in the PMT.

In the plasma focus, the run-down phase allows the transfer of electrical energy from the capacitor bank to the magnetic energy behind the accelerating current sheath a fraction of which is rapidly pumped into the pinch plasma column at the end of radial compression phase in a relatively short time, leading to efficient compression and heating [17]. Under stationary initial gas conditions (unlike in a supersonic gas puff) it is impossible to decouple the final radial compression phase and corresponding plasma phenomena from those occurring during the breakdown and axial run down phases [18]. Therefore, while considering losses in a typical (non-gas-puffed) plasma focus device, the thermal flow down the axis during axial acceleration is an important consideration.

The very high temperature achieved in the plasma focus is mainly the result of the axis-symmetric properties of the imploding shock. Since in the case of the tubular cathode, the outer electrode is an impermeable wall, when there is momentum flowing parallel to the shock, to obtain pressure balance along the shock and near the wall, the plasma density adjacent to the wall must increase. This momentum flowing parallel to the shock thus acts as a sink for the incoming plasma and causes a drop in temperature with increasing radius (as the magnetic pressure falls). With lower temperatures adjacent to the cathode wall and in particular lower electron temperatures, the shock is broadened (with increase in thickness) through resistive diffusion of the magnetic field [19,20]. Aggregation of plasma density near the cathode wall also affects the final temperature that is achieved in the pinch, owing to the fact that compression ratio is mainly dominated by $\rho_{\text{pinch}}/\rho_{\text{shock}}$ and only a partial fraction (about 15%) of the plasma is collected into the ensuing pinch [19]. Hence, in the case of tubular cathodes, due to larger contact area (in comparison with squirrel cage cathode), deleterious effects because of plasma aggregation near the cathode wall are expected to be more pronounced, with a consequent reduction in neutron output.

Another important noticeable observation in the graph shown in Fig. 2 (neutron output vs. filling gas pressure); is the relative shift in the optimum base pressure range with the use of tubular and squirrel cage cathode geometries [21]. The difference in the optimum base pressure range for the two cathode geometries can be explained by the fact that since the geometry of the squirrel cage cathode, allows mass to pass through, during the axial run down phase, the inter-electrode space is relatively clear. In the case of tubular cathodes the outward flow is blocked (due to current sheath canting), then the channel (i.e. the inter electrode space) tends to get constricted due to growing thickness of 'contact layer'. When this layer gets thick enough the channel tends to get loaded/choked. In addition, the outward moving particles are reflected back along with impurities from cathode wall causing substantial increase in thermal bremsstrahlung radiation loss [22] due to impurity addition. In any case, with the use of tubular cathode geometry the cross sectional area of the channel gets effectively reduced, which accounts for loading of current sheath at comparatively lower operating pressure. This observation is corroborated by the measurements shown in Fig. 4, where the variation in time to pinch from the breakdown phase (which includes axial acceleration phase and compression phase, defined as t_p in the current derivative signal shown in the inset), at different filling gas pressures is plotted, for the tubular and squirrel cage cathode geometries. Usually in a typical plasma focus device operation, the characteristic time t_p, increases with the increase in operating pressure due to increased load on the current sheath in the axial phase. In the graph shown, larger slope angle of the operation curve for tubular cathode (by contrast to squirrel cage cathode operation), indicates comparatively higher loading of the current sheath, even at lower pressures. The squirrel cage cathode seems to lessen much of these effects and thus performs with better efficiency resulting in higher yields.

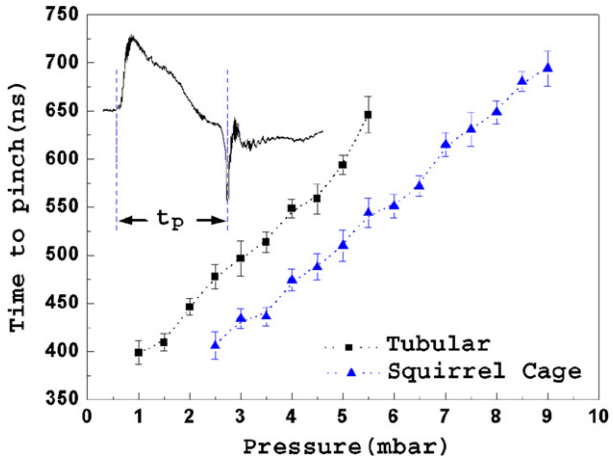

Fig. 4. Time to pinch versus D_2 filling gas pressure for tubular and squirrel cage cathode operation.

Interestingly, it may also be noted that, the 'time to pinch' witnessed for the corresponding cathode geometries (tubular and squirrel cage) at which the neutron yield maximizes is the same i.e. ∼550 ns, while operating at 4 mbar and 6 mbar, respectively. This observation also corroborates the current sheath loading/choking effect with use of tubular cathodes.

Recently, neutron yield scaling has been thoroughly reviewed by S. Lee et al. [23–25], using the five-phase Lee model (RADPFV5.13) [26], and found to follow $Y_n \sim I_{\text{pinch}}^x$ where I_{pinch} is the pinch current that actually participates in the focus pinch phase and x is found to vary in the range of 3–5 for different plasma focus devices. To realistically simulate the experiment using Lee model, firstly the circuit parameters, electrode dimensions, operating voltage and gas pressure are keyed into the code, then the computed current trace is 'fitted' to the experimental peak discharge current trace, by adjusting four 'model parameters'. These four parameters for 'fitting' are axial mass swept-up factor f_m and axial current factor f_c (which characterize axial phase electrodynamics), radial mass factor f_{mr} and radial current factor f_{cr} (which characterize radial phase dynamics). These model parameters are then fine-tuned till the computed trace is in close agreement with the experimentally measured peak discharge current trace [24]. The main objective of using the Lee code is to investigate the changes in the fitting model parameters and electrodynamic behavior for the two cathode geometries to deduce and understand the corresponding changes in plasma dynamics and pinch current. The fine tuned electrical circuit parameters used for the simulation of respective geometries are: 2.4 μF, 32.9 nH and 60 mΩ for tubular cathode operation and 2.4 μF, 31.0 nH and 67 mΩ for squirrel cage cathode operation. A typical 'fitted' trace of squirrel cage cathode operation at 6 mbar gas pressure is shown in Fig. 5. Values of 'model parameters' that have been obtained for 'best fit' with tubular and squirrel cage cathodes (at 4 and 6 mbar, respectively), along with peak/pinch current estimations are summarized in Table 1. The two key differences that can be noticed from Table 1 are (i) for tubular cathode structure, the values of axial mass swept-up factor f_m and radial mass factor f_{mr} are about ∼1.82 and ∼2.2 times higher, respectively, than that obtained for squirrel cage cathode operation which supports the argument and observation of the mass loading of the current sheath for tubular operation and (ii) the estimated pinch current is lower for tubu-

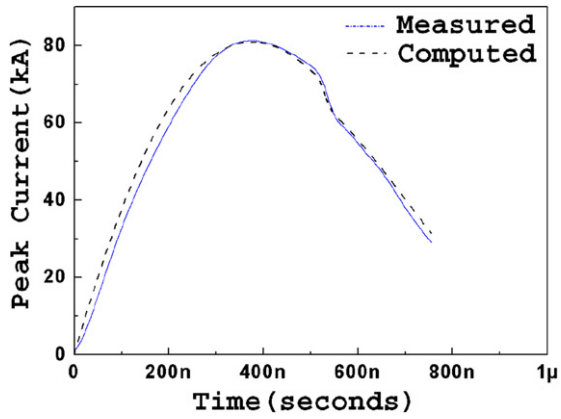

Fig. 5. A "fitted" current trace for squirrel cage cathode operation at 6 mbar filling gas pressure.

Table 1
Model parameters and simulation results

Cathode	f_m	f_{mr}	f_c	f_{cr}	I_{pinch}/I_{peak}
Tubular	0.31	0.33	0.62	0.84	54 kA/81 kA
Squirrel cage	0.17	0.15	0.62	0.89	58 kA/80 kA

lar cathode operation supporting the lower neutron output for this cathode.

In conclusion, our investigation shows a notable enhancement in the neutron output for the squirrel cage geometry as compared to that of a tubular geometry. In a tubular cathode structure, owing to the impermeable wall and relatively larger surface area, the plasma density rises near the cathode wall, causing the shock to be radially broadened through resistive diffusion of the magnetic field. This results in the narrowing of the effective channel cross-section, causing loading of the current sheath along with increased contact layer resistance thereby resulting in lower pinch efficiency. It may also be realized from the Lee model fitting of our experimental results that operation with tubular cathodes also affects the current going out from the main current sheath to the residual plasma as a consequence well-known "current leakage" effect. The fraction of peak discharge current that actually goes from main current sheath to the pinch (i.e. pinch current I_{pinch}) is reduced for tubular cathode operation supporting the lower neutron output for this cathode. Also in operation with tubular cathodes, addition of impurities (due to back reflected particles from the cathode wall) during the axial flow, may result in a substantial drop in temperature due to increased radiation loss which is also consistent with the reduction in neutron output.

Acknowledgements

The authors are grateful to the National Institute of Education/Nanyang Technological University, Singapore, for Scholarship grant and AcRF grant RP 3/06/RSR. One of us, R.V., would like to thank parent organization IPR, Gandhinagar, Gujarat, India for providing study leave to pursue Phd Programme at NTU.

References

[1] V. Gribkov, A. Dubrovsky, L. Karpinski, R. Miklaszewski, M. Paduch, M. Scholz, P. Strzyzewski, K. Tomaszewski, AIP Conf. Proc. 875 (2006) 415.
[2] J.M. Koh, R.S. Rawat, A. Patran, T. Zhang, D. Wong, S.V. Springham, T.L. Tan, S. Lee, P. Lee, Plasma Sources Sci. Technol. 14 (2005) 12.
[3] A. Shyam, R.K. Rout, Phys. Scr. 57 (1998) 290.
[4] F.N. Beg, M. Zakaullah, G. Murtaza, M.M. Beg, Phys. Scr. 46 (1992) 152.
[5] M. Zakaullah, T.J. Baig, S. Beg, G. Murtaza, Phys. Lett. A 137 (1989) 39.
[6] G. Decker, W. Kies, G. Pross, Phys. Lett. A 89 (1982) 393.
[7] M. Zakaullah, A. Waheed, S. Ahmad, S. Zeb, S. Hussain, Plasma Sources Sci. Technol. 12 (2003) 443.
[8] S. Ahmad, S.S. Hussain, M. Sadiq, M. Shafiq, A. Waheed, M. Zakaullah, Plasma Phys. Control. Fusion 48 (2006) 745.
[9] R. Verma, P. Lee, S. Lee, S.V. Springham, T.L. Tan, R.S. Rawat, M. Krishnan, Appl. Phys. Lett. 93 (2008) 101501.
[10] R. Verma, M.V. Roshan, F. Malik, P. Lee, S. Lee, S.V. Springham, T.L. Tan, M. Krishnan, R.S. Rawat, Plasma Sources Sci. Technol. 17 (2008) 045020.
[11] R.K. Rout, P. Mishra, A.M. Rawool, L.V. Kulkarni, S.C. Gupta, J. Phys. D: Appl. Phys. 41 (2008) 205211.
[12] P. Silva, J. Moreno, L. Soto, L. Birstein, R.E. Mayer, W. Kies, Appl. Phys. Lett. 83 (2003) 3269.
[13] M. Milanese, R. Moroso, J. Pouzo, Eur. Phys. J. D 27 (2003) 77.
[14] L. Soto, P. Silva, J. Moreno, M. Zambra, W. Kies, R.E. Mayer, A. Clausse, L. Altamirano, C. Pavez, L. Huerta, J. Phys. D: Appl. Phys. 41 (2008) 205215.
[15] L. Soto, C. Pavez, P. Silva, J. Moreno, M. Barbaglia, A. Clausse, Plasma Sources Sci. Technol. 18 (2009) 015007.
[16] J. Moreno, L. Birstein, R.E. Mayer, P. Silva, L. Soto, Meas. Sci. Technol. 19 (2008) 087002.
[17] M.G. Haines, Philos. Trans. R. Soc. London A 300 (1981) 649.
[18] H. Schmidt, M. Sadowski, L. Jakubowski, E.S. Sadowska, J. Stanislawski, Plasma Phys. Control. Fusion 36 (1994) 13.
[19] D.E. Potter, Phys. Fluids 14 (1971) 1911.
[20] G.J. Pert, J. Phys. D: Appl. Phys. 1 (1968) 1487.
[21] M.A.M. Kashani, T. Miyamoto, AIP Conf. Proc. 651 (2002) 249.
[22] L.H. Li, H.Q. Zhang, J. Phys. D: Appl. Phys. 29 (1996) 2217.
[23] S. Lee, S.H. Saw, Appl. Phys. Lett. 92 (2008) 021503.
[24] S. Lee, P. Lee, S.H. Saw, R.S. Rawat, Plasma Phys. Control. Fusion 50 (2008) 065012.
[25] S. Lee, S.H. Saw, J. Fusion Energy 27 (2008) 292.
[26] http://www.intimal.edu.my/school/fas/UFLF/File7RADPF05.13.9b.xls.